CHAPTER ONE
INTRODUCTION

1.1Background of Study

In recent years, the preparation of activated carbons from several agricultural by-products has been emphasized due to the growing interest in low cost activated carbons from renewable biomass, especially for applications concerning treatment of drinking water and wastewater (Castro *et al.*, 2000).

Consequently, the removal of heavy metals from effluents is one of the major environmental concerns. Therefore, adsorption process has been found to be more effective method for the treatment of heavy metals containing wastewater. The most efficient and commonly used adsorbent is commercial activated carbon which is expensive and has regeneration problems. Recent investigations focused on the effectiveness of low cost adsorbents, like pearl millet husk (Selverani, 2000), wheat straw (Robinson *et al.*, 2002, Verma and Mishra, 2006), sewage sludge (Otero *et al*., 2003), perlite (Dogan *et al.*, 2000), in the removal of heavy metals from wastewater effluent.

Adsorption is a physicochemical process that offers great potential for treating effluents containing undesireable components and renders them safe and reusable (Gupta, *et al.*, 1988, Annadurai, 1996). The major advantage of an adsorption system for water pollution control, are low investment in terms of both initial and land cost, simple design, easy operation and no effects by toxic harmful substances (Annadurai, 1997). Thus, the present work was undertaken to explor the feasibility of finding a low cost effective adsorbent pearnut seed, palm kernel shell, snail shell

and oil bean shell activated carbon, for the treatment of wastewater, heavy metals from aqueous solution. As one of the successful and progressive leading country in palm oil industry, Nigeria produce large amount of waste from palm oil (*Elaeis guineensis*). For every production of 1 million ton of crude palm oil, 11 million tons of waste are produced; palm fiber, palm shell, palm wood and empty fruit bunch (Low, 2011). Only kernel of the fruit and its surrounding fiber (mesocarp) are used for oil extraction. Due to the abundant source of precursor, which is 0.4 million tons palm shell per every million tons of crude palm oil produced, high volatile and carbon contents, palm shell is a suitable precursor to replace conventional activated carbon (AC). Utilizing the palm shell for production of AC will reduce cost, compared to conventional AC. Moreover, it can be said as substitution of waste to wealth. The main advantage is that this material is an agricultural solid waste, available locally and abundantly.

Globally, industrial wastewater represents the main source of water pollution (Akaninwor *et al.*, 2007, Alam *et al*., 2007). Industrial wastewaters are considered among the major sources of environmental pollution, endangering public health through direct use as well as feeding fish that live in the polluted streams.

In most developing countries like Nigeria, most industries dispose their effluents into waters without treatment. These industrial effluents have a hazard effect on water quality, habitat quality, and complex effects on flowing waters (Ethan *et al.*, 2003). Industrial wastes and emission contain toxic and hazardous substances such as heavy metals, most of which are detrimental to human health (Jimena *et al.*,

2008, Rajaram and Ashutost, 2008). The presence of heavy metals in the environment is a potential problem to soil and water quality due to their high toxicity to plants, animals and human life (Meng *et al.*, 2008). Heavy metals have been reported to be carcinogenic (Cossiches, 2002). Apart from being hazardous to living organisms when specific limits are exceeded, they also have accumulating tendencies (Veli, and Alyuz, 2007, Fonseca *et al.*, 2006, Ahmady-Asbchin *et al.*, 2008). Recently, water and wastewater (effluents) contamination by toxic metals has become a global environmental concern because of consequent interference with many uses of water (Ulmanu *et al*., 2003: Aziz *et al.*, 2008). This has led to the enactment of laws worldwide setting discharge limits of these metals from industry (Radojevic and Bashkin, 1999, Lenntech, 2006). In Nigeria, main contributors to the surface and ground water pollution are the by-products of various industries such as textile, metal, dying chemicals, fertilizers, pesticides, cement, petrochemical, energy and power, leather, sugar processing, construction, steel, engineering, food processing, mining, agriculture and others (Idris *et al.*, 2013).

Inability to effectively and efficiently manage vast amount of wastes generated by various anthropogenic activities particularly in developing countries has created one of the most critical problems in our environment. Of more importance is the manner in which industrial effluents are being disposed into the ambient environment, water bodies, fresh water reservoirs being mostly affected. With such activity, these natural resources are rendered unsuitable for both primary and secondary usages (Fakayode, 2005). The major sources of drinking water in Nigeria-inland water

bodies and estuaries-have always been contaminated by the activities of the adjoining populations and industrial establishments (Sangodoyin, 1995).

River systems are the primary means for disposal of industrial effluents, and these have the capacity to alter the physical, chemical and biological nature of the receiving water body (Sangodoyin, 1991). Of recent, there have been pollution stress on surface water bodies as a result of increased industrial activities (Ajayi and Osibanji, 1981). The consequences of this are of great magnitude to public health and the environment (Osibanji *et al*., 2011).

Ideally, effluents from industries are supposed to be properly treated before being discharged into the environment. In Nigeria, there are laws put in place to guide and regulate industrial discharge practices and environmental contamination generally. The Federal Environmental Protection Agency (FEPA) established to check environmental abuses has had little or no impact on pollution control in our environment (Ezeronye and Amogu, 1998).

In Nigeria, cities like Kaduna, Lagos, Kano and Aba depend heavily on their rivers for water supplies. However, the rush by African countries to industrialize has resulted in discharge of partially treated or raw wastes into the surrounding bodies of water since the development of treatment facilities cannot keep pace with the rate at which the wastes are generated by the industries (Nwachuku *et al.*, 1989).

The industrial discharge, constitutes a larger portion of the flow of the river during the dry season, with resultant deteriorated water quality of the river. Uses for which the river is employed involving body contact, expose users to serious hazards owing

to the bacterial infection. Many water bodies in Nigeria experience seasonal fluctuation; leading to a higher concentration of pollutants during the dry season when effluents are least diluted (Kanu *et al.*, 2006).

There are many types of industrial wastewater based on the different industries and the contaminants; each sector produces its own particular combination of pollutants. The metal-working industries discharge chromium, nickel, zinc, cadmium, lead, iron and titanium compounds, among them the electroplating industry is an important pollutants distributor. Photo processing shops produce silver, dry cleaning and car repair shops generate solvent waste, and printing plants release inks and dyes. The pulp and paper industry relies heavily on chlorine-based substances, and as a result, pulp and paper mill effluents contain chloride organics and dioxins, as well as suspended solids and organic wastes. The petrochemical industry discharges a lot of phenols and mineral oils. Also, wastewater from food processing plants is high in suspended solids and organic material (Julie and Stauffer, 1998).

The lack of access to safe drinking water and sanitation is probably directly related to poverty and in many cases to corruption and the inability of governments to develop the political will to provide water and sanitation systems for their citizens. Hence, the public sector has not been successful in meeting the demand for water for residential and commercial uses. For example, out of the 85 million people living in urban and semi-urban areas, less than half have reasonable access to reliable water supply (World Bank and Federal Ministry of Water Resources, 2000). This situation has compelled many households, often the poor, to end up buying

water from water vendors at great expense. This situation has been confirmed by studies of different cities in Nigeria. For instance, despite investments and reforms, Lagos state water authority still lacks adequate treatment capacity to deliver enough clean water for drinking and household use. By the end of 2008, vigorous efforts by the state water authority achieved a water delivery capacity of 200 million gallons per day against a demand of 600 million gallons, a gap of about 66 per cent. This has made households to turn to private wells or street vendors to meet their daily water needs, which has exposed consumers to bacterial infection and heavy metal contamination exceeding local regulatory standards (Stimson Global Health Security, 2013). Similarly, in Nnewi, a town, popular for its commercial and industrial activities in Anambra State, most of the households depend on borehole, well water and 'sachet water' as major potable water sources (Ifenna and Chinedu, 2012). Access to potable water supply in Ibadan is not different from what is obtainable in most cities in Nigeria. Water supply shortages have been very critical in Ibadan city since the 1980s and less than 30% of her residents have access to public water system (Adeniji and Oloukoi, 2012).

There are many technologies that have been developed for purification and treatment of wastewater including chemical precipitation, solvent extraction, oxidation, reduction, dialysis/electrodialysis, electrolytic extraction, reverse osmosis, ion-exchange, evaporation, sedimentation, dilution, adsorption, filtration, flotation, air stripping, steam stripping, flocculation, sedimentation and soil flushing/washing chelation (Mohan and Singh, 2002). The technologies selected

must be analyzed accordingly based on several factors such as available space for construction of treatment facilities, ability of process equipment, limitation of waste disposal, desired final water quality and costs of capital and operating. Mostly, all the technologies listed above are less likely to be selected because they require large financial input and their applications are limited due to the cost factors which predominate the importance of pollution control. Adsorption process is found to be the most suitable technique to remove pollutants from wastewater. It is mostly preferred due to its convenience, ease of operation and simplicity of design. Apart from removing many types of pollutants, it also has wide application in water pollution control. AC is widely used as adsorbent due to its high surface area and pore volume as well as inert properties. However, conventional AC is expensive due to the depletion of coal-based source and especially for producing high quality AC (Mohan and Pittman, 2006).

As substitute to the expensive AC, low cost precursor has been of strong interest to researchers in order to reduce the cost incurred in the purchase of the conventional AC. The factors affecting substitution of raw material are the raw material's high carbon content, low in inorganic content, high density and sufficient volatile content, stability of supply in the countries, potential extent of activation and inexpensive material (Nurul'-Ain, 2007). The AC is mainly comprised of carbon with large surface area, large pore volume and high porosity where the adsorptions take place.

Some studies have reported the use of palm shell, coconut shell, groundnut shell for the production of AC (Jumasiah *et al.*, 2005; Issabayeva *et al*., 2006; Tan *et al*., 2008; Jia and Lua, 2008). However, good number of the studies have been restricted to either type of wastes, preparation procedures, or specific aqueous-phase applications.

1.2 STATEMENT OF PROBLEM

Human activities have led to immense pollution of our environment especially the water bodies. This is as a result of the discharge of inorganic effluents from industries directly into the environment without treatment due to the high cost of establishing or maintaining the effluent treatment plant. These effluents enter the food chain when the aquatic organisms in the water bodies adsorb/absorb them and they are then eaten by human being thereby causing several diseases such as high blood pressure and heart attack. So finding simple and cheap ways of treating these effluents using modified adsorbents from low cost agro-wastes before discharging them into the water bodies forms the purpose of this study. Adsorption which is a phase transfer process has been proved to be one of the best processes in waste management. As a result this study sought to modify some cheap agro-wastes and use them to adsorb the inorganic wastes from industrial effluents before they are discharged into the environment.

1.3 AIM OF THE STUDY

To remove heavy metals from aqueous solutions using activated carbon prepared from agricultural wastes - Oil bean shell, snail shell, palm kernel shell (*Elaeis Guineensisn*) and pear nut seed (*African canarium or African Elemi*).

The Specific Objectives Include:

I. To determine the optimum production conditions of low cost activated carbon from Oil bean shell, snail shell, palm kernel shell (*Elaeis Guineensisn*) and pear nut seed (*African canarium or African Elemi*).

II. To evaluate the effect of chemical activation on the development of pore structure of the activated carbon produced.

III. To optimise the activating conditions for the production of activated carbons.

IV. To characterize the activated carbons produced.

V. To determine their potentials for the removal of Pb^{2+} Cd^{2+}, Mn^{2+} and Ni^{2+} from industrial wastewater.

VI. To test the data obtained from the work on some kinetic models, and

VII. To also determine the isotherm behaviour of the adsorption processes.

1.4 JUSTIFICATION OF STUDY

Due to the continuous urbanization and industrialization in many parts of the world, including Nigeria, metals are continuously being emitted into the environment (water bodies) from the anthropogenic activities of the urban citizens and effluents from manufacturing industries such as battery, petroleum , chemical, textile, cosmetics industries, to the level that may pose a great threat to animal or human health. So, there is need to immobilize these heavy metals from their sources before they enter the food chain and also the need to assess the potentiality of using agro-wastes in the immobilization of these industrial influents (heavy metals). This can be achieved through adsorption. Adsorption which is a surface phenomenon that occur when a gas or liquid solute accumulates on the surface of a solid or liquid

forming a molecular or atomic film (Oyeyemi, 2010), has been described as an effective separation process for treating industrial and domestic effluents. It is widely used as effective physical method of separation in order to eliminate or lower the concentration of a wide range of dissolved pollutants (organics or inorganics) in effluents (Ansari and Mohammad-Khan, 2009). However finding simple and easily performable experiments to illustrate the quantitative aspects of adsorption can be very difficult (Uddin *et al*., 2007). So obtaining effective adsorbents from agricultural wastes through carbonization and activation could be necessary.

1.5 SCOPE OF STUDY

The present work seeks to chemically modify some selected agro-wastes for their use in the removal of heavy metal from aqueous solution, to determine the suitability of the use of AC produced from agro-wastes in the adsorption of metals from industrial effluents, to compare the adsorption efficiency of the AC from these agro-wastes under investigation, and to establish the adsorption capacity of the AC from each of these agro-wastes.

Activated carbon was prepared from two vegetable shells (oil bean and palm kernel), pear nut seed was also carbonised and activated. Snail shell from the sea was carbonised and activated. Carbonisation was carried out at 800°C and 600°C. Therefore, there were eight experimental units. Each portion of the sample was treated three times with different acids. Proximate analysis carried out on each sample were ash, fixed carbon, moisture was determined. The elemental content of each agro-wastes were also determined and these were hydrogen, sodium, oxygen, nitrogen and potassium content. Pore morphology of the activated and unactivated

carbons was determined using scanning electron microscope (SEM) and their pore volumes determined. Surface area of the AC produced was determined. Functional groups present on the surface of the activated carbons were determined before and after usage for adsorption studies using Fourier Transform Infra-Red spectroscopy (FTIR). The adsorption efficiency of the activated carbons was studied using Freundlich, Langmuir, Temkin and Dubinin Radushkevich models and the effect of the initial metal concentration was determined as well. Also, the adsorption kinetics was studied using the first order kinetics and second order kinetic models. Two error functions of non-linear regression basis (HYBRID & MPSD) were employed to find out the most suitable kinetic model to represent the experimental data. Intraparticle diffusion model was also used to study the adsorbate transport from solution phase to the surface of the adsorbent as the rate controlling step.

Characterization of waste water from battery Industry was carried out and the modified agro-wastes were used to remove the Pb present in the wastewater.

CHAPTER TWO
LITERATURE REVIEW

2.1 History of Activated Carbon and Present Day Applications

Activated carbon is a trade name for a carbonaceous adsorbent, which can be manufactured from a variety of carbonaceous materials. The useful properties of activated carbon have been known since ancient times. This traces back to 1500BC when Egyptians used charcoal as an adsorbent for medicinal purposes and a purifying agent. Around 420BC it was observed that Hippocrates dusted wounds with powdered charcoal to remove their odour. Ancient Hindu societies purified their water by filtration through charcoal (Bansal *et al.*, 2005). In 1773, the Swedish chemist Karl Wilhelm Scheele was the first to observe adsorption of gases on charcoal. A few years later activated carbons became popular in applications in the sugar industry as a decolorizing agent for syrup.

In the early 20th century the first plant to produce activated carbon industrially was built for use in sugar refining industry in Germany. Many other plants emerged in the early 1900's to make activated carbons primarily for decolourization. During World War I activated carbon was used in gas masks for protection against hazardous gases and vapours. Today, activated carbons are used to remove colour from pharmaceutical and food products, as air pollution control devices for industrial and automobile exhaust, for chemical purification, and as electrodes in batteries. 500,000 tons per year of activated carbon are produced globally (Jankowska *et al.*, 1991). 80% of this is used for liquid phase applications, and 20% is used for solid phase applications (Bansal *et al.*, 2005).

2.2 Definition of Activated Carbon

Activated carbon is defined as a carbonaceous material with a large internal surface area and highly developed porous structure resulting from the processing of raw materials under high temperature reactions. It is composed of 87% to 97% carbon but also contains other elements depending on the processing method used and raw material it is derived from. Activated carbon's porous structure allows it to adsorb materials from the liquid and gas phase (Jankowska *et al.*, 1991). Its pore volume typically ranges from 0.20 to 0.60cm^3/g, and has been found to be as large as 1.0cm^3/g. Its surface area ranges typically from 800 to 1500m^2/g (Bansal *et al.*, 2005), but has been found to be in excess of 3,000m^2/g. The surface area contains mostly micropores with pore diameters smaller than 2nm (Beguin *et al.*, 2010).

2.3 Development of Micropore Structure in Activated Carbons

During the manufacturing process, macropores are first formed by the oxidation of weak functional groups on the external surface area of the raw material. Mesopores are then formed and are, essentially, secondary channels formed in the walls of the macropore structure. Finally, the micropores are formed by attack of the planes within the structure of the raw material (Cameron carbon Incorperated, 2006). All activated carbons contain micropores, mesopores, and macropores within their structures but the relative proportions vary considerably according to the raw material. A coconut shell based carbon will have a predominance of pores in the micropore range and these accounts for 95% of the available internal surface area. Such a structure has been found ideal for the adsorption of small molecular weight species and low contaminant concentrations. In contrast wood and peat based

carbons are predominantly meso/macropore structures and are, therefore, usually suitable for the adsorption of large molecular species. Such properties are used to advantage in decolorization processes. Coal based carbons, depending on the type of coal used, contain pore structures somewhere between coconut shell and wood (Reinoso *et al.*, 1985).

In general, it can be said that macropores are of little value in their surface area, except for the adsorption of unusually large molecules and are, therefore, usually considered as an access point to micropores. Mesopores do not generally play a large role in adsorption, except in particular carbons where the surface area attributable to such pores is appreciable (usually 400m^2/g or more). Thus, it is the micropore structure of an activated carbon that is the effective means of adsorption. It is, therefore, important that activated carbon should not be classified as a single product but rather a range of products suitable for a variety of specific applications (Reinoso *et al.*, 1985).

2.3.1 Characteristics of Activated Carbon Pore Structure

Almost all materials containing high fixed carbon content can potentially be activated. The most commonly used raw materials are coal (anthracite, bituminous and lignite), coconut shells, wood (both soft and hard), peat and petroleum based residues.

Many other raw materials have been evaluated such as nut shells (Dakiky *et al*., 2002), Oil Palm wastes (Hussein *et al*., 1996, Lua and Guo, 1998), Rice husk (Roy *et al*., 1993), but invariably their commercial limitation lies in raw material supply. This is illustrated by considering that 1,000tons of untreated shell type raw material

will only yield about 100tons of good quality activated carbon. Most carbonaceous materials do have a certain degree of porosity and an internal surface area in the range of 10-15 m^2/g. During activation, the internal surface becomes more highly developed and extended by controlled oxidation of carbon atoms - usually achieved by the use of steam at high temperature. After activation, the carbon will have acquired an internal surface area between 700 and 1,200m^2/g, depending on the plant operating conditions. The internal surface area must be accessible to the passage of a fluid or vapour if a potential for adsorption is to exist. Thus, it is necessary that an activated carbon has not only a highly developed internal surface but accessibility to that surface via a network of pores of differing diameters. As a generalization, pore diameters are usually categorized as micropores <40 Angstroms, mesopores 40 - 5,000 Angstroms and macropores >5,000 Angstroms (typically 5000-20000Å) (Reinoso, *et al.*, 1985).

2.3.2 Porosity of Activated Carbon

During the process of activation, the spaces between the elementary crystallites become cleared of various carbonaceous compounds and non organized carbon. Carbon is also removed partially from the graphitic layers of the elementary crystallites. The resulting voids are termed as pores. Results seem to indicate that, there are pores with a contracted entrance (ink-bottle shaped), pores in the shape of capillaries open at both ends or with one end closed, pores in the shape of more or less regular slits between two planes, v-shaped, tapered pores, and other forms (Smisek & Cerny, 1970). In most cases it is difficult to determine the pore shapes reliably. However, the calculation of diameters of pores assuming cylindrical

capillary shapes yields values which approach the actual dimensions of the pores. Activated carbon usually has pores belonging to several groups, each group having a certain range of values for the effective dimensions.

Pores of an effective diameter larger than about 50nm, are classified as macropores. Their volume in the activated carbon is generally between $0.2cm^3/g$ and $0.5cm^3/g$ and their surface area is $0.5m^2/g$ to $2m^2/g$.

Transitional pores are those in which capillary condensation with the formation of a meniscus of the liquefied adsorbate can take place. This phenomenon usually produces a hysteresis loop on the adsorption isotherm. The effective diameters of transitional pores are in the range of 2nm to 50nm. Their specific surface area is generally around 5% of the total surface area ofthe activated carbon.

Pores with an effective diameter of less than about 2nm are called micropores. The micropore volume is generally around $0.15cm^3/g$ to $0.50cm^3/g$. Usually, the specific surface area of micropores amounts to over 90% of the total specific surface area. Each of these three groups of pores has its specific function in the process of adsorption on activated carbon. According to the type of application, the percentages of the transitional pores and the micropores could bead just edemploying special production procedures (Smisek and Cerny, 1970; Reinoso, *et al*., 1989).

The suitability of active carbon for a particular application depends on the ratio in which pores of different sizes are present. Thus, for the adsorption of vapors and gases from mixtures in which they are present in small concentrations, markedly

microporous active carbons are the most suitable. But active carbons used for the recovery of vapors of industrial organic solvents from waste gases and removal of heavy metals from solutions should contain a certain fraction of transitional pores (Smisek and Cerny, 1970).

2.4 Applications of the Activated Carbon

Due to the high degree of reactivity and high adsorption capacity, activated carbon has a very large area of application. The main application areas of the activated carbon are: Gas/vapour phase adsorption, liquid phase adsorption and using the activated carbon as catalyst or as catalyst support.

2.4.1 Gas/Vapour phase adsorption

Activated carbon for gas-phase adsorption applications is usually used in the form of hard pellets, fibres, monoliths, cloths and hard granules. These adsorbents have a high adsorption capacity per unit volume. One of the parameters that have to be considered in gas-phase applications is humidity of the gas. This will reduce the adsorption effectiveness of the activated carbon. It is highly recommended that the relative humidity of the gases to be treated should be lower than 70% (Harry, 2006).

Gas/vapour phase adsorption has a large area of application. Some of these are: purification of the air for immediate use in the inhabited spaces such as residential buildings and offices, prevention of air pollution from the exhaust gases from various industries and power plants and gas purification by adsorption of impurities such as ammonia, H_2S, amines, mercury and radioactive iodine.

2.4.2 Liquid phase adsorption

Some examples for adsorption of components in an aqueous system by activated carbons include the removal of the heavy inorganic metal ions such as chromium,

mercury, copper, arsenic, uranium, lead or gold from aqueous system in water treatment or industry and power production sites.

Some of the factors that influence the performance of the activated carbon in liquid phase are:

i. The type of compound that has to be removed: compounds with high molecular weight and low solubility can be adsorbed better.

ii. The pH of the waste stream (the stream that has to be filtered): for example, acidic compounds are better removed at lower pH.

iii. The presence of other organic compounds: it causes competition for the available adsorption sites.

iv. The concentration of the compound to be removed: higher concentration of the compound that has to be removed requires higher consumption of the activated carbon.

2.4.3 Activated Carbon as Catalyst and Catalyst Support

Besides the adsorption capacity, activated carbons depending on the different functional molecules existing on their pore surfaces can react with different molecules and catalyse a variety of different reactions. The chemistry of functionality and the nature of the graphene layer play roles in the catalytic capability of the activated carbon. For example the amphoteric nature of the graphene layer in the adsorption of anions from aqueous solutions plays the main role in this catalytic reaction process on the active surface of the activated carbon (Harry, 2006).

Carbon has different roles in different reactions. In some reactions, the size and extension of the active surface area and availability of the active site are important parameters. In some other reactions the presence of the carbon-oxygen surface and the nature of the active surfaces play the dominant roles. Catalytic reactions have been classified into different areas: 1- elimination reactions (catalytic elimination of hydrogen halide, etc.), 2- oxidation reactions (catalytic oxidation of H_2S, Ferrous Ions, etc.), 3- combination (catalytic combination of hydrogen and bromine or catalytic combination of the phosgene and formaldehyde, etc.) and decomposition reactions (catalytic decomposition of benzoyl peroxide).

Activated carbon can also be used as a catalyst support. It provides a much larger distribution of catalytically active atoms than the atoms on the surface of the corresponding metal. Activated carbons are stable in both acidic and basic media. Metals such as silica and alumina are not as stable as activated carbon, for example alumina can be attacked at very low pH and silica can be dissolved at high pH (Auer *et al.*, 1998). An example is the use of activated carbon as a catalyst support for hydrogenation of Cyclohexene.

Applications of Adsorption:

The principle of adsorption is employed in:

1. heterogeneous catalysis.
2. gas masks where activated charcoal adsorbs poisonous gases.
3. in the refining of petroleum and decolouring cane juice.
4. creating vacuum by adsorbing gases on activated charcoal.

5. chromatography to separate the constituents' of a mixture.
6. controlling humidity by the adsorption of moisture on silica gel.
7. certain titrations to determinate the end point using an adsorbent as indicator (Example: Flouroscein).

2.5 Classification of Activated Carbon

Activated carbon materials are usually classified based on their preparation methods or surface characteristics such as effective surface area per gram activated carbon, pore diameter and volume. They can also be classified based on their physical characteristics. (Stoeckli *et al.*,1988). Some examples for these classifications are:

1. Powdered activated carbon (PAC): They are formed as powders or fine granules with a size of less than 1.00mm and the pore diameter is between 15 and 25µm. That is why they have a small diffusion distance and a large ratio of surface area to volume.

2. Bead activated carbon (BAC): They are made with a size of 0.35-0.80mm from petroleum pitch. They have spherical shape, which is suitable for fluidized beds used in water filtration. They have high mechanical strength, low pressure drop and low dust content.

3. Granulated activated carbon (GAC): They can either be granulated or extruded. They have relatively larger size of particles compared to the powdered activated carbon. They have smaller external surface area/g and therefore they are suitable for gases and vapours with high diffusion rate. Granulated carbons are used for water treatment, separation of components of flow system and deodorization.

4. Extruded activated carbons*:* They are made by combining the powdered activated carbon with a binder which fuses together and give them a cylindrical shape with a diameter of 0.8 to 1.30mm. They have high mechanical strength, low pressure drop and low dust content which make them preferable for gas-phase processes.

5. Impregnated AC: They are porous carbons containing several types of the cations such as Al, Fe, Zn, Mn, Ca and Li impregnated by inorganic impregnates such as iodine, silver. They have a large area of application both in gas-phase and liquid phase like drinking water treatment and air pollution control.

6. Polymers coated activated carbon: In this process a porous carbon can be coated with a biocompatible polymer to give a permeable and smooth coat without blocking the pores of the carbon. One of the application areas for this kind of AC is for homo-perfusion which is a medical process used to remove toxic substances from a patient's blood.

7. Spherical activated carbon: In this process, small spherical balls containing pitch are melted in the presence of tetralin or naphthalene and converted into spheres (Stoeckli *et al.*, 1988). Then the naphtha solution extracts naphthalene and creates a porous structure. Subsequently in the presence of an oxidizing agent containing about 30% Oxygen by volume, the spheres are oxidized in the temperature range of 100 and 400°C. Then in the presence of ammonia the spheres are heated to introduce nitrogen into spheres. Finally the spheres are activated by CO_2 or steam. The characteristics with the spherical activated carbon are that they adsorb very well

SO_2 and NO_2 and they have a high mechanical strength, which makes them suitable for use in high temperature processes.

2.6 Evaluation of Activated Carbons

It is difficult for manufacturers to conduct specific tests related to any one application because of the diverse end uses to which a carbon may be applied. A manufacturer can undertake some specialty tests after agreement with the user but this is the exception rather than the rule. The size and number of pores essentially determine a carbon's capacity in adsorbing a specific compound. Since pore size and total pore volume determinations are quite lengthy, they are impractical as a means of quality control during manufacture. It is, therefore, necessary to relate the carbon's surface capabilities to a standard reference molecule (Cameron carbon incorporated, 2006).

2.6.1 Carbon Tetrachloride Activity

The most widely used method is to measure the carbon's capacity to adsorb carbon tetrachloride (referred to as CTC) and express this as a w/w %. This is determined by flowing CTC laden air through a sample of carbon of known weight, under standard conditions, until constant weight is achieved. The apparatus essentially consists of a means to control the supply of air pressure, produce a specified concentration of CTC and control the flow rate of the air/CTC mixture through the sample. The weight of CTC adsorbed is referred to as the carbon's % CTC activity. However, this test does not necessarily provide an absolute or relative measure of the effectiveness of the carbon for other adsorbates or under different conditions. CTC activity is now universally accepted as a means of specifying the degree of

activation or quality of activated carbon. Commercially available carbons range from 20% to 90% CTC activity (Cameron carbon incorporated, 2006).

2.6.2 Surface Area

The internal surface area of a carbon is usually determined by the BET method (Brunauer, Emmett and Teller). This method utilizes the low-pressure range of the adsorption isotherm of a molecule of known dimensions (usually nitrogen). This region of the isotherm is generally attributed to monolayer adsorption. Thus, by assuming the species is adsorbed only one molecule deep on the carbon's surface, the surface area may be calculated using the equation:

$$s = \frac{X_m NA}{M} \tag{2.1}$$

S = specific surface in m^2/g, X_m = sorption value (weight of adsorbed N_2 divided by weight of carbon sample), N = Avagadro's Number, 6.025 $x10^{23}$, A = cross-sectional area of nitrogen molecule in angstroms and M = molecular weight of nitrogen.

Most manufacturers will specify the surface area of their products but as with CTC activity, it does not necessarily provide a measure of their effectiveness, merely demonstrating their degree of activation. It is also impractical to utilize surface area measurement as a means of quality control since this is a very lengthy procedure (Cameron carbon incorporated, 2006).

2.6.3 Adsorption Equilibrium

Carbon atoms are very close to each other as they constitute the surface of the pore site of the activated carbon. This results in the adsorbed molecules being retained

within the pores. Physisorption in contrast to the chemisorption is a reversible process. Physical adsorption is a dynamic process in which some adsorbate molecules are transferred from the fluid phase onto the solid surface, while some are released again to the fluid state. When the rates of two processes (adsorption and desorption) are equal, adsorption equilibrium will be obtained.

Adsorption equilibrium for a physical adsorption processes is a function of:

i. Partial pressures*;* adsorption of the adsorptive and consequently adsorption equilibrium is a function of partial pressure of the molecules in the adsorptive (P/P_0) at constant temperature. (Here P and P_0 are the equilibrium and the saturation pressures of adsorptive molecules at the temperature of adsorption respectively). At constant temperature higher pressure causes higher adsorption and vice versa.

ii. Temperature; as the physical adsorption process is an exothermic process (Harry, 2006) so by increasing the temperature of the adsorption system at constant pressure adsorption capacity decreases and, on the other hand, by decreasing the temperature adsorption capacity increases.

iii. Concentration of molecules in the adsorptive phase; experiments show that by increasing the concentration of the adsorptive wider pores (Centeno *et al.*, 2003), the adsorption capacity of activated carbon increases and this will affect the adsorption equilibrium.

2.6.4 Adsorption Isotherms

In experimental processes adsorption isotherms are commonly used for the determination of the internal surface area of the activated carbon. An Adsorption

isotherm is a plot of the amount of adsorbed molecules (x/m mmol/g) against the relative pressure of adsorptive (p/p_0) at equilibrium. This occurs at constant temperature. The variation of the extent of adsorption (x/m, mmol/g) with respect to temperature at constant relative pressure of the adsorptive (p/p_0) is called adsorption isobar. Figure 2.1 illustrates the relation between the amount of adsorbed molecules and the relative pressure of the adsorptive molecules (a) and the temperature (b).

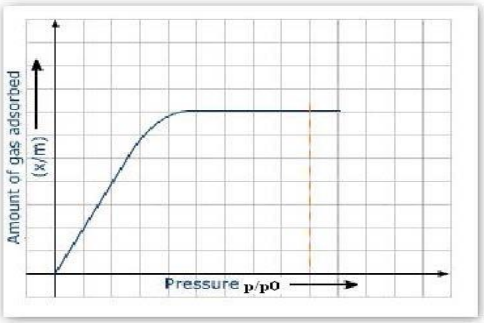

(a)

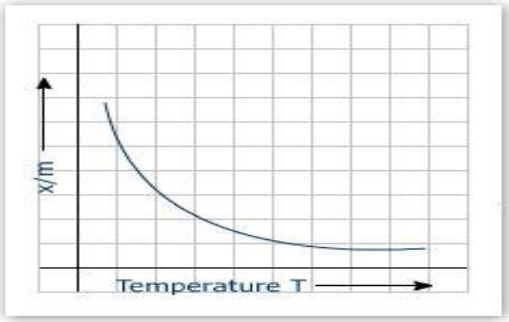

(b)

Figure 2.1: Plot of (a) adsorption isotherm and (b) adsorption isobar (Rigby *et al*., 2004).

The variation of the relative pressure of the adsorptive molecules (p/p_0) with the variation of adsorption temperature (K) under a constant adsorption rate (x/m, mmol/g) is called adsorption isostere.

Among the experimental methods, the adsorption isotherm is the most commonly used method to study the adsorption property of the activated carbons especially when the physical adsorption is of interest. The most commonly used adsorbent for determination of the adsorption isotherms and pore size analysis are (Harry, 2006.)

i. Nitrogen at 77K; can fill the micro, meso and macropores

ii. CO_2 at 273K; can fill the narrow micropores with smaller size which N_2 cannot enter at low temperature (77K)

iii. Argon at 77.35 and 87,27K; can fill micropores of dimension 0.4-0.8nm at a much higher relative pressure due to weaker attractive fluid-wall interactions

iv. Krypton at 77.35K, has been used for the determination of very low surface areas.

2.6.5 Brunauer-Emmett-Teller (BET) equation

The BET equation is the most famous gas adsorption model for describing the solid porosity. The BET equation describes the multilayer adsorption of molecules being formed by physisorption of gases for example adsorption of N_2 at 77K on non-porous surfaces and predicts a value for the monolayer coverage.

Figure 2.2 describes a typical adsorption isotherm and its relation to the adsorption equations.

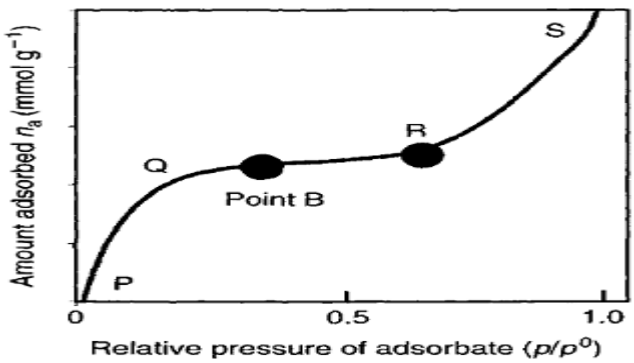

Figure 2.2: A typical adsorption isotherm (Marsh *et al.*, 2006)

The Dubinin Raduskovich (DR) equation extrapolates the initial segment, P to Q, of the isotherm obtained at low relative pressures. The Langmuir equation is based on segment PQB where it is assumed that monolayer coverage takes place, whereas the BET equation linearizes the section of the isotherm that contains the “knee” and extrapolates the initial segment QRS, dealing with pores filling and capillary condensation processes as it is applied to porous solids. For non-porous solids, the segment QRS deals with multilayer formation on open surfaces.

The porous surface area of the carbon from the monolayer coverage can thus be estimated by graphical means by plotting 1/(V [1-P/P_0)]) versus P/P_o using equation (2.2) or the rearranged form equation (2.3).

BET equation:

$$\frac{1}{V[P_O - P]} = \frac{1}{V_m\ C} + \frac{C-1(P/P_o)}{V_m C} \qquad (2.2)$$

Here: V = volume of the adsorbed molecules (cm^3/g) at STP (standard condition for the temperature and pressure), V_m = capacity of the monolayer coverage in volume STP (cm^3/g)

C = is a BET constant which indicates the energy of the adsorption process and calculated from equation 2.4.

The Assumptions Taken into Account for the BET Equation are:

i. The internal surface area of the porous carbon (or solid) is similar to the external surface area of the non-porous solid.

ii. There is no interaction between the adsorption layers.

iii. The gas molecules are adsorbed infinitely on the surface of solid.

iv. The Langmuir theory is applicable on each layer.

To estimate the internal surface area, the value of the monolayer coverage ("n^a_m") [mmol/g] has to be determined. However, it is difficult to measure the adsorption heat of this layer. For this reason a plot of the linear relationship between the left-hand-side of equation (2.2) or (2.3) and the partial pressure (p/p_0) of the adsorbate, a so called BET plot, can be used. It should be noted that this linear relationship is maintained just in the relative pressure range of $0.05 < p/p_0 < 0.35$ (Harry, 2006).

The measured volume of the adsorbed molecules “V” (at STP) at a given relative humidity will give a given relative partial pressure (p/p_0). The different relative

partial pressures are used to derive a linear relationship from the equation (2.2) or (2.3). This plot is illustrated in Figure 2.3.

Equation (2.2) can be re-arranged as:

$$\frac{P/P_O}{V[1-P/P_O} = \frac{1}{V_M C} + \frac{(C-1)(P/P_O)}{V_M C} \qquad (2.3)$$

$$C = \exp^{\frac{(E_1 - E_L)}{RT}} \qquad (2.4)$$

Here:

E_1 is the heat of adsorption of the first layer, E_L is the heat of adsorption of the second and higher layers respectively and (E_L is equal to the heat of liquefaction).

By using $\Psi = p/p_o$ then we can illustrate a linear relationship between the left hand-side of the equation (2.3) and relative pressure of the adsorptive molecules. This plot is called BET plot as is illustrated by Figure 2.3.

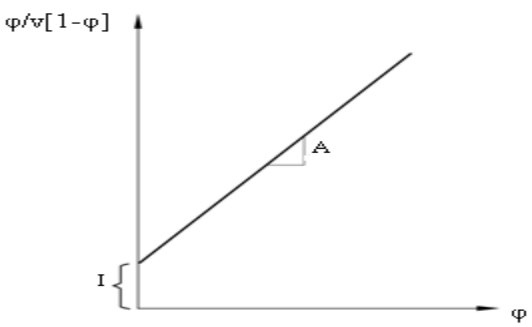

Figure 2.3: A plot of the linier relationship of BET equation 2.2 (Valmari *et al.*, 1999).

Let the slope of the line in the Figure 2.3 be "A" and the intersection of the line with the y-axis "I", then by using the equation 2.3 we have the following relationship and the constant "c" can be determined, using Figure 2.6 and equation 2.5 below:

$$C = 1 + A/I \qquad (2.5)$$

c < 150 has been recorded for adsorption in non-porous carbons and c >> 200 for adsorption in microporous carbons (Marsh *et al.*, 2006). In the same way by using the Figure 2.3, it can be possible to determine the V_m (capacity of the monolayer coverage in volume STP (cm^3/g)).

$$\frac{V_M}{A+1} = 1 \qquad (2.6)$$

Now by the determination of parameter V_m, if we know the cross sectional area of an adsorbed molecule a_m (m^2), which is for example for water $a_m = 0.114\ nm^2$, then we can calculate the total surface area, $S_{BET,Total}$ (m^2), by using the equation 2.7.

$$S_{BET,Total} = (V_m N_a a_m)/V \qquad \text{in } m^2 \qquad (2.7)$$

There N_a is the Avogadro's number which is 6.013×10^{23} elements (atom or molecule per mole). If we know the mass of the adsorbent, m_a (g) we can estimate the specific surface area, S_{BET} (m^2/g) by using equation 2.8 or 2.9.

$$S_{BET} = (S_{BET})/m_a \qquad \text{in } m^2/g \qquad (2.8)$$

$$S_{BET} = n^a{}_m N_a a_m \qquad \text{in } m^2/g \qquad (2.9)$$

2.6.6 Mesh Size

The physical size, or mesh size, of a carbon must be considered in relation to the flow rate in the system it is to be used. Naturally, the smaller the carbon's mesh size, the greater its resistance to flow. Thus, it is usual to select the smallest mesh size carbon that will satisfy the pressure drop limitations of the system (Cameron carbon incorporated, 2006).

2.6.7 Ash Content

Ash content is less important except where the carbon is used as a catalyst support since certain constituents of the ash may interfere or destroy the action of precious metal catalysts. Ash content also influences the ignition point of the carbon—this

may be a major consideration where adsorption of certain solvents is concerned. The density of carbon is, of course, of great importance to many users in estimating the weight required to fill a vessel (Cameron carbon incorporated, 2006).

2.7 Physical Properties of Activated Carbon

Industrial applications of activated carbon always require the determination of the physical properties and adsorption capacity of the activated carbons.

There are many standard testing methods that are in use to determine the physical properties of AC. These methods were developed by some organizations such as, (DIN, 1986) Deutsches Institute fűr Normung, (AWWA, 1990) American Water Works Association, (ASTM, 1992), American Society for Testing Materials and (ISO, 1999) International Organization for Standardization (Marsh *et al*., 2006).

Some physical properties that are usually used by industrial processes to determine the quality of the activated carbons are:

1. Particle size: This property is important because the filterability of the adsorptive flow is directly depending on the size of AC. Furthermore; the rate of adsorption depends inversely on the particle size.

2. Mechanical strength: This is a very important property especially for granular AC. When there is a high pressure drop and carbon loses in the system, it is required that the activated carbon should have a high attrition resistance and mechanical strength.

3. Real density or helium density: This is the mass of the solid carbon skeleton of the activated carbon, excluding the volume of the voids, (empty spaces between the activated carbon particles) and the pore volume.

4. Bulk density: This is the mass per unit volume of the activated carbon in air, which is included the volume of the pores and the empty spaces between the activated carbon particles. This property among others is useful in the determination of the amount of activated carbon needed for a process or determination of the packing volume.

5. Apparent density: This is the mass per unit volume of the activated carbon particles including the pore sites and excluding the voids. Some other properties that are sometimes tested are: ignition temperature and self-ignition temperature, ash content, moisture content and pH value.

2.7.1 Pore Structure of Activated Carbon by Scanning Electron Microscope

A scanning electron microscope (SEM) is a type of electron microscope that images a sample by scanning it with a high-energy beam of electrons in a raster scan pattern. The electrons interact with the atoms that make up the sample producing signals that contain information about the sample's surface topography, composition, and other properties such as electrical conductivity. The types of signals produced by an SEM include secondary electrons, back-scattered electrons (BSE), characteristic X-rays, light (cathode luminescence), specimen current and transmitted electrons. These characteristic X-rays are used to identify the composition and measure the abundance of elements in the sample. In a typical SEM, an electron beam is thermionically emitted from an electron gun fitted with a tungsten filament cathode. Tungsten is normally used in thermionic electron guns because it has the highest melting point and lowest vapour pressure of all metals,

thereby allowing it to be heated for electron emission, and because of its low cost (Subhashree, 2011).

2.8 Preparation of Activated Carbon

Activated carbon is produced from any carbonaceous organic material which contains elemental carbon. Activated carbon can be produced by two main methods: physical activation and chemical activation.

2.8.1 Physical Activation

The production of activated carbon by physical activation can be done using two methods. These methods are called one-step activation and two-step activation depending on whether the carbonization and activation processes occur simultaneous or in the separate steps.

2.8.1.1 Two-step activation method

This method involves two main steps:

1. carbonization of carbonaceous raw material or pyrolysis,

2. activation or gasification of char or carbonized raw material. In two-steps method carbonization and activation are not carried out simultaneously, but in distinct steps.

2.8.1.2 Pyrolysis or carbonization

In this step the carbonaceous raw material is heated up in the absence of oxygen. Almost all of the volatile fractions of the raw material leave the material in the form of permanent gases and tar. The residue that contains mostly carbon is called carbonized material or char. Three products are obtained from the decomposition of raw material namely: char, tar and product gas. To maximize the char fraction in this step, the raw material has to be heated with a slow heating rate and the temperature is usually between 400-850°C (El-Hendawy *et al*., 2001, Girgis *et al*.,

2002). Parameters that determine the characteristic of the pores in this step are heating rate, temperature, properties of the raw material and the type of activating agent. Pores characteristic include the total pore volume, pore diameter and pore size distribution.

The carbonized material needs further treatment because its adsorption capacity is too low for commercial application. Thus the char needs to be treated to increase the porosity and widened the existing micropores and some mesopores. This further treatment process is called activation.

2.8.1.3 Activation

This is the second step in the production of activated carbon by two steps method. In the physical activation process, oxidizing gases such as steam, carbon dioxide or a mixture of both is used for gasification of the carbonized material or char. Physical activation involves the contact between the char and activating agent followed by reaction between the surface carbons on the pores and the activating agent. These agents extract carbon atoms from the structure of the porous carbon. Steam and CO_2 react with surface carbons according to reactions 1 and 2 below.

$C + CO_2 \rightarrow 2CO$ (+163.18 kJ/mole) (Reaction 1)

$C + H_2O \rightarrow CO + H_2$ (+121.33 kJ/mole) (Reaction 2)

The result is that the pores are formed. The most important effects of the activation step are: the formation of micropores and mesopores and the increase of the volume and the diameter of existing pores. The residence time can be controlled to have a larger internal surface area as this is an important indication that determines the quality of the activated carbon. Besides the appropriate oxidizing agent, a suitable

temperature, usually between 800 to 1100°C (Marsh *et al*., 2006) has to be applied. This temperature is usually higher than the pyrolysis temperature. This process requires heat, because the reaction of carbon and these oxidizing gases is endothermic. The high temperature of activation causes a water gas shift reaction that is catalyst by the surface of the carbon according to reaction 3 below (Marsh *et al.*, 2006). It increases the hydrogen content of the gasification product at the expense of carbon monoxide.

$CO + H_2O \leftrightarrow CO_2 + H_2$ (- 41kJ/mole) (Reaction 3)

This is a pre-step in syngas production in the downstream of a gasifier, where the ratio of hydrogen and carbon monoxide in the product gas is critical. This shift reaction is sensitive to temperature, with the tendency to shift towards reactants as temperature increases based on Le Chatelier's principle.

2.8.1.4 One-Step activation

Many studies show that it is possible to produce the activated carbon with physical activation method in one step without pre-carbonization of the raw material (El-Hendawy *et al.*, 2001). One-step activation means that the carbonaceous raw material from the beginning comes in contact with the activation agent, which in most cases is steam or carbon dioxide, so that both carbonization and activation occur simultaneously at the same temperature. Marsh *et al*., 2006 used CO_2 for the activation of almond shells and olive stones by the one-step or direct activation method from the room temperature to 825-850°C. The results were compared with the activated carbon produced by the two-steps method, pre-carbonization followed by activation with CO_2 at 825°C. The result showed that both methods have the

same yield and almost similar surface area and volume of micropores. Other studies (El-Hendawy *et al.*, 2001) used steam as oxidizing agent for the production of activated carbon in one step. In these studies, the carbonaceous raw material was pyrolyzed at temperatures 500-700°C and 700-800°C under the flow of steam. The results shows that the direct contact and reaction of the raw material with steam or CO_2 does not make any considerable differences in the quality of the produced AC as compared to the AC produced by the two-steps method.

2.8.2 Chemical Activation

Chemical activation involves the impregnation of the carbonized material by mixing it with an excess amount of a given chemical, usually in the form of concentrated solution. The commonly used activating agents are: H_2SO_4, $ZnCl_2$, H_3PO_4, KOH and NaOH. Other chemicals that can also be used include ferric iron carbonates of alkali metals and potassium sulphide. Impregnation has to be carried out with special care to ensure an intimate contact between the reagent and the precursor. Impregnation results in the dehydration of the carbon skeleton and swelling of the interior canals of the botanic structure followed by the formation of a porous structure. The residence time and the temperature of the operation for this step are important parameters that have to be considered. The chemically impregnated raw material is then pyrolyzed and carbonized in an inert atmosphere. Then the pyrolyzed product is cooled and washed with distilled water or by mild acid to extrude the rest of the activating agent and the agent is recycled. Impregnation (dehydration) is done at a temperature lower than the boiling temperature for the mixture or water. The temperature range for the activation and carbonization step can be up to 1000°C, but

is usually between 450 to 600°C, which is much lower than those for physical activation (Marsh *et al*., 2006). Chemical activation results in a better development of the porous structure and carbon with higher density. The impregnation process takes up to 24 hours depending on the activating agent, the precursors and the subsequent processes (Paraskeva *et al*., 2008).

The most important function of the activating agents in a chemical activation process is the dehydrating of the carbon skeleton that subsequently influences the pyrolytic decomposition of the raw material. The degree of impregnation (ratio of the activating agent to carbonized raw material) is an important factor that determines the quality and the size distribution of the pores. Larger degree of impregnation yields larger pore diameter and larger active surface area in the product.

2.9 Activated Carbon as an Adsorbent

Adsorption is a process that occurs when a gas, liquid or solid solute accumulates on the surface of a solid or a liquid (adsorbent), forming a molecular or atomic film (the adsorbate). It is different from absorption, in which a substance diffuses into a liquid or solid to form a solution. The term sorption encompasses both processes, while desorption is the reverse process (Oremusová, 2007).

Adsorption is operative in most natural, physical, biological and chemical systems, and is widely used in industrial applications such as in catalysis and water purification. Similar to surface tension, adsorption is a consequence of surface energy. Adsorption is the phenomenon marked by an increase in density of a fluid near the surface, for our purposes, of a solid. In the case of gas adsorption, this

happens when molecules of the gas occasion to the vicinity of the surface and undergo an interaction with it, temporarily departing from the gas phase. Molecules in this new condensed phase formed at the surface remain for a period of time, and then return to the gas phase. The duration of this stay depends on the nature of the adsorbing surface and the adsorptive gas, the number of gas molecules that strike the surface and their kinetic energy (or collectively, their temperature), and other factors (such as capillary forces, surface heterogeneities). Adsorption is by nature a surface phenomenon, governed by the unique properties of bulk materials that exist only at the surface due to bonding deficiencies. The sorbent surface may be thought of as a two-dimensional potential energy landscape, dotted with wells of varying depths corresponding to adsorption sites. A single gas molecule incident on the surface collides in one of two fundamental ways: elastically, where no energy is exchanged, or inelastically, where the gas molecule may gain or lose energy. In the former case, the molecule is likely to reflect back into the gas phase, the system remaining unchanged. If the molecule lacks the energy to escape the surface potential well, it becomes adsorbed for some time and later returns to the gas phase. Inelastic collisions are likelier to lead to adsorption. Shallow potential wells in this energy landscape correspond to weak interactions, for example by Van der Waals forces, and the trapped molecule may diffuse from well to well across the surface before acquiring the energy to return to the gas phase. In other cases, deeper wells may exist which correspond to stronger interactions, as in chemical bonding where an activation energy is overcome and electrons are transferred between the surface

and the adsorbed molecule (Weber Jr, 2001). This kind of well is harder to escape, the chemically bound molecule requiring a much greater increase in energy to return to the gas phase. In some systems, adsorption is accompanied by absorption, where the adsorbed species penetrates into the solid. This process is governed by the laws of diffusion, a much slower mechanism, and can be readily differentiated from adsorption by experimental means.

In the absence of chemical adsorption (chemisorption) and penetration into the bulk of the solid phase (absorption), only the weak physical adsorption (physisorption) case remains. The forces that bring about physisorption are predominantly the attractive "dispersion forces" (named so for their frequency dependent properties resembling optical dispersion) and short-range repulsive forces. In addition, electrostatic (Coulombic) forces are responsible for the adsorption of polar molecules, or by surfaces with a permanent dipole. Altogether, these forces are called "van der Waals forces," named after the Dutch physicist Johannes Diderik van der Waals (Weber Jr, 2001).

Adsorption is integral to a broad spectrum of physical, biological, and chemical processes and operations in the environmental field. Purification of gases by adsorption has played a major role in air pollution control, and adsorption of dissolved impurities from solution has been widely employed for water purification (Weber Jr, 2001). Adsorption is now viewed as a superior method for wastewater treatment and water reclamation. Applications of adsorption for chemical processing, air pollution control and water treatment are well known; applications in

wastewater treatment and water pollution control are generally not as well recognized, nor as well understood. The process has been demonstrated to be widely effective for removing dissolved organic substances from wastewaters, but it should not be viewed as a catholicon for waste treatment, nor should its application be made in an empirical fashion. The purpose of this paper is to develop the details of this application, highlighting advantages over other wastewater purification processes, and defining major factors and considerations involved in its design and use (Weber Jr, 2001).

In a bulk material, all the bonding requirements (be they ionic, covalent or metallic) of the constituent atoms of the material are filled. But atoms on the (clean) surface experience a bond deficiency, because they are not wholly surrounded by other atoms. Thus it is energetically favourable for them to bond with whatever happens to be available. The exact nature of the bonding depends on the details of the species involved, but the adsorbed material is generally classified as exhibiting physisorption or chemisorptions (Oremusová, 2007).

Physisorption or physical adsorption is a type of adsorption in which the adsorbate adheres to the surface only through Van der Waals (weak intermolecular) interactions, which are also responsible for the non-ideal behaviour of real gases.

Chemisorption is a type of adsorption whereby a molecule adheres to a surface through the formation of a chemical bond, as opposed to the Van der Waals forces which cause physisorption (Oremusová, 2007). Adsorption is usually described

through isotherms, that is, functions which connect the amount of adsorbate on the adsorbent, with its pressure (if gas) or concentration (if liquid).

2.9.1 Adsorption Property of Activated Carbon

The description of the adsorption phenomena requires some definitions. In an adsorption system the solid carbon which adheres molecules on its internal surface area and thus adsorb them, is called an adsorbent. Molecules in the gas/vapour or the solute molecules in the solution which has to be adsorbed within the activated carbon are called adsorptives. The portion of the molecules that are absorbed by the activated carbon is called adsorbate.

Adsorption means the adhesion of ions, atoms and molecules of dissolved solids in a liquid-phase or molecules of liquid or gas to the surface of a solid. This results in a higher concentration of the substance in the boundary between the substance and the solid surface than in the bulk of the substance. During the adsorption process a layer (film) of the adsorbate molecules or atoms is created on the surface of the adsorbent. This process is a surface phenomenon, which is caused by surface energy. The fundamental property of carbon adsorbents is that energy is non-uniform on the adsorption space (Marsh *et al*., 2006, Ustinov *et al.*, 1999). Activated carbon is a material filled of holes (spaces, voids, and pores), which make it unique. These holes are special, because they are spaces of zero electron density in which adhesive forces adsorb the other molecules.

Atoms at the surface of a solid such as that of activated carbon have imbalanced forces compared to those within the solid. Consequently, foreign molecules are

attracted to the surface to improve this imbalance. This makes a monolayer of these adsorbate molecules on the surface of the solid.

First, the adsorbate molecules are transferred through the bulk gas-phase to the surface of the solid and then diffuse onto the internal surfaces of the pores in the solid. However, the adsorbent and the adsorbate molecules have also internal motion as well. The internal motion or frequency of vibration increases with increasing temperature of the adsorption system. This enables both the entering of the adsorbate molecules into the pores, as well as their ejection. The ejected adsorbate molecules are replaced by other adsorbate molecules. At equilibrium, the number of molecules leaving the pores is equal to the molecules entering them. On average an adsorbate molecule moves in and out about 1015 times per second. It is also good to notice that in an activated carbon of approximately 1000m^2/g surface area, there are about 10^{20} adsorption sites with different potential energy well (Marsh *et al*., 2006). That is why the adsorption capacity of an activated carbon depends on the total internal surface area, type and size of its pores. They are the adsorption sites in the surface of micropore channels that stands for the major part of the adsorption, despite that the width of the micropores (width < 2nm) are smaller than the width of the macropores (width >50nm) (Marsh, *et al.*, 2006, Centeno *et al.*, 2003).

Activated carbons adsorb a wide variety of substances. Differences in the surface structure make some molecules more easily adsorbed than others. Surface structure of the AC can be affected by different methods of activation (figure 2.4). Their adsorption capacity is between 0.6-0.8cm^3/g. The volume of the pores of an

activated carbons are generally in the range of 0.1cm^3 to 1.0cm^3/g and the width of the pores ranges from 0.3 to several thousand nm (Stoeckli *et al.*, 1988). The internal surface area is generally greater than 400m^2 g-1, it can range between 250 to 2500m^2 (Xu *et al*., 2010). Even production of high surface area MAXORB active carbon with over 3000m^2/g carbon has been reported (Otowa *et al*., 1993).

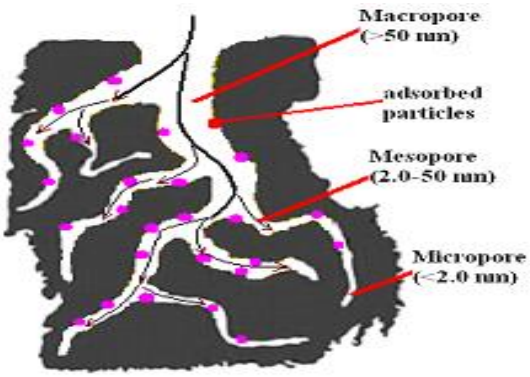

Figure 2.4: Schematic picture of the pores inside the activated carbon (Xu *et al*., 2010)

Due to overlapping of the adsorption potential of opposite walls in micropores there is up to three times more adsorption energies in the micropores than on the nonporous surface of a solid carbon. This results in most of the adsorption occurring in the micropores. At very low relative pressures of the adsorptive, $p/p_0 < 500$ppm, only the finest micropores are involved the adsorption process. By increasing the concentration of the adsorptive and consequently increasing the relative pressure of the adsorptive, wider pores starts to be filled (Centeno *et al.*, 2003).

2.10 Adsorption Processes

Adsorption occurs at least partly as a result of forces active within phase boundaries, or surface boundaries. These forces result in characteristics boundary energies. Classical chemistry defines a system by the properties of its mass. For surface

phenomena the significant properties are those of the surface or boundary. A pure liquid reduces its free surface energy through the action of surface tension, which is quantitatively equal to the amount of work necessary to compensate the natural reduction in free surface energy. A large number of soluble materials can effectively alter the surface tension of a liquid. Detergents, for example, lower surface tension dramatically. If a material which is active at surfaces is present in a liquid system, a decrease in the tension at the surface will occur upon movement of the solute to the surface. Migration of the substance to the surface or boundary results in a reduction of the work required to enlarge the surface area, the reduction being proportional to the concentration of adsorbate at the surface. The energy balance of the system thus favours adsorptive concentration of such surface-active substances at the phase interface. The tendency of an impurity to lower the surface tension of water is referred to as hydrophobicity; that is, the impurity 'dislikes' water (Weber Jr, 1972). Adsorption of an impurity from water on to activated carbon may result from solute hydrophobicity, or it may be caused by a high affinity of the solute for the carbon. For most systems encountered in waste treatment, adsorption results from a combination of these factors. The solubility of a substance in water is significant: solubility in the sense of the chemical compatibility between the water and the solute. The more hydrophilic a substance the less likely it is to be adsorbed. Conversely, a hydrophobic substance will more likely be adsorbed.

In the context of solute affinity for the solid, it is common to distinguish between three types of adsorption. The affinity may be predominantly due to: (I) electrical

attraction of the solute to the adsorbent (exchange adsorption): (2) van der Waals attraction (physical or ideal adsorption): or, (3) chemical reaction (chemisorption or chemical adsorption) (Weber Jr, 1972). Many adsorptions of organic substances by activated carbon result from specific interactions between functional groups on the sorbate and on the surface of the sorbent. These interactions may be designated as 'specific adsorptions'. It is possible for specific adsorptions to exhibit a large range of binding energies, from values commonly associated with 'physical' adsorption to higher energies associated with 'chemisorption'. The adsorptive interactions of aromatic hydroxyl and nitro-substituted compounds with active carbon, for example, are specific adsorption processes resulting from formation of donor-acceptor complexes with surface carbonyl oxygen groups, with adsorption continuing after these sites are exhausted by complexation with the rings of the basal planes of the carbon microcrystallite'(Weber Jr *et al.*, 1972). Adsorption results in the removal of solutes from solution and their concentration at a surface, until the amount of solute remaining in solution is in equilibrium with that at the surface. This equilibrium is described by expressing the amount of solute adsorbed per unit weight of adsorbent q, as a function of C, the concentration of solute remaining in solution. An expression of this type is termed an adsorption isotherm.

2.10.1 Adsorption Mechanism

Adsorption occurs only at the surface of the AC and to recover the material adsorbed, desorption can take place. The mechanism of adsorption is reported by Bhatnagar and Sillanpaa (2010) as below:

1. External mass transfer from bulk solution to adsorbent surface across the boundary layer, surrounding the adsorbent particle. The transfer usually determined by hydrodynamic conditions; increase in mixing speed of batch adsorption creates more turbulence and decrease of boundary layer thickness around particles.

2. Intra-particle diffusion within the internal structure of the particle. Internal diffusion is diffusion of molecules inside the pores and surface diffusion is diffusion of molecules on the surface phase. It controls the transfer of adsorbate from the exterior of the porous adsorbent to the internal surface site.

3. Adsorption at an interior site. This is the step where the particle is attached to the surface of the adsorbent. Adsorption at an interior site is usually considered to be very rapid and is neglected (Choong *et al.*, 2006).

The adsorption occurs in the porous surface of AC. High surface area result in higher adsorption capacity of pollutants. Apart from that, high dosage of adsorbent will offer great availability of exchangeable sites for metal ions (Onundi *et al.*, 2010). There are many researchers' studies on increasing the pore development of palm shell AC (Gua and Luo, 2003; Yin *et al.*, 2007; Owlad *et al.*, 2010). The pore development on AC can be increased by undergoing physical and chemical treatment. Activated carbon can be considered as a material of phenomenal surface area made up of millions of pores - rather like a "molecular sponge".

The process by which such a surface concentrates fluid molecules by chemical and/or physical forces is known as adsorption (whereas, absorption is a process whereby fluid molecules are taken up by a liquid or solid and distributed throughout that liquid

or solid). In the physical adsorption process, molecules are held by the carbon's surface by weak forces known as Van Der Waals Forces resulting from intermolecular attraction. The carbon and the adsorbate are thus unchanged chemically (Wang *et al.,* 1999). However, in the process known as chemisorption molecules chemically react with the carbon's surface (or an impregnate on the carbon's surface) and are held by much stronger forces -chemical bonds. In general terms, to effect adsorption it is necessary to present the molecule to be adsorbed to a pore of comparable size. In this way the attractive forces coupled with opposite wall effect will be at a maximum and should be greater than the energy of the molecule (Wang *et al.,* 1999). For example, a fine pored coconut shell carbon has poor decolorizing properties because colour molecules tend to be larger molecular species and are thus denied access to a fine pore structure. In contrast, coconut shell carbons are particularly efficient in adsorbing small molecular species. Krypton and Xenon, for instance, are readily adsorbed by coconut shell carbon but readily desorbed from large pored carbons such as wood. Maximum adsorption capacity is determined by the degree of liquid packing that can occur in the pores. In very high vapour pressures, multilayer adsorption can lead to capillary condensation even in mesopores. If adsorption capacity is plotted against pressure (for gases) or concentration (for liquids) at constant temperature, the curve so produced is known as an isotherm.

Adsorption increases with increased pressure and also with increasing molecular weight, within a series of a chemical family. Thus, methane (CH_4) is less easily

adsorbed than propane (C_3H_8). This is a useful fact to remember when a particular system has a number of components. After equilibrium, it is generally found that, all else being equal; the higher molecular weight species of a multi-component system are preferentially adsorbed. Such a phenomenon is known as competitive or preferential adsorption - the initially adsorbed low molecular weight species desorbing from the surface and being replaced by higher molecular weight species (Wang *et al.*, 1999).

Physical adsorption in the vapour phase is affected by certain external parameters such as temperature and pressure. The adsorption process is more efficient at lower temperatures and higher pressures since molecular species are less mobile under such conditions. Such an effect is also noticed in a system where moisture and an organic species are present. The moisture is readily accepted by the carbon surface but in time desorbs as the preferred organic molecules are selected by the surface. This usually occurs due to differences in molecular size but can also be attributable to the difference in molecular charge (Wang *et al.*, 1999).

Generally speaking, carbon surfaces dislike any form of charge - since water is highly charged (ionic) relative to the majority of organic molecules the carbon would prefer the organic to be adsorbed. Primary amines possess less charge on the nitrogen atom than secondary amines that in turn have less than tertiary amines. Thus, it is found that primary amines are more readily adsorbed than tertiary amines (Wang *et al.*, 1999).

High levels of adsorption can be expected if the adsorbate is a reasonably large bulky molecule with no charge, whereas a small molecule with high charge would not be expected to be easily adsorbed. Molecular shape also influences adsorption but this is usually of minor consideration.

In certain situations, regardless of how the operating conditions can be varied, some species will only be physically adsorbed to a low level (Examples are ammonia, sulfur dioxide, hydrogen sulfide, mercury vapour and methyl iodide). In such instances, the method frequently employed to enhance a carbon's capability is to impregnate it with a particular compound that is chemically reactive towards the species required to be adsorbed. Since carbon possesses such a large surface (a carbon granule the size of a "quarter" has a surface area in the order of ½ square mile) coating of this essentially spreads out the impregnate over a vast area. This, therefore, greatly increases the chance of reaction since the adsorbate has a tremendous choice of reaction sites. When the adsorbate is removed in this way the effect is known as chemisorptions (Wang *et al.,* 1999).

Unlike physical adsorption the components of the system are changed chemically and the changed adsorbate chemically held by the carbon's surface and desorption in the original form is nonexistent. This principle is applied in many industries, particularly in the catalysis field, where the ability of a catalyst can be greatly increased by spreading it over a carbon surface (Wang *et al.,* 1999).

When adsorbate is contacted with adsorbent, adsorption takes place. If the contacting time is not limited, an equilibrium adsorption can be reached. The equilibrium

adsorption capacity is a function of adsorption pressure and adsorbent temperature, which can be expressed as $X_\infty = f\,(p,\mathrm{T})$. There are several adsorption equations, such as isothermal adsorption $x_\infty = f\,(p)_T$, isobaric adsorption $x_\infty = f\,(\mathrm{T})_p$, isosteric $p = f\,(\mathrm{T})x$ (Wang *et al.*, 1999).

These three adsorption lines can be interchanged; however they are used for different situations. Isothermal adsorption is mainly applied in micro-porous adsorption in industrial equipment. Isobaric adsorption is used in the operation design of generation processes. Isosteric adsorption is suitable for the calculation of heat of adsorption and desorption. In the study of adsorption refrigeration, isobaric adsorption is more important as adsorption and desorption takes place usually under isobaric conditions.

The isothermal or isobaric adsorption equation is the basis for design and simulation of an adsorption refrigeration system. The Dubinin Radushkevich (DR) and Dubinin Astakhov (DA) equations are isobaric adsorption equations used to research mini-pore adsorption phenomena, which are simple, applicable for various pore sizes, and have good agreement for a wide range of temperature and pressure for uniform pore size adsorbent (Rand, 1976). But they are not suitable for non-uniform pore size adsorbent (such as normal activated carbon, zeolite) when they adsorb polar molecules (such as methanol, water, etc.). In this case the DA and DR adsorption equations (Wojsz and Rozwadowski, 1984) should be applied with care.

The adsorption characteristics of adsorption refrigeration pairs are studied in this paper, and improved models of normal DR and DA equations have been applied,

which have better physical meaning, and are in good agreement with experimental results. In addition to the non-uniform pore size adsorption model, a uniform pore size model regarding activated carbon fibre methanol adsorption has also been studied (Wang *et al*., 1999).

2.10.2 ADSORPTION THEORY AND ADSORPTION EQUATION

Activated carbon, zeolite, silica gel, alumina, calcium chloride are used as adsorbents, while water, methanol, ammonia are used as refrigerants in adsorption refrigeration systems. The adsorption of calcium chloride or ammonia is a chemical adsorption, and is a single layer adsorption, which can be described by the Langmuir equation (Wang *et al.*, 1999). Most adsorption refrigeration research is focused on physical adsorption, because of its reversible property, almost unlimited operation time and ease of operation.

The equations for physical adsorption can be classified into three types:

(1) Adsorption equation based on adsorption kinetics, which is based upon single molecular layer adsorption, thereby it is a Langmuir-type equation;

(2) Thermodynamic adsorption equation, which is based on Polanyi adsorption potential theory and the Dubinin mini-pore filling theory. A lot of literature (Dubinin, 1975, Wang *et al*., 1999, Polanyi, 1914) shows that the adsorption of vapour on activated carbon can be well described by such an equation;

(3) Adsorption equation based on capillary condensing theory, which does not consider the effect of energy distribution around the adsorbent surface, but treating the mini-pores as capillaries. There are also some empirical equations, of which one example is based upon the assumption that adsorption capacity is a function of

temperature and pressure, but the two parameters affect the adsorption independently, thus $x = f(T, P) = f_1(T)f_2(p)$ (Wang *et al*., 1999). Among the various adsorption equations, the thermodynamic adsorption equation based on Polanyi adsorption potential theory can well describe adsorption of adsorbates on refrigerants. This is the reason why adsorption potential theory has been adopted in adsorption refrigeration, and is also the basis on which to make further improvement.

Adsorption potential theory is based upon the potential energy distribution around the adsorbent surface, which is a theoretical model to describe multi-molecular layer adsorption. The model was suggested by Polanyi (1914) and the thermodynamic viewpoint is adopted in the model, which pays attention to the influence of adsorption on the changes of Gibbs function of the surface. However, the physical model was not described in detail. Later, this model was further developed by Dubinin (1975), thus this theory is now also called Dubinin Polanyi adsorption potential theory.

Polanyi assumed that the adsorption potential energy ε is independent of temperature over a wide temperature range, that is

$$\left(\frac{\partial \varepsilon}{\partial T}\right)_{V^s} = 0 \qquad (2.10)$$

Where V^S is adsorption volume, the potential function $\varepsilon = f(V^S)$ is suitable for all temperature ranges for a known gas, and is thus called characteristic adsorption function. This assumption was verified for non-polar adsorption and for a polar system with low coverage (Zhang, 1988). Based upon the Polanyi assumption, and

with the assumption that the adsorbed liquid is non-compressible, the work needed to form the liquid film can be neglected, and the gas phase can be treated as an ideal gas. Thus the adsorption potential energy at a distance *l* from the adsorbent surface can be written as

$$\varepsilon_l = RTIn\left(\frac{P_o}{P}\right) \quad (2.11)$$

where P_0 is the saturated pressure of the adsorbate corresponding to the temperature of the adsorbent, P is the equilibrium adsorption pressure.

2.10.3 Components and Conditions of Adsorption

Pressure, extent of adsorbent activation, surface area, temperature of the adsorbate, pH of the adsorbate are some of the components which determine the adsorption capacity of adsorbents as depicted by Adsorption Isotherm. With the increases in pressure, adsorption increases up to a certain extent till saturation level is achieved. After saturation level is achieved no more adsorption takes place no matter how high the pressure is applied (Weber Jr, 1972). Activation of adsorbent surface is done so as to provide more number of vacant sites on surface of adsorbent. This can be done by breaking solid crystal in small pieces, heating charcoal at high temperature, breaking lump of solid into powder or other methods suitable for particular adsorbent. Extent of adsorption is generally proportional to specific surface area, specific surface area being that portion of the total surface available for adsorption (figure 2.5). If the mechanism of uptake is one of adsorption on external sites of a non-porous adsorbent, the rate should vary reciprocally with the first power of the diameter. This holds also for porous adsorbents when the rate is controlled by an external resistance, i.e. 'film transport'. Conversely, for cases in

which intraparticle transport controls, the variation should be with the reciprocal of a higher power of the particle diameter (Weber Jr, 1972).

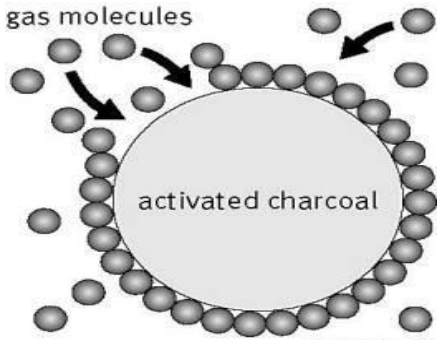

Figure 2.5: Activated carbon and gas adsorption (Weber Jr, 1972)

2.10.3.1 Solute Properties

In general, an inverse relationship between extent of adsorption and water solubility can be anticipated. The water solubility of organic compounds within a particular chemical class decreases with increasing chain length, because the compound becomes more hydrocarbon-like as the number of carbon atoms becomes greater (Weber Jr *et al.*, 1972). Thus, adsorption from aqueous solution increases as homologous series is ascended, largely because the expulsion of increasingly large hydrophobic molecules from water permits an increasing number of water-water bonds to reform. Molecular size is of significance if the adsorption rate is controlled by intraparticle transport, in which case the reaction generally precedes, more rapidly the smaller the adsorbate molecule. It must be emphasized however, that rate dependence on molecular size can be generalized only within a particular chemical class or series of molecules. As shown by Weber and Morris, (1962) large molecules of one chemical class may adsorb more rapidly than smaller ones of another if higher energies (driving forces) are involved (Weber Jr *et al*., 1972).

Many organic compounds exist, or have the potential of existing as ionic species, Fatty acids, phenolic species, amines, and many pesticides are a few materials which ionize under appropriate conditions of pH. Activated carbon commonly has a net negative surface charge: further many of the physical and chemical properties of certain compounds undergo changes upon ionization. Most observations point to the generalization that as long as compounds are structurally simple, adsorption is at a minimum for neutral species. As compounds become more complex, the effect of ionization decreases. Studies of amphoteric compounds indicate an adsorption maximum at the isoelectric point, consistent with other observations that adsorption is at a maximum for neutral species. A polar solute will be strongly adsorbed from a non-polar solvent by a polar adsorbent, but will prefer a polar solvent to a non-polar adsorbent. Polarity of organic compounds is a function of charge separation within the molecule. Almost any asymmetric compound will be more or less polar, but several types of functional groups tend to produce fairly high polarities in compounds. Examples of these are hydroxyl, carboxyl, nitro, nitrile, carbonyl, sulphonate and amine. Thus ethanol, C_2H_5OH, is polar, having an incremental negative charge on the hydroxyl group and a corresponding positive charge on the ethyl group. Because solvation by water involves formation of a hydrogen bond from one of the positively charged hydrogens of the water to a group bearing more or less of a negative charge, along with some bonding in the reverse direction to the water oxygen, water solubility is expected to increase with increasing polarity. It therefore follows that adsorption decreases as polarity increases even though active

carbon is a polar adsorbent. Because hydrogen and hydroxide ions are adsorbed quite strongly, the adsorption of other ions is influenced by the pH of the solution. Further, to the extent to which ionization of an acidic or basic compound affects its adsorption, pH affects adsorption in that it governs the degree of ionization.

In general, adsorption of typical organic pollutants from water is increased with decreasing pH. The organic components of a waste mixture may mutually enhance adsorption, may act relatively independently, or may interfere with one another. Mutual inhibition can be expected if the adsorption affinities of the solutes do not differ by several orders of magnitude and there is no specific interaction between solutes enhancing adsorption. Similarly, because the adsorption of one substance will tend to reduce the number of open sites, and hence, the 'concentration' of adsorbent available, mutually depressing effects on rates of adsorption may be predicted. It should be apparent from the foregoing discussion of the effects of solute character on adsorption that an analytical characterization of the impurities present in a waste is helpful to a thoughtful prediction of the effectiveness of carbon in water purification.

2.10.3.2 Temperature

Adsorption reactions are normally exothermic, thus the extent of adsorption generally increases with decreasing temperature. Changes in enthalpy for adsorption are usually of the order of those for condensation or crystallization reactions, thus small variations in temperature tend not to alter the adsorption process in waste treatment to a significant extent (Weber Jr, 1972). Adsorption process is exothermic

in nature. According to Le Chatleir principle, low temperature conditions would favour the forward direction. $A + B \leftrightarrow AB + Heat$

2.10.3.3 Adsorbent Properties

The properties of different carbons can have profound effects on both rate and capacity for adsorption. The surface chemistry of active carbon has been a subject of much interest for more than a century, yet surprisingly little is known about the nature of the surface functional groups of this material. Recent work has provided an examination of the character of functional groups formed on active carbon under different conditions of activation, using the technique of multiple internal reflectance spectroscopy (MIRS), as a means for characterizing surface functional groups (Weber Jr, 1972). Commercial carbons can be prepared from a variety of raw materials, including wood, lignite, coal, bone, petroleum residues, and nut shells. The raw material is generally activated in an atmosphere of carbon dioxide. Carbon monoxide, oxygen, water vapour, air or other selected gases. At a temperature between 300°C to 1000°C often followed by quenching in air or water. Because of the 'impure' nature of the raw materials used in the production of commercial carbons, and because of the concentration and temperature gradients that develop within the beds of carbon during activation, very heterogeneous or, at best, difficult to characterize surfaces result. Oxygen is known to react to a significant extent with activated carbons. It has been shown that carbons activated in an atmosphere of pure carbon dioxide, or in a vacuum, react with molecular oxygen at room temperature

and below. This affinity for irreversibly 'chemisorbed' oxygen strongly suggests the formation of organic oxygen functional groups on the carbon surface.

Several types of oxygen surface groups have been postulated to explain these phenomena. It is generally thought that two principal types of oxygen functional groups are present on an active carbon surface: those which desorbs as CO. and those which desorbs as CO_2. Several investigators have shown experimentally that carbons activated at higher temperatures are 'basic carbons'. 'Acidic' carbons are defined as carbons which are capable of lowering the pH of neutral or alkaline distilled water, and which are relatively hydrophilic. 'Basic' carbons are not really basic in the acid—base sense, as they interact with acidic solutions in a specific anion adsorption manner, but they are characterized by the ability to raise the pH of a neutral or acidic solution, and by relative hydrophobicity.

We have determined with Mid-infrared Spectroscopy (MIRS) techniques the presence of significant amounts of carbonyl and carboxyl groups on activated carbon surfaces directly substantiating what had long been speculated. The behaviour of active carbon as an adsorbent has to be related to its surface chemistry: the evidence for chemical interaction at the surface between carbonyl and carboxyl groups and organic adsorbates is convincing. Enhancement of the adsorption capacity of active carbon may well be accomplished by increasing the concentration of appropriate surface functional groups (Weber Jr, 1972).

The most characteristic physical property of activated carbon is its extremely large surface area, which is comprised mainly of surfaces bordering inner pore spaces.

The surface area of active carbon is approximately 1000 m^2/g. Relative to the small geometric area of the granules or particles of this material, the large total area requires the existence of a considerable internal surface which can be provided only by small capillaries. In explaining many observed relationships associated with adsorption of materials from solution by carbon, it is essential to consider the physical structure of the adsorbent because the size and arrangement of the capillaries (micropores: 1030Å) and channels or interstices (macropores: 30-100000Å) appear to play a significant role in adsorption processes.

2.10.4 ADSORPTION CAPACITY

Several models that can predict the adsorption capacity have been put forward. A number of such models have been proposed for the adsorption isotherm: the Freundlich isotherm equation (Freundlich, 1926); the Langmuir isotherm (Langmuir, 1916a and 1918b); BET-theory (Brunauer, Emmett and Teller, 1938); the Hacskaylo and LeVan equation (Hackskaylo and LeVan, 1985); the Dubinin-Raduskevish (DR) equation (Dubinin, 1966); and a modification of the DR equation developed by Stoeckli (Stoeckli, 1977a, 1979b). Among the existing predictive equations, the DR equation has been the most widely used to predict organic vapour adsorption onto activated carbon (Wood, 1992, Stoeckli, 1998). It has several advantages:

(a) there is a good data fit over a wide concentration range (b) temperature is included as a parameter (c) it is built around physical parameters (d) it is easy to apply.

Dubinin postulated that the amount of vapour adsorbed (W) by an activated carbon source, at a relative pressure (P/P_s), is a function of the thermodynamic potential (A), with A expressed as

$$A = RTIn(\frac{Ps}{P}) \qquad (2.12)$$

where R is the universal gas constant, T is the absolute temperature, Ps is the saturated vapour pressure at temperature T, and P is the partial pressure of the adsorbate. By examining the adsorption of simple organic compounds, such as benzene, Dubinin concluded that the function was Gaussian. This led to the classical expression of Dubinin and Radushkevich (the D-R equation) (Dubinin, 1975):

$$W = W_O \exp[- (A/\beta E_o)^2] \qquad (2.13)$$

where W_0 is the maximum amount adsorbed, E_0 is the characteristic adsorption energy for a reference vapour on a specific adsorbent. The parameter β is called the affinity coefficient or similarity coefficient, and expresses the ratio of the characteristic free energies of adsorption for the test and reference vapours (Urano *et al.*, 1982; Stoeckli & Morel, 1980). Benzene is, by convention, used as the reference compound for carbonaceous materials, and is, by definition, given the value $\beta = 1$. β is only related to the properties of the adsorbate, and is independent of the adsorbent (Dubinin, 1975). The value of β has a significant influence on adsorption capacities calculated using the DR equation. The influence is most pronounced at low relative pressures.

It has been suggested that the affinity coefficients can be approximated by ratios of:

1) molar polarizabilities (α),

$$\beta = \frac{\alpha}{\alpha ref} \tag{2.14}$$

2) molar volumes (V) of the adsorbates in the liquid state,

$$\beta = \frac{V}{Vref} \tag{2.15}$$

3) ratios of parachors (Ω) of the adsorbate and a reference compound.

$$\beta = \frac{\Omega}{\Omega ref} = \frac{\left[\frac{V\gamma\,1}{4}\right]}{\left[\frac{V\gamma\,1}{4}\right]ref} \tag{2.16}$$

where γ = surface tension and V = molar volume of the adsorbate.

These three expressions have been compared by Wood (2001), who concluded that these three methods give comparatively good predictabilities, but that power functions with exponents less than unity provided slightly better fits for predicting experimental values. The author recommended the molar polarizability correlation parameter. The predictive power of different models and the criteria for selecting reference compound(s) are, however, still under discussion (Reucroft *et al*. 1971, Noll *et al.*, 1989, Golovoy and Braslaw 1981). Reucroft *et al*. and Noll *et al.*, (1989) concluded that the vapours under consideration and the reference vapours should be of similar polarity, while Golovoy and Wood (Wood, 2001), expressed the view that a single reference compound would be sufficient. The equations (2.14) to (2.16) correlate β with one or two parameters of the adsorbate, but these equations sometimes produce very different results. To resolve these problems it is necessary to start with a systematic examination of the inherent nature of the affinity coefficient.

2.10.5 Adsorption Isotherms

Two equations, the Langmuir equation and the Freundlich equation, find common use for describing adsorption isotherms for water and wastewater treatment applications. The Langmuir isotherm is

$$q_e = QbC/(1 + bC) \quad \text{(Weber Jr. } \textit{et al.}\text{, 1972)} \qquad (2.17)$$

in which b is a constant related to the energy or net enthalpy of adsorption, and Q is the ultimate adsorption capacity (maximum value of q).

The Freundlich equation has the general form

$$q_e = K_F C^{1/n} \qquad (2.18)$$

where K_F and n are constants and n> 1. Data are usually fitted to the logarithmic form of the equation, which gives a straight line with a slope of 1/n and an intercept equal to the value of log K_F for C = 1 (log C = 0). The intercept is roughly an indicator of sorption capacity and the slope, 1/n, of adsorption intensity (Weber Jr, *et al.*, 1972). The Freundlich equation generally agrees well with the Langmuir equation and experimental data over moderate ranges of concentration, C. Unlike the Langmuir equation however, it does not reduce to a linear adsorption expression at very low concentrations, nor does it agree well with the Langmuir equation at very high concentrations, since n must reach some limit when the surface is fully covered.

2.10.5.1 Langmuir equation

The Langmuir equation describes the chemical adsorption (chemisorption) phenomena involving monolayer surface coverage (Marsh *et al.*, 2006). The Langmuir equation is derived from the equilibrium between the particle, empty surface sites and the sites filled by particle.

$$\frac{p/p_o}{n^a} = \frac{1}{b n_m^a} + \frac{p/p_o}{n_m^a} \quad (2.19)$$

Here:

p = equilibrium vapour pressure of molecules in adsorbent (Pa), P_0 = saturation vapour pressure (Pa), n^a = amount of molecules adsorbed on the adsorbent surface site (mmol/g), n_m^a = amount of adsorbate which forms a monolayer as a measure of monolayer coverage (mmol/g), b = a constant which describes the average energy adsorption. A plot of n^a against P/P_0 in equation (2.19) gives the value of n^a_m (monolayer coverage) (mmol/g).

Basic assumptions for the Langmuir equation are:

1. The adsorbent has a homogeneous energetic surface; it means that the surface coverage does not have any effect on the heat of adsorption.

2. There is just monolayer coverage (adsorption) that happens during the entire adsorption process.

3. There is no interaction between the adsorbate molecules with other adsorbate molecules (Harry, 2006). The adsorption isotherm is useful for representing the capacity of an activated carbon for adsorbing organics from a waste, and in providing description of the functional dependence of capacity on the concentration of pollutant. The steeper the isotherm, the more effective is the activated carbon; that is, the sharper the rise of the isotherm to a given ultimate capacity as concentration increases, the higher will be the effective capacity at the concentration level desired for the treated water. Experimental determination of the isotherm is routine practice in evaluating the feasibility of adsorption for treatment, in selecting a carbon, and in estimating carbon dosage requirements (Harry, 2006). The

Langmuir and Freundlich equations provide means for mathematical description of the experimentally observed dependence of capacity on concentration. The adsorption isotherm relates to an equilibrium condition, however, and practical detention times used in most treatment applications do not provide sufficient time for true equilibrium to obtain. Rates of adsorption are thus significant, for the more rapid the approach to equilibrium, the greater is the fraction of equilibrium capacity utilized in a given contact time. There are three primary rate steps in the adsorption of materials from solution by granular activated carbon. First is the transport of the adsorbate through a surface film to the exterior of the adsorbent (film diffusion); second is the diffusion of the adsorbate within the pores of the adsorbent (pore diffusion); third is adsorption of the solute on the interior surfaces bounding pore and capillary spaces (Weber Jr *et al.*, 1972). For most operating conditions, transport of adsorbate through the 'surface film' or boundary layer is rate-limiting, if sufficient turbulence is provided, transport of the adsorbate within the porous carbon may control the rate of uptake. The method by which the carbon is contacted with the water determines in large part which of the transport or reaction steps is rate-limiting. For a completely and vigorously mixed batch reactor, pore diffusion may be rate-limiting. For continuous flow systems (e.g. beds of granular carbon) film diffusion is usually rate-limiting for normal flow rates of 2-10gpm/ft^2 (Weber Jr *et al.*, 1972).

In 1916, Irving Langmuir published an isotherm for gases adsorbed on solids, which retained his name. It is an empirical isotherm derived from a proposed kinetic mechanism. It is based on four hypotheses:

1. The surface of the adsorbent is uniform, that is, all the adsorption sites are equal.

2. Adsorbed molecules do not interact.

3. All adsorption occurs through the same mechanism.

4. At the maximum adsorption, only a monolayer is formed: molecules of adsorbate do not deposit on other, already adsorbed, molecules of adsorbate, only on the free surface of the adsorbent. For liquids (*adsorbate*) adsorbed on solids (*adsorbent*), the Langmuir isotherm can be expressed by

$$M = \frac{A_{max}\, kc}{1+kc} \qquad (2.20)$$

here M is the amount of adsorbate adsorbed per gram (or kg) of the adsorbent, the unit of M is $mol.g^{-1}$, resp. $mol.kg^{-1}$. A_{max} is the maximal amount of adsorbate per gram (or kg) of the adsorbent. The unit of A_{max} is $mol.g^{-1}$, resp. $mol.kg^{-1}$. k is the adsorption constant ($mol^{-1}.dm^{3}$); c ($mol.dm^{-3}$) is the concentration of adsorbate in liquid (Oremusová, 2007). In practice, activated carbon is used as an adsorbent for the adsorption of mainly organic compounds along with some larger molecular weight inorganic compounds such as iodine and mercury. Activated carbon, also called activated charcoal or activated coal, is a general term that includes carbon material mostly derived from charcoal. For all three variations of the name, "activated" is sometimes substituted by "active." By any name, it is a material with an exceptionally high surface area. Just one gram of activated carbon has a surface

area of approximately 500m² (for comparison, a tennis court is about 260m²). The three main physical carbon types are granular, powder and extruded (pellet). All three types of activated carbon can have properties tailored to the application. Activated carbon is frequently used in everyday life, in: industry, food production, medicine, pharmacy, military, etc. In pharmacy, activated charcoal is considered to be the most effective single agent available as an emergency decontaminant in the gastrointestinal tract. It is used after a person swallows or absorbs almost any toxic drug or chemical.

2.10.5.2 Freundlich Isotherm

The Freundlich equation assumes that different sites with several adsorption energies are involved in the process of adsorption (Pimentel *et al.*, 2008). It therefore incorporates surface heterogeneity of active sites. The Freundlich isotherm can be derived by applying the Langmuir model and assuming that the heat of adsorption, ΔH, is exponentially dependent on the fractional surface coverage, θ (Sheindorf *et al.*, 1981). This is expressed in the following equation.

$$\theta = aop\left(\frac{-RT}{\Delta Hm}\right) = (aop)\frac{RT}{q_m} \qquad \text{in g/gm} \qquad (2.21)$$

where, $q_m = -\Delta Hm$ (2.22)

$ao = k_a/k_d$ (2.23)

P is the pressure of the adsorbate, R is the universal constant, T is the temperature, g is the amount of adsorbate adsorbed by adsorbent, gm is the amount of adsorbate adsorbed when the surface of the adsorbent is completely covered with a monolayer,

k_a is the rate of adsorption and k_d is the rate of desorption. For purposes of data analysis, the isotherm can be arranged as follows:

$$\ln g = [\ln gm + (\frac{RT}{q_m}) \ln ao] + (\frac{RT}{q_m}) \ln P \quad (2.24)$$

The terms in the brackets are constants at constant temperature. A plot of lng against lnP yields a straight line whose slope is (RT⁄qm), from which qm can be calculated. For liquid adsorbates, the Freundlich relationship is shown as follows:

$$q_e = k_F.C_e^{1/n} \quad (2.25)$$

where, 1/n is a heterogeneity factor, which is a measure of intensity of sorption or affinity of the adsorbate for the adsorbent (Faust and Usman, 1987); k_F is the Freundlich constant. The Freundlich equation can be linearized as shown in equation (2.26).

$$\log q_e = \log k_F + 1/n \log C \quad (2.26)$$

The constants, k_F and n, are determined by plotting log C on the abscissa and log qe on the ordinate. A best fit of the experimental data provides values for kF and n based on the y- intercept and the slope, respectively. The Freundlich equation is useful in cases where the actual identity of the adsorbate is not known (Treybal, 1980).

2.10.5.3 Tempkin Isotherm

The Temkin isotherm assumes that the fall in the heat of sorption is linear rather than logarithmic, as implied in the Freundlich equation (Aharoni and Ungarish, 1977). The isotherm can be derived by assuming that for adsorption at a single site,

the appropriate Langmuir isotherm is as shown in the following equation (Vannice, 2005).

$$\theta/(1 - \theta) = (ka/kd).P \exp(-\Delta H/RT) \quad (2.27)$$

$$\ln \theta/(1 - \theta) = \ln P + (\Delta Ho\alpha\theta)/RT + \ln Ao \quad (2.28)$$

$$\text{where, } Ao = ao \exp(q/RT) \quad (2.29)$$

α is a positive constant. If the variation of lnθ/(1 - θ) is taken to be negligible, then equation (2.29) becomes:

$$\ln P + (\Delta Ho\alpha\theta)/RT + \ln Ao = 0 \quad (2.30)$$

This can be rearranged in the form of equation 2.31:

$$\theta = (RT / qo\alpha) \ln (AoP) = g/gm \quad (2.31)$$

$$\text{where, } qo = -\Delta Ho \quad (2.32)$$

ΔHo is the heat of adsorption at zero coverage. For correlation purposes, the isotherm is expressed as follows:

$$g = (gm\ RT/qo\alpha)\ [\ln ao + (qo/RT)] + (gm\ RT/qo\alpha) \ln P \quad (2.33)$$

A plot of g versus lnP gives a straight line graph whose slope is (gm RT/qoα), from which qo can be calculated.

For liquid adsorbates, the Temkin isotherm model is as follows.

$$qe = (RT)/bT \ln kT + (RT)/bT \ln Ce \quad (2.34)$$

where, bT indicates the adsorption potential of the adsorbent and kT is the Temkin constant (Horsfall & Spiff, 2005). A plot of qe versus lnCe gives a straight line graph if this model is favoured. kT can be calculated from the intercept of the plot while bT can be calculated from the slope.

2.10.5.4. The DR (Dubinin-Radushkevich) isotherm

Many microporous adsorbents including activated carbons contain pores over a

wide range of pore sizes, including micro and mesopores. Hence, the isotherm obtained from such type of adsorbents reveals features from both type I and type IV isotherms. The filling of micropores occurs at very low relative pressures and is entirely governed by the enhanced gas-solid interactions. In addition to the strong adsorption potential a cooperative mechanism may play an important role in the micropore filling process. Dubinin and Radushkevich postulated an equation which allows the micropore volume to be calculated from the adsorption isotherm (Dubinin & Radushkevich, 1989):

$$\text{Logw} = \log (V_oP) - k[\log(p^o/p)]^2 \quad (2.35)$$

where, W is the volume of adsorbate filling micropores, is the density of liquid adsorbate; V_o is the micropore volume and *k* is defined as

$$K = 2.303k(RT/ß)^2 \quad (2.36)$$

Where w is the affinity coefficient, and K is a constant, determined by the shape of the pore size distribution. A plot of log*W* versus $[\log(p^o/p)]^2$ should be a straight line with an intercept to $\log(V_oP)$, from which the micropore volume (V_o) can be calculated. The DR equation of ten fails to linearize when the adsorbent contains heterogeneous micropores. To over come this, a more general equation, known as DA equation, was proposed by Dubinin and Astakhov. The linearized form of DA equation is

$$\ln w = \ln(V_oP) - k[\ln(p^o/p)]^n \quad (2.37)$$

where, *K* is an empirical constant, and *n* is the Dubinin-Astakhov parameter. Depending on the type of micropore system, the value of *n* ranges from 2 to 5, and for adsorbents with homogeneous micropore structure, *n* is usually close to 2.

2.10.5.5 Sorption isotherms

As explained earlier adsorption isotherms are used for the characterization and determination of the pore volume and the internal surface area of the solid carbon. These isotherms have been classified by IUPAC (International Union of Pure and Applied Chemistry) into six types (Marsh *et al*., 2006). Figure 2.6 illustrates these different shapes.

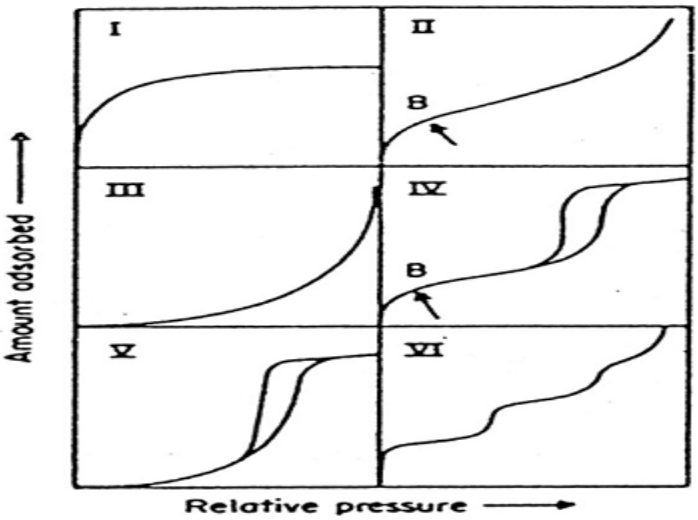

Figure 2.6: IUPAC's classification of the sorption isotherms (Amir, 2012)

Type-I shows adsorption isotherms that reach a maximum value of adsorption without inflections. These isotherms are characteristic of carbons that contain only micropores. The gradient of the first part of the isotherm having a relative pressure (p/p_0) from zero to about 0.05 is an indication for the dimensions of the micropores. The steep initial region is due to very strong adsorption, for example in the micropores. The steeper the gradient the narrower the micropores. The limiting value (plateau) is due to filled pores and essentially zeros external area.

Type-II adsorption isotherms have a knee in the first section of the curve that indicates the approximate location of the monolayer formation. The inflection between the region of relative pressure (p/p_0) > 0.1and p/p_0 > 0.9 indicates that the

extent of the adsorption increases rapidly by multilayer formation in this region. Absence of the hysteresis indicates adsorption on and desorption from a non-porous or open surface with multilayer formation, which is assisted mostly by the condensation of the adsorptive molecules and not by volume filling.

Type-III shows adsorption isotherms that are convex. The lack of a knee indicates extremely weak adsorbate-adsorbent interaction as is the case for adsorption on surfaces of organic polymeric systems such as krypton on polymethyl methacrylate. (BET model is not applicable for these isotherms).

Type-IV isotherms look like the type-II isotherms, but instead of adsorption on open surfaces at high relative pressures ($p/p^0 > 0.9$), adsorption takes place in mesopores. The low slope region in the middle of isotherm plot illustrates the first few multilayers. Activated carbons usually do not exhibit a plateau in the high relative pressure region. Hysteresis indicates capillary condensation in meso and macropores as is the case for activated carbon. (BET and BJH models are applicable for these isotherms).

Type-V represents adsorption isotherms for a low energy, homogeneous solid surface possessing mesopores. The lack of a knee indicates extremely weak adsorbate-adsorbent interaction such as water on black carbon. (BET is not applicable).

Type-VI represents the adsorption isotherms for surfaces with an extremely homogeneous structure such as pyrolytic graphite that uses methane and argon as adsorbate but not N_2.

Hysteresis is indicative of the presence of mesopores. The pore size distribution can be calculated from the adsorption isotherm, as well as, desorption isotherm branches.

2.11 Adsorption Kinetics of Activated Carbon

Various kinetic models are used in determining the mechanism of an adsorption process and the potential rate controlling steps. Some of these models are discussed in the following section.

2.11.1 Bhattacharya-Venkobachar Model

The Bhattacharya-Venkobachar equation is as follows:

$$\log [1 - (U)T] = (kB/2.303)\ t \qquad (2.38)$$

where

$$(U)T = (C_o - C_t)/ (Co - C_e) \qquad (2.39)$$

KB is the Bhattacharya-Venkobachar's constant (min^{-1}); C_o is the initial concentration (mg/l); C_t is the concentration at time, t (mg/l) and C_e is the concentration at equilibrium (mg/l). A plot of log [1- (U)T] versus t should yield a straight line, if the sorption process obeys this model. From the slope of the plot, KB can be determined. The Bhattacharya-Venkobachar equation is based on the assumption that the adsorption process is controlled by intra-particle diffusion (Israel and Ekwumemgbo, 2008).

2.11.2 Lagergren Pseudo First Order Model

The Lagergren pseudo first order equation is generally expressed as follows:

$$dq_t/d_t = k1\ (q_e - q_t) \qquad (2.40)$$

where, q_e and q_t are the adsorption capacity at equilibrium and at time t, respectively ($mg.g^{-1}$) and k_1 is the rate constant of pseudo first order adsorption

(min^{-1}). The integrated rate law, after applying the initial condition of $q_t = 0$ at $t = 0$, is as follows (Ibraham *et al.*, 2006):

$$\log (q_e - q_t) = \log (q_e) - (k_1 t)/2.303 \quad (2.41)$$

A plot of $\log (q_e - q_t)$ versus t should give a straight line, if the sorption is controlled by this model. k_1 and q_e can be determined from the slope and intercept of the plot, respectively. The experimental qe should tally with the estimated one. Generally, higher values of k_1 suggest greater adsorption (Igwe and Abia, 2007). The assumption with this model is that the rate of adsorption is proportional to the difference between the adsorption capacity (q_e) at equilibrium and the capacity at any time t (Ibrahim, *et al*., 2006). According to Sağ and Aktay, (2002), if the experimental results do not follow equation (2.41), then $k_1(q_e - q_t)$ does not represent the number of available adsorption sites and $\log q_e$ is not equal to the intercept of the plot of $\log(q_e - q_t)$ against t.

2.11.3 Pseudo-second Order Model

The pseudo second order adsorption kinetic rate equation as expressed by Ho *et al.*, (2000) is shown in equation (2.42).

$$dq_t/dt = k_2 (q_e - q_t)^2 \quad (2.42)$$

where, k_2 is the rate constant of pseudo second order adsorption ($g.mg^{-1}.min^{-1}$). From the boundary conditions t = 0 to t = t and $q_t = 0$ to $q_t = q_t$, the integrated form of equation (2.42) becomes equation (2.43).

$$1/(q_e - q_t) = 1/q_e + k_2 t \quad (2.43)$$

This is the integrated rate law for a pseudo second order reaction. Equation (2.43) can be rearranged to obtain equation (2.44), which has a linear form.

$$t/q_t = 1/(k_2 qe^2) + t/qe \quad (2.44)$$

A plot of t/q_t versus t should give a straight line if this model is obeyed by the sorption process. From the slope and intercept of the plots, q_e and k_2 are determined, respectively. The experimental qe should tally with the estimated one. Decrease in the values of k_2 suggests increased adsorption (Debnath and Ghosh, 2008).

The main assumptions of the pseudo-second order kinetic model is that rate limiting step is chemical sorption involving bond formation through sharing or exchange of electrons between the adsorbate and adsorbent. It also assumes that sorption follows the Langmuir equation (Ho and McKay, 2000).

2.12 Review of Major Literatures

2.12.1 Sorption involving Lead and other ions

(a1) Olugbenga *et al*. (2010) in the paper ‘’Sorption studies of Pb^{2+} onto activated carbon produced from oil-palm fruit fibre’’ examined the batch sorption removal of Pb^{2+} from aqueous solution using treated oil palm fruit fibre. The oil palm fruit fibre was obtained from a local oil palm mill in Yoaco Area, Ogbomoso, Oyo State, Nigeria.

The adsorption equilibrium and kinetic studies of Pb^{2+} on such fibre were then examined at 25°C. Adsorption isotherms of Pb^{2+} on the activated carbon produced from treated oil palm fibre were determined and correlated with common isotherm equations. The equilibrium data for Pb^{2+} adsorption fitted well to the Langmuir equation more than the Freundlich equation with maximum monolayer adsorption capacity of 588.24 mg/g. The batch sorption model, based on a pseudo-second-order mechanism, was applied to predict the rate constant of sorption, the equilibrium capacity and the initial sorption rate with the effects of the initial solution pH and

fibre dose. The adsorption capacity at equilibrium increases from 75.48 to 439.06 mg/g with an increase in the initial lead concentration from 100 to 500mg/l. Equilibrium concentrations were evaluated with the equilibrium capacity obtained from the pseudo-second-order rate equation. The adsorption data was found to fit the pseudo second order model more than the pseudo first order model.

Oguegbulu *et al*. (2013), evaluated the adsorption isotherm of activated charcoal used in pharmaceutical medicine from some Nigerian plant parts, corn cobs, the wooden parts of *Mangifera indica and Azandirachta indica* collected from the University of Port Harcourt, community in Rivers State, Nigeria. It was observed that M. indica (K – 0.076), showed the highest adsorption capacity while at the same time was statistically significant, followed by A. Indica (K - 0.026) whereas corn cobs (K – 0.013) and standard (K – 0.013) ranked equally with the lowest specific adsorption property. Activated charcoal with excellent performance as well as cost-effective for use in pharmaceutical medicine can be sourced from local plants and farm wastes.

Ademiluyi *et al*. (2012), studied the effect of Chemical Activation on the Adsorption of Heavy Metals Using Activated Carbons from Waste Materials.

(a2) The effect of chemical activation on the adsorption of metals ions (Cr^{2+}, Cu^{2+}, Ni^{2+}, Pb^{2+}, Fe^{2+}, and Zn^{2+}) using waste Nigerian based bamboo, coconut shell, and palm kernel shell was investigated. The bamboo, coconut, and palm kernel shell were carbonized at 400^0C - 500^0C and activated at 800^0C using six activating agents. Chemical activation had significant effect on the iodine number and

invariably increased the micropores and macropores of the activated carbons produced from bamboo, coconut, and palm kernel shell. It also affected the adsorption of metal ions and the type of carboneous material used for activation. The highest metal ions adsorbed were obtained from bamboo activated with HNO_3. The cellulose nitrite formed during the activation of bamboo with HNO_3 combined with high pore volume and low ash content of bamboo effectively create more reaction sites for adsorption of different metal ions. This shows that waste bamboo activated with HNO_3 can effectively be used to remove metal ions from waste streams and in different metal recovery processes than activated carbon from coconut shell and palm kernel shell (Ademiluyi *et al*., 2012).

Amuda *et al*. (2007), looked at the removal of heavy metal from industrial waste water using modified activated coconut shell carbon. Adsorption data fitted well with the Langmuir and Freundlich models. However, Langmuir isotherm displayed a better fitting model than Freundlich isotherm because of the higher correlation coefficient that the former exhibited, thus, indicating to the applicability of monolayer coverage of the zinc (II) on the surface of adsorbent. Desorption studies were carried out with NaOH and quantitative recovery of the metal was evident. The dominant sorption mechanism is ion exchange. The use of agricultural waste (coconut shell) and aquatic waste (chitin) to produce activated carbon potentially leads to the production of a highly effective adsorbent generated from less expensive raw materials that are from renewable resources.

Elaigwu (2009), studied the adsorption of Pb(II) from Aqueous solution by activated carbon prepared from cow dung. Chemical activation utilizes such as H_2SO_4, H_3PO_4, ZnCl , KOH, and CaCl , which have dehydrating and oxidation characteristics (Kim *et al*., 2001) Carbonization and activation are usually carried out simultaneous in chemical activation process (Kobya *et al*., 2005). The fresh cow dung was obtained from a cattle ranch at Sango along Jebba road, Ilorin, Kwara state, Nigeria. The fresh cow dung was sun dried and grinded and sieved to the desired size prior to activation. Chemical activation using H_2SO_4 at moderate temperatures produces a high surface area and high degree of micro porosity (Demirbas, 2003). The method of Kobya *et al.*, 2005 was adopted. 100g of the sieved material was mixed in a 1:1 wt ratio with concentrated H_2SO_4 placed in an oven and heated to 200°C for 24hrs. After this, the sample was allowed to cool to room temperature, washed with distilled water and soaked in 1% $NaHCO_3$ solution to neutralize any remaining acid. The sample was filtered and washed with distilled water until a pH of 7.0 was attained, dried at 105°C for 5hrs and sieved to obtain the desired sample size (1.00-1.25mm). Batch experiments were conducted to investigate the effects of pH, adsorbent dosage, absorbate concentration, contact time and temperature on the adsorption of Pb on the activated cow dung. All reagent used were of AR grade. $Pb(NO_3)_2$ salt was used in the preparation of the stock solutions by dissolving it at a known concentration in distilled water. The initial concentration of metal ion and corresponding concentrations after fixed time periods were measured by atomic adsorption spectrophotometer (UNICAM 919). The metal

concentration retained in the adsorbent phase (q, mg/g) was calculated by using the following equation.

$$Q = \frac{(C_o - C)V}{W} \quad (2.45)$$

Where C_o is the initial metal ion concentration in mg/l, C is the equilibrium concentration of metal ions in mg/l, V is the volume of the solution (l) and W is the mass of the adsorbent (g). Each of the experiment was carried out in duplicate and the average of two values was used in the calculations.

Awoyale *et al.* (2013), conducted and investigated the production and experimental efficiency of activated carbon from local waste bamboo gotten from construction sites of the rain forest belt of the Niger Delta region of Nigeria for a typical adsorption and treatment of wastewater from a typical refinery. The experiment showed that both adsorbents can be effectively used for the treatment and removal of Pb and Cu from a typical refinery wastewater stream for re-use. The tests' utmost operating conditions for carbon dosage and pH also gave a 100% removal of both metal ions. Thus the effective observation on using activated carbon produced from local bamboo for the adsorption process was quite efficient and could be employed for other adsorption purposes.

Ameh (2013), studied the 'Modelling of the Adsorption of Cu (II) and Cd (II) from Aqueous Solution by Iraqi Date-Palm Activated Carbon (IPDAC)' which Batch adsorption studies were used to evaluate the adsorption capacity of Iraqi Palm Date in the removal of Cd(II) and Cu(II) ions from synthetic aqueous solutions. The

present data confirms that Iraqi Palm Date may be used as efficient adsorbent for the removal of cadmium (II) and copper (II) ions from aqueous solution.

(a3) Agbozu and Emoruwa (2014) evaluated the efficiency of metals (Cu, Fe, Pb, Cr and Cd) removal from mixed metal ions solution using coconut husk as adsorbent. The effects of varying contact time, initial metal ion concentration, adsorbent dose and pH on adsorption process of these metals were studied using synthetically prepared wastewater. The percentage removal of metals increased with increasing weight (0.4-1.2 g) in 50 ml of adsorbent dose and the observed trend was: Cr > Cu > Pb > Fe > Cd. The adsorption efficiency increased with increasing initial metal ion concentration (0.3-0.9 mg/l) and the observed trend was: Cr > Cu > Cd > Fe > Pb. Similarly, percentage removal of metal ions increased with increasing pH of the mixed metal ions solution (pH values of 2, 6 and 10). The observed trend of percentage adsorption of metals by varying pH was: Cd > Fe > Cr > Cu > Pb. The effect of contact time on the adsorption efficiency at different time intervals of 20, 40 and 60min in mixed metal ions solution showed that the removal of tested metals was rapidly achieved during a short interval of 20min. Generally, the study showed that coconut husk (a waste material) is a viable material for removal of metals from waste water as the percentage adsorbed varies from 95.2-98.8, 91.1-99.3 and 75.0-98.5% for Cd, Cr and Cu, respectively while the percentage removal of Fe and Pb from the waste water varies from 84.9-97.0 and 81.1-98.7%, respectively. Isothermal studies showed that the experimental data are best fitted on Langmuir model.

Akiode *et al.* (2015) in adsorption of Cu (II) ions by untreated sugarcane bagasse (USCB) and treated sugarcane bagasse (TSCB) was investigated. Sugarcane bagasse was treated with 0.1M oxalic acid prior to TSCB adsorption studies. Dependence of Cu (II) adsorption on pH, contact time, temperature and initial concentration of adsorbate solution were also investigated. Optimum pH 2 and contact time of 100 minutes were observed for both USCB and TSCB, while Cu II sorption increased with temperature. Under optimum condition, TSCB adsorbed Cu (II) ions better than USCB (1.854mgg^{-1} and 0.556mgg^{-1} respectively). Thermodynamic investigations showed that Cu (II) adsorption was feasible, spontaneous and endothermic. Kinetic data was adequately described by Ho's pseudo-second-order kinetic model while intra-particle diffusion model described a slow adsorption affinity. It was concluded that Cu (II) adsorption by sugarcane bagasse is a favourable chemisorption process and was well explained by both Langmuir and Freundlich isotherms.

Quek *et al.* (1998), in their study on the use of sago waste for the sorption of lead and copper. Sago processing waste, which is both a waste and a pollutant, was used to adsorb lead and copper ions from solution. The sorption process was examined in terms of its equilibria and kinetics. The most effective pH range was found to be 4 to 5.5 for both metals. The equilibria data for both metals fitted both the Langmuir and the Freundlich models and based on the Langmuir constants, the sago waste had a greater sorption capacity for lead (46.6mg g^{-1}) than copper (12.4mg g^{-1}). The

kinetic studies showed that the sorption rates could be described well by a second-order expression than by the more commonly applied Lagergren equation.

Kadirvelu *et al.* (2003) studied on utilization of various agricultural wastes for activated carbon preparation and application for the removal of dyes and metal ions from aqueous solution. Mercury(II) and nickel(II) were used in the study for various adsorbents. Activated carbon was prepared from agricultural solid wastes such as, silk cotton hulls, coconut tree sawdust, sago waste, maize cob and banana pitch.

Erhan Demirbas *et al.* (2004) reported that the batch removal of Cr (VI) from aqueous solution using low-cost adsorbents such as cornelian cherry, apricot stone and almond shell under different experimental conditions was investigated in this study. The influences of initial Cr (VI) ion concentration (20 to 300 mg•L-1), pH (1 to 4) and particle size (0.63 to 1.60 mm) have been reported. Adsorption of Cr (VI) is highly pH-dependent and the results indicate that the optimum pH for the removal was found to be 1 for all types of carbon. A comparison of kinetic models applied to the adsorption of Cr (VI) ions on the adsorbents was evaluated for the pseudo first-order, the pseudo second-order, Elovich and intraparticle diffusion kinetic models, respectively. Results show that the pseudo second-order kinetic model was found to correlate the experimental data well.

In the investigation of Hema Krishna *et al.* (2011), the powder of mosambi fruit peelings (PMFP) was used as an inexpensive and efficient adsorbent for Ni (II) removal from aqueous solutions. The influence of physico-chemical key parameters such as the initial metal ion concentration, pH, agitation time, particlesize and

adsorbent dosage has been considered in batch tests. Sorbent ability to adsorb Ni (II) ions was examined and the mechanism involved in the process investigated. The optimum results were determined at an initial metal ion concentration of 50 (mg L^{-1}), pH=4, agitation time – 90 min, an adsorbent dose (125 mg/50 ml) and the particle size (0.6 mm). The % adsorption, Langmuir constants [Q_0=29.41 mg g^{-1} and b=0.4789 L mg^{-1}], Freundlich constant K_f= 23.92 mg g^{-1} and n=2.24 L mg^{-1}, Lagergren rate constants [K_{ad}=4.37x10^{-2} min^{-1}] for [Ni(II)] 50 mg L^{-1}, were determined for the adsorption system as a function of sorbate concentration. The equilibrium data obtained were tested using Langmuir, Freundlich adsorption isotherm models, and the kinetic data obtained were fitted to pseudo first order model.

The study of Koel Banerjee *et al.* (2012), deals with the application of watermelon shell, an agricultural waste, for the adsorptive removal of Cu(II) from its aqueous solutions. The adsorption behavior of the Cu(II) has been studied using Freundlich, Langmuir and Tempkin adsorption isotherm models. The monolayer adsorption capacity determined from the Langmuir adsorption equation has been found as 111.1mg g^{-1}. Kinetic measurements suggest the involvement of pseudo-second-order kinetics in adsorptions and is controlled by a particle diffusion process. Adsorption of Cu(II) on adsorbents was found to increase on decreasing initial concentration, increasing pH up to 8, increasing temperature, increasing agitation speed and decreasing particle size. Overall, the present findings suggest that

watermelon outer shell is environmentally friendly, efficient and low-cost biosorbent which is useful for the removal of Cu(II) from aqueous media.

Halim *et al*. (2003) studied on removal of lead ions from industrial wastewater by different types of natural materials. From the research done it was reported that at lead concentration of 4 mgL^{-1} and pH 6 the adsorption capacity is maximum for Nile rose plant powder at 80% removal and at the same concentration and pH it was also reported that bone powder removed 98.8% of lead.

Tan *et al.* (1993), studied on removal of chromium (VI) from solution by coconut husk and palm pressed fibres and it was investigated using batch and column techniques. For both substrates, the optimum pH for maximum removal is at 2.0 which corresponds to >80% removal.

Sarin *et al.* (2006), reported that removal of poisonous hexavalent form of chromium from solutions was possible using selected adsorbents. Eucalyptus bark (EB) was the most effective for which the removal reached more than 99% for Cr(VI) at concentration of 200 ppm and at pH 2. Increase in the dose of adsorbent, initial concentration of Cr(VI) and increase in contact time upto 2h are favorable for all increase the adsorption of Cr(VI). The kinetic of the Cr(VI) adsorption on EB was found to follow first order mechanism. The Gibbs free energy was obtained for each system. It was found to be -1.884 kJ mol^{-1} for Cr(VI) and -3.872 kJ mol^{-1} for Cr(III) for removal from industrial effluent. The adsorption data can be satisfactorily explained by Freundlich isotherm. Higher sorption capacity of this sorbent indicates that eucalyptus bark can be used for the treatment of chromium effluent.

2.13 Agricultural Wastes as Low Cost Metal Adsorbents

2.13.1 Bagasse

Bagasse, an agricultural waste from sugar industry, has been found as low cost metal adsorbent. Mohan and Singh (2009), studied potentiality of activated carbon (AC) derived from bagasse for removal of Cd (II) and Zn (II) from aqueous solutions in single as well as multi-metal systems. Cd (II) adsorption was slightly more than Zn (II) and increased sorption capacity was reported with increase in temperature. Adsorption on bagasse-based AC occurs through a film diffusion mechanism at all concentrations. Using bagasse-based carbon, Ayyappan et al., (2005) studied adsorbent of Pb (II) under batch adsorption. Desorption of Pb (II) from sorbed carbon was achieved by eluting with 0.1M HNO_3. Carbon was retrieved by washing with 0.1M $CaCl_2$ solution and reused.

2.13.2 Cassava Waste

Cassava tuber, a major staple food in Africa and many other parts of world (Osagie, 1998), generates enormous waste biomass. Pure activated and differentially thiolated cassava waste biomass19 (0.5M and 1M thiolation level respectively), studied using equilibrium sorption, removed metals from aqueous solutions at following sorption rates: Cd (II), 0.2303, 0.109; Cu (II), 0.0051, 0.0069; and Zn (II), 0.0040min^{-1}, 0.0367min^{-1}. Increased thiolation led to increased incorporation or availability of more binding groups onto cellulosic matrix, which improved adsorptivity of cassava waste biomass. Cassava tuber bark wastes (Abia *et al.*, 2003, Horsfall *et al.*, 2003, Horsfall *et al.*, 2003), (CTBW) in pure and chemically modified forms had good potential as metal ion adsorbents from aqueous solutions and industrial effluents. From solutions containing 100 mg l^{-1} of metal, CTBW

removed: Cd, 45.61; Cu, 54.21; and Zn, 28.95 mg g^{-1}. Acid treatment of biomass enhanced sorption capacity (Horsfall *et al.*, 2006) (> 50%).

2.13.3 Coconut Wastes

Coconut Shell and Fibre Coconut shell based AC (Guikwad, 2004), removed 66% Cd (II) from water within 80min at pH 6. Coconut shell charcoal (CSC) oxidized with nitric acid had higher Cr adsorption capacities (10.88mg g-1) than that oxidized with sulfuric acid (4.05mg g^{-1}) or coated with chitosan (3.65mg g^{-1}). Surface modification of CSC with a strong oxidizing agent and treatment of chitosan generated more adsorption sites on its surface for metal adsorption (Babel and Kurniawan, 2004). Regeneration of CSC with NaOH and HNO_3 enabled the same column for multiple uses in subsequent cycle with more than 95% regeneration efficiency (Kurniawan, 2002, Shukla *et al.*, 2006), found that metal uptake of H_2O_2 modified coir fibres was 4.33, 7.88 and 7.49mg g^{-1} for Ni (II), Zn (II) and Fe (II), respectively as against 2.51, 1.83 and 2.84mg g^{-1} respectively for unmodified ones due to generation of carboxylic acid groups on fibre. Lowering of pH decreases metal uptake. Unground and unmodified coir (Conrad and Hansen, 2007) in batch sorption removed Zn (91%) and Pb (97%).

2.13.4 Oil Palm Waste

Palm oil industry generates huge amounts of palm shell. Most research on palm shell carbon is focused on carbonization and activation (Hussein *et al*., 1996, Lua and Guo, 1998, Guo and Lua, 2000). Oil palm shell, because of inherent high densities and carbon content (Hussein *et al.*, 1996, Guo and Lua, 2000, Guo and Lua, 2000, Normah *et al.*, 1995), produced high quality AC. Othman *et al.* (1994)

investigated adsorption of Cd (II) and Pb on modified oil palm shell. Chu and Hashin (2002a), Chu and Hashin, (2002b) reported application of palm oil fuel ash for removal of Cr and Zn (II) from aqueous solutions. Biosorbent prepared by coating chitosan onto acid treated oil palm shell charcoal (AOPSC) was studied for Cr removal from industrial wastewater (Nomanbhay and Palanisamy, 2005). AOPSC (particle size 100-150µm) with approx. 21% w/w chitosan loading gave sorption of 154mg Cr g^{-1} of chitosan used at 25°C. Palm shell AC (Issabayera *et al*., 2006) showed high adsorption capacity for Pb ions (95.2 mg g^{-1}) at pH 5.0. Addition of boric acid to the solution improved total metal uptake, while malonic acid decreased uptake due to formation of Pb-malonate complex.

2.13.5 Orange Wastes

Orange peel adsorbed heavy metals from wastewater (Selvakumari *et al.,* (2002), Azab and Perkeson (1989). Ajmal *et al*. (2000), employed orange peel for Ni (II) removal from simulated wastewater. Maximum metal removal (158 mg g^{-1}) occurred at pH 6.0 and 50°C. This result was significantly higher than a similar study by Annadurai *et al.* (2003), suggesting that adsorption capacity of an adsorbent depends on initial concentration of adsorbate. Pavan *et al.* (2006), using Ponkan mandarin (*Citrus reticulata Blanco*) peel as biosorbent got maximum adsorption at pH 4.8 from aqueous solutions as follows: Ni (II), 1.92; Co (II), 1.37; and Cu (II) 1.31mmol g^{-1}.

2.13.6 Rice Husk

Rice husk has good metal affinity and has potential for use as a low cost sorbent Kumar and Baudyopadhyay (2006)., Roy *et al*. (1993), demonstrated applicability

of ground rice hulls for adsorption of heavy metals [As, Cd, Cr, Pb (>99%) and Sr (94%)]. Maximum Cr (VI) removal (23.4 mg g^{-1}) by rice husk AC from aqueous solution is reported (Bishnoi *et al*., 2004) at pH 2.0. Chemical pretreatment of rice husk showed varied degree of effects in adsorbing heavy metal from solution (Bishnoi *et al*., 2004, Ajumal *et al*., 2003). Daifullah *et al.* (2003), used rice husk in removal of metals from a complex matrix containing six heavy metals (Fe, Mn, Zn, Cu, Cd and Pb) and metal removal efficiency of sorbent was approximately 100%.

2.13.7 Sawdust

Several reseachers Shukla *et al.* (2003), Vaish *et al.* (1991), Shukla *et al.* (1991), reviewed sawdust as adsorbent for metals and other pollutants from water. Ajmal *et al*. (1996), observed that phosphate treatment of sawdust from mango tree, used for Cr (VI) removal from electroplating wastewater, improved adsorption capacity (100% adsorption at pH<2 and initial concentration of 8-50 mg l^{-1}). Almost 87% of sorbed chromium was recovered by treating with 0.01M NaOH. Adsorption-desorption cycles (Mavin and Ayele, 2003) showed that Cu (II) binding capacity of sawdust stabilized at $3.1x10^{-2}$ $meqg^{-1}$. Competitive ion exchange exhibited in adsorption from mixture of ions showed order of affinity for sawdust as Ni (II) < Zn (II) < Cd (II) <Cu (II) < Pb (II).

2.13.8 Wastes from Tree Nuts

Hasar *et al*., (2002), found maximum Ni(II) adsorption from simulated solution using almond husk AC at pH 5.0. Ni(II) adsorption capacity of almond husk (37.17mg g^{-1}) was almost four times than that of Cr(VI) adsorption by almond shell (10.67mg g^{-1}) (Dakiky *et al.*, 2002), because cell walls of almond husk contain a

higher concentration of cellulose, silica and lignin than those of almond shell. Almond husk has more hydroxyl and carboxylic groups than almond shell for metal adsorption, resulting in higher metal removal by almond husk (Hasar *et al.,* 2002). AC from almond husks (Hasar *et al.,* (2003), at optimum conditions (initial metal concentration 20mgl^{-1}, pH 5.5, temp. 700°C, contact time 60 min and adsorbent conc. 4g l^{-1}) removed 92% of Zn(II) ions. Demirbas *et al.* (2002), observed that hazelnut shell AC removed from simulated solution maximum Ni (II) (initial metal concentration 15mg l^{-1}) at pH 3.0 with metal adsorption capacity of 10.11mg g^{-1}.

Oil Bean

The African oil bean popular in Nigeria (its local name Ugba) is a tropical tree in the family of leguminose. It is native to tropical Africa, although it exists in south and Central America. It is found in southern rain forest zone of West Africa. The tree produces flowers between March and April and also between June and November. The fruit is a long green pod which slowly darkens with maturity 36 – 46cm long and 5 – 10cm broad. Each pod contain up to 10seeds and at maturity, the pod splits open explosively scattering its seeds up to a distance of 20m from the tree. The seeds are flat in shape, hard but smooth in texture, brown in colour and about 6cm long (Achinewhu, 1982).

Peanut Seed Shell (African elemi)

African elemi (*Canarium schweinfurthii*) is one of the tropical trees whose fruits contain oils in its pulp and seed kernel. The tree is grown widely in the tropics and is abundantly available in Sub-Sahara Africa, including Nigeria (Burkill, 1994; Keay, 1989; Orwa *et al.*, 2009., Hafchinson and Dalziel, 1954). The pulp is

commonly eaten raw or cooked; it is also usually processed for the constituent oil which is popularly referred to as atile oil in some parts of northern Nigeria. The seed (stone) which contains the kernel oil is either thrown away or used as local beads for feet (Burkill, 1994). Also called Mbele, Nde and white mahagony is a wild growing tree which produces fruit similar to Olive. The trees grow wild in forests and common lands. Local people gather the fruits which have a ready market. An enormous deciduous tree up to 50m high, branching beginning at 7m or more, giving the tree the appearance of a flagpole. The Fruit is about the size of a Olive and resembles one when eaten; a thin dark-bluish skin surrounds a 3mm layer of flesh that is the edible portion. The seed is hard, five-sided 2cm long and 1cm wide, kernel edible and often eaten. It is propagated by seed which has a very had coat (Eromosele, 1994).

Snail Shell

It is part of the body of snail/gastropod, a kind of mollusk. The shell is an external skeleton (exoskeleton) which may serve for protection from predators, mechanical damage and dehydration, but also for muscle attachment and calcium storage. Snail shell is made up of 3 layers: the calcareous central layer, the ostracum which is made of calcium carbonate precipitated into organic matrix Conchiolin. The outermost layer is the periostracum which is resistant to abrasion and provides most shell coloration, the body of snail contacts the innermost smooth layer that may be composed of mother-of-pearl shell Nacre, a dense horizontally packed form of Conchiolin, which is layered upon the periostracum as the snail grows (Goodfriend, 1986).

Palm Kernel Shell

Palm kernel shells are the shell fractions left after the nut has been removed after crushing in the palm oil mill. Kernel shells are fibrous material and can be easily handled in bulk directly from the product line to the end use. Large and small shell fractions are mixed with dust-like fractions and fibres. Moisture content in palm kernel shell is low compared to other biomass residues with different sources suggesting values between 11% to 13%. The demand for palm kernel shells has increased considerably in Malaysia, Indonasia, Nigeria and Thailand resulting in price close to that of coal. Nowadays, cement industries are using palm kernel shells to replace coal mainly because of clean development mechanism (CDM) benefits (Salman Zafar, 2015).

CHAPTER THREE
MATERIALS AND METHODS

3.0 List of Apparatus

The following apparatus were used in the course of the research: Digital pH meter (Labtech 4620), Weighing balance (Metler MP301), Digital Muffle furnace (Labtech 201), platinium crucible, Seive (ASTM-E11 No. 80 Mesh, 180microns), Desiccator, thermometer, whatmann filter paper no 1, fume cupboard, funnels, FTIR (Buck 530 FTIR), SEM (Aspex 3020 PSEM2), and Atomic Absorption Spectrophotometry (AAS varian AA240). Magnetic stirrer, BOD incubator, BOD Hanna instrument, Hot Plate, conductivity meter, TDS meter (Dist 1),

3.1 List of Reagents

The reagents used were analar and laboratory grade reagents made by Sigma-Aldrich Germany and Titan Biotech Ltd, India. They include: Hydrochloric acid (HCl), phosphoric acid (H_3P0_4), sulphuric acid (H_2SO_4), sodium hydroxide (NaOH), deionized water, barium chloride ($BaCl_2$), cadmium chloride monohydrate ($CdCl_2.H_2O$), manganese sulphate monohydrate ($MnSO_4.H_2O$), nickel chloride hexahydrate ($NiCl_2.6H_2O$), lead Nitrate ($Pb(NO_3)_2$), selenium powder and perchloric acid $HClO_4$, bromocresol blue, BOD nutrient buffer, boric acid, HNO_3, petroleum ether (60 – 80^oC), Standard Potassium Dichromate, Sulphuric Acid, Standard Ferrous, Ammonium Sulphate, Ferroin Indicator, Phenolphthalein indicator, Methyl orange indicator, Silver nitrate solution, Sodium chloride standard solution, Potassium Chromate indicator, 0.01M EDTA, NaOH, Erichrome black T, NH_4Cl-NH_4OH

3.2 Sampling

The four types of agricultural wastes chosen as precursor were: (i) Pear nut shell (African elemi or Canarium seed, Ube Mgba in Imo state, Ube Okpoko in Enugu State), (ii) Palm Kernel shell, (iii) Oil bean shell (*Pentaclethra Macrophylla*, Ugba or Ukpaka in Igbo land) and (iv) snail shell. The oil bean shell (Plate 2.1, 2.2), Palm Kernel shell (plate 2.9) and African Canarium seed (plate 2.3, 2.4) were collected from Obollo Afor in Enugu State while the Snail Shell (plate 2.7) was collected from Marina road, Eket, Akwa Ibom State. Dirt was removed from the samples after which they were washed and sun dried.

In this study, four Agro-wastes were selected and they include: Snail shell, Pearnut seed, Palm kernel shell and Oil bean shell (Plates 2.1 to 2.9).

Plate 3.1: Oil bean shell

Plate 3.2: Smashed Oil Bean Fruit

Plate 3.3: African Canarium

Plate 3.4: African Canarium seed

Plate 3.5: Smashed African Canarium seed

Plate 3.6: Carbonized African Canarium Seed

Plate 3.7: Snail Shells

Plate 3.8: Smashed Snail Shells

Plate 3.9: Palm Kernel shell

3.2.1 Wastewater Sampling

Wastewater sample was collected from the effluent channel of Ibeto Battery Factory Nnewi, on May 8 using plastic cup into a six liters plastic rubber. The factory is

situated at No. 60/61 Igwe Orizu Road, Nnewi, Anambra State. The pH and temperature of the sample were determined immediately as well as the TDS using hand-held Hanna instrument. The colour was brownish and it had an unpleasant odour.

3.3 Carbonization and activation

The procedure by Grigis *et al.* (1999), with slight modifications was used. The Shell was removed and washed with deionized water. It was dreid under the sun for about three weeks and crushed using locally made grinder. The crushed precursors were divided into two portions and one portion was carbonized at 800^0C and the other portion at 600^0C for 30mins respectively. The carbonized precursors were further divided into three portions and each portion was mixed with 20% of three different activating agents (H_2S0_4, HCl and H_3P0_4) at a ratio of 1:1 (Acid: char). This impregnation at 80^0C was done simultaneously with continuous stirring for 2hours. After that, the sample was then washed with deionized water and dried overnight at 120^0C in oven. This was sieved to about 180microns (ASTM E11 mesh Number). The Activated carbon was gradually cooled to room temperature and washed severally using deionized water until the washing deionized water had a pH of about 7.0. Each prepared activated carbon was dried at 120^0C overnight, cooled and stored for further studies.

3.4 Determination of the Carbonization Yield

The carbonization yield was determined as follows:

$$\text{Yield (\%)} = \frac{\text{weight of carbon produced}}{\text{weight of raw sample used}} \times 100$$

3.5 Analysis of Activated Carbon

3.5.1 Carbon Content Determination

Carbon content determination was performed according to AOAC, (1984). Platinum Crucible was washed, dried and the weight was noted. 2g of wet sample was weighed into the Platinum Crucible and placed in a Muffle furnace at 850^0C for 3hours. The sample was cooled in a desiccator after burning and was weighed.

Calculations: % Ash content = $\frac{W_3 - W_1}{W_2 - W_1} \times \frac{100}{1}$ (3.1a)

Where W_1 = weight of empty Platinum Crucible, W_2 = weight of Platinum Crucible and sample before burning, W_3 = weight of Platinum and carbon.

3.5.2 Nitrogen Content Determination

The method by AOAC, (1984) was used for nitrogen determination. The principle of the method involves the digestion of sample with hot concentrated sulphuric acid in the presence of a metallic catalyst (Selenium powder), and then the Organic nitrogen in the sample is reduced to ammonia which is retained in the solution as ammonium sulphate. When the solution is made alkaline, and then distilled the ammonia is then trapped in dilute sulphuric acid and then titrated.

About 1g of each sample was weighed into a kjehdal flask containing 30ml of conecentrated H_2SO_4 (this was gently done to prevent the sample from touching the walls of the Flask), and 1g of kjedahl catalyst mixture was added and then the flask was closed (stoppered) and shaken. The mixture was heated in a digestion rack under fire until a clear solution was seen. The clear solution was then allowed to stand for 30minutes in order for it to cool. After cooling about 100ml of deionized water was added to avoid caking and then transferred to the kjedahl digestion apparatus. A 500ml receiver flask containing 5ml of boric acid indicator was placed

under a condenser of the distillation apparatus so that the tap was about 20cm inside the solution. Then 10ml of 40% sodium hydroxide was added to the digested sample in the apparatus and distillation commenced immediately until distillation reached the 35ml mark of the receiver flask, after which it was titrated to pink colour using 0.01N Hydrochloric acid.

% Nitrogen = Titre value x 0.01 x atomic mass of Nitrogen x 4. (3.1b)

Where 0.01 = normality of the acid.

3.5.3 Sulphur Content Determination

The method by Adrian, (1973) was used to determine the sulphur content. 10g of the dried sample was weighed into a digestion flask and 20ml of the acid mixture (650ml of concentrated HNO_3; 80ml Perchloric acid; 20ml concentrated H_2SO_4) was added. The flask was heated until a clear digest was obtained. The digest was then diluted with distilled water to the 250ml mark. Appropriate dilutions were then made for each element to be determined. Sulphate was analysed according to APHA standard method (APHA; 1998). A 250ml of the sample was evaporated to dryness on a dish. The residue was moistened with a few drops of conc. HCl and 30ml distilled water. The mixture was boiled and then filtered. The dish was rinsed and the filter paper washed with distilled water severally and both filterate and washings added together. This was heated to boiling and then 10ml of 10% $BaCl_2$ solution was added, drop by drop with constant stirring. The mixture was digested for about 30minutes, filtered and the filter paper washed with warm distilled water. It was then ignited, cooled and weighed in a pre-weighed crucible.

Sulphur = mg of $BaS0_4$ x 411.5ml of water sample (3.1c)

3.5.4 Moisture Content

A petri-dish was washed and dried in the oven and exactly 2g of the sample was weighed into the petri dish. The weight of the petri dish and sample was recorded before drying in the oven. The petridish and sample were put in the oven for 30minutes and the weight was noted. The drying procedure was continued until a constant weight was obtained.

$$\% \text{ moisture content} = \frac{W_1 - W_2}{\text{Weight of sample (2g)}} \times 100 \qquad (3.2)$$

Where w_1 = weight of petri dish and sample before drying and W_2 = weight of petri dish and sample after drying.

3.5.5 Ash Content

Ash content was determined according to AOAC, (1984). A Platinum Crucible was washed, dried and the weight was recorded. About 2g of the sample was weighed into the Platinum Crucible and placed in the muffle furnace at 500^0C for 3hours. The sample was cooled in a Desiccator after burning and it was weighed and weight recorded.

$$\% \text{ Ash content} = \frac{W_3 - W_1}{W_2 - W_1} \times \frac{100}{1} \qquad (3.3)$$

Where: W_1 = weight of empty platinum crucible, W_2 = weight of platinum crucible and sample before burning and W_3 = weight of platinum and ash.

3.5.6 Determination of the Percent fixed carbon

Percentage fixed carbon was calculated as 100 minus the percentage ash content and other components of the sample.

% Fixed carbon =100 – (% ash content + moisture content + volatile matter) (3.4)

3.5.9 Determination of Nitrogen Content

Crude protein content was determined according to AOAC, 1984. About 1g of sample was weighed into a kjehdal flask containing 30ml of concentrated H_2SO_4 (gently to prevent the sample from touching the walls of the flask) and then the

flasks were stoppered and shaken. Then 1g of the kjedahl catalyst mixture was added. The mixture was heated cautiously in a digestion rack under fire until a clear solution was seen. The clear solution was then allowed to stand for 30minutes and allowed to cool. After cooling, about 100ml of deionized water was added to avoid caking and then 50ml was transferred to the kjedahl dstillation apparatus. A 100ml receiver flask containing 5ml of 2% boric acid and indicator mixture containing 5 drops of Bromocresol blue and 1 drop of methlene blue was placed under a condenser of the distillation apparatus so that the tap was about 20cm inside the solution. 5ml of 40% sodium hydroxide was added to the digested sample in the apparatus and distillation commenced immediately until 50 drops gets into the receiver flask, after which it was titrated to pink colour using 0.01N Hydrochloric acid.

% Nitrogen = Titre value x 0.01 x 14 x 4. (3.5)

3.5.10 Surface Area Measurement

The surface area of each activated carbon was estimated according to the method of Al-Qodah and Shawarbkah (2009). 1.5g of activated carbon was agitated in 100ml of HCl of pH 3. Then 30g of NaCl was added while stirring the suspension. The volume was then made up to 150ml with de-ionized water resulting in the change of the pH to 4.0. NaOH (0.1N) was used to raise the pH from 4 to 9 and the volume of NaOH used, V, recorded. The surface area was then calculated using the following equation:

$$S = 32V - 25 \quad (3.6)$$

where S is the surface area (m^2/g).

3.6 INSTRUMENTAL PHYSICAL ANALYSIS

These assays involve instrumentation such as scanning electron microscope (SEM), Fourier Transform Infra red Spectroscopy (FTIR) and atomic absorption spectrophotometer (AAS).

3.6.1 Determination of the Pore Structure by Scanning Electron Microscope

Each sample was ground into fine particles and then sieved using mechanical mesh (300micrometer pore sizes). The SEM machine was powered on and allowed to warm up for about 10minutes. The resolution required was selected and about 1g of the sample was taken and transferred onto the SEM machine sample plate chamber for SEM analysis. Then, the run command was selected and the computer system gave out the morphology of the sample.

3.6.2 Determination of the Surface Functional Group by FTIR

The samples were first ground into fine particles. About 1g of the sample was mixed with 0.1g of KBr and few drops of Nujol. The mixture was then put on the KBr bolt (sample cell) and the KBr bolt was then placed on the sample cell compartment and the FTIR was ran at 600 – 4000cm^{-1}. Finally, the read out (computer system) gave the spectrum and it was then printed.

3.6.3 Determination of Pore Volume

Pore volume was determined according to Veria, (2012). 1g of each activated carbon was immersed in water and boiled for 15minutes in order to displace air from the pores of the activated carbon. The samples were superficially dried and reweighed. The pore volume was calculated from the difference in weight (dw) divided by the density of water (e) at room temperature.

$$\text{Pore Volume} = dw/e_{t25} \qquad (3.7)$$

3.7 Experimental Determination

3.7.1 Isotherm Studies

The batch technique was selected to obtain equilibrium data because of its simplicity. Batch adsorption was performed at the room temperature and different initial metal concentrations to obtain equilibrium isotherms. For isotherm studies, 1g of the activated carbon sample was measured into a 50ml flask and 10ml of 35mg/l of metal ion stock solution prepared from $CdCl_2.H_2O$, $MnSO_4.H_2O$, $NiCl_2.6H_2O$, $Pb(NO_3)_2$ by dividing the molecular mass of the compound by the molar mass of the metal and and then dissolving it in 1L of distilled water to give 1000mg/l, from which difference concentration of the metals (35mg/l to 150mg/l) was prepared by serial dilution. The mixture was placed in a mechanical shaker and then shook for about 1hour. Thereafter, the flask was removed and the content filtered through a whatmann no.1 filter paper into a 20ml sample bottle. AAS (Varian AA240) was used to determine the concentration of the metal in the filtrate using 228.8nm, 232.0nm, 283.3nm and 279.5nm wavelenghts for Cd, Ni, Pb and Mn respectively. This procedure was repeated for other initial metal concentrations prepared which ranged from 35mg/l to 150mg/l. In order to obtain the adsorption capacity, the amount of metal ions adsorbed per mass unit of activated carbon sample (mg/g) was evaluated using the following expression:

$$q_e = (C_0 - C_e)V/m \qquad (3.8)$$

where q_e is the amount adsorbed at equilibrium (mg/g), C_0 is the initial metal ions concentration (mg/l), C_e is the equilibrium metal ions concentration (mg/l), V is the

volume of the aqueous phase (L), and m is the amount of the activated carbon used in gram.

The data obtained was then subjected to Freundlich, Langmuir, Temkin and Dubinin Radushkovich isotherm models to determine sorption parameters and identify the model which best fit or describes the adsorption by these prepared activated carbons.

The Freundlich model is a case for heterogeneous surface energies and it gives an exponential distribution of active sites present in the activated carbon (Hutson & Yang, 2000). This form of the equation was used to relate the amount of heavy metal ions sorbed from the metal solutions and the linear form of the model is

$$\log q_e = \log K_f + 1/n \log C_e \qquad (3.9)$$

where q_e is the amount of sorbed metal ions in mg/g, C_e is the equilibrium concentration of the metal ions. n and K_f are the Freundlich constants which respectively indicates the adsorption intensity and the adsorption capacity of the AC (Uddin *et al*., 2007; Khan, *et al*., 2005). They are calculated from the slope and intercept of the plot of $\log q_e$ versus $\log C_e$.

The Langmuir Adsorption Isotherm model describes quantitatively the formation of monolayer adsorbate on the outer surface of the adsorbent. It is represented as

$$1/qe = 1/Q^o + 1/Q^o b C_e \qquad (3.10)$$

Where C_e is the equilibrium concentration of adsorbate (mg/L), q_e is the amount of metal adsorbed per gram of the adsorbent at equilibrium (mg/g), Q^o is the maximum monolayer coverage capacity (mg/g) and b is the Langmuir isotherm constant (L/mg). Q^o and b were calculated from the slope and intercept of the Langmuir plot

of 1/qe versus $1/C_e$. The separation constant (R_L) was also determined using $R_L = 1/1+(1+bC_e)$, where C_e is the highest initial metal concentration (Langmuir, 1918).

Temkin isotherm model is a case that contains a factor that explicitly taking into account of adsorbent-adsorbate interactions by ignoring the extremely low and large value of concentrations. The model assumes that heat of adsorption of all molecules in the layer would decrease linearly rather than logarithmic with coverage (Temkin & Pyzhev, 1940, Aharoni and Ungarish, 1977).

It is represented as $qe = (RT/b_T)\ln A_T + (RT/b_T)\ln C_e$ (3.11)

Where R is universal gas constant (8.314J/mol/K), b_T is Temkin isotherm constant related to heat of sorption (J/mol), T is temperature (298K), A_T is Temkin isotherm equilibrium binding constant (L/mg). The constants were calculated from the slope and intercept of the plot of q_e against $\ln C_e$.

Dubinin Radushkevich isotherm model is generally applied to express the adsorption mechanism with Gaussian energy distribution onto a heterogeneous surface (Gunay *et al*., 2007, Dabrowski, 2001). The model is expressed as

$Lnq_e = \ln(q_s) - (K_{ad}\varepsilon^2)$ (3.12)

Where q_e, q_s, K_{ad} and ε are amount of adsorbate in the adsorbent at equilibrium (mg/g), theoretical isotherm saturation capacity (mg/g), Dubini-Radushkevich isotherm constant (mol^2/kJ^2) and Dubinin-Radushkevich isotherm constant which is $RT\ln[1+1/C_e]$ respectively. The constants were calculated from the plot of lnqe against ε^2.

3.7.2 Determination of the Adsorption Efficiency

Stock solution of heavy metals was prepared by dissolving required quantity of the salts in deionized water. The salts used were cadmium chloride monohydrate ($CdCl_2.H_2O$), manganese sulphate monohydrate ($MnSO_4.H_2O$), nickel Chloride

hexahydrate ($NiCl_2.6H_2O$), lead nitrate ($Pb(NO_3)_2$), for Cd(II), Mn(II), Ni(II), and Pb(II) respectively, for the preparation of stock solution. The stock solution was further diluted with deionized water to desired concentration for obtaining the test solutions while using NaOH for pH adjustments.

The method by Grigis *et al*. (1999), with slight modification was used to study the adsorption capacity of each activated carbon prepared at different time from each of the agro-waste. 2g of the activated carbon was mixed with 10ml of the prepared initial metal solution whose concentration ranged from 35mg/l to 150mg/l. the mixeture was shaked for 2h at about 120rpm. After that it was filtered and the metal concentration in the filtrate was determined using AAS and the adsorption efficiency calculated as

Adsorption Efficiency = $C_0 – C/C_0$ x 100. (3.13)

Where C = concentration at equilibrium heavy metal and C_o = initial concentration of the heavy metal.

3.7.3 Kinetic Studies

Kinetic experiment was conducted according to Ho and McKay, (1998), on each type of activated carbon produced. 4g of each of the activated carbon was weighed into 100ml flask and 60ml of different initial metal concentration (ranging from 35mg/l to 150mg/l) was measured into the 100ml flask as well. The mixture was shaken and for every 20minutes intervals, 10ml aliquots of the solution was withdrawn from the mixture and then filtered. The filtrate was analysed with AAS for the metal concentration retained. This was done until about 100minutes to allow

for equilibrium adsorption. It was repeated for the four metals (Mn, Pb, Cd, Ni) that were studied.

Pseudo First-order rate equation and pseudo second-order rate equation were then applied to calculate the rate constants and the empirical adsorption capacity of each of the activated carbons produced.

The Pseudo First-order and pseudo second-order expressions were employed to calculate the first and second order rate constants and the first and second order adsorption capacities. The pseudo first order and pseudo second order equations are expressed as follows:

Pseudo First-order rate equation: $\text{Log}\,(q_e - q_t) = \text{Log}q_e - K_1 t/2.303$ (3.14)

Pseudo Second-order rate equation: $t/q_t = 1/(K_2 q_e^2) + t/q_e$ (3.15)

Where K_1 and K_2 are respectively first-order and second-order rate constants, t is time, q_e is equilibrium concentration (empirical adsorption capacity), q_t is equilibrium concentration at time t. The amount of metal ion sorbed, q_t, was calculated from

$$q_t = \frac{(C_o - C_t)V}{M} \quad (3.16)$$

Where q_t (mg/g) is the equilibrium adsorption capacity at time t, C_o and C_t are the initial and equilibrium concentration of metal ion solution, V (L) is the volume of metal solution and M(g) is the weight of the adsorbent (AC).

From the expressions, $\text{Log}q_e$ is the intercept while $K_1/2.303$ is the slope for the first order rate equation, while the second order rate equation gives $1/(k_2 q_e^2)$ as the intercept and $1/q_e$ as the slope, from which q_{e1}, q_{e2} (empirical adsorption capacity

from the first and second order rate equation respectively) and K_1, K_2 (rate constant for the first and second order rate equations respectively) were calculated.

The Pseudo-first order and second-order model equations were fitted to model the kinetics of metals adsorption onto activated carbons prepared. The linearity of each model when plotted (Log $q_e - q_t$ against time for first-order and t/q_t against time for second order), indicated whether the model suitably described the adsorption process or not (Jain *et al.*, 1979).

Intraparticle diffusion model by Weber and Morris, (1963) was applied to predict the rate –limiting step in the adsorption of these metal under consideration. For a solid-liquid sorption process of this nature, the solute transfer is usually chracterised by externl mass transfer (boundary layer diffusion), intraparticle diffusion or both.

Intraparticle diffusion model is given by

$$q_t = K_{id}t^{0.5} + C \qquad (3.17)$$

Where q_t = adsorption at time t, K_{id} = intraparticle diffusion rate constant (mg/g $min^{1/2}$) and C = constant that gives idea about the thickness of the boundary layer, that is the larger the values of C, the greater the boundary layer effects.

A plot of q_t versus $t^{0.5}$ gives a straight line from the origin for the sorption process to be controlled by intraparticle diffusion.

3.7.4 ERROR ANALYSIS

Two error functions of non-linear regression basis were examined in order to be able to evaluate the fit of the kinetic models to represent the experimental data (Kapoor and Yang, 1989, Marquardt, 1963). They are the Hybrid Fractional Error Function (HYBRID), which is given as

$$HYBRID = [\frac{100}{n-p}\frac{\sum[q_{e.exp} - q_{e.cal}]}{q_{e.exp}}] \quad (3.18)$$

and Marquardt's Percent Standard Deviation (MPSD) Error function which is also given as

$$MPSD = \frac{100\sqrt{\frac{1}{n-p}\sum[q_{e.exp} - q_{e.cal}]^2}}{q_{e.exp}} \quad (3.29)$$

where $q_{e.exp}$ = experimental equilibrium adsorption capacity, $q_{e.cal}$ = theoretical equilibrium adsorption capacity, n = number of experimental data points and p = the number of parameters in each isotherm model.

HYBRID was developed to improve the fit of the square of errors function at low concentration values while the MPSD is similar in some respects to a geometric mean error distribution modified according to the number of degrees of freedom of the system.

3.8 WASTEWATER CHARACTERIZATION

3.8.1 Determination of Dissolved Oxygen (DO)

Disolved oxygen was determined according to Montgomery *et al.,* (1964). Dissolved oxygen is a very important parameter in waste water analysis. It is determined in waste water in other to know the amount of oxygen present so as to determine its availability for organism's uptake. DO was determined according to Alkaline-azide Modification of Winkler's Method**.**

About 300ml of sample was collected using the BOD bottle avoiding air bubbles being trapped. Magnesium sulphate powder and alkaline iodide-azide was added and immediately stoppered so that air is not trapped in the bottle. The bottle was inverted severally for proper mixing. The sample became orange-brown and flocculent precipitate formed. It was kept for the solution to settle and after about

2minutes, sulfanic acid powder pillow was added and stoppered again making sure air is not trapped. It was inverted again to dissolve the precipitate. 100ml was measured out and transferred into 250ml flask. It was titrated with sodium thiosulphate to a pale yellow colour using about 3drops of starch solution as indicator (dark blue colour). It was titrated further to colourless end point. The concentration of the DO in the sample is equivalent to the number of millilitres of titrant used. Each ml of sodium thiosulphate added is equal to 1mg/l of DO.

DO (mg/l) = Titre value x 10 = mg/l O_2 (3.20)

3.8.2 Determination of Biochemical Oxygen Demand (BOD)

BOD was determined according to Kwok *et al.* (2005), using Trek instrument. BOD is the amount of oxygen consumed at 20°C and in darkness during a period of 5days to cause oxidation of the biodegradable organic matter present in waste water. The greater the decomposable matter in the waste water, the greater the oxygen demand and the greater the BOD value. 420ml of the sample was measured into the sample amber bottle and magnetic stirring bar was placed into each bottle. BOD nutrient buffer was added into each and stoppered. 1 lithium hydroxide powder pillow was added to each bottle using funnel. The bottles were placed on the chassis of the machine and appropriate tube was connected to each bottle firmly with a chamber number. The BOD Trek was started.The duration and concentration was selected following the steps below:

i. The left and right arrow keys were simultaneously pressed and held until menu appeared
ii. Channel 6 was pressed to activate the test length parameter

iii. The arrow keys were used to choose a 5 days test

iv. Off button was pressed to save and exit the menu

v. Then test was started by pressing the channel number corresponding to the button

vi. The ON key was pressed and the menu for BOD range was displayed and the range was selected

vii. Then ON key was pressed and test started and a graph was displayed

viii. The BOD result was read directly from the display by pressing the key corresponding to each sample

ix. Hot swampy water was used to clean all sample bottles and other items and then rinsed with distilled water

x. The BOD Trek with the sample was placed inside the incubator set at $20^{o}C$ for 5days. The result was read after 5days.

3.8.3 Chemical Oxygen Demand (COD)

The COD was determined according to Clair (2003). Most of the organic matters are destroyed when boiled with a mixture of potassium dichromate and sulphuric acid producing carbon dioxide and water. A sample is refluxed with a known amount of potassium dichromate in sulphuric acid medium and the excess of dichromate is titrated against ferrous ammonium sulphate. The amount of dichromate consumed is proportional to the oxygen required to oxidize the oxidizable organic matter.

0.4g of $HgSO_4$ was placed in a reflux tube. 20ml or an aliquot of the sample diluted to 20ml with distilled water was added and mixed well, so that chlorides are converted into poorly ionized mercuric chloride, 10ml standard $K_2Cr_2O_7$ solution was added and added slowly was 30ml sulphuric acid containing silver sulphate were added slowly and mixed well. The tubes were connected tothe condensers and then refluxed for 2h at 150°C. It was cooled and washed down the condensers with 60ml of distilled water. It was titrated against standard ferrous ammonium sulphate

using ferroin as indicator. Near the end of the titration, the colour changed sharply from green-blue to wine red. Reagent blank was refluxed simultaneously with the sample under identical conditions.

$$\text{COD, mg/l} = \frac{(V_1 - V_2)\ N \times 8000}{V_o} \quad (3.21)$$

Where

V_1 = volume of Fe $(NH_4)_2$ $(SO_4)_2$ required for titration against the blank, in ml

V_2 = volume of $Fe(NH_4)_2$ $(SO_4)_2$ required for titration against the sample, in ml

N = Normality of $Fe(NH_4)_2$ $(SO_4)_2$, V_0 = volume of sample taken for testing, in ml.

3.8.4 Determination of Alkalinity

The alkalinity was determined according to Snoeyink (1980) as described in UNEP/WHO method. 100ml of the sample was mixed with three drops of phenolphthalein indicator in a conical flask over a white surface. As the colour changed to pink, it was titrated with standard 0.01M HCl acid until the pink colour disappeared. The end point was recorded as phenolphthalein alkalinity. We went further to determine the total alkalinity. A few drops of methyl orange indicator was added to the sample and as the colour turned yellow, it was titrated with 0.01M HCl acid until the first perceptible colour changed towards orange was observed.

$$\text{Total alkalinity in mgl}^{-1}\text{ as } CaCO_3) = \frac{\text{titre value} \times 100{,}000 \times \text{conc. of acid}}{\text{Volume of sample}} \quad (3.22)$$

3.8.5 Determination of Chloride

The chloride content was determined accordeing to APHA (1998). 100ml of the sample was measured into a conical flask and the pH was checked. The pH was brought to 8.0 and a small amount of calcium carbonate was added and stirred.

1ml of potassium chromate indicator solution was added and stirred until the solution turned to a reddish colour. The solution was titrated with silver nitrate

solution with constant stirring until only the slightest perceptible reddish colour persisted. Steps 1 to 3 were repeated on 100ml distilled water blank to allow for the presence of chloride for the solubility of silver chromate.

$$\text{Chloride as } Cl^{-1} = \frac{1000\,(v_1 - v_2)}{100} \qquad (3.23)$$

Where V_1 = Volume of silver nitrate required by the sample (ml)

V_2 = Volume of silver nitrate required by the blank (ml)

3.8.6 Determination of Conductivity

Electrical conductivity of the wastewater was determined conductrimetrically using Hanna conductivity meter. The conductivity meter was first calibrated against a 0.1M KCl solution according to the manufacturer's instruction. The meter was powered on and then the mode was changed to scm^{-1} or μscm^{-1}. The sample was poured into the beaker. The electrode was dipped into the beaker containing the sample. The conductivity value was recorded.

3.8.7 Determination of Total Hardness

The method by Sawyer *et al.* (2000), was used to determine the total hardness. Water hardness is caused by the presence of bicarbonates, sulphates and chlorides of calcium and magnesium. It was determined usin EDTA Titrimetric Method.

50ml of water sample was measured into a clean 250ml conical flask. 1ml of NH_4Cl-NH_4OH buffer solution was added and thoroughly mixed with the sample. 2 drops of erichrome black 'T' indicator was added. It was titrated with standard 0.1M EDTA solution until the colour changed from wine red to pure blue end points

$$\text{Total hardness, mg/l } CaCO_3 = \frac{\text{titre value x 1000}}{\text{Volume of sample}} \qquad (3.24)$$

3.8.8 Determination of Total Solids

The method by Sawyer *et al.* (2000), was used to determine the total solids. Total solids give an empirical estimate of water quality by measuring the amount of foreign materials present. It was determined by gravemetric method. The metal dish was clean dried at 105°C in an oven and then cooled to room temperature in a dessicator. The weight of the metal dish was recorded as (w_1), 100ml of the sample was measured into the beaker, poured into the dish and then placed on water bath. It was evaporated to dryness and the residue was dried in an oven for about an hour. It was then transferred into the dessicator and cooled and weighed. It was dried further, cooled and weighed again. Then the weight was taken (w_2)

$$\text{Total solids (mg/l)} = \frac{w_2 - w_1}{\text{ml of sample}} \times 1000 \qquad (3.25)$$

3.8.9 DETERMINATION OF HEAVY METALS IN WASTE WATER USING ATOMIC ABSORPTION SPECTROPHOTOMETER (AAS)

100ml of sample was measured and 10ml of concentrated HNO_3 was added. It was boiled to about 30ml and then cooled. It was then made up to 100ml with deionised water. The AAS was switched on and gas was turned on as well and left for about 3minutes. Then distilled water was passed through the nebulizer for sometimes to allow the flame to get stabilized. The cathode for the required metal was inserted for calibration and the required parameter was highlighted on the readout (computer). Already prepared standards was used to calibrate the AAS, and after the calibration, the sample was then aspirated and the concentration was obtained.

3.8.10 pH Determintion

The pH was determined using hand held Hanna pH meter. The pH electrode was dipped into 50ml of the wastewater sample in a plastic beaker, and powered on. The reading was allowed to stabilize and then the reading was recorded.

3.8.11 Total Dissolved Solid (TDS)

The TDS was also calculated using hand held Hanna TDS meter and the procedure followed that of pH meter.

3.8.12 DETERMINATION OF SULPHATE IN WASTE WATER BY TITRIMETRIC METHOD

20ml of sample was measured and the pH was adjusted to 5.5. Equal volume of acetone was added and 2 to 3 drops of sulphonazo (iii) indicator solution was also added, It was titrated against barium perchlorate solution. The colour changed to greenish-blue, but after some shaking, the colour returned to red leaving a white precipitate of $BaSO_4$ settling out. It was further titrated with shaking till the colour changed to light blue .

$$\text{Sulphate (as } SO_4^{2-}\text{), percent by mass} = \frac{V \times 0.96 \times 100}{V_1} \qquad (3.26)$$

Where V = Titre Volume
V_1 = Volume of sample used

CHAPTER FOUR
RESULTS AND DISCUSSION

4.1 Proximate and Elemental Results

The result of the proximate analysis of the four agro-wastes studied is presented in Table 4.1.

Table 4.1: The Proximate Analysis of the Samples

Sample Name	Sample code	pH	Sulphur (mg/g)	%Ash	% N_2	% Moisture
Pearnut seed	A	6.31	41.15	5.00	0.616	5.5
Palm kernel shell	B	6.62	382.695	3.5	0.448	13.5
Oil bean shell	C	6.71	37.035	1.50	0.392	56.5
Snail shell	D	6.82	20.575	4.00	0.56	5.5

A = Pear nut seed, B = Palm kernel shell, C = Oil Bean shell and D = Snail shell.

It was observed that the pH values of the samples ranged from 6.31 to 6.82 indicating slightly acidic to neutral samples. According to Okiemmen *et al.* (2007), activated carbons of pH 6 – 8 are useful for most applications. Therefore, all the prepared activated carbons could be acceptable for most applications involving adsorption from aqueous solutions. Also, according to Ahmedna *et al.* (2006), it should be noted that distinctively acidic activated carbons are not desirable. It was also observed that sample B had high sulphur content (382.695mg/g), while the sulphur content of other samples were relatively low. The trend is as follows: B > A > C > D. Activated carbon contains about 95% of carbon and other heteroatoms like S, N_2, H and O_2. These heteroatoms react with activating agents during the activation process and change the functional groups present in the AC which inturn affect the adsorption behaviour of the AC according to Zheng *et al.* (2014). Also, the percentage ash, fat, fibre, nitrogen and protein contents were relatively low for all the samples and they are comparable to literature values found in Daud and Ali, (2004), Ademiluyi *et al*., (2012). Sample C had high moisture content, 56.5% but

recorded low percentage carbohydrate unlike other samples that had their percentage carbohydrate above 50%. High ash content is undesireable for AC since it reduces the mechanical strength of the AC and affects the adsorptive capacity as well. Moisture content according to Aziza *et al.* (2008), has a relationship with porosity of AC. Adsorbents with high moisture content is expected to swell less, and so retard pore size expansion for adsorbate uptake.

The elemental analysis of the samples (Table 4.2 appendix B and Figure 4.1), showed that sample D recorded the highest carbon content (0.453mg/g), indicating that it may be a good adsorbent. Sodium was not detected in sample A, but it had the highest oxygen content (0.029mg/g). These hereatoms affect the functional groups present in the carbons during their activation.

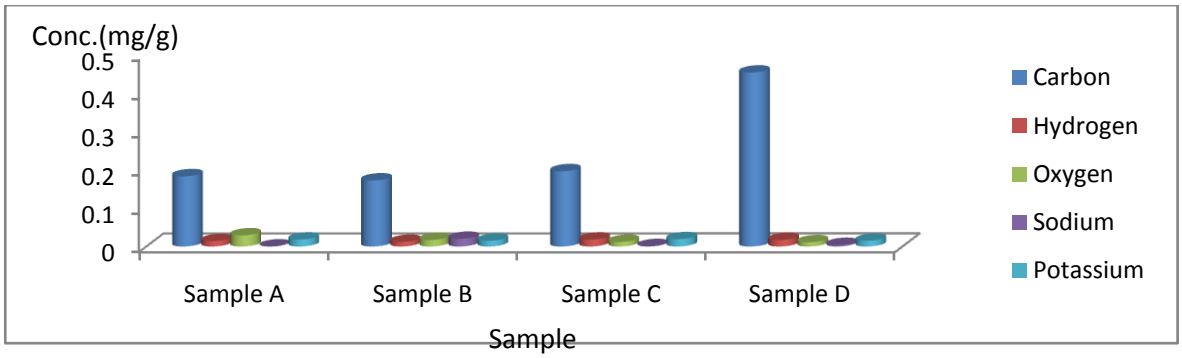

Figure 4.1: The Elemental Content of the Samples

From Figure 4.2 (Table 4.3 appendix B), percentage yield after carbonization, it was observed that all the samples had a low percentage yield below 35% after carbonization except for sample D which had a percentage yield of 61.85% and 86.11% at carbonization temperatures of 800°C and 600°C respectively. This was in line with the results reported by Abechi *et al*., (2013). This is also an evidence of the high carbon content recorded by sample D in the elemental analysis presented in

Table 4.2 (appendix B). It can also be observed that the percentage yield at a higher temperature is lower than that at lower temperature. This is because increase in temperature resulted in more volatile components of the precursor materials being lost, and hence a decreasing percentage carbon yield. This was also advanced by Abechi *et al.* (2013).

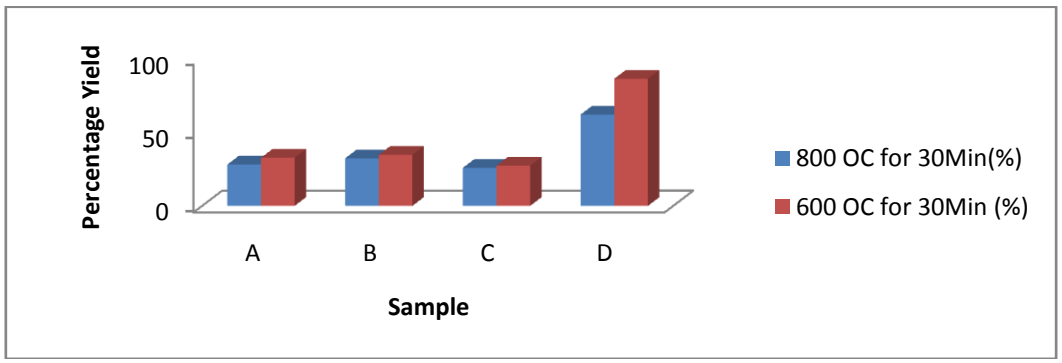

Figure 4.2: Percentage Yield of the Carbonized Sample

Figure 4.3 showed the percentage yield after chemical activation of the produced carbon. After chemical activation, the percentage yield Table 4.4 (appendix B) was very high in all the samples and at the temperatures used, though it was better for H_3PO_4, in both temperatures. This could be attributed to the ionization constant (Ka) of the activating agents (Ka for HCl > H_2SO_4 > H_3PO_4), an indication of their acid strenght. The activation time does not influence the yield remarkably, relative to the activation temperature. This can easily be seen from figure 4.3a and b. The percentage yield of Palm Kernel activated at 800°C with H_3PO_4 and $ZnCl_2$ using activating agent as reported by Abechi *et al*. (2013), was 46.33%. This suggested that activation with H_3PO_4, HCl and H_2SO_4 gave better yield compared to Abechi's method.

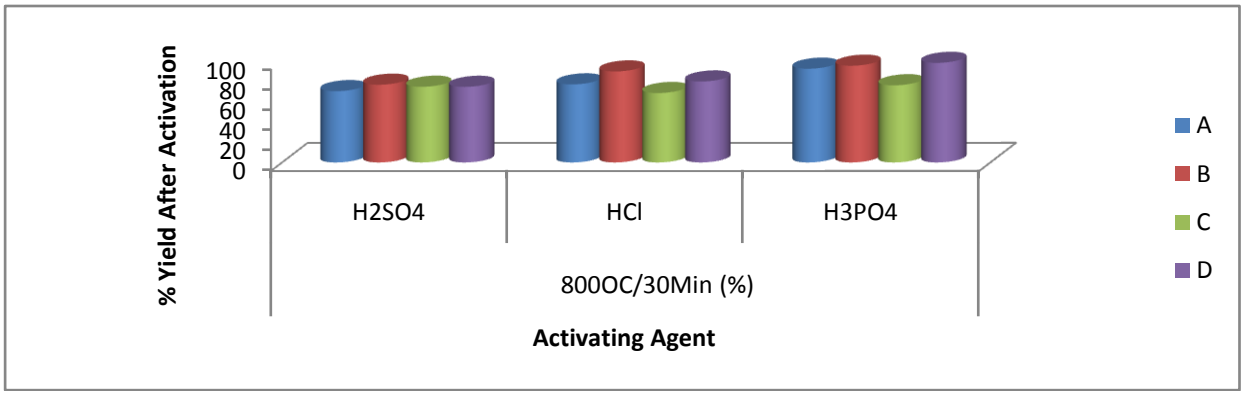

Figure 4.3a: Percentage Yield after Chemical Activation

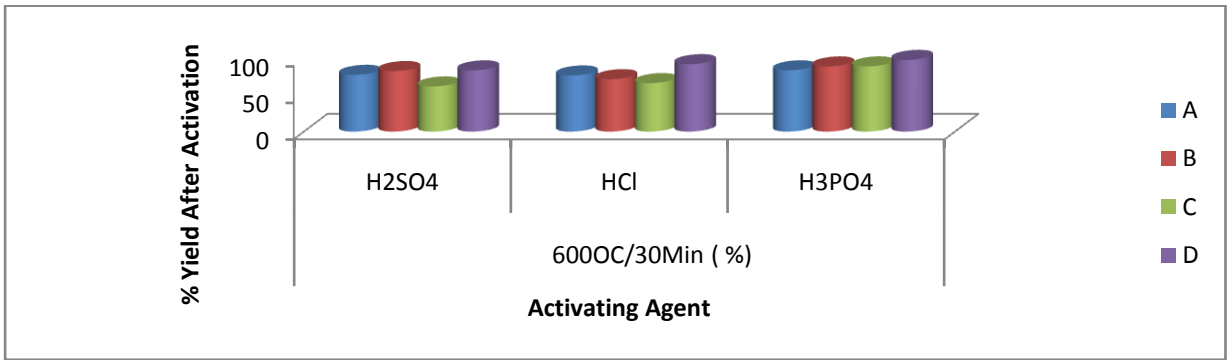

Figure 4.3b: Percentage Yield after Chemical Activation

Table 4.5 outlined the characterization result of wastewater collected from Ibeto Battery company liquid waste channel. The physicochemical properties of the effluent were observed to have met most of the standards but failed others. The pH values and the Pb contents are not within the standards set by federal environmental protection agency (FEPA, 1991). Pb have been observed to affect the development of the brain and nervous system in children and causes high blood pressure and kidney damage in adults even at low concentration (UNEP, 2016).

Table 4.5: Characteristics of effluent sample from Ibeto Battery Company

S/N	PARAMETER	RESULT	FEPA LIMITS
1	Temperature	28^oC	$<4^oC$
2	pH at 28^oC	$4.8\ ^oC$	$6 – 9\ ^oC$
3	Odour	Not offensive	Odourless
4	Colour	Cloudy	Clear
5	Conductivity	1023µs/cm	1000 µs/cm
6	Dissolved oxygen	34.67mg/l	Min 4 mg/l
7	Biochemical oxygen demand (BOD^5_{20})	16.1mg/l	50 mg/l
8	Chemical oxygen demand(COD)	26.7mg/l	150 mg/l
9	Total solid	0.13mg/l	30 mg/l
10	Total Dissolve Solid (TDS)	414mg/l	500 mg/l
11	Total Hardness ($CaCO_3$)	625.3mg/l	-
12	Alkalinity ($CaCO_3$)	248.3mg/l	-
13	Sulphate	4.211mg/l	500 mg/l
14	Manganase (Mn)	0.002±0.50 mg/l	<1 mg/l
15	Cadmium (Cd)	ND	<1 mg/l
16	Nickel (Ni)	0.063±0.70 mg/l	<1 mg/l
17	Zinc (Zn)	0.4565±0.11 mg/l	<1 mg/l
18	Cobalt (Co)	0.005±0.001 mg/l	<1 mg/l
19	Lead (Pb)	17.95±1.20 mg/l	<1 mg/l
20	Cupper (Cu)	0.034±0.01 mg/l	<1 mg/l
21	Arsenic (As)	0.001±0.00 mg/l	<1 mg/l
22	Chromium (Cr)	ND	<1 mg/l
23	Chloride	159.67mg/l	600 mg/l

ND = below detection limit of the AAS.

4.2 Surface Chemistry Study

The type and net charge of functional groups bonded to the carbon surface is important in understanding the mechanism of adsorption of ionic adsorbates on activated carbons (Nale *et al*., 2012). The adsorption capacity of activated carbon is influenced by functional groups on the carbon surface. They do not only affect the adsorption behavior but also dominate the adsorption mechanism. They reduce the binding energy while increasing the uptake kinetics at a lower coverage (monolayer coverage) (Zheng *et al.*, 2014).

TABLE 4.6: FTIR Analysis Result OF Oil Bean (in Nujol and KBr as Solvents)

Activated Oil Bean Shell Carbon		Used Activated Carbon	OBAC/600°C/HCl	OBAC/600°C/ H_3PO_4	OBAC/600°C/H_2SO_4	OBAC/800°C/HCl	OBAC/800°C/ H_3PO_4	OBAC/800°C/ H_2SO_4
Wave number	**Possible Assignments**	**Wave number**	**Possible Assignments**	**Possible Assignments**	**Possible Assignments**	**Possible Assignments**	**Possible Assignments**	**Possible Assignments**
822.92	Aromatic C – H stretching	860 – 680				Aromatic C – H Bending	Aromatic C – H Bending	Aromatic C – H Bending
958.1954		1780 – 1710	C = O Str. of COOH, Ketones, Esters	C = O Str. of COOH, Ketones, Esters	C = O Str. of COOH, Ketones, Esters.			
1177.18	Carboxylic acid C=0 stretch	1700 – 1500	Aromatic C = C Bending	Aromatic C = C Bending	Aromatic C = C Bending	Aromatic C = C Bending	Aromatic C = C Bending	Aromatic C = C Bending
1265.15		1680 – 1620	C = C Str. of Alkenes		C = C Str. of Alkenes	C = C Str. of Alkenes.		C = C Str. of Alkenes
1423.69		1690 – 1630	Amide, C = O Str.		Amide, C = O Str.	Amide, C = O Str.		Amide, C = O Str.
1574.504	Aromatic C=C bending	1750 – 1735	Aromatic C = H Bending	Aromatic C = H Bending	Aromatic C = H Bending	Aromatic C = H Bending	Aromatic C = H Bending	Aromatic C = H Bending
1806.151		1740 – 1690		Aldehyde C,= O Str.			Aldehyde C,= O Str.	
1882.47		1750 – 1680		Ketone C = O Str			Ketone C = O Str.	
2158.96	Alkyl C = C Stretch	2950 – 2850	C – H Str. of Alkanes	C – H Str. of Alkanes	C – H Str. of Alkanes	C – H Str. of Alkanes	C – H Str. of Alkanes	C – H Str. of Alkanes
2237.413	Nitrile C=N Strech	2260 – 2100	C = C Str. of Nitriles	C = C Str. of Nitriles	C = C Str. of Nitriles	C = C Str. of Nitriles	C = C Str. of Nitriles	C = C Str. of Nitriles
2905.61	Alkyl C-H Stretch							
3170.13	Alkyl C-H Stretch	3100 – 3010	C – H Str. of Aromatic ring				C – H Str. of Aromatic ring	C – H Str. of Aromatic ring
3223.80	Alcohol, phenol O - H stretch	3000 – 2500	O – H Str. of COOH, phenols, OH	O – H Str. of COOH, phenols, OH	O – H Str. of COOH, phenols, OH	O – H Str. of COOH, phenols, OH	O – H Str. of COOH, phenols, OH	O – H Str. of COOH, phenols, OH.
3351.445	Alcohol/phenol O-H stretch	3500 – 3300	N – H Str. of Amines			N – H Str. of Amines	N – H Str. of Amines	N – H Str. of Amines
3550.973	Amide N –H Stretch	3550 – 3200	O – H, Str. Of Phenol			O – H, Str. Of Phenol	O – H, Str. Of Phenol	O – H, Str. Of Phenol
3714.78	Amide N-H Stretch	3700 – 3500	Amide, N – H Str.			Amide, N – H Str.	Amide, N – H Str.	Amide, N – H Str.

The functional groups on the surface of activated carbon analysed by the FTIR demonstrated the existence of carboxyl, hydroxyl, amine groups, amide groups, alkyl, aromatic C = C, nitrile, phenol and carboxylic groups (Tables 4.6 to 4.9). The FTIR spectra of the activated carbon of both used and unused carbons showed some differences from each other. This demonstrates that after the adsorption, shifting occurred both to higher and lower wave numbers. This shifting indicated that binding processes took place on the surfaces of the activated carbons during adsorption. FTIR spectra were obtained on a JASCO FTIR-3500 spectrometer. The analysis conditions used were 16 scans at a resolution of $4cm^{-1}$ measured between 400 and $4000cm^{-1}$.

The FTIR spectra of both activated and used OBAC revealed complex surfaces as shown by the presence of several peaks (Table 4.6). The activated carbons showed less peaks than the used Oil Bean shell activated carbons. This was an indication that some reorganisation of the surface oxides on subjection to adsorption (Appendix F). The peak observed around $1177cm^{-1}$ for the activated OBAC shifted to around $1780cm^{-1}$ in the used OBAC. Similarly, the C = C aromatic bonding observed around $1574cm^{-1}$ on the activated Oil Bean carbon shifted to $1750cm^{-1}$. The O – H stretch observed around $3223.80cm^{-1}$ in the activated carbon and the C – H observed at $822.92cm^{-1}$ also went through various shifts as well. These results are similar to the ones reported for sawdust (Huang *et al.*, 2005). These functional groups could act as chemical binding agents where carboxyl, hydroxyl and amine groups could dissociate negatively charged active surface. This means that these

functional groups could attract the positively charged objects such as heavy metal ions (Nale *et al*., 2012). Looking at appendix F, the FTIR spectra showed that there was modification of chemical structure of activated carbon which is as a result of adsorption.

Functional groups are formed during activation by interaction of free radicals on the carbon surface with atoms such as oxygen and nitrogen, both from within the precursor and from the atmosphere (Zawadski, 1989). The functional groups render the surface of activated carbon chemically reactive and influence its adsorptive properties (McEnaney and Mays, 1989). Surface oxidation is an inherent feature of activated carbon production. It results in hydroxyl (-OH), carbonyl (=CO), and carboxylic (-COOH) groups imparting an amphoteric character to the activated carbon. So it can be either acidic or basic.

In the FTIR analysis of PKAC (Appendix F), there were peaks observed on the unused activated and used activated carbon as well. As it was for OBAC, the peaks observed on the unused activated carbon was less than that observed on the used activated carbon. This also indicates a reorganisation of the chemical bonds on the surfaces of the activated carbons prepared. There was shifting of peaks on the activated carbon surfaces. It can also be deduced from Table 4.7 that more peaks were observed with the activating agents, H_2SO_4 and H_3PO_4 in all the activated carbon types prepared.

TABLE 4.7: FTIR Analysis of Palm kernel (in Nujol and KBr as Solvents)

Activated Palm Kernel Carbon		Used Activated Carbon	PKAC/600°C/HCl	PKAC/600°C/ H_3PO_4	PKAC/600°C/ H_2SO_4	PKAC/800°C/ HCl	PKAC/800°C/ H_3PO_4	PKAC/800°C/H_2SO_4
Wave number	**Possible Assignments**	**Wave Number**	**Possible Assignments**	**Possible Assignments**	**Possible Assignments**	**Possible Assignments**	**Possible Assignments**	**Possible Assignments**
688.985		860 – 680	Aromatic C – H Bending	Aromatic C – H Bending			Aromatic C – H Bending	
1081.167		1700 – 1500	Aromatic C = C Bending	Aromatic C = C Bending	Aromatic C = C Bending	Aromatic C = C Bending	Aromatic C = C Bending	Aromatic C = C Bending
1242.046		1680 – 1620		C = C Str. of Alkenes			C = C Str. of Alkenes.	C = C Str. of Alkenes
1492.60		1690 – 1630						Amide, C = O Str.
1689.91	Alkenes C – H stretch	1740 – 1690						
1975.51		2260 – 2220	C = C Str. of Nitriles	C = C Str. of Nitriles	C = C Str. of Nitriles	C = C Str. of Nitriles	C = C Str. of Nitriles	C = C Str. of Nitriles
2314.015		2950 – 2850	C – H Str. of Alkanes	C – H Str. of Alkanes	C – H Str. of Alkanes	C – H Str. of Alkanes	C – H Str. of Alkanes	C – H Str. of Alkanes
2544.58	Carboxylic Acid O-H Stretch	2260 – 2100		C = C Str. of Nitriles			C = C Str. of Nitriles.	
2882.934	Alkyl C-H Stretch	3300						
3139.709	Alkyl C-H Stretch	3030						
3234.794	Amine N - H Stretch							
3488.52	Amine N - H Stretch	3100 – 3010				C – H Str. of Aromatic ring	C – H Str. of Aromatic ring	C – H Str. of Aromatic ring.
3591.79		3000 – 2500	O – H Str. of COOH, phenols, OH	O – H Str. of COOH, phenols, OH	O – H Str. of COOH, phenols, OH	O – H Str. of COOH, phenols, OH	O – H Str. of COOH, phenols, OH	O – H Str. of COOH, phenols, OH
3665.27		3500 – 3300		N – H Str. of Amines	N – H Str. of Amines		N – H Str. of Amines	N – H Str. of Amines
3817.802		3550 – 3200	O – H, Str. Of Phenol	O – H, Str. Of Phenol	O – H, Str. Of Phenol	O – H, Str. Of Phenol	O – H, Str. Of Phenol	O – H, Str. Of Phenol
		3700 – 3500	Amide, N – H Str.	Amide, N – H Str.	Amide, N – H Str.	Amide, N – H Str.		Amide, N – H Str.

This might be attributed to the presence of the oxygen atoms as earlier mentioned. The O – H stretch of the carboxylic, phenol and alcohol group shifted from around 2544.58cm^{-1} to around 3000 – 2500cm^{-1} wave number. Such shift was observed for several other functional groups. This was in line with the observation made by Abechi *et al*., (2013). A similar observation was also made for the PNAC prepared (Table 4.8). There was reorganisation of the surface oxides of the activated carbons when subjected to adsorption. There was also shifting of observed peaks as a result of the adsorption. For instance, the O – H stretch of COOH, phenol and alcohol groups observed at 2671.554cm^{-1} in the activated peanut seed carbon shifted to around 3000 – 2500cm^{-1} in the used activated PNAC prepared. Equally, it was observed for amine N – H stretch, but the alkyl C – H stretch disappeared on subjection of the carbon to adsorption processess. *African canarium or African elemi* (Peanut seed) is known to contain phenolic group, carboxylic as well as saponins and terpenes (Mogana and Wiart, 2011).

TABLE 4.8: FTIR Analysis of Pear nut seed (in Nujol and KBr as Solvents)

Activated Peanut Seed Carbon		Used Activated Carbon	PNAC/600°C/HCl	PNAC/600°C/ H_3PO_4	PNAC/600°C/H_2SO_4	PNAC/800°C/HCl	PNAC/800°C/ H_3PO_4	PNAC/800°C/ H_2SO_4
Wave number	**Possible Assignments**	**Wave number**	**Possible Assignments**	**Possible Assignments**	**Possible Assignments**	**Possible Assignments**	**Possible Assignments**	**Possible Assignments**
690.814		860 – 680	Aromatic C – H Bending	Aromatic C – H Bending	Aromatic C – H Bending	Aromatic C – H Bending	Aromatic C – H Bending	Aromatic C – H Bending
871.512		1780 – 1710	C = O Str. of COOH, Ketones, Esters					
991.405		1700 – 1500	Aromatic C = C Bending	Aromatic C = C Bending	Aromatic C = C Bending	Aromatic C = C Bending	Aromatic C = C Bending	Aromatic C = C Bending
1119.63		1680 – 1620		C = C Str. of Alkenes				C = C Str. of Alkenes
1245.066		1690 – 1630			Amide, C = O Str.			Amide, C = O Str.
1591.75		1740 – 1690		Aldehyde C,= O Str.	Aldehyde C,= O Str.			
1814.838		1750 – 1680		Ketone C = O Str.	Ketone C = O Str.			
2066.413		2260 – 2220	C = C Str. of Nitriles	C = C Str. of Nitriles	C = C Str. of Nitriles	C = C Str. of Nitriles	C = C Str. of Nitriles	
2307.56		2950 – 2850			C – H Str. of Alkanes			C – H Str. of Alkanes
2671.554	Carboxylic Acid O-H Stretch							
2764.64	Alkyl C-H Stretch	3300						
2870.199	Alkyl C-H Stretch	3030						
3248.346	Amine N-H Stretch	3100 – 3010	C – H Str. of Aromatic ring		C – H Str. of Aromatic ring			
3498.979	Amine N-H Stretch	3000 – 2500	O – H Str. of COOH, phenols, OH	O – H Str. of COOH, phenols, OH	O – H Str. of COOH, phenols, OH	O – H Str. of COOH, phenols, OH	O – H Str. of COOH, phenols, OH	O – H Str. of COOH, phenols, OH
3694.003		3500 – 3300	N – H Str. of Amines	N – H Str. of Amines	N – H Str. of Amines	N – H Str. of Amines	N – H Str. of Amines	N – H Str. of Amines
3830.064		3550 – 3200	O – H, Str. Of Phenol	O – H, Str. Of Phenol	O – H, Str. Of Phenol	O – H, Str. Of Phenol	O – H, Str. Of Phenol	O – H, Str. Of Phenol
3948.219		3700 – 3500	Amide, N – H	Amide, N – H	Amide, N – H	Amide, N – H	Amide, N – H	Amide, N – H

The FTIR spectra of both activated and the used snail shell carbon also revealed complex surface due to the presence of several peaks (Table 4.9). The activated snail shell carbon showed less peaks than the used snail shell carbon. This was an indication of the strong surface oxide reorganisation resulting from the interactions of the atoms of the activating agents (HCl, H_2SO_4 and H_3PO_4) used. There was shifting of peaks as well as disappearance of some previously observed peaks in the activated snail shell carbon prepared after the adsorption. The C = O of the aldehyde functional group was not observed in the activated carbon but was found in the used SSAC. Similar observation was made for C = C aromatic stretch (Appendix F).

TABLE 4.9: FTIR Analysis of Snail shell (in Nujol and KBr as Solvents)

Activated Snail Shell Carbon		Used Activated Carbon	SSAC/600°C/HCl	SSAC/600°C/ H_3PO_4	SSAC/600°C/ H_2SO_4	SSAC/800°C/HCl	SSAC/800°C/ H_3PO_4	SSAC/800°C/H_2SO_4
Wave number	**Possible Assignments**	**Wave number**	**Possible Assignments**	**Possible Assignments**	**Possible Assignments**	**Possible Assignments**	**Possible Assignments**	**Possible Assignments**
761.209		860 – 680	Aromatic C – H Bending	Aromatic C – H Bending	Aromatic C – H Bending	Aromatic C – H Bending	Aromatic C – H Bending	Aromatic C – H Bending
945.987		1780 – 1710	C = O Str. of COOH, Ketones, Esters					
1127.46		1700 – 1500	Aromatic C = C Bending	Aromatic C = C Bending				Aromatic C = C Bending
1495.913		1690 – 1630		Amide, C = O Str.	Amide, C = O Str.			Amide, C = O Str.
1751.494		1740 – 1690	Aldehyde C,= O Str.					
1987.339		2260 – 2220	C = C Str. of Nitriles	C = C Str. of Nitriles	C = C Str. of Nitriles		C = C Str. of Nitriles	
2544.37	Carboxylic Acid C –H Stretch	3300						
2873.69	Alkyl C –H Stretch							
3207.012	Amine N-H Stretch	3000 – 2500	O – H Str. of COOH, phenols, OH	O – H Str. of COOH, phenols, OH	O – H Str. of COOH, phenols, OH	O – H Str. of COOH, phenols, OH	O – H Str. of COOH, phenols, OH	O – H Str. of COOH, phenols, OH
3332.85	Amine N-H Stretch	3500 – 3300	N – H Str. of Amines	N – H Str. of Amines		N – H Str. of Amines	N – H Str. of Amines	N – H Str. of Amines
3474.62	Amine N-H Stretch	3550 – 3200	O – H, Str. Of Phenol	O – H, Str. Of Phenol	O – H, Str. Of Phenol	O – H, Str. Of Phenol	O – H, Str. Of Phenol	O – H, Str. Of Phenol
3614.68		3700 – 3500	Amide, N – H	Amide, N – H		Amide, N – H	Amide, N – H	

4.3 Deductions from SEM Images of the Activated Carbons

The scanning electron microscope results of the carbonized oil Bean are presented in plate 4.1 and 4.2.

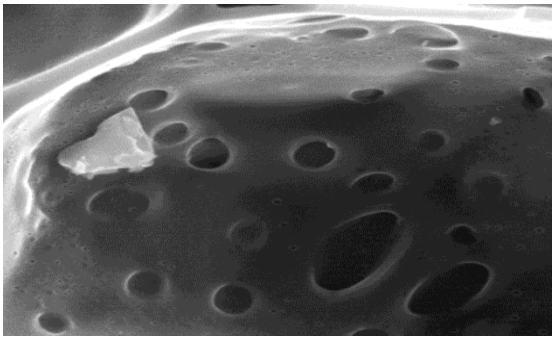

15.0kv. mag =5000x. 20µm. wd = 16.0mm at 600°C

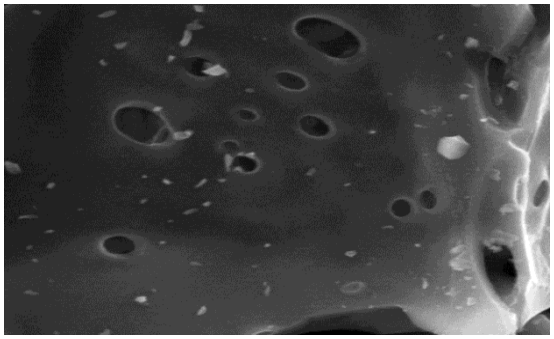

15.0kv. mag =5000x. 20µm. wd = 16.0mm at 800°C

Plate 4.1: SEM image of Oil Bean Carbonised at 600°C and 800°C

Plate 4.1 showed the SEM images of char samples produced by pyrolysis of Oil Bean as activated carbon precursor at different temperatures. Comparing SEM images of the char samples produced under the two temperatures (600°C & 800°C), it can be seen that the pore development on the surfaces of the carbon were similar in their pores and the pores were not evenly distributed as well. That carbonized at 600°C developed more pores than its counterpart but that at 800°C had larger pore size than the 600°C carbon.

Plate 4.2 presents the SEM results of the activated Oil Bean carbons.

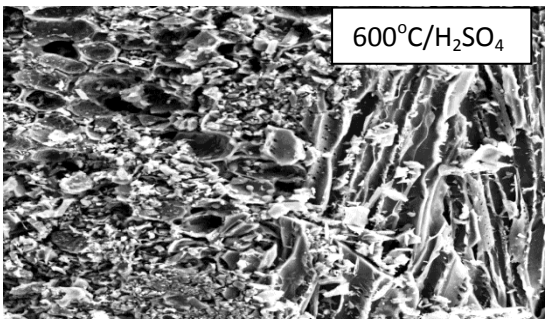

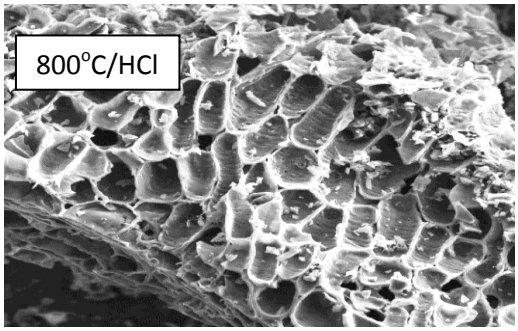

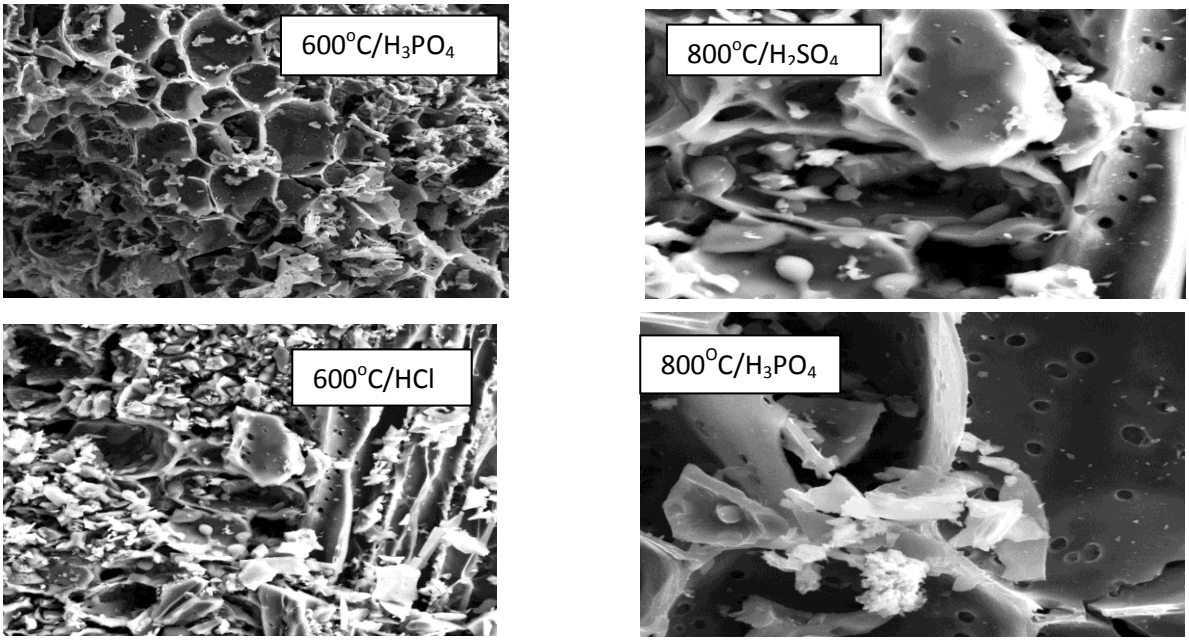

15.0kv. mag =5000x. 20µm. wd = 16.0mm

Plate 4.2: SEM image of Oil Bean Carbonised at 600°C & 800°C and Activated with acids.

Looking at the Plate 4.2, it could be seen that activation of the carbons produced with acid developed more micropores pores as well expanded the initial pores created during carbonization. After the activation the pores were eveningly distributed especially for those carbonized at 600°C but with a rough surface.

Plate 4.3 presents the SEM results of the carbonized Palm Kernel at 600°C and 800°C.

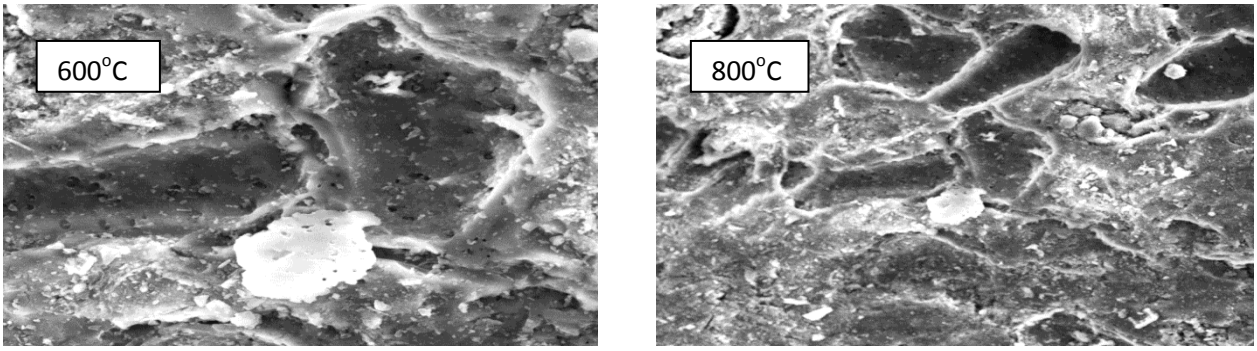

15.0kv. mag =5000x. 20µm. wd = 16.0mm

Plate 4.3: SEM image of Palm Kernel Carbonised at 600°C and 800°C

For Palm Kernel carbons produced, there was a poor pore development before activation but after activation, several pores were developed (Plate 4.4). This may be due to removal of impurities like tars that could have clogged the pores before the activation. The pores developed were not evenly distributed and was of macro and micro sizes. From Plate 4.3, it can be deduced that carbonized at 800°C had better pores than its counterpart at 600°C.

Presented in Plate 4.4 is the SEM results of the activated Pear nut seed carbons.

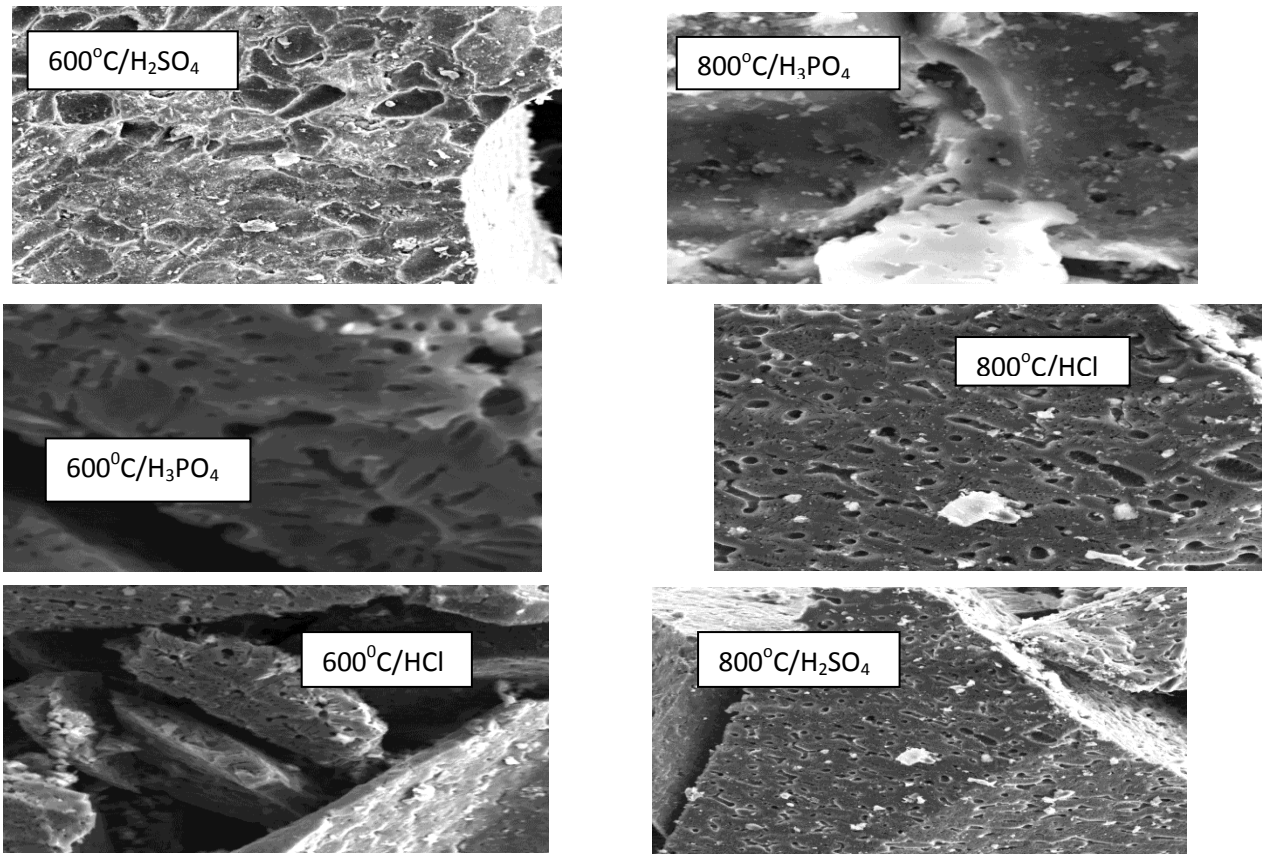

15.0kv. mag =5000x. 20µm. wd = 16.0mm

Plate 4.4: SEM image of Paim Kernel Carbonised at 600°C & 800°C and Activated with acids.

Plate 4.5 presents the SEM results of the carbonized Pear nut Seed at 600°C and 800°C.

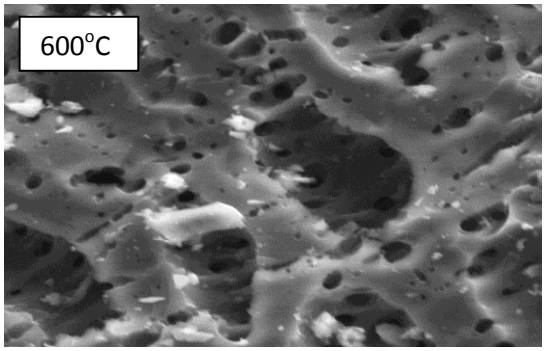

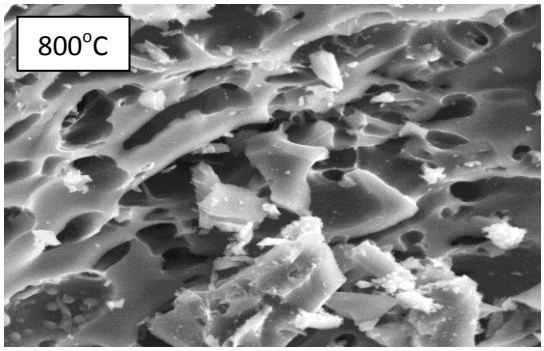

15.0kv. mag =5000x. 20µm. wd = 16.0mm

Plate 4.5: SEM image of Peanut Seed Carbonised at 600°C and 800°C

The morphological structure of the pear nut seed activated carbon has honeycomb-like structures as shown in plate 4.5, 4.6. The SEM photograph is characterised by a rough surface with many non orderly pores developed. The pores on the activated carbon were finely structured unlike that unactivated carbon produced from Pear nut seed. There was not much physical difference between the different types of activated carbons produced. This indicates that there adsorption capacity will be somewhat close to each other. Those activated with H_2SO_4 irrespective of the carbonization temperatures showed better and larger pores than others.

Plate 4.6 presents the SEM results of the activated Pear nut seed carbons.

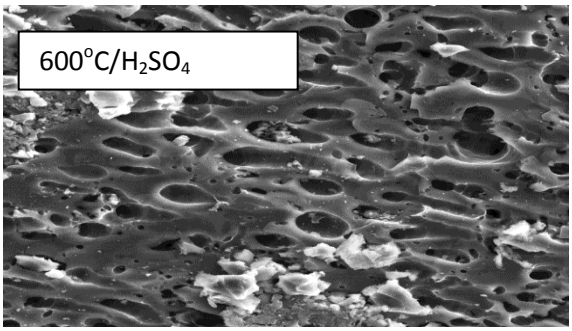

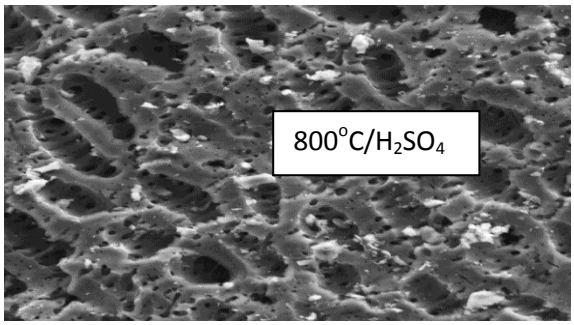

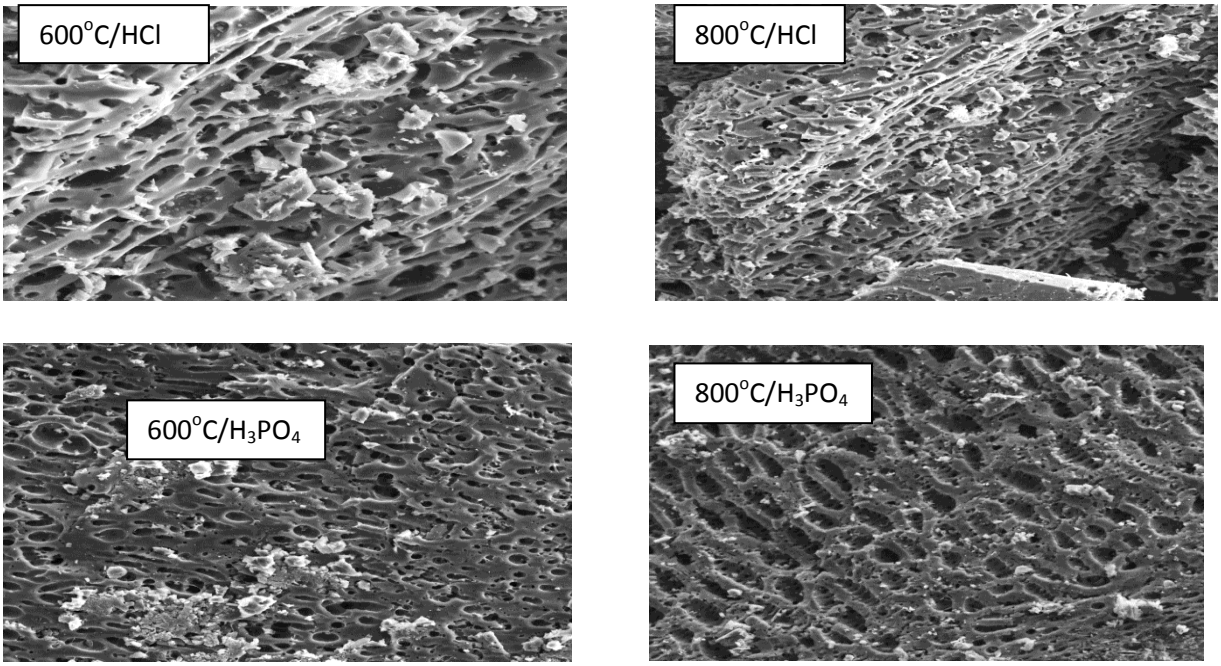

15.0kv. mag =5000x. 20µm. wd = 16.0mm

Plate 4.6: SEM image of Peanut Seed Carbonised at 600°C & 800°C and Activated with acids.

Plate 4.7 presents the SEM results of the carbonized Snail shell at 600°C and 800°C

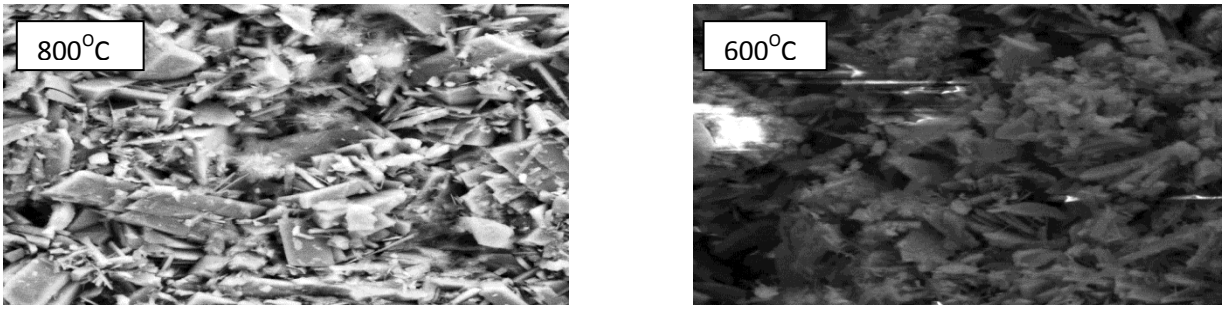

15.0kv. mag =5000x. 20µm. wd = 16.0mm

Plate 4.7: SEM image of Snail Shell Carbonised at 600°C and 800°C

The SEM photograph of the snail shell activated carbon showed no visible pores.

This might be as a result of presence of impurities such as tar which may have clogged the pores developed by the shell which inhibited the pores structure development (plate 4.7, 4.8).

Plate 4.8 presents the SEM results of the activated Snail shell carbons.

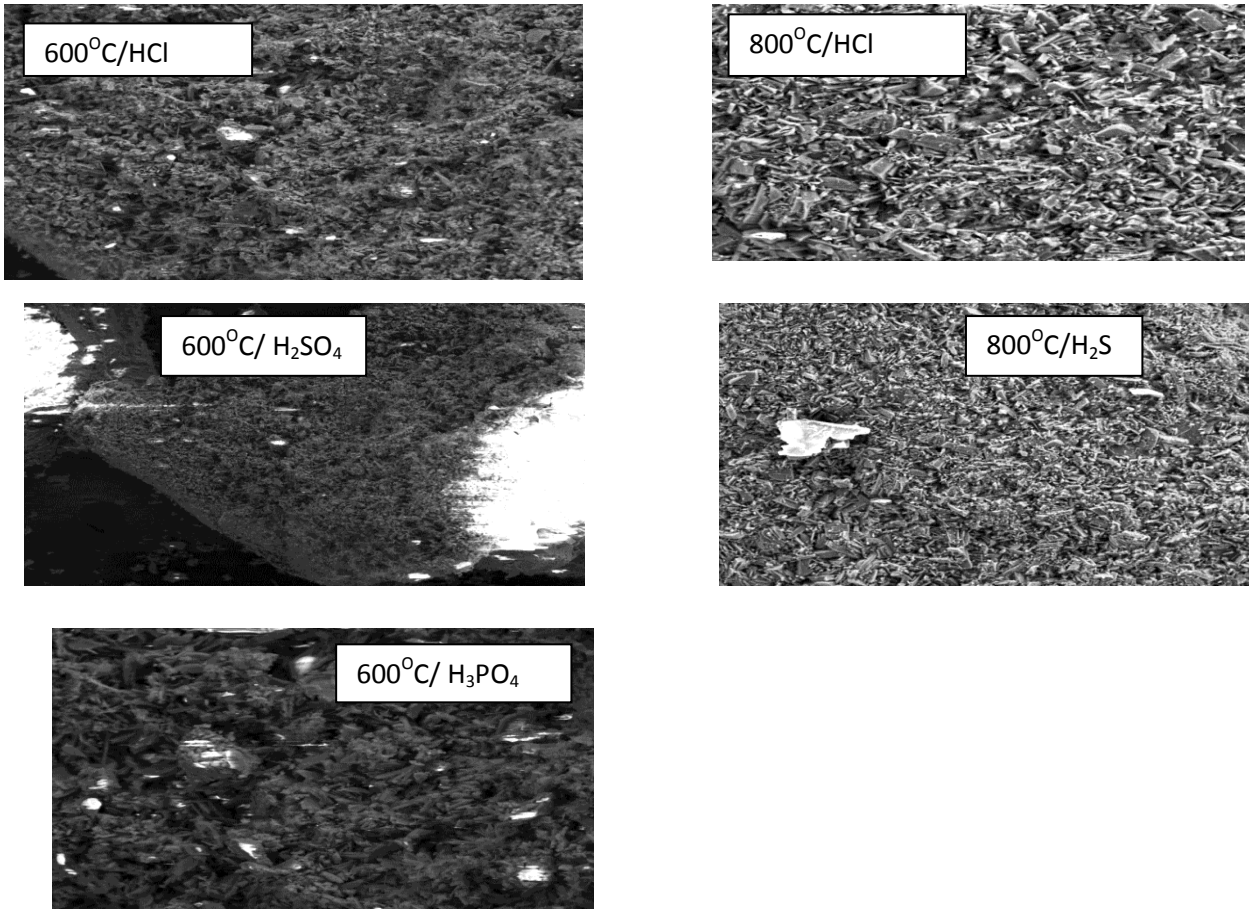

15.0kv. mag =5000x. 20µm. wd = 16.0mm

Plate 4.8: SEM image of Snail Shell Carbonised at 600°C & 800°C and Activated with acids.

4.4 Pore Volume and Surface Area of Activated Carbons

Table 4.10 showed the pore volumes and surface areas of the carbons produced. The pore volumes of the activated carbons were larger than the unactivated carbons in all the type of carbon produced. The activated carbons had good pore volumes as a result of the increased surface area during activation which is a good adsorptive property for activated carbons. The observed trend for the Oil Bean activated carbon pore volume is OBAC/600^{0}C/H_2SO_4 > OBAC/800^{0}C/H_2SO_4 = OBAC/800^{0}C/H_3PO_4 > OBAC/800^{0}C/HCl = OBAC/600^{0}C/HCl while for Pear nut Seed activated carbon the trend is PNAC/800^{0}C/H_3PO_4 = PNAC/800^{0}C/H_2SO_4 > PNAC/800^{0}C/HCl > PNAC/600^{0}C/H_3PO_4 = PNAC/600^{0}C/H_2SO_4 > PNAC/600^{0}C/HCl. For Palm Kernel Shell the trend is PKAC 600^{0}C HCl > PKAC/600^{0}C/H_2SO_4 > PKAC/600^{0}C/H_3PO_4 = PKAC/800^{0}C/HCl = PKAC/800^{0}C/H_3PO_4 = PKAC/800^{0}C/H_2SO_4 while for Snail Shell activated carbon the trend is SSAC/600^{0}C HCl > SSAC/800^{0}C/HCl >

SSAC/800^{0}C/H_2SO_4 > SSAC/800^{0}C/H_3PO_4 > SSAC/600^{0}C/H_3PO_4 > SSAC/600^{0}C/H_2SO_4. Larger pore volumes are advantageous in removing larger heavy metals from aqueous media.

Table 4.10: Pore Volume and Surface Area of both activated and unactivated carbons

Activated Carbon Type	Pore Volume (m^3/g)	Surface Area(m^2/g)
OBAC 600^{0}C	3.9 X 10^{-5}	
OBAC 800^{0}C	3.5 X 10^{-5}	
OBAC 600^{0}C HCl	2.9 X 10^{-5}	812
OBAC 600^{0}C H_2SO_4	2.4 X 10^{-5}	839
OBAC 600^{0}C H_3PO_4	2.6 X 10^{-5}	888
OBAC 800^{0}C HCl	2.9 X 10^{-5}	912
OBAC 800^{0}C H_2SO_4	2.5 X 10^{-5}	815
OBAC 800^{0}C H_3PO_4	2.5 X 10^{-5}	901
PNAC 600^{0}C	3.3 X 10^{-5}	
PNAC 800^{0}C	3.1 X 10^{-5}	
PNAC 600^{0}C HCl	2.8 X 10^{-5}	923
PNAC 600^{0}C H_2SO_4	2.6 X 10^{-5}	865
PNAC 600^{0}C H_3PO_4	2.6 X 10^{-5}	923
PNAC 800^{0}C HCl	2.4 X 10^{-5}	886
PNAC 800^{0}C H_2SO_4	2.3 X 10^{-5}	789
PNAC 800^{0}C H_3PO_4	2.3 X 10^{-5}	945
PKAC 600^{0}C	3.8 X 10^{-5}	
PKAC 800^{0}C	3.8 X 10^{-5}	
PKAC 600^{0}C HCl	2.6 X 10^{-5}	1006
PKAC 600^{0}C H_3PO_4	2.8 X 10^{-5}	1010
PKAC 600^{0}C H_2SO_4	2.7 X 10^{-5}	987
PKAC 800^{0}C HCl	2.9 X 10^{-5}	998
PKAC 800^{0}C H_3PO_4	2.9 X 10^{-5}	912
PKAC 800^{0}C H_2SO_4	2.9 X 10^{-5}	877
SSAC 600^{0}C	8.7 X 10^{-6}	
SSAC 800^{0}C	7.9 X 10^{-6}	
SSAC 600^{0}C HCl	6.2 X 10^{-6}	312
SSAC 600^{0}C H_3PO_4	7.1 X 10^{-6}	267
SSAC 600^{0}C H_2SO_4	7.3 X 10^{-6}	298
SSAC 800^{0}C HCl	6.7 X 10^{-6}	288
SSAC 800^{0}C H_3PO_4	6.9 X 10^{-6}	315
SSAC 800^{0}C H_2SO_4	6.8 X 10^{-6}	312

The surface area obtained ranged from 267 to 1010m^2/g. Most of the samples had a large surface area especially the PKAC. The large surface area shows the possibility

of high adsorption of metals and other pollutants from industrial waste. Surface area is an important attribute for consideration in the application of activated carbon (Rao et al., 2003). The values of the surface area estimated followed the trend PKAC > OBAC > PNAC > SSAC.

4.5 Quantitative Description of Sorption Isotherm

Traditionally, the sorption of ions by adsorbents has been quantitatively described by parameters obtained either directly from isotherms or by least square analysis with sorption isotherms. The data from this study was subjected to Freundlich, Langmuir, Temkin and Dubinin Radushkovich isotherm models to determine sorption parameters and identify the model which best fit or describes the adsorption by these prepared activated carbons.

The Freundlich model is a case for heterogeneous surface energies and it gives an exponential distribution of active sites present in the activated carbon (AC). This form of the equation was used to relate the amount of heavy metal ions sorbed from the metal solutions and the linear form of the model is

$$\log q_e = \log K_f + 1/n \log C_e \qquad (4.1)$$

where q_e is the amount of sorbed metal ions in mg/g, C_e is the equilibrium concentration of the metal ions. n and K_f are the Freundlich constants which respectively indicates the adsorption intensity and the adsorption capacity of the AC (Uddin *et al*., 2007; Khan, *et al*., 2005). They are calculated from the slope and intercept of the plot of $\log q_e$ versus $\log C_e$.

Figues 4.4 to 4.11 presents the adsorption of Ni on OBAC carbonized at both 600°C and 800°C for 30min and activated with HCl, H_2SO_4 and H_3PO_4. The parameters for the plot of the freundlich, Langmuir, Temkin and Dubinin-Radushkevich isotherm models are also presented in appendix C.

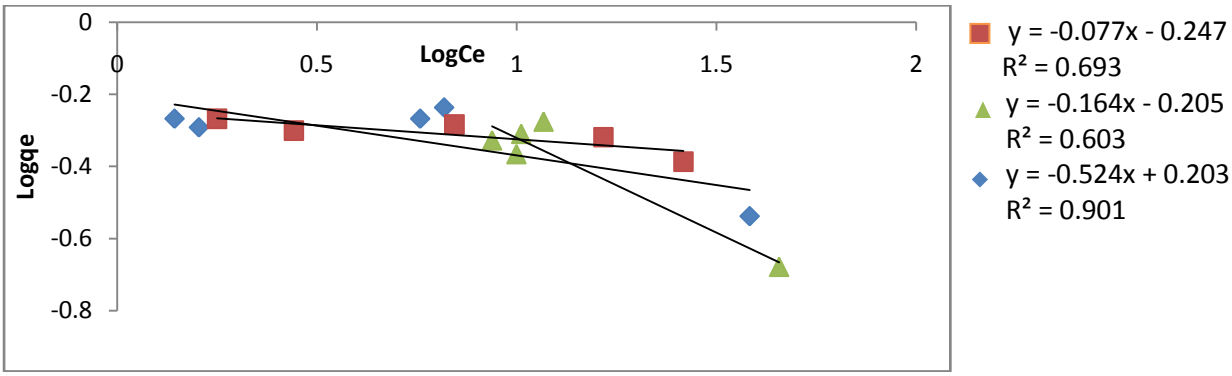

Figure 4.4: Freundlich isotherm plot for Ni onto OBAC Carbonized at 600°C and activated with HCl, H_3PO_4, H_2SO_4

Figure 4.4 showed the result of the adsorption isotherm for Ni on OBAC carbonised at 600°C and activated with HCl, H_2SO_4 and H_3PO_4 at the same temperature. From the figure, the straight line plot indicated the occurrence of Ni metal adsorption from the sample. The graph showed the adsorption isotherm is of relative good fit on Freundlich model. This is indicated by the coefficient of determination (R^2) ranging from 0.603 to 0.901. The goodness of fit of an experimental data is measured by the determination coefficient (R^2) (Zaid and Mohammed, 2008). The R^2 for all the isotherms are presented in Table 4.122. The slope of the linear plot is also good and suitable for testing the adsorption effectiveness. The value of n obtained from the slope of the linear plot ranged from 1.91 to 15.9 which indicated the strength of the OBAC as an adsorbent. When n > 1, the adsorption coefficient

increases with increasing concentration of the solution which lead to an increase in hydrophobic surface characteristic after monolapisan and when n < 1, K_f decreases with concentration (Hamidi-Aziz *et al*., 2003). Appendix G showed the Atomic Absorption Spectrophotometer (AAS) results of the heavy metal analysis.

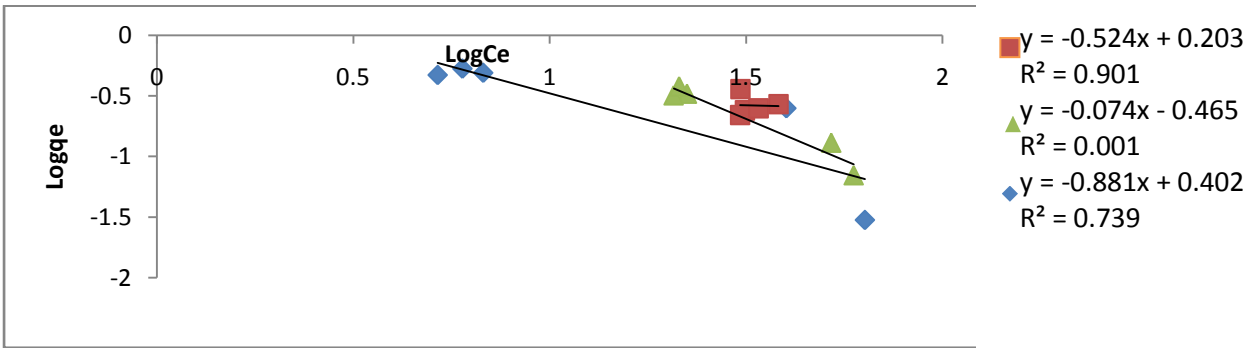

Figure 4.5: Freundlich isotherm plot for Ni onto OBAC Carbonized at 800°C and activated with HCl, H_3PO_4, H_2SO_4

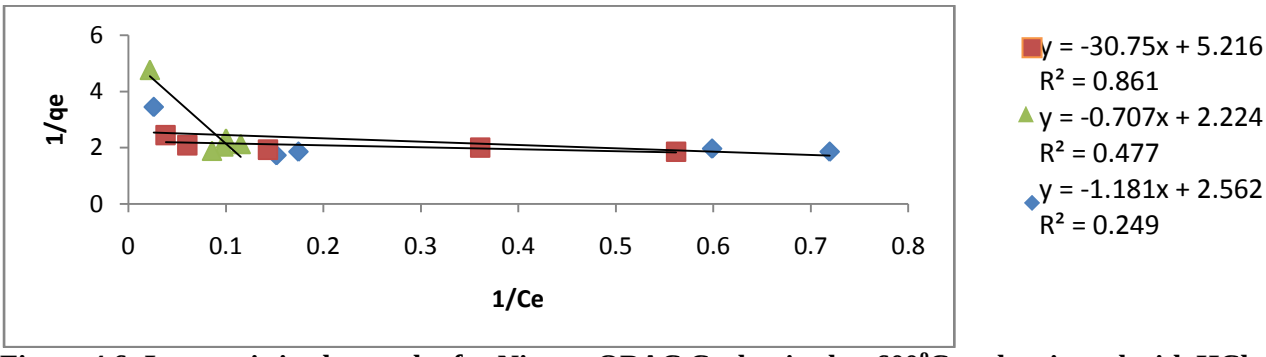

Figure 4.6: Langmuir isotherm plot for Ni onto OBAC Carbonized at 600°C and activated with HCl, H_3PO_4, H_2SO_4

The Langmuir isotherm model suggested that sorption occured on homogeneous surface by monolayer sorption without interaction between sorbed ions. The linear form of Langmuir isotherm equation is as presented below:

$$1/q_e = 1/Q^o + 1/bQ^o 1/C_e \qquad (4.2)$$

Where Ce is the equilibrium concentration (mg/l), q_e is the amount of metal ions adsorbed at equilibrium (mg/g) and the Q^o and b are the Langmuir isotherm constants which gives the adsorption capacity and the energy of adsorption

respectively (Uddin, 2007). The linear plot of $1/q_e$ versus $1/C_e$ indicated the Langmuir model plot and the values of Q^o and b were calculated from the slopes and intercepts of the Langmuir plots respectively.

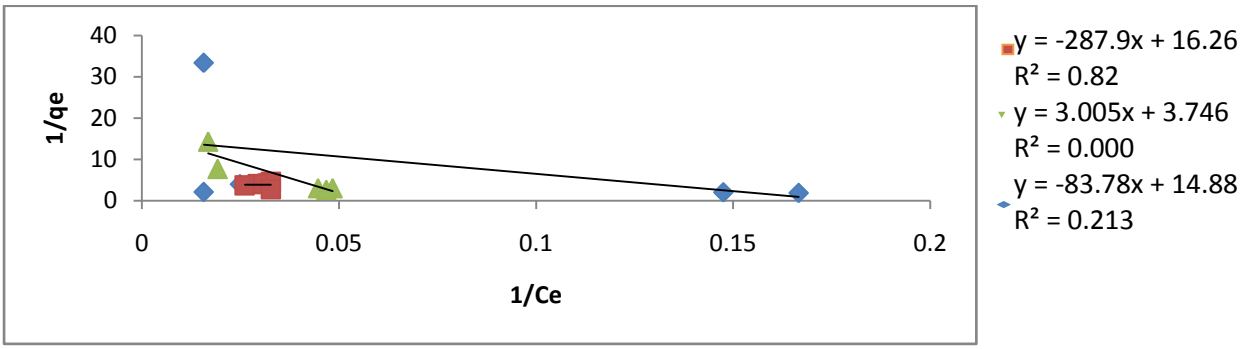

Figure 4.7: Langmuir isotherm plot for Ni onto OBAC Carbonized at 800°C and activated with HCl, H_3PO_4, H_2SO_4

In Figures 4.6 and 4.7, the determination coefficient did not show a good fit and the Langmuir adsorption capacity (Q^o) of the three type of OBAC for Ni ranged from 0.035 to 1.4144l/kg, while the Langmuir energy of adsorption (b) ranged from 0.32 to 5.895 which reflect the retention intensity and the number of sites available for a sorbate.

For the adsorption of Ni by OBAC carbonised at 800°C, the K_f ranged from 2.5 to 2.9 which was an indication of good adsorptive capacity. Also, the adsorption intensity ranged from 0.001 to 0.739. The determination coefficient of the Freundlich plot indicated poor fit except for that activated with HCl.

The adsorption data for OBAC carbonised at 600°C had a better fit for the Freundlich model and so indicated heterogeneous nature of the activated carbon surface energies. The Freundlich intensity of adsorption (n) of Ni on OBAC was

relatively high, but the reverse was the case for the Freundlich adsorption capacity of the (K_f) values for OBAC.

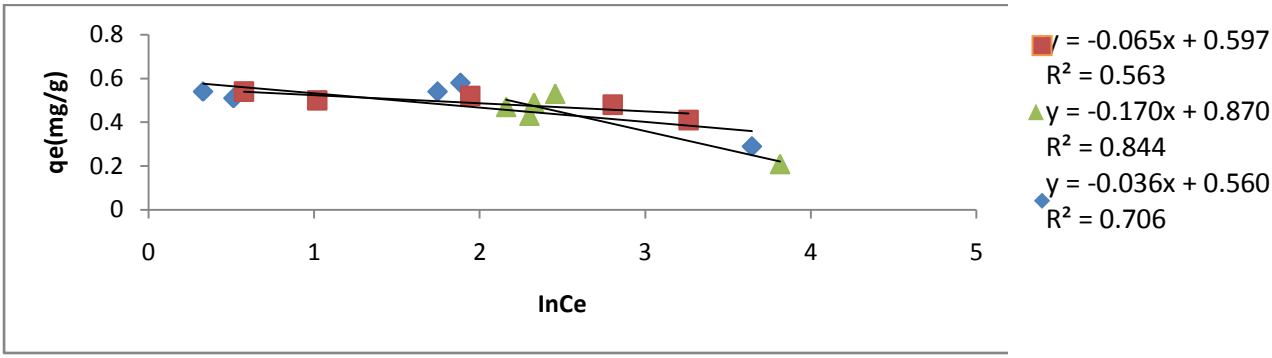

Figure 4.8: Temkin isotherm plot for Ni onto OBAC Carbonized at 600°C and activated with HCl, H_3PO_4, H_2SO_4

The data obtained from the Ni adsorption onto OBAC fitted well on the Temkin model as indicated by the determination coefficients except for that carbonized at 800°C and activated with H_2SO_4, $R^2 = 0.010$ (Figure 4.9).

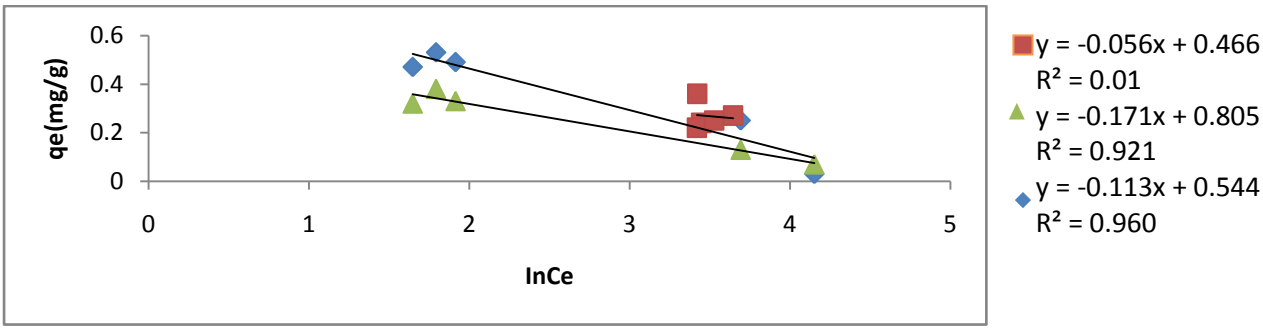

Figure 4.9: Temkin isotherm plot for Ni onto OBAC Carbonized at 800°C and activated with HCl, H_3PO_4, H_2SO_4

The determination coefficients for the adsorption of Ni onto OBAC showed the data fitted poorly on the D-R isotherm model except for that activated with H_3PO_4 (Figure 4.10 and 4.11).

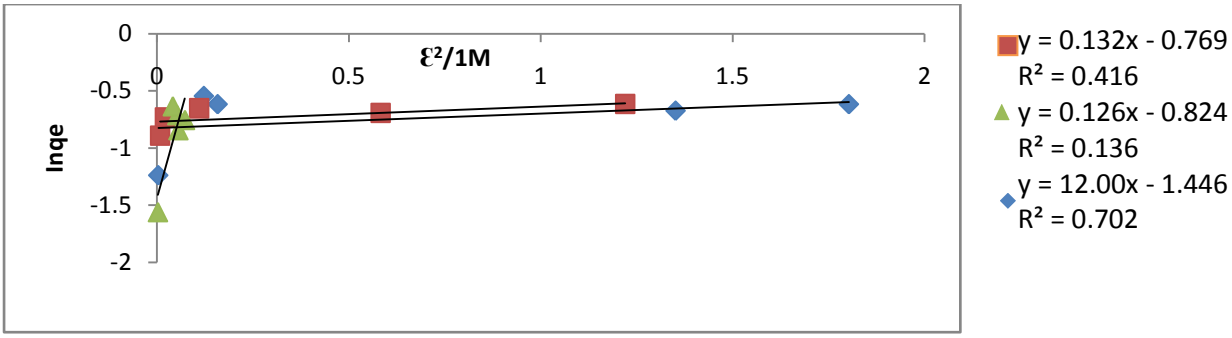

Figure 4.10: Dubinin Rudushkevich isotherm plot for Ni onto OBAC Carbonized at 600°C and activated with HCl, H_3PO_4, H_2SO_4

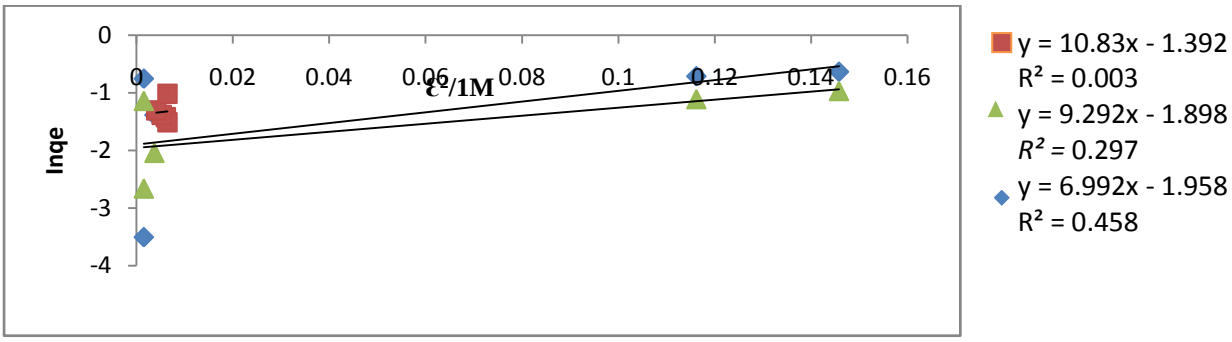

Figure 4.11: Dubinin Rudushkevich isotherm plot for Ni onto OBAC Carbonized at 800°C and activated with HCl, H_3PO_4, H_2SO_4

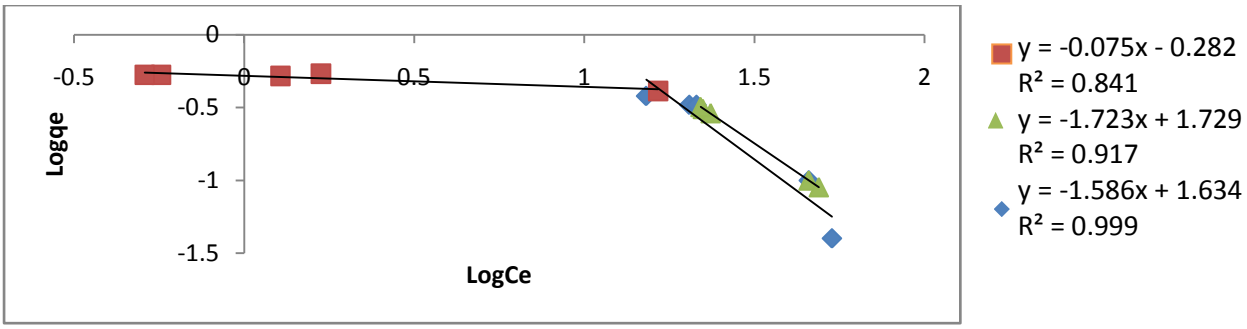

Figure 4.12: Freundlich isotherm plot for Cd onto OBAC Carbonized at 600°C and activated with HCl, H_3PO_4, H_2SO_4

The data obtained from the adsorption of Cd onto OBAC fitted well on the Freundlich model as indicated by the determination coefficients except for that carbonized at 800°C and activated with H_2SO_4, $R^2 = 0.022$ (Figures 4.12 and 4.13). This is an indication of heterogeneous adsorption as suggested by Freundlich model.

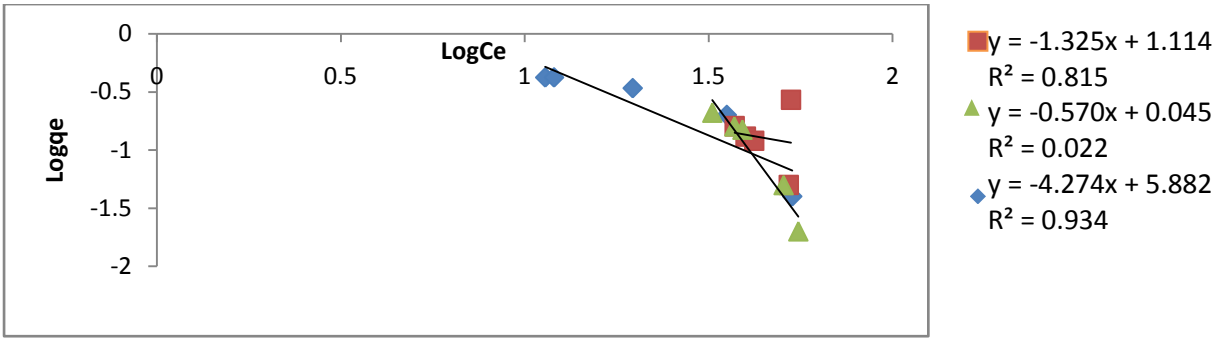

Figure 4.13: Freundlich isotherm plot for Cd onto OBAC Carbonized at 800°C and activated with HCl, H_3PO_4, H_2SO_4

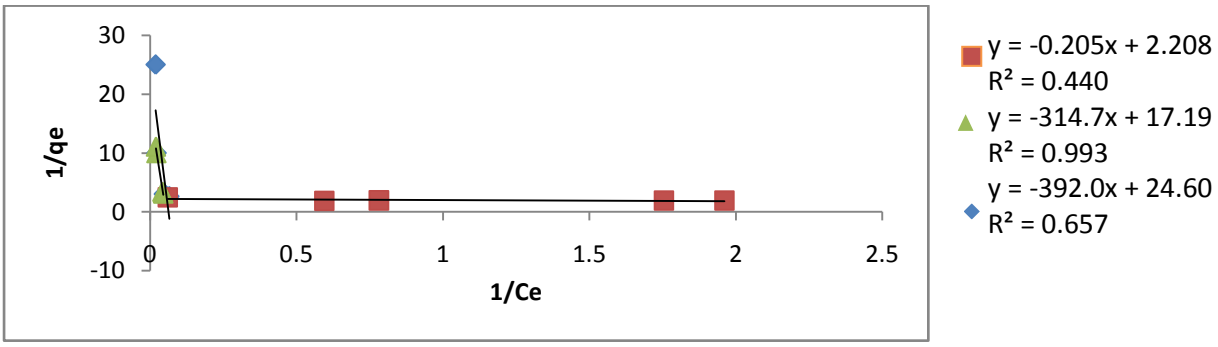

Figure 4.14: Langmuir isotherm plot for Cd onto OBAC Carbonized at 600°C and activated with HCl, H_3PO_4, H_2SO_4

The data obtained for the adsorption of Cd onto OBAC fitted poorly on the Langmuir isotherm model as indicated by R^2 and this is an indication that its adsorption does not follow monolayer coverage as suggested by Langmuir model.

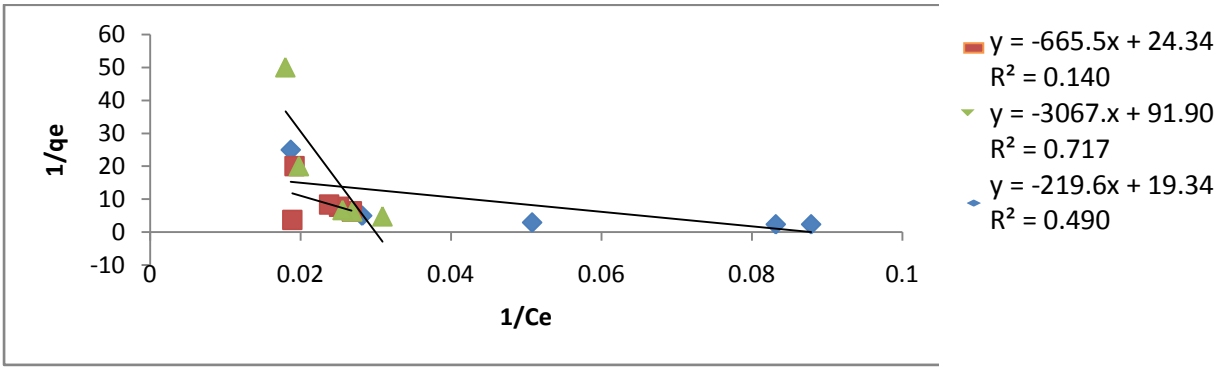

Figure 4.15: Langmuir isotherm plot for Cd onto OBAC Carbonized at 800°C and activated with HCl, H_3PO_4, H_2SO_4

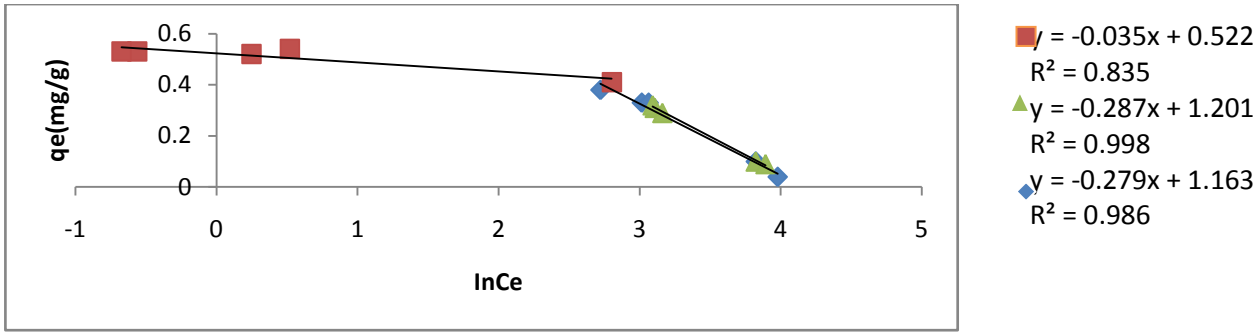

Figure 4.16: Temkin Isotherm plot for Cd onto OBAC Carbonized at 600°C and activated with HCl, H_3PO_4, H_2SO_4

Figures 4.16 and 4.17 presents the Temkin isotherm plot for Cd adsorption onto OBAC at both activation temperatures. The R^2 showed that the data fitted well with the model in most of them having ranged from 0.835 to 0.998 for those carbonized at 600°C and 0.019 to 0.998 for those carbonized at 800°C respectively.

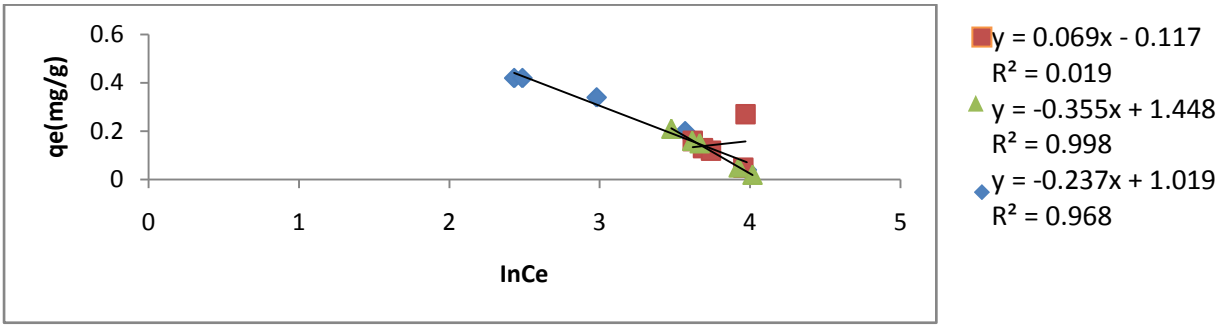

Figure 4.17: Temkin Isotherm plot for Cd onto OBAC Carbonized at 800°C and activated with HCl, H_3PO_4, H_2SO_4

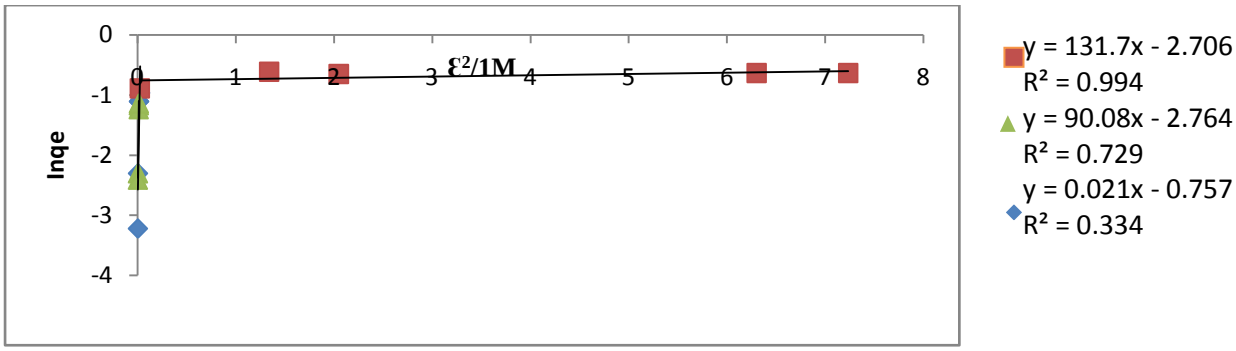

Figure 4.18: Dubinin Rudushkevich Isotherm plot for Cd onto OBAC Carbonized at 600°C and activated with HCl, H_3PO_4, H_2SO_4

Presented in Figures 4.18 and 4.19 are the D-R plot for the adsorption of Cd onto OBAC at 600°C and 800°C respectively. The fitness of the data on the model is

relatively good for both temperatures of activation considering the determination coefficients but those of Temkin were better.

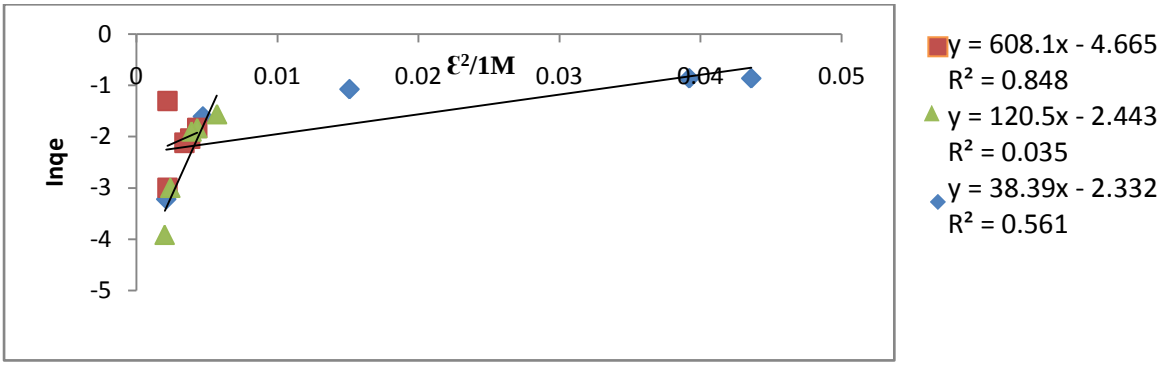

Figure 4.19: Dubinin Rudushkevich Isotherm plot for Cd onto OBAC Carbonized at 800°C and activated with HCl, H_3PO_4, H_2SO_4

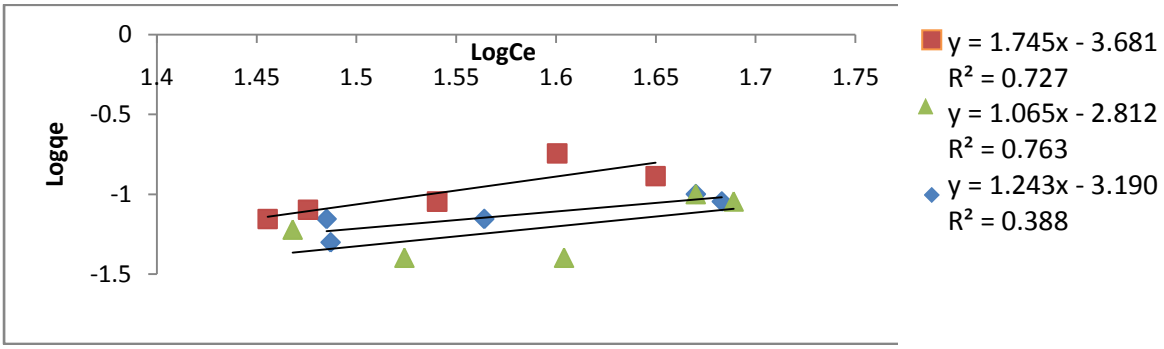

Figure 4.20: Freundlich isotherm plot for Pb onto OBAC Carbonized at 600°C and activated with HCl, H_3PO_4, H_2SO_4

Figures 4.20 and 4.21 showed the freundlich adsorption isotherms for Pb adsorption onto OBAC at both 600°C and 800°C respectively. They all had good determination coefficients except for those activated with H_3PO_4 at both carbonization temperatures.

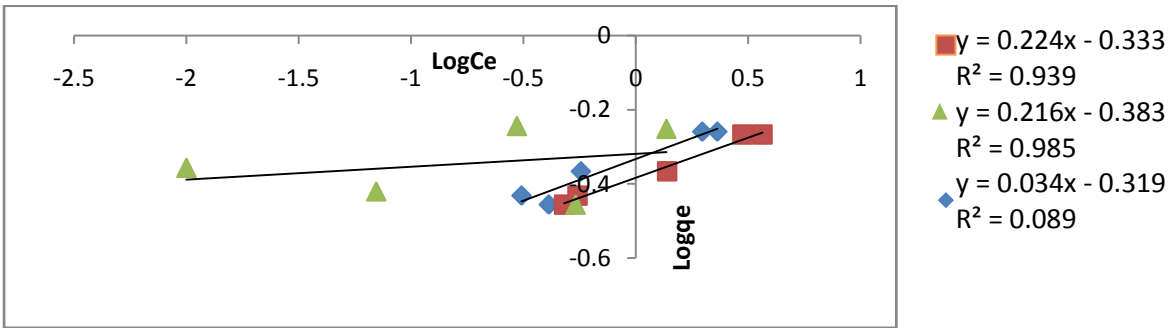

Figure 4.21: Freundlich isotherm plot for Pb onto OBAC Carbonized at 800°C and activated with HCl, H_3PO_4, H_2SO_4

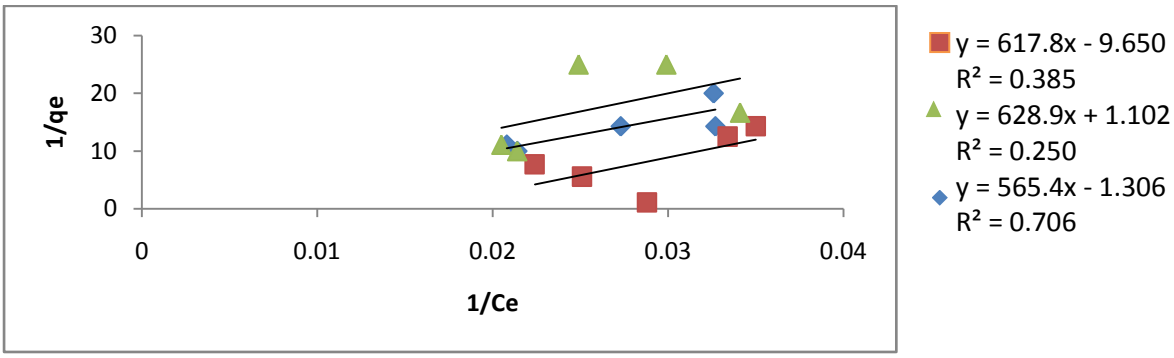

Figure 4.22: Langmuir isotherm plot for Pb onto OBAC Carbonized at 600°C and activated with HCl, H_3PO_4, H_2SO_4

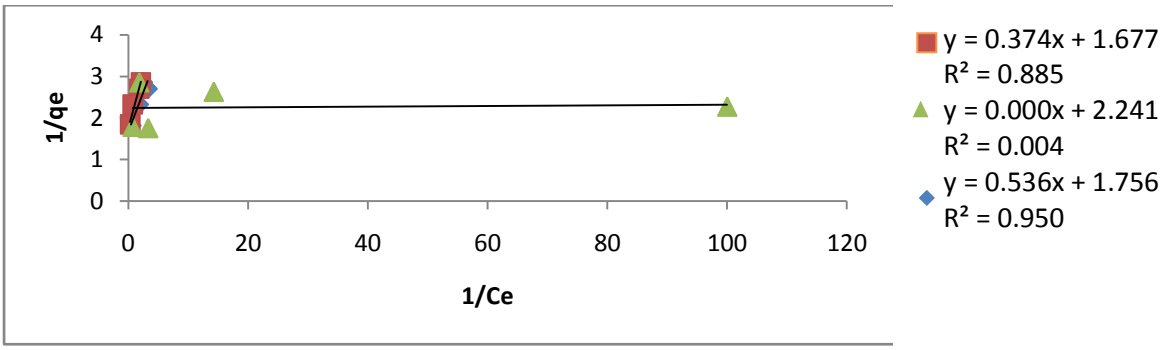

Figure 4.23: Langmuir isotherm plot for Pb onto OBAC Carbonized at 800°C and activated with HCl, H_3PO_4, H_2SO_4

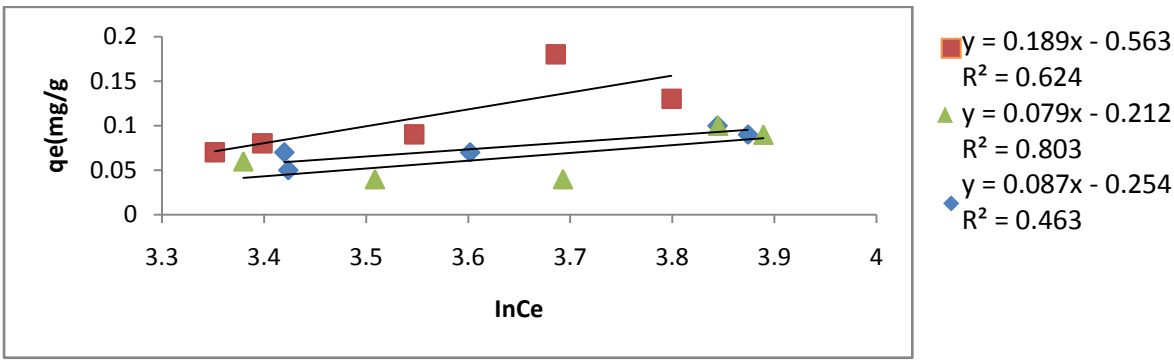

Figure 4.24: Temkin Isotherm plot for Pb onto OBAC Carbonized at 600°C and activated with HCl, H_3PO_4, H_2SO_4

Figures 4.24 and 4.25 presents the Temkin adsorption isotherms for Pb adsorption onto OBAC at both 600°C and 800°C respectively. They all had good determination coefficients except for those activated with H_2SO_4 at both carbonization temperatures.

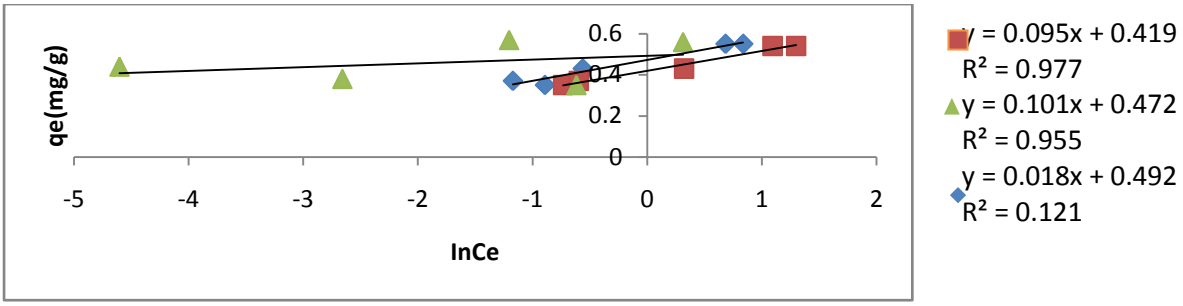

Figure 4.25: Temkin Isotherm plot for Pb onto OBAC Carbonized at 800°C and activated with HCl, H_3PO_4, H_2SO_4

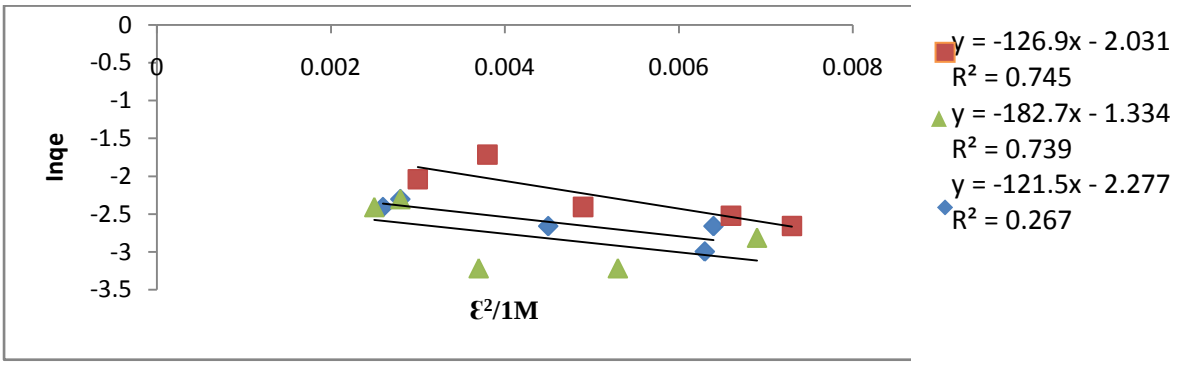

Figure 4.26: Dubinin Rudushkevich Isotherm plot for Pb onto OBAC Carbonized at 600°C and activated with HCl, H_3PO_4, H_2SO_4

The adsorption data obtained for Pb on D-R model showed good fit for both carbonization temperatures except for those activated with H_2SO_4 (Figures 4.26 and 4.27).

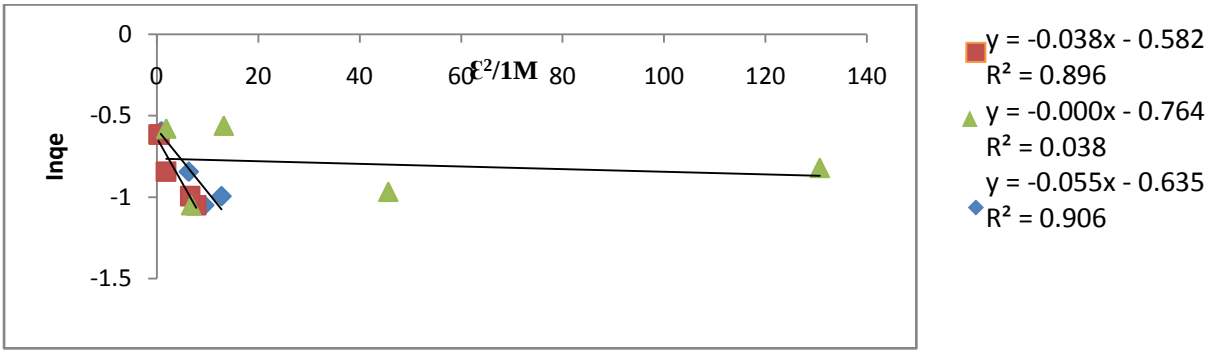

Figure 4.27: Dubinin Rudushkevich Isotherm plot for Pb onto OBAC Carbonized at 800°C and activated with HCl, H_3PO_4, H_2SO_4

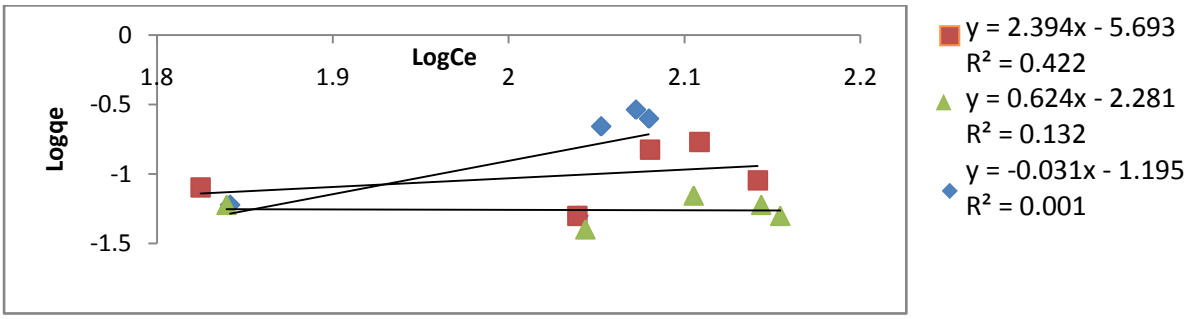

Figure 4.28: Freundlich Isotherm plot for Mn onto OBAC Carbonized at 600°C and activated with HCl, H_3PO_4, H_2SO_4

Figures 4.28 and 4.29 presents the isotherm plot, equation of the plot, as well as the determination coefficients for the fit of Freundlich model by the data obtained. It showed that all the activated carbon fitted poorly on the adsorption of Mn except for the carbonization at 800°C and HCl activation.

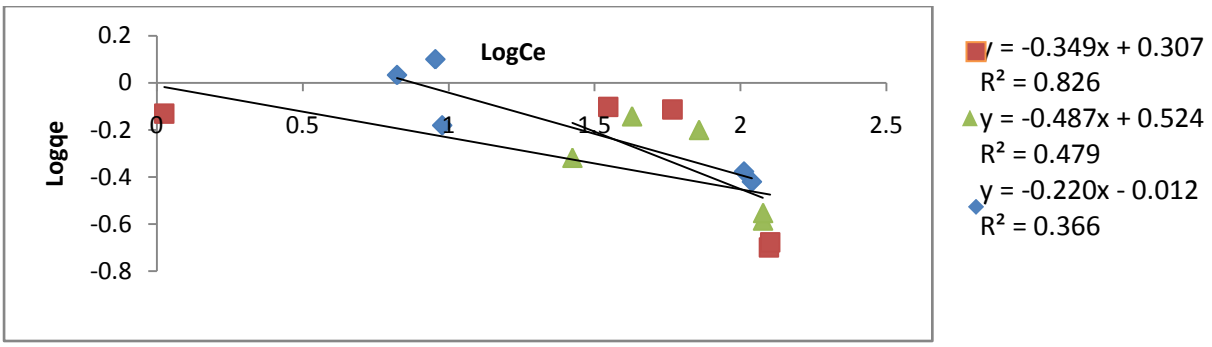

Figure 4.29: Freundlich Isotherm plot for Mn onto OBAC Carbonized at 800°C and activated with HCl, H_3PO_4, H_2SO_4

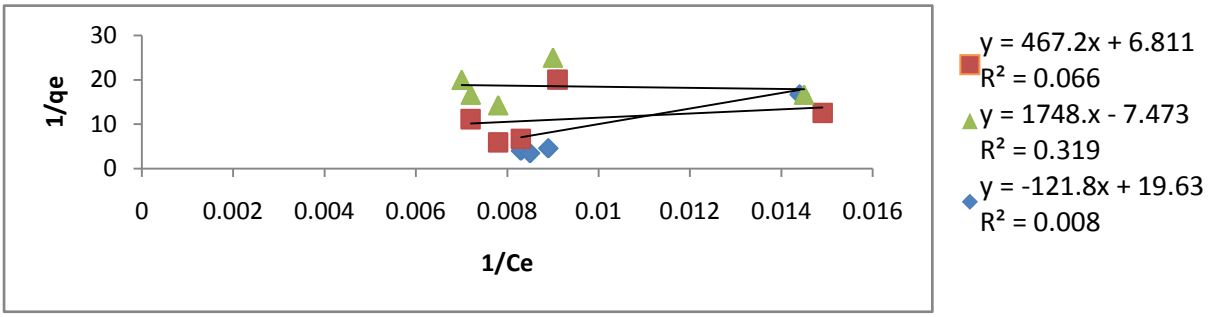

Figure 4.30: Langmuir Isotherm plot for Mn onto OBAC Carbonized at 600°C and activated with HCl, H_3PO_4, H_2SO_4

Mn adsorption on to OBAC also did not follow Langmuir model as shown by the having had poor determination coefficients in all except for the carbonization at 800°C which showed improved fitness with HCl activation (Figures 4.30 and 4.31).

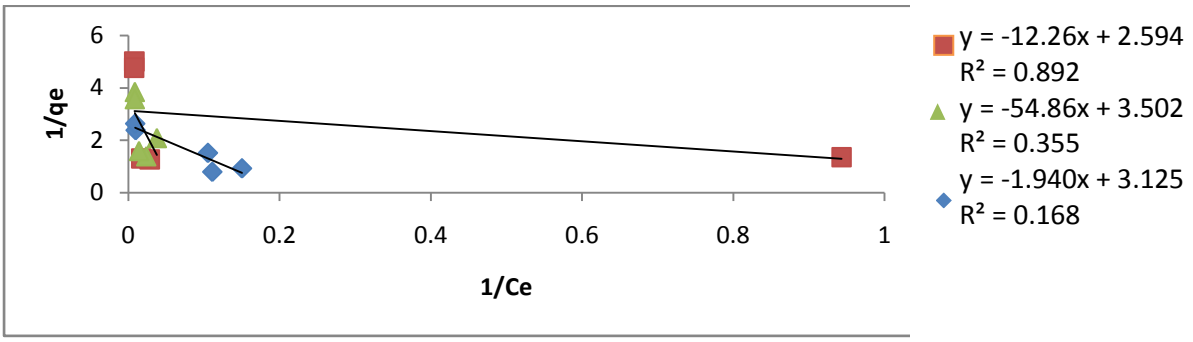

Figure 4.31: Langmuir Isotherm plot for Mn onto OBAC Carbonized at 800°C and activated with HCl, H_3PO_4, H_2SO_4

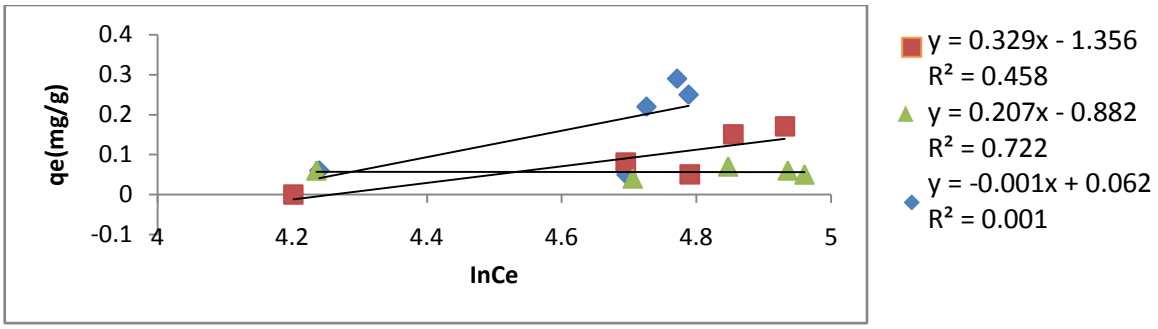

Figure 4.32: Temkin Isotherm plot for Mn onto OBAC Carbonized at 600°C and activated with HCl, H_3PO_4, H_2SO_4

From figure 4.32 and 4.33 the data for adsorption of the metals fitted well on the Temkin model except for those carbonized at 800°C and activated with H_2SO_4 for Ni, Cd and Pb but for Mn.

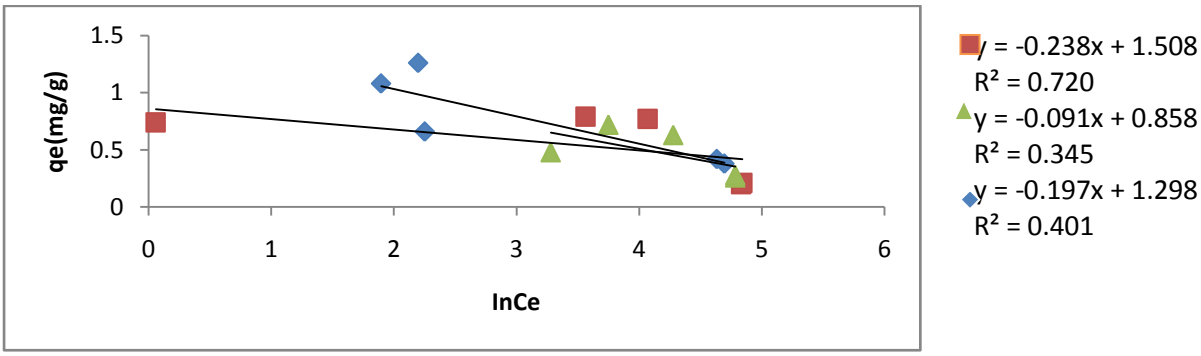

Figure 4.33: Temkin Isotherm plot for Mn onto OBAC Carbonized at 800°C and activated with HCl, H_3PO_4, H_2SO_4

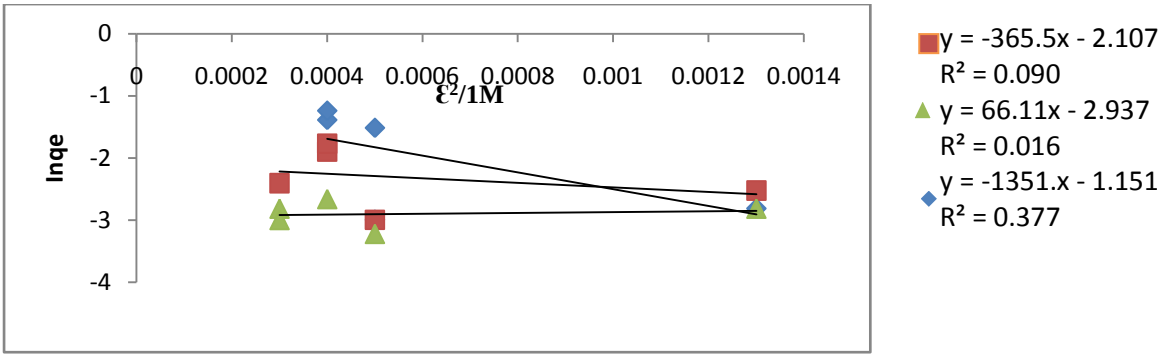

Figure 4.34: Dubinin Rudushkevich Isotherm plot for Mn onto OBAC Carbonized at 600°C and activated with HCl, H_3PO_4, H_2SO_4

For the Dubinin Rudushkevich Isotherm model, the data generally speaking, did not fit well for all the metals studied.

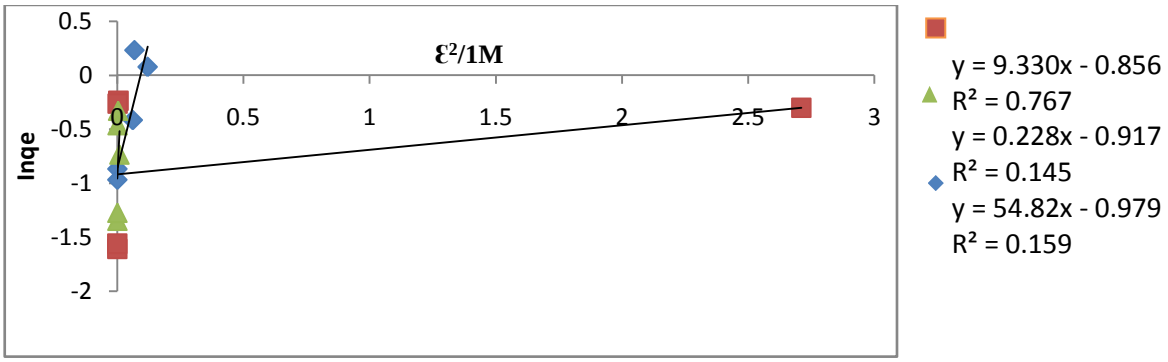

Figure 4.35: Dubinin Rudushkevich Isotherm plot for Mn onto OBAC Carbonized at 800°C and activated with HCl, H_3PO_4, H_2SO_4

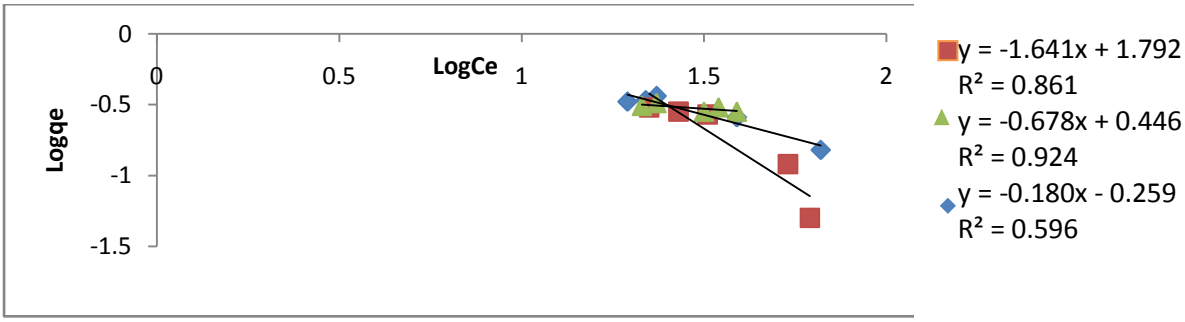

Figure 4.36: Freundlich Isotherm plot for Ni onto PNAC Carbonized at 600°C and activated with HCl, H_3PO_4, H_2SO_4

The adsorption of Ni on PNAC for both carbonization temperatures showed high values for the determination coefficients indicating good fit of the data obtained on the four isotherm models tested (Figures 4.36, 4.43).

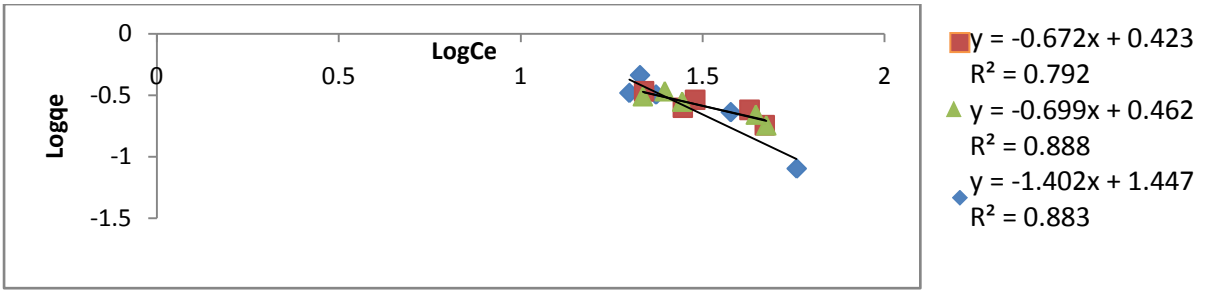

Figure 4.37: Freundlich Isotherm plot for Ni onto PNAC Carbonized at 800°C and activated with HCl, H_3PO_4, H_2SO_4

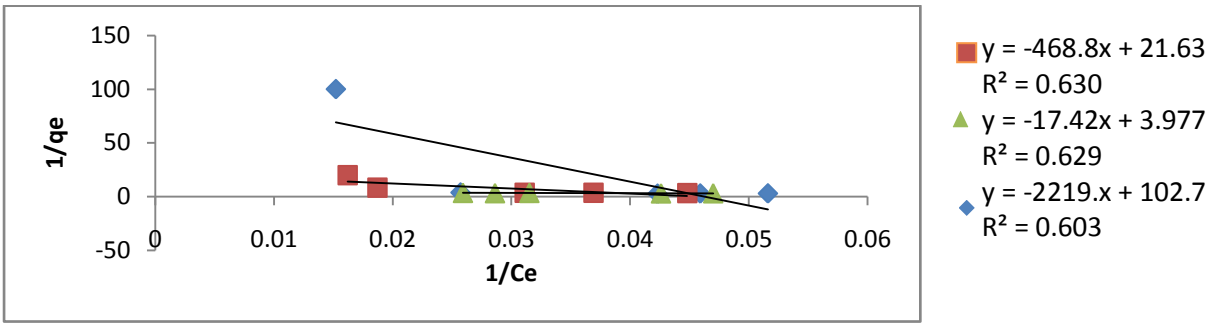

Figure 4.38: Langmuir Isotherm plot for Ni onto PNAC Carbonized at 600°C and activated with HCl, H_3PO_4, H_2SO_4

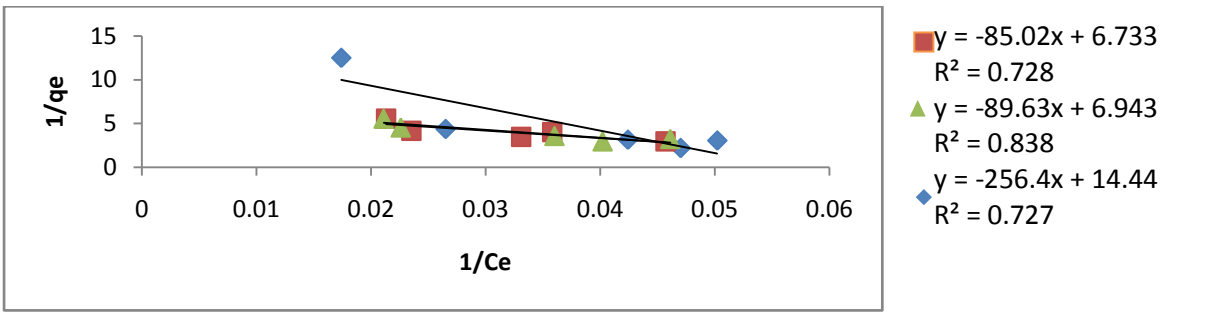

Figure 4.39: Langmuir Isotherm plot for Ni onto PNAC Carbonized at 800°C and activated with HCl, H_3PO_4, H_2SO_4

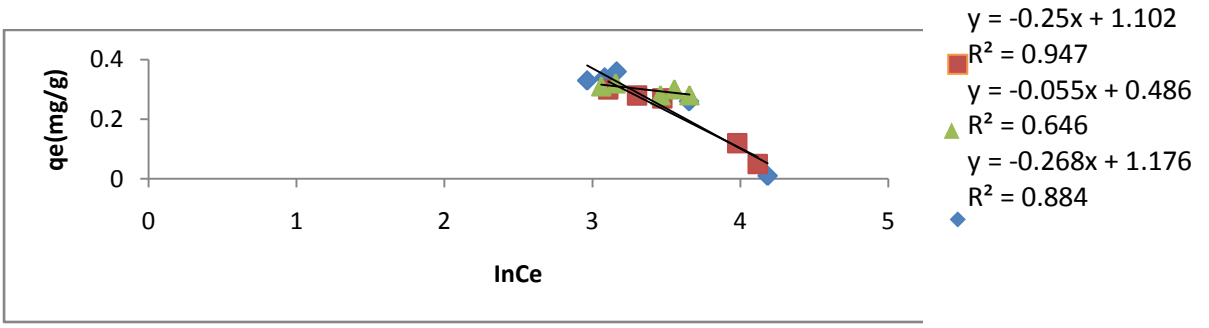

Figure 4.40: Temkin Isotherm plot for Ni onto PNAC Carbonized at 600°C and activated with HCl, H_3PO_4, H_2SO_4

Ni adsorption data onto PNAC fitted well by the Temkin model for both carbonization temperatures as indicated by the determination coefficients recorded from the isotherm plot (Figure 4.40 and 4.41).

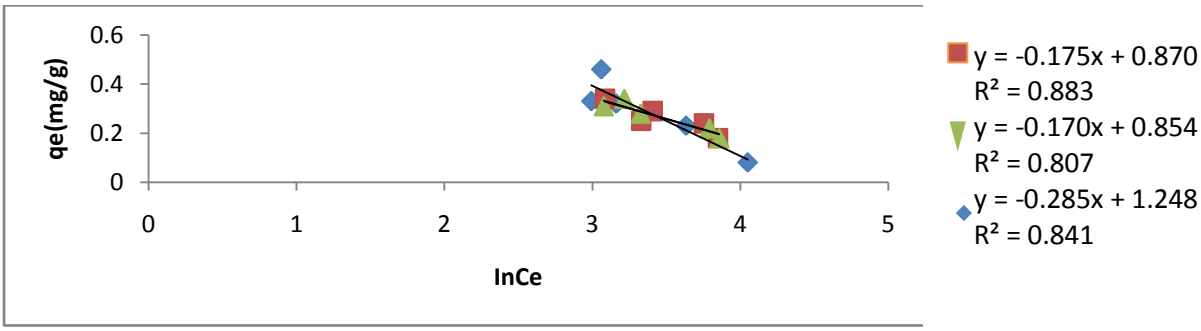

Figure 4.41: Temkin Isotherm plot for Ni onto PNAC Carbonized at 800°C and activated with HCl, H_3PO_4, H_2SO_4

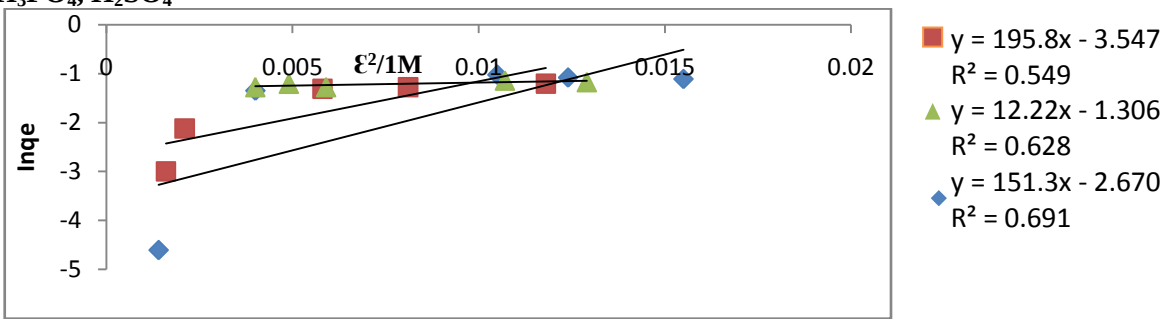

Figure 4.42: Dubinin Rudushkevich Isotherm plot for Ni onto PNAC Carbonized at 600°C and activated with HCl, H_3PO_4, H_2SO_4

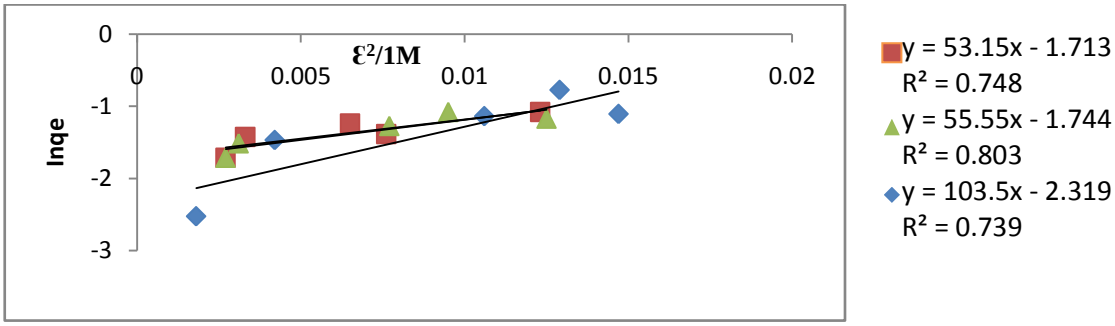

Figure 4.43: Dubinin Rudushkevich Isotherm plot for Ni onto PNAC Carbonized at 800°C and activated with HCl, H_3PO_4, H_2SO_4

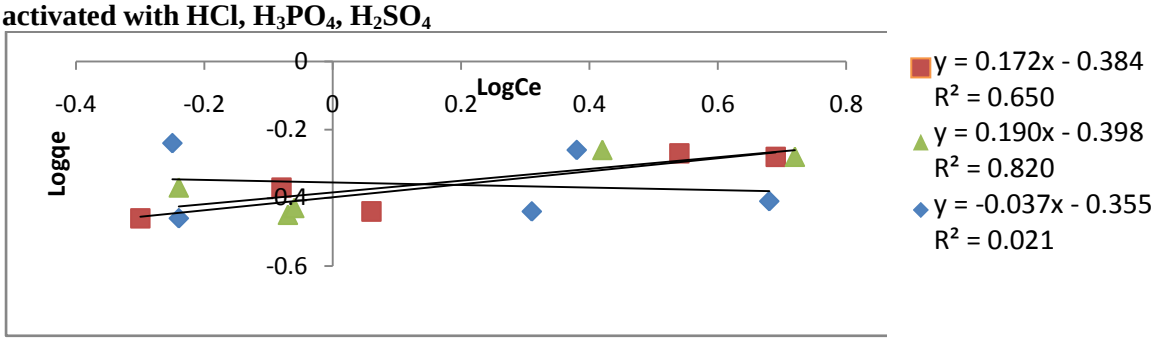

Figure 4.44: Freundlich Isotherm plot for Pb onto PNAC Carbonized at 600°C & activated with HCl, H_3PO_4, H_2SO_4

The adsorption of Pb on PNAC for both carbonization temperatures also showed high values for the determination coefficients indicating good fit of the data obtained on the four isotherm models tested (Figures 4.44 to 4.51).

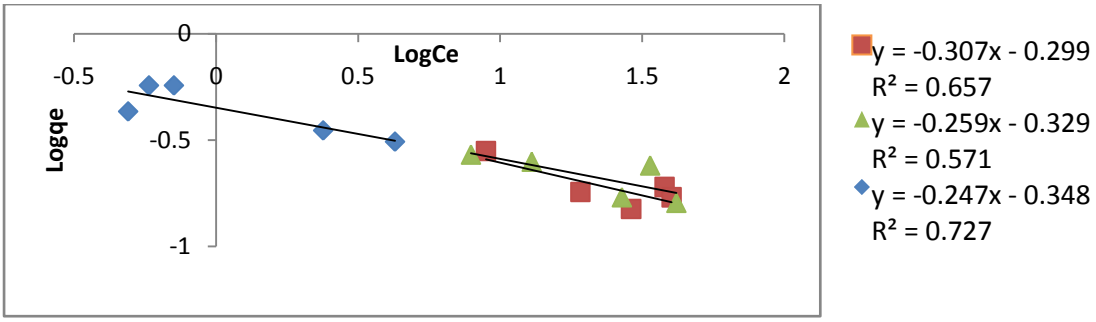

Figure 4.45: Freundlich Isotherm Plot for Pb onto PNAC Carbonized at 800°C and activated with HCl, H_3PO_4, H_2SO_4

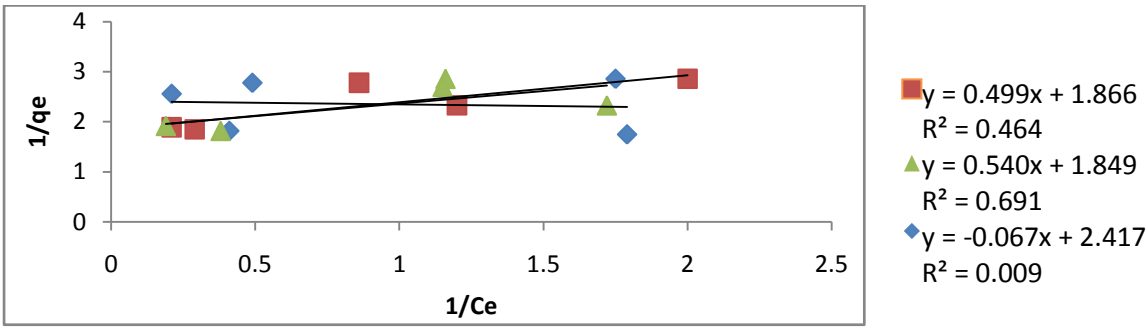

Figure 4.46: Langmuir Isotherm plot for Pb onto PNAC Carbonized at 600°C and activated with HCl, H_3PO_4, H_2SO_4

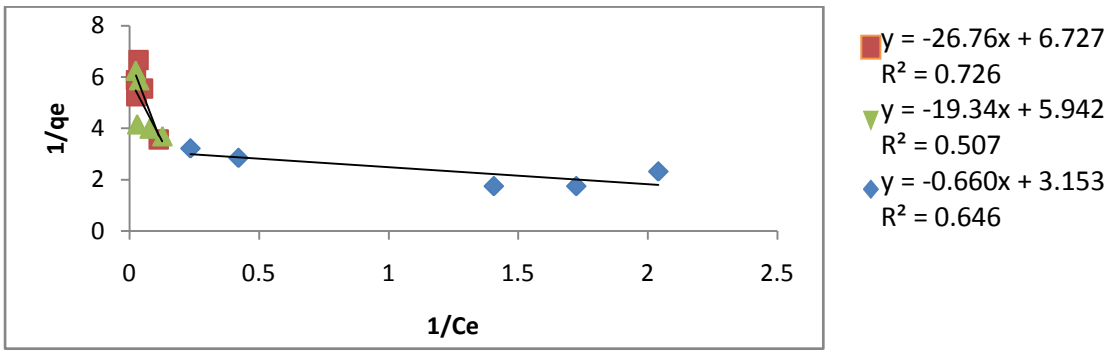

Figure 4.47: Langmuir Isotherm plot for Pb onto PNAC Carbonized at 800°C and activated with HCl, H_3PO_4, H_2SO_4

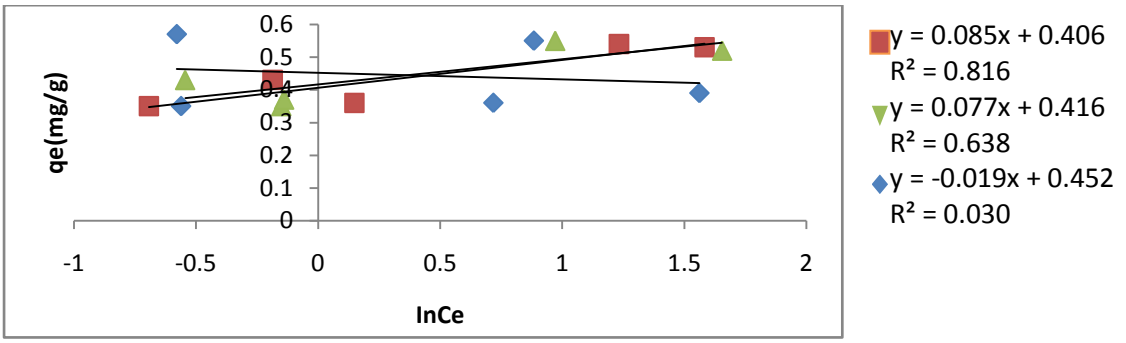

Figure 4.48: Temkin Isotherm plot for Pb onto PNAC Carbonized at 600°C and activated with HCl, H_3PO_4, H_2SO_4

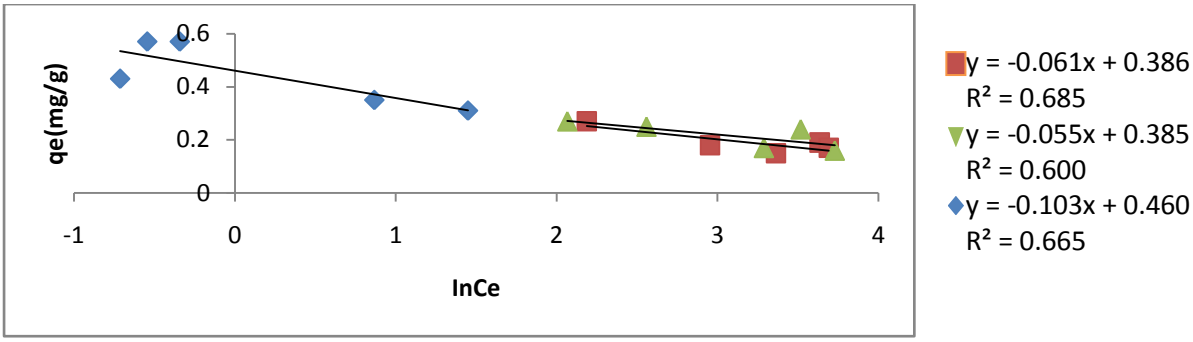

Figure 4.49: Temkin Isotherm plot for Pb onto PNAC Carbonized at 800°C and activated with HCl, H_3PO_4, H_2SO_4

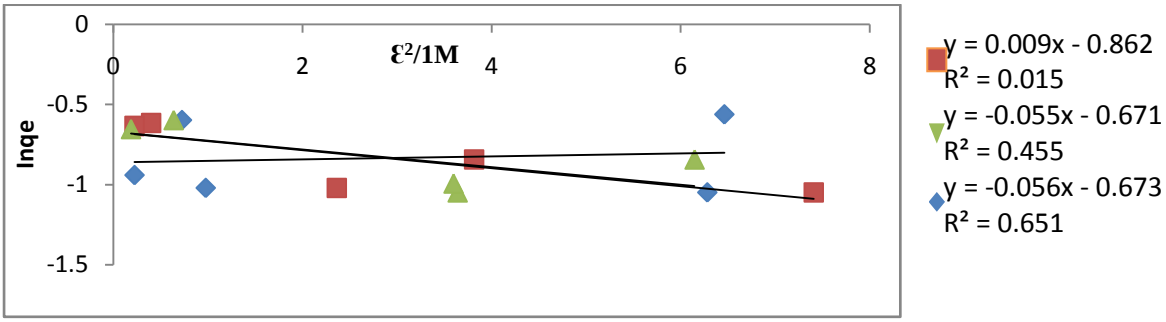

Figure 4.50: Dubinin Rudushkevich Isotherm plot for Pb onto PNAC Carbonized at 600°C and activated with HCl, H_3PO_4, H_2SO_4

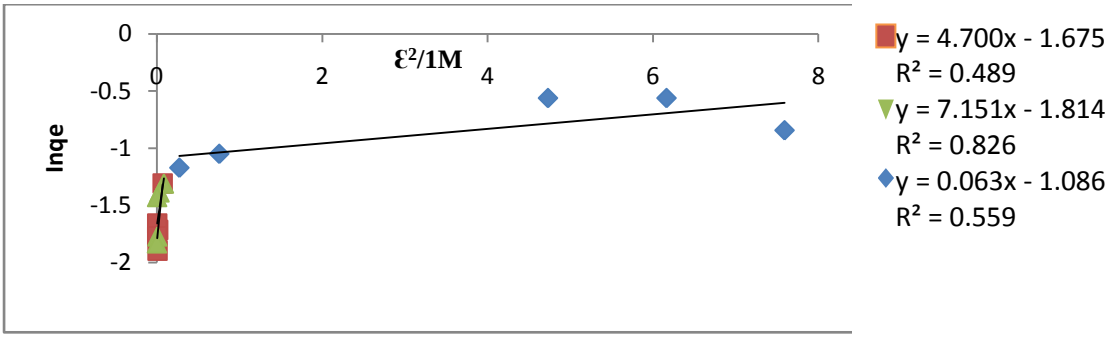

Figure 4.51: Dubinin Rudushkevich Isotherm plot for Pb onto PNAC Carbonized at 800°C and activated with HCl, H_3PO_4, H_2SO_4

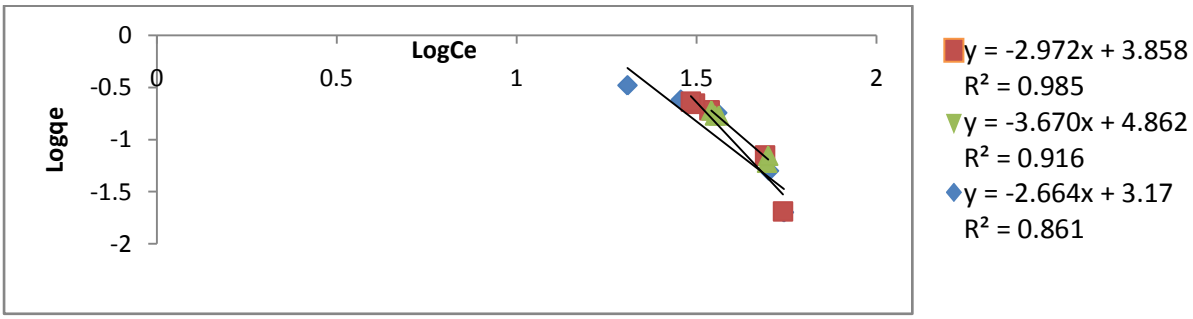

Figure 4.52: Freundlich Isotherm plot for Cd onto PNAC Carbonized at 600°C and activated with HCl, H_3PO_4, H_2SO_4

Figures 4.52 to 4.59 present the adsorption of Cd onto PNAC for both carbonization temperatures and they showed high values for the determination coefficients

indicating good fit of the data obtained on the four isotherm models that were tested.

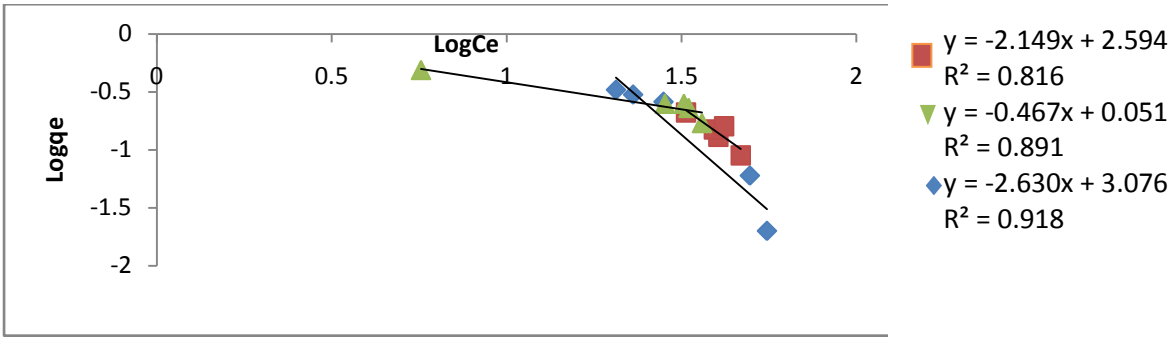

Figure 4.53: Freundlich Isotherm plot for Cd onto PNAC Carbonized at 800°C and activated with HCl, H_3PO_4, H_2SO_4

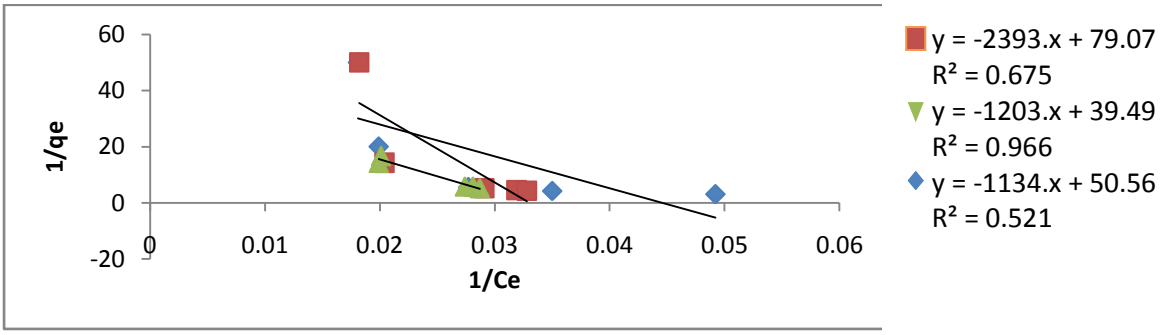

Figure 4.54: Langmuir Isotherm plot for Cd onto PNAC Carbonized at 600°C and activated with HCl, H_3PO_4, H_2SO_4

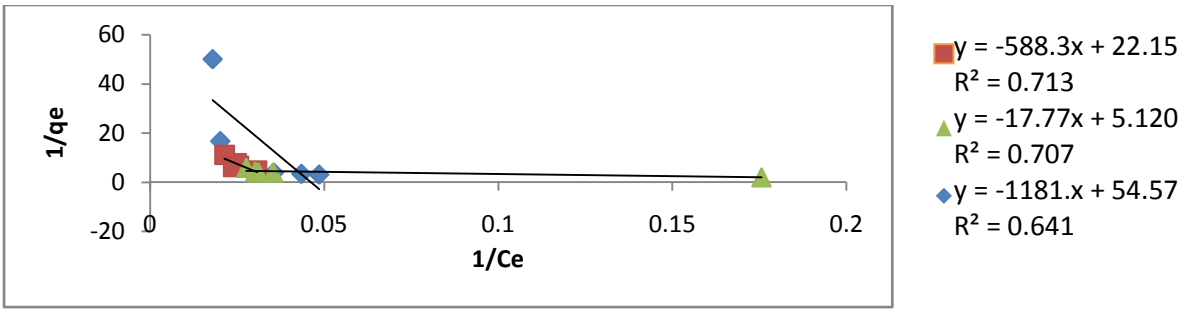

Figure 4.55: Langmuir Isotherm plot for Cd onto PNAC Carbonized at 80(
HCl, H_3PO_4, H_2SO_4

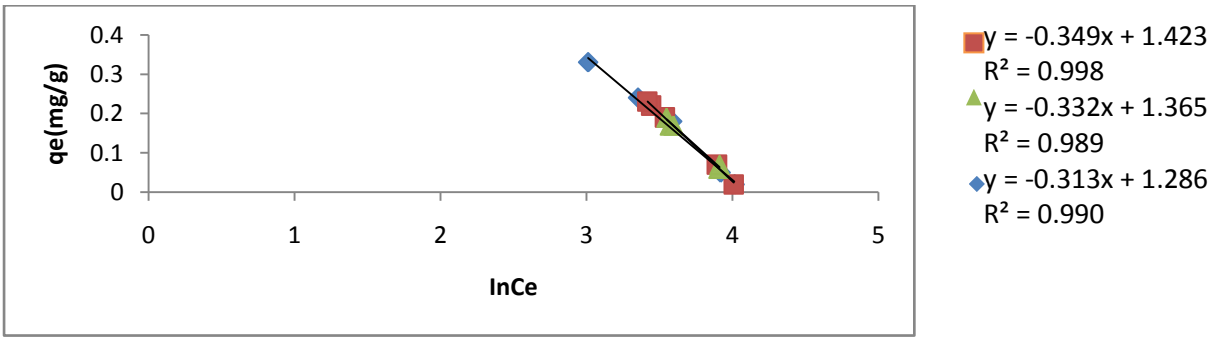

Figure 4.56: Temkin Isotherm plot for Cd onto PNAC Carbonized at 600°C and activated with HCl, H_3PO_4, H_2SO_4

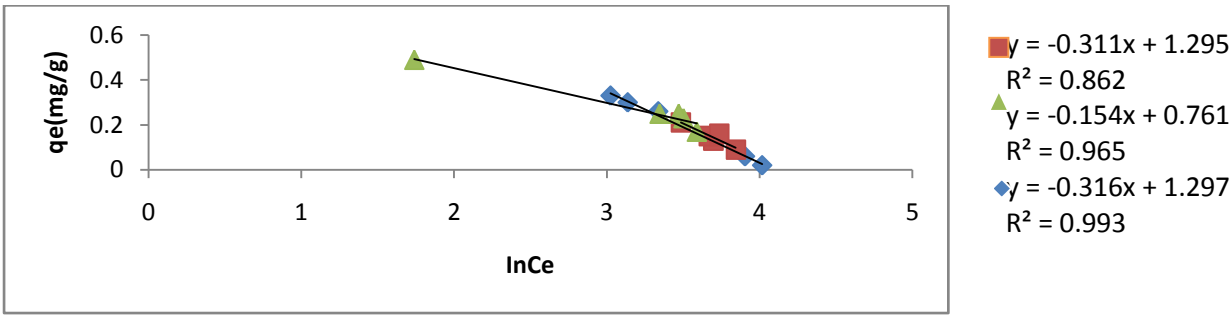

Figure 4.57: Temkin Isotherm plot for Cd onto PNAC Carbonized at 800°C and activated with HCl, H_3PO_4, H_2SO_4

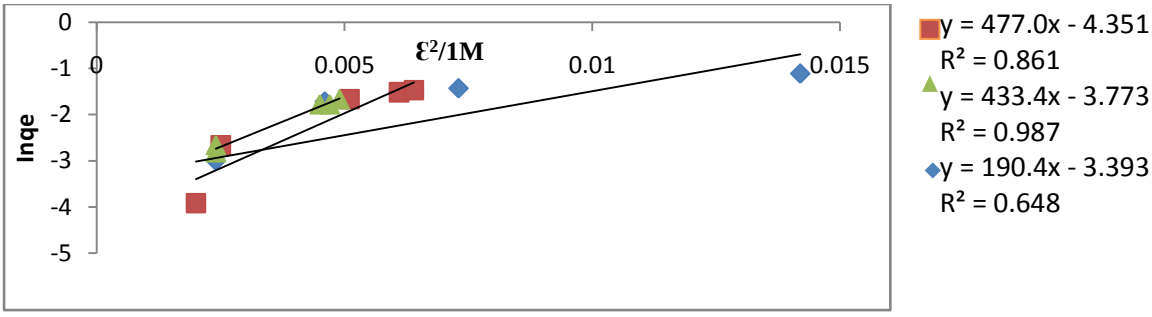

Figure 4.58: Dubinin Rudushkevich Isotherm plot for Cd onto PNAC Carbonized at 600°C and activated with HCl, H_3PO_4, H_2SO_4

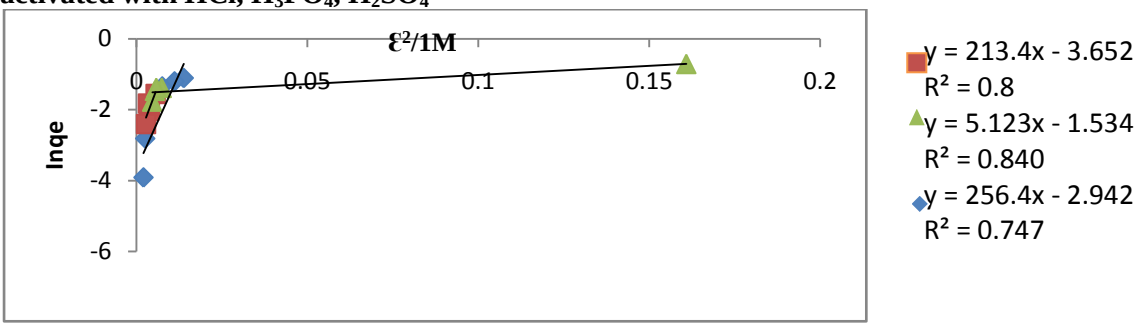

Figure 4.59: Dubinin Rudushkevich Isotherm plot for Cd onto PNAC Carbonized at 800°C & activated with HCl, H_3PO_4, H_2SO_4

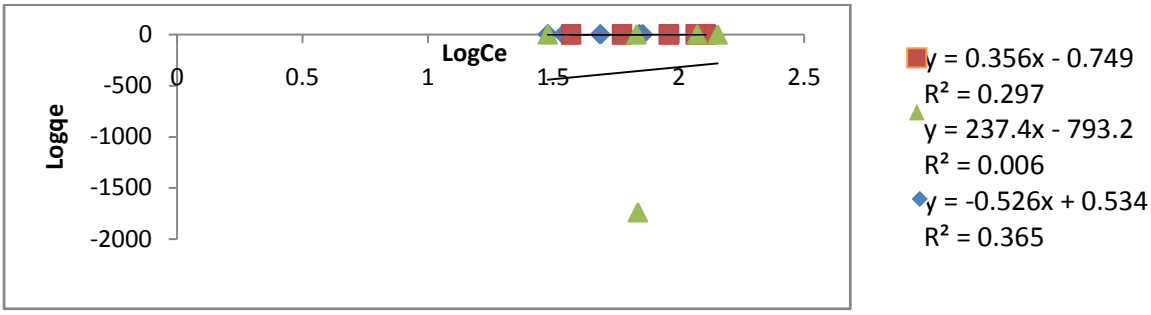

Figure 4.60: Freundlich Isotherm plot for Mn onto PNAC Carbonized at 600°C and activated with HCl, H_3PO_4, H_2SO_4

For the adsorption of Mn onto PNAC for both carbonization temperatures, the data obtained for the plot of the four isotherm models did not fit well as shown by the $R^{2'}$s at both temperatures of carbonization (Figures 4. 60 to 4.67).

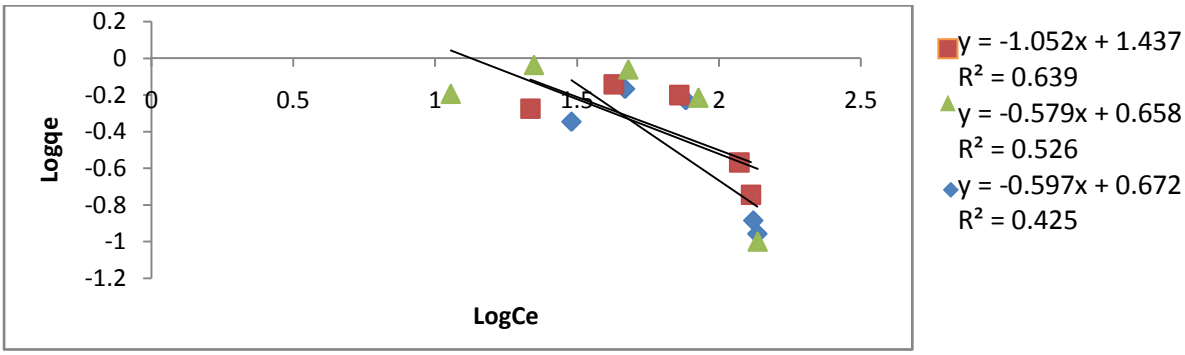

Figure 4.61: Freundlich Isotherm plot for Mn onto PNAC Carbonized at 800°C and activated with HCl, H_3PO_4, H_2SO_4

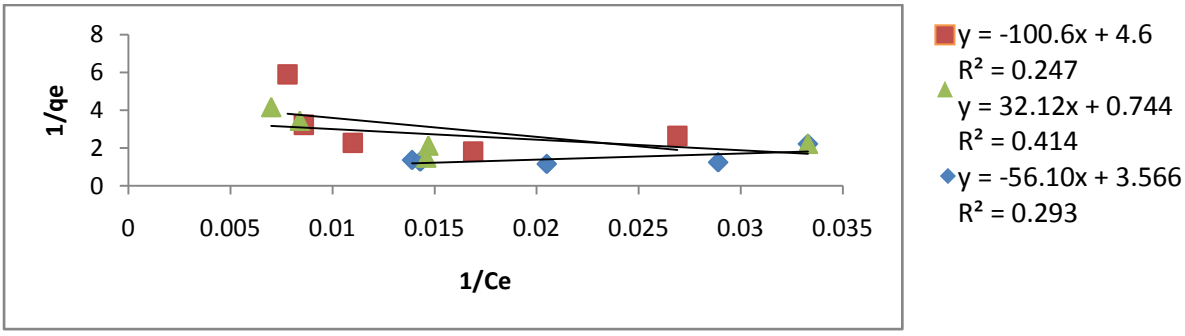

Figure 4.62: Langmuir Isotherm plot for Mn onto PNAC Carbonized at 600°C and activated with HCl, H_3PO_4, H_2SO_4

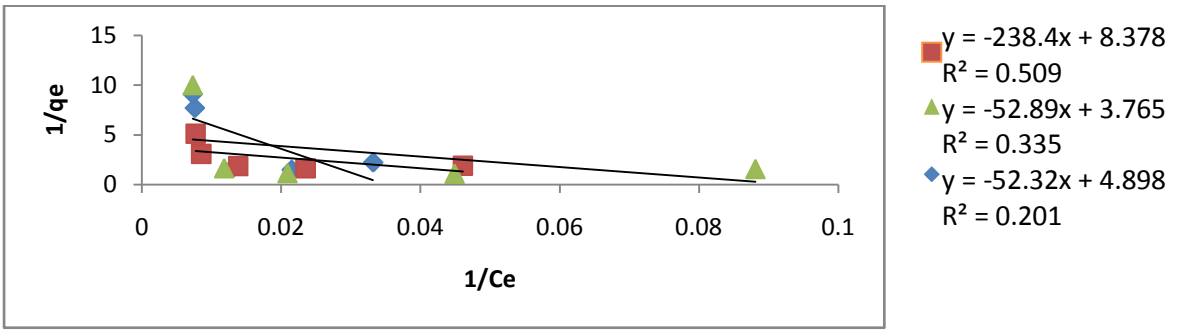

Figure 4.63: Langmuir Isotherm plot for Mn onto PNAC Carbonized at 800°C and activated with HCl, H_3PO_4, H_2SO_4

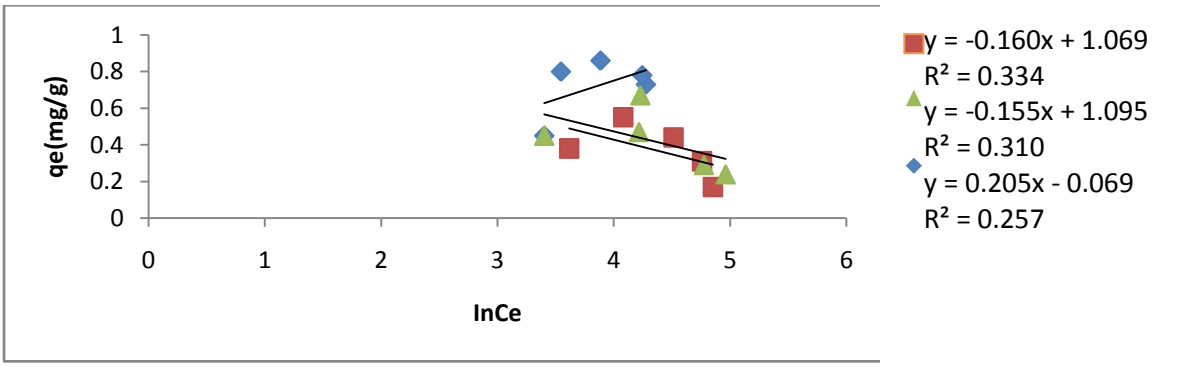

Figure 4.64: Temkin Isotherm plot for Mn onto PNAC Carbonized at 600°C and activated with HCl, H_3PO_4, H_2SO_4

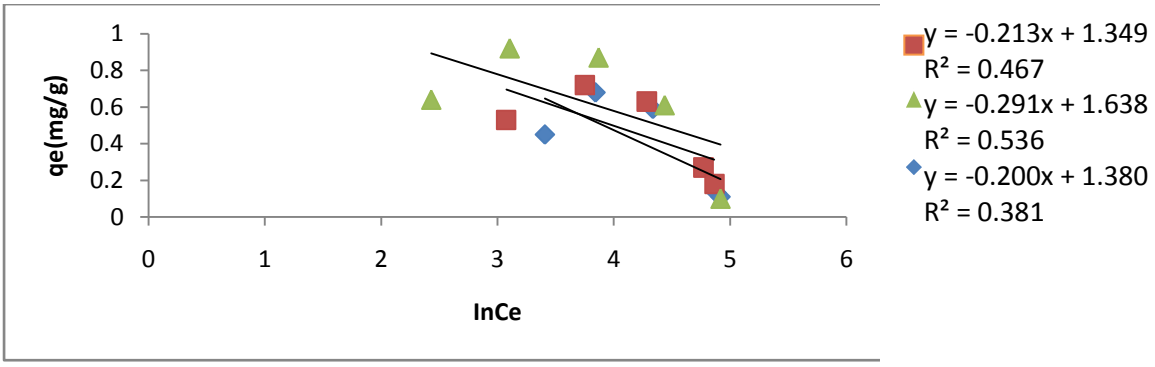

Figure 4.65: Temkin Isotherm plot for Mn onto PNAC Carbonized at 800°C and activated with HCl, H_3PO_4, H_2SO_4

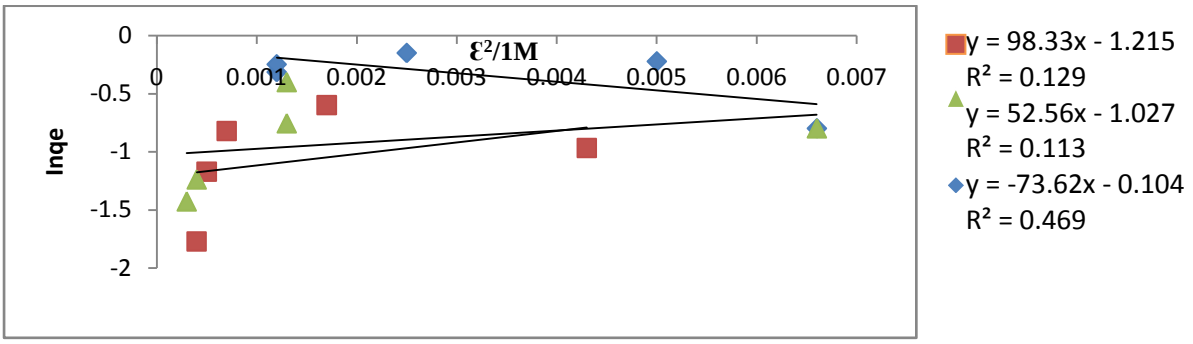

Figure 4.66: Dubinin Rudushkevich Isotherm plot for Mn onto PNAC Carbonized at 600°C and activated with HCl, H_3PO_4, H_2SO_4

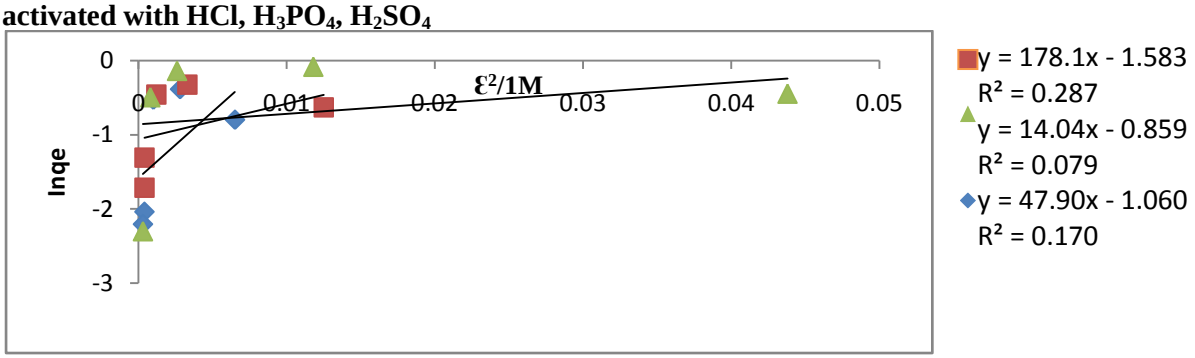

Figure 4.67: Dubinin Rudushkevich Isotherm plot for Mn onto PNAC Carbonized at 800°C and activated with HCl, H_3PO_4, H_2SO_4

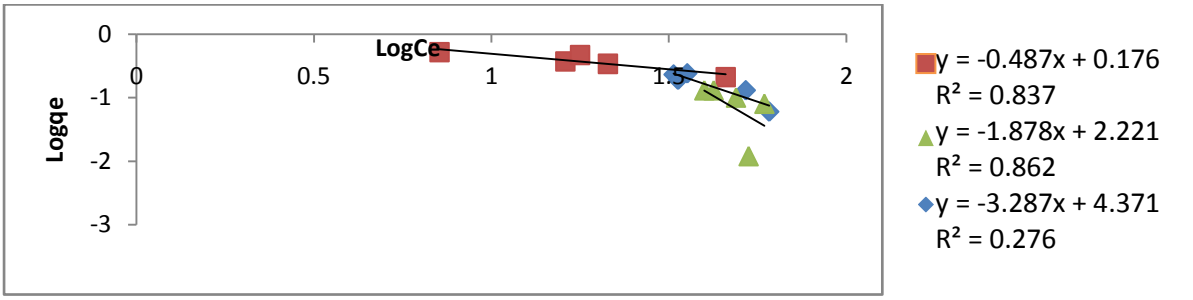

Figure 4.68: Freundlich Isotherm plot for Ni onto PKAC Carbonized at 600°C and activated with HCl, H_3PO_4, H_2SO_4

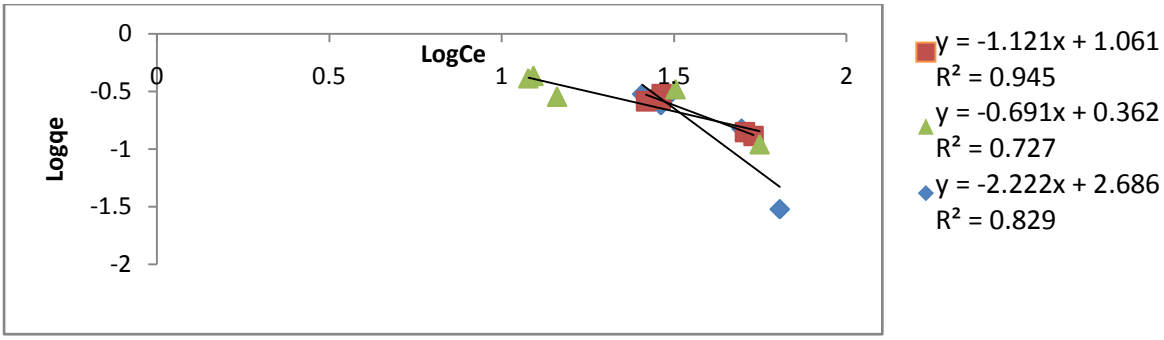

Figure 4.69: Freundlich Isotherm plot for Ni onto PKAC Carbonized at 800°C and activated with HCl, H_3PO_4, H_2SO_4

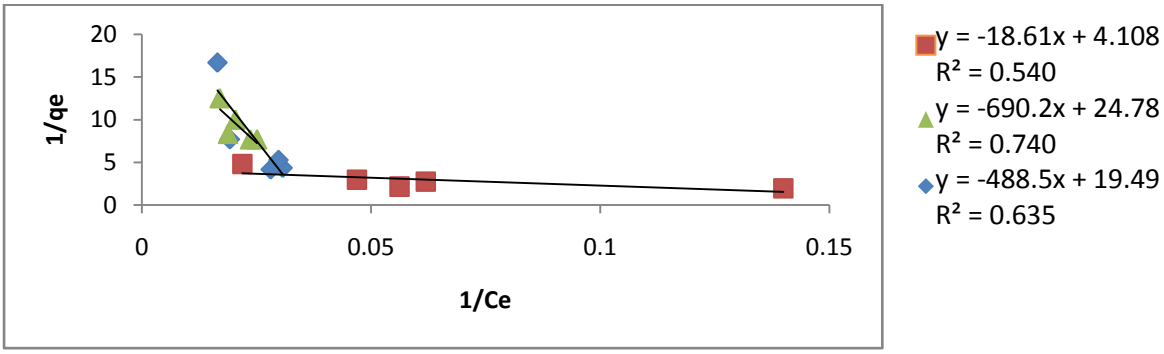

Figure 4.70: Langmuir Isotherm plot for Ni onto PKAC Carbonized at 600°C & activated with HCl, H_3PO_4, H_2SO_4

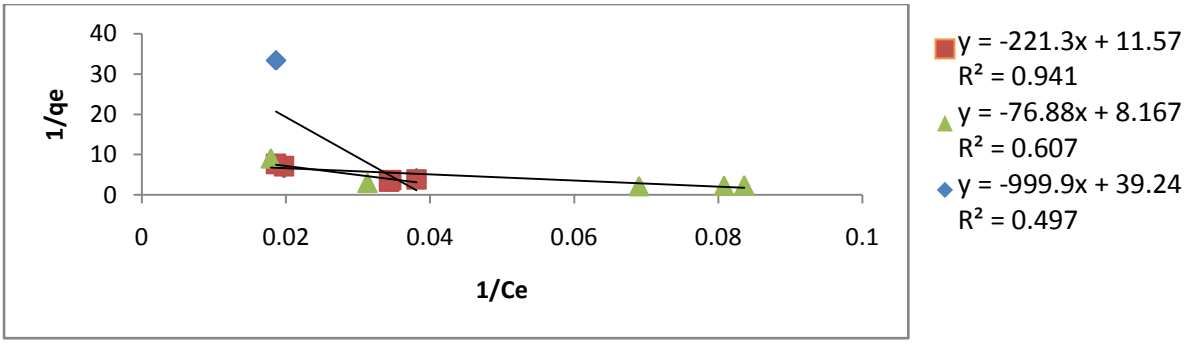

Figure 4.71: Langmuir Isotherm plot for Ni onto PKAC Carbonized at 800°C and activated with HCl, H_3PO_4, H_2SO_4

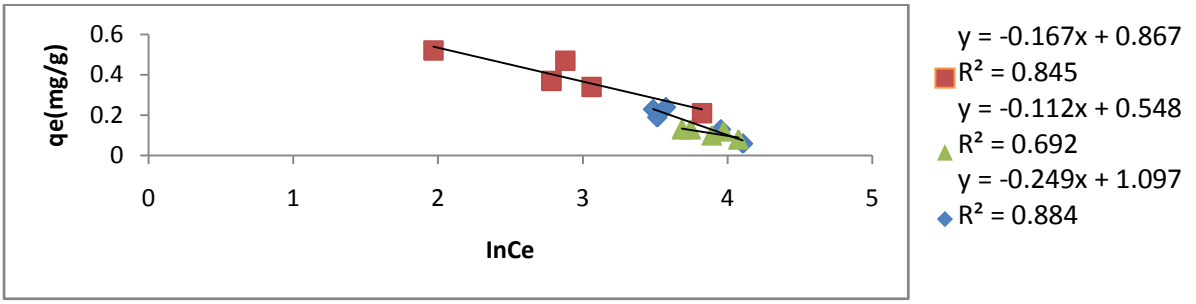

Figure 4.72: Temkin Isotherm plot for Ni onto PKAC Carbonized at 600°C and activated with HCl, H_3PO_4, H_2SO_4

The determination coefficients for the adsorption of Ni onto PKAC were generally high indicating a good fit of the adsorption data on the Temkin isotherm model (Figures 4.72 and 4.73). A similar result was also obtained for Pb and Cd. For Mn adsorption, the R^2 values were all very low indicating a poor fit of the data onto the model except for that carbonized at 600°C and activated with HCl.

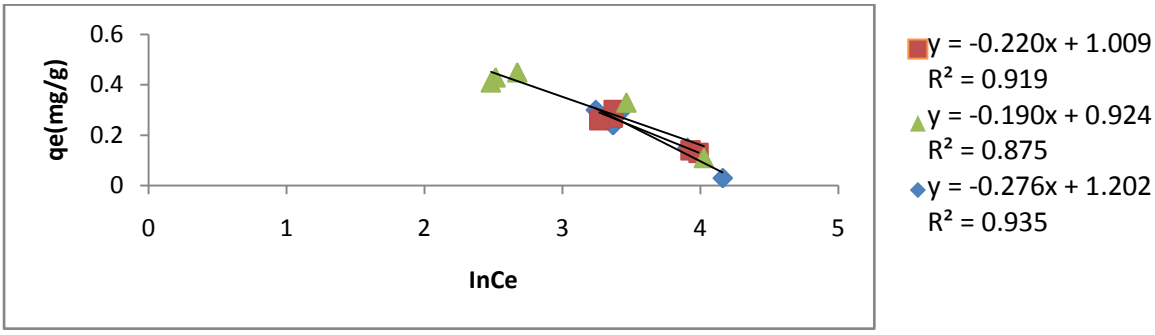

Figure 4.73: Temkin Isotherm plot for Ni onto PKAC Carbonized at 800°C and activated with HCl, H_3PO_4, H_2SO_4

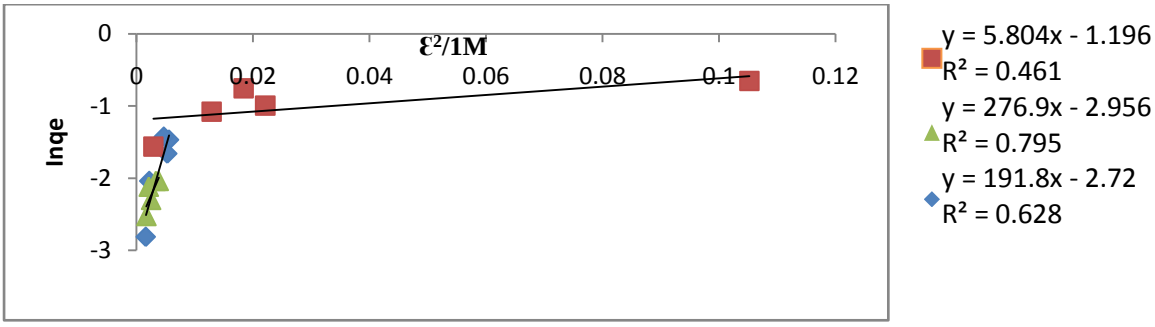

Figure 4.74: Dubinin Rudushkevich Isotherm plot for Ni onto PKAC Carbonized at 600°C and activated with HCl, H_3PO_4, H_2SO_4

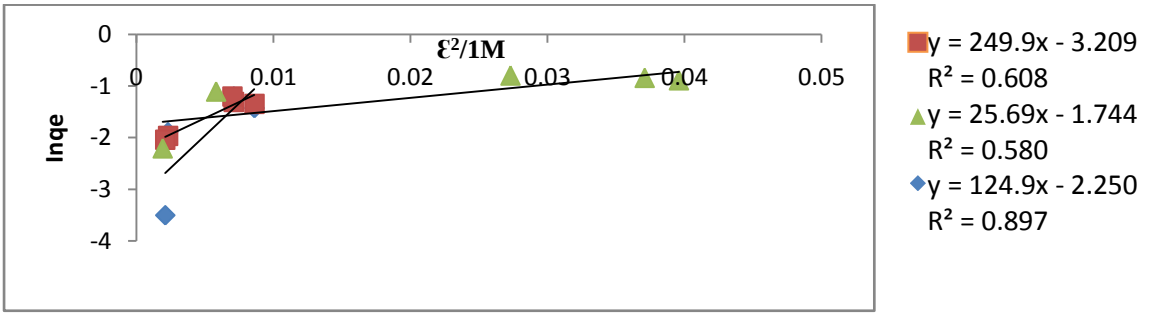

Figure 4.75: Dubinin Rudushkevich Isotherm plot for Ni onto PKAC Carbonized at 800°C and activated with HCl, H_3PO_4, H_2SO_4

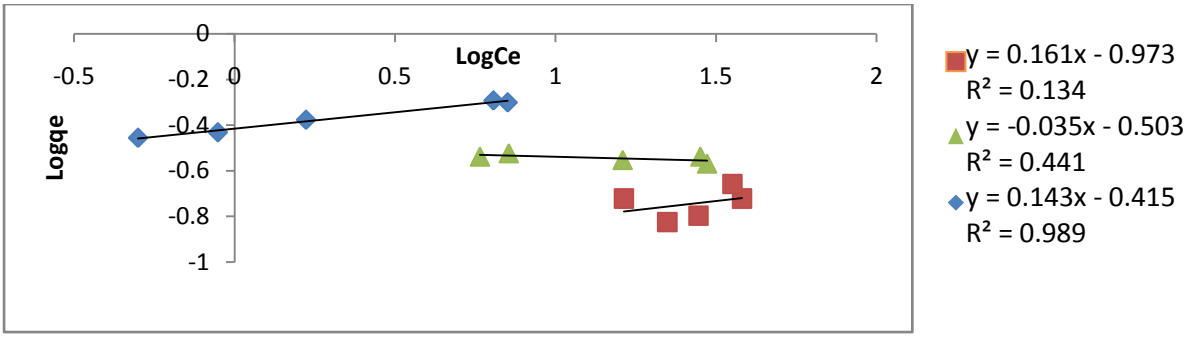

Figure 4.76: Freundlich Isotherm plot for Pb onto PKAC Carbonized at 600°C and activated with HCl, H_3PO_4, H_2SO_4

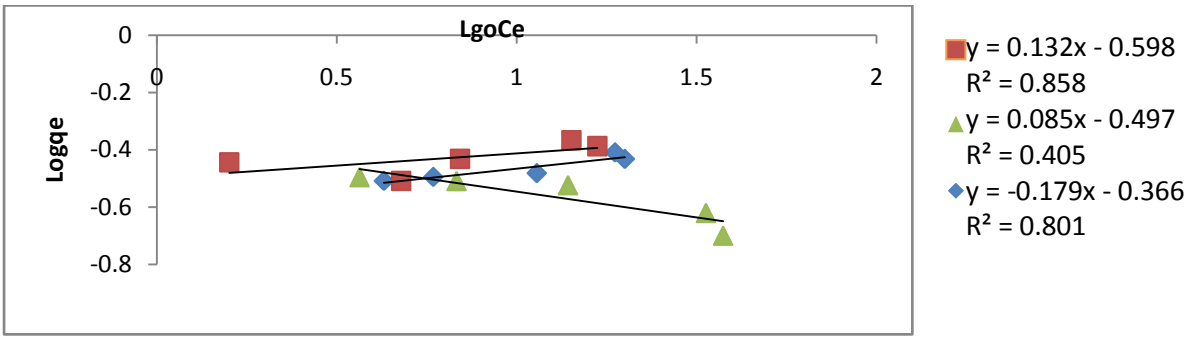

Figure 4.77: Freundlich Isotherm plot for Pb onto PKAC Carbonized at 800°C and activated with HCl, H_3PO_4, H_2SO_4

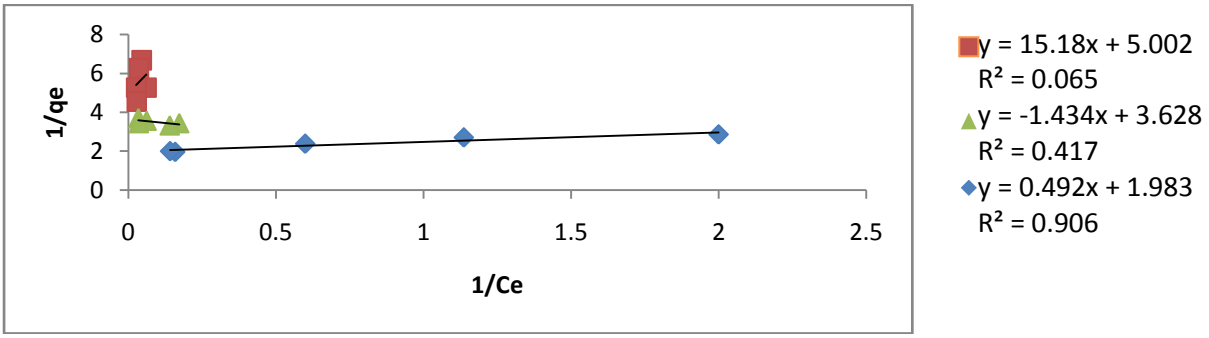

Figure 4.78: Langmuir Isotherm plot for Pb onto PKAC Carbonized at 600°C and activated with HCl, H_3PO_4, H_2SO_4

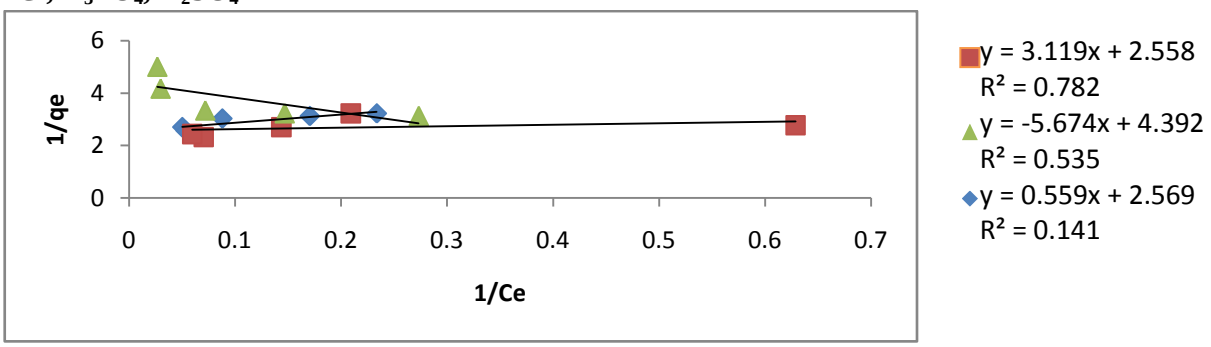

Figure 4.79: Langmuir Isotherm plot for Pb onto PKAC Carbonized at 800°C and activated with HCl, H_3PO_4, H_2SO_4

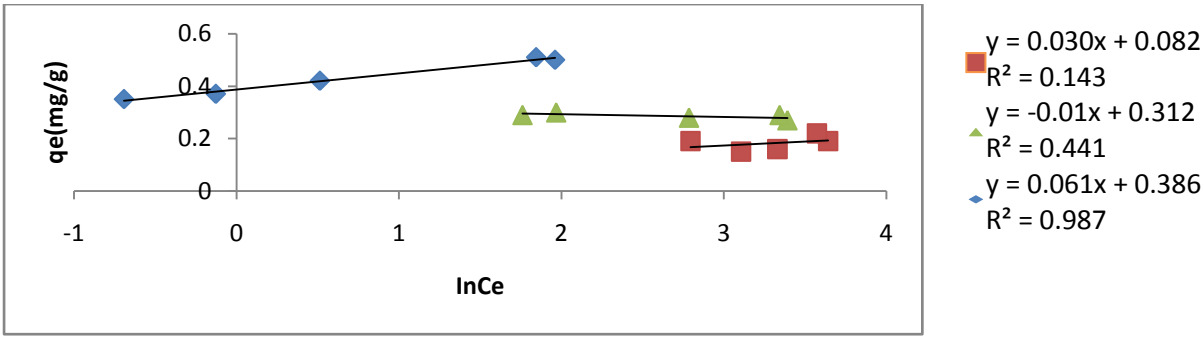

Figure 4.80: Temkin Isotherm plot for Pb onto PKAC Carbonized at 600°C and activated with HCl, H_3PO_4, H_2SO_4

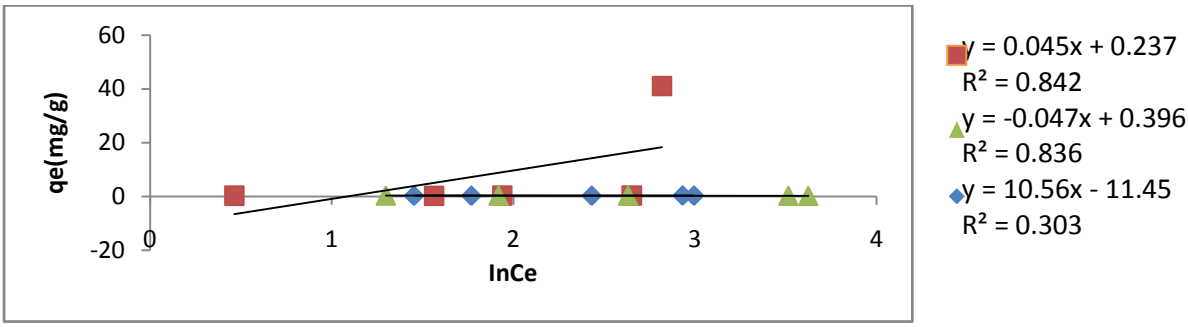

Figure 4.81: Temkin Isotherm plot for Pb onto PKAC Carbonized at 800°C and activated with HCl, H_3PO_4, H_2SO_4

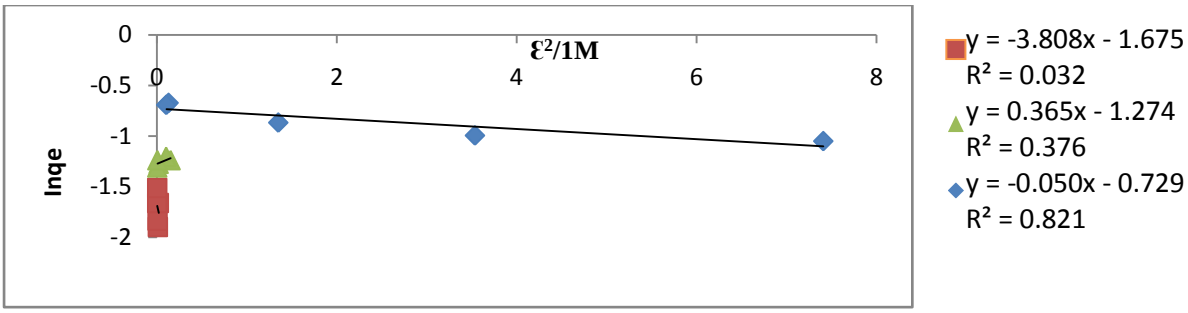

Figure 4.82: Dubinin Rudushkevich Isotherm plot for Pb onto PKAC Carbonized at 600°C and activated with HCl, H_3PO_4, H_2SO_4

The adsorption data for Ni, Pb, Mn and Cd onto PKAC, generally did not followed the Dubinin Rudushkevich isotherm model having had relatively Low determination coefficient values in almost all the adsorption plots (Figures 4.73, 4.74, 4.81, 4.82, 4.89, 4.90).

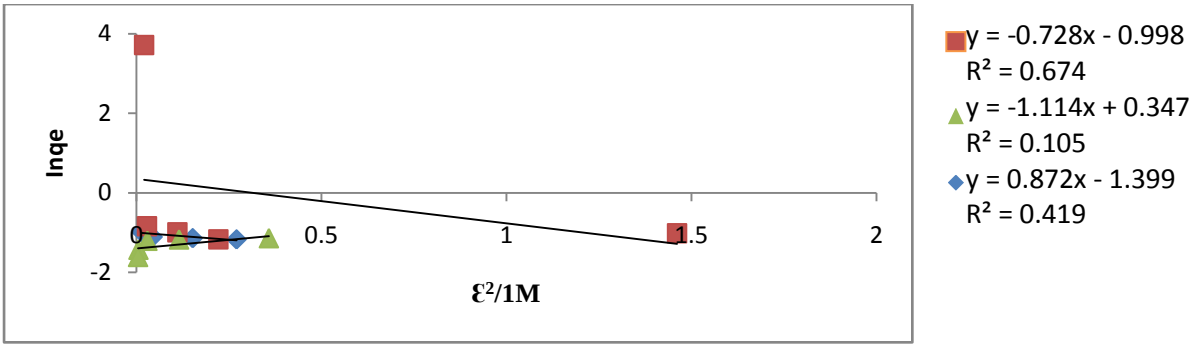

Figure 4.83: Dubinin Rudushkevich Isotherm plot for Pb onto PKAC Carbonized at 800°C and activated with HCl, H_3PO_4, H_2SO_4

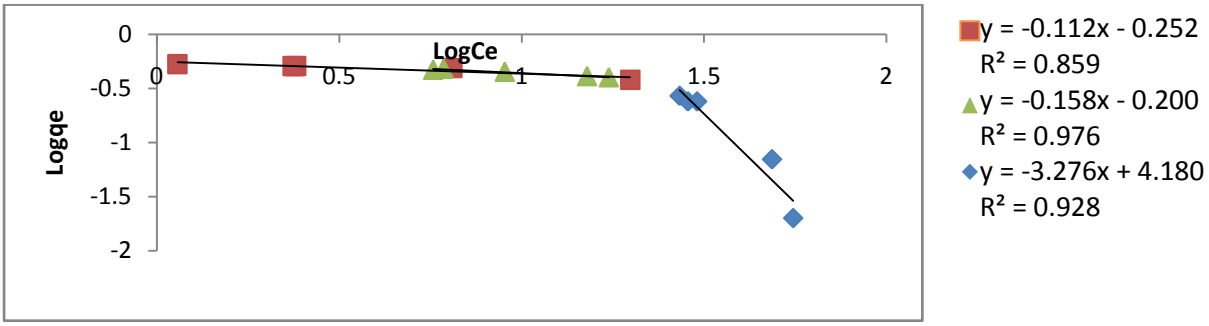

Figure 4.84: Freundlich Isotherm plot for Cd onto PKAC Carbonized at 600°C and activated with HCl, H_3PO_4, H_2SO_4

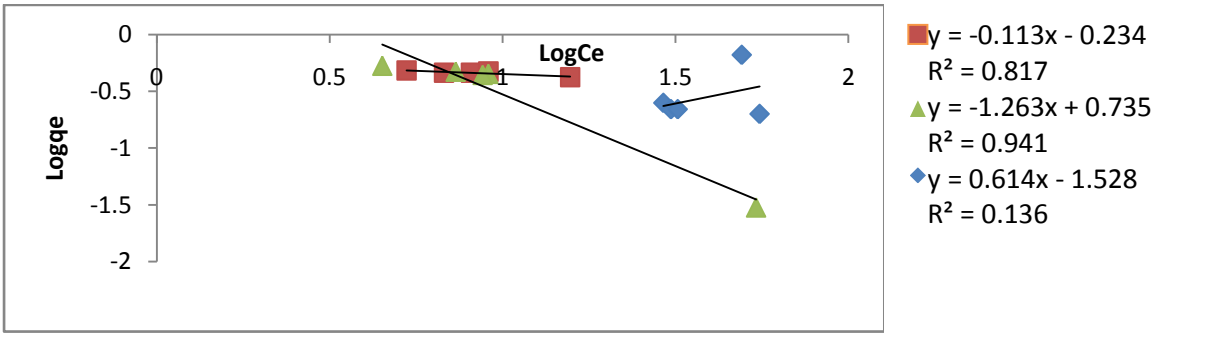

Figure 4.85: Freundlich Isotherm plot for Cd onto PKAC Carbonized at 800°C and activated with HCl, H_3PO_4, H_2SO_4

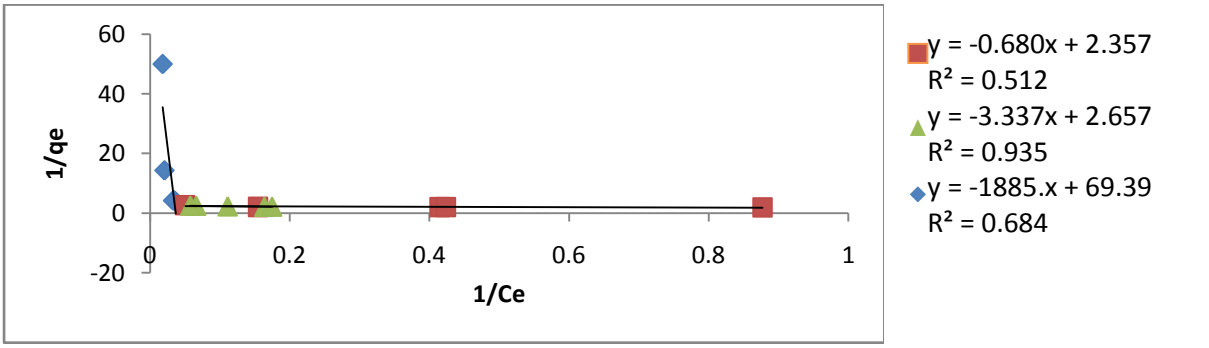

Figure 4.86: Langmuir Isotherm plot for Cd onto PKAC Carbonized at 600°C and activated with HCl, H_3PO_4, H_2SO_4

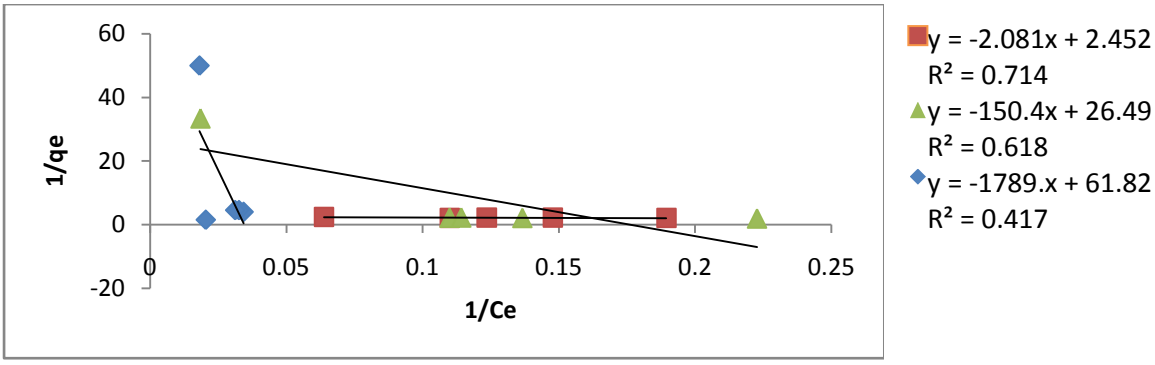

Figure 4.87: Langmuir Isotherm plot for Cd onto PKAC Carbonized at 800°C and activated with HCl, H_3PO_4, H_2SO_4

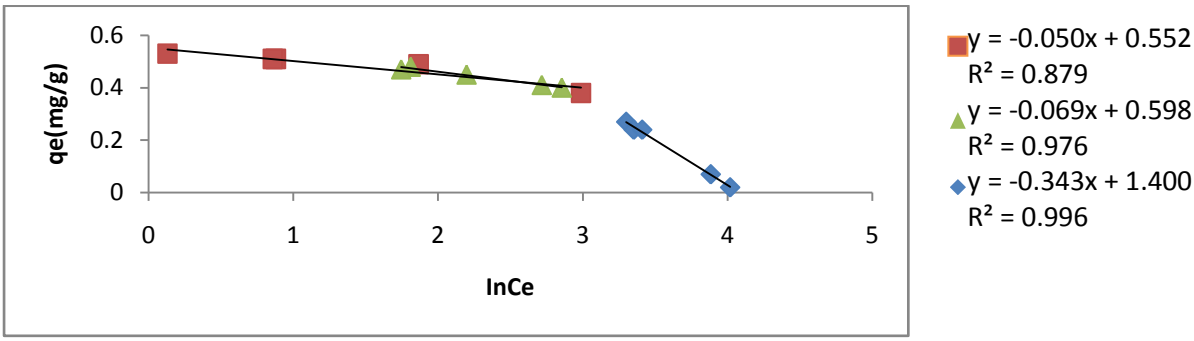

Figure 4.88: Temkin Isotherm plot for Cd onto PKAC Carbonized at 600°C and activated with HCl, H_3PO_4, H_2SO_4

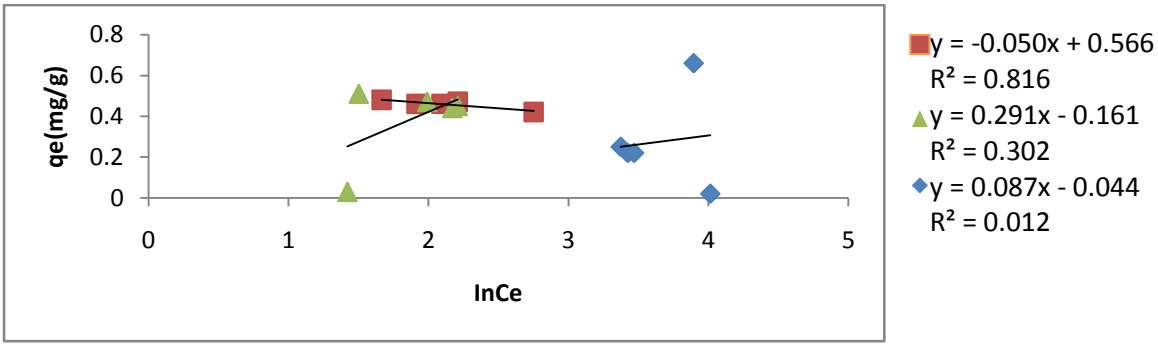

Figure 4.89: Temkin Isotherm plot for Cd onto PKAC Carbonized at 800°C and activated with HCl, H_3PO_4, H_2SO_4

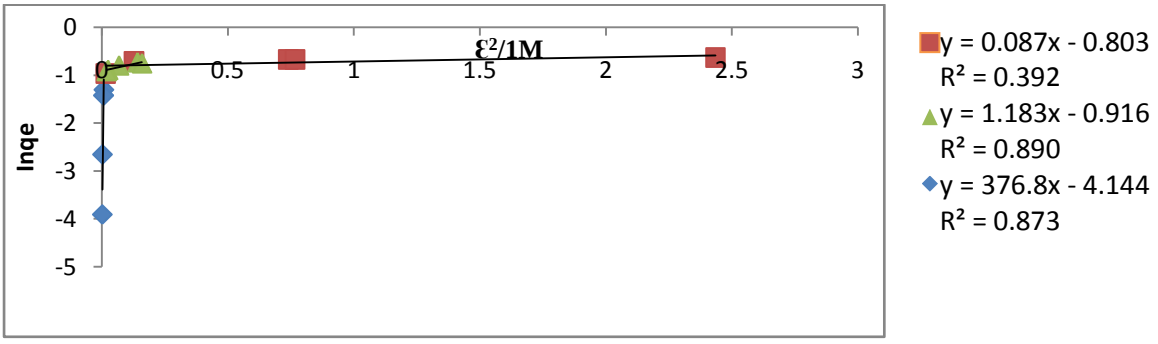

Figure 4.90: Dubinin Rudushkevich Isotherm plot for Cd onto PKAC Carbonized at 600°C and activated with HCl, H_3PO_4, H_2SO_4

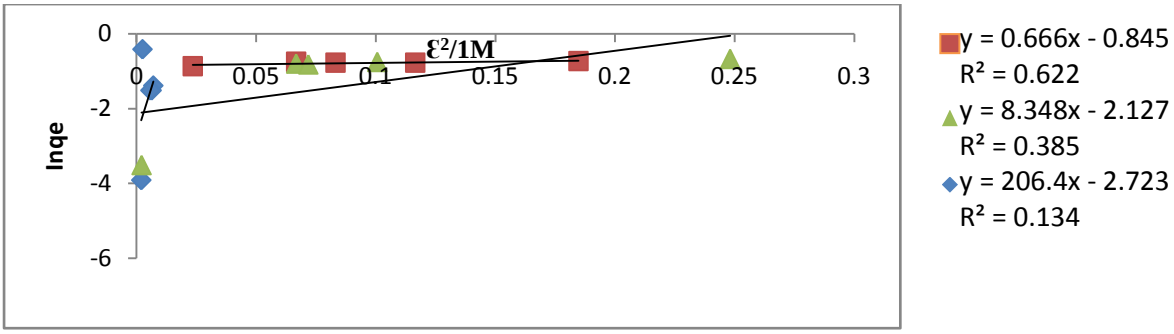

Figure 4.91: Dubinin Rudushkevich Isotherm plot for Cd onto PKAC Carbonized at 800°C and activated with HCl, H_3PO_4, H_2SO_4

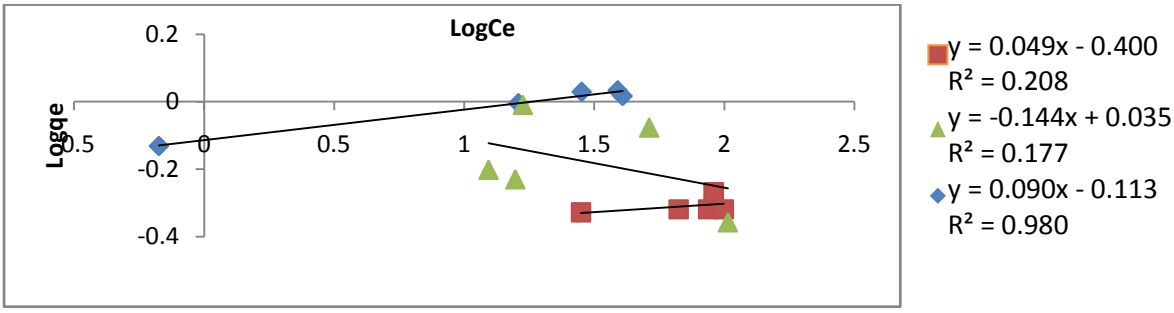

Figure 4.92: Freundlich Isotherm plot for Mn onto PKAC Carbonized at 600°C and activated with HCl, H_3PO_4, H_2SO_4

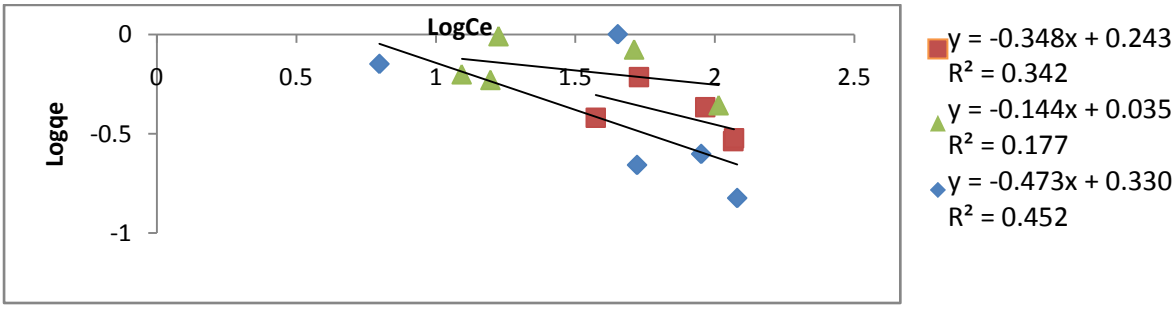

Figure 4.93: Freundlich Isotherm plot for Mn onto PKAC Carbonized at 600°C and activated with HCl, H_3PO_4, H_2SO_4

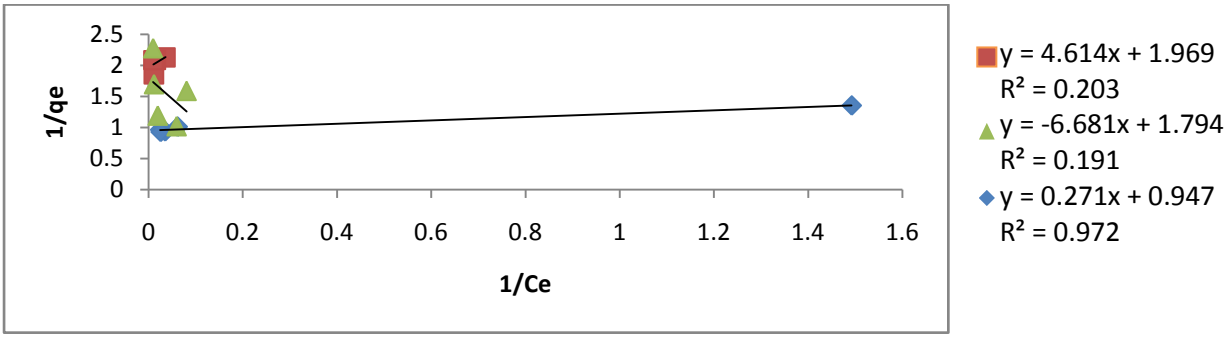

Figure 4.94: Langmuir Isotherm plot for Mn onto PKAC Carbonized at 600°C and activated with HCl, H_3PO_4, H_2SO_4

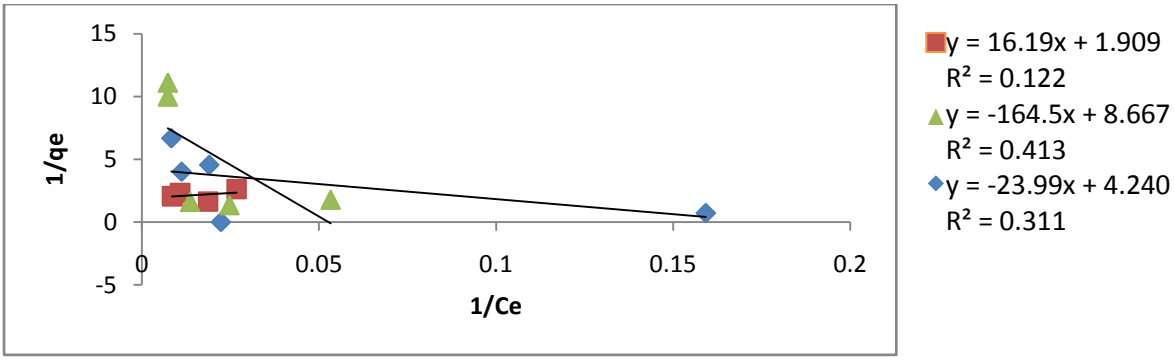

Figure 4.95: Langmuir Isotherm plot for Mn onto PKAC Carbonized at 800°C and activated with HCl, H_3PO_4, H_2SO

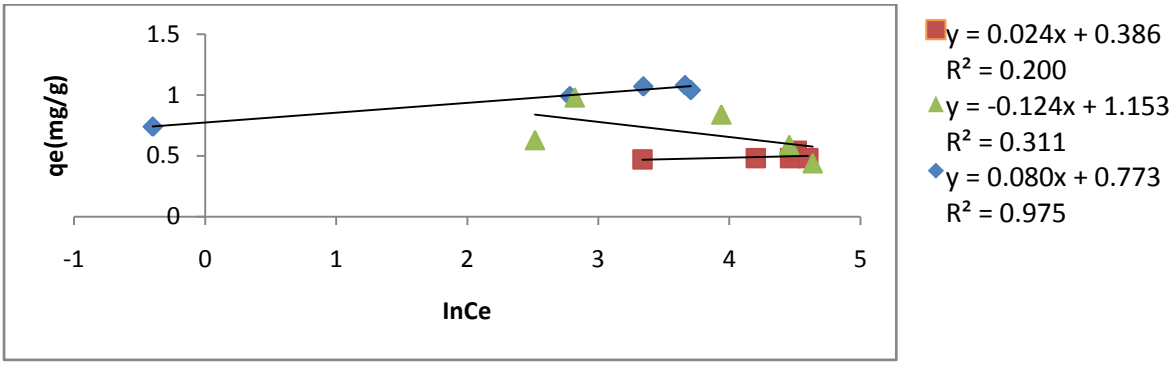

Figure 4.96: Temkin Isotherm plot for Mn onto PKAC Carbonized at 600°C and activated with HCl, H_3PO_4, H_2SO_4

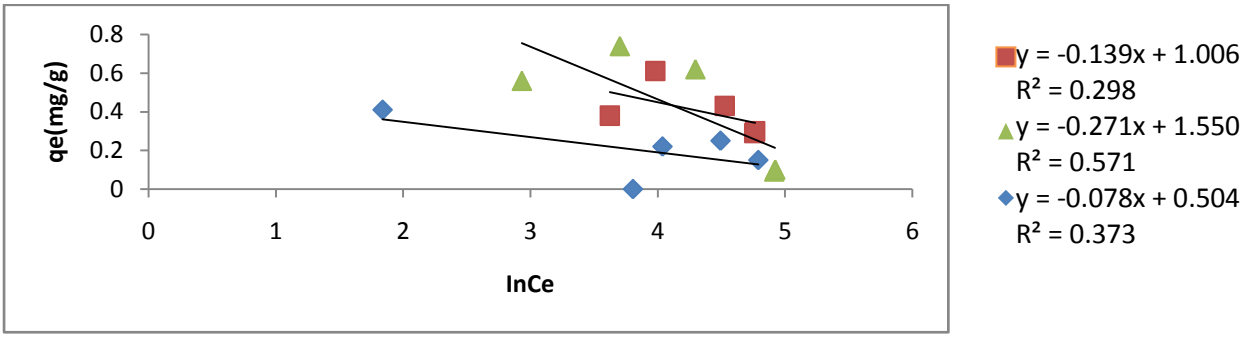

Figure 4.97: Temkin Isotherm plot for Mn onto PKAC Carbonized at 800°C & activated with HCl, H_3PO_4, H_2SO_4

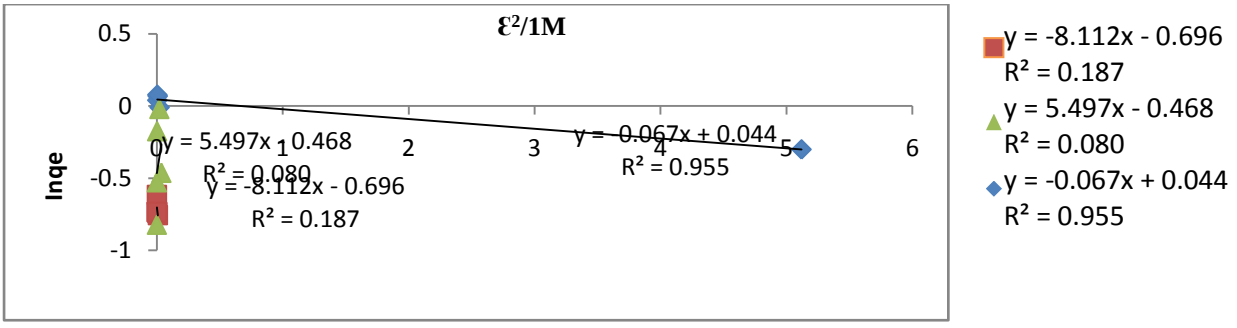

Figure 4.98: Dubinin Rudushkevich Isotherm plot for Mn onto PKAC Carbonized at 600°C and activated with HCl, H_3PO_4, H_2SO_4

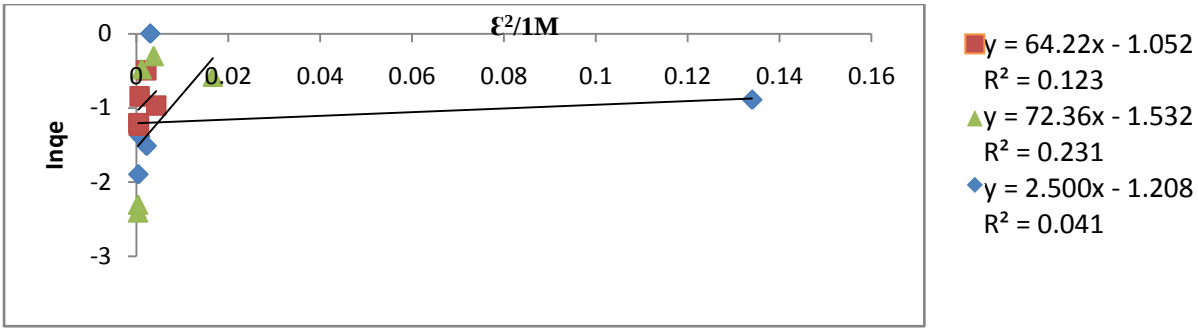

Figure 4.99: Dubinin Rudushkevich Isotherm plot for Mn onto PKAC Carbonized at 800°C and activated with HCl, H_3PO_4, H_2SO_4

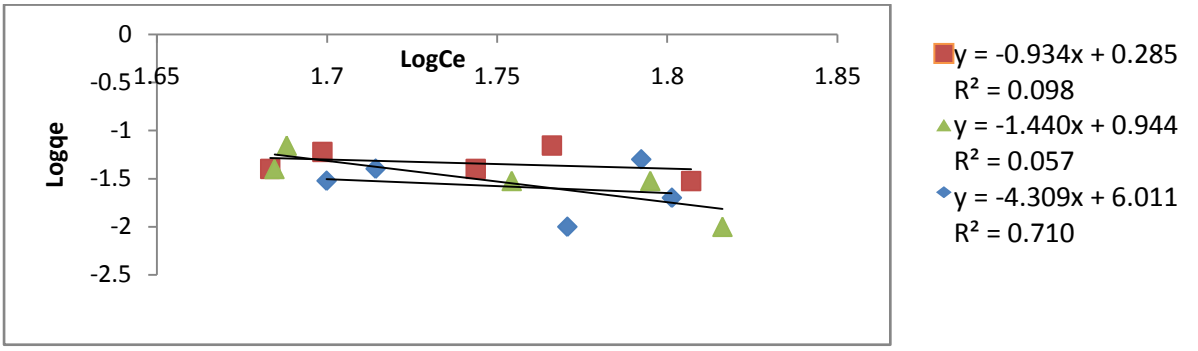

Figure 4.100: Freundlich Isotherm plot for Ni onto SSAC Carbonized at 600°C and activated with HCl, H_3PO_4, H_2SO_4

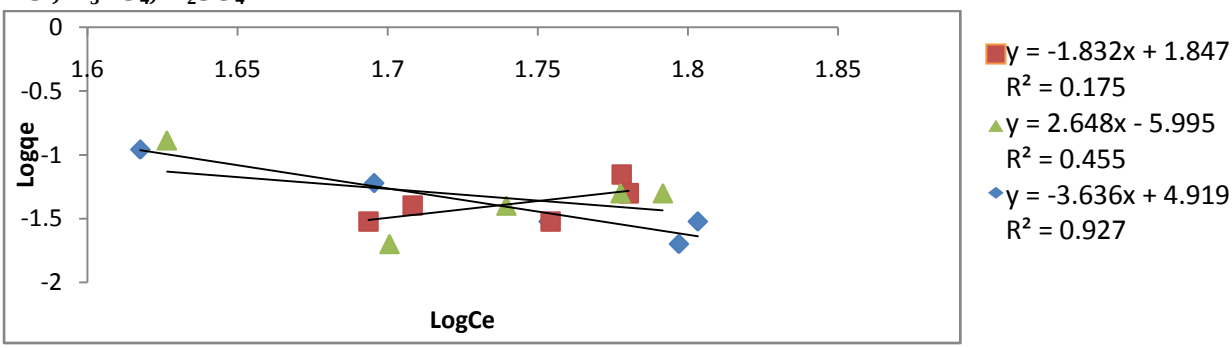

Figure 4.101: Freundlich Isotherm plot for Ni onto SSAC Carbonized at 800°C and activated with HCl, H_3PO_4, H_2SO_4

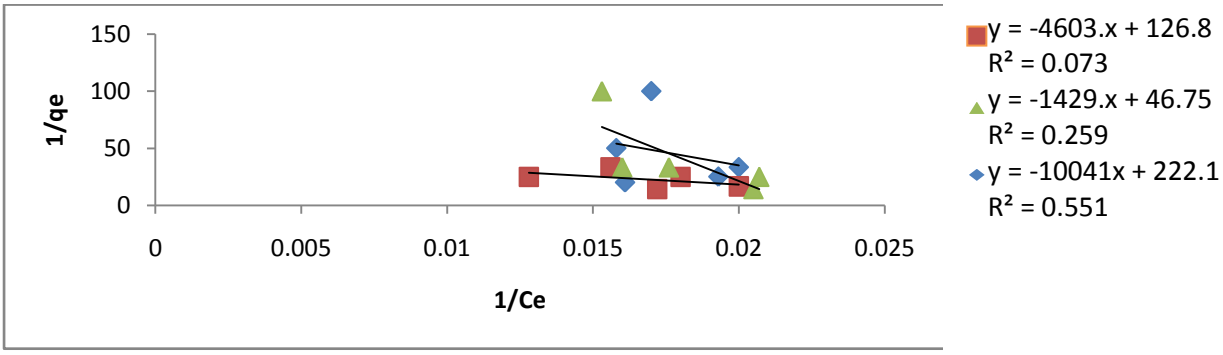

Figure 4.102: Langmuir Isotherm plot for Ni onto SSAC Carbonized at 600°C and activated with HCl, H_3PO_4, H_2SO_4

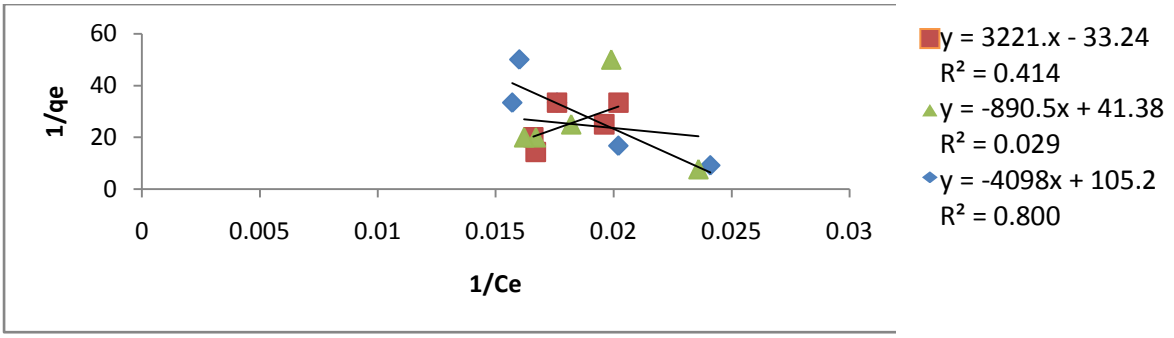

Figure 4.103: Langmuir Isotherm plot for Ni onto SSAC Carbonized at 800°C and activated with HCl, H_3PO_4, H_2SO_4

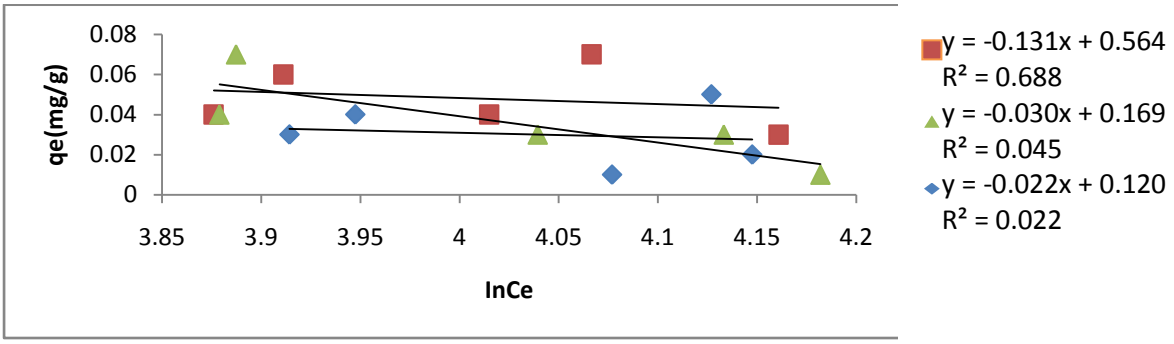

Figure 4.104: Temkin Isotherm plot for Ni onto SSAC Carbonized at 600°C and activated with HCl, H_3PO_4, H_2SO_4

The Temkin model was not suitable to describe the data obtained from the adsorption of all the metals under consideration as indicated by the poor fit of the determination coefficients (Figures 4. 102, 4.103, 4.109, 4.110, 4.117, 4.118).

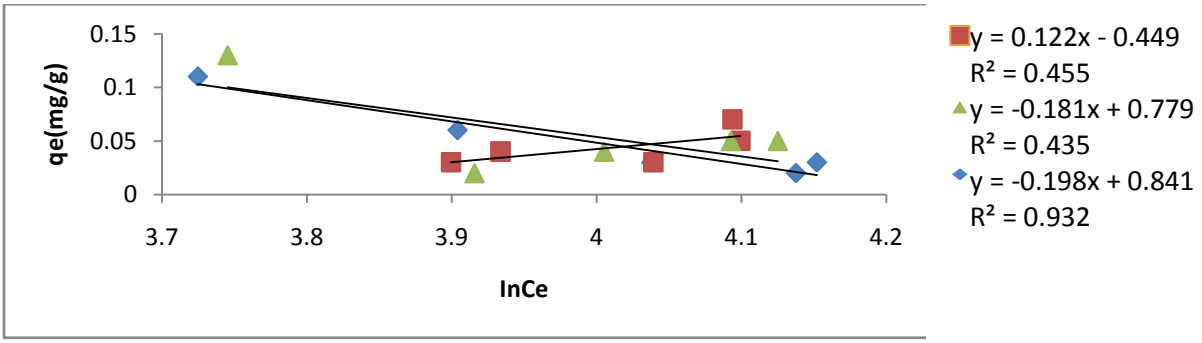

Figure 4.105: Temkin Isotherm plot for Ni onto SSAC Carbonized at 800°C and activated with HCl, H_3PO_4, H_2SO_4

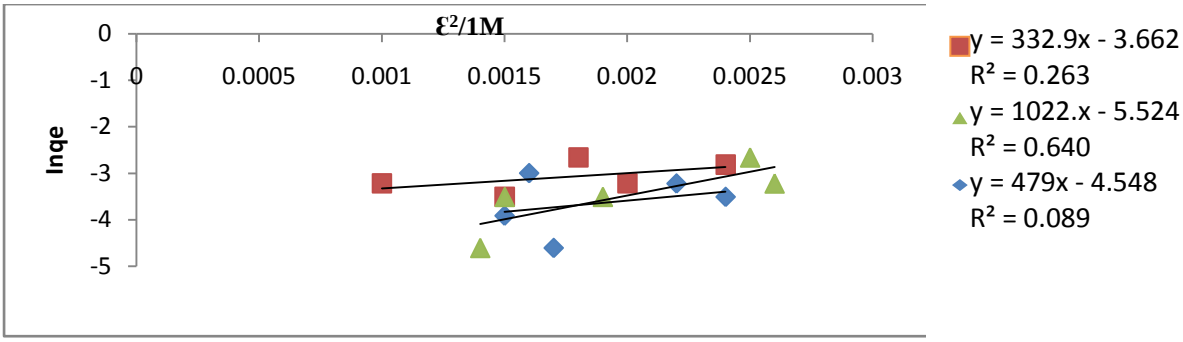

Figure 4.106: Dubinin Rudushkevich Isotherm plot for Ni onto SSAC Carbonized at 600°C and activated with HCl, H_3PO_4, H_2SO_4

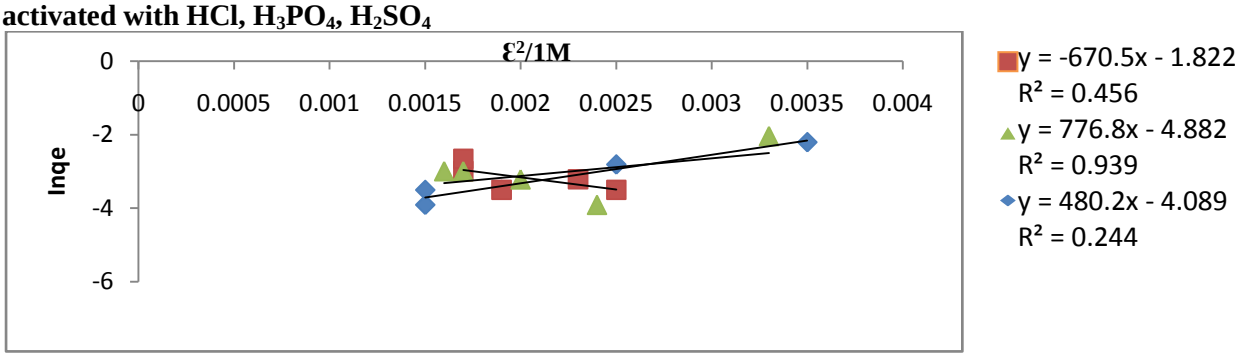

Figure 4.107: Dubinin Rudushkevich Isotherm plot for Ni onto SSAC Carbonized at 800°C and activated with HCl, H_3PO_4, H_2SO_4

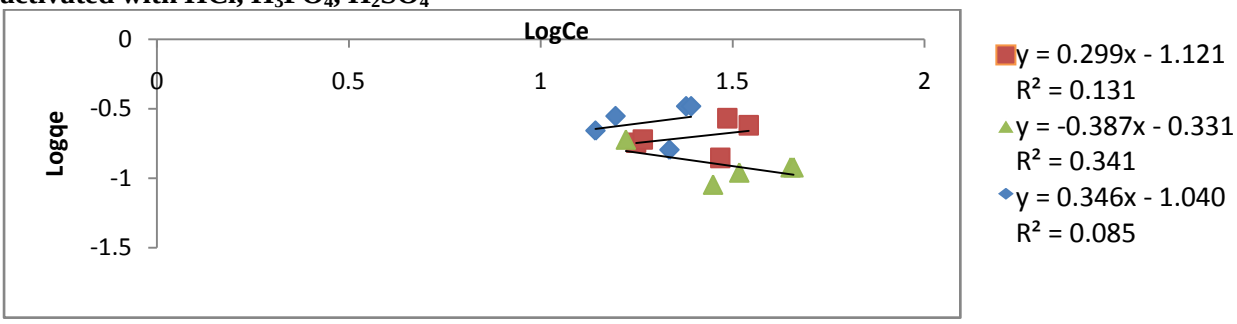

Figure 4.108: Freundlich Isotherm plot for Pb onto SSAC Carbonized at 600°C and activated with HCl, H_3PO_4, H_2SO_4

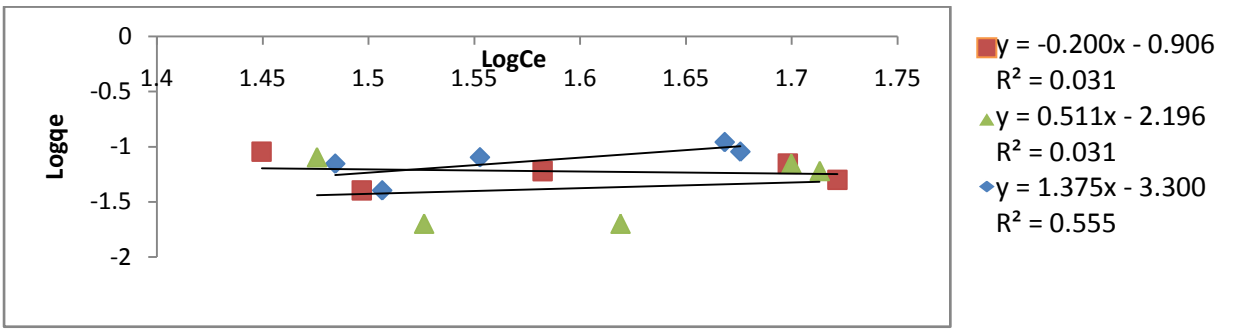

Figure 4.109: Freundlich Isotherm plot for Pb onto SSAC Carbonized at 800°C and activated with HCl, H_3PO_4, H_2SO_4

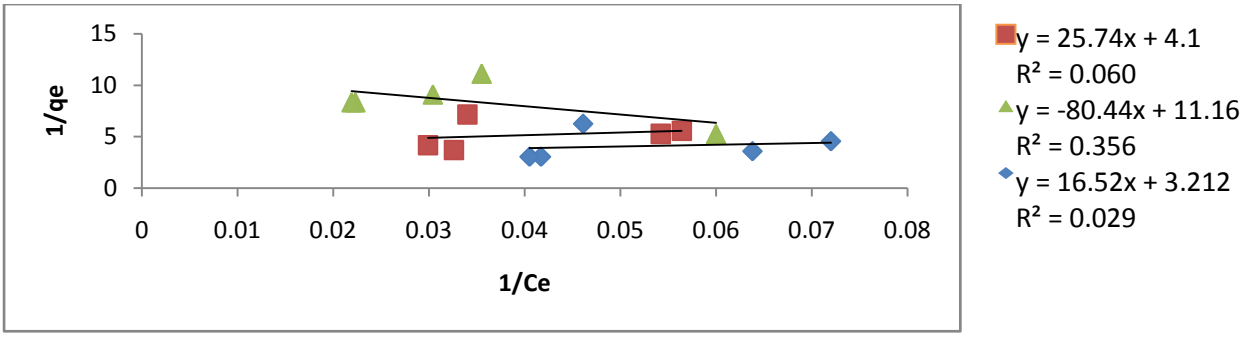

Figure 4.110: Langmuir Isotherm plot for Pb onto SSAC Carbonized at 600°C and activated with HCl, H_3PO_4, H_2SO_4

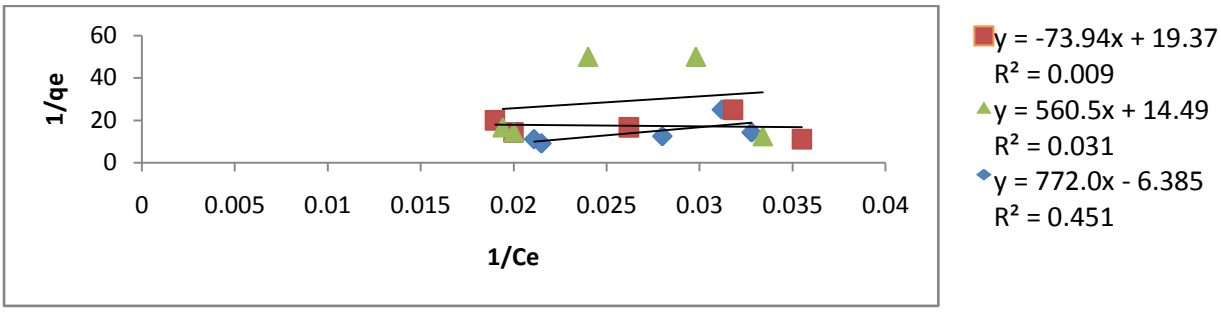

Figure 4.111: Langmuir Isotherm plot for Pb onto SSAC Carbonized at 800°C and activated with HCl, H_3PO_4, H_2SO_4

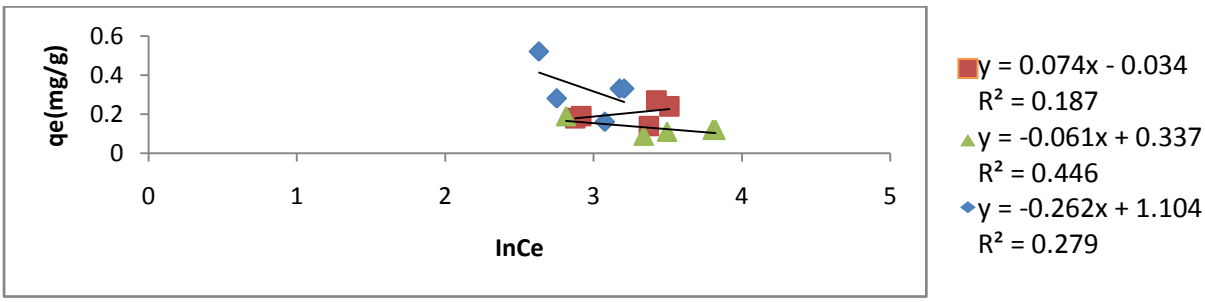

Figure 4.112: Temkin Isotherm plot for Pb onto SSAC Carbonized at 600°C and activated with HCl, H_3PO_4, H_2SO_4

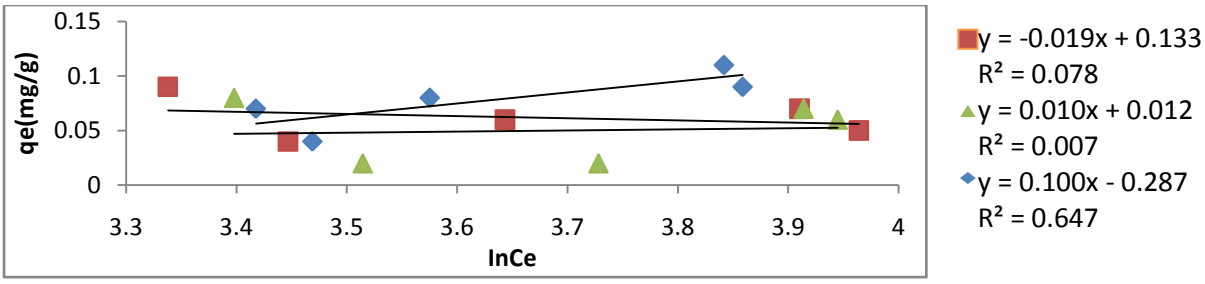

Figure 4.113: Temkin Isotherm plot for Pb onto SSAC Carbonized at 800°C
H_3PO_4, H_2SO_4

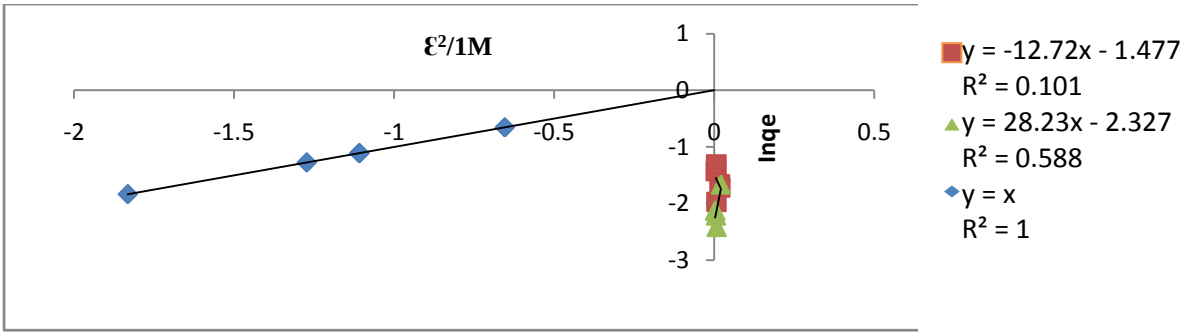

Figure 4.114: Dubinin Rudushkevich Isotherm plot for Pb onto SSAC Carbonized at 600°C and activated with HCl, H_3PO_4, H_2SO_4

The Dubinin Rudushkevich Isotherm model also was not suitable to describe the data obtained from the adsorption of Ni, Pb, Cd, and Mn as indicated by the low values of the determination coefficients (Figures 4. 104, 4.105, 4.111, 4.112, 4.119, 4.120).

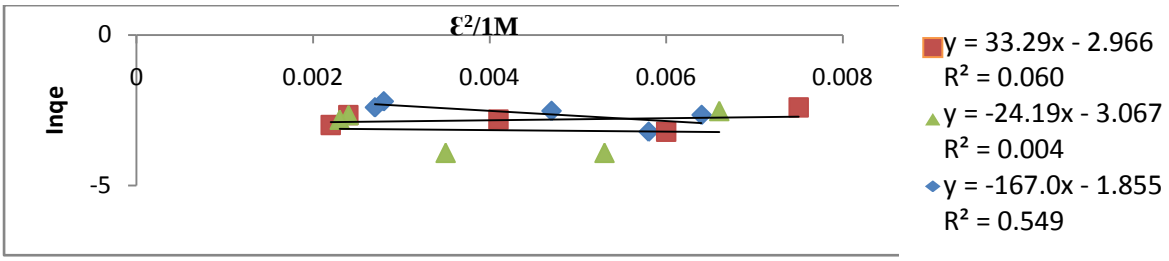

Figure 4.115: Dubinin Rudushkevich Isotherm plot for Pb onto SSAC Carbonized at 800°C and activated with HCl, H_3PO_4, H_2SO_4

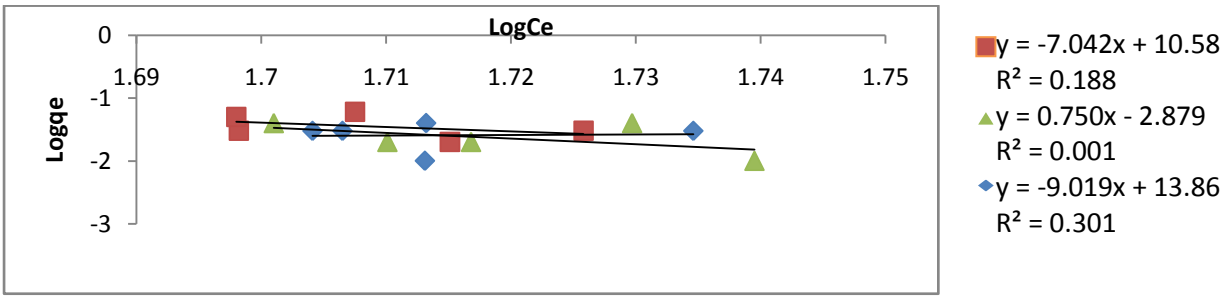

Figure 4.116: Freundlich Isotherm plot for Cd onto SSAC Carbonized at 600°C and activated with HCl, H_3PO_4, H_2SO_4

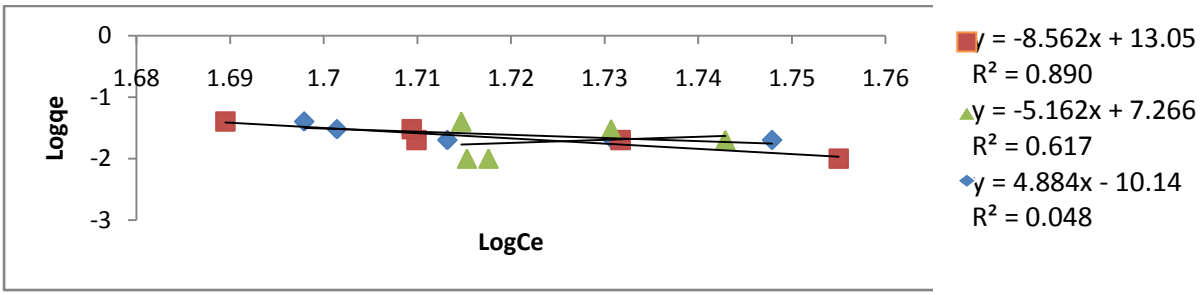

Figure 4.117: Freundlich Isotherm plot for Cd onto SSAC Carbonized at 800°C and activated with HCl, H_3PO_4, H_2SO_4

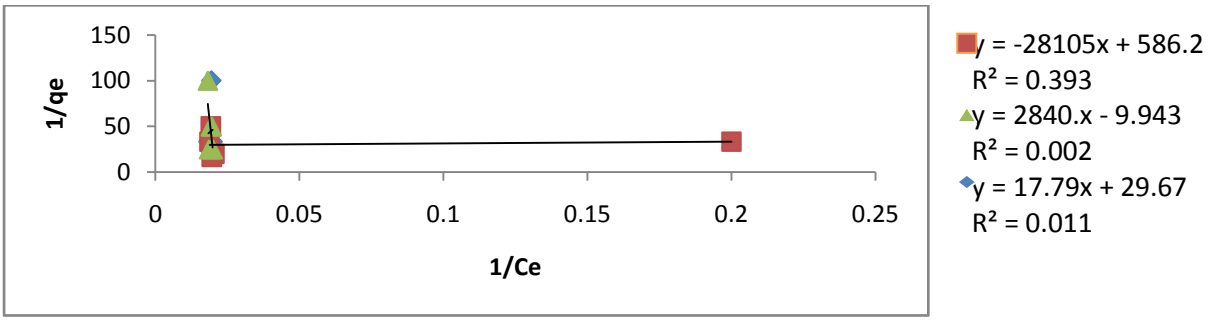

Figure 4.118: Langmuir Isotherm plot for Cd onto SSAC Carbonized at 600°C and activated with HCl, H_3PO_4, H_2SO_4

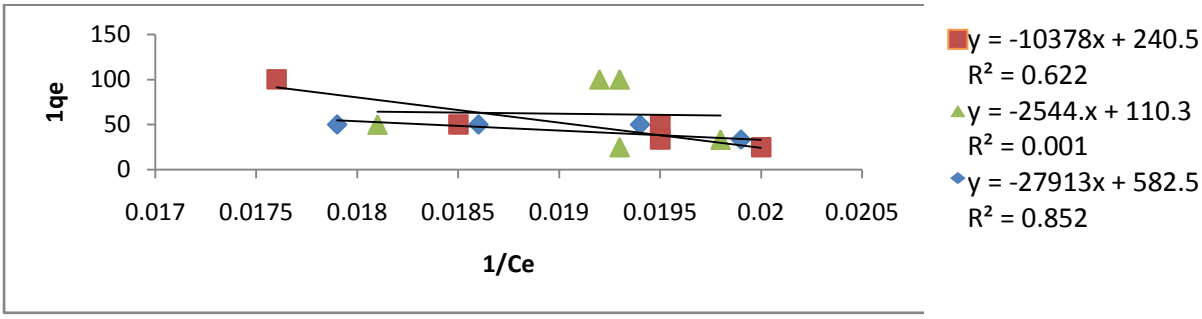

Figure 4.119: Langmuir Isotherm plot for Cd onto SSAC Carbonized at 800°C and activated with HCl, H_3PO_4, H_2SO_4

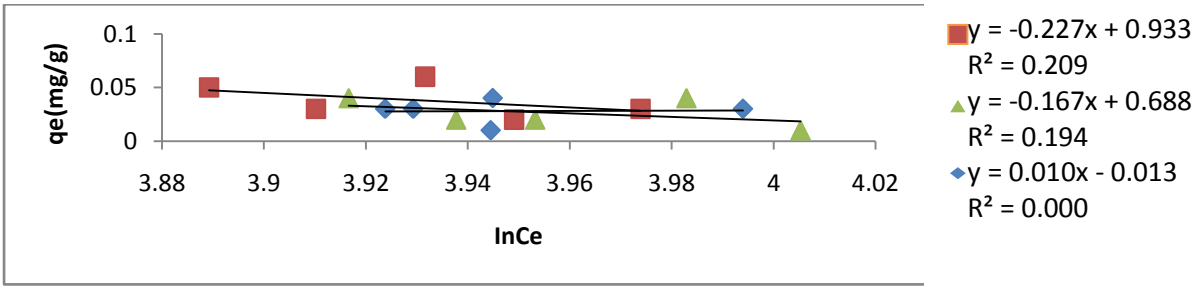

Figure 4.120: Temkin Isotherm plot for Cd onto SSAC Carbonized at 600°C and activated with HCl, H_3PO_4, H_2SO_4

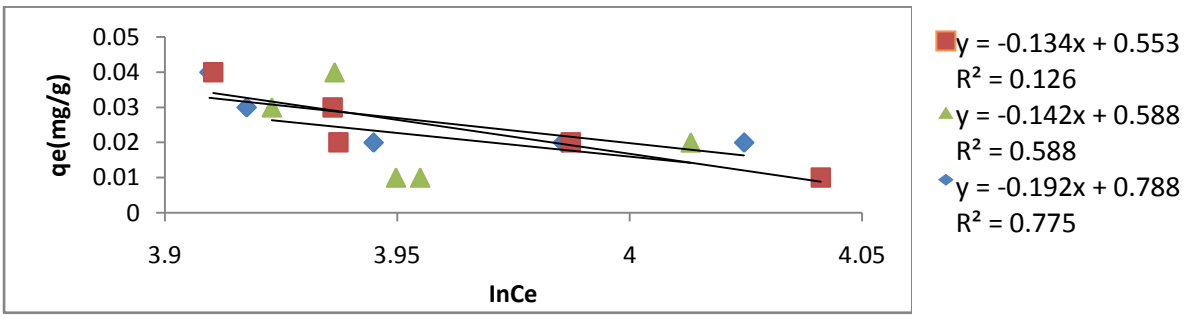

Figure 4.121: Temkin Isotherm plot for Cd onto SSAC Carbonized at 800°C and activated with HCl, H_3PO_4, H_2SO_4

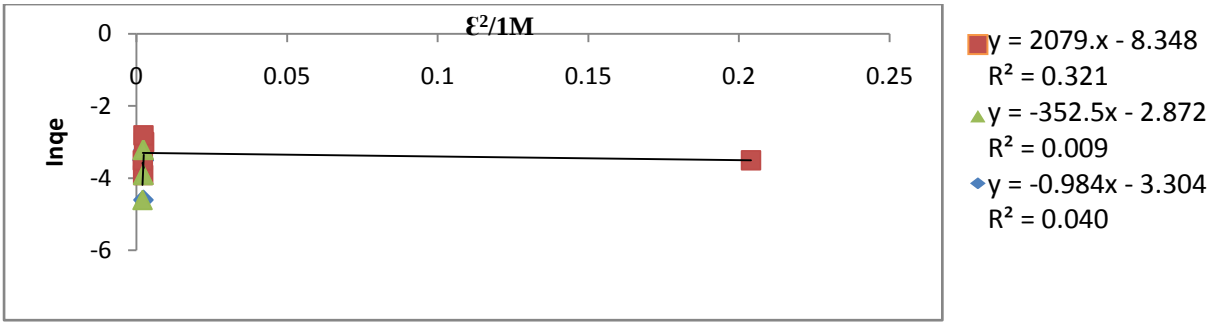

Figure 4.122: Dubinin Rudushkevich Isotherm plot for Cd onto SSAC Carbonized at 600°C and activated with HCl, H_3PO_4, H_2SO_4

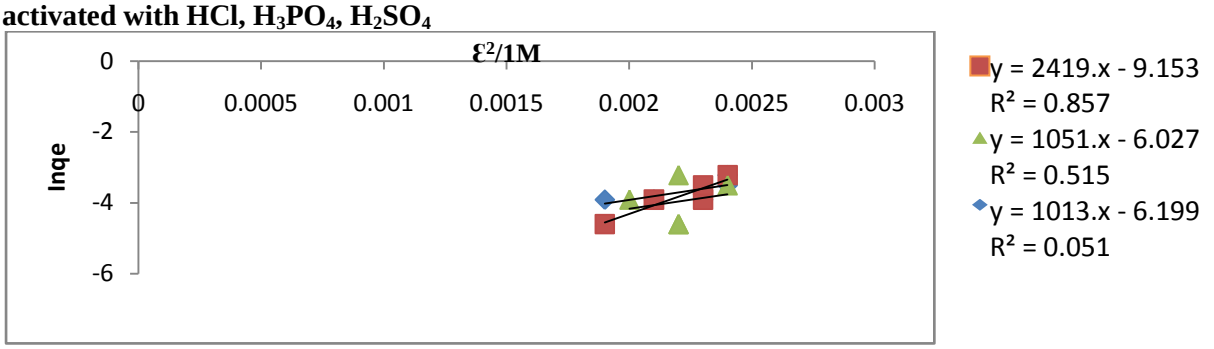

Figure 4.123: Dubinin Rudushkevich Isotherm plot for Cd onto SSAC Carbonized at 800°C and activated with HCl, H_3PO_4, H_2SO_4

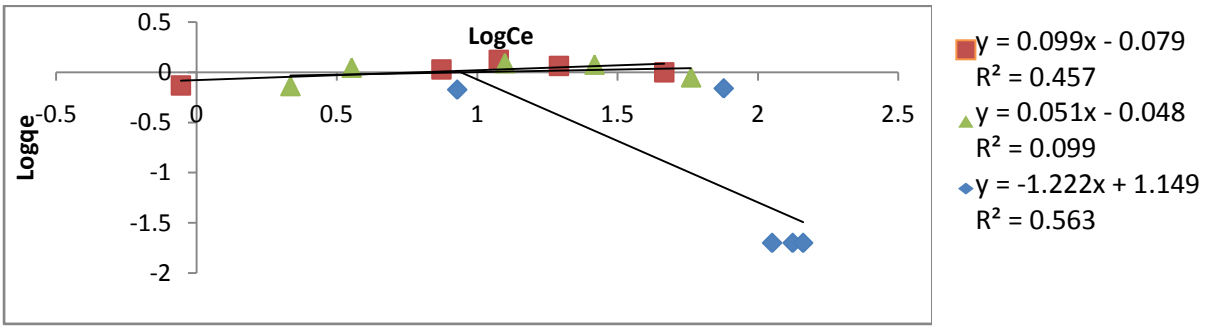

Figure 4.121: Freundlich Isotherm plot for Mn onto SSAC Carbonized at 600°C and activated with HCl, H_3PO_4, H_2SO_4

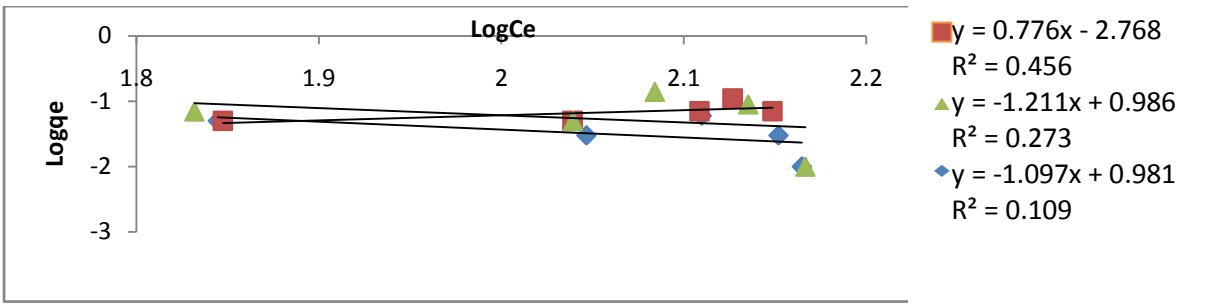

Figure 4.124: Freundlich Isotherm plot for Mn onto SSAC Carbonized at 800°C and activated with HCl, H_3PO_4, H_2SO_4

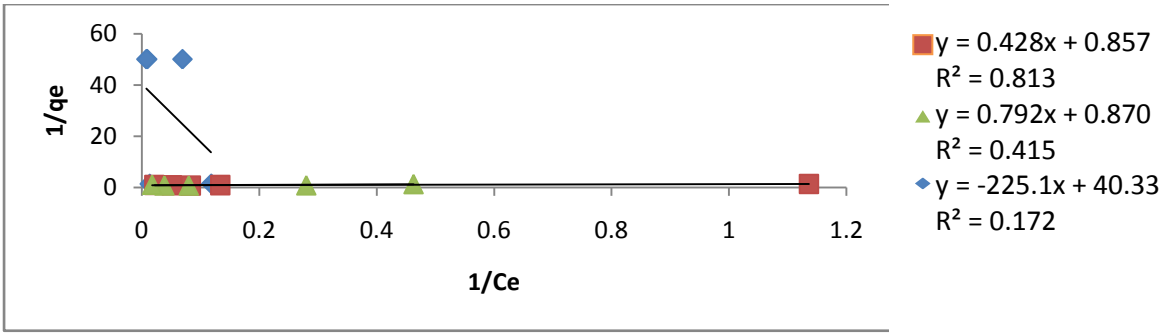

Figure 4.125: Langmuir Isotherm plot for Mn onto SSAC Carbonized at 600°C and activated with HCl, H_3PO_4, H_2SO_4

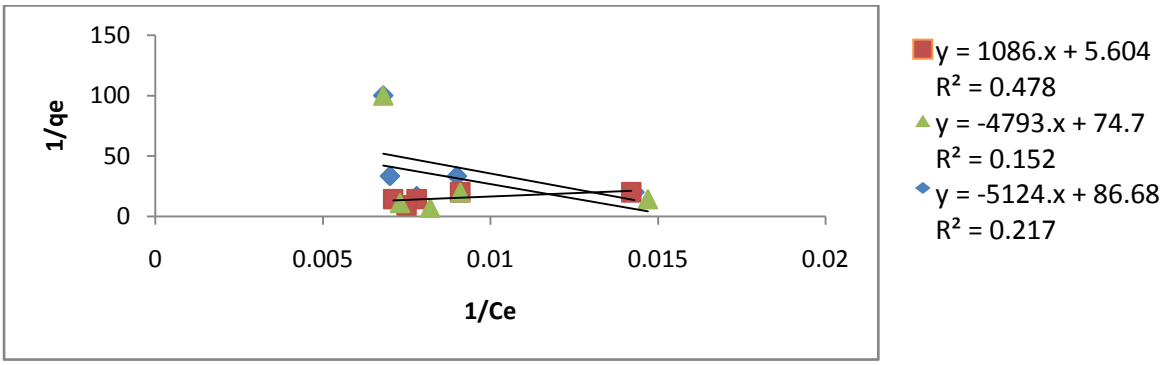

Figure 4.126: Langmuir Isotherm plot for Mn onto SSAC Carbonized at 600°C and activated with HCl, H_3PO_4, H_2SO_4

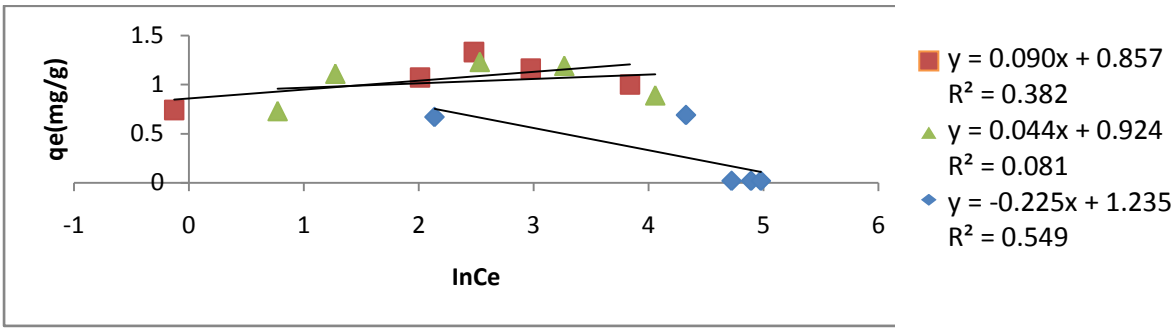

Figure 4.127: Temkin Isotherm plot for Mn onto SSAC Carbonized at 600°C and activated with HCl, H_3PO_4, H_2SO_4

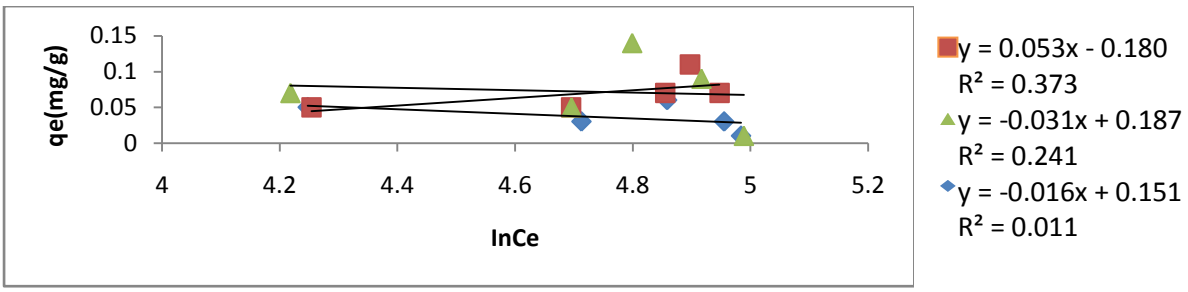

Figure 4.128: Temkin Isotherm plot for Mn onto SSAC Carbonized at 800°C and activated with HCl, H_3PO_4, H_2SO_4

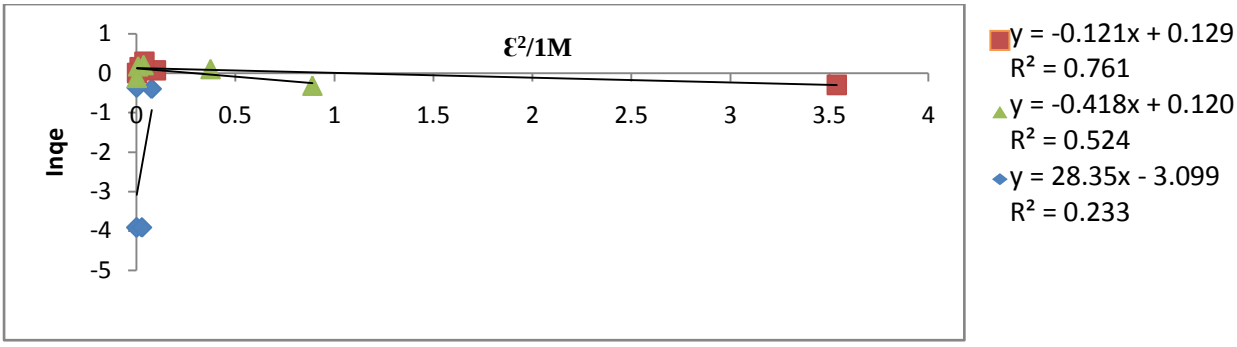

Figure 4.129: Dubinin Rudushkevich Isotherm plot for Mn onto SSAC Carbonized at 600°C and activated with HCl, H_3PO_4, H_2SO_4

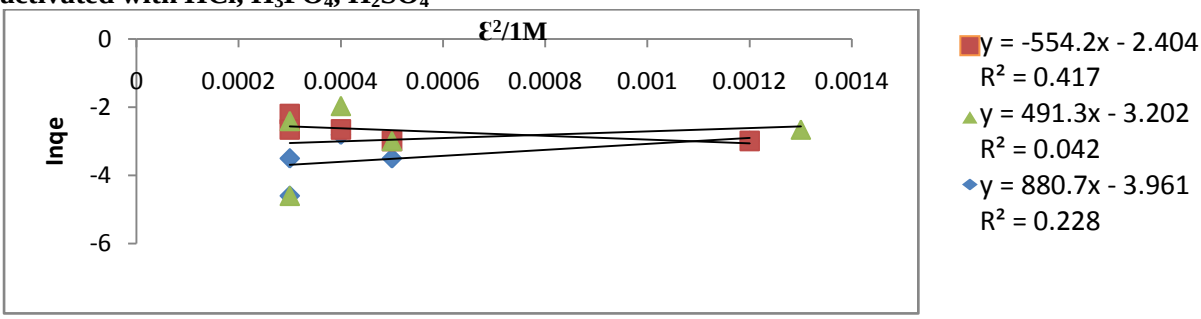

Figure 4.130: Dubinin Rudushkevich Isotherm plot for Mn onto SSAC Carbonized at 800°C and activated with HCl, H_3PO_4, H_2SO_4

4.6 Summary of Isotherm Parameters

Freundlich isotherm model as earlier mentioned is a case for heterogeneous surface energies and it gives an exponential distribution of active sites. The Freundlich constants n and K_f which respectively indicated the adsorption intensity and adsorption capacity were calculated from the slope and intercept of the plot of $\log q_e$ versus $\log C_e$ presented in section 4.5 and these parameters are summarized in Table 4.107.

The Freundlich binding capacities for Activated carbon produced from Oil Bean ranged from 1.0 to 7.6×10^5 (Table 4.107). The increasing value indicated greater adsorption capacity. The value of n is a function of the strength of the adsorbent materials used and it gives an indication of the favourability of adsorption. As n > 1, favourable adsorption condition was observed (Gupta *et al*., 1999). When the value of n is high, it showed the adsorption bond was weak and when n > 1, the

absorption coefficient increases with increasing concentration of the solution which lead to an increase in the surface characteristic after monolayer adsorption. When the value of n < 1 K_f decreased with concentration in most of the activated carbon types, and this was in line with Hamidi *et al*. (2003), observation.

Tables 4.107 to 4.110 presented the OBAC, PNAC, PKAC and SSAC adsorption data fitted on Freundlich Isotherm model and their respective parameters.

Table 4.107: Freundlich Adsorption Isotherm Constants for OBAC

S/N	AC Type	Equation (Y=)	R^2	n	K_f
1	Ni OBAC 600^0C HCl	-0.524x+0.203	0.901	-1.91	1.60
2	Ni OBAC 600^0C H_2SO_4	-0.077x-0.247	0.693	-12.99	0.57
3	Ni OBAC 600^0C H_3PO_4	-0.164x-0.205	0.603	-6.10	0.62
4	Ni OBAC 800^0C HCl	-0.881x+0.402	0.739	-1.14	2.52
5	Ni OBAC 800^0C H_2SO_4	0.044x-0.71	0.726	22.73	0.19
6	Ni OBAC 800^0C H_3PO_4	-1.364x+1.356	0.944	-0.73	22.70
7	Cd OBAC 600^0C HCl	-1.723x1.729	0.917	-0.58	53.58
8	Cd OBAC 600^0C H_2SO_4	-0.075x-0.282	0.841	-13.33	0.52
9	Cd OBAC 600^0C H_3PO_4	-1.586x+1.634	0.999	-0.63	43.05
10	Cd OBAC 800^0C HCl	-1.325x+1.114	0.815	-0.75	13.00
11	Cd OBAC 800^0C H_2SO_4	-0.57x+0.045	0.022	-1.75	1.11
12	Cd OBAC 800^0C H_3PO_4	-4.274x+5.882	0.984	-0.23	7E+5
13	Pb OBAC 600^0C HCl	1.065x-2.812	0.753	0.94	0.00
14	Pb OBAC 600^0C H_2SO_4	1.745x-3.681	0.727	0.57	0.00
15	Pb OBAC 600^0C H_3PO_4	1.243x-3.19	0.388	0.80	0.00
16	Pb OBAC 800^0C HCl	0.224x-0.333	0.939	4.46	0.46
17	Pb OBAC 800^0C H_2SO_4	0.216x-0.383	0.985	4.63	0.41
18	Pb OBAC 800^0C H_3PO_4	0.034x-0.319	0.089	29.41	0.48
19	Mn OBAC 600^0C HCl	2.394x-5.693	0.422	0.42	0.00
20	Mn OBAC 600^0C H_2SO_4	0.624x-2.281	0.132	1.60	0.01
21	Mn OBAC 600^0C H_3PO_4	-0.031x-1.195	0.001	-32.26	0.06
22	Mn OBAC 800^0C HCl	-0.349x+0.307	0.826	-2.87	2.03
23	Mn OBAC 800^0C H_2SO_4	-0.22x-0.012	0.366	-4.55	0.97
24	Mn OBAC 800^0C H_3PO_4	-0.487x+0.524	0.479	-2.05	3.34

The goodness of fit of an experimental data is measured by the determination coefficients or data realiability (R^2) (Zaid and Mohammed, 2008). The R^2 for the isotherm studied as summarized in Table 4.107 showed that the Freundlich model

had a good fit for all the oil bean activated carbon except for Cd/OBAC/800^{0}C/H_3PO_4, Mn/OBAC/600^{0}C/H_2SO_4, Ni/OBAC/800^{0}C/H_2SO_4, Pb/OBAC/800^{0}C/H_2SO_4 and Mn/OBAC/600^{0}C/H_3PO_4.

Freundlich adsorption capacities for Activated carbon produced from Peanut seed ranged from 1.1 to 7.2x10^4 (Table 4.108). For Mn/PNAC/600^{0}C/H_3PO_4, the K_f value tends towards infinity but looking at the determination coefficient (0.006), it showed that the Freundlich isotherm did not have a good fit and so it gave a doubtful value for the K_f. This showed that it is better to use more than a single

Table 4.108: Freundlich Adsorption Isotherm Constants for Peanut Activated Carbon

S/N	AC Type	Equation (Y=)	R^2	n	K_f
1	Ni PNAC 600^{0}C HCl	-0.678x+0.446	0.924	-1.47	2.79
2	Ni PNAC 600^{0}C H_2SO_4	-1.641x+1.792	0.861	-0.61	61.94
3	Ni PNAC 600^{0}C H_3PO_4	-0.18x-0.269	0.596	-5.56	0.54
4	Ni PNAC 800^{0}C HCl	-1.402x+1.447	0.883	-0.71	27.99
5	Ni PNAC 800^{0}C H_2SO_4	-0.672x+0.423	0.792	-1.49	2.65
6	Ni OBAC 800^{0}C H_3PO_4	-0.699x+0.462	0.888	-1.43	2.90
7	Pb PNAC 600^{0}C HCl	-0.037x-0.355	0.021	-27.03	0.44
8	Pb PNAC 600^{0}C H_2SO_4	-0.19x-0.398	0.820	-5.26	0.40
9	Pb PNAC 600^{0}C H_3PO_4	-0.172x-0.384	0.650	-5.81	0.41
10	Pb PNAC 800^{0}C HCl	-0.247x-0.348	0.727	-4.05	0.45
11	Pb PNAC 800^{0}C H_2SO_4	-0.307x-0.299	0.657	-3.26	0.50
12	Pb PNAC 800^{0}C H_3PO_4	-0.259x-0.329	0.571	-3.86	0.47
13	Cd PNAC 600^{0}C HCl	-0.664x+3.17	0.861	-1.51	1479.11
14	Cd PNAC 600^{0}C H_2SO_4	-3.67x+4.862	0.916	-0.27	72777.98
15	Cd PNAC 600^{0}C H_3PO_4	-2.972x+3.858	0.985	-0.34	7211.07
16	Cd PNAC 800^{0}C HCl	-2.63x+3.076	0.918	-0.38	1191.24
17	Cd PNAC 800^{0}C H_2SO_4	-2.149x+2.594	0.816	-0.47	392.64
18	Cd PNAC 800^{0}C H_3PO_4	-0.467x+0.051	0.891	-2.14	1.12
19	Mn PNAC 600^{0}C HCl	0.356x-0.749	0.297	2.81	0.18
20	Mn PNAC 600^{0}C H_2SO_4	-0.526x+0.534	0.365	-1.90	3.42
21	Mn PNAC 600^{0}C H_3PO_4	237.4x-793.2	0.006	0.00	0.00
22	Mn PNAC 800^{0}C HCl	-1.052x+1.437	0.639	-0.95	27.35
23	Mn PNAC 800^{0}C H_2SO_4	-0.579x+0.658	0.526	-1.73	4.55
24	Mn PNAC 800^{0}C H_3PO_4	-0.597x+0.672	0.425	-1.68	4.70

error measurement to confirm the goodness of fit between the data and the Freundlich Isotherm model, as there are instances where one parameter indicates a poor fit and the other indicates a good fit (Coles *et al*., 2006). The goodness of fit of an experimental data is measured by the determination coefficients (R^2) (Zaid and Mohammed, 2008). The R^2 for the isotherm studied are as summarised in Table 4.108, and it could be deduced from this table that the Freundlich model showed a good fit for all the Pear nut seed activated carbon except for Pb/PNAC/600^{0}C/HCl, Mn/PNAC/600^{0}C/HCl, Mn/PNAC/800^{0}C/H_2SO_4, Mn/PNAC/600^{0}C/H_2SO_4 and Mn/PNAC/600^{0}C/H_3PO_4.

The value of n is a function of the strength of the adsorbent materials used. When the value of n is high, it showed the adsorption bond was weak and when n > 1, the absorption coefficient increases with increasing concentration of the solution which lead to an increase in the surface characteristic after monolayer adsorption. From the results obtained, n < 1and K_f decreased with concentration in most of the activated carbon types. This is also in line with Hamidi *et al*., (2003) observation.

The Freundlich isotherm model showed a good fit for virtually all the type of activated carbon produced from Palm kernel shell except for Ni/PKAC/600^{0}C/H_2SO_4, Pb/PKAC/600^{0}C/H_3PO_4, Pb/PKAC/600^{0}C/H_2SO_4, Cd/PKAC/800^{0}C/HCl, Mn/PKAC/600^{0}C/H_3PO_4, Mn/PKAC/600^{0}C/H_2SO_4, Mn/PKAC/800^{0}C/HCl, Mn/PKAC/800^{0}C/H_3PO_4. R^2 ranged from 0.134 to 0.989. The adsorption intensity parameter ranged from 0.30 to 28.6, n being greater than one is also an indication of the favourability of heavy metal adsorption (Gupta *et al.*,

1999). This showed relative high adsorption intensities for the Palm kernel activated carbons. Similar observation was obtained for the Freundlich adsorption capacity parameter which had a range of 1.1 to $2.3x10^4$ (Table 4.109).

Table 4.109: Freundlich Adsorption Isotherm Constants for Palm Kernel Activated Carbon

S/N	AC Type	EquationY(=)	R^2	n	K_f
1	Ni PKAC 600^0C HCl	-1.878x+2.221	0.862	-0.53	166.34
2	Ni PKAC 600^0C H_3PO_4	-0.487x+0.176	0.837	-2.05	1.50
3	Ni PKAC 600^0C H_2SO_4	-3.287x+4.371	0.276	-0.30	23496.33
4	Ni PKAC 800^0C HCl	-2.222x+2.686	0.829	-0.45	485.29
5	Ni PKAC 800^0C H_3PO_4	-1.121x+1.061	0.945	-0.89	11.51
6	Ni PKAC 800^0C H_2SO_4	0.691x+0.362	0.727	1.45	2.30
7	Pb PKAC 600^0C HCl	0.143x-0.415	0.989	6.99	0.38
8	Pb PKAC 600^0C H_3PO_4	0.161x-0.973	0.134	6.21	0.11
9	Pb PKAC 600^0C H_2SO_4	-0.035x-0.503	0.441	-28.57	0.31
10	Pb PKAC 800^0C HCl	0.132x-0.598	0.858	7.58	0.25
11	Pb PKAC 800^0C H_3PO_4	0.085x-0.497	0.405	11.76	0.32
12	Pb PKAC 800^0C H_2SO_4	-0.179x-0.366	0.801	-5.59	0.43
13	Cd PKAC 600^0C HCl	-3.276x-4.18	0.928	-0.31	0.00
14	Cd PKAC 600^0C H_3PO_4	-0.112x-0.252	0.859	-8.93	0.56
15	Cd PKAC 600^0C H_2SO_4	-0.158x-0.2	0.976	-6.33	0.63
16	Cd PKAC 800^0C HCl	0.614x-1.528	0.136	1.63	0.03
17	Cd PKAC 800^0C H_3PO_4	-0.113x-0.234	0.817	-8.85	0.58
18	Cd PKAC 800^0C H_2SO_4	-1.263x+0.731	0.941	-0.79	5.38
19	Mn PKAC 600^0C HCl	0.096x-0.113	0.980	10.42	0.77
20	Mn PKAC 600^0C H_3PO_4	0.049x-0.4	0.208	20.41	0.40
21	Mn PKAC 600^0C H_2SO_4	-0.144x+0.035	0.177	-6.94	1.08
22	Mn PKAC 800^0C HCl	-0.463x+40.33	0.452	-2.16	2.13796E+40
23	Mn PKAC 800^0C H_3PO_4	-0.348x-0.243	0.342	-2.87	0.57
24	Mn PKAC 800^0C H_2SO_4	-0.144x+0.035	0.177	-6.94	1.08

The Freundlich adsorption intensity (n) for the OBAC carbonised at 600^oC ranged from 1.14 to 15.6 (Table 4.122). The higher the value of n, the stronger the bond between the adsorbent and the adsorbate, a desired parameter in waste water treatment (Yakubu *et al*., 2008). n is > 1 for Ni adsorption on each OBAC (Table 4.122). A similar result was obtained for coconut shell carbon adsorption of Methylene Blue (Okeola *et al.*, 2010).

Table 4.110 showed the Freundlich adsorption isotherm parameters for the adsorption of Ni, Pb, Cd and Mn by the activated carbons produced from Snail shell. The Freundlich model fitted very poorly virtually in all the types of activated carbons under consideration. This in turn affected the values of their respective

Table 4.110: Freundlich Adsorption Isotherm Constants for Snail Shell Activated Carbon

S/N	AC Type	Equation (Y=)	R^2	n	K_f
1	Ni SSAC 600^0C HCl	-1.44x+0.944	0.057	-0.69	8.79
2	Ni SSAC 600^0C H_3PO_4	-0.934x+0.285	0.098	-1.07	1.93
3	Ni SSAC 600^0C H_2SO_4	-4.309x+6.011	0.710	-0.23	1E+6
4	Ni SSAC 800^0C HCl	-3.636x+4.919	0.927	-0.28	8E+4
5	Ni SSAC 800^0C H_3PO_4	2.648x-5.995	0.455	0.38	0.00
6	Ni SSAC 800^0C H_2SO_4	-1.832x+1.847	0.175	-0.55	70.31
7	Pb SSAC 600^0C HCl	0.346x-1.042	0.085	2.89	0.09
8	Pb SSAC 600^0C H_3PO_4	0.299x-1.121	0.131	3.34	0.08
9	Pb SSAC 600^0C H_2SO_4	-0.387x	0.341	-2.58	0.47
10	Pb SSAC 800^0C HCl	1.375x-0.331-3.3	0.555	0.73	0.00
11	Pb SSAC 800^0C H_3PO_4	-0.2x-0.906	0.031	-5.00	0.12
12	Pb SSAC 800^0C H_2SO_4	0.511x-2.198	0.031	1.96	0.01
13	Cd SSAC 600^0C HCl	0.75x-2.879	0.001	1.33	0.00
14	Cd SSAC 600^0C H_3PO_4	-7.04x2+10.58	0.188	-0.14	3E+10
15	Cd SSAC 600^0C H_2SO_4	-9.019x+13.86	0.301	-0.11	7E+13
16	Cd SSAC 800^0C HCl	-5.162x+7.266	0.617	-0.19	1.18E+8
17	Cd SSAC 800^0C H_3PO_4	-8.562x+13.05	0.890	-0.12	1.12E+13
18	Cd SSAC 800^0C H_2SO_4	4.884x-10.14	0.048	0.20	0.00
19	Mn SSAC 600^0C HCl	-1.222x+1.149	0.563	-0.82	14.09
20	Mn SSAC 600^0C H_3PO_4	0.099x-0.079	0.457	10.10	0.83
21	Mn SSAC 600^0C H_2SO_4	0.051x-0.048	0.099	19.61	0.90
22	Mn SSAC 800^0C HCl	-1.211x+0.986	0.273	-0.83	9.68
23	Mn SSAC 800^0C H_3PO_4	0.776x-2.768	0.456	1.29	0.00
24	Mn SSAC 800^0C H_2SO_4	-1.097x+0.987	0.109	-0.91	9.71

adsorption intensities as well as their adsorption capacities.

Table 4.111 presents the determination coefficients, the Langmuir constants (b and Q^o) after experimental data were fitted and the separation factor (R_L).

The Langmuir isotherm model suggested that sorption occurs on homogeneous surface by monolayer sorption without interaction between sorbed ions. The values of b and Q^o were evaluated from the slopes and intercepts respectively for the 24

types of OBAC. It was deduced from Table 4.111 that the coefficient of determinations were all poorly fitted into the Langmuir model equation except for few of them. The range of the R^2 values was 0.008 to 0.993 with most falling below 0.500. Pb/OBAC/800^{0}C/H_2SO_4 was very poorly fitted with R^2 being 0.004 and this might have led to the high value of b (2801.9l/mg). Most of the Langmuir isotherm constants had negative values indicating the inadequacy of the model to explain the adsorption process, since these constants represent the surface binding energy and monolayer coverage or that the tested systems does not follow the assumptions of the Langmuir approach (Kiurski *et al.*, 2012, Kiurski *et al.*, 2011). This is in line with the observation of Konduru, (1996).

Table 4.111: Langmuir Adsorption Isotherm Constants for Oil Bean Activated Carbon

S/N	AC Type	Equation (Y=)	R^2	Q^o (mg/g)	b (l/mg)	R_L
1	Ni OBAC 600^{0}C HCl	-1.181x+2.562	0.249	0.39	-2.17	-0.01
2	Ni OBAC 600^{0}C H_2SO_4	-0.707x+2.224	0.477	0.45	-3.15	0.00
3	Ni OBAC 600^{0}C H_3PO_4	-30.75x+5.216	0.861	0.19	-0.17	-0.10
4	Ni OBAC 800°C HCl	-83.78x+14.88	0.213	0.07	-0.18	-0.09
5	Ni OBAC 800°C H_2SO_4	3.005x+3.746	0.000	0.27	1.25	0.01
6	Ni OBAC 800°C H_3PO_4	-287.9x+16.26	0.820	0.06	-0.06	-0.36
7	Cd OBAC 600^{0}C HCl	-392x+24.6	0.657	0.04	-0.06	-0.38
8	Cd OBAC 600^{0}C H_2SO_4	-0.20x5+2.208	0.440	0.45	-10.77	0.00
9	Cd OBAC 600^{0}C H_3PO_4	-3147x+17.19	0.993	0.06	-0.01	1.46
10	Cd OBAC 800°C HCl	-219.6x+19.34	0.490	0.05	-0.09	-0.25
11	Cd OBAC 800°C H_2SO_4	-665.5x+21.34	0.140	0.05	-0.03	-1.19
12	Cd OBAC 800°C H_3PO_4	-3067x+91.9	0.717	0.01	-0.03	-1.39
13	Pb OBAC 600^{0}C HCl	565.4x-1.306	0.706	-0.77	0.00	1.15
14	Pb OBAC 600^{0}C H_3PO_4	617.8x-9.65	0.385	-0.10	-0.02	9.77
15	Pb OBAC 600^{0}C H_2SO_4	628.9x-1.102	0.250	-0.91	0.00	1.11
16	Pb OBAC 800^{0}C HCl	0.374x+1.677	0.885	0.60	4.48	0.00
17	Pb OBAC 800^{0}C H_3PO_4	0.536x+1.756	0.950	0.57	3.28	0.01
18	Pb OBAC 800^{0}C H_2SO_4	0.000x+2.241	0.004	0.45	0	0
19	Mn OBAC 600^{0}C HCl	17x48+7.473	0.319	0.13	0.00	0.61
20	Mn OBAC 600^{0}C H_3PO_4	467x.2+6.811	0.066	0.15	0.01	0.32
21	Mn OBAC 600^{0}C H_2SO_4	-121.x8+19.63	0.008	0.05	-0.16	-0.04
22	Mn OBAC 800^{0}C HCl	-12.26x+2.594	0.892	0.39	-0.21	-0.03
23	Mn OBAC 800^{0}C H_3PO_4	-1.94x+3.125	0.168	0.32	-1.61	0.00
24	Mn OBAC 800^{0}C H_2SO_4	-54.86x+3.502	0.355	0.29	-0.06	-0.12

The essential characteristics of Langmuir isotherm can be expressed in terms of a dimensionless equilibrium parameter (R_L) called Separation Factor (Hall *et al*., 1966, Adamson, 2001), which is defined as: $R_L = 1/ (1 + bC_o)$. Where b =

Table 4.112: Langmuir Adsorption Isotherm Constants for Peanut Seed Activated Carbon

S/N	AC Type	Equation (Y=)	R^2	$Q^{o(mg/g)}$	b (l/mg)	R_L
1	Ni PNAC 600^0C HCl	-2219x+102.7	0.603	0.01	-0.05	-0.48
2	Ni PNAC 600^0C H_3PO_4	-468.8x+21.63	0.630	0.05	-0.05	-0.48
3	Ni PNAC 600^0C H_2SO_4	-17.42x+3.977	0.629	0.25	-0.23	-0.07
4	Ni PNAC 800^0C HCl	-256.4x+14.44	0.727	0.07	-0.06	-0.36
5	Ni PNAC 800^0C H_3PO_4	-85.02x+6.733	0.728	0.15	-0.08	-0.23
6	Ni PNAC 800^0C H_2SO_4	-89.63x+6.943	0.838	0.14	-0.08	-0.24
7	Pb PNAC 600^0C HCl	-0.067x+2.417	0.009	0.41	-36.07	0.00
8	Pb PNAC 600^0C H_3PO_4	0.54x+1.849	0.691	0.54	3.42	0.01
9	Pb PNAC 600^0C H_2SO_4	0.499x+1.866	0.464	0.54	3.74	0.00
10	Pb PNAC 800^0C HCl	-0.66x+3.153	0.646	0.32	-4.78	0.00
11	Pb PNAC 800^0C H_3PO_4	-26.76x+6.727	0.726	0.15	-0.25	-0.07
12	Pb PNAC 800^0C H_2SO_4	-19.36x+5.942	0.507	0.17	-0.31	-0.06
13	Cd PNAC 600^0C HCl	-1134x+50.56	0.521	0.02	-0.04	-0.64
14	Cd PNAC 600^0C H_3PO_4	-2393x+79.07	0.675	0.01	-0.03	-1.11
15	Cd PNAC 600^0C H_2SO_4	-1203x+39.49	0.966	0.03	-0.03	-1.13
16	Cd PNAC 800^0C HCl	-1181x+54.57	0.641	0.02	-0.05	-0.60
17	Cd PNAC 800^0C H_3PO_4	-588.3x+22.15	0.713	0.05	-0.04	-0.86
18	Cd PNAC 800^0C H_2SO_4	-17.77x+5.12	0.707	0.20	-0.29	-0.06
19	Mn PNAC 600^0C HCl	32.12x+0.744	0.414	1.34	0.02	0.23
20	Mn PNAC 600^0CH_2SO_4	-100.6x+4.6	0.247	0.22	-0.05	-0.17
21	Mn PNAC 600^0C H_3PO_4	-56.1x+3.566	0.293	0.28	-0.06	-0.12
22	Mn PNAC 800^0C HCl	-238.4x+8.378	0.909	0.12	-0.04	-0.24
23	Mn PNAC 800^0C H_3PO_4	-52.89x+3.766	0.335	0.27	-0.07	-0.11
24	Mn PNAC 800^0C H_2SO_4	-52.32x+4.898	0.201	0.20	-0.09	-0.08

Langmuir constant and C_o is the highest initial metal concentration (mg/l). The value of R_L indicated the type of the isotherm to be either unfavourable ($R_L > 1$), linear ($R_L = 1$), favourable ($0 < R_L < 1$) or irreversible ($R_L = 0$). The Langmuir isotherm model for the adsorption of Ni, Pb, Cd and Mn on OBAC generally had

low determination coefficients (Table 4.111). It showed that the Langmuir isotherm plot did not have a good fit in most of the plots.

The essential characteristics of Langmuir isotherm (separation factor) R_L, showed that most isotherm were negatives buttressing the inadequacy of the Langmuir model applicability to the tested systems. The separation factors for the OBAC that had positive b were generally within the favourable adsorption ($0 < R_L < 1$).

Table 4.113: Langmuir Adsorption Isotherm Constants for Palm Kernel shell Activated Carbon

S/N	AC Type	Equation (Y=)	R^2	$Q^{o(mg/g)}$	b (l/mg)	R_L
1	Ni PKAC 600^0C HCl	-690.2x+24.78	0.740	0.04	-0.04	-0.72
2	Ni PKAC 600^0C H_3PO_4	-18.61x+4.108	0.540	0.24	-0.22	-0.07
3	Ni PKAC 600^0C H_2SO_4	-488.5x+19.49	0.635	0.05	-0.04	-0.60
4	Ni PKAC 800^0C HCl	-99.9x+39.24	0.497	0.03	-0.39	-0.04
5	Ni PKAC 800^0C H_3PO_4	-221.3x+11.57	0.941	0.09	-0.05	-0.40
6	Ni PKAC 800^0C H_2SO_4	-76.88x+8.167	0.607	0.12	-0.11	-0.16
7	Pb PKAC 600^0C HCl	0.492x+1.983	0.906	0.50	4.03	0.00
8	Pb PKAC 600^0C H_3PO_4	15.18x+5.002	0.065	0.20	0.33	0.05
9	Pb PKAC 600^0C H_2SO_4	-1.434x+3.628	0.417	0.28	-2.53	-0.01
10	Pb PKAC 800^0C HCl	3.119x+2.558	0.782	0.39	0.82	0.02
11	Pb PKAC 800^0C H_3PO_4	0.559x+2.559	0.141	0.39	4.58	0.00
12	Pb PKAC 800^0C H_2SO_4	-5.674x+4.392	0.535	0.23	-0.77	-0.02
13	Cd PKAC 600^0C HCl	-1885x+69.39	0.684	0.01	-0.04	-0.90
14	Cd PKAC 600^0C H_3PO_4	-0.68x+2.357	0.512	0.42	-3.47	-0.01
15	Cd PKAC 600^0C H_2SO_4	-3.337x+2.657	0.935	0.38	-0.80	-0.02
16	Cd PKAC 800^0C HCl	-1789x+61.82	0.417	0.02	-0.03	-1.01
17	Cd PKAC 800^0C H_3PO_4	-2.081x+2.452	0.714	0.41	-1.18	-0.01
18	Cd PKAC 800^0C H_2SO_4	-150.4x+26.49	0.618	0.04	-0.18	-0.11
19	Mn PKAC 600^0C HCl	0.271x+0.947	0.972	1.06	3.49	0.00
20	Mn PKAC 600^0C H_3PO_4	4.614x+1.969	0.203	0.51	0.43	0.02
21	Mn PKAC 600^0C H_2SO_4	-6.681x+1.794	0.191	0.56	-0.27	-0.03
22	Mn PKAC 800^0C HCl	-23.99x+4.24	0.311	0.24	-0.18	-0.04
23	Mn PKAC 800^0C H_3PO_4	16.19x+1.909	0.122	0.52	0.12	0.05
24	Mn PKAC 800^0C H_2SO_4	-164.5x+9.667	0.413	0.10	-0.06	-0.13

Considering the determination coefficients for the Pear nut activated carbons prepared, it showed that the Langmuir isotherm had a good fit when compared with that of the OBAC (Table 4.112). The extent of adsorption of Ni, Pb, Cd and Mn on

the prepared Pear nut seed activated carbon which was tested by the essential feature of the Langmuir isotherm model (R_L), showed that their adsorption were mostly negative indicating the inadequacy of the model to explain the adsorption process.

The adsorption of those that had positive adsorption constants, were all favourable ($0<R_L<1$). The lack of fitness of experiment data into the Langmuir isotherm model indicated the heterogeneous nature of the adsorbent surface. The result also demonstrated the formation of multilayer coverage of Ni, Pb, Cd and Mn ions at the outer layer of the adsorbents (Hameed *et al*., 2006).

Table 4.114: Langmuir Adsorption Isotherm Constants for Snail Shell Activated Carbon

S/N	AC Type	Equation (Y=)	R^2	$Q^{o(mg/g)}$	b (l/mg)	R_L
1	Ni SSAC 600^0C HCl	-4603x+126.8	0.073	0.01	-0.03	-1.19
2	Ni SSAC 600^0C H_3PO_4	-1429x+46.75	0.259	0.02	-0.03	-0.84
3	Ni SSAC 600^0C H_2SO_4	-10041x+222.2	0.551	0.00	-0.02	-2.09
4	Ni SSAC 800^0C HCL	-4098x+105.2	0.800	0.01	-0.03	-1.40
5	Ni SSAC 800^0C H_3PO_4	3221x-33.24	0.414	-0.03	-0.01	3.22
6	Ni SSAC 800^0C H_2SO_4	-890.5x+41.38	0.029	0.02	-0.05	-0.48
7	Pb SSAC 600^0C HCl	16.52x+3.212	0.029	0.31	0.19	0.08
8	Pb SSAC 600^0C H_3PO_4	25.74x+4.1	0.060	0.24	0.16	0.10
9	Pb SSAC 600^0C H_2SO_4	-80.44x+11.16	0.356	0.09	-0.14	-0.14
10	Pb SSAC 800^0C HCl	772x-6.385	0.451	-0.16	-0.01	1.90
11	Pb SSAC 800^0C H_3PO_4	-73.94x+19.37	0.009	0.05	-0.26	-0.07
12	Pb SSAC 800^0C H_2SO_4	560.5x+14.4	0.031	0.07	0.03	0.40
13	Cd SSAC 600^0C HCl	2840x-9.943	0.002	-0.10	0.00	1.25
14	Cd SSAC 600^0C H_3PO_4	17.79x+29.67	0.011	0.03	1.67	0.01
15	Cd SSAC 600^0C H_2SO_4	-28105x+586.2	0.393	0.00	-0.02	-5.03
16	Cd SSAC 800^0C HCl	-10378x+240.5	0.622	0.00	-0.02	-3.01
17	Cd SSAC 800^0C H_3PO_4	-27913x+582.5	0.852	0.00	-0.02	-5.02
18	Cd SSAC 800^0C H_2SO_4	-2544x+110.3	0.001	0.01	-0.04	-0.67
19	Mn SSAC 600^0C HCl	-225.1x+40.33	0.172	0.02	-0.18	-0.04
20	Mn SSAC 600^0C H_3PO_4	0.428x+0.857	0.813	1.17	2.00	0.00
21	Mn SSAC 600^0C H_2SO_4	0.792x+0.87	0.415	1.15	1.10	0.01
22	Mn SSAC 800^0C HCl	-5124x+86.68	0.271	0.01	-0.02	-0.67
23	Mn SSAC 800^0C H_3PO_4	1086x+5.604	0.478	0.18	0.01	0.57
24	Mn SSAC 800^0C H_2SO_4	-4793x+74.7	0.151	0.01	-0.02	-0.77

The Langmuir isotherm constants determined from the slopes and intercepts of the respective plot for PKAC are summarized in Table 4.113. A similar observation as for OBAC, PNAC was made for PKAC.

In the Table 4.114 which is the summarized Langmuir isotherm model constants for snail shell (SSAC) activated carbon, it showed that they generally had a poor fit as most of the R^2 are below 0.500 unlike that of the OBAC, PNAC and PKAC. The Langmuir factors were also negative in most of the tested systems as obseved in OBAC.

Table 4.115: Temkin Adsorption Isotherm Constants for OBAC

S/N	AC Type	Equation (Y=)	R^2	$b_{T\ (J/mol)}$	$A_{T(L/mg)}$	$B_{\ (J/mol)}$
1	Ni OBAC 600^0C HCl	-0.065x+0.597	0.563	-38116.5	0.00	-0.065
2	Ni OBAC 600^0C H_2SO_4	-0.036x+0.56	0.706	-68821.4	0.00	-0.036
3	Ni OBAC 600^0C H_3PO_4	-0.17x+0.87	0.844	-14574.0	0.01	-0.17
4	Ni OBAC 800^OC HCl	-0.171x+0.805	0.921	-14488.7	0.01	-0.171
5	Ni OBAC 800^OC H_2SO_4	-0.056x+0.466	0.010	-44242.4	0.00	-0.056
6	Ni OBAC 800^OC H_3PO_4	-0.113x+0.544	0.960	-21925.4	0.01	-0.113
7	Cd OBAC 600^0C HCl	-0.279x+1.168	0.986	-8880.2	0.02	-0.279
8	Cd OBAC 600^0C H_2SO_4	-0.035x+0.522	0.835	-70787.8	0.00	-0.035
9	Cd OBAC 600^0C H_3PO_4	-0.287x+1.201	0.998	-8632.7	0.02	-0.287
10	Cd OBAC 800^OC HCl	-0.237x+1.019	0.968	-10453.9	0.01	-0.237
11	Cd OBAC 800^OC H_2SO_4	-0.069x-0.117	0.019	-35906.8	5.45	-0.069
12	Cd OBAC 800^OC H_3PO_4	-0.355x+1.448	0.998	-6979.1	0.02	-0.355
13	Pb OBAC 600^0C HCl	0.079x-0.212	0.803	31361.7	0.07	0.079
14	Pb OBAC 600^0C H_3PO_4	0.189x-0.563	0.624	13108.8	0.05	0.189
15	Pb OBAC 600^0C H_2SO_4	0.087x-0.254	0.463	28477.8	0.05	0.087
16	Pb OBAC 800^0C HCl	0.101x+0.462	0.955	24530.4	96.96	0.101
17	Pb OBAC 800^0C H_3PO_4	0.095x+0.419	0.977	26079.7	82.31	0.095
18	Pb OBAC 800^0C H_2SO_4	0.018x+0.492	0.121	137642.9	7.42E+9	0.018
19	Mn OBAC 600^0C HCl	0.329x-1.356	0.456	7530.6	0.02	0.329
20	Mn OBAC 600^0C H_3PO_4	0.207x-0.882	0.722	11968.9	0.01	0.207
21	Mn OBAC 600^0C H_2SO_4	-0.001x+0.062	0.001	-2477572.0	0.00	-0.001
22	Mn OBAC 800^0C HCl	-0.238x+1.508	0.720	-10410.0	0.00	-0.238
23	Mn OBAC 800^0C H_3PO_4	-0.091x+0.858	0.345	-27226.1	0.00	-0.091
24	Mn OBAC 800^0C H_2SO_4	-0.197x+1.298	0.401	-12576.5	0.00	-0.197

Temkin isotherm model assumes that heat of adsorption (function of temperature) of all molecules in the layer of AC would decrease linearly rather than logarithmic

with coverage (Temkin, 1940, Aharoni, 1977), due to adsorbent-adsorbate interactions, and that the adsorption is characterized by a uniform distribution of the binding energies, up to some maximum binding energy. Temkin equation is given as $q_e = (RT/b_T)\ln A_T + (RT/b_T)\ln C_e$ where A_T is the equilibrium binding constant which corresponds to the maximum binding energy, $RT/b_T = B$ is related to the heat of adsorption, q_e is equilibrium adsorption and C_e is the initial metal concentration. From the results obtained for OBAC (Table 4.115) adsorption of Ni, Pb, Cd and Mn, it can be seen that the binding energy (A_T) which holds these metals to the surface of the OBAC were generally low in almost all the metals except for Pb

Table 4.116: Temkin Adsorption Isotherm Constants for PNAC

S/N	AC Type	Equation (Y=)	R^2	$b_{T(J/mol)}$	$A_{T(L/mg)}$	$B_{(J/mol)}$
1	Ni PNAC 600^0C HCl	-0.268x+1.176	0.884	-9244.7	0.01	-0.268
2	Ni PNAC 600^0C H_3PO_4	-0.25x+1.102	0.947	-9910.3	0.01	-0.25
3	Ni PNAC 600^0C H_2SO_4	-0.055+0.486	0.646	-45046.8	0.00	-0.055
4	Ni PNAC 800^0C HCl	-0.285x+1.248	0.841	-8693.2	0.01	-0.285
5	Ni PNAC 800^0C H_3PO_4	-0.17x+0.854	0.807	-14574.0	0.01	-0.17
6	Ni PNAC 800^0C H_2SO_4	-0.175x+0.87	0.883	-14157.6	0.01	-0.175
7	Pb PNAC 600^0C HCl	-0.019x+0.452	0.030	-130398.5	0.00	-0.019
8	Pb PNAC 600^0C H_3PO_4	0.085x+0.406	0.816	29147.9	118.68	0.085
9	Pb PNAC 600^0C H_2SO_4	0.077x+0.416	0.638	32176.3	221.98	0.077
10	Pb PNAC 800^0C HCl	-0.103x+0.46	0.665	-24054.1	0.01	-0.103
11	Pb PNAC 800^0C H_3PO_4	-0.016x+0.386	0.685	-154848.3	0.00	-0.016
12	Pb PNAC 800^0C H_2SO_4	-0.055x+0.382	0.600	-45046.8	0.00	-0.055
13	Cd PNAC 600^0C HCl	-0.313x+1.286	0.990	-7915.6	0.02	-0.313
14	Cd PNAC 600^0C H_3PO_4	-0.349x+1.423	0.998	-7099.1	0.02	-0.349
15	Cd PNAC 600^0C H_2SO_4	-0.332x+1.365	0.989	-7462.6	0.02	-0.332
16	Cd PNAC 800^0C HCl	-0.316x+1.297	0.993	-7840.4	0.02	-0.316
17	Cd PNAC 800^0C H_3PO_4	-0.311x+1.295	0.862	-7966.5	0.02	-0.311
18	Cd PNAC 800^0C H_2SO_4	-0.154x+0.761	0.965	-16088.1	0.01	-0.154
19	Mn PNAC 600^0C HCl	0.205x+-0.069	0.257	12085.7	0.71	0.205
20	Mn PNAC 600^0CH_2SO_4	-0.16x+1.069	0.334	-15484.8	0.00	-0.16
21	Mn PNAC 600^0C H_3PO_4	-0.155x+1.095	0.310	-15984.3	0.00	-0.155
22	Mn PNAC 800^0C HCl	-0.291x+1.638	0.536	-8514.0	0.00	-0.291
23	Mn PNAC 800^0CH_3PO_4	-0.213x+1.349	0.467	-11631.8	0.00	-0.213
24	Mn PNAC 800^0CH_2SO_4	-0.2x+1.38	0.384	-12387.9	0.00	-0.2

which was relatively high (ranging from 0.05 to 7.42E+9). b_T which indicates the heat of adsorption were almost all negative showing the non-suitability of this model to describe the heat of adsorption associated with the adsorbate-adsorbent interactions at the prevailing condition of room temperature during the adsorption study. The determination coefficients (R^2), were reasonably high in most of the OBAC studied. The constant related to heat of sorption (B) in J/mol indicates the heat of sorption of these metals on OBAC and from the values it can be inferred that the low values suggest physiosorption adsorption process according to Oladoja *et al*., (2008).

Table 4.117: Temkin Adsorption Isotherm Constants for PKAC

S/N	AC Type	Equation (Y=)	R^2	$b_{T(J/mol)}$	$A_{T(L/mg)}$	$B_{(J/mol)}$
1	Ni PKAC 600^0C HCl	-0.249x+1.097	0.884	-9950.1	0.01	-0.249
2	Ni PKAC 600^0C H_3PO_4	-0.167x+0.867	0.845	-14835.8	0.01	-0.167
3	Ni PKAC 600^0C H_2SO_4	-0.112x+0.548	0.692	-22121.2	0.01	-0.112
4	Ni PKAC 800^0C HCl	-0.276x+1.202	0.935	-8976.7	0.01	-0.276
5	Ni PKAC 800^0C H_3PO_4	-0.22x+1.009	0.919	-11261.7	0.01	-0.22
6	Ni PKAC 800^0C H_2SO_4	0.19x+0.924	0.875	13039.9	129.43	0.19
7	Pb PKAC 600^0C HCl	0.061x+0.385	0.987	40615.9	550.86	0.061
8	Pb PKAC 600^0C H_3PO_4	0.03x+0.082	0.143	82585.7	15.38	0.03
9	Pb PKAC 600^0C H_2SO_4	-0.01x+0.312	0.441	-247757.2	0.00	-0.01
10	Pb PKAC 800^0C HCl	0.045x+0.237	0.842	55057.2	193.77	0.045
11	Pb PKAC 800^0C H_3PO_4	10.56x+-11.45	0.303	234.6	0.34	10.56
12	Pb PKAC 800^0C H_2SO_4	-0.047x+0.396	0.836	-52714.3	0.00	-0.047
13	Cd PKAC 600^0C HCl	-0.343x+1.4	0.996	-7223.2	0.02	-0.343
14	Cd PKAC 600^0C H_3PO_4	-0.05x+0.552	0.879	-49551.4	0.00	-0.05
15	Cd PKAC 600^0C H_2SO_4	-0.069x+0.598	0.976	-35906.8	0.00	-0.069
16	Cd PKAC 800^0C HCl	0.087x+-0.044	0.012	28477.8	0.60	0.087
17	Cd PKAC 800^0C H_3PO_4	-0.05x+0.566	0.816	-49551.4	0.00	-0.05
18	Cd PKAC 800^0C H_2SO_4	0.291x+-0.161	0.302	8514.0	0.58	0.291
19	Mn PKAC 600^0C HCl	0.08x+0.773	0.975	30969.7	1.5717E+2	0.08
20	Mn PKAC 600^0C H_3PO_4	0.024x+0.386	0.200	103232.2	9.65E+4	0.024
21	Mn PKAC 600^0C H_2SO_4	-0.124x+1.153	0.311	-19980.4	0.00	-0.124
22	Mn PKAC 800^0C HCl	-0.078x+0.504	0.373	-31763.7	0.00	-0.078
23	Mn PKAC 800^0C H_3PO_4	-0.139x+1.006	0.298	-17824.3	0.00	-0.139
24	Mn PKAC 800^0C H_2SO_4	-0.271x+1.55	0.571	-9142.3	0.00	-0.271

Similar results were obtained for PNAC and PKAC as presented in Tables 4.116 and 4.117 respectively. For SSAC (Table 4.118), low determination coefficient values (R^2) was obtained ranging from 0.000 to 0.932.

Generally, Dubinin-Radushkevich isotherm model is applied to express the adsorption mechanism (Gunay, 2007) with a Gaussian energy distribution onto a heterogeneous surface (Dabrowski, 2001). The approach was usually applied to distinguish the physical and chemical adsorption of metal ions (Dubinin, 1960), with its mean free energy, E per molecule of adsorbate (for removing a molecule from its location in the sorption space to the infinity) can be computed by the relationship (Hubson, 1969). $E = 1/\sqrt{2K_{ad}}$ Where K_{ad} = is isotherm constant.

Table 4.118: Temkin Adsorption Isotherm Constants for SSAC

S/N	AC Type	Equation (Y=)	R^2	$b_{T(J/mol)}$	$A_{T(L/mg)}$	$B_{(J/mol)}$
1	Ni SSAC 600^0C HCl	-0.022x+0.12	0.022	-112616.9	0.00	-0.022
2	Ni SSAC 600^0C H_3PO_4	-0.03x+0.169	0.045	-82585.7	0.00	-0.03
3	Ni SSAC 600^0C H_2SO_4	-0.131x+0.0564	0.688	-18912.8	0.65	-0.131
4	Ni SSAC 800^0C HCl	-0.198x+0.841	0.932	-12513.0	0.01	-0.198
5	Ni SSAC 800^0C H_3PO_4	0.122x-0.449	0.455	20308.0	0.03	0.122
6	Ni SSAC 800^0C H_2SO_4	-0.181x+0.779	0.435	-13688.2	0.01	-0.181
7	Pb SSAC 600^0C HCl	-0.262x+1.104	0.279	-9456.4	0.01	-0.262
8	Pb SSAC 600^0C H_3PO_4	0.074x-0.034	0.187	33480.7	0.63	0.074
9	Pb SSAC 600^0C H_2SO_4	-0.061x+0.337	0.446	-40615.9	0.00	-0.061
10	Pb SSAC 800^0C HCl	0.1x-0.287	0.647	24775.7	0.06	0.1
11	Pb SSAC 800^0C H_3PO_4	-0.6x19+0.133	0.078	-4002.5	0.81	-0.619
12	Pb SSAC 800^0C H_2SO_4	0.01x+0.012	0.007	247757.2	3.32	0.01
13	Cd SSAC 600^0C HCl	0.01x-0.013	0.000	247757.2	0.27	0.01
14	Cd SSAC 600^0C H_3PO_4	-0.227+x0.933	0.209	-10914.4	0.02	-0.227
15	Cd SSAC 600^0C H_2SO_4	-0.167x+0.688	0.194	-14835.8	0.02	-0.167
16	Cd SSAC 800^0C HCl	-0.142x+0.588	0.588	-17447.7	0.02	-0.142
17	Cd SSAC 800^0C H_3PO_4	-0.192x+0.788	0.775	-12904.0	0.02	-0.192
18	Cd SSAC 800^0C H_2SO_4	-0.134x+0.553	0.126	-18489.3	0.02	-0.134
19	Mn SSAC 600^0C HCl	-0.235x+1.235	0.549	-10542.9	0.01	-0.235
20	Mn SSAC 600^0C H_3PO_4	0.09x+0.857	0.382	27528.6	1.36E+2	0.09
21	Mn SSAC 600^0C H_2SO_4	0.044x+0.924	0.081	56308.5	1.31E+7	0.044
22	Mn SSAC 800^0C HCl	-0.031x+0.187	0.241	-79921.7	0.00	-0.031
23	Mn SSAC 800^0C H_3PO_4	0.053x-0.18	0.373	46746.6	0.03	0.053
24	Mn SSAC 800^0C H_2SO_4	-0.016x+0.151	0.011	-154848.3	0.00	-0.016

From the results of energy of activation, E obtained for OBAC (Table 4.119), it can be said that the adsorption followed physiosorption since E in all the activated carbon types are less than 8kJ/mol, and according to Ozean, et al., (2005), which says that if the energy of activation is less than 8kJ/mol, the adsorption follows physiosorption and if it is 8-16kJ/mol, then it is chemorsorption in nature. From the result, it implies that at room temperature, the adsorption of Pb, Mn, Cd and Ni onto OBAC followed physical adsorption.

Table 4.119: Dubinin Rudushkevich Adsorption Isotherm Constants for OBAC

S/N	AC Type	Equation (Y=)	R^2	K_{ad} (mol^2/kJ^2)	q_s mg/g	qe mg/g (exp)	E (J/mol)
1	Ni OBAC 600^0C HCl	0.126x-0.824	0.136	0.126	0.44	0.58	1.99
2	Ni OBAC 600^0C H_2SO_4	0.132x-0.769	0.416	0.132	0.46	0.53	1.95
3	Ni OBAC 600^0C H_3PO_4	12x-1.446	0.702	12.000	0.24	0.54	0.20
4	Ni OBAC 800^OC HCl	9.292x-1.898	0.297	9.292	0.15	0.53	0.23
5	Ni OBAC 800^OC H_2SO_4	10.83x-1.392	0.003	10.830	0.25	0.38	0.21
6	Ni OBAC 800^OC H_3PO_4	6.992x-1.958	0.458	6.992	0.14	0.36	0.27
7	Cd OBAC 600^0C HCl	90.08x-2.764	0.729	90.080	0.06	0.38	0.07
8	Cd OBAC 600^0C H_2SO_4	0.021x-0.757	0.334	0.021	0.47	0.54	4.88
9	Cd OBAC 600^0C H_3PO_4	131.7x-2.706	0.994	131.700	0.07	0.32	0.06
10	Cd OBAC 800^OC HCl	38.39x-2.332	0.561	38.390	0.10	0.42	0.11
11	Cd OBAC 800^OC H_2SO_4	120.5x-2143	0.035	120.500	0.00	0.21	0.06
12	Cd OBAC 800^OC H_3PO_4	608.1x-4.665	0.846	608.100	0.01	0.27	0.03
13	Pb OBAC 600^0C HCl	-126.9x-2.031	0.745	-126.900	0.13	0.1	0.00
14	Pb OBAC 600^0C H_3PO_4	-182.7x-1.334	0.739	-182.700	0.26	0.1	0.00
15	Pb OBAC 600^0C H_2SO_4	-121.5x-2.277	0.267	-121.500	0.10	0.18	0.00
16	Pb OBAC 800^0C HCl	-0.038x-0.582	0.896	-0.038	0.56	0.55	0.00
17	Pb OBAC 800^0C H_3PO_4	-0.055x-0.635	0.906	-0.055	0.53	0.57	0.00
18	Pb OBAC 800^0C H_2SO_4	0x-0.764	0.038	0.000	0.47	0.54	0.00
19	Mn OBAC 600^0C HCl	-1351x-1.51	0.377	-1351.000	0.22	0.29	0.00
20	Mn OBAC 600^0C H_3PO_4	-365.5x-2.107	0.090	-365.500	0.12	0.17	0.00
21	Mn OBAC 600^0C H_2SO_4	66.11x+2.937	0.016	66.110	18.86	0.07	0.09
22	Mn OBAC 800^0C HCl	9.33x-0.856	0.767	9.330	0.42	1.26	0.23
23	Mn OBAC 800^0C H_3PO_4	0.228x-0.917	0.145	0.228	0.40	0.79	1.48
24	Mn OBAC 800^0C H_2SO_4	54.82x-0.979	0.159	54.820	0.38	0.72	0.10

The result of energy of activation, E obtained for PNAC (Table 4.120), PKAC (Table 4.121) and SSAC (Table 4.122) also followed physiosorption adsorption type having had less than 8kJ/mol of energy of activation.

The theoretical adsorption capacity, q_s obtained from the application of D-R isotherm model equation ranged from 0.00mg/g to 18.86mg/g for OBAC, 0.01mg/g to 0.90mg/g for PNAC, 0.02mg/g to 1.41mg/g for PKAC and 0.00mg/g to 1.14mg/g for SSAC. Comparing the q_s result with the q_e experimental (q_e exp), it was seen that both adsorption capacity were close in almost all the activated carbon types prepared. A similar result was obtained for PNAC, PKAC and SSAC.

Table 4.120: Dubinin Rudushkevich Adsorption Isotherm Constants for PNAC

S/N	AC Type	Equation (Y=)	R^2	K_{ad} (mol^2/kJ^2)	q_s mg/g	q_e mg/g (exp)	E (J/mol)
1	Ni PNAC 600^0C HCl	195.8x-3.547	0.549	195.80	0.03	0.34	0.05
2	Ni PNAC 600^0C H_3PO_4	151.3x-2.67	0.691	151.30	0.07	0.30	0.06
3	Ni PNAC 600^0C H_2SO_4	12.22x-1.306	0.628	12.22	0.27	0.32	0.20
4	Ni PNAC 800^0C HCl	103.5x-2.319	0.739	103.50	0.10	0.46	0.07
5	Ni PNAC 800^0C H_3PO_4	53.15x-1.713	0.748	53.15	0.18	0.34	0.10
6	Ni PNAC 800^0C H_2SO_4	55.55x-1.744	0.803	55.55	0.17	0.34	0.09
7	Pb PNAC 600^0C HCl	0.009x-0.863	0.015	0.01	0.42	0.57	7.45
8	Pb PNAC 600^0C H_3PO_4	-0.056x-0.673	0.651	-0.06	0.51	0.54	0.00
9	Pb PNAC 600^0C H_2SO_4	-0.055x-0.671	0.455	-0.06	0.51	0.55	0.00
10	Pb PNAC 800^0C HCl	0.063x-1.086	0.559	0.06	0.34	0.57	2.82
11	Pb PNAC 800^0C H_3PO_4	7.151x-1.814	0.826	7.15	0.16	0.27	0.26
12	Pb PNAC 800^0C H_2SO_4	4.7x-1.675	0.489	4.70	0.19	0.27	0.33
13	Cd PNAC 600^0C HCl	190.4x-3.393	0.648	190.40	0.03	0.33	0.05
14	Cd PNAC 600^0C H_3PO_4	477x-4.351	0.861	477.00	0.01	0.23	0.03
15	Cd PNAC 600^0C H_2SO_4	433.4x-3.773	0.987	433.40	0.02	0.19	0.03
16	Cd PNAC 800^0C HCl	213.4x-3.652	0.800	213.40	0.03	0.33	0.05
17	Cd PNAC 800^0C H_3PO_4	216.4x-2.942	0.747	216.40	0.05	0.21	0.05
18	Cd PNAC 800^0C H_2SO_4	5.123x-1.534	0.840	5.12	0.22	0.49	0.31
19	Mn PNAC 600^0C HCl	-73.62x-0.104	0.469	-73.62	0.90	0.86	0.00
20	Mn PNAC 600^0CH_2SO_4	98.33x-1.219	0.129	98.33	0.30	0.55	0.07
21	Mn PNAC 600^0C H_3PO_4	52.56x-1.027	0.113	52.56	0.36	0.67	0.10
22	Mn PNAC 800^0C HCl	178.1x-1.583	0.287	178.10	0.21	0.68	0.05
23	Mn PNAC 800^0CH_3PO_4	47.9x-1.06	0.170	47.90	0.35	0.72	0.10
24	Mn PNAC 800^0CH_2SO_4	14.04x-0.859	0.079	14.04	0.42	0.92	0.19

The determination coefficients obtained for the activated carbon types were relatively high and that indicates a good fit of the data obtained except for SSAC.

Table 4.121: Dubinin Rudushkevich Adsorption Isotherm Constants for PKAC

S/N	AC Type	Equation (Y=)	R^2	K_{ad} (mol^2/kJ^2)	q_s mg/g	qe mg/g (exp)	E (J/mol)
1	Ni PKAC 600^0C HCl	276.9x-2.956	0.795	276.90	0.05	0.24	0.04
2	Ni PKAC 600^0C H_3PO_4	5.804x-1.196	0.461	5.80	0.30	0.52	0.29
3	Ni PKAC 600^0C H_2SO_4	191.8x-2.72	0.628	191.80	0.07	0.13	0.05
4	Ni PKAC 800^0C HCl	249.9x-3.209	0.608	249.90	0.04	0.30	0.04
5	Ni PKAC 800^0C H_3PO_4	124.9x-2.25	0.897	124.90	0.11	0.30	0.06
6	Ni PKAC 800^0C H_2SO_4	25.69x-1.744	0.580	25.69	0.17	0.45	0.14
7	Pb PKAC 600^0C HCl	-0.05x-0.729	0.821	-0.05	0.48	0.51	0.00
8	Pb PKAC 600^0C H_3PO_4	-3.803x-1.675	0.032	-3.80	0.19	0.22	0.00
9	Pb PKAC 600^0C H_2SO_4	0.365x-1.274	0.576	0.37	0.28	0.30	1.17
10	Pb PKAC 800^0C HCl	-0.728x-0.998	0.674	-0.73	0.37	0.39	0.00
11	Pb PKAC 800^0C H_3PO_4	-1.114x+0.347	0.105	-1.11	1.41	0.43	0.00
12	Pb PKAC 800^0C H_2SO_4	0.872x-1.399	0.419	0.87	0.25	0.32	0.76
13	Cd PKAC 600^0C HCl	376.8x-4.144	0.873	376.80	0.02	0.27	0.04
14	Cd PKAC 600^0C H_3PO_4	0.087x-0.803	0.392	0.09	0.45	0.53	2.40
15	Cd PKAC 600^0C H_2SO_4	1.183x-0.916	0.890	1.18	0.40	0.48	0.65
16	Cd PKAC 800^0C HCl	206.4x-2.723	0.134	206.40	0.07	0.66	0.05
17	Cd PKAC 800^0C H_3PO_4	0.666x-0.845	0.644	0.67	0.43	0.48	0.87
18	Cd PKAC 800^0C H_2SO_4	8.348x-2.127	0.385	8.35	0.12	0.51	0.24
19	Mn PKAC 600^0C HCl	-0.067x+0.044	0.955	-0.07	1.04	1.08	0.00
20	Mn PKAC 600^0C H_3PO_4	-8.112x-0.696	0.187	-8.11	0.50	0.54	0.00
21	Mn PKAC 600^0C H_2SO_4	5.497x-0.468	0.080	5.50	0.63	0.98	0.30
22	Mn PKAC 800^0C HCl	2.5x-1.208	0.041	2.50	0.30	0.41	0.45
23	Mn PKAC 800^0C H_3PO_4	64.22x-1.052	0.123	64.22	0.35	0.61	0.09
24	Mn PKAC 800^0C H_2SO_4	72.36x-1.532	0.213	72.36	0.22	0.74	0.08

Table 4.122: Dubinin Rudushkevich Adsorption Isotherm Constants for SSAC

S/N	AC Type	Equation (Y=)	R^2	K_{ad} (mol^2/kJ^2)	q_s mg/g	qe mg/g (exp)	E (J/mol)
1	Ni SSAC 600^0C HCl	479x-4.548	0.089	479.00	0.01	0.05	0.03
2	Ni SSAC 600^0C H_3PO_4	332.9x-3.662	0.263	332.90	0.03	0.07	0.04
3	Ni SSAC 600^0C H_2SO_4	1022x-5.524	0.640	1022.00	0.00	0.07	0.02
4	Ni SSAC 800^0C HCl	776.8x-4.882	0.939	776.80	0.01	0.11	0.03
5	Ni SSAC 800^0C H_3PO_4	-670.5x-1.822	0.456	-670.50	0.16	0.07	0.00
6	Ni SSAC 800^0C H_2SO_4	480.2x-4.089	0.244	480.20	0.02	0.13	0.03
7	Pb SSAC 600^0C HCl	y = x	1.000	y = x	1.00	0.52	0.00
8	Pb SSAC 600^0C H_3PO_4	-12.72x-1.477	0.101	-12.72	0.23	0.27	0.00
9	Pb SSAC 600^0C H_2SO_4	28.23x-2.327	0.588	28.23	0.10	0.19	0.13
10	Pb SSAC 800^0C HCl	-167x-1.855	0.549	-167.00	0.16	0.11	0.00
11	Pb SSAC 800^0C H_3PO_4	33.29x-2.966	0.060	33.29	0.05	0.09	0.12
12	Pb SSAC 800^0C H_2SO_4	-24.19x-3.067	0.004	-24.19	0.05	0.08	0.00
13	Cd SSAC 600^0C HCl	-352.5x-2.872	0.009	-352.50	0.06	0.04	0.00
14	Cd SSAC 600^0C H_3PO_4	-0.984x-3.304	0.040	-0.98	0.04	0.06	0.00
15	Cd SSAC 600^0C H_2SO_4	2079x-8.348	0.321	2079.00	0.00	0.04	0.02
16	Cd SSAC 800^0C HCl	1051x-6.027	0.515	1051.00	0.00	0.04	0.02
17	Cd SSAC 800^0C H_3PO_4	2419x-9.153	0.857	2419.00	0.00	0.04	0.01
18	Cd SSAC 800^0C H_2SO_4	1013x-6.199	0.051	1013.00	0.00	0.04	0.02
19	Mn SSAC 600^0C HCl	28.35x-3.099	0.233	28.35	0.05	0.69	0.13
20	Mn SSAC 600^0C H_3PO_4	-0.12x+0.129	0.761	-0.12	1.14	1.33	0.00
21	Mn SSAC 600^0C H_2SO_4	-0.418x+0.12	0.524	-0.42	1.13	1.23	0.00
22	Mn SSAC 800^0C HCl	880.7x-3.961	0.228	880.70	0.02	0.06	0.02
23	Mn SSAC 800^0C H_3PO_4	-554.2x-2.404	0.417	-554.20	0.09	0.11	0.00
24	Mn SSAC 800^0C H_2SO_4	491.3x-3.202	0.042	491.30	0.04	0.14	0.03

4.7 Percentage Adsorption of Metals on Activated Carbon

Tables 4.123 - 4.126 and Figures 4.131 – 4.134 outlined the percentage adsorption of Ni, Cd, Pb and Mn respectively on OBAC. IMC = Initial Metal Conc.

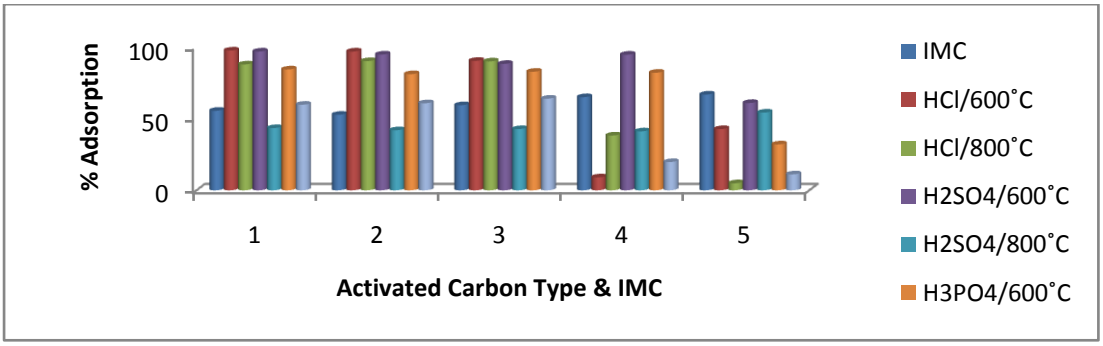

Figure 4.131: Percentage Adsorption of Ni by OBAC

From Table 4.131 as well as from Figure 4.131, it could be deduced that carbonization at 600^0C gave a better percentage adsorption compare to those of 800^0C irrespective of the activating agents.

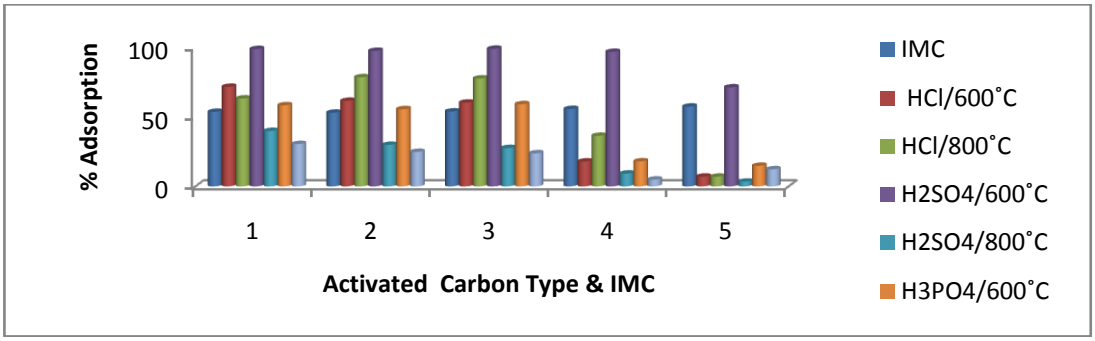

Figure 4.132: Percentage Adsorption of Cd by OBAC

In the adsorption of Cd by the OBAC, there was a better adsorption by those carbonized at 600^0C since most of the percentage adsorption are higher than those of their counter parts except for some that were activated with HCl (Table 4.124 and Figure 4.132).

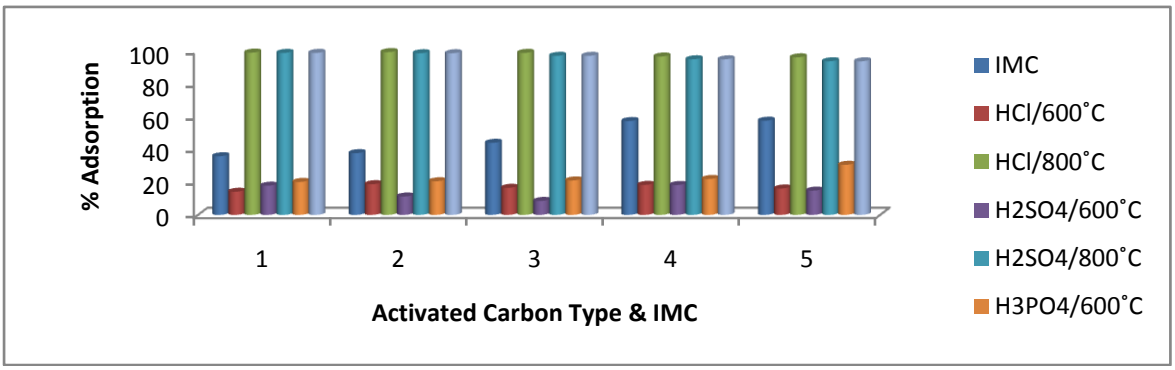

Figure 4.133: Percentage Adsorption of Pb by OBAC

In Table 4.125 Pb adsorbed better in OBAC carbonized at 800^0C and as well had a high percentage of adsorption. This is shown pictorially by Figure 4.133.

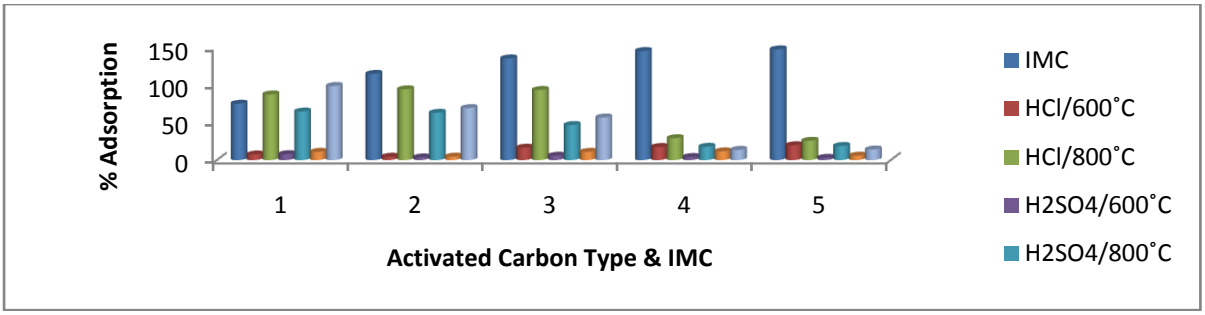

Figure 4.134: Percentage Adsorption of Mn by OBAC

Just like Pb adsorption by OBAC, Mn was adsorbed better by those carbonized at 800^0C even though the percentage adsorption was not that high (Table 4.126).

Tables 4.127 – 4.130 and Figures 4.134 – 4.138 presents the percentage adsorption of Ni, Pb, Cd and Mn respectively on PNAC.

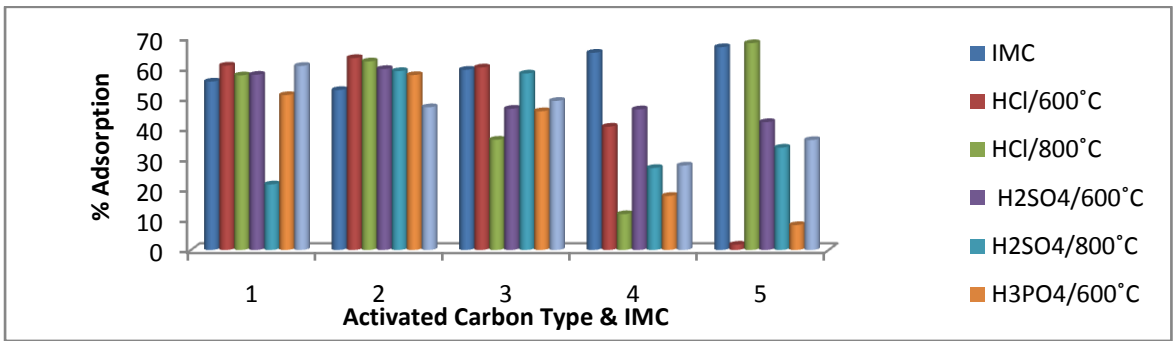

Figure 4.135: Percentage Adsorption of Ni by PNAC

From Table 4.127 and Figure 4.135 which is the percentage adsorption of Ni by PNAC, Ni adsorption by those activated with HCl and carbonized at 600^0C were better adsorbent, so also it was for those activated with H_2SO_4 and H_3PO_4 except for few of them.

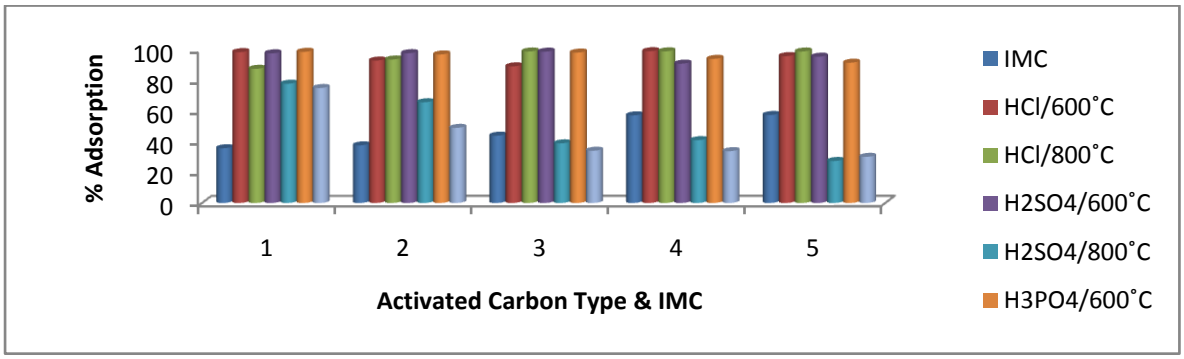

Figure 4.136: Percentage Adsorption of Pb by PNAC

Table 4.128 shows the percentage adsorption of Pb by peanut seed activated carbon. It could be deduced from this Table that those carbonized at 600^oC was better than

their counterpart except for 93.6% and 98.8% for HCl activated carbons that were carbonized at 800°C. This can easily be seen in Figure 4.136.

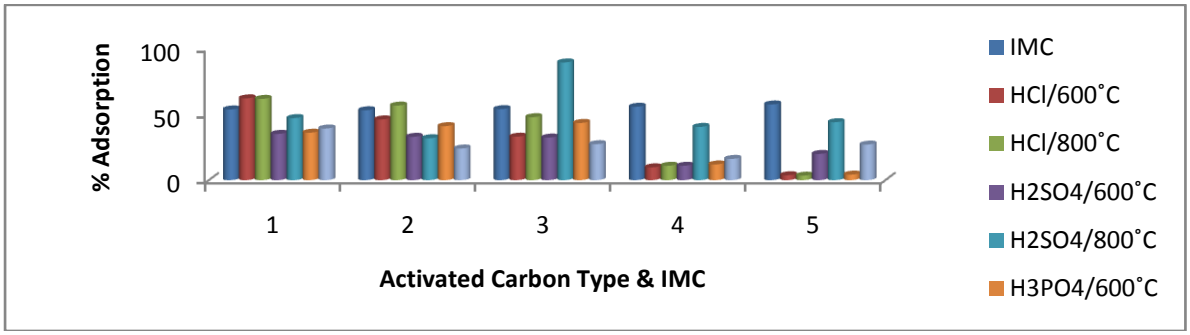

Figure 4.137: Percentage Adsorption of Cd by PNAC

In the adsorption of Cd by the Pear nut seed activated carbon, those carbonized at 800°C and activated with H_2SO_4 and H_3PO_4 were better adsorbents in most of the produced activated carbon as indicated by the percentage values of the adsorption. Generally they all had low percentage of adsorption since their values ranged between 3.4% to 62.1% except for the carbonization at 800°C with H_2SO_4 activation (Table 4.129 and Figure 4.137).

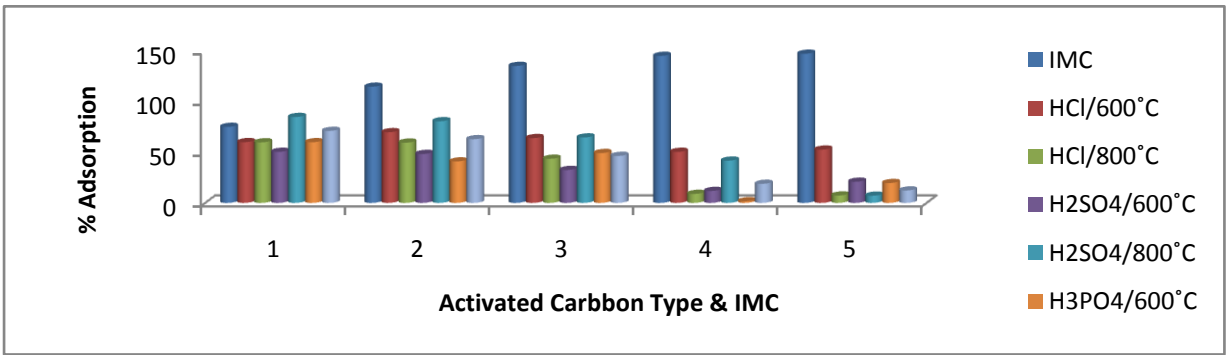

Figure 4.138: Percentage Adsorption of Mn by PNAC

The percentage Mn adsorption by PNAC as shown in Table 4.130 and Figure 4.138 indicated that those carbonized at 800°C were mostly better than their counterpart except for all those activated with HCl, 7.1% for those activated with H_2SO_4 and 46.4%, 12.3% for those activated with H_3PO_4. In general, their overall adsorptions were of average values.

Tables 4.131 – 4.134 and figures 4.139 – 4.142 outlined the percentage adsorption of Ni, Pb, Cd and Mn respectively on PKAC.

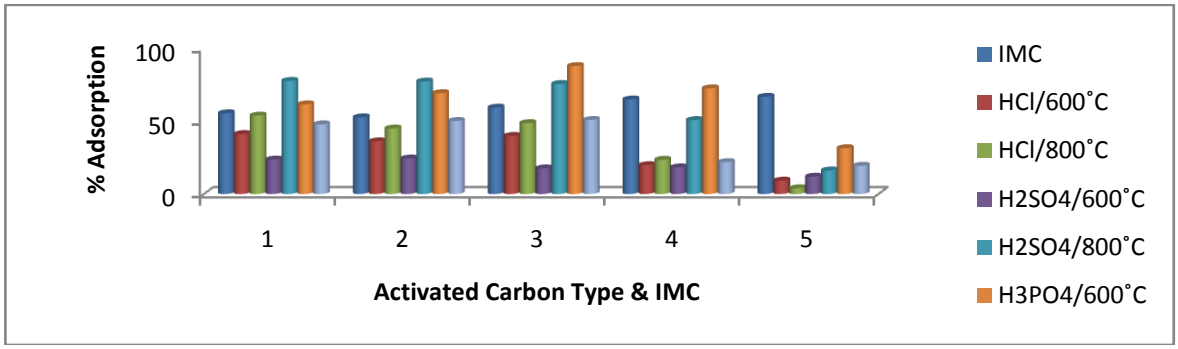

Figure 4.139: Percentage Adsorption of Ni by PKAC

The adsorption by palm Kernel shell activated carbon where generally of average and those carbonized at 800°C had a better percentage adsorption especially for the H_2SO_4 and HCl, but in the case of H_3PO_4 activated carbon, the reverse was the case in all the respective initial metal concentration (Table 4.131, Figure 4.139).

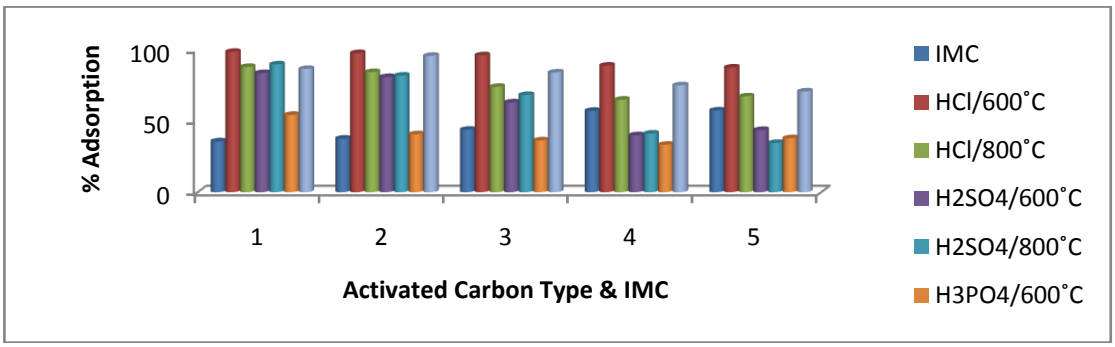

Figure 4.140: Percentage Adsorption of Pb by PKAC

From Table 4.132 and Figure 4.140, the PKAC activated with HCl and carbonized at 600°C were better adsorbent for Pb while for those activated with H_2SO_4 and H_3PO_4, and carbonized at 800°C were better adsorbents. Generally, they all had a high percentage of adsorption except for few.

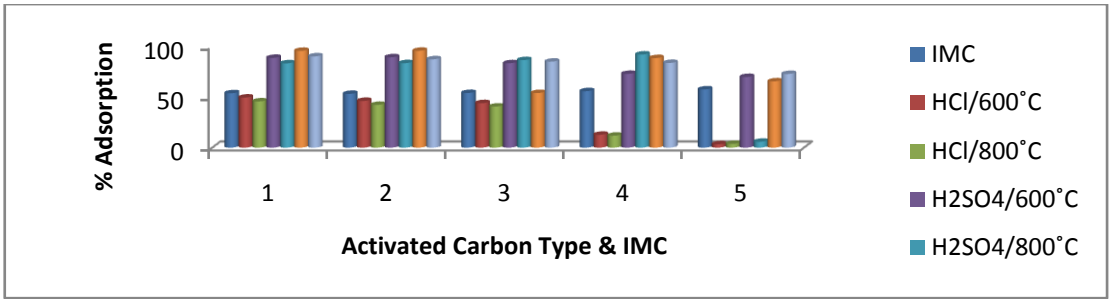

Figure 4.141: Percentage Adsorption of Cd by PKAC

In the adsorption of Cd by PKAC, those carbonized at 600°C had a better percentage adsorption in all except for 86.4%, 91.9% for those activated with H_2SO_4 and 84.9%, 72.7% for those activated with H_3PO_4. Also the percentage adsorption of the Cd was generally high (Table 4.133 and Figure 4.141).

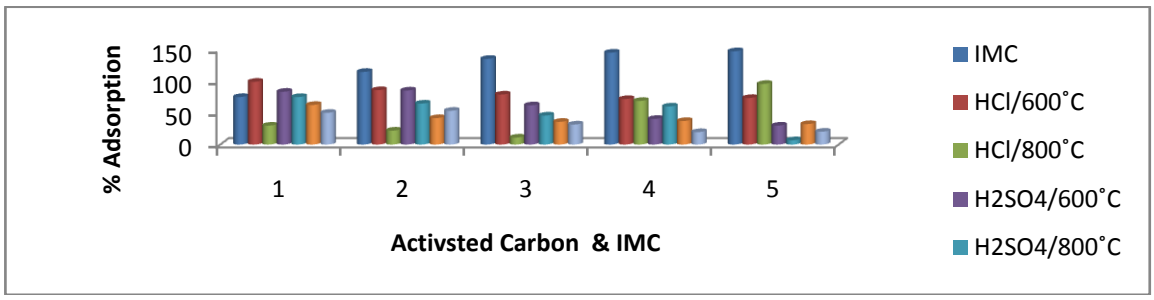

Figure 4.142: Percentage Adsorption of Mn by PKAC

The palm kernel AC had a high percentage adsorption of Mn almost in all, but those carbonized at 600°C were better of except 95.7% for those activated with HCl, 60.1% for those activated with H_2SO_4 and 53.3% for those activated with H_3PO_4 (Table 4.134, Figure 4.142). Tables 4.136 – 4.138 and Figures 4.143 – 4.146 presented the percentage adsorption of Ni, Pb, Cd and Mn onto SSAC.

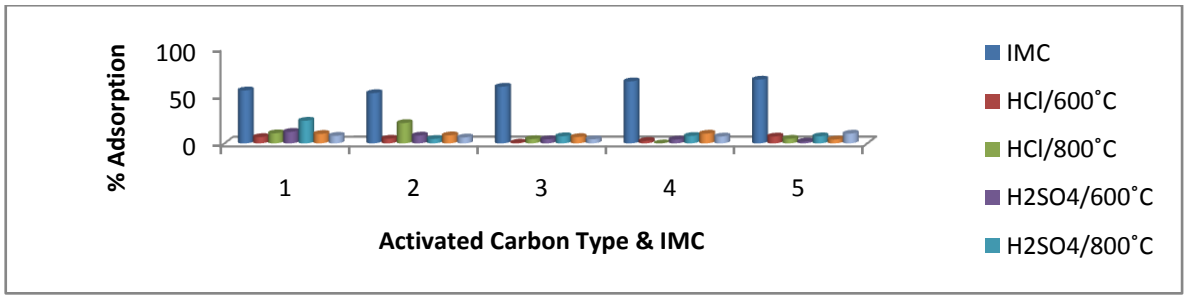

Figure 4.143: Percentage Adsorption of Ni by SSAC

The AC carbonised at 800°C had a better percentage of adsorption except for those activated with H_3PO_4, but they all generally had a low percentage of adsorption and are not suitable for the removal of Ni from industrial effluents or liquid wastes (Table 4.135 and Figure 4.143).

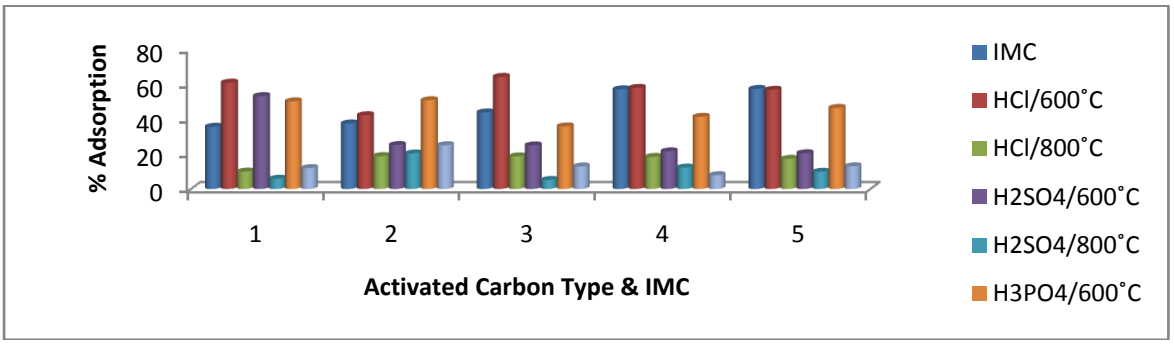

Figure 4.144: Percentage Adsorption of Pb by SSAC

In the adsorption of Pb by SSAC, the AC carbonized at 600°C had a better percentage adsorption irrespective of the activating agent used though they all had low percentage of adsorption. This showed that it is not viable for use in the removal of Pb from waste (Table 4.136 and Figure 4.144).

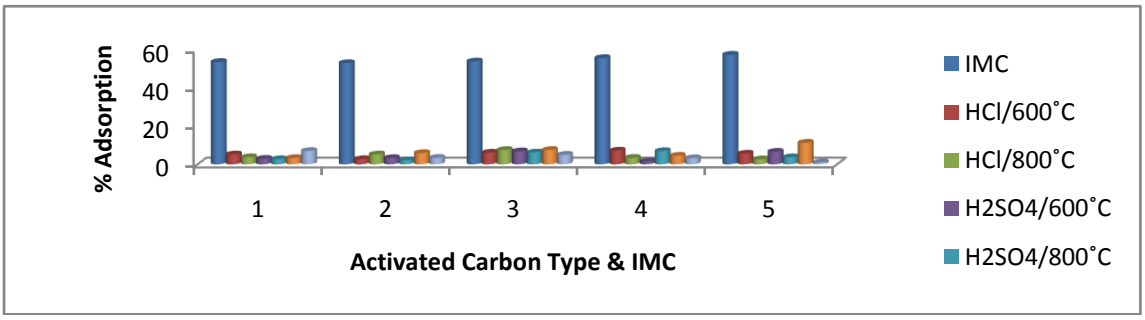

Figure 4.145: Percentage Adsorption of Cd by SSAC

The adsorption of Cd by SSAC carbonized at both temperature values and activated with different reagents/acids was very low in all, though those carbonized at 600°C had a better percentage adsorption in most. Based on the aforesaid reason, they are not suitable to be used in the removal of Cd from liquid industrial effluents (Table 4.137, Figure 4.145).

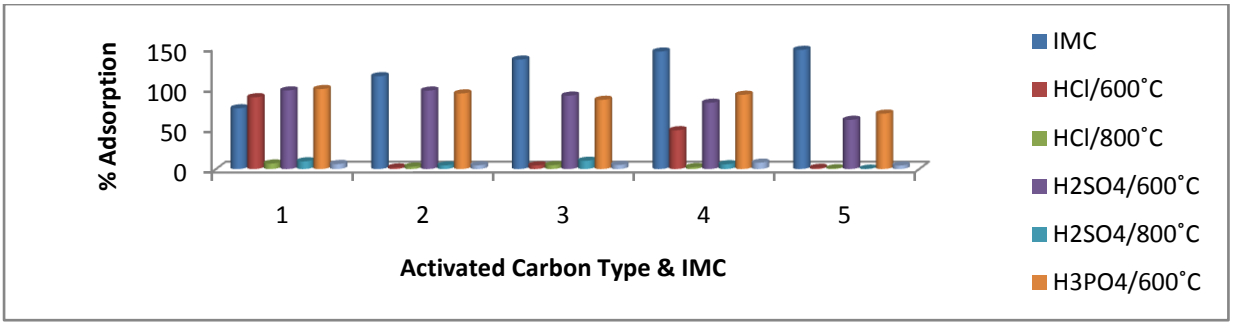

Figure 4.146: Percentage Adsorption of Mn by SSAC

The percentage adsorptions of Mn by SSAC were generally low though those carbonized at 600°C had a better adsorption especially those activated with H_3PO_4 and H_2SO_4. Therefore, it is not recommended for use in the treatment of liquid industrial effluents contaminated with metals (Table 4.139).

4.8 Effects of Initial metal Concentration on Adsorption

The effect of initial concentration on the extent of adsorption of Ni(II), Cd(II), Pb(II) and Mn (II) metal ions onto activated carbon from Pear nut seed shell, Palm kernel shell, Snail shell and Oil bean shell was determined by plotting the initial metal concentration against the percentage adsorption (Tables 4.11 to 4.106, appendix C), and are presented in Figures 4.147 to 4.160. It was evident that metal ion removal decreased with an increase in the initial metal concentration. This may be attributed to the fact that the adsorbents have limited number of active sites which become saturated at a certain concentrations of the metals. This was also noted by Azouaou *et al.*, (2013).

From the figures, it can be seen that the uptake of the metals ion was rapid within the first few minutes and that rapid uptake gave a way to much slower adsorption after the first few minutes.

A similar result was obtained for almost all the activated carbon types that were prepared.

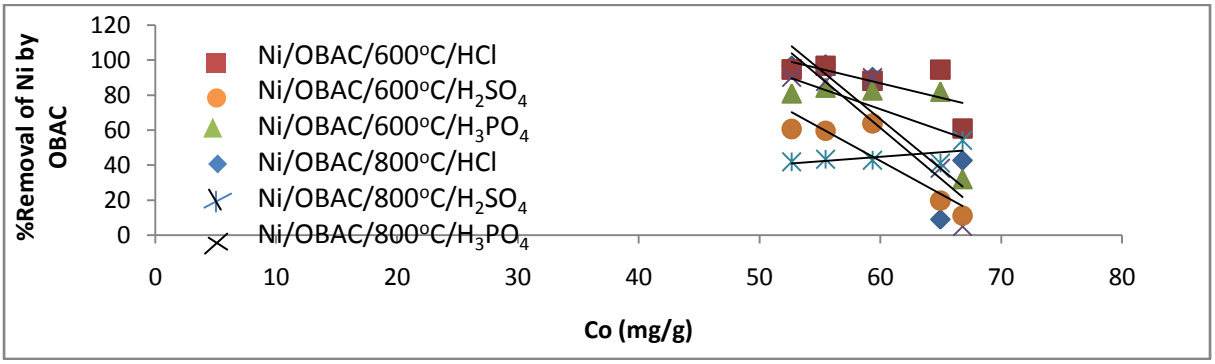

Figure 4.147: Effect of Initial Ni Concentration on the Adsorption by OBAC

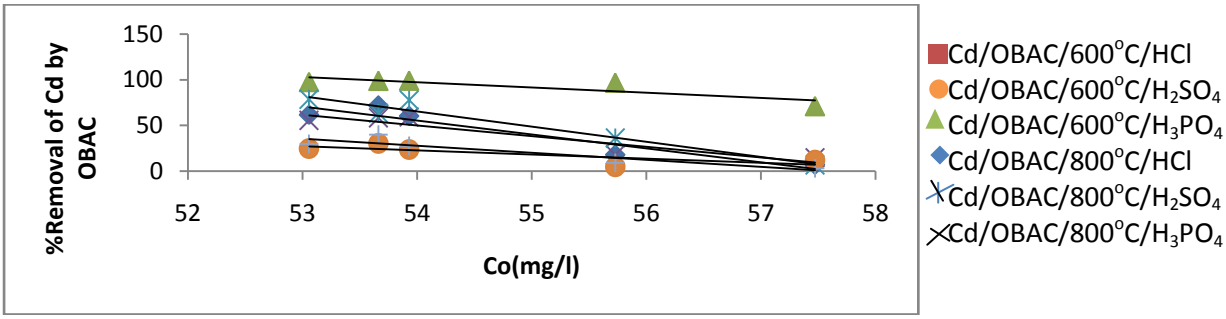

Figure 4.148: Effect of Initial Cd Concentration on the Adsorpt

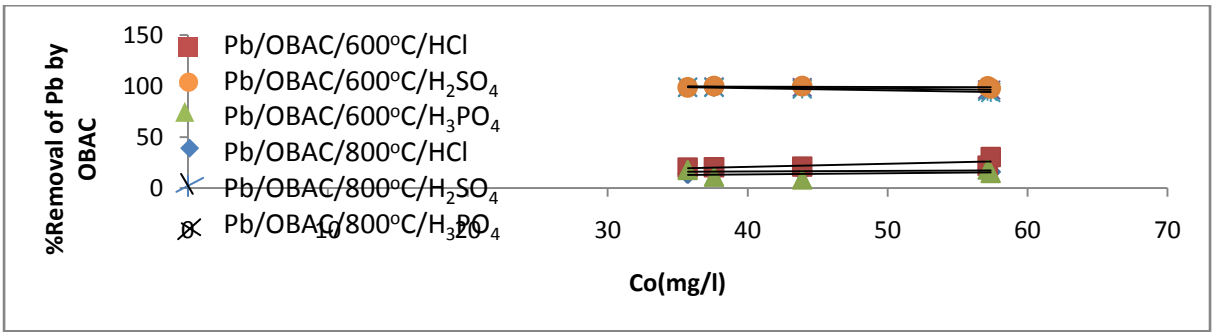

Figure 4.149: Effect of Initial Pb Concentration on the Adsorption by OBAC

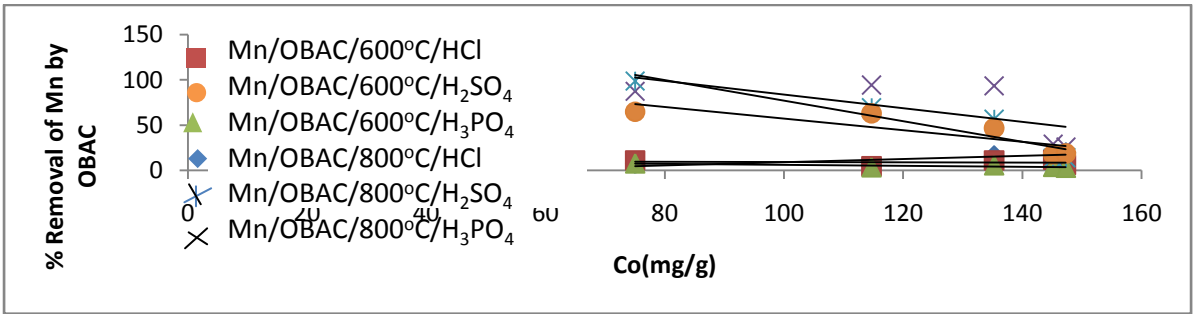

Figure 4.150: Effect of Initial Mn Concentration on the Adsorption by OBAC

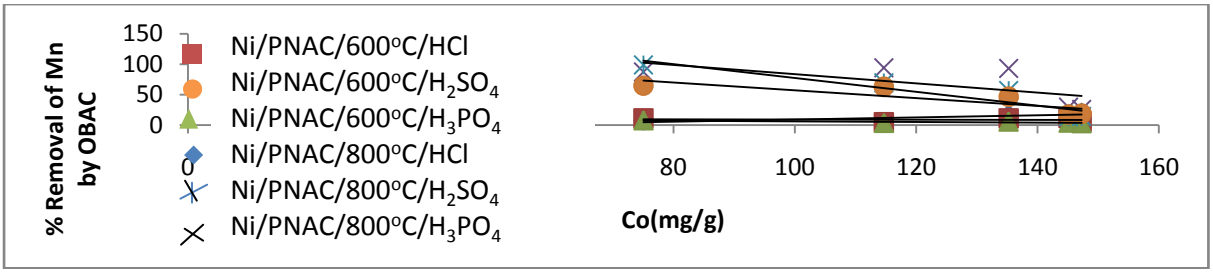

Figure 4.151: Effect of Initial Ni Concentration on the Adsorption by PNAC

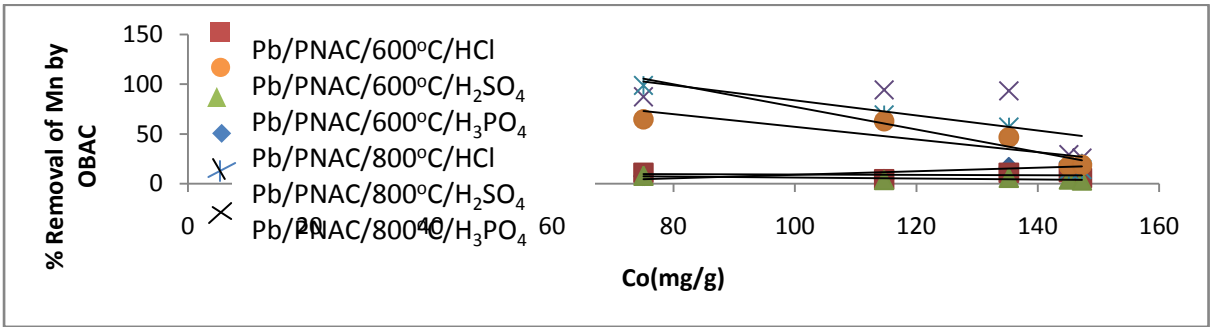

Figure 4.152: Effect of Initial Pb Concentration on the Adsorption by PNAC

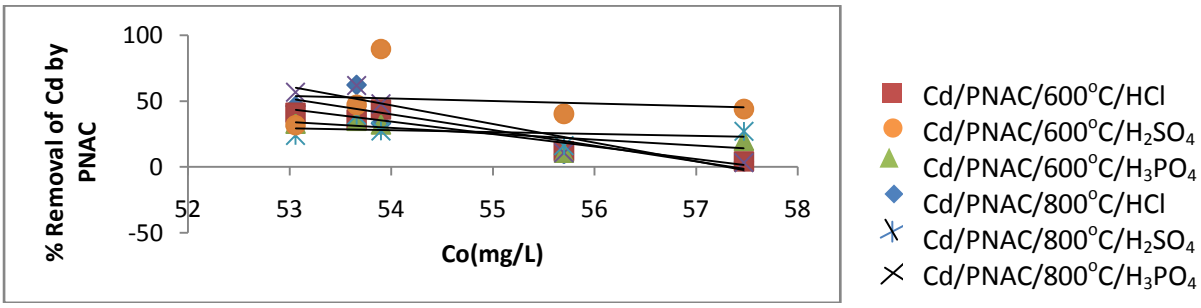

Figure 4.153: Effect of Initial Cd Concentration on the Adsorption by PNAC

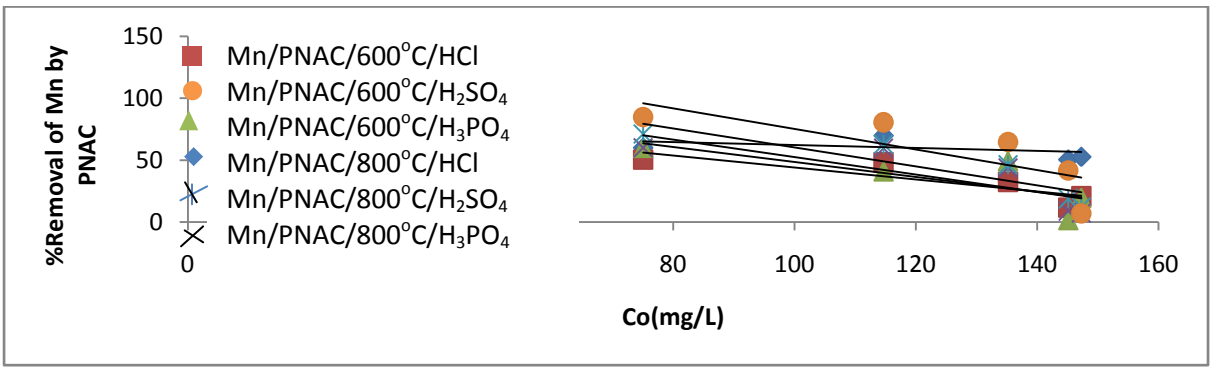

Figure 4.154: Effect of Initial Mn Concentration on the Adsorption by PNAC

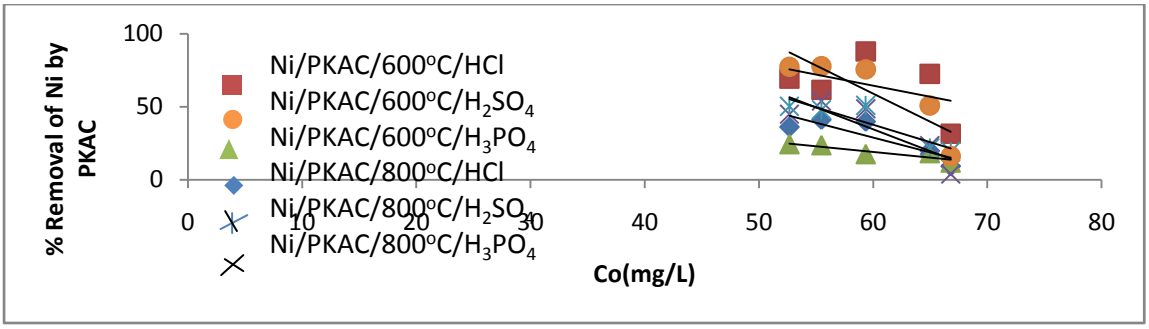

Figure 4.155: Effect of Initial Ni Concentration on the Adsorption by PKAC

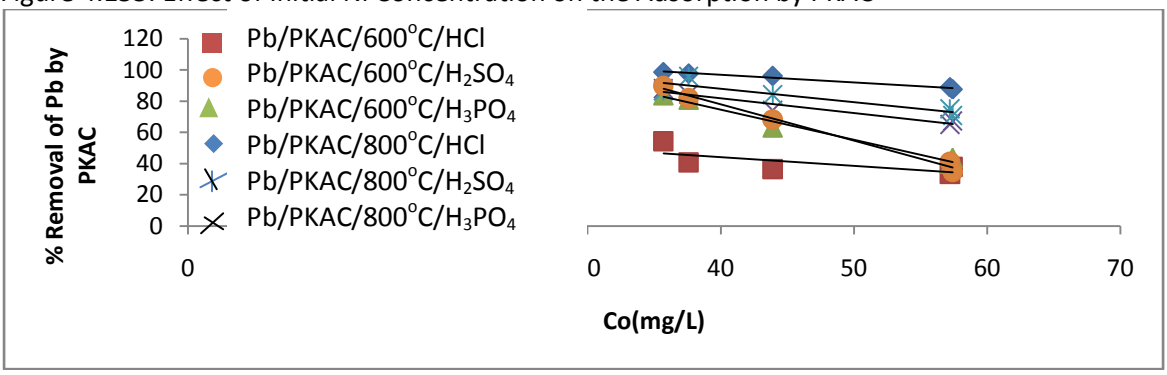

Figure 4.156: Effect of Initial PbConcentration on the Adsorption by PKAC

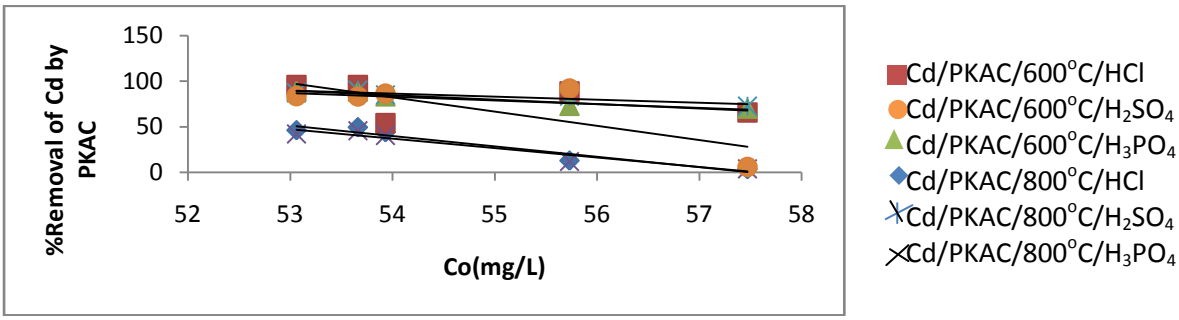

Figure 4.157: Effect of Initial Cd Concentration on the Adsorption by PKAC

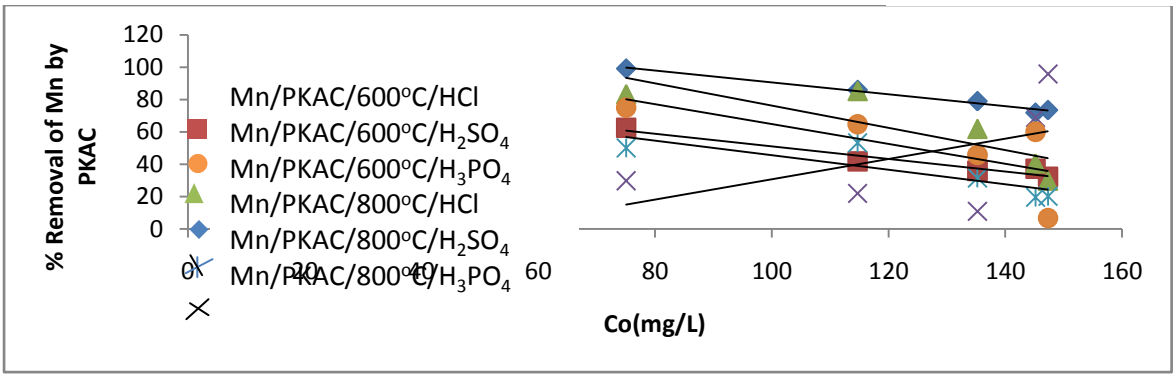

Figure 4.158: Effect of Initial Mn Concentration on the Adsorption by PKAC

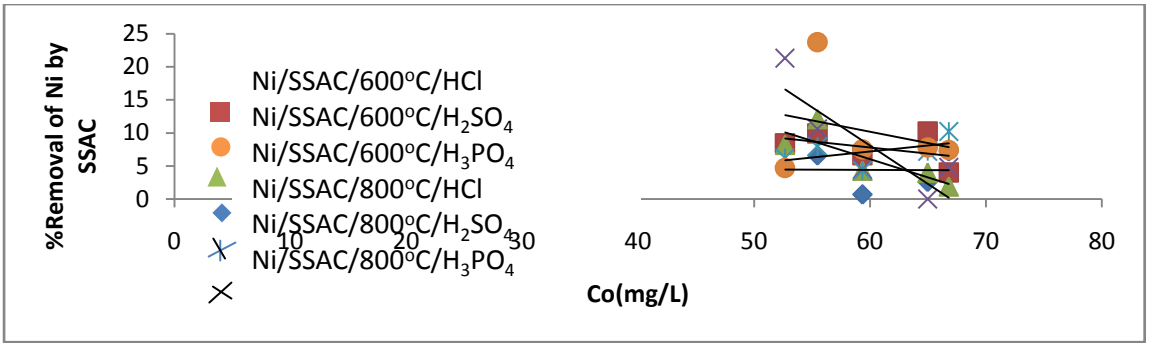

Figure 4.159: Effect of Initial Ni Concentration on the Adsorption by SSAC

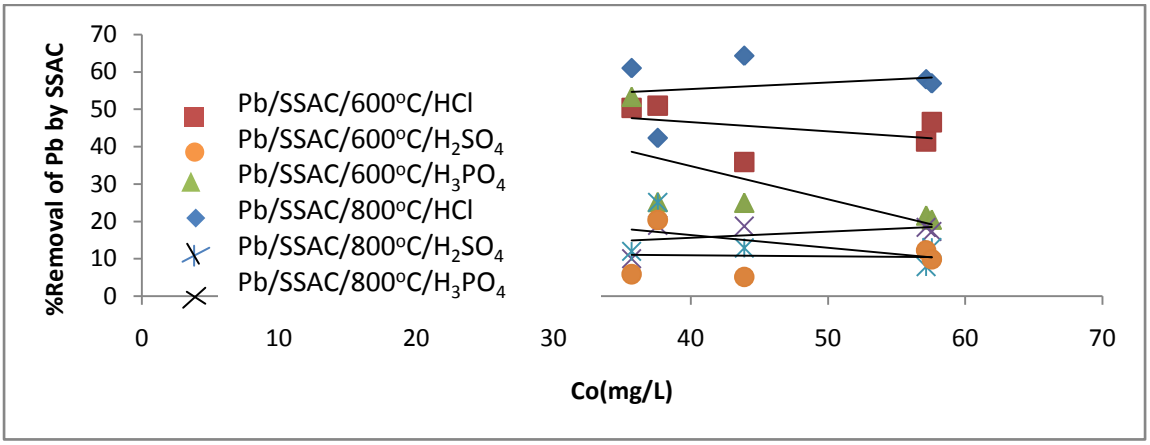

Figure 4.160: Effect of Initial Pb Concentration on the Adsorption by SSAC

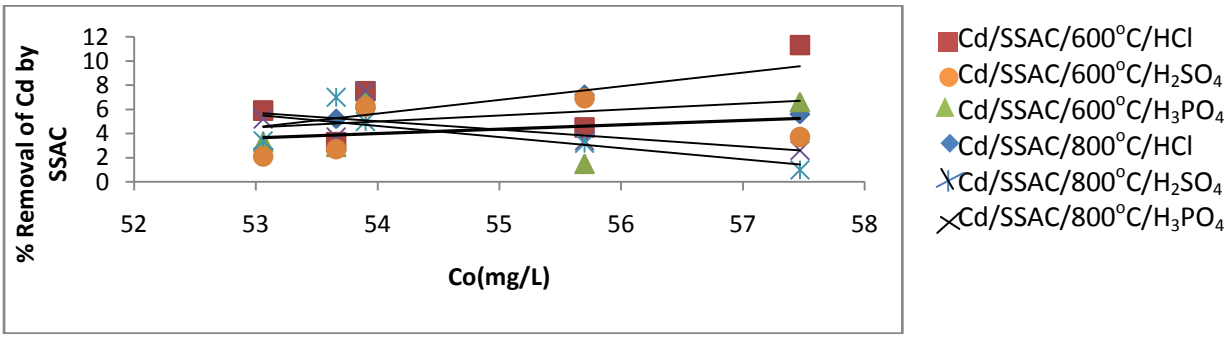

Figure 4.161: Effect of Initial Cd Concentration on the Adsorption by SSAC

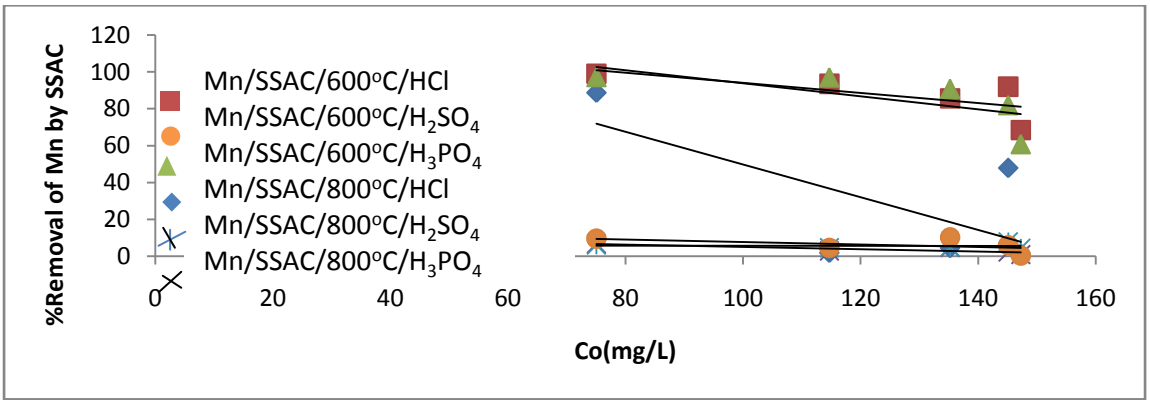

Figure 4.162: Effect of Initial Mn Concentration on the Adsorption by SSAC

4.9 Adsorption of Pb from Industrial Waste

Table 4.139 presented the percentage of Pb adsorbed from Ibeto Battery company liquid waste by the carbon samples.

Table 4.139: Percentage of Pb adsorbed from Ibeto Battery waste by the AC

Activated Carbon Type	Initial Pb Conc. (mg/l)	Amount Adsorbed (mg/g)	Percentage Adsorbed
PNAC/600^{0}C/HCl	17.95	0.95	5.3
PNAC/600^{0}C/H_2SO_4	17.95	1.17	6.5
PNAC/600^{0}C/H_3PO_4	17.95	1.99	11.1
PNAC/800^{0}C/HCl	17.95	6.75	37.6
PNAC/800^{0}C/H_2SO4	17.95	8.08	45.0
PNAC/800^{0}C/H_3PO_4	17.95	1.35	7.5
OBAC/600^{0}C/HCl	17.95	2.90	16.2
OBAC/600^{0}C/H_2SO_4	17.95	4.77	26.6
OBAC/600^{0}C/H_3PO_4	17.95	2.89	16.1
OBAC/800^{0}C/HCl	17.95	3.69	20.6
OBAC/800^{0}C/H_2SO_4	17.95	3.52	19.6
OBAC/800^{0}C/H_3PO_4	17.95	0.47	2.6
PKAC/600^{0}C/HCl	17.95	0.39	2.2
PKAC/600^{0}C/H_2SO_4	17.95	0.81	4.5
PKAC/600^{0}C/H_3PO_4	17.95	1.44	8.0
PKAC/800^{0}C/HCl	17.95	3.56	19.8
PKAC/800^{0}C/H_2SO_4	17.95	5.79	32.3
PKAC/800^{0}C/H_3PO_4	17.95	2.67	15.3
SSAC/600^{0}C/HCl	17.95	0.90	5.0
SSAC/600^{0}C/H_2SO_4	17.95	0.11	0.6
SSAC/600^{0}C/H_3PO_4	17.95	0.02	0.1
SSAC/800^{0}C/HCl	17.95	0.88	4.9
SSAC/800^{0}C/H_2SO_4	17.95	0.40	2.2
SSAC/800^{0}CH_3PO_4	17.95	0.03	0.2

PNAC = Pear nut Activated carbon, OBAC = oil bean activated carbon, PKAC = palm kernel shell activated carbon and SSAC = snail shell activated carbon.

The waste water collected from Ibeto Battery factory (Nnewi) was characterized and because Pb concentration was discovered to be at elevated concentration, it was the only metal studied with the prepared ACs. Other metal concentrations were very low and so we did not study their adsorption because when adsorbed by the ACs, we may not be able to establish the correct percentage adsorption of those metals

since the adsorbent will take up all the metal in the effluent. From the result (Table 4.139) it could be deduced that all the prepared activated carbons were good Pb adsorbents. The PNAC adsorption capacity ranged from 5.3% to 45.0% with PNAC/800^0C/H_2SO_4 recording the highest adsorbed Pb concentration. The adsorption capacity of OBAC for Pb on waste water ranged from 2.6% to 26.6%, while that of PKAC and SSAC were 2.2% to 32.3% and 0.1% to 5.0% respectively. The observed trend for the average adsorption of Pb on to the various activated carbons is PNAC > OBAC > PKAC > SSAC. This showed that when Pear nut seed is carbonized at 800^oC and activated with H_2SO_4, it serves as a good adsorbent for the treatment of waste water from Battery industries. So also it is for oil bean activated carbon, but for Palm kernel shell that was activated with HCl when carbonized at 600^oC was far better.

4.10 Kinetic Studies

The kinetics of adsorption describes the rate of metal ions uptake on the activated carbon and this rate control the equilibrium time. The kinetics of adsorbate uptake is required for selecting optimum operating conditions for the full-scale batch adsorption process (Gupta *et al.*, 2003). The kinetic parameter, which is helpful for the prediction of adsorption rate, gives important information for designing and modelling the processes. Thus the effects of initial concentration and contact time were analysed from the kinetic point of view. Preliminary studies on the adsorption rate showed that the amount adsorbed increased with increase in metal concentration. The maximum amount of metal ions was adsorbed within 80min

(90% of the total metal ions adsorbed) and thereafter, the adsorption proceeds at a slower rate until equilibrium was reached. The equilibrium time was found to be around 80 to 100min for the initial metal ion concentration range studied.

The kinetics of the adsorption data was analysed using different kinetic models such as pseudo-first-order and pseudo-second-order models. Also, intraparticle diffusion model (Weber and Morris, 1962), was applied to describe the competitive adsorption. Figures 4.145 to 4.156 outlined the pseudo-first-order, pseudo-second-order kinetic plots for PNAC used in adsorption of Pb, Ni, Cd and Mn. Tables 4.140 to 4.164 (Appendix E) present the parameters. C_t is the initial metal concentration (in mg/g), q_e is the equilibrium concentration (in mg/g), q_t is the concentration of metal at time t (in mg/l) and time T in minutes.

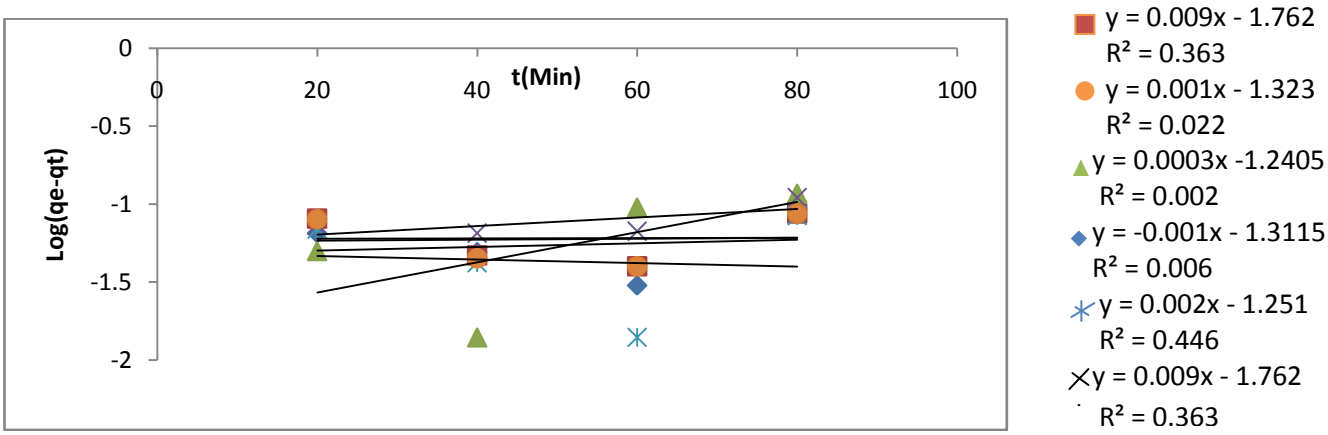

Figure 4.163: Pseudo First-order Kinetics for Pb Adsorption onto PNAC

From Figures 4.161 and 4.162, it can be deduced that the second order kinetics had a better fit of the data obtained from the adsorption of Pb on PNAC as it had higher values for the determination coefficients unlike the first order kinetics. Similar results were obtained for Cd, Mn and Ni adsorption onto PNAC.

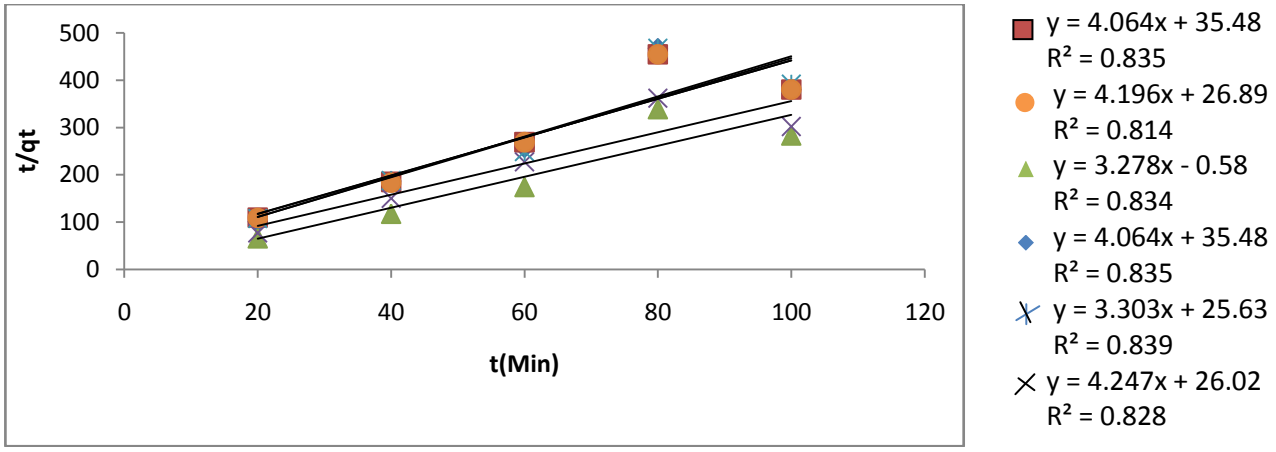

Figure 4.164: Pseudo Second-order Kinetics for Pb Adsorption onto PNAC

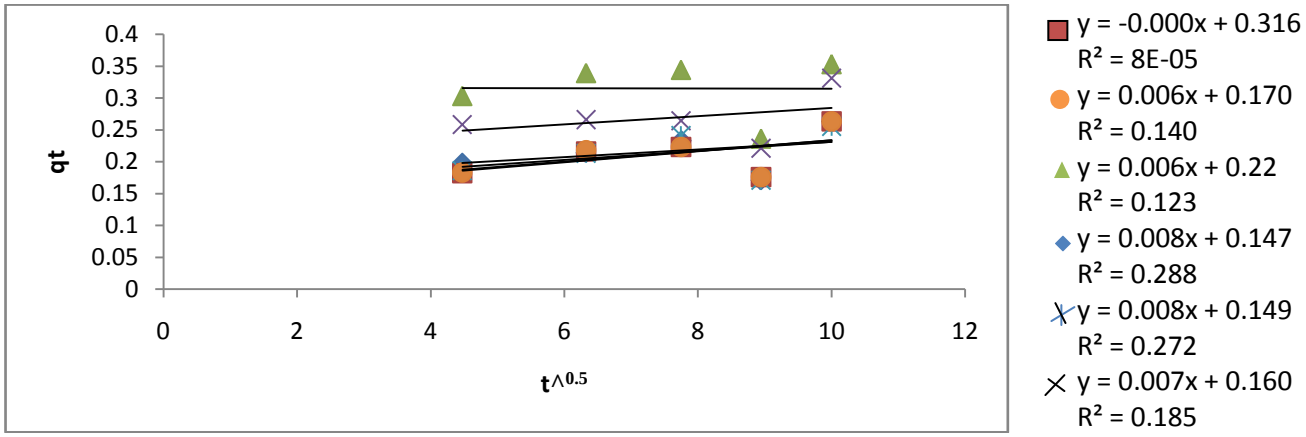

Figure 4.165: Intraparticle Diffusion for the Adsorption of Pb onto PNAC

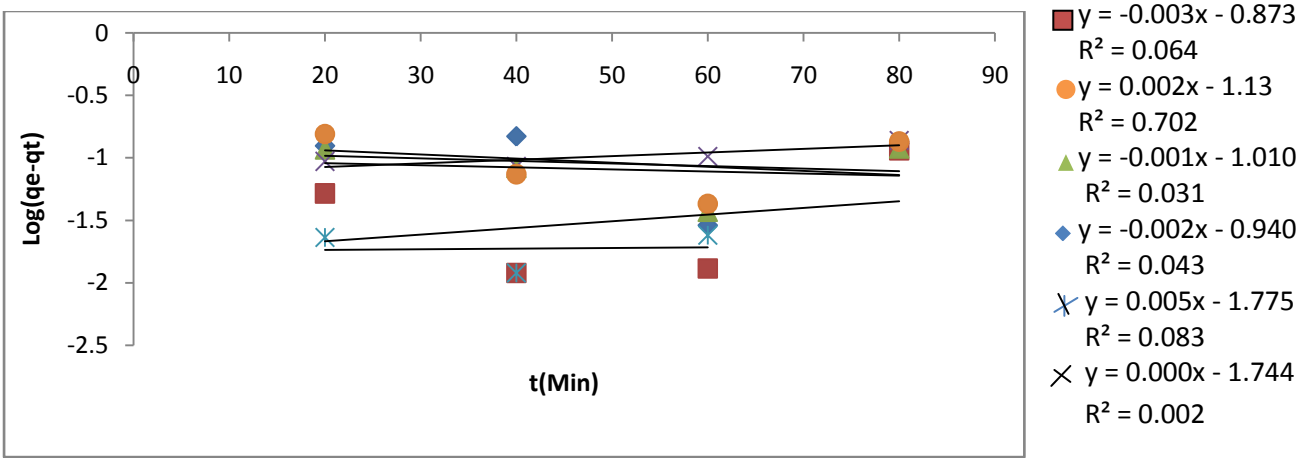

Figure 4.166: Pseudo First-order Kinetics for Ni Adsorption onto PNAC

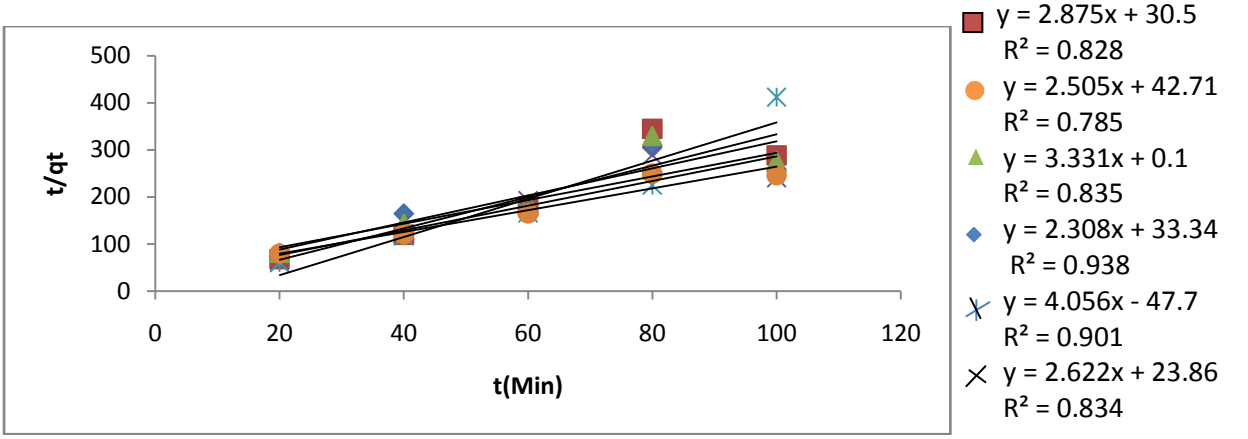

Figure 4.167: Pseudo Second-order Kinetics for Ni Adsorption onto PNAC

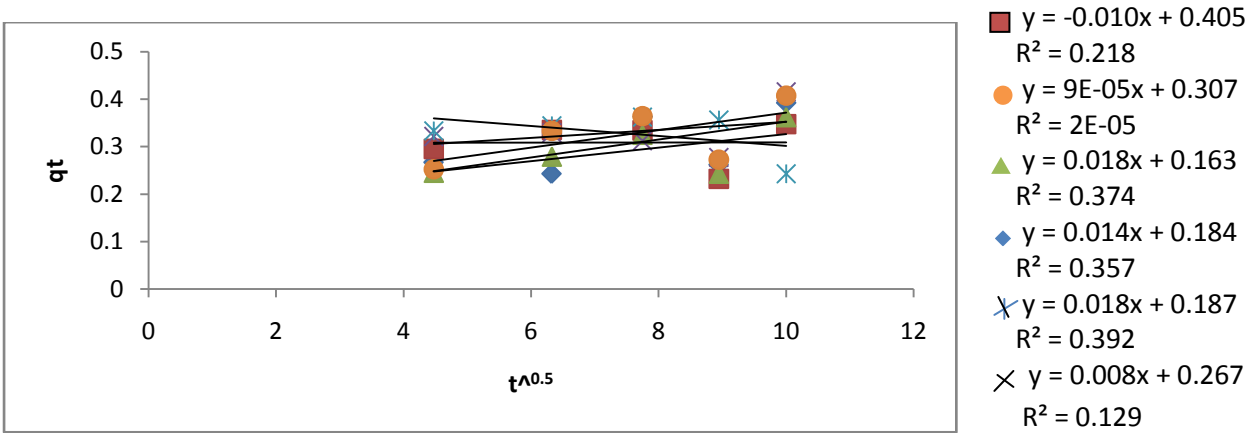

Figure 4.168: Intraparticle Diffusion for the Adsorption of Ni onto PNAC

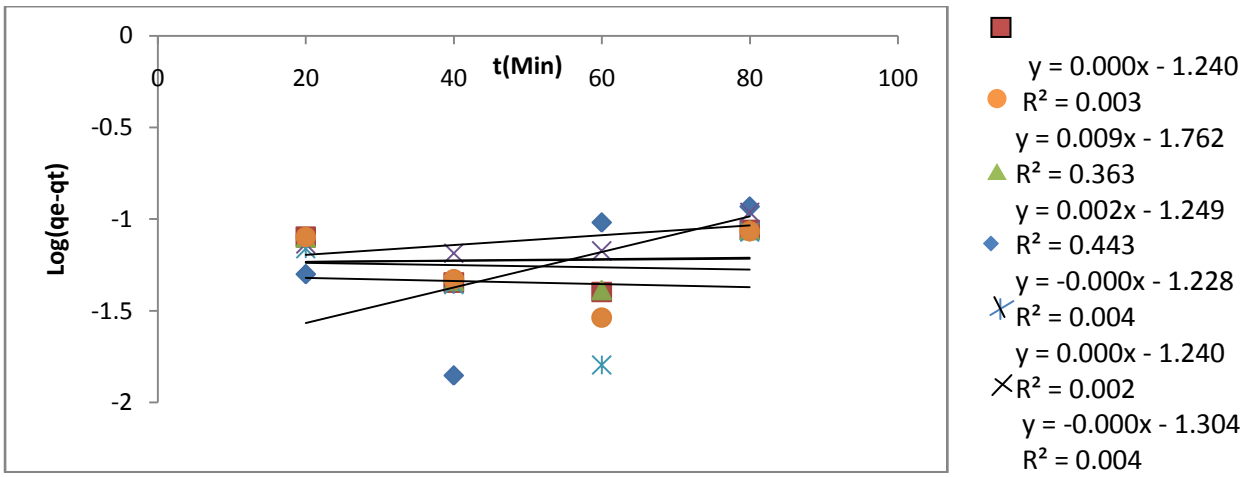

Figure 4.169: Pseudo First-order Kinetics for Cd Adsorption onto PNAC

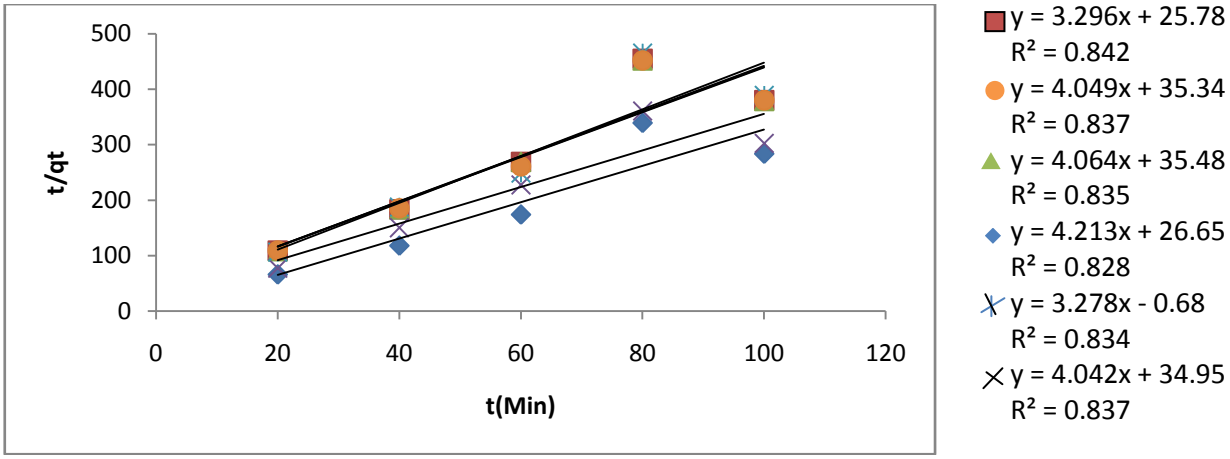

Figure 4.170: Pseudo Second-order Kinetics for Cd Adsorption onto PNAC

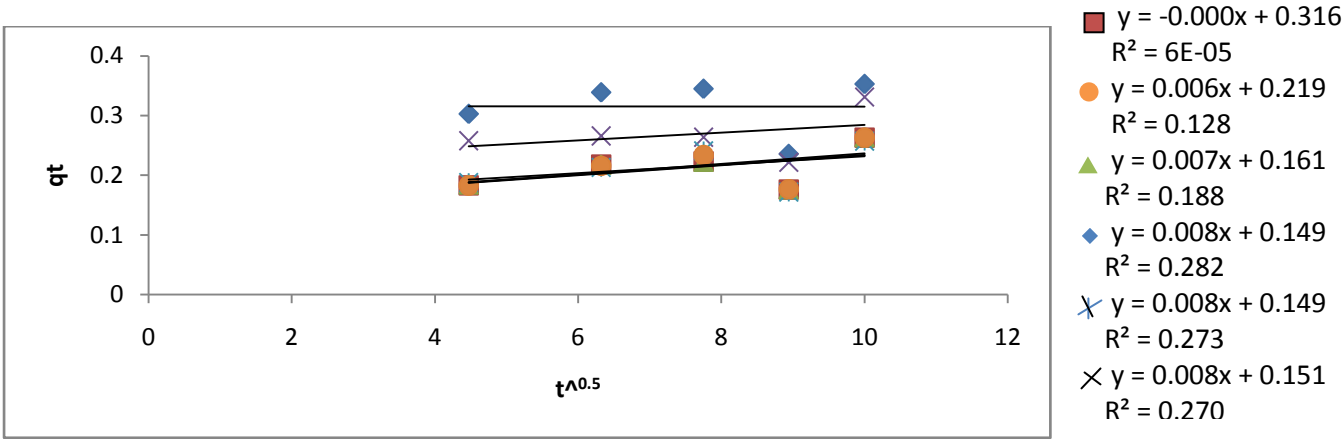

Figure 4.171: Intraparticle Diffusion for the Adsorption of Cd onto PNAC

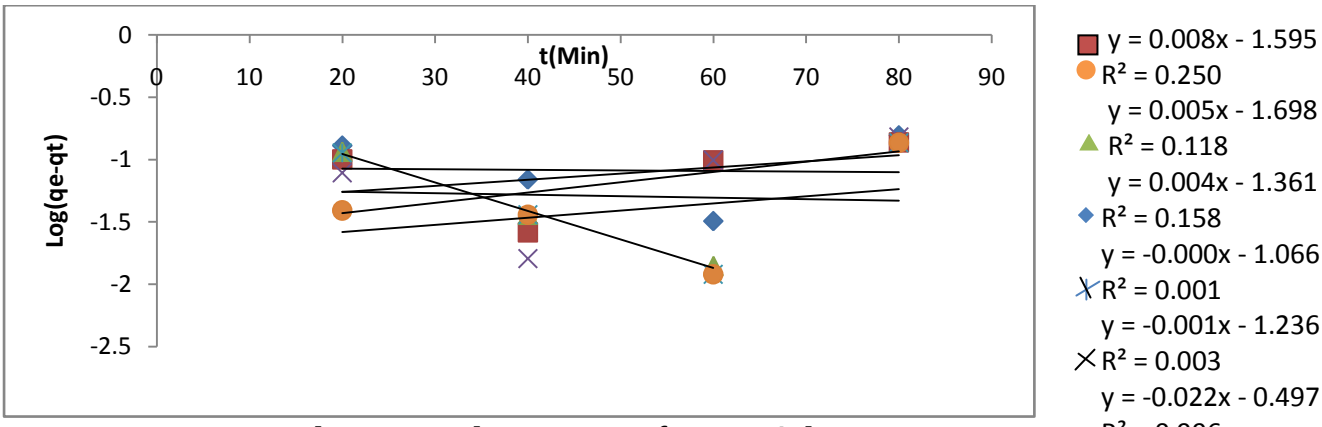

Figure 4.172: Pseudo First-order Kinetics for Mn Adsorption onto PNAC

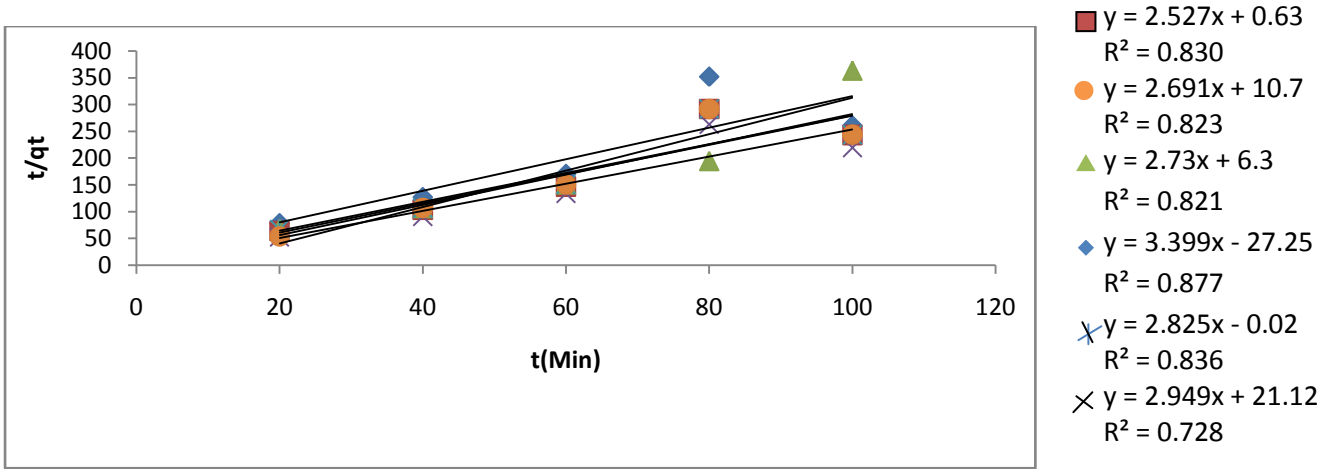

Figure 4.173: Pseudo Second-order Kinetics for Mn Adsorption onto PNAC

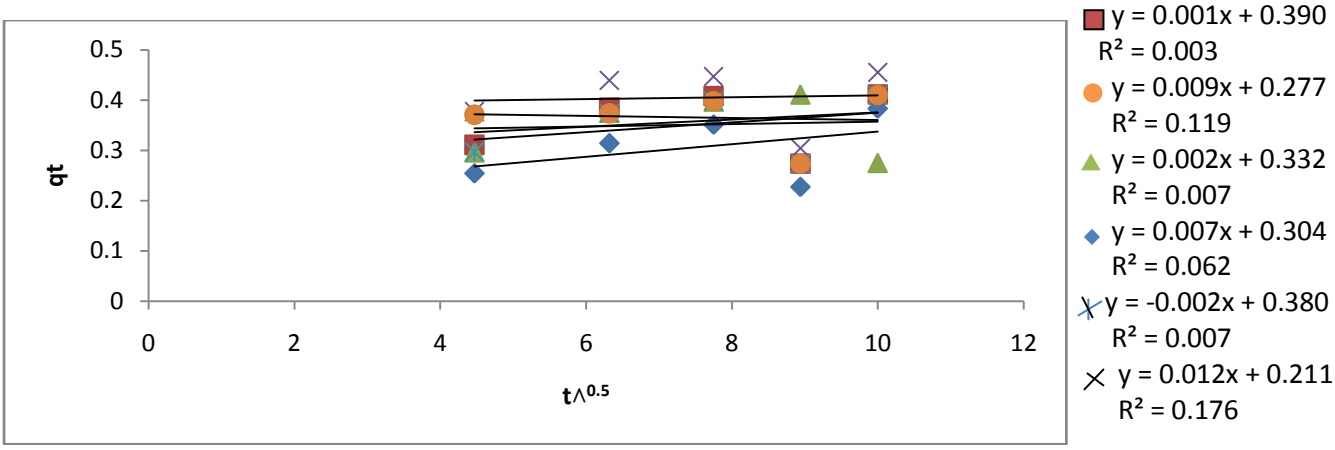

Figure 4.174: Intraparticle Diffusion for the Adsorption of Mn onto PNAC

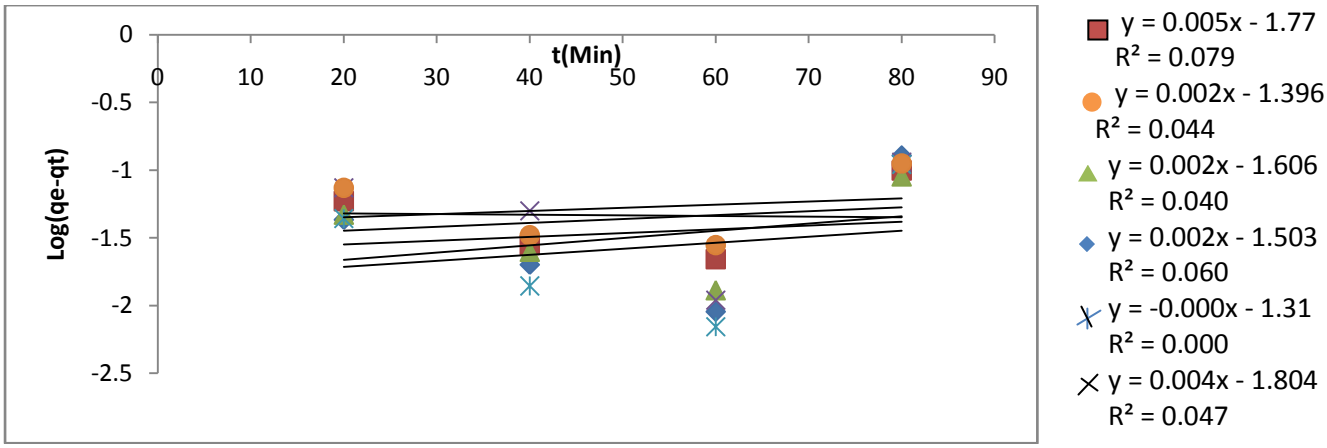

Figure 4.175: Pseudo First-order Kinetics for Ni Adsorption onto PKAC

Figures 4.157 and 4.158, present the first order and second order kinetic plots for the adsorption of Ni onto PKAC and it showed that the determination coefficients

for the second order kinetics were higher than those of the first order kinetics indicating the suitability of the second order kinetics to explain the adsorption kinetics that took place. Similar results were obtained for Cd, Mn and Ni adsorption onto PKAC.

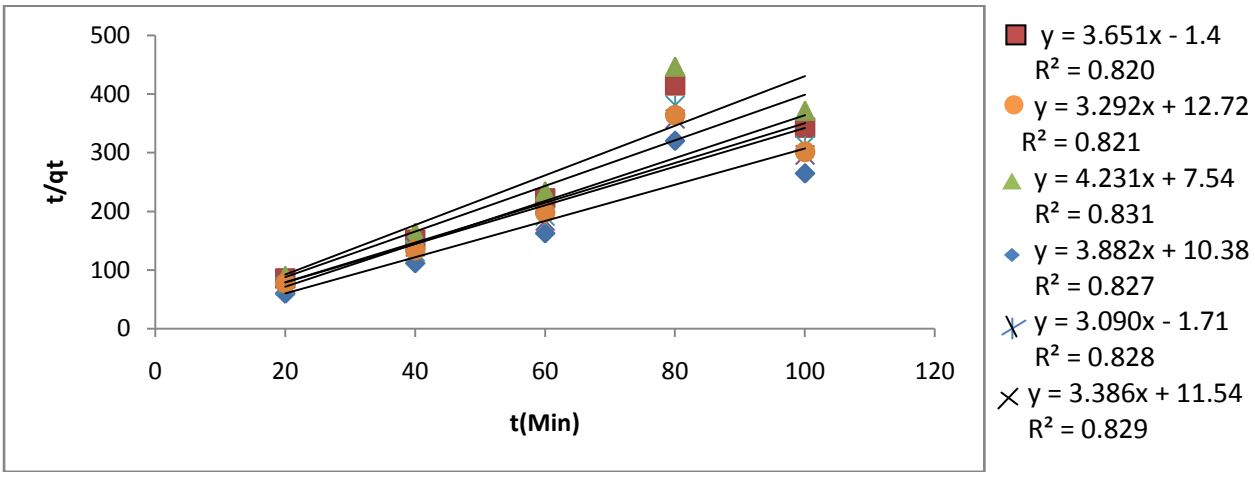

Figure 4.176: Pseudo Second-order Kinetics for Ni Adsorption onto PKAC

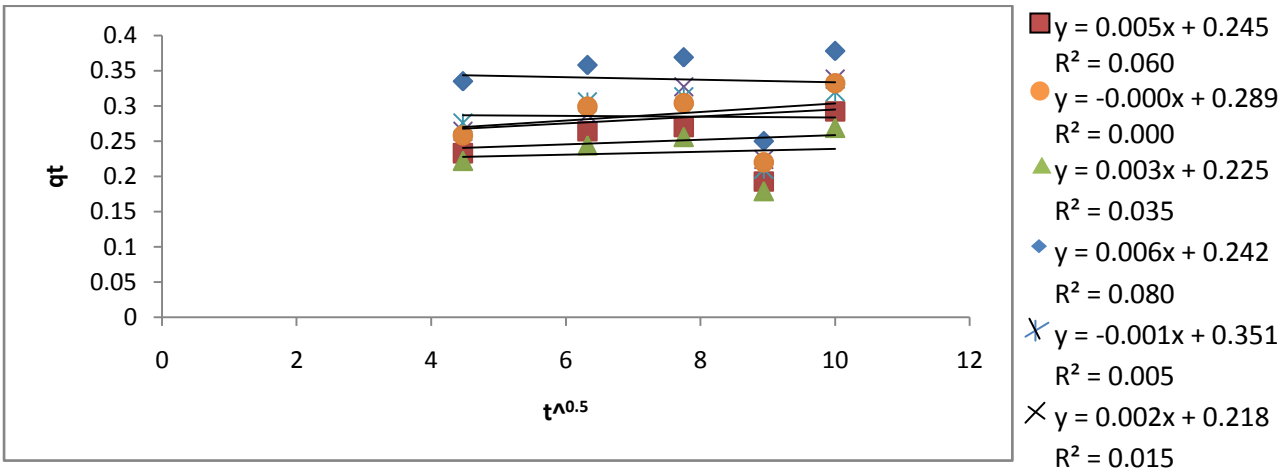

Figure 4.177: Intraparticle Diffusion for the Adsorption of Ni onto PKAC

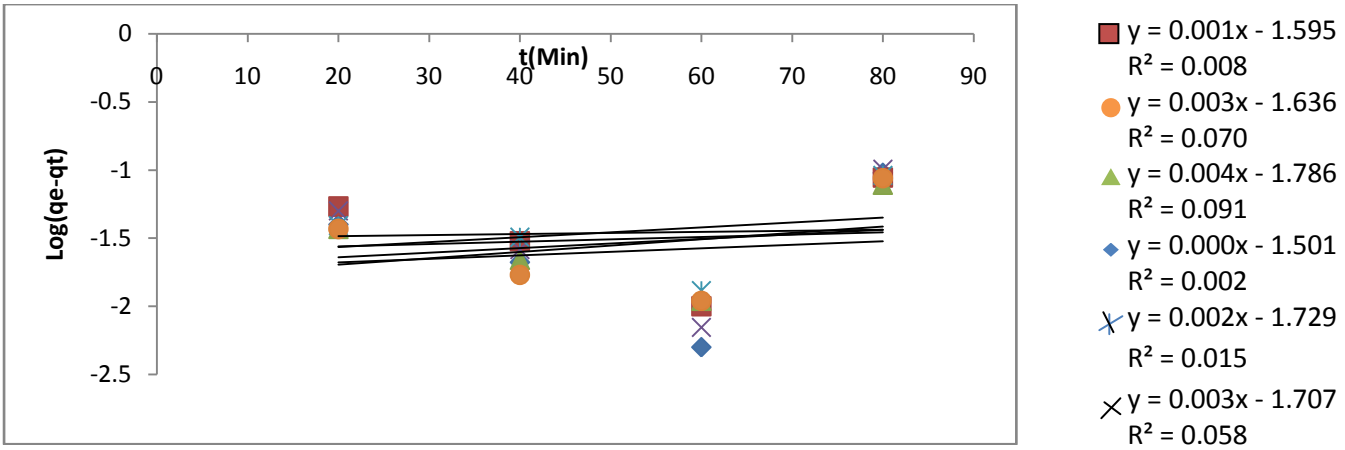

Figure 4.178: Pseudo First-order Kinetics for Pb Adsorption onto P

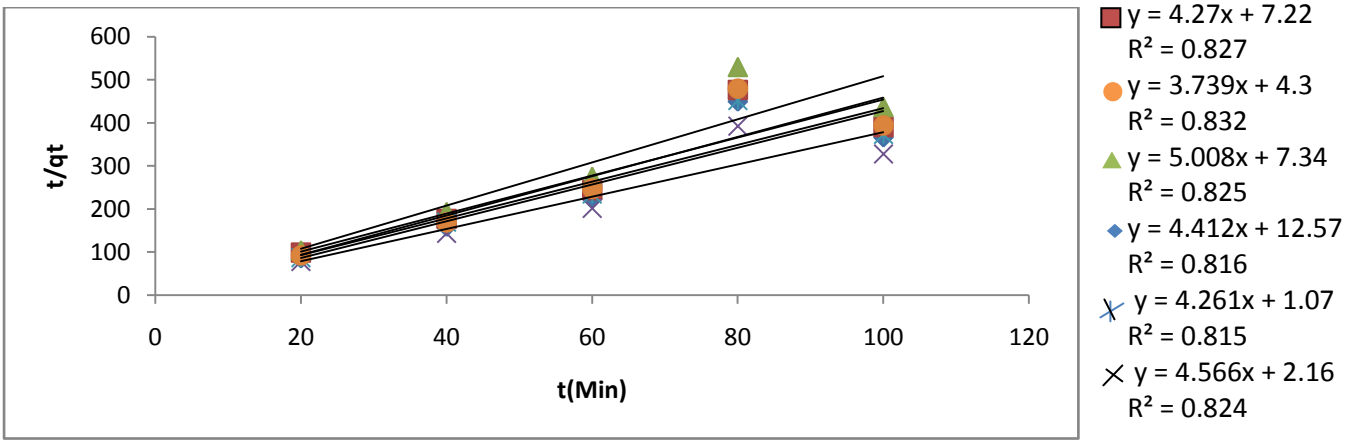

Figure 4.179: Pseudo Second-order Kinetics for Pb Adsorption onto PKAC

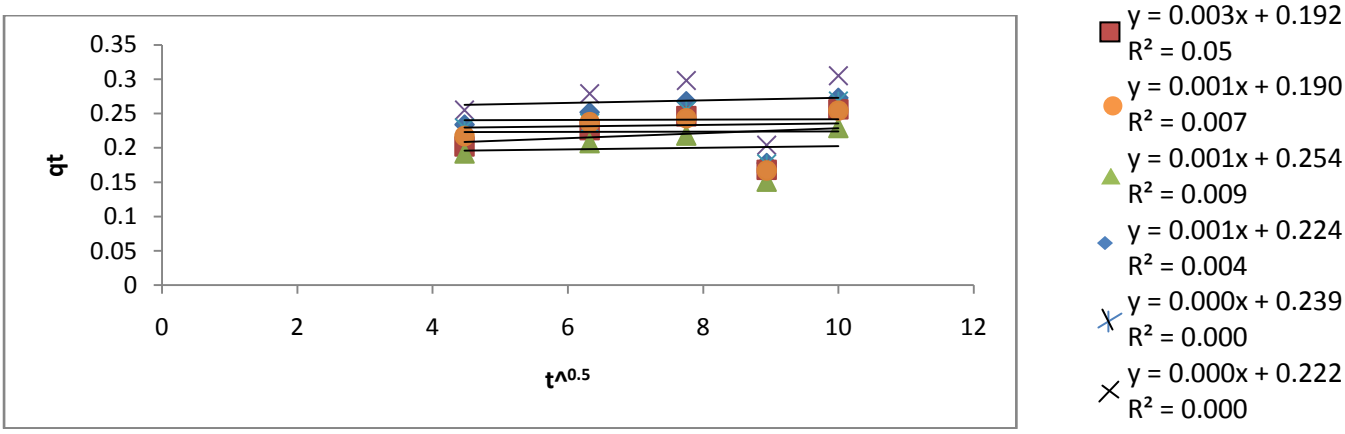

Figure 4.180: Intraparticle Diffusion for the Adsorption of Pb onto PKAC

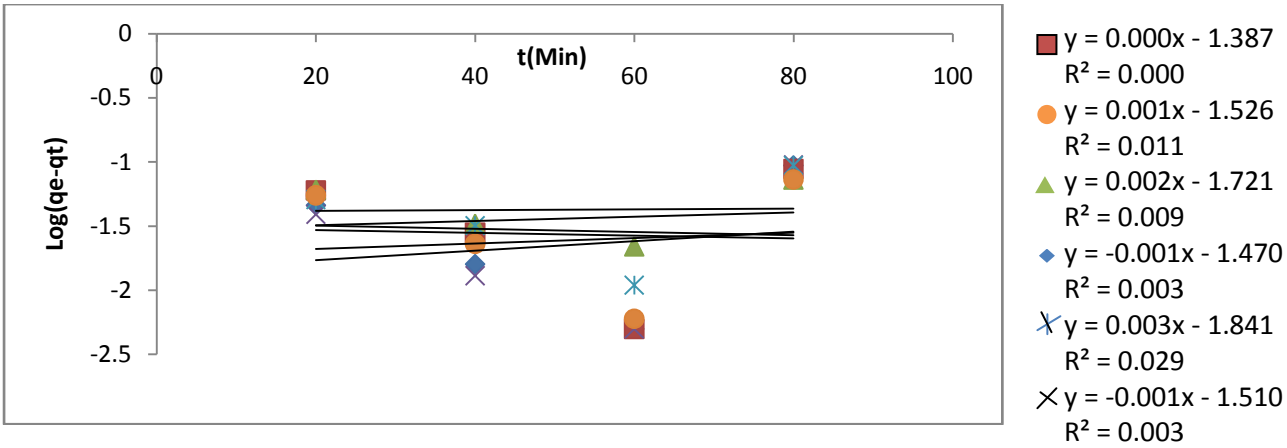

Figure 4.181: Pseudo First-order Kinetics for Cd Adsorption onto PKAC

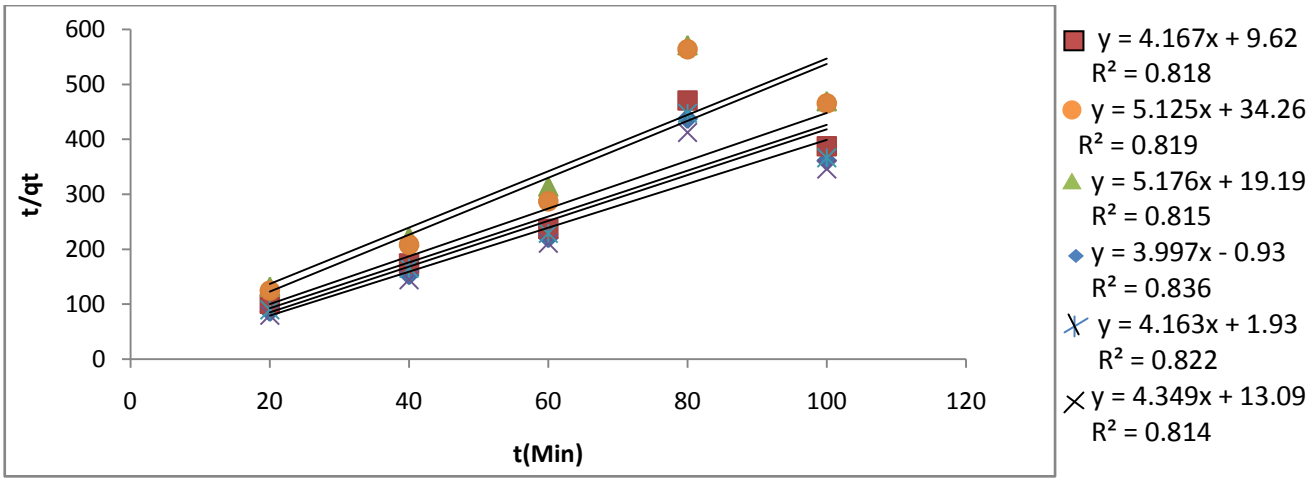

Figure 4.182: Pseudo Second-order Kinetics for Cd Adsorption onto PKAC

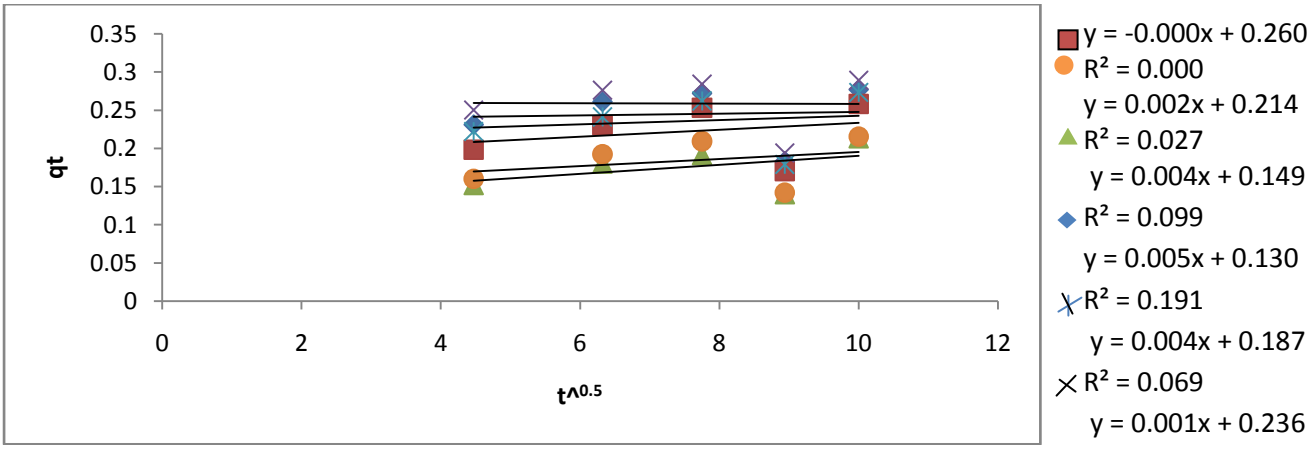

Figure 4.183: Intraparticle Diffusion for the Adsorption of Cd onto PKAC

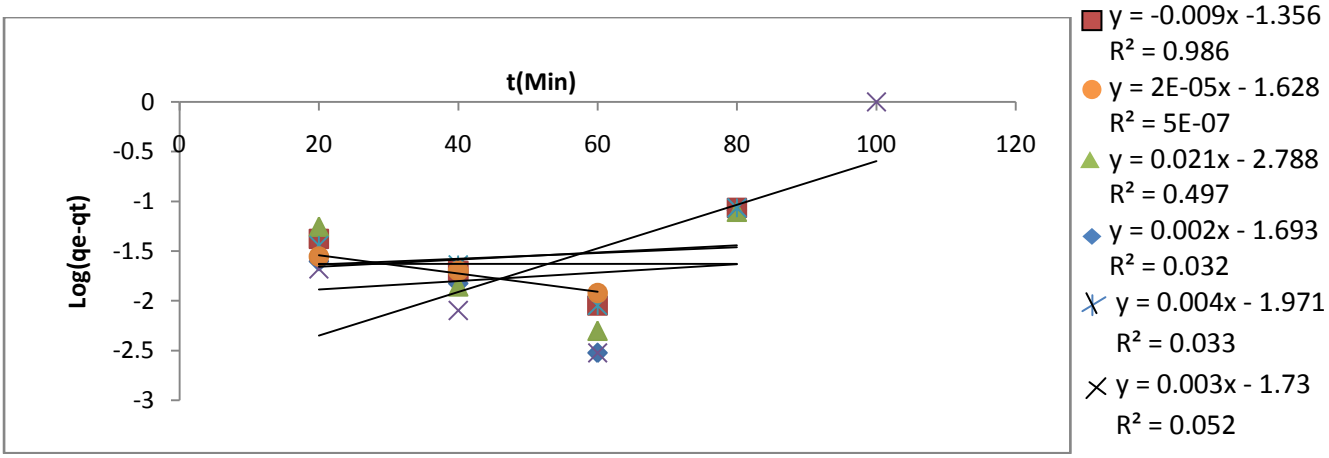

Figure 4.184: Pseudo First-order Kinetics for Mn Adsorption onto PKAC

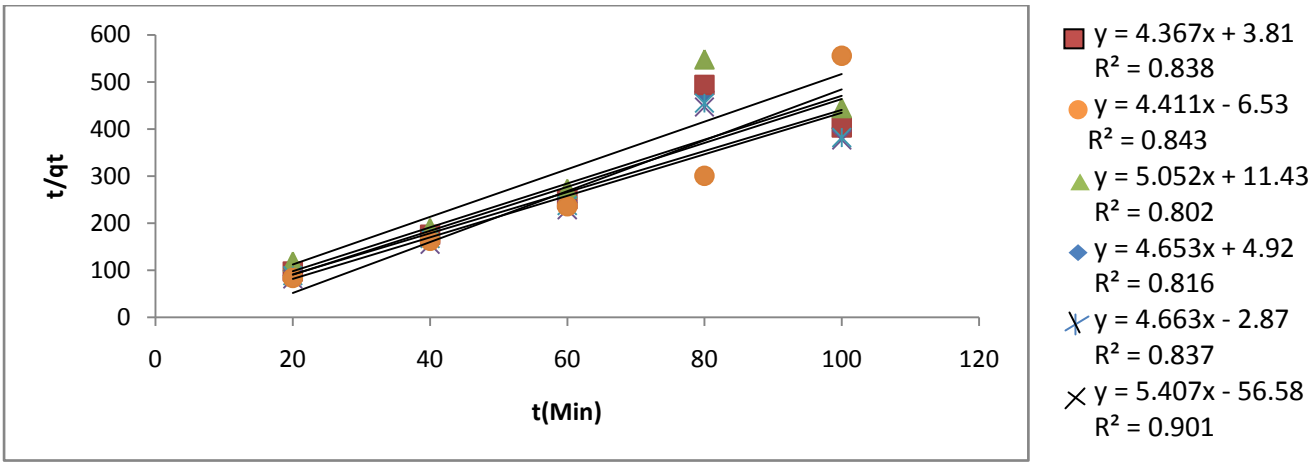

Figure 4.185: Pseudo Second-order Kinetics for Mn Adsorption onto PKAC

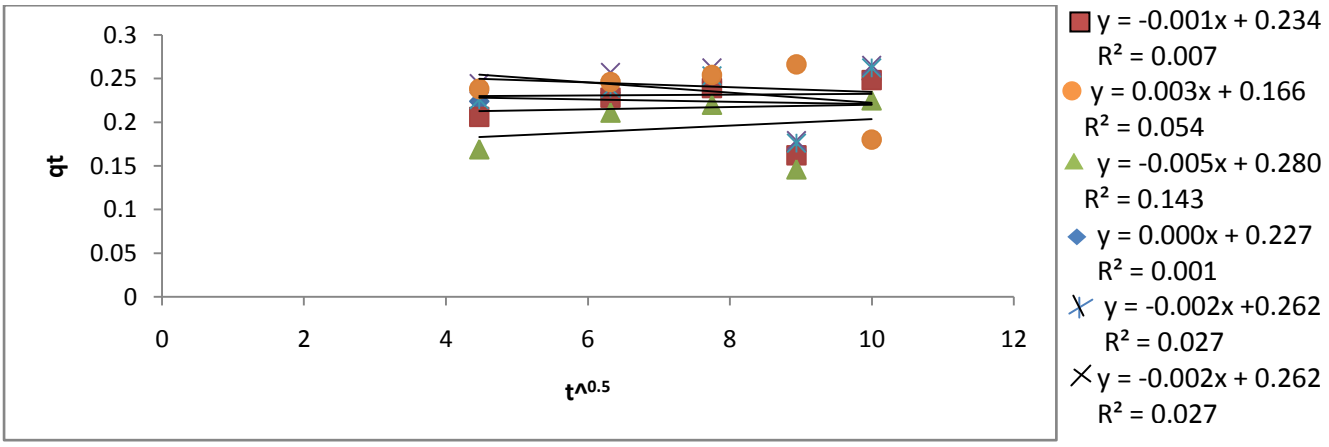

Figure 4.186: Intraparticle Diffusion for the Adsorption of Mn onto PKAC

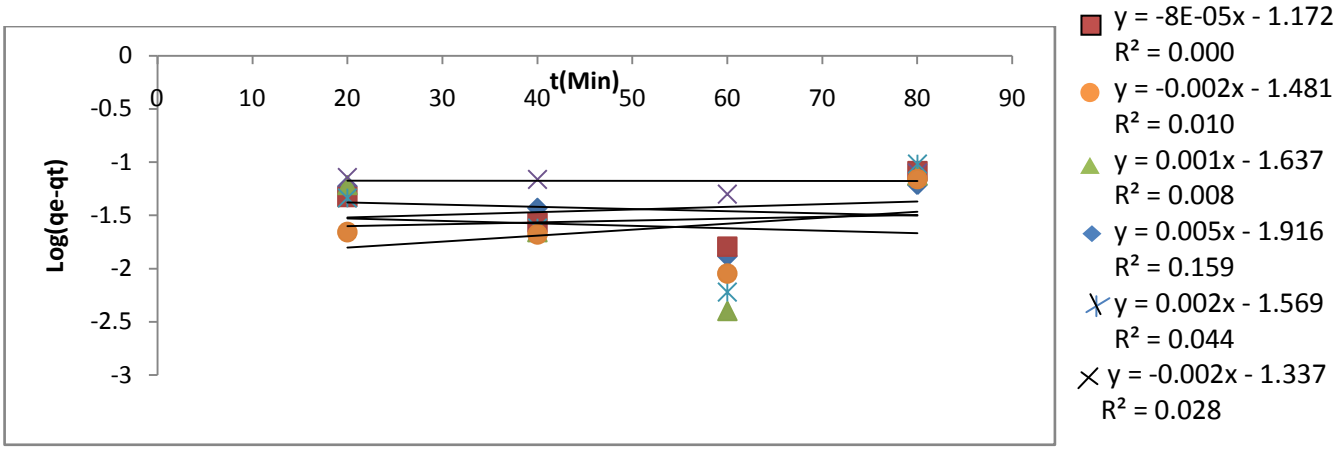

Figure 4.187: Pseudo First-order Kinetics for Pb Adsorption onto OBAC

Figures 4.185 and 4.186, present the first order and second order kinetic plots for the adsorption of Pb onto OBAC and it showed that the determination coefficients for the second order kinetics were higher than those of the first order kinetics indicating the suitability of the second order kinetics to explain the adsorption kinetics taking place. Similar results were also obtained for Cd, Mn and Ni adsorption onto OBAC.

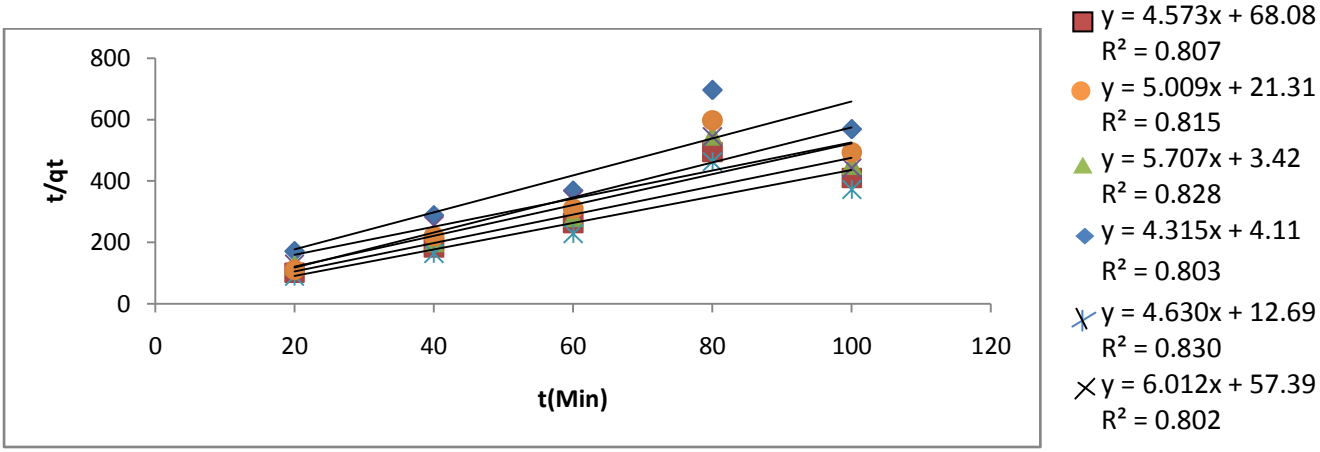

Figure 4.188: Pseudo Second-order Kinetics for Pb Adsorption onto OBAC

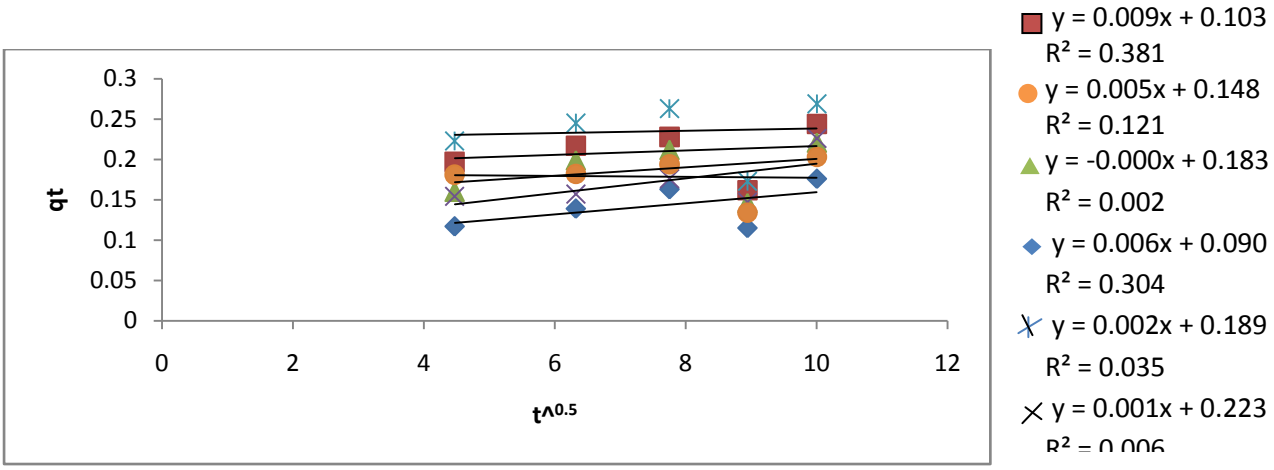

Figure 4.189: Intraparticle Diffusion for the Adsorption of Pb onto OBAC

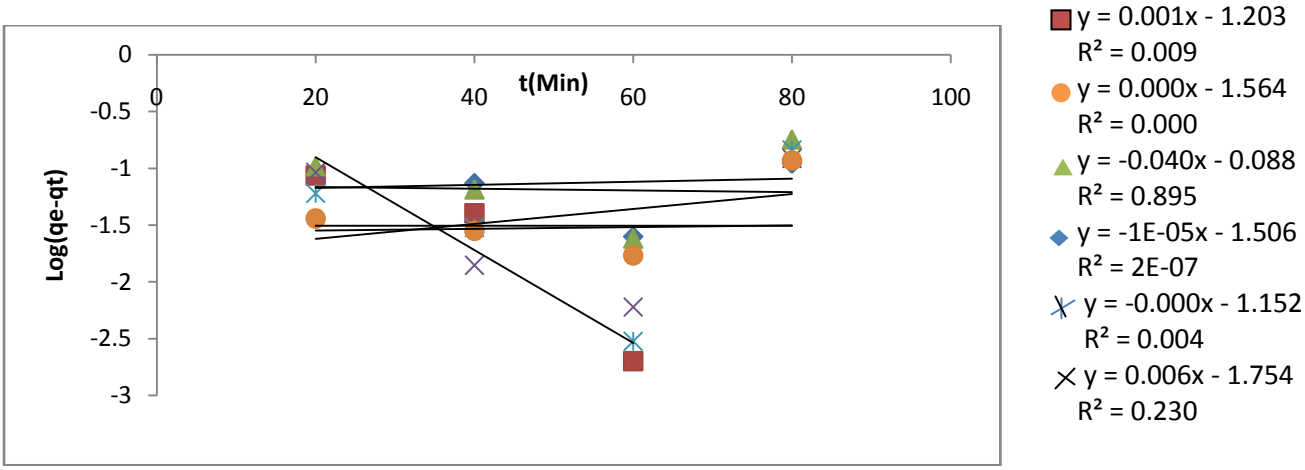

Figure 4.190: Pseudo First-order Kinetics for Ni Adsorption onto OBAC

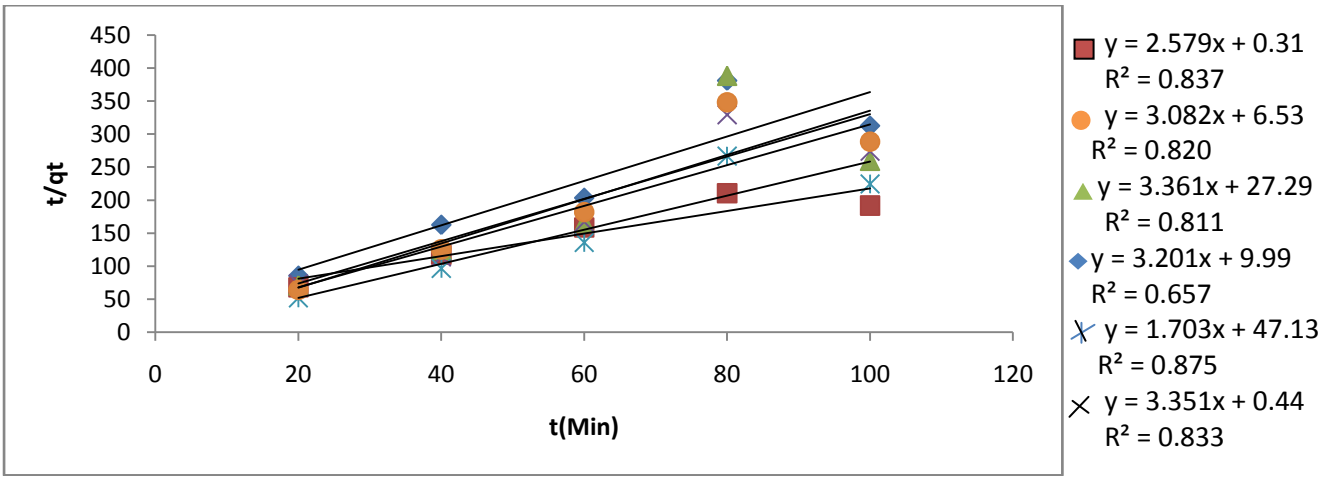

Figure 4.191: Pseudo Second-order Kinetics for Ni Adsorption onto OBAC

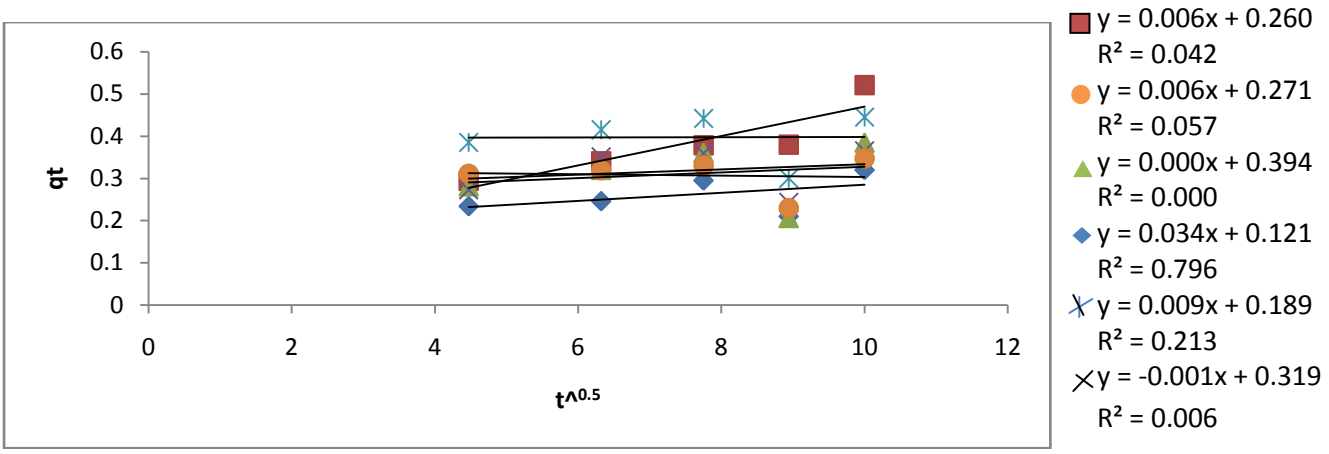

Figure 4.192: Intraparticle Diffusion for the Adsorption of Ni onto OBAC

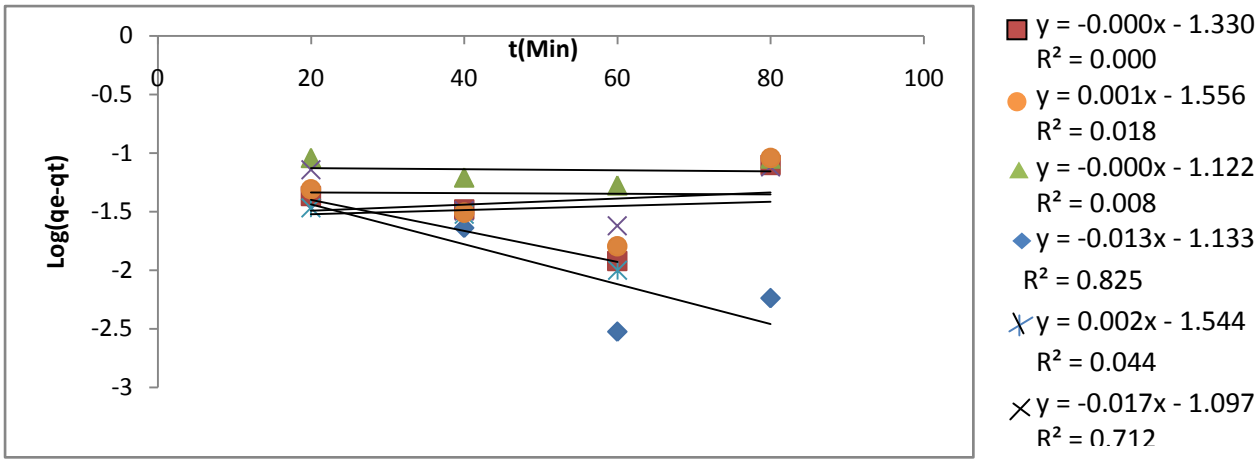

Figure 4.193: Pseudo First-order Kinetics for Cd Adsorption onto OBAC

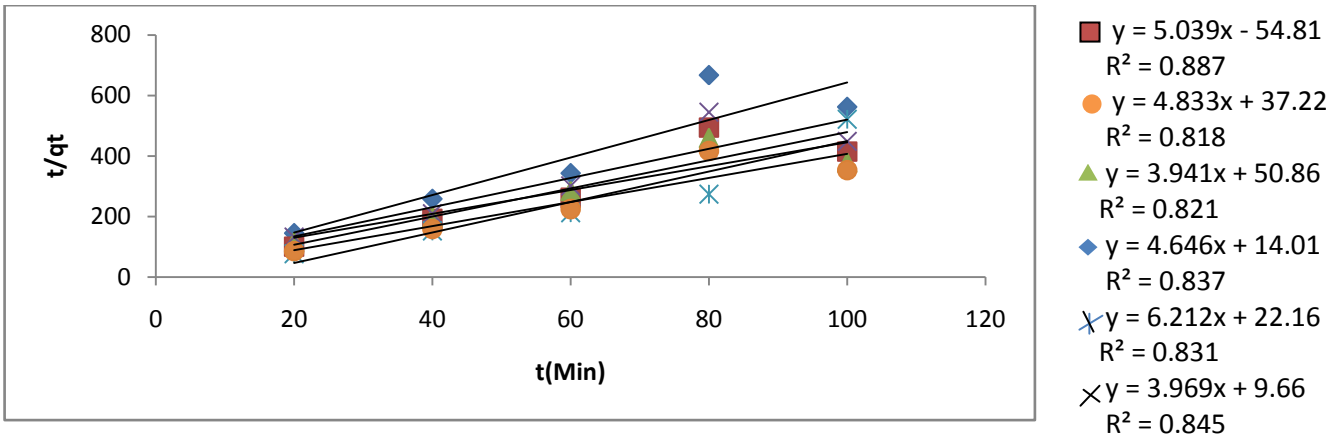

Figure 4.194: Pseudo Second-order Kinetics for Cd Adsorption onto OBAC

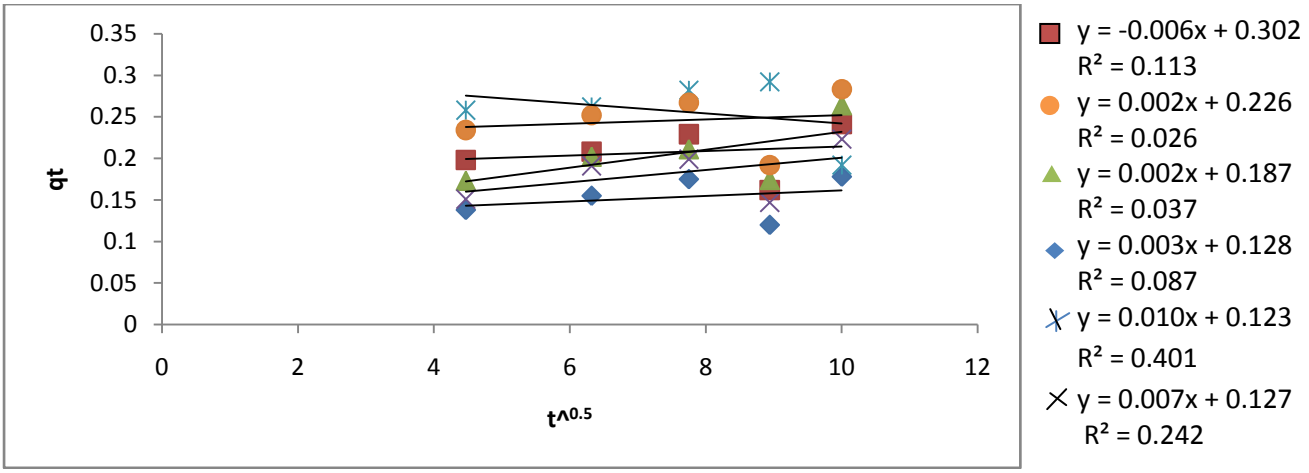

Figure 4.195: Intraparticle Diffusion for the Adsorption of Cd onto OBAC

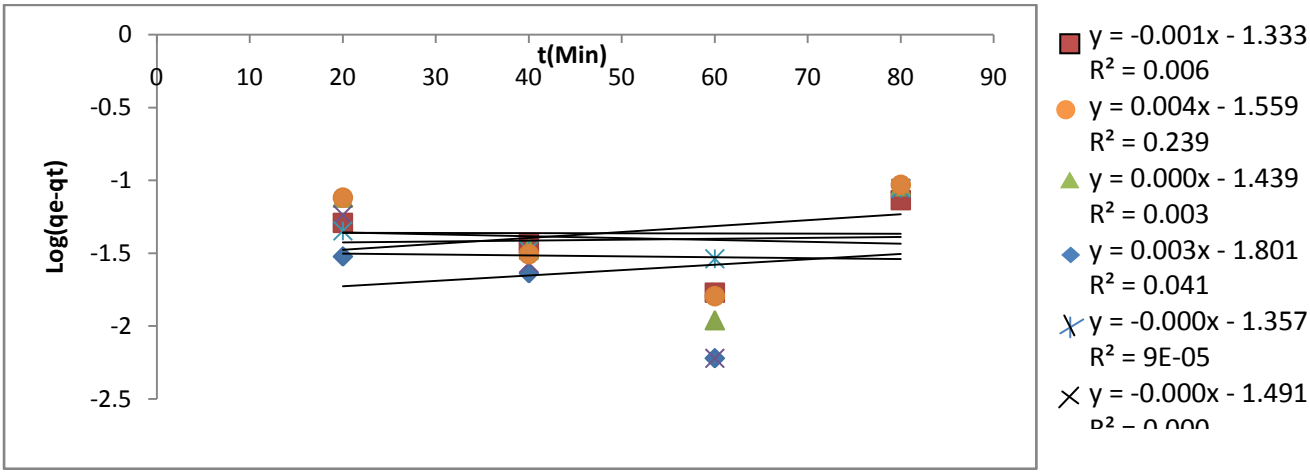

Figure 4.196: Pseudo First-order Kinetics for Mn Adsorption onto OBAC

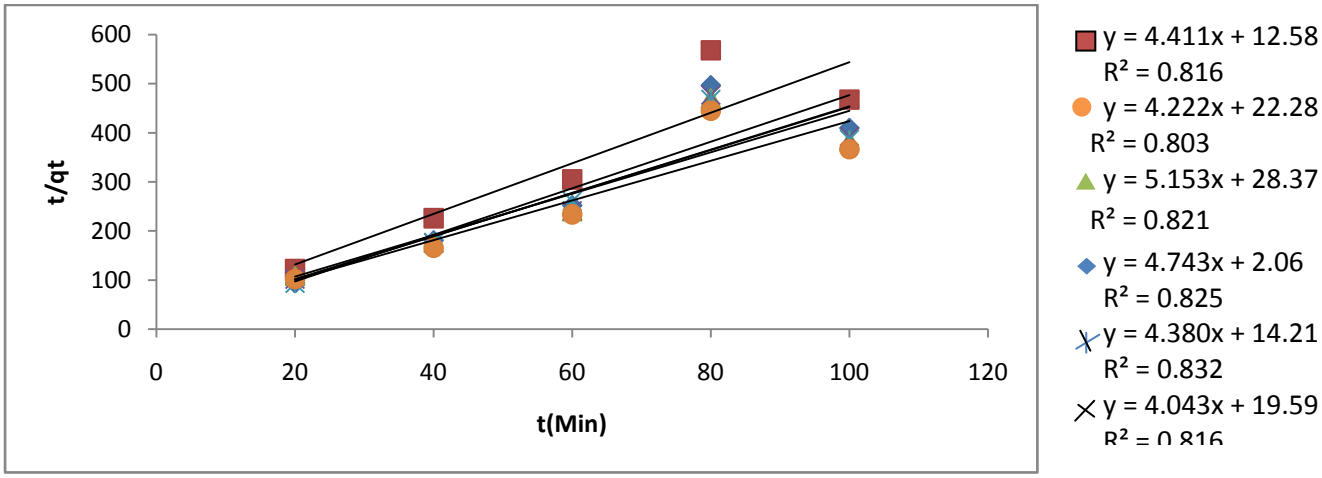

Figure 4.197: Pseudo Second-order Kinetics for Mn Adsorption onto OBAC

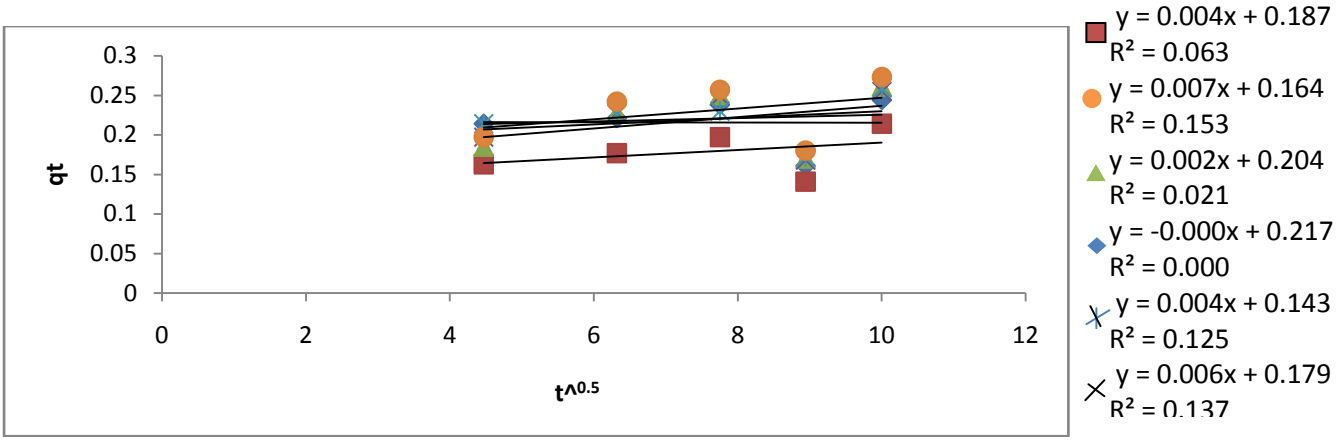

Figure 4.198: Intraparticle Diffusion for the Adsorption of Mn onto OBAC

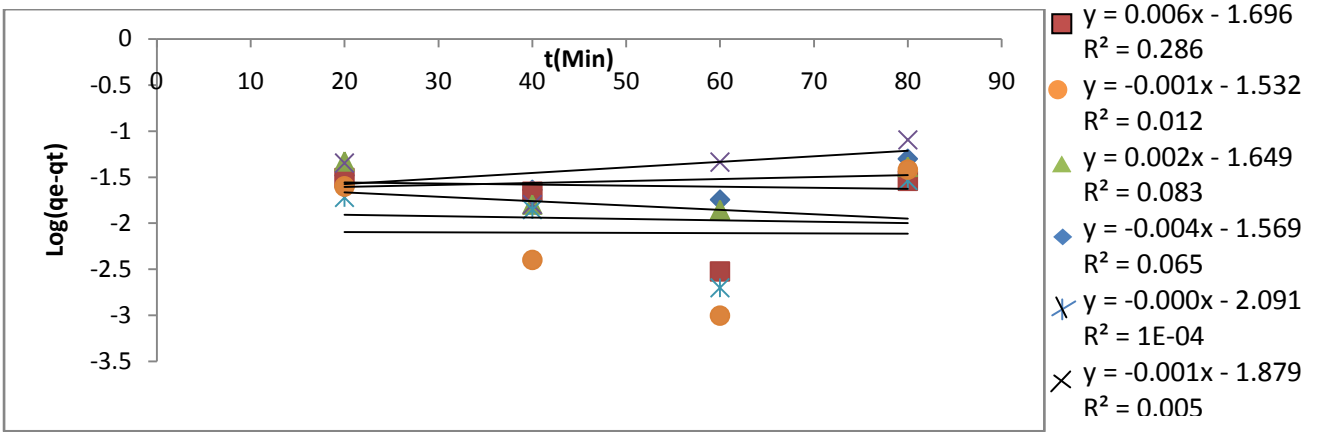

Figure 4.199: Pseudo First-order Kinetics for Ni Adsorption onto SSAC

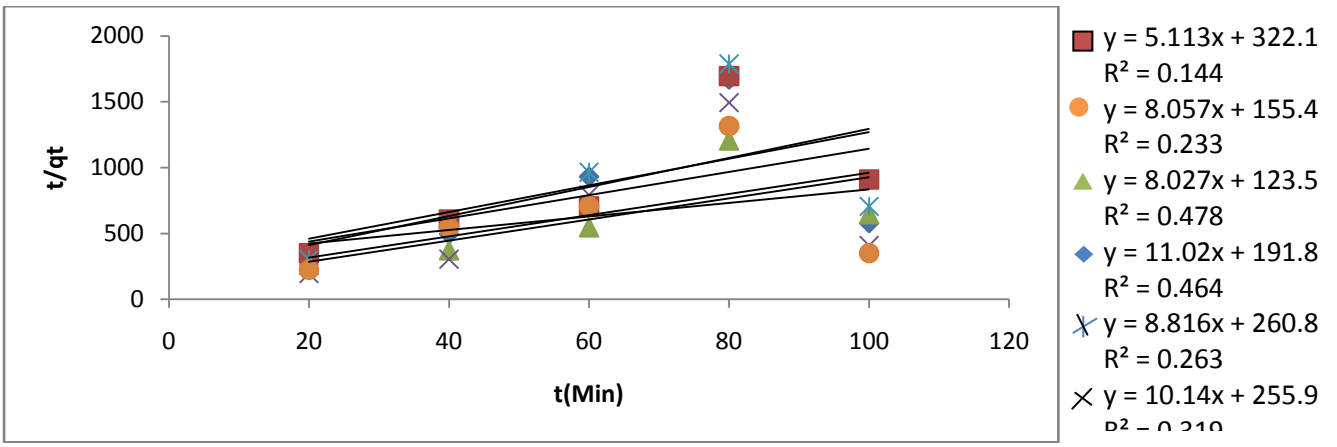

Figure 4.200: Pseudo Second-order Kinetics for Ni Adsorption onto SSAC

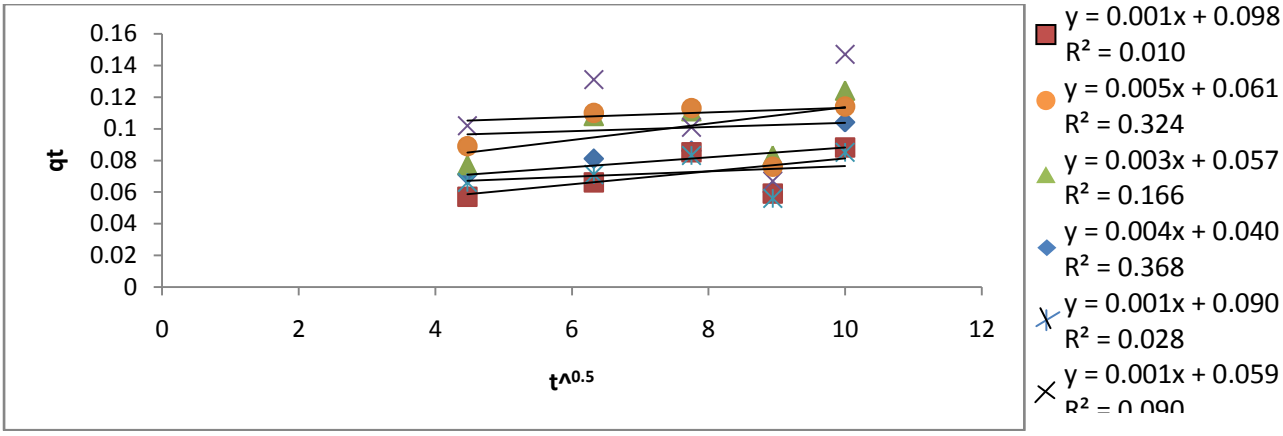

Figure 4.201: Intraparticle Diffusion for the Adsorption of Ni onto SSAC

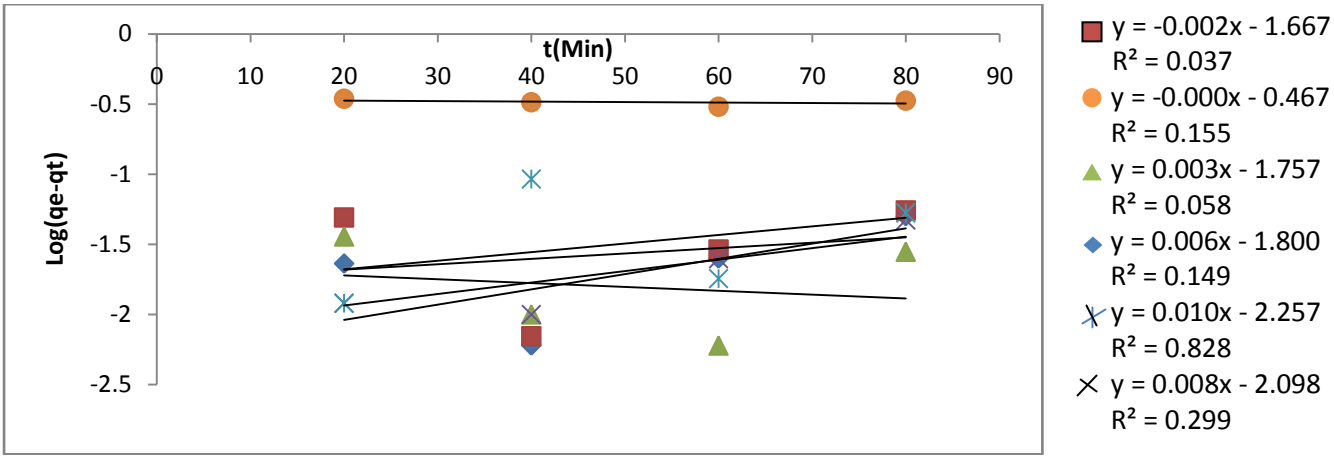

Figure 4.202: Pseudo First-order Kinetics for Pb Adsorption onto SSAC

Presented in Figures 4.200 and 4.201 are the first order and second order kinetic plots for the adsorption of Pb onto SSAC and it showed that the determination coefficients for the second order kinetics were higher than those of the first order kinetics (even though both were low), indicating the suitability of the second order kinetics to explain the adsorption kinetics. Similar results were obtained for Cd, Mn and Ni adsorption onto SSAC.

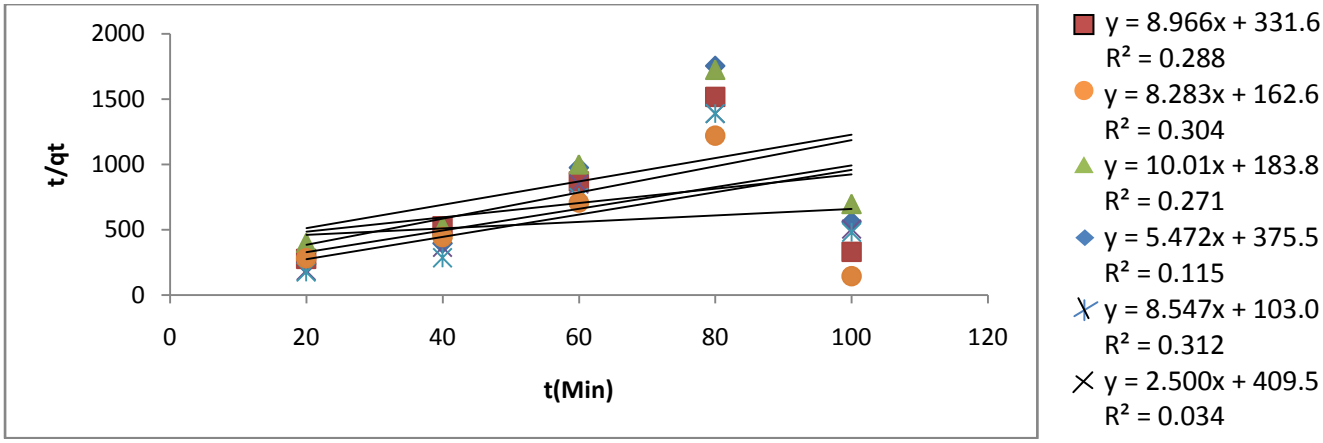

Figure 4.203: Pseudo Second-order Kinetics for Pb Adsorption onto SSAC

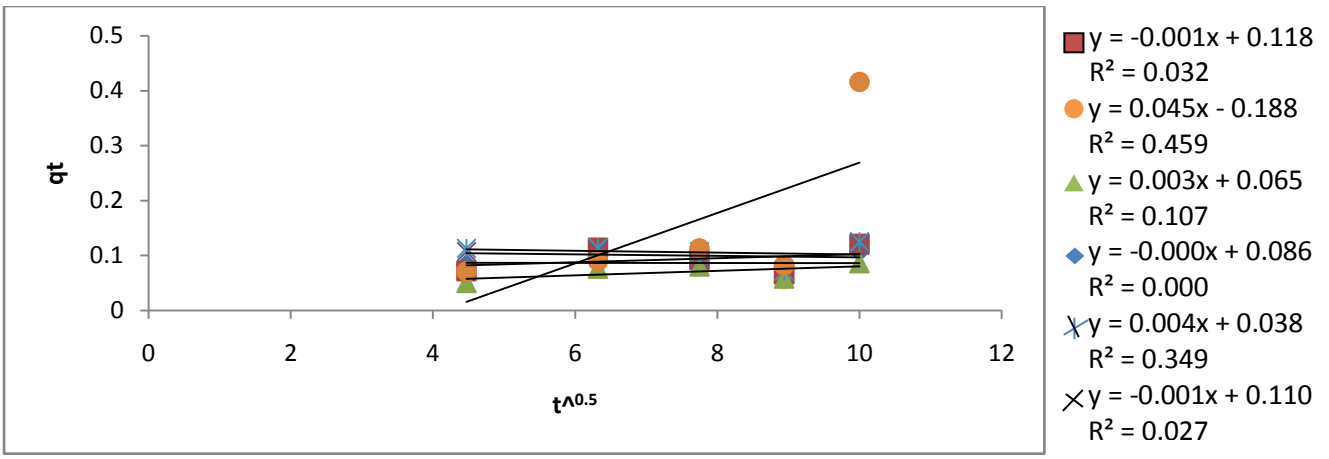

Figure 4.204: Intraparticle Diffusion for the Adsorption of Pb onto SSAC

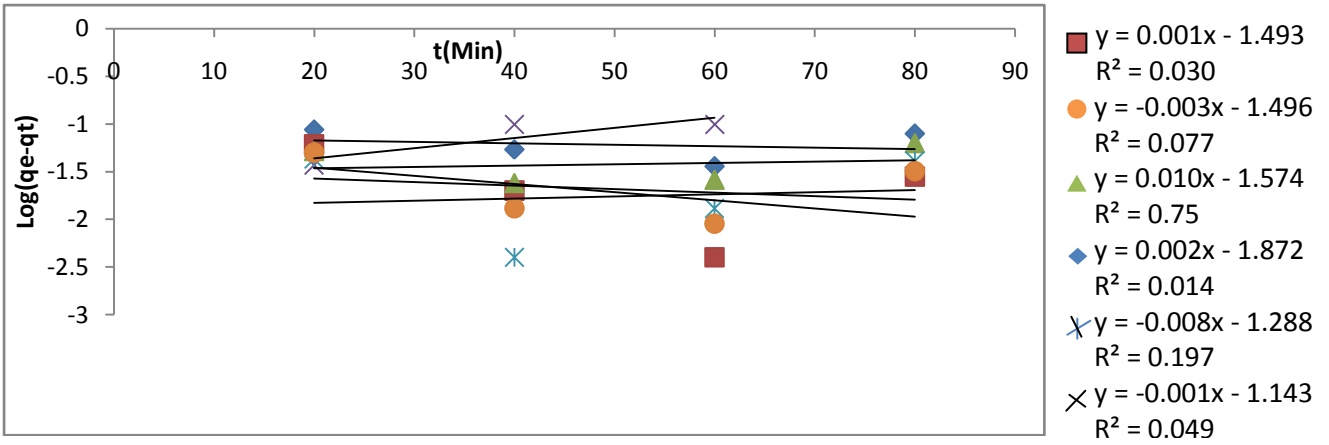

Figure 4.205: Pseudo First-order Kinetics for Cd Adsorption onto SSAC

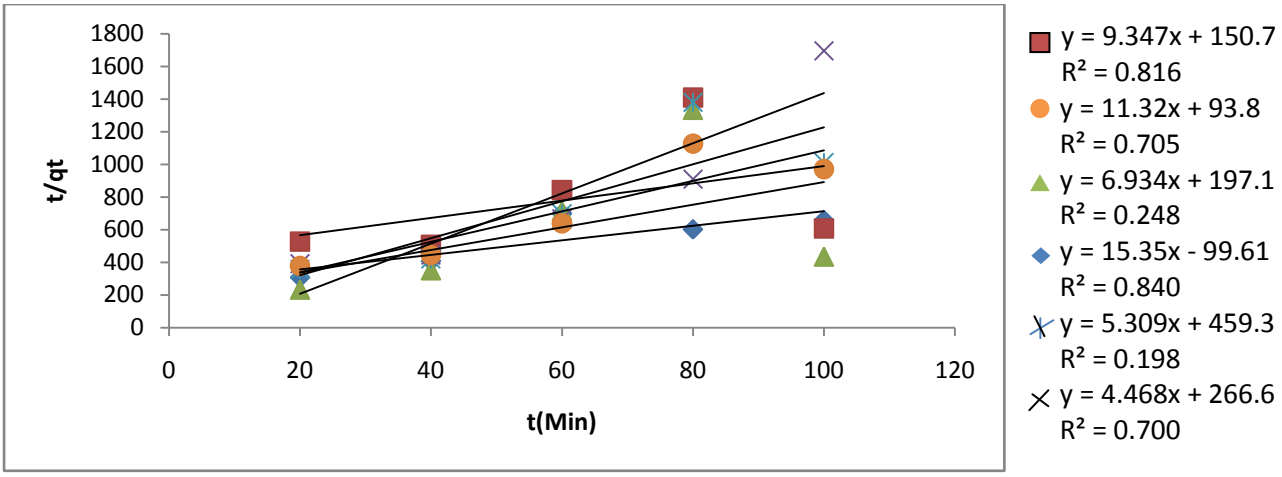

Figure 4.206: Pseudo Second-order Kinetics for Cd Adsorption onto SSAC

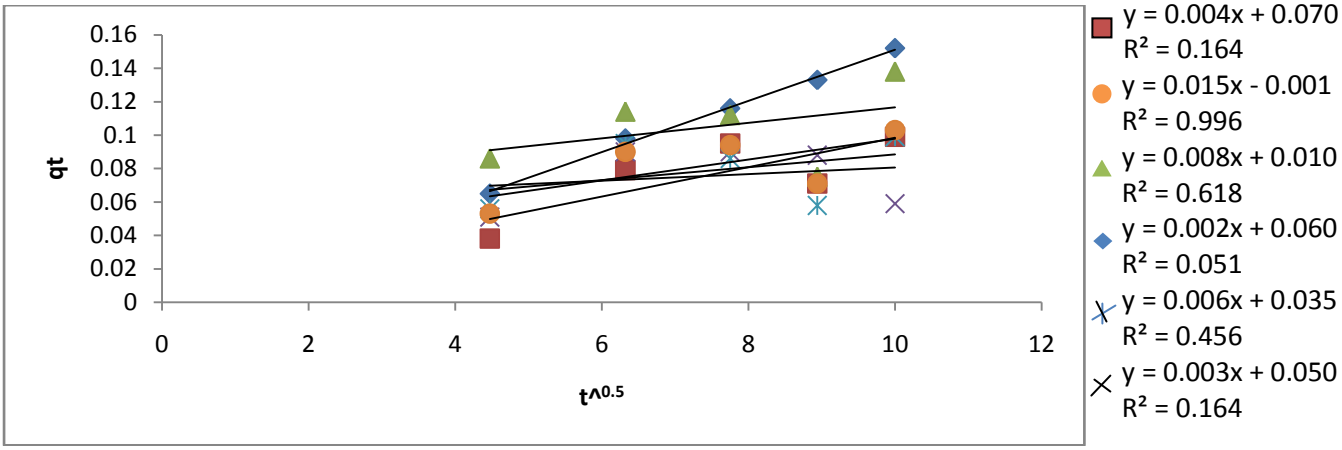

Figure 4.207: Intraparticle Diffusion for the Adsorption of Cd onto SSAC

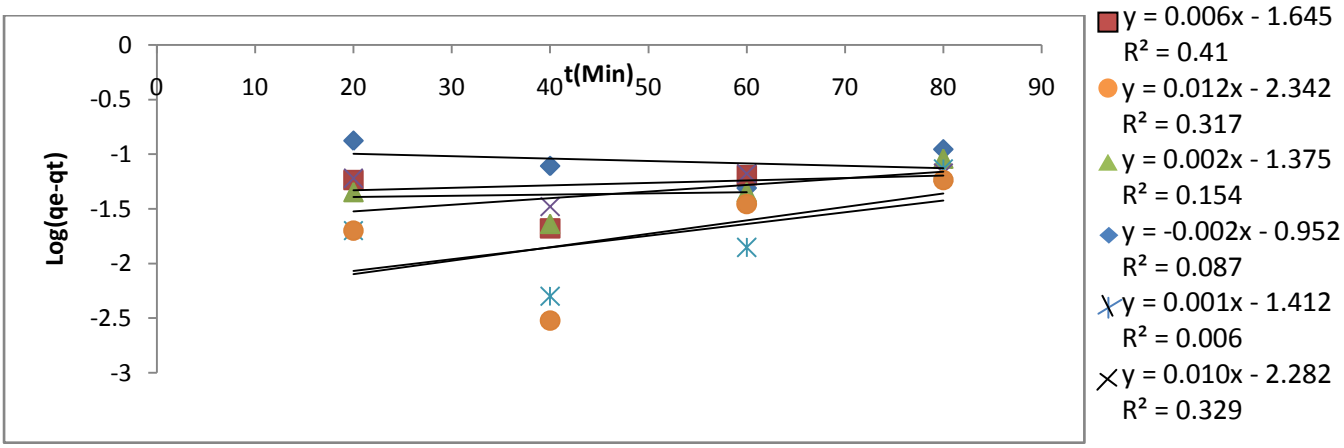

Figure 4.208: Pseudo First-order Kinetics for Mn Adsorption onto SSAC

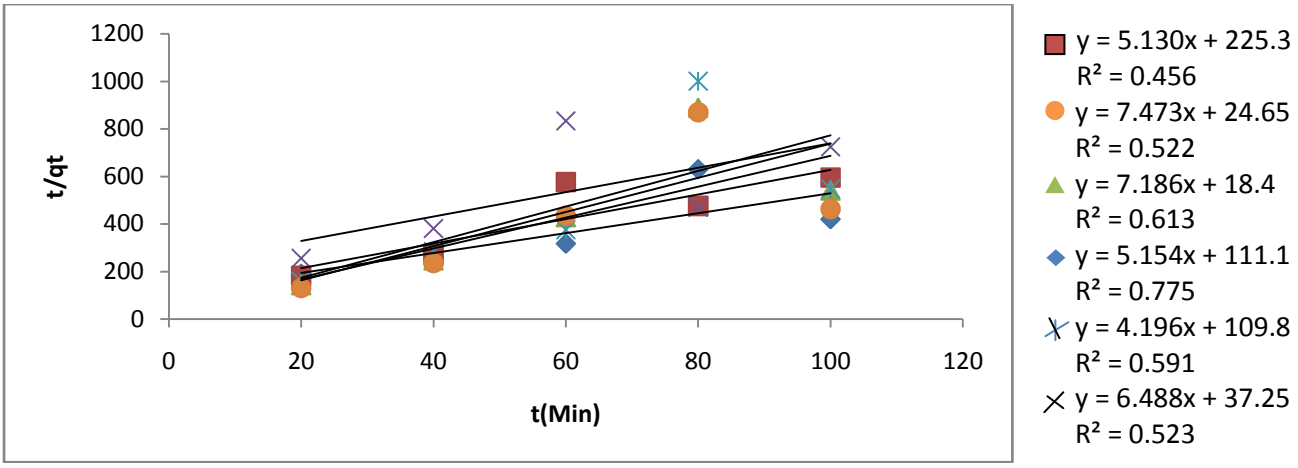

Figure 4.209: Pseudo Second-order Kinetics for Mn Adsorption onto SSAC

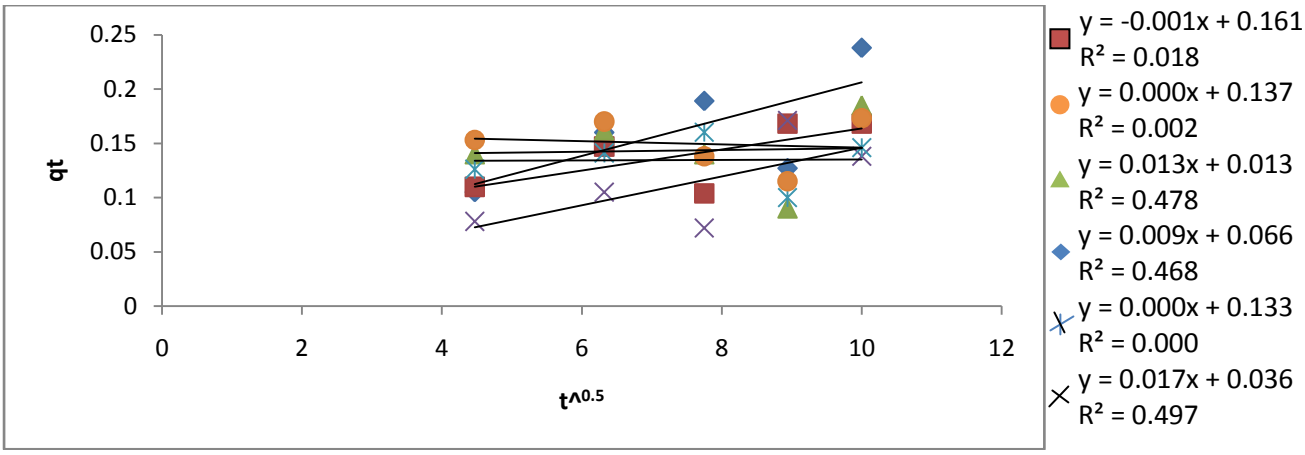

Figure 4.210: Intraparticle Diffusion for the Adsorption of Mn onto SSAC

The first-order equation did not apply throughout all the contact times in this work. It was applicable over certain initial sorption period. Plot of log (q_e-q_t) against time at different adsorbate concentrations deviated considerably from the data after a short period. The calculated slopes and intercepts from the plots were used to determine the rate constants k_1 and k_2 and equilibrium capacities.

It was observed in almost all the type of activated carbon prepared that the first-order model fits well for the first 60mins and thereafter the data deviated from the theory. Thus, the model represents that the initial stages where rapid adsorption

occurs well but cannot be applied to the entire adsorption process. A similar trend was observed by Ho and McKay (1998).

From the results of the fitted data in kinetic plot (Figures 4.161 to 4.208), it was clear that pseudo-second-order reaction model yielded very good straight lines compared to the pseudo-first-order reaction model, which was significantly scattered (non linear). The determination coefficient (R^2) of the plots is another evidence showing the linearity of the Pseudo second-order kinetic. In addition, the calculated (theoretical) values of qe for Pseudo second-order reaction model are closer to the experimental value of q_e (Tables 4.237 to 4.240). These facts suggest that the adsorption of heavy metals by activated carbons from these precursors follows the Pseudo-second-order reaction model, which was as a result of chemisorptions. In chemisorptions (chemical adsorption), the heavy metals stick to the adsorbent surface by forming a chemical (usually covalent) bond and tends to find sites that maximize their coordination number with the surface.

Tables 4.237 to 4.240 summarized the results of pseudo-first-order and pseudo-second-order equations, their respective determination coefficients (R^2), the first and second order rate constants (k_1, k_2), the calculated adsorption capacities from the first and second order kinetic models and the experimental adsorption capacities of all the prepared activated carbons.

For PKAC, the determination coefficients of the second order model indicated good fit (ranging from 0.8028 to 0.8470) unlike the first order dtermination coefficients

which ranged from $5x10^7$ to 0.1949 (Table 4.237). The adsorption capacities calculated from the pseudo-secondorder model were higher than its counterparts and were also closer to the experimental adsorption capacities in almost all the PKAC types prepared. For instance, for Cd/PKAC/600^0C/HCl, q_{e1} was 0.019 mg/g, q_{e2} was 0.240 mg/g and q_e was 0.270mg/g.

Table 4.237: Rate Constants, Theoretical and Experimental Adsorption Capacities of Palm Kernel Activated Carbons

AC Type	EQU 1st order(Y =)	EQU 2nd 0rder(Y =)	R^2 1st order	R^2 2nd 0rder	K_1 (min^{-1})	K_2 (g/mgmin)	qe_1 mg/g (calculated)	qe_2 mg/g (calculated)	qe mg/g (experimental)	1st Order HYBRID	2nd Order HYBRID	1st Order MPSD	2nd Order MPSD
Ni PKAC 600^0C HCl	0.0054x-1.777	3.0905x-1.71	0.0798	0.8282	-5.605	$-1.24x10^{-2}$	0.017	0.323	0.24	30.9722	-11.5278	53.6455	19.9667
Ni PKAC 600^0C H_3PO_4	0.0028x-1.606	4.231x+7.54	0.0405	0.8311	-2.381	$6.45x10^{-3}$	0.025	0.236	0.52	31.7308	18.2051	54.9593	31.5322
Ni PKAC 600^0C H_2SO_4	0.0028x-1.5305	3.882x+10.38	0.0602	0.8277	-1.447	$6.45x10^{-3}$	0.031	0.258	0.13	25.3846	-32.8205	43.9674	56.8468
Ni PKAC 800^0C HCl	0.0005x-1.31	3.292x+12.72	0.0008	0.8213	-0.850	$1.15x10^{-3}$	0.049	0.304	0.30	27.8889	-0.4444	48.3050	0.7698
Ni PKAC 800^0C H_3PO_4	0.0023x-1.396	3.386x+11.54	0.0446	0.8290	-0.996	$5.29x10^{-3}$	0.040	0.295	0.30	28.8889	0.5556	50.0370	0.9623
Ni PKAC 800^0C H_2SO_4	0.0045x-1.8045	3.651x-1.400	0.0474	0.8209	-9.514	$-1.04x10^{-2}$	0.016	0.274	0.45	32.1481	13.0370	55.6822	22.5808
Pb PKAC 600^0C HCl	0.0026x-1.729	4.2615x+1.07	0.0152	0.8150	-16.923	$5.99x10^{-3}$	0.019	0.235	0.51	32.0915	17.9739	55.5841	31.1316
Pb PKAC 600^0C H_3PO_4	0.0034x-1.707	5.008x+7.34	0.0581	0.8254	-3.440	$7.83x10^{-3}$	0.019	0.199	0.22	30.4545	3.1818	52.7488	5.5111
Pb PKAC 600^0C H_2SO_4	0.0008x-1.5015	4.4125x+12.57	0.0026	0.8165	-1.544	$1.84x10^{-3}$	0.031	0.227	0.30	29.8889	8.1111	51.7691	14.0489
Pb PKAC 800^0C HCl	0.0017x-1.5955	3.739x+4.30	0.0082	0.8323	-3.262	$3.92x10^{-3}$	0.025	0.267	0.39	31.1966	10.5128	54.0341	18.2087
Pb PKAC 800^0C H_3PO_4	0.0046x-1.7865	4.566x+2.16	0.0914	0.8242	-9.653	$1.06x10^{-2}$	0.016	0.219	0.43	32.0930	16.3566	55.5868	28.3304
Pb PKAC 800^0C H_2SO_4	0.0036x-1.636	4.27x+7.220	0.0704	0.8270	-2.529	$8.29x10^{-3}$	0.023	0.234	0.32	30.9375	8.9583	53.5853	15.5163
Cd PKAC 600^0C HCl	0.0021x-1.7215	4.1635x+1.93	0.0097	0.8229	-8.995	$4.84x10^{-3}$	0.019	0.240	0.27	30.9877	3.7037	53.6722	6.4150
Cd PKAC 600^0C H_3PO_4	0.0003x-1.387	5.125x+34.26	0.0009	0.8190	-0.768	$6.91x10^{-3}$	0.041	0.195	0.53	30.7547	21.0692	53.2687	36.4929
Cd PKAC 600^0C H_2SO_4	0.0012x-1.4705	4.349x+13.09	0.0034	0.8149	-1.457	$2.76x10^{-4}$	0.034	0.229	0.48	30.9722	17.4306	53.6455	30.1906
Cd PKAC 800^0C HCl	0.0037x-1.841	3.9975x-0.93	0.0299	0.8364	-17.204	$-8.52x10^{-3}$	0.014	0.250	0.66	32.6263	20.7071	56.5103	35.8657
Cd PKAC 800^0C H_3PO_4	0.0011x-1.5105	5.1765x+19.19	0.0032	0.8157	-1.399	$2.53x10^{-3}$	0.031	0.193	0.48	31.1806	19.9306	54.0063	34.5207
Cd PKAC 800^0C H_2SO_4	0.0017x-1.526	4.167x+9.62	0.0118	0.8180	-1.820	$3.92x10^{-3}$	0.029	0.239	0.51	31.4379	17.7124	54.4521	30.6788
Mn PKAC 600^0C HCl	0.0042x-1.971	4.6635x-2.87	0.0338	0.8372	-7.608	$-9.67x10^{-3}$	0.011	0.214	1.08	32.9938	26.7284	57.1470	46.2949
Mn PKAC 600^0C H_3PO_4	2e-05x-1.628	5.0525x+11.43	5E.07	0.8028	-2.232	$4.61x10^{-3}$	0.024	0.198	0.54	31.8519	21.1111	55.1690	36.5655
Mn PKAC 600^0C H_2SO_4	0.0029x-1.6935	4.653x+4.92	0.0323	0.8167	-4.400	$6.67x10^{-5}$	0.020	0.215	0.98	32.6531	26.0204	56.5568	45.0687
Mn PKAC 800^0C HCl	0.0071x-2.1935	4.4115x-6.53	0.0859	0.8436	-2.972	$-1.6x10^{-2}$	0.006	0.227	0.41	32.8455	14.8780	56.8901	25.7695
Mn PKAC 800^0CH_3PO_4	0.0064x-1.9096	5.407x-56.58	0.3597	0.9012	-0.015	$-5.17x10^{-1}$	81.200	0.185	0.61	-4403.825	23.2240	7627.649	40.2252
Mn PKAC 800^0C H_2SO_4	0.0036x-1.73	4.3675x+3.81	0.0528	0.8387	-4.927	$8.29x10^{-3}$	0.019	0.229	0.74	30.9722	-11.5278	53.6455	19.9667

From Table 4.237, the error functions (HYBRID and MPSD) corresponding to the minimized deviations between the experimental and calculated kinetic models suggest pseudo-second order kinetics as the best (the lowest values of the error functions) according to Srenscek-Nazzal *et al.* (2016), and this suggest that the adsorption is chemosorption unlike what Temkin and Dubini-Radushkovick Isotherm models predicted earlier on the adsorption of these metals by the activated carbons prepared. Similar results were also obtained for other activated carbon types under consideration.

Table 4.238: Rate Constants, Theoretical and Experimental Adsorption Capacities of Pearnut Seed Activated Carbons

AC Type	EQUATION 1st order (Y =)	EQUATION 2nd 0rder (Y =)	R^2 1st order	R^2 2nd 0rder	K_1 (min^{-1})	K_2 (g/mgmin)	qe_1 mg/g (calculated)	qe_2 mg/g (calculated)	qe mg/g (experimental)	1st Order HYBRID	2nd Order HYBRID	1st Order MPSD	2nd Order MPSD
Ni PNAC 600^0C HCl	-0.0033x-0.8735	2.5505x+43.31	0.0649	0.7889	0.145030	$7.5X10^{-3}$	0.134	0.399	0.34	20.1961	-5.7843	34.9806	10.0187
Ni PNAC 600^0C H_3PO_4	-0.0016x-1.0105	2.875x+30.50	0.0315	0.8284	0.270730	$3.6X10^{-3}$	0.097	0.348	0.30	22.5556	-5.3333	39.0674	9.2376
Ni PNAC 600^0C H_2SO_4	0.0054x-1.775	0.331x+0.100	0.0833	0.8353	-111.1110	$1.2X10^{-2}$	0.017	0.300	0.32	31.5625	2.0833	54.6679	3.6084
Ni PNAC 800^0C HCl	0.0029x-1.13	2.622x+23.86	0.7022	0.8345	-0.288721	$6.6X10^{-3}$	0.074	0.381	0.46	27.9710	5.7246	48.4472	9.9154
Ni PNAC 800^0C H_3PO_4	-0.0021x-0.9405	2.308x+33.34	0.0439	0.9388	0.159977	$4.8X10^{-3}$	0.115	0.433	0.34	22.0588	-9.1176	38.2070	15.7922
Ni PNAC $800^0CH_2SO_4$	0.0101x-2.0883	4.056x-47.70	0.6998	0.9014	-0.023300	$-3.4X10^{-1}$	122.5	0.247	0.34	-1E+4	9.1176	2E+4	15.7922
Pb PNAC 600^0C HCl	0.0097x-1.762	3.278x-0.580	0.3632	0.8345	-18.534135	$-2.2X10^{-2}$	0.017	0.305	0.57	32.3392	15.4971	56.0131	26.8417
Pb PNAC 600^0C H_3PO_4	0.0012x-1.3235	4.1965x+26.89	0.0225	0.8142	-0.656531	$2.7X10^{-3}$	0.047	0.238	0.54	30.4321	18.6420	52.7099	32.2888
Pb PNAC 600^0C H_2SO_4	0.0001x-1.226	4.0495x+36.81	0.0004	0.8353	-0.445434	$2.3X10^{-4}$	0.059	0.247	0.55	29.7576	18.3636	51.5416	31.8068
Pb PNAC 800^0C HCl	0.0027x-1.251	3.3035x+25.63	0.4468	0.8394	-0.424989	$6.2X10^{-3}$	0.056	0.303	0.57	30.0585	15.6140	52.0628	27.0443
Pb PNAC 800^0C H_3PO_4	0.0003x-1.2405	4.064x+35.48	0.0020	0.8356	-0.465766	$6.9X10^{-4}$	0.057	0.246	0.27	26.2963	2.9630	45.5465	5.1320
Pb PNAC 800^0C H_2SO_4	0.0011x-1.3115	4.247x+26.02	0.0068	0.8285	-0.696378	$2.5X10^{-3}$	0.049	0.235	0.27	27.2840	4.3210	47.2572	7.4842
Cd PNAC 600^0C HCl	0.0097x-1.762	3.278x-0.680	0.3633	0.8341	-15.873015	$-2.2X10^{-2}$	0.017	0.305	0.33	31.6162	2.5253	54.7608	4.3739
Cd PNAC $600^0CH_3PO_4$	0.0004x-1.2405	4.049x+35.34	0.0036	0.8378	-0.463821	$9.2X10^{-4}$	0.057	0.247	0.23	25.0725	-2.4638	43.4268	4.2674
Cd PNAC $600^0CH_2SO_4$	0.0003x-1.2405	4.064x+35.48	0.0020	0.8356	-0.465766	$6.9X10^{-4}$	0.057	0.246	0.19	23.3333	-9.8246	40.4145	17.0166
Cd PNAC 800^0C HCl	0.0027x-1.249	3.296x+25.78	0.4437	0.8422	-0.422475	$6.2X10^{-3}$	0.056	0.303	0.33	27.6768	2.7273	47.9376	4.7238
Cd PNAC $800^0CH_3PO_4$	-0.0006x-1.228	4.0425x+34.95	0.0047	0.8375	0.469043	$1.3X10^{-3}$	0.059	0.247	0.21	23.9683	-5.8730	41.5142	10.1724
Cd PNAC $800^0CH_2SO_4$	-0.0008x-1.304	4.2135x+26.65	0.0046	0.8280	0.158328	$1.8X10^{-3}$	0.050	0.237	0.49	29.9320	17.2109	51.8437	29.8101
Mn PNAC 600^0C HCl	-0.0004-1.066	2.949x+21.12	0.0013	0.7280	0.412031	$9.2X10^{-4}$	0.086	0.339	0.86	30.0000	20.1938	51.9615	34.9767
Mn PNAC $600^0CH_2SO_4$	0.0049x-1.361	2.815x-0.500	0.1581	0.7105	-15.87300	$-1.1X10^{-2}$	0.044	0.355	0.55	30.6667	11.8182	53.1162	20.4697
MnPNAC$600^0CH_3PO_4$	0.0018x-1.3745	3.3995x-27.25	0.0175	0.8770	-0.004140	$-4.2X10^{-2}$	23.68	0.294	0.67	-1E+3	18.7065	1E+3	32.4006
Mn PNAC 800^0C HCl	0.0083x-1.5955	2.5275x+0.63	0.2505	0.8305	-10.10100	$1.9X10^{-2}$	0.025	0.396	0.68	32.1078	13.9216	55.6124	24.1129
Mn PNAC $800^0CH_3PO_4$	0.0058x-1.698	2.825x-0.02	0.1189	0.8368	-333.3330	$-1.3X10^{-2}$	0.020	0.354	0.72	32.4074	16.9444	56.1313	29.3486
Mn PNAC $800^0CH_2SO_4$	-0.0012x-1.236	2.691x+10.7	0.0038	0.8230	0.675220	$2.7X10^{-3}$	0.058	0.372	0.92	20.1961	-5.7843	34.9806	10.0187

From Table 4.238, it could be deduced that for pearnut seed based activated carbons, the R^2 for the second-order were better than R^2 for the first-order rate model. Similar observation was made between the calculated adsorption capacities. q_{e2} were closer to the experimental adsorption capacities q_e. For example, for Cd/PNAC/800°C/HCl, q_{e1} = 0.056mg/g, q_{e2} = 0.303mg/g while q_e = 0.33mg/g. for Ni/PNAC/600°C/H_2SO_4, q_{e1} = 0.017mg/g, q_{e2} = 0.300mg/g while q_e = 0.32mg/g.

Table 4.239: Rate Constants, Theoretical and Experimental Adsorption Capacities of Oil Bean Shell Activated Carbons

AC Type	EQU 1st order(Y =)	EQU 2nd 0rder(Y =)	R^2 1st order	R^2 2nd 0rder	K_1 (min^{-1})	K_2 (g/mgmin)	qe_1 mg/g (calculated)	qe_2 mg/g (calculated)	qe mg/g (experimental)	1st Order HYBRID	2nd Order HYBRID	1st Order MPSD	2nd Order MPSD
Pb OBAC 600^0C HCl	-0.0021x-1.3375	6.013x+57.39	0.0289	0.0825	0.00484	0.6299	0.046	0.16	0.58	30.6897	24.1379	53.1560	41.8081
Pb OBAC 600^0C H_2SO_4	0.0025x-1.5695	4.631x+12.69	0.0446	0.8302	-0.00580	1.6896	0.027	0.21	0.53	31.6352	20.1258	54.7938	34.8589
Pb OBAC 600^0C H_3PO_4	-0.0024x-1.4815	5.010x+21.31	0.0109	0.8159	0.00553	1.1776	0.033	0.19	0.54	31.2963	21.6049	54.2068	37.4209
Pb OBAC 800^OC HCl	-8e-05x-1.1725	4.573x+68.08	0.0006	0.8076	0.00018	0.3071	0.067	0.21	0.53	29.1195	20.1258	50.4364	34.8589
Pb OBAC 800^OC H_2SO_4	0.0018x-1.6375	4.3155x+4.11	0.0080	0.8030	-0.00415	4.5312	0.022	0.23	0.38	31.4035	13.1579	54.3925	22.7901
Pb OBAC 800^OC H_3PO_4	0.0056x-1.9165	5.707x+3.420	0.1592	0.8286	-0.01290	9.5233	0.012	0.17	0.36	32.2222	17.5926	55.8105	30.4713
Cd OBAC 600^0C HCl	-0.017x-1.0975	6.212x+22.16	0.7123	0.8314	0.00392	1.7413	0.079	0.16	0.38	26.4035	19.2982	45.7322	33.4255
Cd OBAC 600^0C H_2SO_4	0.0018x-1.5565	4.647x+14.01	0.0180	0.8373	-0.00415	1.5410	0.028	0.21	0.54	31.6049	20.3704	54.7414	35.2825
Cd OBAC 600^0C H_3PO_4	-0.0004x-1.122	3.941x+50.86	0.0083	0.8219	0.00092	0.3053	0.076	0.25	0.32	25.4167	7.2917	44.0230	12.6295
Cd OBAC 800^OC HCL	0.0003x-1.3305	4.833x+37.22	0.0008	0.8180	-0.00069	0.6280	0.047	0.20	0.42	29.6032	17.4603	51.2742	30.2422
Cd OBAC $800^OCH_2SO_4$	0.0055x-1.8007	5.0395x-54.81	0.2113	0.8873	-0.01270	-0.4634	63.19	0.20	0.21	-9E+3	1.5873	1E+4	2.7493
Cd OBAC 800^OC H_3PO_4	0.0026x-1.544	3.969x+9.660	0.0443	0.8459	-0.00599	1.6310	0.029	0.25	0.27	29.7531	2.4691	51.5339	4.2767
Ni OBAC 600^0C HCl	0.0008x-1.152	3.362x+27.29	0.00046	0.8114	-0.00184	0.4140	0.070	0.29	0.10	10.0000	-63.333	17.3205	109.6966
Ni OBAC 600^0C H_3PO_4	0.0014x-1.203	3.2015x+9.99	0.0093	0.6575	-0.00322	1.0260	0.063	0.31	0.10	12.3333	-70.000	21.3620	121.2436
Ni OBAC 600^0C H_2SO_4	0.0014x-1.5881	1.704x+47.13	0.0032	0.8752	-0.00322	0.0616	38.73	0.59	0.18	-7138.8	-75.925	12364.91	131.5076
Ni OBAC 800^0C HCl	-1e-05x-1.506	3.0825x+6.53	$2.0x10^{-7}$	0.8202	0.00230	1.4551	0.031	0.32	0.55	31.4545	13.9394	54.4809	24.1437
Ni OBAC 800^0C H_3PO_4	0.0066x-1.7545	3.351x+0.440	0.2304	0.8330	-0.01520	25.521	0.018	0.29	0.57	32.2807	16.3743	55.9118	28.3611
Ni OBAC 800^0C H_2SO_4	0.0007x-1.564	2.280x+0.310	0.0007	0.8370	-0.00161	21.464	0.027	0.38	0.54	31.6667	9.8765	54.8483	17.1067
Mn OBAC 600^0C HCl	0.0037x-1.8015	4.743x+2.060	0.0415	0.8251	-0.00852	10.920	0.016	0.21	0.29	31.4943	9.1954	54.5496	15.9269
Mn OBAC 600^0C H_3PO_4	0.0013x-1.333	4.222x+22.28	0.0062	0.8031	-0.00299	0.8000	0.046	0.23	0.17	24.3137	-11.764	42.1126	20.3771
Mn OBAC 600^0C H_2SO_4	0.0006x-1.4395	5.154x+28.37	0.0037	0.8211	-0.00138	0.9362	0.036	0.19	0.07	16.1905	-57.142	28.0427	98.9743
Mn OBAC 800^0C HCl	-0.0006x-1.4915	4.411x+12.58	0.0090	0.8160	0.00138	1.5467	0.032	0.22	1.26	32.4868	27.5132	56.2687	47.6543
Mn OBAC 800^0C H_3PO_4	0.0001x-1.3575	4.044x+19.59	0.00009	0.8168	-0.00230	0.8346	0.044	0.24	0.79	31.4768	23.2068	54.5194	40.1953
Mn OBAC 800^0C H_2SO_4	0.0041x-1.5595	4.3805x+14.21	0.2398	0.8320	-0.00944	1.3504	0.028	0.22	0.72	32.0370	23.1481	55.4898	40.0938

The adsorption data for OBAC fitted well on the pseudo-second order kinetic as reflected in the values of R^2 for the pseudo-second order kinetic plot (Table 4.239). The similar thing was observed between the kinetic rate constants k_1 and k_2 as well as between the calculated qe_1 and qe_2 when compared. The calculated respective qe_2 values were closer to the experimental values in almost all the OBAC prepared irrespective of the metal adsorbed. As the adsorption model obeyed pseudo-second order kinetic, this suggested that the overall rate of the adsorption process is most likely to be controlled by chemosorption process, and that the rate of the reaction is directly proportional to the number of active sites on the surface of the activated carbons (Singha, 2013).

Table 4.240: Rate Constants, Theoretical and Experimental Adsorption Capacities of Snail Shell Activated Carbons

AC Type	EQU 1st order(Y =)	EQU 2nd 0rder(Y =)	R^2 1st order	R^2 2nd 0rder	K_1 (min^{-1})	K_2 (g/mgmin)	qe_1 mg/g (calculated)	qe_2 mg/g (calculated)	qe mg/g (experimental)	1st Order HYBRID	2nd Order HYBRID	1st Order MPSD	2nd Order MPSD
Ni SSAC 600^0C HCl	0.0022x - 1.6495	8.8165x + 260.87	0.0835	0.2635	$-5.0x10^{-3}$	$2.9x10^{-1}$	0.022	0.110	0.05	18.6667	-40.0000	32.3316	69.2820
Ni SSAC 600^0C H_3PO_4	-0.0012x - 1.5325	8.0270x + 123.50	0.0124	0.4780	$2.7x10^{-3}$	$5.2x10^{-1}$	0.029	0.120	0.07	19.5238	-23.8095	33.8162	41.2393
Ni SSAC 600^0C H_2SO_4	0.0048x - 1.5690	11.0260x + 191.82	0.0651	0.4646	$-1.1x10^{-2}$	$6.3x10^{-1}$	0.026	0.091	0.07	20.9524	-10.0000	36.2906	17.3205
Ni SSAC 800^0C HCl	0.0060x - 1.6965	8.0570x + 155.42	0.2863	0.2334	$-1.3x10^{-2}$	$4.2x10^{-1}$	0.020	0.120	0.11	27.2727	-3.0303	47.2377	5.2486
Ni SSAC 800^0C H_3PO_4	-0.0030x - 2.0910	5.1135x + 322.15	1E -04	0.1441	$6.9x10^{-4}$	$8.1x10^{-2}$	0.008	0.190	0.07	29.5238	-57.1429	51.1367	98.9743
Ni SSAC 800^0C H_2SO_4	0.0015x - 1.8790	10.1410x + 255.95	0.0055	0.3190	$-3.4x10^{-3}$	$4.0x10^{-1}$	0.013	0.098	0.13	30.0000	8.2051	51.9615	14.2117
Pb SSAC 600^0C HCl	0.0082x - 2.0985	10.0180x + 183.88	0.2990	0.2718	$-1.8x10^{-2}$	$5.5x10^{-1}$	0.008	0.099	0.52	32.8205	26.9872	56.8468	46.7432
Pb SSAC 600^0C H_3PO_4	-0.0027x - 1.6675	8.9660x + 331.66	0.0371	0.2884	$6.2x10^{-3}$	$2.4x10^{-1}$	0.021	0.110	0.27	30.7407	19.7531	53.2445	34.2133
Pb SSAC 600^0C H_2SO_4	0.0038x - 1.7575	5.4725x + 375.55	0.0580	0.1154	$-8.7x10^{-3}$	$7.9x10^{-1}$	0.017	0.180	0.19	30.3509	1.7544	52.5693	3.0387
Pb SSAC 800^0C HCl	0.0109x - 2.2570	8.2830x + 162.62	0.8280	0.3043	$-2.5x10^{-2}$	$4.2x10^{-1}$	0.005	0.120	0.11	31.8182	-3.0303	55.1107	5.2486
Pb SSAC 800^0C H_3PO_4	0.0004x - 0.4675	15.3850x - 105.85	0.1550	0.9376	$-9.2x10^{-4}$	$-2.2x10^{0}$	0.340	0.064	0.09	-92.5926	9.6296	160.3751	16.6790
Pb SSAC 800^0C H_2SO_4	0.0061x - 1.8005	8.5470x + 103.02	0.1490	0.3125	$-1.4x10^{-2}$	$7.1x10^{-1}$	0.015	0.110	0.08	27.0833	-12.5000	46.9097	21.6506
Cd SSAC 600^0C HCl	0.0015x - 1.1430	4.4685x + 266.69	0.0496	0.7002	$-3.4x10^{-3}$	$7.4x10^{-2}$	0.071	0.220	0.04	-25.8333	-150.0000	44.7446	259.8076
Cd SSAC 600^0C H_3PO_4	0.0014x - 1.4935	6.9340x + 197.14	0.0302	0.2484	$-3.2x10^{-3}$	$2.4x10^{-1}$	0.032	0.140	0.06	15.5556	-44.4444	26.9430	76.9800
Cd SSAC 600^0C H_2SO_4	0.0086x - 1.2880	10.5010x + 147.82	0.1975	0.7761	$-1.9x10^{-2}$	$7.5x10^{-1}$	0.051	0.095	0.04	-9.1667	-45.8333	15.8771	79.3857
Cd SSAC 800^0C HCl	0.0026x - 1.1029	15.352x -99.6100	0.0989	0.8408	$-6.0x10^{-3}$	$-0.2x10^{-1}$	12.67	0.065	0.04	-1E+4	-20.8333	1E+4	36.0844
Cd SSAC 800^0C H_3PO_4	-0.0037x - 1.4965	9.3470x + 150.74	0.0777	0.8163	$0.5x10^{-3}$	$5.9x10^{-1}$	0.031	0.100	0.04	7.5000	-50.0000	12.9904	86.6025
Cd SSAC 800^0C H_2SO_4	0.0023x - 1.8725	11.3210x + 93.80	0.0143	0.7059	$-5.2x10^{-3}$	$1.4x10^{0}$	0.013	0.088	0.04	22.5000	-40.0000	38.9711	69.2820
Mn SSAC 600^0C HCl	-0.0022x - 0.9525	4.1965x + 109.83	0.0879	0.5915	$5.0x10^{-3}$	$1.6x10^{-1}$	0.110	0.230	0.69	28.0193	22.2222	48.5309	38.4900
Mn SSAC 600^0C H_3PO_4	0.0060x - 1.6455	7.1860x + 18.400	0.4100	0.6132	$-1.3x10^{-2}$	$2.8x10^{0}$	0.022	0.130	1.33	32.7820	30.0752	56.7800	52.0918
Mn SSAC 600^0C H_2SO_4	0.0013x - 1.2842	5.1545x + 111.17	0.0397	0.7753	$-2.9x10^{-3}$	$2.4x10^{-1}$	0.051	0.190	1.23	31.9512	28.1843	55.3411	48.8166
Mn SSAC 800^0C HCl	0.0022x - 1.3755	5.1305x + 225.33	0.1547	0.4569	$-5.0x10^{-3}$	$1.2x10^{-1}$	0.042	0.190	0.06	10.0000	-72.2222	17.3205	125.0926
Mn SSAC 800^0C H_3PO_4	0.0123x - 2.3420	6.4885x + 37.25	0.3174	0.5234	$-2.8x10^{-2}$	$1.1x10^{0}$	0.00005	0.150	0.11	33.3182	-12.1212	57.7088	20.9946
Mn SSAC 800^0C H_2SO_4	0.0107x - 2.2825	7.4735x + 24.650	0.3294	0.5225	$-2.4x10^{-2}$	$2.3x10^{0}$	0.0054	0.130	0.14	32.0476	2.3810	55.5081	4.1239

The observation made on the kinetic study of SSAC, tolls the line of OBAC as well as PKAC except in the values of the calculated q_e and the experimented where the q_{e1} was closer to q_e in most of the activated carbon types (Table 4.240).

Table 4.241: Intraparticle Diffusion constants for PNAC

S/N	AC Type	Intraparticle Diffusion plot Equ. (Y =)	R^2	K_{id}	C
1	Ni PKAC 600^0C HCl	0.018x+0.168	0.374	0.018	0.168
2	Ni PKAC 600^0C H_3PO_4	0.014x+0.184	0.357	0.014	0.184
3	Ni PKAC 600^0C H_2SO_4	9.00E-05x+	2.00E-05	9.00E-05	0.307
4	Ni PKAC 800^0C HCl	0.008x+0.307	0.129	0.008	0.267
5	Ni PKAC 800^0C H_3PO_4	0.018x+0.187	0.392	0.018	0.187
6	Ni PKAC 800^0C H_2SO_4	-0.010x+0.405	0.218	-0.010	0.405
7	Pb PKAC 600^0C HCl	0.000x+0.316	8.00E-05	0.000	0.316
8	Pb PKAC 600^0C H_3PO_4	0.006x+0.170	0.140	0.006	0.170
9	Pb PKAC 600^0C H_2SO_4	0.008x+0.147	0.288	0.008	0.147
10	Pb PKAC 800^0C HCl	0.006x+0.220	0.123	0.006	0.220
11	Pb PKAC 800^0C H_3PO_4	0.008x+0.149	0.272	0.008	0.149
12	Pb PKAC 800^0C H_2SO_4	0.007x+0.160	0.185	0.007	0.160
13	Cd PKAC 600^0C HCl	0.000x+0.316	6.00E-05	0.000	0.316
14	Cd PKAC 600^0C H_3PO_4	0.008x+0.151	0.270	0.008	0.151
15	Cd PKAC 600^0C H_2SO_4	0.008x+0.149	0.273	0.008	0.149
16	Cd PKAC 800^0C HCl	0.006x+0.219	0.128	0.006	0.219
17	Cd PKAC 800^0C H_3PO_4	0.008x+0.149	0.282	0.008	0.149
18	Cd PKAC 800^0C H_2SO_4	0.007x+0.161	0.188	0.007	0.161
19	Mn PKAC 600^0C HCl	0.012x+0.211	0.178	0.012	0.211
20	Mn PKAC 600^0C H_3PO_4	0.007x+0.204	0.062	0.007	0.204
21	Mn PKAC 600^0C H_2SO_4	0.002x+0.332	0.007	0.002	0.332
22	Mn PKAC 800^0C HCl	0.001x+0.390	0.003	0.001	0.390
23	Mn PKAC 800^0CH_3PO_4	-0.002x+0.380	0.007	-0.002	0.380
24	Mn PKAC 800^0C H_2SO_4	0.009x+0.277	0.119	0.009	0.277

Intraparticle diffusion model by Weber and Morris, (1963) was applied to predict the rate–limiting step in the adsorption of these metals under consideration. For a solid-liquid sorption process of this nature, the solute transfer is usually chracterised by externl mass transfer (boundary layer diffusion), intraparticle diffusion or both.

Table 4.242: Intraparticle Diffusion constants for PKAC

S/N	AC Type	Intraparticle Diffusion plot Equ. (Y =)	R^2	K_{id}	C
1	Ni PNAC 600^0C HCl	-0.001x+0.351	0.005	-0.001	0.351
2	Ni PNAC 600^0C H_3PO_4	0.002x+0.218	0.015	0.002	0.218
3	Ni PNAC 600^0C H_2SO_4	0.003x+0.225	0.035	0.003	0.225
4	Ni PNAC 800^0C HCl	0.006x+0.242	0.080	0.006	0.242
5	Ni PNAC 800^0C H_3PO_4	0.005x+0.245	0.060	0.005	0.245
6	Ni PNAC $800^0CH_2SO_4$	0.000x+0.289	0.000	0.000	0.289
7	Pb PNAC 600^0C HCl	0.000x+0.239	0.000	0.000	0.239
8	Pb PNAC 600^0C H_3PO_4	0.001x+0.190	0.007	0.001	0.190
9	Pb PNAC 600^0C H_2SO_4	0.003x+0.192	0.050	0.003	0.192
10	Pb PNAC 800^0C HCl	0.001x+0.254	0.009	0.001	0.254
11	Pb PNAC 800^0C H_3PO_4	0.000x+0.222	0.000	0.000	0.222
12	Pb PNAC 800^0C H_2SO_4	0.001x+0.190	0.004	0.001	0.190
13	Cd PNAC 600^0C HCl	0.001x+0.236	0.003	0.001	0.236
14	Cd PNAC $600^0CH_3PO_4$	0.005x+0.130	0.191	0.005	0.130
15	Cd PNAC $600^0CH_2SO_4$	0.004x+0.187	0.069	0.004	0.187
16	Cd PNAC 800^0C HCl	0.000x+0.260	0.000	0.000	0.260
17	Cd PNAC $800^0CH_3PO_4$	0.004x+0.149	0.099	0.004	0.149
18	Cd PNAC $800^0CH_2SO_4$	0.002x+0.214	0.027	0.002	0.214
19	Mn PNAC 600^0C HCl	-0.001x+0.234	0.007	-0.001	0.234
20	Mn PNAC $600^0CH_2SO_4$	0.003x+0.166	0.054	0.003	0.166
21	MnPNAC$600^0CH_3PO_4$	0.001x+0.207	0.006	0.001	0.207
22	Mn PNAC 800^0C HCl	-0.002x+0.262	0.027	-0.002	0.262
23	Mn PNAC $800^0CH_3PO_4$	-0.005x+0.280	0.143	-0.005	0.280
24	Mn PNAC $800^0CH_2SO_4$	0.000x+0.227	0.001	0.000	0.227

The result (figure 4.145 to 4.192) obtained showed that the plot of q_t versus $t^{0.5}$ did not give a straight line graph which starts from the origin and this suggests that intraparticle diffusion is not the only rate limiting step involved in the adsorption of these metals on the activated carbons obtained, according to Weber and Morris, (1963). The variation from the origin may be due to the variation of mass transfer in the initial and final stage adsorption according to Pandey *et al.*, (1986), Mohanty *et al.*, (2005). This indicates that overall adsorption process may be controlled either by one or more steps such as external diffusion, pore diffusion, surface diffusion and

adsorption on the pore surface or a combination of more than one step. Similar result was obtained for almost all the activated carbon types prepared.

Table 4.243: Intraparticle Diffusion constants for OBAC

S/N	AC Type	Intraparticle Diffusion plot Equ. (Y =)	R^2	K_{id}	C
1	Pb OBAC 600^0C HCl	0.006x+0.090	0.305	0.006	0.090
2	Pb OBAC 600^0C H_2SO_4	0.002x+0.189	0.035	0.002	0.189
3	Pb OBAC 600^0C H_3PO_4	0.005x+0.148	0.121	0.005	0.148
4	Pb OBAC 800^OC HCl	0.009x+0.103	0.381	0.009	0.103
5	Pb OBAC 800^OC H_2SO_4	0.001x+0.223	0.006	0.001	0.223
6	Pb OBAC 800^OC H_3PO_4	0.000x+0.183	0.002	0.000	0.183
7	Cd OBAC 600^0C HCl	0.003x+0.128	0.087	0.003	0.128
8	Cd OBAC 600^0C H_2SO_4	0.002x+0.187	0.037	0.002	0.187
9	Cd OBAC 600^0C H_3PO_4	0.010x+0.123	0.401	0.010	0.123
10	Cd OBAC 800^OC HCl	0.007x+0.127	0.242	0.007	0.127
11	Cd OBAC 800^OCH_2SO_4	-0.006x+0.302	0.113	-0.006	0.302
12	Cd OBAC 800^OC H_3PO_4	0.002x+0.226	0.026	0.002	0.226
13	Ni OBAC 600^0C HCl	0.009x+0.189	0.213	0.009	0.189
14	Ni OBAC 600^0C H_3PO_4	0.006x+0.260	0.042	0.006	0.260
15	Ni OBAC 600^0C H_2SO_4	0.034x+0.121	0.796	0.034	0.121
16	Ni OBAC 800^0C HCl	0.006x+0.271	0.057	0.006	0.271
17	Ni OBAC 800^0C H_3PO_4	0.001x+0.319	0.006	0.001	0.319
18	Ni OBAC 800^0C H_2SO_4	0.000x+0.394	0.000	0.000	0.394
19	Mn OBAC 600^0C HCl	0.000x+0.217	0.000	0.000	0.217
20	Mn OBAC 600^0C H_3PO_4	0.007x+0.164	0.153	0.007	0.164
21	Mn OBAC 600^0C H_2SO_4	0.004x+0.143	0.125	0.004	0.143
22	Mn OBAC 800^0C HCl	0.004x+0.187	0.063	0.004	0.187
23	Mn OBAC 800^0C H_3PO_4	0.006x+0.179	0.137	0.006	0.179
24	Mn OBAC 800^0C H_2SO_4	0.002x+0.204	0.021	0.002	0.204

Table 4.244: Intraparticle Diffusion constants for SSAC

S/N	AC Type	Intraparticle Diffusion Plot Equ. (Y =)	R^2	K_{id}	C
1	Ni SSAC 600^0C HCl	0.003x+0.057	0.166	0.003	0.057
2	Ni SSAC 600^0C H_3PO_4	0.005x+0.061	0.324	0.005	0.061
3	Ni SSAC 600^0C H_2SO_4	0.004x+0.040	0.368	0.004	0.040
4	Ni SSAC 800^0C HCl	0.001x+0.098	0.010	0.001	0.098
5	Ni SSAC 800^0C H_3PO_4	0.001x+0.090	0.028	0.001	0.090
6	Ni SSAC 800^0C H_2SO_4	0.001x+0.059	0.090	0.001	0.059
7	Pb SSAC 600^0C HCl	0.000x+0.086	0.000	0.000	0.086
8	Pb SSAC 600^0C H_3PO_4	0.004x+0.038	0.349	0.004	0.038
9	Pb SSAC 600^0C H_2SO_4	0.003x+0.065	0.107	0.003	0.065
10	Pb SSAC 800^0C HCl	-0.001x+0.110	0.027	-0.001	0.110
11	Pb SSAC 800^0C H_3PO_4	0.045x+0.188	0.459	0.045	0.188
12	Pb SSAC 800^0C H_2SO_4	-0.001x+0.118	0.032	-0.001	0.118
13	Cd SSAC 600^0C HCl	0.015x-0.001	0.996	0.015	-0.001
14	Cd SSAC 600^0C H_3PO_4	4.000x+0.070	0.164	4.000	0.070
15	Cd SSAC 600^0C H_2SO_4	0.008x+0.010	0.618	0.008	0.010
16	Cd SSAC 800^0C HCl	0.002x+0.060	0.051	0.002	0.060
17	Cd SSAC 800^0C H_3PO_4	0.006x+0.035	0.456	0.006	0.035
18	Cd SSAC 800^0C H_2SO_4	0.003x+0.050	0.164	0.003	0.050
19	Mn SSAC 600^0C HCl	0.017x+0.036	0.497	0.017	0.036
20	Mn SSAC 600^0C H_3PO_4	0.000x+0.137	0.002	0.000	0.137
21	Mn SSAC 600^0C H_2SO_4	0.009x+0.066	0.468	0.009	0.066
22	Mn SSAC 800^0C HCl	0.013x+0.013	0.478	0.013	0.013
23	Mn SSAC 800^0C H_3PO_4	-0.001x+0.161	0.018	-0.001	0.161
24	Mn SSAC 800^0C H_2SO_4	0.000x+0.133	0.000	0.000	0.133

CHAPTER FIVE
CONCLUSION AND RECOMMENDATIONS

5.1 Conclusion

(1) In this research, Oil bean shell, Pearnut seed, Palm kernel shell and snail shell have shown to be potential adsorbent in solving waste water pollution problem at low cost.

(2) The FTIR spectra of the carbons indicated the presence of various types of functional groups such as OH group, alkenes, CO, aldehydes, ketones, carboxylic acid group on the surface of the adsorbents. There was higher percentage yield at 600°C both before activation and after activation with the activating agents.

(3) The SEM result showed that wide varieties of pores were present in the activated carbons and that more pores existed on the activated carbon than the unactivated carbons as reflected in the pore sizes of the activated carbons.

(4) There was a great effect of the chemical activation process on the pore development in virtually all the activated carbon types produced as shown by the pore volumes of the AC indicated by both activated carbon before and activated carbon after activation. The ACs showed high surface area but did not show a direct relationship with the pore volumes obtained.

(5) The experimental data obtained were subjected to four isotherm models, Freundlich, Langmuir, Temkin and Dubinin-Radushkevich and out of which the Freundlich and Temkin isotherm were the most appropriate for the experimental data (higher determination coefficients) which suggest heterogeneous surface energies and gives an exponential distribution of active sites.

(6) Three kinetic models were also studied but the results showed extremely higher coefficients of determination when it was fitted to the pseudo-second order kinetic models. Also, the two non-linear regression error functions (HYBRID and MPSD) and the calculated (theoretical) values of q_{e2} for Pseudo second-order reaction model which are closer to the experimental value of q_e suggests that pseudo-second kinetic model best explains the kinetics of adsorption by these activated carbons. These facts suggest that the adsorption of heavy metals by activated carbons from these precursors followed the Pseudo-second-order reaction model, which was as a result of chemisorptions. In chemisorptions, the metals stick to the adsorbent surface by forming a chemical (usually covalent) bond and tends to find sites that maximize their coordination number with the surface. The rate of sorption was also found not to be controlled by a singular rate limiting step as noted from the Weber Morris Intraparticle diffusion model conducted.

(7) PNAC carbonized at 800^0C and activated with H_2SO_4 gave the highest percentage adsorption of Pb from the wastewater examined while the least was shown by SSAC carbonized at 800^0C and activated with H_3PO_4.

(8) Finally, the best adsorbent for Ni and Pb adsorption was OBAC carbonized at 600^oC and 800^oC and activated with HCl respectively. But for Cd, it was PKAC carbonized at 800^oC and activated with HCl, while for Mn, it was SSAC carbonized at 600^oC and activated with H_3PO_4. In all generally, H_3PO_4 was observed to be the best activating agent followed by H_2SO_4 while HCl was the least.

5.2 Recommendations

(1) More carbonization temperatures and different activating agents should be investigated and further characterization of the activated carbons produced in such case should be carried out.

(2) There should be focus on the full scale implementations, the preparation of activated carbons from these agro-wastes to be scaled up from laboratory to pilot plant while considering the suggestions in the adsorption study.

(3) There is need to do an economic analysis to determine the cost of preparation of activated carbons from the by-products of oil bean, palm kernel shell, snail shell and pear nut seed shell in order to have a complete idea about the economic viability of application of these adsorbents.

There is also the need for the study of desorption and regeneration of the activated carbon so that it could be reused, saving cost and avoiding environmental problem with its disposal.

5.3 Contribution to Knowledge

(1) Although some agricultural wastes have been modified to activated carbons and as well used to remove heavy metals from aqueous solutions, the agricultural waste has not been sufficiently exhausted in its use to produce AC. Thus some important agro-wastes have not been fully utilized and their adsorption capacities have not been established. In this research, oil bean shell and pear nut seed has actually been modified to activated carbon which can be used to remove heavy metals from aqueous effluents.

(2) We did not only establish that these agro-wastes can be converted to activated carbons at these temperatures and time, but this study has shown that at a lower

temperatures of carbonization, higher AC yield from these agro-wastes even when carbonized for a longer period could bbe obtained.

(3) The study has also established that carbonization at high temperatures (600°C and 800°C) over a period of time aids heavy metal adsorptions from aqueous solutions.

(4) To date, a considerable body of research has sought to establish the best conditions for carbonization and activation of raw materials (agro-wastes) and this study has shown that fact that at 600°C and 800°C, oil bean shell, palm kernel shell, peanut seed and snail shell can be carbonized for 30minutes and activated with H_2SO_4, HCl and H_3PO_4 and efficiently used to remove heavy metals from aqueous solution.

(5) The study has established that the best condition to remove Ni from industrial effluent using Oil bean based activated carbon is carbonization at 600°C for 30min and activation with HCl. Also for Pb, using oil bean based activated carbon, carbonization at 800°C for 30min and activation with HCl gives the best adsorption.

(6) The study also established that palm kernel based activated carbon carbonized at 800°C for 30min and activated with HCl best removes Cd from industrial effluents.

(7) Also established is the fact that Mn can best be removed from industrial waste using Snail shell based activated carbon when carbonized at 600°C for 30min and activated with H_3PO_4.

(8) Finally, from this study it has established that oxidation of activated carbon by acid is directly proportional to the acid strength on these agrowastes.

REFERENCES

Abaje, I.B., Ati, O.F. and Ishaya, S. (2009). "Nature of Potable Water Supply and Demand in Jema'a Local Government Area of Kaduna State, Nigeria," Research. *Journal of Environment and Earth Sciences*, 1(1), 16-21.

Abechi, S.E., Gimba, C.E., Uzairu, A. and Dallatu, Y.A. (2013). Preparation and characterization of Activated carbon from Palm Kernel shell by chemical Activation. *Research Journal of chemical sciences*. 3(7), 54-61

Abia, A. A., Horsfall, M. and Didi, O. (2003). The use of chemically modified and unmodified cassava waste for the removal of Cd, Cu, and Zn ions from aqueous solution. *Bioresources Technology*, 90, 345- 348.

Achinewhu, S.C. (1982). Composition and food potentials of the African oil bean (Pentaclethra Macrophylla) and Velvet bean (Mucuna Uriens). Journal of Science, 47: 1736 – 1737.

Adeniji-Oloukoi, G. (2012). Assessment of the Quality of Spring Water in Ibadan, Nigeria. *Journal of Applied Sciences in Environmental Sanitation*, 7 (4), 263-268.

Adrian, W. J. (1973). A comparison of a wet pressure digestion method with other commonly used wet and dry-ashing methods. *Analyst*, *98*, 213-216.

Adaikpoh, E. O., Nwajei, G.E. and Iogala, J. E. (2005). Heavy metals concentrations in coal and sediments from River Ekulu in Enugu, Coal City of Nigeria. *Journal of AppliedScience and Environmental Management, 9*(3), 5 – 8.

Adamson, A. W. (2001). Physical chemistry of surfaces, 5th edition, Wisley, New York. *Pigments, 51, 25 – 40*.

Ademoroti, C.M.A. (1986). Levels of heavy metals on bark and fruit of trees in Benin City, Nigeria. *Environmental pollution. 11,* 241-243.

Ademoroti, C.M.A. (1996). Environmental Chemistry and toxicology. March prints and Consultancy. Foludex Press Ltd. Ibadan. pp. 177-195.

Ademiluyi, F.T. and David-West, E.O. (2012). Effect of Chemical Activation on the Adsorption of Heavy Metals Using Activated Carbons from Waste Materials. *International Scholarly Research Network (ISRN) Chemical Engineering. 5,*

Ademiluyi, F.T., Amadi, S.A. and Amakama, N.J. (2009). Adsorption and treatment of organic contaminants using activated carbon from waste Nigerian bamboo. *Journal of AppliedScience and Environmental Management, 13*(3), 39-47

Adinata, D., Daud, W. M.A.W. and Mohd Kheireddine, A. (2007). Preparation and characterization of activated carbon from palm shell by chemical activation with K_2CO_3. *Bioresource Technology*. *98*, 145-149.

Agbo, S., (1997). Effects of lead poisoning in children. In: Proceeding at a workshop on vehicular emission and lead poisoning in Nigeria. *Friends of the environment*. pp. 20-28.

Agbozu, I. E. and Emoruwa, F.O. (2014). Batch adsorption of heavy metals (Cu, Pb, Fe, Cr & Cd) from aqueous solutions using Coconut husk. *African Journal of Environmental Science and Technology*, 8(4), 239-246.

Aharoni, C. and Ungarish, M. (1977). Kinetics of activated chemosorption, Part 2. Teoretical models. *Journal of chemical society Faraday Trans*. 73, 456- 464.

Ahmad, A.L., Harris, W.A., Syafiie and Seng, O.B. (2002). Removal of dye from wastewater of textile industry using membrane technology. *Journal of Technology*, 36, 31-44.

Ahmedna, M., Clark, S. J., Rao, R.M., Mashall, W.E. and Johns, M.M. (2006). Use of filtration and buffers in raw sugar colour measurement. Journal of Science Food and Agriculture, 75, 109- 116.

Ahmady-Asbchin, S., Andres, Y., Gerente, C. and Cloirec, P. (2008). Biosorption of Cu(II) from aqueous solution by Fucus serratus: Surface characterization and sorption mechanisms. *Bioresources Technology*, 99, 6150-6155.

Ajao, E.A. and Anurigwo, S. (2002). Land-based sources of pollution in the Niger Delta, Nigeria. AMBIO: *Journal of the Human Environment. 31*(5), 442–445.

Ajiwe, V. I. E., Okereke, C. A., Ogbuagu, J. O., Ojukwu, U. and Onwukema, V. I. (1998). Characterisation and applications of oils extracted from Canarium schweinfurthii, Vitex doniana and Xylopia aethiopica fruit/seeds. *Bioresources Technology*, 64 (3), 249-252.

Ajmal, M., Rao, R. A. K., Ahmad, R. and Ahmad, J. (2000). Adsorption studies on Citrus reticulata (fruit peel of orange) removal and recovery of Ni (II) from electroplating wastewater. *Journal of Hazard Materials*, 79, 117– 131.

Ajmal, M, Rao, R A. K. and Siddiqui, B. A. (1996). Studies on removal and recovery of Cr (VI) from electroplating wastes. *Water Resources*, 30, 1478-1482.

Ajmal, M., Rao, R. A. K., Anwar, S., Ahmad, J. and Ahmad, R. (2003). Adsorption studies on rice husk: removal and recovery of Cd(II) from wastewater.

Bioresources Technology, 86, 147-149.

Akan, B.W. and Abiola, R.K. (2008). Assesment of trace metal levels in fish species of Lagos Lagoon. Conference Proceedings of Chemical Society of Nigeria. *31st Annual International Conference and Exhibition*, Warri. 22nd-26th 2008. Delta State Nigeria. pp. 394-399.

Akaninwor, J. O., Onyeike, E. N. and Ifemeje, J.C. (2005). Trace metal levels in raw and heat processed Nigerian staple foods from oil-producing areas of Rivers and Bayelsa States. *Journal of Applied Sciences and Environmental Management. 10*(2), 23-27.

Akaninwor, J.O. Anosike, E.O. and Egwim, O. (2007). Effect of indomie industrial effluent discharge on microbial properties of new Calabar river. *Science Resource Essay*, 2, 1–25

Akiode, O.K. Idowu, M.A. Omeike, S.O. and Akinwunmi, F. (2015). adsorption and kinetics studies of cu (ii) ions removal from aqueous solution by untreated and treated sugarcane bagasse. *Global NEST Journal*, 17(3), 583-593.

Alamu, O. (2005). Watershed management to meet water quality standards and emerging TMDL (Total maximum daily load). *Proceedings of the Third Conference 5-9 March 2005 (Atlanta, Georgia USA). American Society of Agricultural and Biological Engineers*, St. Joseph, Michigan. www.asabe.org, 701P0105.

Alam, J.B. Hossain, A. Khan, S.K. Banik, B.K. Islam, M.R. and Muyen, Z. (2007). Deterioration of water quality of Surma River. *Envirnmental Monitoring and Assessment*, 134(1–3), 233–242

Alicia Leung and Deepak Sinha., (1998). Brewery Industry China Hong Kong Management Case Study, Management Development Center of Hong Kong, Hong Kong.

Al-Asheh, S. and Banat, F. (2001). Adsorption of Zn (II) and Cu (II) Ions by the solid waste of the olive oil industry. *Adsorption Science Technology*, 19, 117-129.

Al-Qodah, Z. and Shawarbkah, R. (2009). "Production and characterization of granular Activated carbon from activated sludge." *Brazilian Journal of Chemical Engineering, 26 (1), 127 - 136.*

Alturkmani, A. (2004). Industrial wastewater. http://www.4enveng.com/. Retrieved 23/04/2014

Amusan, A.A., Bada, S.B. and Salami, A.T. (2003). Effect of traffic density on heavy

metal content of soil and vegetation along roadsides in Osun State, Nigeria. *West African Journal of Applied Ecology. 4,* 107-114.

American Public Health Association (APHA), (1998). Standards methods for examination of water and waste water. 20th edition, American Public Health Association Inc,Washington D. C.

Amuda, O. S., Giwaa, A. A. and Bello, I. A. (2007). Removal of heavy metal from industrial waste water using modified activated coconut shell carbon. *Biochemical Engineering Journal 36*, 174 – 181.

Amuda, O.S. and Ibrahim, A.O. (2006). Industrial wastewater treatment for chemical oxygen demand (COD) using natural material as adsorbent. *African Journal of Biotechnology, 5*(16), 1483–1487.

Ameh, P.O. (2013*).* Modelling of the Adsorption of Cu (II) and Cd (II) from Aqueous Solution by Iraqi Palm-Date Activated Carbon (IPDAC). *International Journal of Modern Chemistry, 5*(3), 136-144

Ameh, P. O. and Odoh, R., (2013). Iraqi Palm-date as Adsorbent for Removal of Pb(II) and Ni(II) Ions from Aqueous Solution. *International Journal of Modern Chemistry, 4*(1), 11-18.

Amir, S., (2012). Production of activated carbon within the indirect gasification process. Master's Thesis within the Sustainable Energy Systems Programme (MPSES), *Chalmers University of Technology, Gothenburg*, Sweden.

Anirudhan, T. S. and Krishnan, K. A. (2003). Removal of Cd^{2+} from aqueous solution by steam-activated sulphurised carbon prepared from sugar-cane bagase pith: kinetic and equilibrium studies, *Water SA.*, 29(2), 147-156.

Anderson, R.A. (1998). Effects of chromium on body composition and weight loss. *Nutrient Revelation*. 56(9), 266- 270.

Annadurai, Krishnan. (1996). Adsorption of basic dye using chitin. *Industrial Journal of Environmental Protection,* 16(6), 444-449.

Annadurai, A., Juang, R. S. and Lee, D. J. (2003). Adsorption of heavy metals from water using banana and orange peels. *Water Science Technology*, 47, 185-190.

Annadurai, Krishnan. (1996). Batch kinetic studies of adsorption of reactive dye using chitosan. *Industrial Journal of Environmental Protection*, 17(5), 328-333.

AOAC. (1984). Official methods of analysis: Association of Official Analytical

Chemists' 14th edition, Washington D. C.

APHA, (1998). Standard Methods for the Examination of Water and Wastewater. American Public Health Association, Washington, DC, New York, USA,

ASTM, (2007). International Standard Test Method for Determination of Additive Elements in Lubricating Oils by Inductively Coupled Plasma Atomic Emission Spectrometry. *Annual Book of ASTM Standards*, 5(03), ASTM D4951-02.

Auer, E., Freund, A. pietsch, J. and Tacke, T. (1998). Carbons as supports for industrial precious metal catalysts. *Applied Catalysis A: General, 173*(2), 259-271.

Ayyappan, R., Carmalin-Sophia, A., Swaminathan, K. and Sandhya, S. (2005). Removal of Pb (II) from aqueous solution using carbon derived from agricultural wastes. *Process Biochemistry*, 40, 1293-1299.

Ayodele, J.T., Momoh, R.U. and Amm, M. (1996). Determination of heavy metals in Sharada Industrial effluents, in water quality monitoring and environmental status in Nigeria. *Proceedings of the National Seminar on Water Quality Monitoring and Status in Nigeria, organized by Federal Environmental Protection Agency and National Water Resources Institute*. October 16-18. pp. 158-166.

Ayodele, R.I., Dawodu, M. and Akande, Y. (2007). Heavy metal contamination of topsoil and dispersion in the vicinities of reclaimed auto repair workshops in Iwo, Nigeria. *Research Journal of Applied Sciences, 2*(11),1106-1115.

Awoyale, A.A., Eloka-Eboka, A.C. and Odubiyi, O.A. (2013). Production and experimental efficiency of activated carbon from local waste bamboo for waste water treatment. *International Journal of Engineering and Applied Sciences, 3*(2), 8 – 19.

Arami-Niya, A., Daud, W.M.A.W. and Farouq, S.M. (2010). Using granular activated carbon prepared from oil palm shell by ZnCl2 and physical activation for methane adsorption. *Journal of Analytical and Applied Pyrolysis*, *89*,197-203

Azouaou, N., Belmedani, M., Mokaddem, H. and Sadaoui, Z. (2013). Adsorption of Pb from aqueous solution onto untreated Orange Barks. *Chemical engineering Transactions,* 32, 55 – 60.

Aziz, H.A, Adlan, M.N and Ariffin, K.S. (2008). Heavy metals (Cd, Pb, Zn, Ni, Cu and Cr(III)) removal from water in Malaysia: Post treatment by high quality limestone. *Bioresources Technology*. 99, 1578-1583.

Azab, M. S. and Peterson, P. J. (1989). The removal of Cd (II) from water by the use of biological sorbents. *Water Science & Technology.* 21, 1705-1706.

Bansal, M., Singh, D., Garg, V.K. and Pawan R. (2009). Use of agricultural waste for the removal of Nickel ions from aqueous solutions: equilibrium and kinetic studies, *Proceedings of International Conference on energy and Environment*, 19-21.

Bansal, R.C. and Goyal, M. (2005). *Activated Carbon Adsorption*. Boca Raton, FL: CRC Press.

Barałkiewicz, D. and Siepak, J. (1999). Chromium, nickel and cobalt in environmental samples and existing legal norms. *Polish Journal of Environmental Studies, 8(*4), 201-208.

Baumbach, G.U., Vogt, K.R.G., Hein, A.F., Oluwole, O.J., Ogunsola, H.B. and Akeredolu, F.A. (1995). Air pollution in large tropical city with high traffic density: results of measurements in Lagos, Nigeria. *Science of Total Environment, 169,* 25-31.

Bayly, G.R., Braithwaite, R.A., Sheehan, T.M.T., Dyer, N.H., Grimley, C. and Ferner, R.E. (1995). Lead poisoning from Asian traditional remedies in the West Midlands- report of a series of five cases. *Human Experimental Toxicology, 14,* 24-28.

Babel, S. and Kurniawan, T. A. (2004). Cr (VI) removal from synthetic wastewater using coconut shell charcoal and commercial activated carbon modified with oxidizing agents and/or chitosan. *Chemosphere*, 54, 951-967.

Bansode, R. R, Losso, J. N., Marshall, W. E., Rao, R. M. and Portier, R. J. (2003). Adsorption of metal ions by pecan shell-based granular activated carbons. *Bioresources Technology*, 89, 115-119.

Banerjee, K., Ramesh, S. T., Gandhimathi, R., Nidheesh, P. V., and Bharathi, K. S. (2012). A novel agricultural waste adsorbent, watermelon shell for the removal of copper from aqueous solutions. *Iran Journal of Energy & Environment,* 3(2), 143-156.

Bakircioglu, Y., Bakircioglu, D. and Akman, S. (2003). Solid phase extraction of bismuth and chromium by rice husk. *Journal of Trace & Microprobe Technique*, 21, 467-478.

Beguin, F. and Frackowiak, E. (2010). *Carbons for Electrochemical Energy Storage and Conversion Systems*, CRC Press.

Bhaskaran, T. R. (1998). Tannery Wastes, Guidelines for the Control of Industrial Wastes, *WHO/WD*/ 73.14.

Bhatnagar, A. and Sillanpaa, M. (2010). Utilization of agro-industrial and municipal waste materials as potential adsorbents for water treatment—A review. *Chemical Engineering Journal, 157***,** 277-296.

Bhattacharya, A. K., Mandal, S. N. and Das, S. K. (2006). Adsorption of Zn(II) from aqueous solution by using different adsorbents. *Chemical Engineering Journal*, 123, 43-51.

Bishnoi, N. R., Bajaj, M., Sharma, N. and Gupta, A. (2004). Adsorption of Cr (VI) on activated rice husk carbon and activated alumina. *Bioresources Technology*, 91, 305-307.

Bond, R. G. and Straub, C. P. (1974). Handbook of environmental control. Vol. iv waste water: treatment and disposal. CRC Press, Cleveland, Ohio, p. 905.

Boudrahem, F., Aissani-Benissad, F. and Ait-Amar, H. (2009). Batch sorption dynamics and equilibrium for the removal of lead ions from aqueous phase using activated carbon developed from coffee residue activated with zinc chloride. *Journal of Environmental Management, 90*(10), 3031-3039,

Boehm, H.P. (1990). Surface Oxides on Carbon. *High Temp-High Pressures*, *22*, 275-288.

Boleslav, T. and Roman, M. (2011). Immobilization of Heavy Metal Ions on Coals and Carbons, Waste Water - Treatment and Reutilization, Prof. Fernando SebastiÃ¡n GarcÃa Einschlag (Ed.), ISBN: 978- 953-307-249-4, InTech, Available from: http://www.intechopen.com/books/waste-water-treatment-and-reutilization/immobilization-of-heavy-metal-ions-on-coals-and-carbons

Brunauer, S., Emmett, P.H. and Teller, E. (1938). Adsorption of gases in multimolecular layers. *Journal of American Chemical Society, 60*, 309-319.

Burkill, H. M. (1994). Useful plants of west tropical Africa. Vol. 2. Families E-I. Kew: Royal Botanical Gardens.

Cay, S, Uyanik, A. and Ozai, K. A., (2004). Single and binary component adsorption of Cu (II) and Cd (II) from aqueous solutions using tea-industry waste, *Separation and Purification Technoogyl, 38, 273-280.*

Castro, J., Bonelli, P., Cerrella, E. and Cukierman, A. (2000). Phosphoric acid activation of agricultural residues and bagasse from sugar cane: influence of

the experimental conditions on adsorption characteristics of activated carbons. *Industrial Engineering Chemical Resources.* 39, 4166-4170.

Cameron carbon Incorperated, (2006). Activated carbon manufacture, structure and properties. Havre de Grace, USA.Retrieved from www.cameroncarbon.com

Centeno, T.A., Marbán, G. and Fuertes, A.B. (2003). Importance of micropore size distribution on adsorption at low adsorbate concentrations. *Carbon, 41*(4), 843-846.

Chamarthy, S., Chung, W. S. and Marshall, W. E. (2001). Adsorption of selected toxic metals by modified peanut shells. *Journal Chemical Technology and Biotechnology*, 76, 593-597

Chu, K. H. and Hashim, M. A. (2002). Adsorption and desorption characteristics of Zn(II) on ash particles derived from oil palm waste. *Journal of Chemical Technology & Biotechnology*, 77, 685-693.

Chu, K. H. and Hashim, M. A. (2002). Adsorption characteristics of trivalent chromium on palm oil fuel ash. *Clean Technology & Environmental Policy*, 4 8-15.

Clair, N.S, Perry, L.M., and Gene, F.P. (2003). Chemistry for environmental engineering and science (5th ed.), New York McGraw-hill.

Choong, T.S.Y., Wong, T.N., Chuah, T.G. and Idris, A. (2006). Film-pore-concentration-dependent surface diffusion model for the adsorption of dye onto palm kernel shell activated carbon. *Journal of Colloid and Interface Science, 301*, 436-440.

Conrad, K. and Hansen, H. C. B. (2007). Sorption of Zn (II) and lead on coir, *Bioresources Technology*, 98, 89-97.

Cossiches, P. Taveres, C. R. G. and Ravangnani, T. M. K. (2002). Biosorption of chromium (III) by Sargassum sp. biomass. *Elec. Journal of Biotechnology*. 5(2), 133-140.

Cynthia A. Coles and Raymond N. Yong. (2006). Use of equilibrium and initial metal concentrations in determining Freundlich isotherms for soils and sediments. *Engineering Geology*, 85, 19 – 25.

Czysz, W. and Schneider, W. (1989). Waste Water Technology: Origin, Collection, Treatment and Analysis of Waste Water, Springer-Verlag Berlin Heidelberg, New York, pp103-109

Dabrowski, A. (2001). Adsorption-from theory to practice. *Advanced colloid*

interface science, 93, 135- 224

Daifullah, A. A. M., Girgis, B. S. and Gad, H. M. H. (2003). Utilization of agro-residues (rice husk) in small waste water treatment plans. *Materials Letter*, 57, 1723-1731.

Dakiky, M., Khamis, M., Manassra, A. and Mer'eb, M. (2002). Selective adsorption of chromium (VI) in industrial wastewater using low-cost abundantly available adsorbents. *Advanced Environmental Resources*, 6,533-540.

Daud, W. M. A. W., Ali, W. S. W. and Sulaiman, M. Z. (2002). Effect of activation temperature on pore development in activated carbon produced from palm shell, Journal of Chemical Technology & Biotechnology, 78, 1-5.

Daud, W.M. A. W and Ali, W. S.W. (2004). Comparison on pore development of activated carbon produced from palm shell and coconut shell. *Bioresource Technology*, 93, 63-69.

De Rosa, M., Zarrilli, S., Paesano, L., Carbone, U., Boggia, B., Petretta, M., Masto, A., Cimmino, F., Puca, G., Colao, A. and Lombardi, G. (2003). Traffic pollutants affect infertility in men. *Human Reproduction, 18*, 1055-1061.

Devenyi, A.G., Barron, T.F. and Mamourian, A.C. (1994). Dystonia, hyperintense basal ganglia, and whole blood manganese levels in Alagille's syndrome. *Gastroenterology, 106*, 1068-1071.

Demirbas, E., Kobya, M., Senturk, E., and Ozkan, T. (2004). Adsorption kinetics for the removal of chromium (VI) from aqueous solutions on the activated carbons prepared from agricultural wastes. *Water SA*, 30(4), 533-540.

Demirbas, E., Kobya, M., Oncel, S. and Sencan, S. (2002). Removal of Ni (II) from aqueous solution by adsorption onto hazelnut shell activated carbon: equilibrium studies. *Bioresources Technology*, 84, 291-293.

Debnath, S. and Ghosh, U. C. (2008). "Kinetics, isotherm and thermodynamics for Cr (III) and Cr (VI) adsorption from aqueous solutions by crystalline hydrous titanium oxide", *Journal Chemical Thermodynamics*, 40, 67–77.

Demirbas, E. (2003). Adsorption of Cobalt (II) from Aqueous Solution onto Activated Carbon Prepared from Hazelnut Shells. *Adsorption Science and Technology, 21*, 951-963.

Dhakal, R. P., Ghimire, K. N. and Inoue, K. (2005) Adsorptive separation of heavy metals from an aquatic environment using orange waste. H*ydrometallurgy*, 79, 182-190.

Dina, D.J.D., Ntieche A.R., Nti, J.N. and Ketcha M.J. (2012). Adsorption of acetic acid onto activated carbons obtained from maize cobs by chemical activation with zinc chloride. *Resources Journal of Chemical Science, 2*(9), 42-49.

Dogan, M. Alkan, M. and Onganer, Y. (2000). Adsorption of methylene blue from aqueous solution onto perlite. *Water Air & Soil Pollution*, 120, 229-248.

Dubinin, M. M. (1975). Programmed Surface Membrane, *Sciences*, 9, 10.

Dubinin, M.M., and Walker, P.L. (1966). Chemistry and physics of carbon, Vol. 2, Marcel Dekker, New York, pp 151-120.

Dubinin, M. M. (1975). Physical adsorption of gases and vapors in micropores. *Progress in surface and membrane science,* 9,1-70.

Ekhaise, F.O. and Anyasi C.C. (2005), Influence of breweries effluent discharge on the microbiological and physicochemical quality of Ikpoba river, Nigeria. *African Journal of Biotechnology*, 4(10), 1062–1065.

EPA, (1984a). Health assessment document for chromium. Research Triangle Park, NC: Environmental Assessment and Criteria Office, U.S. Environmental Protection Agency. EPA 600/8-83-014F.

EPA, (1987). Toxic air pollutant/source crosswalk: A screening tool for locating possible sources emitting toxic air pollutants. Research Triangle Park, NC: U.S. *Environmental Protection Agency*, Office of Air Quality Planning and Standards. EPA-450/4-87-023a.

Elaigwu, S. E., Usman, L. A., Awolola, G. V., Adebayo, G. B. and Ajayi, R. M. K. (2009). Adsorption of Pb(II) from Aqueous Solution by Activated Carbon Prepared from Cow Dung. *Advances in Natural and Applied Sciences, 3*(3), 442-446.

Elinder, C.G. (1985). Cadmium: uses, occurrence and intake. In: Friberg, L., Elinder, C.G., Kjellstrom, P. et al eds. Cadmium and health: A toxicological and epidermiological appraisal. Vol. 1. Exposure, dose and metabolism. Effects and response. Boca Raton, FL. CRS. Press. Pp. 23-64.

El-Hendawy, A.-N.A., Samra, S.E. and Girgis, B.S. (2001). Adsorption characteristics of activated carbons obtained from corncobs. Colloids and Surfaces A*: Physicochemical and Engineering Aspects, 180*(3), 209-221.

Emission estimation technique manual for lead acid battery manufacturing, National pollutant inventory, (1999).

Emoyan, O.O., Ogban, F.E. and Akarah, E. (2005). Evaluation of heavy metals loading in River Ijana in Ekpa-Warri, Nigeria. *Journal of Applied Sciences and environmental management, 10*(2),121-127.

Energy Ministry, (2008). Business summary 21st to 28th, 2008. Accessed from www.bpeng,org/NR/rdonlyres on 15/1/09.

Eromosele, A.O., Eromosele, C.O., Akintye, A.O. and Komolafe, T.O. (1994). Characteristics of oils and chemical analysis of the seed of wild plants. Plant Food for Human Nutrition, 46: 361 – 365.

Essoka, P.A., Ubogu, A.E. and Uzu, L. (2006). An overview of oil pollution and heavy metal concentration in Warri area, Nigeria. *Management of environmental quality, 10*(2), 209-215.

European Committee for Standardization (ECS), (2006). Fat and oil derivatives -Fatty acid methyl ester (FAME) -Determination of Ca, K, Mg and Na content by optical emission spectral analysis with inductively coupled plasma (ICP-OES). EN 14538.

Enemari, E. (2001). Vehicular emissions: Environmental and health implications. National Conference on the Phase-out Leaded Gasoline in Nigeria.

Ethan, J. N., Richard, W. M. and Michael, G. K. (2003). The effect of an industrial effluent on an urban stream benthic community: water quality vs. habitat quality. *Environmental Pollution*.123(1), 1-13.

Fakayode, S. O. and Olu-Owolabi, B. I. (2003b). Trace metal content and estimated daily human intake from chicken eggs in Ibadan, Nigeria. Archives of Environmental Health. http:www.encyclopedia.com/beta/doc/IGI-111732614.

Fakayode, S. O. and Olu-Owolabi, B. I. (2003a). Heavy metal contamination of roadside topsoil in Osogbo, Nigeria: its relationship to traffic density and proximity to highways. *Environmental Geology, 44(*2), 150-157.

Faust, S.D. and Osman, M.A. (1987). "Adsorption process for water treatment." London: Butterworths. p.15.

Federal Environmental Protection Agency (FEPA) Act, (1991). Guidelines and standards for Industrial effluent, gaseous emissions and hazardous waste management in Nigeria.

FEPA, (1991). Guidelines and standards for environmental pollution control in Nigeria. Federal environmental protection agency, Lagos.

Final Report to the President and the Congress of the United States. (1973). National Water Commission, Water Policies for the Future, pp 64-70.

Fiol, N., Villaescusa, I., Martínez, M., Miralles, N., Poch, J. and Serarols, J. (2006). Sorption of Pb (II), Ni (II), Cu (II) and Cd (II) from aqueous solution by olive stone waste. *Separation and Purification Technology, 5*0, 132-140.

Flegal, A.R. and Smith, D.R. (1995). Measurements of environmental lead contamination and human exposure. *Revelation Environmental Contaminants and Toxicology, 143,*1-45.

Fonseca, M. G., Oliveira, M. M. and Arakaki, L. N. H. (2006). Removal of cadmium, zinc, manganese and chromium cations from aqueous solution by clay mineral. *Journal Hazardous Materials* B137, 288-292.

Forbes, G.M. and Forbes, A. (1997). Micronutrient status in patients receiving home parenteral nutrition. *Nutrition, 13,* 941-944.

Fiyyaz A, Zill-i-humanazli, and Waseemahmad, S. (2000). Conversion of some agro-industrial wastes into useful industrial products. *Pak Journal of Agricultural Science Tbi; 37*, 3-4.

Food and Agricultural Organisation (FAO). (2007). Coping with water scarcity, 2007 World Water Day, 22nd March, Available on 127 017 2010 from: http://www.fao.org/nr/water7docs/wwd07brochure.pdf. Retrieved 23/04/2014

Freundlich, H. (1926). Colloid and Capillary Chemistry. Methuen, London, P.120.

Fu, F. and Wang, Q. (2011). Removal of heavy metal ions from wastewaters: a review. *Journalof Environmental Management, 92,* 407-18.

Gaikwad, R. W. (2004). Removal of Cd (II) from aqueous solution by activated charcoal derived from Coconut shell, Electron. *Journal of Environmental Agriculture and Food Chemistry*, 3, 702-709.

Galadima, A., Garba, Z.N., Leke, L., Almustapha, M. N. and Adam, I. K. (2011). Domestic water pollution among local communities in Nigeria – causes and consequences. *European journal of scientific Research, 52*(4), 592 – 603.

Gerbeding, J.L. (2005a). Toxicological profile for lead. Public health service, Agency for toxic substances and diseases. Atlanta Georgia. pp 3-5, 31, 113-130, 224-228 and 312-350.

Gerbeding, J.L. (2005b). Toxicological profile for nickel. Public health service.

Agency for toxic substances and diseases. Atlanta Georgia. pp. 27, 79, 134-144, 166-167.

Giraldo-Gutierrez, L. and Moreno-Pirajan, J.C. (2008). Pb(II) and Cr(VI) adsorption from aqueous solution on activated carbons obtained from sugar cane husk and sawdust. *Journal of Analytical and Applied Pyrolysis, 81*(2), 278-284,

Grigis. B. S. and Ishak, M. F. (1999). Activated carbon from cotton stalks by Impregnated with phosphoric acid. *Material Letters*, (39),107-114.

Grigis, B.S., Yunis, S.S. and Soliman, A.M. (2002). Characteristics of activated carbon from peanut hulls in relation to conditions of preparation. *Materials Letters, 57*(1),164-172.

Goodfriend, G.A. (1986). Variation in land-snail shell form and size and its causes – a review. Systematic Zoology, 35: 204 – 223.

Government of the People's Republic of Bangladesh, (2000). The Environment Conservation Rules 1997, Unofficial translation Ministry of Environment and Forests, Dhaka.

Guo, J. and Lua, A. C. (2000). Preparation and characterization of adsorbents from oil palm fruit solid wastes. *Journalof Oil Palm Resources*, 12, 64-70.

Guo, J. and Lua, A. C. (2000). Adsorption of sulphur dioxide onto activated carbons prepared from oil palm shells impregnated with potassium hydroxide. *Journal of Chemical Technology and Biotechnology*, 75 971-976.

Guo, J. and Lua, A.C. (2002). Characterization of adsorbent prepared from oil-palm shell by CO2 activation for removal of gaseous pollutants. *Material Letters, 55,* 334-339.

Guo, J. and Lua, A.C. (2003). Adsorption of sulphur dioxide onto activated carbon prepared from oil-palm shells with and without pre-impregnation. *Separation and Purification Technology, 30,* 265-273.

Guo, J., Xu, W.S., Chen, Y.L. and Lua, A.C. (2005). Adsorption of NH_3 onto activated carbon prepared from palm shells impregnated with H_2SO_4. *Journal of Colloid and Interface Science, 281,* 285-290.

Guo, J., Luo, Y., Chi, R.A., Chen, Y.L., Bao, X.T., and Xiang, S.X. (2007). Adsorption of hydrogen sulphide (H_2S) by activated carbons derived from oil-palm shell. *Carbon, 45,* 330-336.

Guo, J. and Lua, A. C. (2003). Textural and chemical properties of adsorbent

prepared from palm shell by phosphoric acid activation. *Material Chemistry and Physics*, 80, 114-119.

Guo, G. (2002). The effect of local hydrodynamics on mass transfer in disordered porous media, Ph.D Dissertation, Louisiana State University, USA.

Gunay, A., Arslankaya, E. and Tosun, I. (2007). Lead removal from aqueous solution by natural and pretreated clinoptilolite: adsorption equilibrium and kinetics. J*ournal of hazardous materials*, 146, 362-371

Gupta, V. K. and Sharma, S. (2003). Removal of Zinc from aqueous solutions using bagasse fly ash - a low cost adsorbent. *Industrial Engineering Chemical Resources*, 42, 6619.

Gupta, V. K., Mohan, D. Sharma, S. and Park, K. T. (1999). Removal of Cr(iv) from electroplating industry waste water using baggasse fly ash a sugar industry waste materials. *Environmental, 19, 129*.

Gupta, G. S., Prasad, G. and Singh, V.N. (1988b). Removal of chrome dye from aqueous solutions on Fly ash. *Water, Air, Soil Pollution*, 37, 13-24.

Gunkel, G. J., Kosmol, M., Sobral, H., Rohn, S. and Montenegro, J. (2007). Aureliano Sugar cane industry as a source of water pollution – case study on the situation in Ipojuca river, Pernambuco. *Brazil Water, Air, Soil Pollution*, 180(1–4), 261–269.

Hamza, S.A and Galadima, A. (2010). Arsenic level speciation in fresh water from Karaye Local Government Area, Kano State, Nigeria. *International Journal of Chemistry, India, 20*(2),113-117.

Hamidi Abdul Aziz Mohd Suffian Yussof, Mohd Nordin Adlan, Nurul Hidayah Adnan and Salina Alias. (2003). *Physico-chemical removal of iron from semi-aerobic landfill leachate by limestone filter*. pp 53-64.

Hackskaylo, J.J. and Levan, M.D. (1985).Correlation of adsorption equilibrium data using a modified Antonie equation: a new approach for pore-filling models. *Langmuir*, 1, *97-100.*

Hamad, B.K., Noor, A.M., Afida, A.R. and Mohd Asri, M.N. (2010). High removal of 4-chloroguaiacol by high surface area of oil palm shell-activated carbon activated with NaOH from aqueous solution. *Desalination, 257*, 1-7.

Hazdat, (2005). Hazdat data base. ASTDR's. Hazardous substance release and health effect data base. Atlanta. Agency for toxic substance and disease registry. www.astsdr.cdc.gov/hazdat-html. Retrieved April 13, 2005.

Hasar, H. (2003) Adsorption of nickel (II) from aqueous solution onto activated carbon prepared from almond husk. *Journal of Hazardous Materials*, B97 49-57.

Hall, K. R. Eagleton, L.C. Acrivos, A. and Vermeulen, T. (1966). Poor and solid diffusion kinetic in fixed bed adsorption under constant parttern conditions. *Industrial and engineering chemistry fundamentals, 5 (2), 212-223.*

Hammed, B.H., Din, A.M. and Almed, A.L. (2006). Adsorption of Methylene Blue onto Bamboo based Activated Carbon: kinetic and equilibrium studies. *Hazard material, 137(3), 695-699.*

Hafchinson, J., and J. M. Dalziel. (1954). Floral of West Africa. 2nd ed. Vol. 1, Part1. London: Crown Agents for Overseas Administrations

Harry Marsh, F.R.-R. (2006). Activated carbon. Vol. 1. Amesterdam Boston, London, new york, Elsevier. P.536.

Hanafiah, M.A.K.; Ibrahim, S. C. and Yahaya, M.Z.A. (2006). Equilibrium adsorption study of lead ions onto sodium hydroxide modified lalang (Imperata cylindrical) leaf powder. *Journal of Applied Science Resources, 2,* 1169-1174.

Hasar, H., Cuci, Y., Obek, E. and Fatih-Dilekoglu, M., (2003). Removal of Zn (II) by activated carbon prepared from almond husks under different conditions. *Adsorption Science and Technology, 21,* 799-808.

Halim, S. H. A., Shehata, A. M. A. and El-Shahat, M. F. (2003). Removal of lead ions from industrial waste water by different types of natural materials.*Water Resources*, 37, 1678–1683.

Hema Krishna, R., and Swamy, A. V. V. S. (2011). Studies on the removal of Ni (II) from aqueous solutions using powder of mosambi fruit peelings as a low cost sorbent. *Chemcical Sciences Journal*, 31, 1-13.

Horsfall, M Jr, Abia, A. A. and Spiff, A. I. (2003). Removal of Cu (II) and Zn (II) ions from wastewater by cassava waste biomass (Manihot esculenta Cranz), *African Journal of Biotechnology*, 2, 360-364.

Horsfall, J., M. and Spiff, A. L. (2005). "Equilibrium sorption study of Al, Co and Ag in aqueous solutions by fluted pumpkin (Telfairia occidentalis Hook f.) waste biomass." *Acta. Chim. Slov*., 52, 174 – 181.

Ho, Y.S. and McKay, (1998). Sorption of dyes from aqueous solution by peat.

Chemical Engineering Journal, 70, 115.

Ho, Y.S., McKay, G., Wase, D.A.J and Forster, C.F. (2000). "Study of the sorption of divalent metal ions onto peat." *Adsorption Science and Technology*, 18, 639 - 650.

Ho, Y.S. and McKay, G. (2000). "The kinetics of sorption of divalent metal ions onto sphagnum moss peat." *Water Resources*, 34, 735– 742.

Hossain, M.A., Ngo, H.H., Guo, W.S. and Nguyen, T.V. (2011). Palm oil fruit shells as biosorbent for copper removal from water and wastewater: experiments and sorption models. *Bioresource Technology, 24*(11), 2-6.

Horsfall, M. Jr, Abia, A. A. and Spiff, A. I. (2006). Kinetic studies on the adsorption of Cd^{2+}, Cu^{2+} and Zn^{2+} ions from aqueous solutions by cassava (Manihot esculenta Cranz) tuber bark waste. *Bioresources Technology, 97*, 283-291.

Hussein, M. Z., Tarmizi, R. S. H., Zainal, Z., Ibrahim, R. and Badri, R. M. (1996). Preparation and characterization of active carbons from oil palm shells. *Carbon*, 34, 1447-1453.

Huang, G.F, Wu, Q.T, Wong, J.W.C, and Nagar, B.B. (2005). Transformation of organic matter during co-composting of pig manure with sawdust, *Bioresource Technology 35*, 132-137.

Hughes, W.W. (1996). Essentials of environmental toxicology. The effects of environmental hazardous substances on human health. Loma, Lind Califonia. Tay and Francais Publishers. 3, 87-95.

Hutson, N. N. D. and Yang, R. T. (2000). Adsorption. *Advanced colloid ingerface science*, 189.

Hubson, J. P. (1969). Physical adsorption isotherms extending from ultra high vacuum to vapour pressure. *Journal of physical chemistry, 73*, 2720 – 2727.

Ibrahim, S.C, Hanafiah M.A.K.M and Yahya, M.Z.A. (2006). "Removal of cadmium from aqueous solutions by adsorption onto sugarcane bagasse." American-Eurassian. *Journal of Agriculture and Environmental Science* 1(3), 179 – 184.

IARC, (1990). IARC (International Agency for Research on Cancer) monographs on the evaluation of carcinogenic risks to humans. Chromium, nickel and welding. Lyon, France: *International Agency for Research on Cancer. World Health Organization. 49*, 257-445.

Ibeto, C. N. and Okoye C. O. B. (2009). Elevated Cadmium Levels in Blood of the Urban Population in Enugu State Nigeria. *World Applied Sciences Journal 7*(10), 1255- 1262, 2009.

Ibeto, C.N. and Okoye, C.O.B. (2010a). High levels of heavy metals in blood of the urban population in Nigeria. *Research Journal of Environmental Sciences. 4* (4): 371-382.

Ibeto, C. N. and Okoye C. O. B. (2010b). Elevated Levels of Lead in Blood of Different Groups in the Urban Population of Enugu State, Nigeria. International Journal of Human and Ecological Risk Assessment. Human and Ecological Risk Assessment: *An International Journal, 16*(5), 1133 — 1144.

Ifenna, I. and Chinedu, O. (2012). Heavy Metal Levels and Physico-Chemical Parameters of Potable Water in Nnewi, Anambra State, Nigeria. *Archives of Applied Science Research*, 4(5), 2094-2097.

Igwe, J.C. and Abia, A.A. (2007). Adsorption kinetics and intraparticulate diffusivities for bioremediation of Co (II), Fe (II) and Cu (II) ions from waste water using modified and unmodified maize cob. *International Journal of Physical Sciences* 2 (5), 119 – 127.

Idris, M. A., Kolo, B. G., Garba, S. T. and Waziri, I. (2013). Pharmaceutical Industrial Effluent: Heavy Metal Contamination of Surface waterin Minna, Niger State, Nigeria. *Bulletin of Environment, Pharmacology and Life Science*, 2(3), 40-44.

Imamoglu, M. and Tekir, O. (2008). Removal of copper (II) and lead (II) ions from aqueous solutions by adsorption on activated carbon from a new precursor hazelnut husks. *Desalination, 228*(1-3), 108-113,

Ikem, A., Osibanjo, O., Sridhar, M. K. C. and Sobande, A. (2002). Evaluation of groundwater quality characteristics near two waste sites in Ibadan and Lagos, Nigeria. *Water, air and soil pollution, 140*(1-4), 307-*333*.

Issabayeva, G., Aroua, M.K. and Sulaiman, N.M.N., (2006). Removal of lead from aqueous solutions on palm shell activated carbon. *Bioresource Technology*, *97*, 2350-2355.

Issabayeva, G., Aroua, M. K. and Sulaiman, N. M. N. (2006). Removal of lead from aqueous solution on palm shell activated carbon. *Bioresources Technology*, 97, 2350-2355.

Issabayeva, G., Aroua, M.K. and Sulaiman, N.M. (2008). Continuous adsorption of lead ions in a column packed with palm shell activated carbon. *Journal of*

Hazardous Materials, 155, 109-113.

Israel, O.K and Ekwumemgbo, P.A. (2008). "Kinetics of the Removal of Ovalbumin from White Wine Model Solution." Book of Proceedings. S.H.O Egboh et al (eds.), *Chemical Society of Nigeria*. 22nd – 26th Sept., 2008. p. 413 – 418.

Jain, K.K., Guru, P. and Singh, V. (1979). Heavy metals removal from industrial wastewater. *Journal of Chemical Technology and Biotechnology*, 29, 36 – 38

Jasim, M. d. Uddin, Pritom Kumar Mondal, Hasibur Rahman Lemon, M.d. and Atiqur Rahman, M.d., (2013). An Approach to Reduce waste in Lead Acid Battery Industry. *Global Journal of Research in Engineering Industrial Engineering*, (2), *13*

Jankowska, H., Swiatkowski, A. and Choma, J. (1991). *Active Carbon*: Ellis Horwood Limited.

Jeon, C., and Park, K. H. (2005). Adsorption and desorption characteristics of mercury(II) ions using aminated chitosan bead. *Water Resources*, 36, 3938–3944.

Johns, M. M., Marshall, W. E. and Toles, C. A. (1998). Agricultural by products as granular activated carbons for adsorbing dissolved metals and organics. *Journal of Chemical Technology*, 71, 131-140.

Jimena, M. G., Roxana, O., Catiana, Z., Margarita, H., Susana, M. and Ines-Isla. (2008). Industrial effluents and surface waters genotoxicity and mutagenicity evaluation of a river of Tucuman, Argentina. *Journal of hazardous Material*. 155(3), 403-406.

John, H., Cheryl, H., Richerd, S. and Christine, S. (1991). Toxics A-Z- A guide to everyday pollution hazards. University of Califonia, Press. Berkley. Angeles. Oxford. pp. 47-104.

Jonathan, T. (2008). Leaded fuels update. Press information - Thursday 15th May 2008. Accessed from www.bayfordgroup.co.uk and www.leadedpetrol.co.uk. on the 24th of January 2014.

Julie, Stauffer, (1998). The Water Crisis: Constructing Solution to Freshwater Pollution, Earthscan Publications Limited, London UK.

Jumasiah, A., Chuah, T.G., Gimbon, J., Choong, T.S.Y. and Azni, I. (2005). Adsorption of basic dye onto palm kernel shell activated carbon: sorption equilibrium and kinetic studies. *Desalination*, 186, 57-64.

Kadirvelu, K., Kavipriya, M., Karthika, C., Radhika, M., Vennilamani N. and Pattabhi, S. (2003). Utilization of various agricultural wastes for activated carbon preparation and application for the removal of dyes and metal ions from aqueous solutions. *Bioresources Technology*, 87(1), 129-132.

Karthika, C. and Sekar, M. (2013). Comparison studies of Adsorption Properties on Ni(II) Removal by strong and weak acid cation-exchange Resins. *Resources Journal of Chemical science*, 3(3), 65-69.

Kapoor, A. and Yang, R. T. (1989). Correlation of equilibrium, adsorption data of condensible vapours on porous adsorbents. *Gas separation and purification*, 3(4), 187-192.

Keay, R. W. J. (1989). Trees of Nigeria. 2nd ed. Oxford: C. Krendon Press. pp 335-336.

Khan, A. R., Tahir, H. Uddin, F. and Uzma, H. (2005). Adsorption of methylene blue from aqueous solution on the surface of wool fiber and cotton fiber. *Journal of Applied Science and environmental Management*, 9(2), 29-35.

Kim, J.W., Myoung, H.S., Dong, S.K., Seung, M.S. and Young, S.K. (2001). Production of Granular Activated Carbon from Waste Walnut Shell and its Adsorption Characteristic for Cu^{2+} ion. *Journal of Hazard Material, B85*, 301-315.

Kiurski, J., Adamoric, S., Oros, I., Krstic, J. and Kovacevic, I. (2012). Adsorption Feasibility in the Cr(total) ions removal from waste printing developer. *Global NEST Journal*, 14(1), 18-23.

Kiurski, J., Adamoric, S., Oros, I., Krstic, J. and Vojinovic, M. (2011). Adsorption efficiency of low-cost materials in the removal of Zn(II) ions from printing developer. *ACTA Techinica Corviniensis-Bulettin of Engineering, 4, 61-66.*

Kobya, M. (2004) Removal of Cr (VI) from aqueous solutions by adsorption onto hazelnut shell activated carbon: kinetic and equilibrium studies. *Bioresources Technology*, 91, 317-321.

Kobya, M., Demirbas, E., Oncel, M. S. & Encan, S. S. (2002). Adsorption kinetic models applied to nickel ions on hazelnut shell activated carbons. *Adsorption Science and Technology*, 20, 179-188.

Kobya, M., Demirbas, E. and Senturk, M. (2005). Adsorption of Heavy Metal ions from aqueous solutions by activated carbon prepared from apricot stone. *Bioresource Technology, 96,* 1518-1521

Konduru, R. R. and Viraraghavan, T. (1996). Dye Removal Using Peat. *American Dyestuff Reporter*, 28-34

Kontturi, V., Hyvärinen, S., García, A., Carmona, R., Yu Murzin, D., Mikkola, J.P. and Peiponen, K.E. (2011). Simultaneous detection of the absorption spectrum and refractive index ratio with a spectrophotometer: monitoring contaminants in bioethanol. *Measurement Science and Technology. 22*(5), 055 - 803

Koplan, J.H. (2000a). Toxicological profile for manganese. Public health service. Agency for toxic substances and disease registry. Atlanta Georgia. pp. 21-50, 175-207 and 295-400.

Koplan, J.H. (2000b). Toxicological profile for chromium. Public health service. Agency for toxic substances and disease registry. Atlanta Georgia. pp. 1-9, 16-50, 122-157 and 301-315.

Koplan, J.P. (1999). Toxicological profile for cadmium. Public health service. Agency for Toxic Substance and Disease Registry (ATSDR). Atlanta Georgia. pp. 126-140, 207 and 260- 270.

Kumar, U. and Bandyopadhyay, M. (2006). Sorption of Cd (II) from aqueous solution using pretreated rice husk, *Bioresources Technology*, 97, 104-109.

Kurniawan, T. A. (2002). A research study on Cr (VI) removal from electroplating wastewater using chemically modified low-cost adsorbents and commercial activated carbon, Master thesis, Sirindhorn International Institute of Technology (SIIT), Thammasat University, Bangkok,

Kwok, N.Y., Dung, S. Lo, W. and Wong, K.Y. (2005). An optical biosensor for multisample determination of BOD . *sensor actuators B: chemistry*, 110 (2), 289 – 298.

Langmuir, I. (1918). The adsorption of gases on plane surfaces of glass, mica and platinum. *Journal of American chemical society*, 40, 1362-1403.

Lao, C.X., Zeledon, Z., Gamisans, X. and Solé, M. (2005). Sorption of Cd(II) and Pb(II) from aqueous solutions by a low-rank coal (leonardite). *Separation and Purification Technology, 45*(2), 79-85,

Lennard-Jones, J. E. (1932). Processes of adsorption and diffusion on solid surfaces, *Trans. Faraday Society*, 28, 333-359.

Lee, C.C. and Lin. S.D. (1999). Handbook of Environmental Engineering Calculations. McGraw Hill, New York,.

Lenntech, (2006). "Water treatment and air purification" In: http://www.Lenntech.com/heavy-metals.htm.

Lim, Y.N., Shaaban, M.G. and Yin, C.Y. (2009). Treatment of landfill leachate using palm shell-activated carbon column: Axial dispersion modeling and treatment profile. *Chemical Engineering Journal*, *146,* 86-89.

Linskens, H. F. and Jackson J. F. (1999). Modern Methods of Plant Analysis Vol. 20 Analysis of Plant Waste Materials, Springer- Verlag, Berlin Heidelberg, pp 41-42.

Lim,W.C., Srinivasakannan, C., and Balasubramanian, N. (2010). Activation of palm shells by phosphoric acid impregnation for high yielding activated carbon. *Journal of Analytical and Applied Pyrolysis*, *88,* 181-186.

Li, Q.Z., Chai, L.Y., Yang, Z.H. and Wang, Q. (2009). Kinetics and thermodynamics of Pb(II) adsorption onto modified spent grain from aqueous solutions. *Applied Surface Science*, *255(*7), 4298-4303,

Low, L. (2011). Converting Palm Waste to Wealth, *Rediscover Renewable Energy in the Palm Oil Industry To Create A Green Economy*. BELL Group of Companies, unpublished

Low, K.S., Lee, C.K. and Liew, S.C. (2000). Sorption of cadmium and lead from aqueous solution by spent grain. *Process Biochemistry*, 36, 59-64.

Lockitch, G., (1993). Prospective on lead toxicity. *Clinical Biochemistry*, *26*,371-81.

Lua, A.C., Lau, F.Y. and Guo, J. (2006). Influence of pyrolysis conditions on pore development of oil-palm-shell activated carbons. *Journal of Analytical and Applied Pyrolisis*, *76,* 96-102.

Lua, A. C. and Guo. J. (1998). Preparation and characterization of chars from oil palm Waste. *Carbon*, 36, 1663-1670.

Lytle, C.M., Smith, B.N. and Mckinwu, C.Z. (1995). Manganese accumulation along the Utah roadways. A possible indication of motor exhaust pollution. *Science of the Total Environment*, *162,* 1056-109.

Malkoc, E., Nuhoglu, Y. and Dundar, M. (2006). Adsorption of chromium (VI) on pomace-An olive oil industry waste: Batch and column studies. *Journal of Hazardous Materials*, 138, 142-151.

Malkoc, E. and Nuhoglu, Y. (2005). Investigations of nickel (II) removal from aqueous solutions using tea factory waste. *Journal of Hazardous Materials*, 127, 120-128.

Marin, J. and Ayele, J. (2003). Removal of some heavy metal cations from aqueous solutions by spruce sawdust II: Adsorption-desorption through column experiments. *Environmental Technology*, 24, 491-502.

Marsh, H. and Reinoso, F.R. (2006). Activated Carbon. Materials & Mechanical: Elsevier Science Ltd. 1-554.

Marsh, H. and Rodríguez-Reinoso, F. (2006). Characterization of Activated Carbon, in Activated Carbon, Elsevier Science Ltd: Oxford. pp. 143-242.

Marsh, H. and Rodríguez-Reinoso, F. (2006). Applicability of Activated Carbon, in Activated Carbon, Elsevier Science Ltd: Oxford. pp. 383-453.

Manocha, S. (2002). Activated carbons from waste biomass. Project Report, UGC Project

Manocha, S., Chauha, *V.B.* and Manoch*a, L.M. (*2002). Studies on development of porosity in carbons from different types of biowastes. *Carbon Science, 3(1),1-5*.

Manocha, S. (2003). Porous carbons, *Sadhana. 28*, Parts 1 & 2, 335–348. February/April

Marquardt, D. W. (1963). An algorithm for least-squares estimation of non-linear parameters. *Journal of society for industrial applications of mathematics*, 11(2), 431-441.

Machida, M., Yamazaki, R., Aikawa, and Tatsumoto, H. (2005). Role of minerals in carbonaceous adsorbents for removal of Pb(II) ions from aqueous solution. *Separation and Purification Technology, 46(*1-2), 88-94.

Maduabuchi, J.M.U., Nzegwu, C.N., Adigba, E.O., Aloke, R.U., Ezomike, C.N. Okocha, C.E., Obi, E. and Orisakwe, O.E. (2006): Lead and cadmium exposures from canned and non-canned beverages in Nigeria: A public health concern. *Science of the Total Environment. 366*(2-3), 621-626.

Matte, T.D., Proops, D., Palazeulos, E., Graef, J. and Avila, H.A. (1994). Acute high dose lead exposure from beverage contaminated from traditional Mexican pottery. *Lancet, 344*, 1064-1065.

Meng, X., Christodoulatos, C. and Boddu, V. M. (2008). Biosorption mechanism of nine different heavy metals Krishnani, K. K., onto biomatrix from rice husk. *Journal of Hazardous Materials*, 153, 1222-1234.

Meybeck, M., Chapman, V.D. and Helmer, R. (1990). Global Freshwater Quality (A First Assessment), Published on behalf of the WHO and UNEP, Blackwell Ltd., USA.

McEnaney, B. and Mays, T.J. (1989). Introduction to Carbon Science, Butterworths, London.

Mishra, D.K., Mudgal, M., Padmakaran, M. and chakradhar, P. (2009). Performance Evaluation of an Effluent treatment plant for a pulp and paper mill, *Indian Journal of Chemical Technology, 16*, 79-83

Mohan, D. and Singh, K. P. (2002). Single- and multi-component adsorption of Cd(II) and Zn(II) using activated carbon derived from Bagasse—an agricultural waste, *Water Resources*, 36, 2304- 2318.

Moriyama, T., Taguchi, Y., Watanabe, H. and Joh, T. (2002). Changes in the cadmium content of wheat during the milling process (in Japanese). In: Report on Risk Evaluation of Cadmium in Food, Research on Environmental Health, Health Sciences Research Program, Ministry of Health, Labour and Welfare, pp. 153–160.

Mohan, D. and Singh, K.P. (2002). Single- and multi-component adsorption of cadmium and zinc using activated carbon derived from bagasse – an agricultural waste. *Water Research*, *36*, 2304-2318.

Mohan, D. and Pittman, C.U.J. (2006). Activated carbons and low cost adsorbents for remediation of tri- and hexavalent chromium from water. *Journal of Hazardous Materials*, *B137*, 762-811.

Mogana, R. and Wiart, C. (2011). Canarium L.: A Phytochemical and Pharmacological Review. *Journal of Pharmacy research, 4(8), 2482-2489.*

Montgomery, H.A.C., Thom, N.S. and Cockburn, A. (1964). Determination of dissolved oxygen by the winkler method and the solubility of oxygen in pure water and sea water. *Journal of applied chemistry*, 14: 280 – 296

Muta'a Hellandendu, J. (2012)." Health Implications of Water Scarcity in Nigeria," *European Scientific Journal*, 8(18), 111-117.

National Summary of Water Quality Conditions, Inventory Report to Congress, 1994. URL: http://www.epa.gov/305b/execsum.html

National Environmental Protection Regulations, Federal Republic of Nigeria. (1988). Supplement to Official Gazette Extraordinary - Part B. 78 (42): B15 – 31. Federal Environmental Protection Agency (FEPA) Guidelines and

Standards for environmental pollution control in Nigeria. Decree 58 p. 238.

Nale, B. Y., Kagbu, J.A., Uzairu, A., Nwankwere, E.T., Saidu, S. and Musa, H. (2012). Kinetic and Equilibrium studies of the adsorption of Lead (II) and Nickel(II) ions from aqueous solutions on activated carbon prepared from Maize Cob. *Pelagia Research Library*, 3(2), 302-312.

Nair, C.I., Jayachandran, K. and Shashidhar, S. (2008). Biodegradation of phenol. *African Journal of Biotechnology, 7,* 4951-4958.

Namasivayam, C., Sangeetha, D. and Gunasekaran, R. (2007). Removal of Anions, Heavy Metals, Organics and Dyes from Water by Adsorption onto a New Activated Carbon from Jatropha Husk, an Agro-Industrial Solid Waste. *Process Safety and Environmental Protection*, *85,* 181-184.

Namasivayam, C. and Periasamy, K. (1993). Bicarbonate treated peanut hull carbon for mercury (II) removal from aqueous solution. *Water Resources*, 27, 1663-1668.

Namasivayam, C. and Kadirvelu, K. (1994). Coir pith an agricultural by product for the treatment of dyeing wastewater. *Bioresources Technology*, 48, 79-81.

Namasivayam, C. and Sangeetha, D. (2006). Recycling of agricultural solid waste, coir pith: Removal of anions, heavy metals, organics and dyes from water by adsorption onto ZnCl2 activated coir pith carbon. *Journal of Hazardous Materials*, 135, 449- 452.

Nduka, J.K.C., Orisakwe, O.E., Ezenweke, L.O., Abiakam, C.A., Nwanguma, C.K. and Maduabuchi, U.J.M. (2006). Metal contamination and infiltration into the soil at refuse dump sites in Awka, Nigeria. *Archives of Environmental and Occupational Health, 61*(5), 197 – 204.

Nganje, T. N. Edet, A. E. and Ekwere, S. J. (2007). Concentrations of heavy metals and hydrocarbons in groundwater near petrol stations and mechanic workshops in Calabar metropolis, southeastern Nigeria. *Environmental Geosciences, 14* (1), 15-29.

Nriagu, J.O. (1996). History of global metal pollution. *Sciences,* 272, 223-224.

Nriagu, J. O., Blankson, M. L. and Ocran, K. (1996). Childhood lead poisoning in Africa: a growing public health problem. *Journal of Science of the Total Environment, 181(2,15):93-100.*

Nriagu, J.O. and Pacyna, J.M. (1988). Quantitative assessment of worldwide contamination of air, water and soils by trace metals. *Nature, 333,*134-139.

Nriagu, J., Oleru, N.T., Cudjo, C. and Chino, A. (1997). The Science of the Total Environment, *197*, 13-19.

Nomanbhay, M.S and Palanisamy, K. (2005). Removal of heavy metal from industrial waste using chitosan coated oil palm shell charcoal, *Electronic Journal of Biotechnology, 8,* 43–53.

Nur Azreen, B. F., Saadi, A. I., and Kamriah, N. I. (2012). Review Study for Activated Carbon from Palm kernel shell used for Waste water. *Journal of Purity, Utility Reaction and Environment, 1*(5), 252 – 266.

Normah, M., Teo, K. C. and Watkinson, A. P. (1995). Preparation and characterization of activated carbon derived from oil palm shells using a fixed bed pyrolyser, in Bioproducts Processing: Technologies for the Tropics, edited by M A Hashim (Institute of Chemical Engineers, Rugby, United Kingdom), 93.

Niewolak, S. (2000). Bacteriological monitoring of river water quality in the North area of Wigry National Park. *Pollution Journal of Environmental Study*, 9(4), 291–299.

Nicolaou, M. and Hadjivassilis, I. (1992). Treatment of wastewater from the textile industry. *Water Science and Technology*, 25(1), 31-35.

Nwabanne, J. T. and Igbokwe, P. K. (2012). Modelling of heavy metals adsorption on fixed bed column. *International Journal of Environmental Resources, 6*(4), 945 - 952

Olaoye, O.A. and Onulide, A.A. (2009). Assessment of microbial quality of sachet-packaged drinking water in western Nigeria and its public health significance. *Public Health, 123,* 729-734.

Oladoja, N. A., Aboluwoye, C. O. and Oladimeji, Y. B. (2008). Kinetics and Isotherm studies on methylene blue adsorption onto ground palm kernel coat, *Turkish Journal of engineering & environmental science, 32, 303-312.*

Onianwa, P. C.; Jaiyeola, O. M. and Egekenze, R. N. (2001). Heavy metals contamination of topsoils in the vicinities of auto-repair workshops, gas stations and motor parks in a Nigeria city. *Toxicological and Environmental Chemistry, 84*(1-4), 33 -39.

Onnes, H. K. (1901). Expression of the equation of state of gases by means of series, Proc. Sect. Sci. Konink. Akad. Weten. Amsterdam, 4, 125-147.

Ohwo, O. (2011). Spatial Analysis of the Quality of Borehole Water Supply in

Warri-Effurun Metropolis, Delta State, Nigeria," Ikogho: *A Multi-disciplinary Journal*, 9(2 &3), 91-103.

Ohwo, O. (2012.) Quality of Water Supply from Hand-Dug Wells in Warri-Effurun Metropolis, Delta State, Nigeria. *Nigerian Geographical Journal*, 8(2), 73-86.

Okigbo, B. (1984). Improved permanent production systems as an alternative to shifting intermittent cultivation. In; Improved production systems as an alternative to shifting cultivation, FAO Soils Bulletin No. 53, Rome.

Ofoefule, A.U., Uzodinma, E.O. and Anyanwu C.N. (2010). Studies on the effect of Anaerobic digestion on the microbial flora of animal wastes 2: Digestion and modelling of process parameters. *Trends in Applied Science Resources, 5*(1), 39-47.

Okeola, F. O. and Odebunmi, E. O. (2010). Freundlich and Langmuir Isotherm Parameters for Adsorption of Methylene Blue by Activated Carbon Derived from Agrowastes. *Advances in Natural and Applied Sciences*, 4(3), 281-288.

Onundi Y.B., Mamun, A. A., Al Khatib, M. F., and Ahmed, Y.M. (2010). Adsorption of copper, nickel and lead ions from synthetic semiconductor industrial wastewater by palm shell activated carbon. *International journal of Environmental Science and Technology*, 7, 751-758.

Okiemmen, F., Okiemen, C. and Wuana, (2007. Preparation and characterization of AC from rice husk. *Journal of Chemical Society of Nigeria*, 32, 126-136.

Okoye, C.O.B. (1991). Heavy metals and organisms in the Lagos lagoon. *International Journal of Environmental studies, 37,* 285-292.

Okoye, C.O.B. (1994). Lead and other metals in dried fish from Nigerian markets. *Bulletinof Environmental Contaminant and Toxicology, 52, 825 – 832.*

Okoye, C.O.B. (2001). Trace metal concentrations in Nigerian fruits and vegetables. *International Journal of Environmental Studies, 58,* 501-509.

Okoye, C.O.B. and Ibeto C.N. (2008). Determination of Bioavailable Metals in Soils of Three Local Government Areas in Enugu State, Nigeria. Proceedings of the 31st Annual International Conference and Exhibition, Delta Chem, 2008. Petroleum Training Institute (PTI), Conference Centre Complex, Effurun-Warri, Delta State, Nigeria, pp. 767-771.

Okoye, C.O.B. and Ibeto C.N. (2009). Analysis of different brands of fruit juice with

emphasis on their sugar and trace metal content. *Bioresearch Journal, 7*(2), 493-495.

Okoye, C. O. B., Aneke A.U., Ibeto, C. N. and Ihedioha, J. N. (2011). Heavy Metals Analysis of Local and Exotic Poultry Meat. *International Journal of Applied Environmental Sciences, 6*(1), 49-55.

Okoye, C.O.B., Ugwu, J.N. and Ibeto, C.N. (2010). Characterization of rural water resources for potable water supply in some parts of South-eastern Nigeria. *Journal of Chemical Society of Nigeria, 35(1), 83-88.*

Okuo, J.M., Okonji, E.I. and Omeyerere, F.R. (2007). Hydrophysico-chemical assessment of the Warri coastal aquifer, Southern Nigeria. *Journal of Chemical Society of Nigeria, 32*(2), 53-64.

Orwa, C., Mutua, A., Kindt, R., Jamnadass, R. and Simons, A. (2009). Agroforestree Database: a tree reference and selection guide version 4.0 http://www.worldagroforestry.org/af/treedb/): accessed April, 2014.

Osibanjo, O. and Ajayi, S.O. (1989). Trace metal analysis of petroleum products by flame atomic absorption spectrophotometry. *Nigeria Journal of Nutritional Health, 4,* 33- 40.

Onundi Y.B., Mamun, A.A., Al Khatib, M.F., and Ahmed, Y.M. (2010). Adsorption of copper, nickel and lead ions from synthetic semiconductor industrial wastewater by palm shell activated carbon. *International journal of Environmental Science and Technology, 7,* 751-758.

Olugbenga, S. B., Mary. A. O. and Abimbola M. O. (2010). Sorption studies of Pb^{2+} onto activated carbon produced from oil-palm fruit fibre. *Stem Cell, 1(1),14-29.*

Oguegbulu, E. N. and Okumiahor, J. (2013). Evaluation of the adsorption isotherm of activated charcoal used in pharmaceutical medicine from some Nigerian plant parts, corn cobs, the wooden parts of Mangifera indica and Azandirachta indica. *Advancement in Medicinal Plant Research, 1(4), 72-76.*

Owlad, M., Aroua, M.K., and Daud, W.M.A.W. (2010). Hexavalent chromium adsorption on impregnated palm shell activated carbon with polyethyleneimine. *Bioresource Technology*, 101, 5098-5103.

Oremusová, J. (2007). Manual for laboratory practice in physical chemistry for students of pharmacy, Department of Physical Chemistry, Faculty of Pharmacy, Comenius University, Bratislava, in Slovak

Otowa, T., Tanibata, R. and Itoh, M. (1993). Production and adsorption characteristics of MAXSORB: High-surface-area active carbon. *Gas Separation & Purification, 7(4),* 241-245.

Oubagaranadin, J.U.K. and Murthy, Z.V.P. (2009). Removal of Pb(II) from aqueous solutions by carbons prepared from Sal wood (Shorea robusta). *European Journal of Wood and Wood Products, 67*(2), 197-206.

Otero, M. M., Rozada, L.F., Calvo, A.I. and Garcia, A. Moran, (2003). Kinetic and Equilibrium modeling of meth- ylene blue from solution by adsorbent materials produced from sewage sludges. *Biochemical and Engineering Journal*, 15, 59-68.

Othman, F., Salim, M. R. and Ahmad, R. (1994). MOPAS for metal removal, in 20th WEDC Conf (Colombo, Sri Lanka), 292-294.

Osagie, A. U. (1998). Antinutritional Factors in Nutritional Quality of Plants (University of Benin press), 221-244.

Osuide, S. (1990). Environmental pollution in Nigeria. *Habitat International, 14*(1), 5-15.

Oyeyemi, S. M. and Gaiya, S. (2010). Adsorption of Radon at different gamma energies using different activated carbon. *Report and opinion, 2*(6), 23 – 27.

Ozer, A., Tanyildizi, M. S. and Tumen, F. (1998). Study of Cd (II) adsorption from aqueous solution on activated carbon from sugar beet pulp, *Environmental Technology*, 19, 1119-1125.

Parab, H., Joshi, S., Shenoy, N., Lali, A., Sarma, U. S and Sudersanan, M. (2006). Determination of kinetic and equilibrium parameters of the batch adsorption of Co (II), Cr (III) and Ni (II) onto coir pith. *Process Biochem*, 41, 609-615.

Pagnanelli, F, Toro, L and Veglio, F. (2002). Olive mill solid residues as heavy metal sorbent material: a preliminary study, *Waste Managment*, 22, 901-907.

Pagnanelli, F., Mainelli, S., Veglio, F. and Toro, L. (2003). Heavy metal removal by olive pomace, biosorbent characterization and equilibrium modeling, Chemical Engr. Science, 58, 4709-4717.

Pavan, F. A., Lima, I. S., Lima, E. C., Airoldi, C. and Gushikem, Y. (2006). Use of Ponkan mandarin peels as biosorbent for toxic metals uptake from aqueous solutions. *Journal of Hazardous Materials*, 137, 527-533.

Patrick, J.W. (1995). Porosity in carbons, Characterisation and applications #

(London: Edward Arnold)

Preparation of the technical guidelines for the environmentally sound management of waste lead-acid batteries, technical working group of the Basel Convention. Twentieth session Geneva, (2002).

Periasamy, K and Namasivayam, C. (1994). Process development for removal and recovery of Cd (II) from wastewater by a low cost adsorbent: adsorption rate and equilibrium studies. *Industrial Engineering and Chemical Resources*, 33, 317-320.

Periasamy, K. and Namasivayam, C. (1995). Adsorption of Pb (II) by peanut hull carbon from aqueous solution, Separation Science Technology, 30, 2223-2237.

Periasamy, K. and Namasivayam, C., (1995). Removal of nickel (II) from aqueous solution and nickel planting industry wastewater using agriculture waste: peanut hulls. *Waste management*, 15, 63- 68.

Periasamy, K. and Namasivayam, C. (1996). Removal of Cu (II) by adsorption onto peanut hull carbon from wastewater and Cu (II) plating industry wastewater. *Chemosphere*, 32, 769-789.

Pehlivan, E., Cetin, S. and Yanik, B. H. (2006). Equilibrium studies for the sorption of Zn (II) and Cu (II) from aqueous solutions using sugar beet pulp and fly ash. *Journal of Hazardous Materials*, 135, 193-199.

Pimentel, P.M., Melo, M.A.F, Melo, D.M.A, Assuncao, A.L.C, Henrique, D.M, Silva, C.N and Gonzalez, G. (2008). "Kinetics and thermodynamics of Cu (II) adsorption on oil shale wastes*." Fuel Processing Technology*, 89, 62 – 67.

Polanyi, M. (1914). Uber die Adsorption vom Standpunkt des dritten Wairmesatzes, Verh Dtsch. *Physics Ges. 16*, 1012-1016.

Quek, S. Y., Wase, D. A. J. and Forster, C. F., (1998). Water S.A. 24(3), 251-256.

Rao, M., Parawate, A. V. and Bhole, A. G. (2002). Removal of Cr^{6+} and Ni^{2+} from aqueous solution using Bagasse and fly ash. *Waste Managment*, 22, 821-830.

Rao, R.M., Bansode, R.R., Losso, J.N., Marshall, W.E. and Portier, R.J. (2003). Adsorption of volatile organic compounds by pecan shell and almond shell-based granular activated carbons. *Bioreources Technology*, 90, 2629 – 2635.

Rajaram, T. and Ashutost, D. (2008). Water pollution by industrial effluents in India: discharge scenario and case for participatory ecosystem specific local

regulation. *Envronmental Journal, 40*(1), 56-69.

Radojevic, M. and Bashkin, V. N. (1999). Practical Environmental Analysis. The Royal Society of Chemistry, Cambridge Pp.463

Rahman, S., Khalid, N. Zaidi, J.H., Ahmad, S. and Iqbal, M. Z. (2006): Non occupational lead exposure and hypertension in Pakistani adults. *Journal of Zhepang University Science, B9,*732-737.

Ramakrishnaiah, H. and Somashekar, R.K. (2002). Heavy metal contamination in roadside soil and their mobility in relations to pH and organic Carbon. Soil and sediment contamination: *An International Journal,11*(5), 643 – 654.

Rahangdale, R. V., Kore, S.V. and Kore, V.S. (2012). Waste Management in Lead-Acid Battery Industry: A Case Study. *World Journal of Applied Environmental Chemistry, 1*(1), 7 – 12.

Rand, B., (1976). On the empirical nature of the Dubinin Radushkevich equation of adsorption. *Journal of Colloid Interface Science, 56,*337–346

Rao. R.M., Ahmedna, M. and Marshall, W.E. (2000). Surface properties of granular activated carbons from agricultural by-products and their effects on raw sugar decolorization, *Bioresource Technology*, 71,103-112.

Reeves, P.G. and Vanderpool, R.A. (1997). Cadmium burden in men and women who report regular consumption of confectionery sunflower kernels containing a natural abundance of cadmium. *Environmental Health Perspective, 105*(10), 98-104.

Reinoso, R.F., Martines, M.J.M., and Sabio, M.M. (1985). A comparison of the porous texture of two CO_2 activated botanic materials. *Carbon,* 23, 19-24.

Reinoso, R.F., and Linares-Solano, A. (1989). Microporous structure of activated carbons as revealed by adsorption methods. *Chemistry and physics of carbon,* 21, 1-146

Reddad, Z., Gerente, C., Andres, Y., Ralet, M. C., Thibault, J. F., and Cloirec, P. L. (2002). Ni (II) and Cu (II) binding properties of native and modified sugar beet pulp. *Carbohyd Polym*, 49 23-31.

Ricardo, C., Tarley, T. and Arruda, M. A. Z. (2004). Biosorption of heavy metals using rice milling by-products, Characterization and application for removal of metals from aqueous effluents. *Chemosphere,* 54, 987-995.

Rigby, P.S., Fletcher, R.S. and Riley, S.N. (2004). Characterisation of porous solids

using integrated nitrogen sorption and mercury porosimetry. *Chemical Engineering Science, 59*(1), 41-51.

Romero, L. C., Bonomo, A. and Gonzo, E. E. (2004). Peanut shell activated carbon: Adsorption capacities for Copper (II), zinc (II), nickel (II) and chromium (VI) ions from aqueous solutions. *Adsorption Science Technology, 22*, 237-243.

Robinson, T. B. and Chandaran, P. Nigam (2002). Removal of dyes from a synthetic dye effluent by biosorption on wheat straw. *Water Resources*, 36, 2830-2842.

Roy, D., Greenlaw, P. N. and Shane, B. S. (1993). Adsorption of heavymetals by green algae and ground rice hulls. *Journal of Environ Science and Health* A, 28, 37-50.

Rodriguez, R. (1995). Chemistry and physics of carbon. P A Thrower, vol. 21, p.1.

Saeed, A., Iqbal, M. and Akhtar, M. W. (2005). Removal and recovery of lead (II) from single and multimetal (Cd, Cu, Ni, Zn) solutions by crop milling waste (black gram husk). *Journal of Hazardous Materials*, 117, 65-73.

Saeed, A., Akhtar, M. W. and Iqbal, M. (2005). Affinity relationship of heavy metal biosorption by the husk of Cicer arietinum (chickpea var. black gram) with their atomic weights and structural features. *Fresenius Environ Bull*, 14, 219-223.

Santhy, K. and Selvapathy, P. (2004). Removal of heavy metals from wastewater by adsorption on coir pith activated carbon. *Separation Science Technology*, 39, 3331-3351.

Salman Zafar (2015). Palm kernel shells as biomass resources. Bioenergy consult.

Sawyer, C.N. McCatty, P.L. and Parkin, G.F. (2000). Chemistry for environmental engineering. Fourth edition, McGraw-Hill, Inc., New York.

Sağ, Y. and Aktay, Y. (2002). Kinetic studies on sorption of Cr (VI) and Cu (II) ions by chitin, chitosan and rhizopus arrhizus. *Biochemical Engineering Journal*, 12, 143 – 153.

Sarin, V. and Pant K. K. (2006). Removal of chromium from industrial waste by using eucalyptus bark. *Bioresource Technology*, 97, 15–20.

Samiya, A., Alexandra, C., Matthew, C. and Kelvin, T. (1997). Choosing an effluents treatment plant. Government of the People's Republic of Bangladesh. pp. 1-33

Selvakumari, G., Murugesan, M., Pattabi, S. and Sathishkumar, M. (2002). Treatment of electroplating industry effluent using maize cob carbon. *Bull Environ. Contam. Toxicology*, 69, 195-202.

Selverani, K. (2000). Studies on low cost adsorbents for the removal of organics and inorganic from wastewater, Ph.D. Thesis, REC, Tiruchirapalli, India.

Sciban, M., Radetic, B., Kevresan, Z. and Klasnja, M. (2007). Adsorption of heavy metals from electroplating wastewater by wood sawdust, *Bioresources Technology*, 98, 402-409.

Sheindorf, C.H., Rebhun, M. and Sheintuch, M. (1981) "A Freundlich-type multicomponent isotherm." *Journal of Colloid and Interface Science*, 79(1), 136 – 142.

Shen, W., Li Z. and Liu Y. (2008). Surface chemical functional groups modification of porous carbon, *Recent Patents on Chemical Engineering*, 1, 24-40.

Shy, C. M. (1990). Lead in petrol. The mistake of the 20th century. World health statistics, *Quaterly, 43*, 168-176.

Singha, B. and Das, S.K. (2013). Adsorptive removal of Cu(II) from aqueous solution and industrial effluentusing natural/agricultural wastes. *Colloids surface Biointerfaces*, 107, 97-106.

Sing, K.S.W, Everett, D.H, Haul, R.A.W, Moscou, L, Pierotti, R.A, Rouquerol, J, and Sieminiewska, C. (1985). Presentation of physisorption data from gas/solid systems, *Pure and Applied Chemistry, 57*, 603– 619.

Shukla, A., Zhang, Y. H., Dubey, P., Margrave, J. L. and Shukla, S. S. (2003). The role of sawdust in the removal of unwanted materials from water. *Journal of Hazardous Materials*, 95, 137-152.

Shukla, S. R. and Sakhardande, V. D. (1991). Novel method of using reactive dyestuff for effluent treatment. *Am Dyest Rep*, 41, 38-42.

Snoeyink, V, and Jenkins, D. (1980). Water chemistry. John wiley and sons New York.

Shukla, S. R., Pai, R. S. and Shendarkar, A. D. (2006). Adsorption of Ni (II), Zn (II) and Fe (II) on modified coir fibers, *Separationa and Purification Technology*, 47, 141-147.

Slobodan, K. M. (2007). A consideration of the correct calculation of thermodynamic parameters of adsorption. *Journal of the Serbian*

Chemical Society, 72(12), 1363-1367.

Song, X.L., Liu, H.Y., Cheng, L. and Qu, Y. (2010). Surface modification of coconut-based activated carbon by liquid-phase oxidation and its effects on lead ion adsorption. *Desalination, 255*(1-3), 78-83,

Sidnei, G. S. and Fábio, P.R. (2010). A flow injection procedure based on solenoid micro-pumps for spectrophotometric determination of free glycerol in biodiesel. *Talanta, 83*(2), 15, 559-564.

Spiff, A. I. and Horsfall. M. Jnr. (2004). Trace metal concentrations in inter-tidal flate sediments of the upper new Calabar River in the Niger Delta area of Nigeria. *Scientia African, 3*, 19-28.

Sposito, G. (1989). The chemistry of soils, Oxford University Press, New York.

Stoeckli, H.F. and Roop Chand Bansal, J.-B.D. (1988). Active Carbon, New York: Marcel Dekker, INC.

Stoeckli, H.F. (1977). A Generalization of the Dubinin-Radushkevich Equation for the Filling of Heterogeneous Micropore Systems. *Journal of Colloid and Interface Science, 59*, 184-185.

Stimson Global Health Security, (2012).” Lagos: Growth without infrastructure,” The Stimson Centre, [Online]. Available: http://www.stimson.org, Accessed Jul. 24, 2013.

Subhashree, P. (2011). Production and characterisation of activated carbon produced from a suitable industrial sludge. A thesis submitted to the department of chemical engineering, National Institute of Technology, Rourkela.

Sulaiman, F., Abdullah, N., Gerhauser, H., and Shariff, A. (2011). An outlook of Malaysian energy, oil palm industry and its utilization of wastes as useful resources Biomass and Bioenergy. *Journal of Purity, Utility Reaction and Environment, 1(5), 252-266*

Sumathi, S., Bhatia, S., Lee, K.T. and Mohamed, A.R. (2010). Cerium impregnated palm shell activated carbon (Ce/PSAC) sorbent for simultaneous removal of SO_2 and NO – Process study. *Chemical Engineering Journal*, *162*, 51-57

Srenscek, J., Narkiewicz, U., Morawski, A. W. and Wrobel, R. (2016). Modification of commercial activated carbon for CO_2 adsorption. *ACTA Physica Polonica A., 129(3), 394-400.*

Tang, P. L., Lee, C. K., Low, K. S. and Zainal, Z. (2003). Sorption of Cr (VI) and Cu (II) in aqueous solution by ethylenediamine modified rice hull. *Environmental Technology*, 24, 1243-1251.

Tan, W. T., Ooi, S. T., and Lee, C. K., Environ. Technol., 1993, 14, 277-282.

Tan, I.A.W., Ahmad, A.I. and Hameed, B.H. (2008). Enhancement of basic dye adsorption uptake from aqueous solutions using chemically modified oil palm shell activated carbon. *Colloids and Surfaces A. Physicochemical* and *Engineering Aspects, 318,* 88-96.

Tan, I.A.W., Ahmad, A.L., and Hameed, B.H. (2009). Fixed-bed adsorption performance of oil palm shell-based activated carbon for removal of 2,4,6-trichlorophenol. *Bioresource Technology, 100,* 1494-1496.

Taylor, A., Branch, S. Halls, D.J., Owen, L.M.W. and White, M. (2000). Atomic Spectrometry update: Clinical and biological material, food and beverages. *Journal of Analytical Atomic Spectrum, 15,* 451-487.

Temkin, M. I. and Pyzhev, V. (1940). Kinetics of ammonia synthesis on promoted iron catalyst. *Acta Phys. Chim. USSR*, 12, 327-356.

Treybal, R.E. (1980). Mass Transfer Operations. 3rd ed. New York: McGraw-Hill. Pp. 581– 582.

Technical Guidelines on Management of used lead acid batteries Central Environmental Authority (CEA), (2005).

Tinggi, U., Reilly, C., and Patterson, C., (1997). Determination of manganese and chromium in food by atomic absorption spectromety after wet digestion. *Food Chemistry, 60,* 123-128.

Tong, J. S. and Li, J. (1982). *Calculation of ¹hermo-physical Properties of Fluids* (in Chinese), Tsinghua University Press.

Thornton, I. (1992). Sources and pathways of cadmium in the environment. *IARC Science Publication, 118,* 149-162.

Thomas, V. and Kwong, A. (2001). Ethanol as a Replacement: Phasing out leaded gasoline in Africa. *Energy Policy, 29,* 1133-1143.

Todorovska, N., Karadjova, I. and Stafilov, T. (2002). ETAAS determination of nickel in serum and urine. *Analytical and Bioanalytical Chemistry, 373*(4-5), 310-313.

Ulmanu, M. M., Fernandez, Y., Castrillon, L., Anger, I. and Dumitriu, D. (2003). Removal of copper and cadmium ions from diluted aqueous solutions by low cost and waste material adsorbents. *Water, Air and Soil Pollut*ion, 142, 357-373.

Uddin, M. T., Islam, M.S. and Abedin, M.Z. (2007). Adsorption of phenol from aqueous solution by water hyacinth ash. *ARPN Journal of Engineering and Applied Sciences, 2(2), 121-128.*

UNEP. (2016). Leaded petrol phase-out: Global status as at June, 2016. Nairobi, United Nations Environmental Programme.

U.S. EPA Planning Workshop to Develop Recommendations for a Ground Water Protection Strategy. 1980b. Appendixes. Washington DC. pp 171.

U.S. EPA Handbook, Ground Water Vol. 1: Ground Water and Contamination. 1990. Office of Research and Development. Washington DC. EPA/625/6-90/016a.

U.S. EPA. (1993). Clean Water Act, sec. 503, vol. 58, no. 32. (U.S. Environmental Protection Agency Washington, D.C.).

United Nations. (2006). Interim review of scientific information on lead. Overview of existing and future national actions, including legistation, relevant to lead. Appendix. Acessed from http://www.chem.unep.ch/pb_and_cd/SR/Files/Interim_reviews/UNEP-Lead-review-Interim-APPENDIX-Oct 2006.doc on December 20th 2013.

Uzodinma, E.O. Ofoefule, A.U. and Enwere N.J. (2011). Optimization of biogas fuel production from blending maize bract with biogenic wastes. *American Journal of Food and Nutrition, 1*(1), 1-6.

Umeh, J.C. (1989). Farmer co-operative union and rural life quality in Nigeria. *Journal of Rural Co-operation, 17,* 151-166.

Umeh, J.C., Amali, O., and Umeh, E.U. (2004). The socio-economic effects of tropical diseases in Nigeria. *Economics and Human Biology, 2,* 245-263.

Ustinov, E., Polyakov, N. and Petukhova, G. (1999). Statistical interpretation of the Dubinin-Radushkevich equation. *Russian Chemical Bulletin, 48*(2), 261-265.

Vaishya, R. C. and Prasad, S. C. (1991). Adsorption of Cu (II) on sawdust. *Indian Journal of Environmental Protection*, 11, 284-289.

Vannice, M.A. (2005). Kinetics of Catalytic reactions. USA: Springer

Science+Business Media Inc., p.100

Valmari, T., Lind, T.M., Kauppinen, E.I., Sfiris, G., Nilsson, K. and Willy, M.U. (1999). Field study on ash behavior during circulating fluidized-bed combustion of biomass. 2. Ash deposition and alkali vapor condensation. *Energy & Fuels, 13(2)*, 390-395.

Verma, V.K. and Mishra, A.K. (2006). Removal of dyes by the wheat straw carbon. *Ecology, Environment & Conservation*, 12(4), 755-757.

Veglio, F., Beolchini, F. and Prisciandaro, M. (2003). Sorption of Cu (II) by olive mill residues. *Water Resources*, 37, 4895-4903.

Verlag, Berlin Heidelberg, (1999). Modern Methods of Plant Analysis Vol. 20 Analysis of Plant Waste Materials, Springer-, pp 41-42.

Veli, S. and Alyuz, B. (2007). Adsorption of copper and zinc from aqueous solutions by using natural clay. *Journal of Hazardous Materials, 149*, 226-233.

Veria, A.W., Horsfall (Jnr), M., Veria, E.N., Spiff, A.I. and Ekpete, O.A. (2012). Preparation and characterization of activated carbon from Fluted Pumpkin (Telfairia Occidentalis Hook.F) Seed Shell. *Asian Journal of Natural & Applied Sciences*, 1(3), 39 – 50

Viraraghavan, T. and Maria-alfaro, F.D. (1998). Adsorption of phenol from wastewater by peat, fly ash and bentonite. *Journal of Hazardous Materials, 57*, 59-70

Volpe, A., Lopez, A. and Pagano, M. (2003). Olive husk: an alternative sorbent for removing heavy metals from aqueous streams, *Applied Biochemistry & Biotechnology*, 110, 137-150.

Wang, R. Z. and Wang, Q. B. (1999). Adsorption mechanism and improvements of the adsorption equations for adsorption refrigeration pairs. *International journal of Energy Reaserch, 23*, 887-898.

Wafwoyo, W., Chung, W. S. and Marshall, W. E. (1999). Utilization of peanut shells as adsorbents for selected metals. *Journal of Chemical Technology Biotechnology*, 74, 1117-1121.

Weber Jr. W. J. (1972). Physicochemical Processes for Water Quality Control. Wiley-lnterscience New York.

Weber Jr. W. J. (1966). 'Fluid—carbon columns for sorption of persistent organic pollutants'. Proceedings of the Third International Conference on Water

Pollution Research. *Vol. I. Water Pollution Control Federation: Washington, DC (1966).*

World Bank Group. (1998). Pollution prevention and abatement handbook. Project Guidelines: Industry Sector Guidelines. pp. 298-301

WHO. (1996). Trace elements in human nutrition and health. International atomic energy agency. WHO Library Publication Data. Geneva. pp. 194-215, 256-259.

WHO. (1982). Rapid Assessment of sources of Air, Water and Land pollution. Offset Publication, 62, 7.

WHO (IPCS). (1983). Environmental Health Criteria 27: Guidelines on Studies in Environmental Epidemiology. WHO, Geneva. pp. 351

World Health Organization (WHO). (1996a). Trace elements in human nutrition and health. WHO, Geneva. pp. 343.

Woods, G.D. and Fryer, F.I. (2007). Direct elemental analysis of biodiesel by inductively coupled plasma-mass spectrometry. *Analytical and Bioanalytical Chemistry, 389*(3), 753-761.

Wu, T.N., Yang, G.Y., Shen, C.Y. and Liou, S.H., (1995). Lead contamination of candy: an example of crisis management in public health. *Lancet, 346*, 1437-1442.

World Water Council, "Water supply and sanitation," (2005). [Online]. Available: http://www.worldwatercouncil.org/index.php?id [Accessed Nov.13, 2007].

World Bank," World water challenge," The Punch, Friday, March 23, 2007.

World Health Organization, "Cost and benefits of water and sanitation improvements," 2004 [Online], vailable:http://www.who.int/watersanitationhealth/wsh0404 summary/en/index.html [Accessed Nov.13, 2007].

World Health Organization and United Nations Children Fund, "Water and Sanitation Report," The Guardian, Monday, December 4, 2006.

Wilson, K., Yang, H., Seo, C. W.and Marshall, W. E. (2006). Select metal adsorption by activated carbon made from peanut shells. *Bioresources Technology*, 97, 2266-2270.

World Bank and Federal Ministry of Water Resources, "Water supply and sanitation interim strategy note on Nigeria," 2000 [Online]. Available: http://siter resources world bank. Org/NIGERIA EXTN/Resources/wss 1100, [Accessed

Nov.13, 2007].

Wojsz, R., and Rozwadowski, M. (1984). *Carbon*, 22, 437.

Yakubu, M., Gumel, K. and Abdullah, M. S. (2008). Use of activated carbon from date seeds to treat textile and tannery effluents, *African Journal of Science and Technology, 9(1), 31-40.*

Yin, C.Y., Aroua, M.K., and Daud, W.M.A.W. (2007). Impregnation of palm shell activated carbon with polyethyleneimine and its effects on Cd^{2+} adsorption. *Colloids and Surfaces A, 307,*128-136.

Zaid Ahmed Al-Anber, and Mohammed A. S. Al-Anber. (2008). Thermodynamics and Kinetics Studies of Iron (III) Adsorption by Olive Cake in a Batch System. *Journal of Mexico Chemical Society, 52, 108 - 115.*

Zawadzki J. (1988). Infrared spectroscopy in surface chemistry of carbons. *in chemistry and physics of carbon;* Thrower PA. Ed.; Marcel Dekker: New York, 21, 147-386.

Zawadzki, J. (1989). Chemistry and Physics of Carbon, Vol. 21, Marcel Dekker, Inc., New York, 79 – 88.

Zhang, Y. H. (1988). *Adsorption* (in Chinese), Shanghai Press of Science and Technology, pp54 - 120

Zheng, J. Zhao, Q. and Ye, Z. (2014). Preparation and characterization of Activated Carbon Fibre (ACF) from cotton woven waste. *Applied Surface Science Journal,* 299, 86-91

Zulkali, M. M. D., Ahmed, A. L. and Norulakmal, N. H. (2006). Oryza sativa L. husk as heavy metal adsorbent: Optimization with lead as model solution. *Bioresources Technology*, 97, 21-25.

APPENDIX A

DETERMINATION OF DISSOLVED OXYGEN (ALKALINE-AZIDE MODIFICATION OF WINKLER'S METHOD)

CALCULATION:

DO, mg/l = Titre value x 10 = mg/l O_2

RESULT

	1st	2nd	3rd
Final volume	3.40	3.50	3.50
Initial volume	0.00	0.00	0.00
Titre (ml)	3.40	3.50	3.50

$$\text{Average titre} = \frac{3.4 + 3.5 + 3.5}{3} = 3.467\text{ml}$$

DO, mg/l = 3.467 x 10 = 34.67mg/l

CHEMICAL OXYGEN DEMAND (COD)

Standardization of Ferrous Ammonium Sulphate

10.0ml of standard $K_2Cr_2O_7$ solution was diluted to about 100ml. 30 ml of concentrated H_2SO_4 was added and cooled. 3-4 drops of ferroin indicator was added and titrated with ferrous ammonium sulphate till the colour changed to wine red.

$$\text{Normality of Ferrous ammonium sulphate} = \frac{10 \times 0.25}{V}$$

Where

V = volume of Fe $(NH_4)_2$ $(SO_4)_2$ required for titration, in ml.

CALCULATION

Sample titration

	1st	2nd	3rd
Final volume	15.6	15.6	15.6
Initial volume	0.00	0.00	0.00
Titre (ml)	15.6	15.6	15.6

Blank titration

	1st	2nd	3rd
Final volume	15.6	15.6	15.6
Initial volume	0.00	0.00	0.00
Titre (ml)	15.6	15.6	15.6

V = 13.2ml

$$\text{Normality of Ferrous ammonium sulphate} = \frac{10 \times 0.25}{26.2} = 0.0954\text{N}$$

$$\text{N COD, mg/l} = \frac{(V_1 - V_2)\text{ N} \times 8000}{V_o}$$

Where

V_1 = volume of Fe $(NH_4)_2$ $(SO_4)_2$ required for titration against the blank, in ml

V_2 = volume of $Fe(NH_4)_2$ $(SO_4)_2$ required for titration against the sample, in ml

N = Normality of $Fe(NH_4)_2$ $(SO_4)_2$

V_0 = volume of sample taken for testing, in ml.

$$\text{COD in mg/l of } O_2, = \frac{(15.6 - 14.9) \times 0.0954 \times 8000}{20} = 26.7\text{mg/l}$$

DETERMINATION OF ALKALINITY IN WASTE WATER BY UNEP/WHO METHOD

CALCULATION:

Run	Initial Reading	Final Reading	Titre (ml)
1	0.00	24.9	24.9
2	0.00	24.8	24.8
3	0.00	24.8	24.8

Average Titre = (24.9 + 24.8 + 24.8)/3 = 24.83ml

$$\text{Total alkalinity in mgl}^{-1} \text{ as } CaCO_3) = \frac{\text{titre value} \times 100{,}000 \times \text{conc. of acid}}{\text{Volume of sample}}$$

$$= \frac{24.83 \times 100000 \times 0.01}{100} = 248.3\text{mg/l}$$

DETREMINATION OF CHLORIDE IN WASTE WATER

CALCULATION:

SAMPLE

	Initial Reading	Final Reading	Titre
1	0.00	13.30	13.30
2	0.00	13.50	13.50
3	0.00	13.50	13.50

$$\text{Average Titre} = \frac{13.3 + 13.5 + 13.5}{3} = 13.433\text{ml}$$

BLANK

	Initial Reading	Final Reading	Titre
1	0.00	30.0	30.0
2	0.00	29.1	29.1
3	0.00	29.1	29.1

$$\text{Average Titre} = \frac{30.0 + 29.1 + 29.1}{3} = 29.4\text{ml}$$

$$\text{Chloride as } Cl^{-1} = \frac{1000\,(v_1 - v_2)}{100}$$

Where V_1 = Volume of silver nitrate required by the sample (ml)

V_2 = Volume of silver nitrate required by the blank (ml)

$$\frac{1000 \times 29.4 - 13.433}{100} = 159.67 mg/l$$

DETERMINATION OF TOTAL HARDNESS (EDTA TITRIMETRY METHOD) IN WASTE WATER

CALCULATION:

Total hardness, mg/l $CaCO_3$ = $\frac{\text{titre value} \times 1000}{\text{Volume of sample}}$

RESULT

Run	Initial Reading	Final Reading	Titre (ml)
1	0.00	31.3	31.3
2	0.00	31.2	31.2
3	0.00	31.3	31.3

Average titre = (31.3+ 31.2+ 31.3)/3 = 31.267ml

Total hardness = $\frac{31.267 \times 1000}{50}$ = 625.33mg/l

DETERMINATION OF TOTAL SOLIDS BY GRAVEMETRIC METHOD

CALCULATION:

Total solids (mg/l) = $\frac{w_2 - w_1}{\text{ml of sample}} \times 1000$

w_1 = 23.202g

w_2 = 23.215g

ml of sample = 100ml

$= \frac{23.215 - 23.202}{100} \times 1000 = 0.13 mg/l$

DETERMINATION OF SULPHATE WASTE WATER BY TITRIMETRIC METHOD

CALCULATIONS

	1st	2nd	3rd
Initial volume	0.00	0.00	0.00
Final volume	87.80	87.7 0	87.70
Titre (ml)	87.80	87.70	87.7 0

Average titre volume = (87.8 + 87.7 + 87.7)/ 3 = 87.73

1ml of Barium perchlorate solution is = 0.96mg of SO_4^{2-}

Sulphate (as SO_4^{2-}), percent by mass = $\frac{V \times 0.96 \times 100}{V_1}$

Where V = Titre Volume = 87.73 ml

V_1 = Volume of sample used = 20ml

Sulphate (as SO_4^{2-}), percent by mass = $\frac{87.7 \times 0.96}{20}$ = 4.211mg/l

APPENDIX B

Table 4.2 and figure 4.1 showed the initial elemental analysis of the four samples.

Table 4.2: The Elemental Analysis of the Samples

Elements (mg/g)	Sample A	Sample B	Sample C	Sample D
Carbon	0.183	0.172	0.196	0.453
Hydrogen	0.014	0.012	0.018	0.017
Oxygen	0.029	0.017	0.012	0.011
Sodium	0.00	0.020	0.001	0.004
Potassium	0.018	0.015	0.019	0.015

Table 4.3 and figure 4.2 depicted the percentage yield of carbon after the carbonization of each sample.

Table 4.3: Percentage Yield of Carbon after Carbonization

SAMPLE	800 ^{O}C for 30Min(%)	600 ^{O}C for 30Min (%)
A	28.01	32.61
B	32.19	34.58
C	25.79	27.27
D	61.85	86.11

Table 4.4: Percentage Yield after Chemical Activation

SAMPLE	800°C/30Min (%)			600°C/30Min (%)		
	H_2SO_4	HCl	H_3PO_4	H_2SO_4	HCl	H_3PO_4
A	70.27	76.93	92.40	77.74	76.86	83.90
B	76.61	89.67	95.31	82.88	71.74	89.28
C	74.59	68.42	76.02	61.85	66.40	89.32
D	74.52	79.80	98.15	83.85	92.35	98.21

APPENDIX C

Table 4.11: Ni Adsorption by Oil Bean Carbonized at 600°C and Activated with HCl

C_o (mg/l)	C_e (mg/l)	q_e (mg/g)	E (%)	$logq_e$	$logC_e$	$1/q_e$	$1/C_e$	Inq_e	ε^2	InC_e	$\varepsilon^2/1m$
55.472	1.39	0.54	97.5	-0.268	0.143	1.852	0.7194	-0.6162	1803066.3	0.3293	1.8031
52.672	1.67	0.51	96.8	-0.292	0.204	1.961	0.5988	-0.6733	1351659.6	0.5128	1.3517
59.352	5.73	0.54	90.3	-0.268	0.758	1.852	0.1745	-0.6162	158801.4	1.7457	0.1588
64.965	6.58	0.58	8.99	-0.237	0.818	1.724	0.152	-0.5447	122903.1	1.8840	0.1229
66.797	38.26	0.29	42.7	-0.538	1.583	3.448	0.0261	-1.2379	4074.9	3.6444	0.0041

C_o = initial metal concentration, C_e = equilibrium metal concentration, q_e = metal adsorbed per gram activated carbon and E = Percentage adsorption efficiency, $\varepsilon^2/1m = \varepsilon^2/1{,}000{,}000$

Table 4.12: Ni Adsorption by Oil Bean Carbonized at 600°C and Activated with H_2SO_4

Co (mg/l)	Ce (mg/l)	qe (mg/g)	E (%)	logqe	logCe	1/qe	1/Ce	Inqe	ε^2	InCe	$\varepsilon^2/1m$
55.472	1.78	0.54	96.8	-0.268	0.25	1.8519	0.5618	-0.6162	1220137.3	0.5766	1.2201
52.672	2.77	0.5	94.7	-0.301	0.442	2	0.361	-0.6931	583140.8	1.0188	0.5831
59.352	6.98	0.52	88.2	-0.284	0.844	1.9231	0.1433	-0.6539	110086.9	1.9430	0.1101
64.965	16.5	0.48	94.6	-0.319	1.217	2.0833	0.0606	-0.7340	21248.1	2.8034	0.0212
66.797	26.1	0.41	60.9	-0.387	1.417	2.439	0.0383	-0.8916	8671.1	3.2619	0.0087

Table 4.13: Ni Adsorption by Oil Bean Carbonized at 600°C and Activated with H_3PO_4

C_o (mg/l)	C_e (mg/l)	q_e (mg/g)	E (%)	$logq_e$	$logC_e$	$1/q_e$	$1/C_e$	Inq_e	ε^2	InC_e	$\varepsilon^2/1m$
55.472	8.67	0.47	84.3	-0.328	0.938	2.128	0.1153	-0.755	73095.2	2.1599	0.0731
52.672	9.98	0.43	81	-0.366	0.999	2.326	0.1002	-0.844	55974.	2.3006	0.0560
59.352	10.26	0.49	82.7	-0.31	1.011	2.041	0.0975	-0.713	53130.5	2.3283	0.0531
64.965	11.66	0.53	82	-0.276	1.067	1.887	0.0858	-0.635	41594.1	2.4562	0.0416
66.797	45.36	0.21	32	-0.678	1.657	4.762	0.022	-1.561	2906.9	3.8146	0.0029

Table 4.14: Ni Adsorption by Oil Bean Carbonized at 800°C and Activated with HCl

C_o (mg/l)	C_e (mg/l)	q_e (mg/g)	E (%)	$logq_e$	$logC_e$	$1/q_e$	$1/C_e$	Inq_e	ε^2	InC_e	$\varepsilon^2/1m$
55.472	6.78	0.49	87.8	-0.31	0.831	2.0408	0.1475	-0.7133	116198.1	1.9140	0.1162
52.672	5.19	0.47	90.1	-0.328	0.715	2.1277	0.0157	-0.7550	1489.6	1.6467	0.0015
59.352	6.003	0.53	89.9	-0.276	0.778	1.8868	0.1666	-0.6349	145754.3	1.7923	0.1458
64.965	40.13	0.25	38.2	-0.602	1.603	4.0000	0.0249	-1.3863	3713.2	3.6921	0.0037
66.797	63.53	0.03	4.9	-1.523	1.803	33.333	0.0157	-3.5066	1489.6	4.1515	0.0015

Table 4.15: Ni Adsorption by Oil Bean carbonized at 800°C and Activated with H_2SO_4

C_o (mg/l)	C_e (mg/l)	q_e (mg/g)	E (%)	$logq_e$	$logC_e$	$1/q_e$	$1/C_e$	Inq_e	ε^2	InC_e	$\varepsilon^2/1m$
55.472	31.38	0.24	43.4	-0.62	1.497	4.1667	0.0319	-1.4271	6052.9	3.4462	0.0061
52.672	30.56	0.22	41.9	-0.658	1.485	4.5455	0.0327	-1.5141	6355.3	3.4197	0.0064
59.352	34.01	0.25	42.7	-0.602	1.532	4.0000	0.0294	-1.3863	5153.9	3.5267	0.0052
64.965	38.27	0.27	41.1	-0.569	1.583	3.7037	0.0261	-1.3093	4074.9	3.6447	0.0041
66.797	30.6	0.36	54.2	-0.444	1.486	2.7778	0.0327	-1.0217	6355.3	3.4210	0.0064

Table 4.16: Ni Adsorption by Oil Bean Carbonized at 800°C and Activated with H_3PO_4

C_o (mg/l)	C_e (mg/l)	q_e (mg/g)	E (%)	$logq_e$	$logC_e$	$1/q_e$	$1/C_e$	Inq_e	ε^2	InC_e	$\varepsilon^2/1m$
55.472	22.37	0.33	59.7	-0.481	1.35	3.03	0.0447	-1.1087	11738.3	3.1077	0.0117
52.672	20.68	0.32	60.7	-0.495	1.316	3.025	0.0484	-1.1394	13713.1	3.0292	0.0137
59.352	21.38	0.38	63.9	-0.42	1.33	2.632	0.0468	-0.9676	12841.2	3.0625	0.0128
64.965	52.17	0.13	19.7	-0.886	1.717	7.692	0.0192	-2.0402	2220.2	3.9545	0.0022
66.797	59.38	0.07	11.1	-1.155	1.774	14.286	0.0168	-2.6593	1703.8	4.0840	0.0017

Table 4.17: Cd Adsorption by Oil Bean Carbonized at 600°C and Activated with HCl

C_o (mg/l)	C_e (mg/l)	q_e (mg/g)	E (%)	$logq_e$	$logC_e$	$1/q_e$	$1/C_e$	Inq_e	ε^2	InC_e	$\varepsilon^2/1m$
53.662	15.19	0.38	71.7	-0.42	1.182	2.6316	0.0658	-0.9676	24927.7	2.7206	0.0249
53.057	20.37	0.33	61.6	-0.481	1.309	3.0303	0.0491	-1.1087	14103.1	3.0141	0.0141
53.93	21.38	0.33	60.3	-0.481	1.33	3.0303	0.0468	-1.1087	12841.2	3.0625	0.0128
55.728	45.74	0.10	17.9	-1.000	1.66	10.0000	0.0219	-2.3026	2880.8	3.8230	0.0029
57.47	53.426	0.04	7.04	-1.398	1.728	25.0000	0.0187	-3.2189	2107.1	3.9783	0.0021

Table 4.18: Cd Adsorption by Oil Bean Carbonized at 600°C and Activated with H_2SO_4

C_o (mg/l)	C_e (mg/l)	q_e (mg/g)	E (%)	$logq_e$	$logC_e$	$1/q_e$	$1/C_e$	Inq_e	ε^2	InC_e	$\varepsilon^2/1m$
53.662	0.57	0.53	98.9	-0.276	-0.244	1.8868	1.7544	-0.6349	6301480.8	-0.5621	6.3015
53.057	1.28	0.52	97.6	-0.284	0.107	1.9231	0.7813	-0.6539	2046072.6	0.2469	2.0461
53.93	0.51	0.53	99.1	-0.276	-0.292	1.8868	1.9608	-0.6349	7232356.4	-0.6733	7.2324
55.728	1.681	0.54	96.9	-0.268	0.226	1.8519	0.5949	-0.6162	1337626.3	0.5194	1.3376
57.47	16.47	0.41	71.3	-0.387	1.217	2.439	0.0607	-0.8916	21316.3	2.8015	0.0213

Table 4.19: Cd Adsorption by Oil Bean Carbonized at 600°C and Activated with H_3PO_4

C_o (mg/l)	C_e (mg/l)	q_e (mg/g)	E (%)	$logq_e$	$logC_e$	$1/q_e$	$1/C_e$	Inq_e	ε^2	InC_e	$\varepsilon^2/1m$
53.662	22.33	0.31	58.4	-0.509	1.349	3.2258	0.0448	-1.1712	11789.8	3.1059	0.0118
53.057	23.56	0.29	55.6	-0.538	1.372	3.4483	0.0424	-1.2379	10584.9	3.1596	0.0106
53.93	21.99	0.32	59.2	-0.495	1.342	3.125	0.0455	-1.1394	12152.9	3.0906	0.0122
55.728	45.67	0.1	18	-1	1.66	10	0.0219	-2.3026	2880.8	3.8214	0.0029
57.47	48.96	0.09	14.8	-1.046	1.69	11.1111	0.0204	-2.4079	2503.4	3.8910	0.0025

Table 4.20: Cd Adsorption by Oil Bean Carbonized at 800°C and Activated with HCl

C_o (mg/l)	C_e (mg/l)	q_e (mg/g)	E (%)	$logq_e$	$logC_e$	$1/q_e$	$1/C_e$	Inq_e	ε^2	InC_e	$\varepsilon^2/1m$
53.662	19.690	0.34	63.3	-0.469	1.294	2.9412	0.0508	-1.0788	15072.0	2.9801	0.0151
53.057	11.380	0.42	78.6	-0.377	1.056	2.381	0.0879	-0.8675	43569.7	2.4319	0.0436
53.930	12.022	0.42	77.7	-0.377	1.080	2.381	0.0832	-0.8675	39206.6	2.4867	0.0392
55.728	35.452	0.20	36.4	-0.699	1.550	5.000	0.0282	-1.6094	4747.3	3.5682	0.0047
57.470	53.407	0.04	6.96	-1.398	1.728	25.000	0.0187	-3.2189	2107.1	3.9779	0.0021

Table 4.21: Cd Adsorption by Oil Bean Carbonized at 800°C and Activated with H_3PO_4

C_o (mg/l)	C_e (mg/l)	q_e (mg/g)	E (%)	$logq_e$	$logC_e$	$1/q_e$	$1/C_e$	Inq_e	ε^2	InC_e	$\varepsilon^2/1m$
53.662	37.28	0.16	30.5	-0.796	1.571	6.25	0.0268	-1.8326	4293.5	3.6185	0.0043
53.057	39.9	0.13	24.8	-0.886	1.601	7.6923	0.0251	-2.0402	3772.3	3.6864	0.0038
53.93	42.1	0.12	23.8	-0.921	1.624	8.3333	0.0238	-2.1203	3396.0	3.7400	0.0034
55.728	53	0.27	4.9	-0.569	1.724	3.7037	0.0189	-1.3093	2151.9	3.9703	0.0022
57.47	52.18	0.05	12.3	-1.301	1.718	20	0.0192	-2.9957	2220.2	3.9547	0.0022

Table 4.22: Cd Adsorption by Oil Bean Carbonized at 800°C and Activated with H_2SO_4

C_o (mg/l)	C_e (mg/l)	q_e (mg/g)	E (%)	$logq_e$	$logC_e$	$1/q_e$	$1/C_e$	Inq_e	ε^2	InC_e	$\varepsilon^2/1m$
53.662	32.33	0.21	39.9	-0.678	1.51	4.7619	0.0309	-1.5606	5684.9	3.4760	0.0057
53.057	37.16	0.16	29.9	-0.796	1.57	6.25	0.0269	-1.8326	4325.2	3.6152	0.0043
53.93	39.04	0.15	27.6	-0.824	1.592	6.6667	0.0256	-1.8971	3922.2	3.6646	0.0039
55.728	50.59	0.05	9.2	-1.301	1.704	20	0.0198	-2.9957	2359.7	3.9238	0.0024
57.47	55.49	0.02	3.4	-1.699	1.744	50	0.018	-3.9120	1953.6	4.0162	0.0020

Table 4.23: Pb Adsorption by Oil Bean Carbonized at 600°C and Activated with HCl

C_o (mg/l)	C_e (mg/l)	q_e (mg/g)	E (%)	$logq_e$	$logC_e$	$1/q_e$	$1/C_e$	Inq_e	ε^2	InC_e	$\varepsilon^2/1m$
35.724	30.68	0.05	14.1	-1.301	1.487	20	0.0326	-2.9957	6317.1	3.4236	0.0063
37.606	30.56	0.07	18.7	-1.155	1.485	14.2857	0.0327	-2.6593	6355.3	3.4197	0.0064
43.912	36.66	0.07	16.5	-1.155	1.564	14.2857	0.0273	-2.6593	4453.0	3.6017	0.0045
57.167	46.72	0.1	18.3	-1	1.67	10	0.0214	-2.3026	2752.1	3.8442	0.0028
57.381	48.14	0.09	16.1	-1.046	1.683	11.1111	0.0208	-2.4079	2601.5	3.8741	0.0026

Table 4.24: Pb Adsorption by Oil Bean Carbonized at 600°C and Activated with H_3PO_4

C_o (mg/l)	C_e (mg/l)	q_e (mg/g)	E (%)	$logq_e$	$logC_e$	$1/q_e$	$1/C_e$	Inq_e	ε^2	InC_e	$\varepsilon^2/1m$
35.724	28.55	0.07	20.1	-1.1549	1.4556	14.2857	0.035	-2.6593	7264.5	3.3517	0.0073
37.606	29.91	0.08	20.5	-1.0969	1.4758	12.5	0.0334	-2.5257	6625.8	3.3982	0.0066
43.912	34.71	0.09	21	-1.0458	1.5405	1.1111	0.0288	-2.4079	4948.5	3.5470	0.0049
57.167	44.66	0.13	21.9	-0.8861	1.6499	7.6923	0.0224	-2.0402	3012.4	3.7991	0.0030
57.381	39.87	0.18	30.5	-0.7447	1.6006	5.5556	0.0251	-1.7148	3772.3	3.6856	0.0038

Table 4.25: Pb Adsorption by Oil Bean Carbonized at 600°C and Activated with H_2SO_4

C_o (mg/l)	C_e (mg/l)	q_e (mg/g)	E (%)	$logq_e$	$logC_e$	$1/q_e$	$1/C_e$	Inq_e	ε^2	InC_e	$\varepsilon^2/1m$
35.724	29.36	0.06	17.8	-1.222	1.468	16.666	0.0341	-2.8134	6901.7	3.3796	0.0069
37.606	33.4	0.04	11.2	-1.398	1.524	25.000	0.0299	-3.2189	5328.1	3.5086	0.0053
43.912	40.16	0.04	8.5	-1.398	1.604	25.000	0.0249	-3.2189	3713.2	3.6929	0.0037
57.167	46.76	0.1	18.2	-1	1.67	10.000	0.0214	-2.3026	2752.1	3.8450	0.0028
57.381	48.88	0.09	14.8	-1.046	1.689	11.111	0.0205	-2.4079	2527.7	3.8894	0.0025

Table 4.26: Pb Adsorption by Oil Bean Carbonized at 800°C and Activated with HCl

C_o (mg/l)	C_e (mg/l)	q_e (mg/g)	E (%)	$logq_e$	$logC_e$	$1/q_e$	$1/C_e$	Inq_e	ε^2	InC_e	$\varepsilon^2/1m$
35.724	0.41	0.35	98.9	-0.4559	-0.3872	2.8571	2.439	-1.0498	9365125	-0.8916	9.3651
37.606	0.31	0.37	99.2	-0.4318	-0.5086	2.7027	3.2258	-0.9943	12749884	-1.1712	12.7499
43.912	0.57	0.43	98.7	-0.3665	-0.2441	2.3256	1.7544	-0.8440	6301480	-0.5621	6.3015
57.167	1.98	0.55	96.5	-0.2596	0.2967	1.8182	0.5051	-0.5978	1026125	0.6831	1.0261
57.381	2.31	0.55	96	-0.2596	0.3636	1.8182	0.4329	-0.5978	794208	0.8372	0.7942

Table 4.27: Pb Adsorption by Oil Bean Carbonized at 800°C and Activated with H_3PO_4

C_o (mg/l)	C_e (mg/l)	q_e (mg/g)	E (%)	$logq_e$	$logC_e$	$1/q_e$	$1/C_e$	Inq_e	ε^2	InC_e	$\varepsilon^2/1m$
35.724	0.48	0.35	98.7	-0.4559	-0.3188	2.8571	2.08333	-1.0498	7782823.9	-0.7340	7.7828
37.606	0.55	0.37	98.5	-0.4318	-0.2596	2.7027	1.8182	-0.9943	6589531.8	-0.5978	6.5895
43.912	1.38	0.43	96.9	-0.3665	0.1399	2.3256	0.7246	-0.8440	1823214.8	0.3221	1.8232
57.167	2.99	0.54	94.8	-0.2676	0.4757	1.8519	0.3344	-0.6162	510845.1	1.0953	0.5108
57.381	3.67	0.54	93.6	-0.2676	0.5647	1.8519	0.2725	-0.6162	356473.4	1.3002	0.3565

Table 4.28: Pb Adsorption by Oil Bean Carbonized at 800°C and Activated with H_2SO_4

C_o (mg/l)	C_e (mg/l)	q_e (mg/g)	E (%)	$logq_e$	$logC_e$	$1/q_e$	$1/C_e$	Inq_e	ε^2	InC_e	$\varepsilon^2/1m$
35.724	0.54	0.35	98.5	-0.4559	-0.2676	2.8571	1.8519	-1.0498	6741601.3	-0.6162	6.7416
37.606	0.07	0.38	99.8	-0.4202	-1.1549	2.6316	14.2857	-0.9676	45645361.0	-2.6593	45.6454
43.912	0.01	0.44	99.9	-0.3565	-2	2.2727	100	-0.8210	130743064.9	-4.6052	130.7431
57.167	0.3	0.57	99.5	-0.2441	-0.5288	1.7544	3.3333	-0.5621	13198228.4	-1.2040	13.1982
57.381	1.37	0.56	97.6	-0.2518	0.1367	1.7857	0.7299	-0.5798	1843802.9	0.3148	1.8438

Table 4.29: Mn Adsorption by Oil Bean Carbonized at 600°C and Activated with HCl

C_o (mg/l)	C_e (mg/l)	q_e (mg/g)	E (%)	$logq_e$	$logC_e$	$1/q_e$	$1/C_e$	Inq_e	ε^2	InC_e	$\varepsilon^2/1m$
75.046	69.42	0.06	7.5	-1.2218	1.8415	16.6667	0.0144	-2.8134	1254.8	4.2402	0.0013
114.686	109.55	0.05	4.5	-1.301	2.0396	20	0.0091	-2.9957	503.7	4.6964	0.0005
135.24	112.86	0.22	16.5	-0.6576	2.0525	4.5455	0.0089	-1.5141	481.9	4.7261	0.0005
145.137	120.14	0.25	17.5	-0.6021	2.0797	4	0.0083	-1.3863	419.4	4.7887	0.0004
147.28	118.11	0.29	19.8	-0.5376	2.0723	3.4483	0.0085	-1.2379	439.8	4.7716	0.0004

Table 4.30: Mn Adsorption by Oil Bean Carbonized at 600°C and Activated with H_3PO_4

C_o (mg/l)	C_e (mg/l)	q_e (mg/g)	E (%)	$logq_e$	$logC_e$	$1/q_e$	$1/C_e$	Inq_e	ε^2	InC_e	$\varepsilon^2/1m$
75.046	66.81	0.08	11	-1.0969	1.8248	12.5	0.0149	-2.5257	1342.7	4.2019	0.0013
114.686	109.4	0.05	4.6	-1.301	2.039	20	0.0091	-2.9957	503.7	4.6950	0.0005
135.24	120.3	0.15	11	-0.8239	2.0803	6.6667	0.0083	-1.8971	419.4	4.7900	0.0004
145.137	128.34	0.17	11.6	-0.7695	2.1084	5.8824	0.0078	-1.7720	370.6	4.8547	0.0004
147.28	138.56	0.09	5.9	-1.0458	2.1416	11.1111	0.0072	-2.4079	315.9	4.9313	0.0003

Table 4.31: Mn Adsorption by Oil Bean Carbonized at 600°C and Activated with H_2SO_4

C_o (mg/l)	C_e (mg/l)	q_e (mg/g)	E (%)	$logq_e$	$logC_e$	$1/q_e$	$1/C_e$	Inq_e	ε^2	InC_e	$\varepsilon^2/1m$
75.046	69.12	0.06	7.9	-1.2218	1.8396	16.6667	0.0145	-2.8134	1272.1	4.2358	0.0013
114.686	110.56	0.04	3.6	-1.3979	2.0436	25	0.009	-3.2189	492.8	4.7056	0.0005
135.24	127.4	0.07	5.8	-1.1549	2.1052	14.2857	0.0078	-2.6593	370.6	4.8473	0.0004
145.137	139.2	0.06	4.1	-1.2218	2.1436	16.6667	0.0072	-2.8134	315.9	4.9359	0.0003
147.28	142.7	0.05	3.1	-1.301	2.1544	20	0.007	-2.9957	298.7	4.9607	0.0003

Table 4.32: Mn Adsorption by Oil Bean Carbonized at 800°C and Activated with HCl

C_o (mg/l)	C_e (mg/l)	q_e (mg/g)	E (%)	$logq_e$	$logC_e$	$1/q_e$	$1/C_e$	Inq_e	ε^2	InC_e	$\varepsilon^2/1m$
75.046	9.51	0.66	87.3	-0.1805	0.9782	1.5151	0.1052	-0.4155	61415.9	2.2523	0.0614
114.686	6.66	1.08	94.2	0.0334	0.8235	0.9259	0.1502	0.0770	120201.7	1.8961	0.1202
135.24	9.011	1.26	93.3	0.1004	0.9548	0.7937	0.111	0.2311	68011.7	2.1984	0.0680
145.137	102.9	0.42	29.1	-0.3768	2.0124	2.381	0.0097	-0.8675	572.0	4.6338	0.0006
147.28	109.5	0.38	25.7	-0.4202	2.0394	2.6316	0.0091	-0.9676	503.7	4.6959	0.0005

Table 4.33: Mn Adsorption by Oil Bean Carbonized at 800°C and Activated with H_3PO_4

C_o (mg/l)	C_e (mg/l)	q_e (mg/g)	E (%)	$logq_e$	$logC_e$	$1/q_e$	$1/C_e$	Inq_e	ε^2	InC_e	$\varepsilon^2/1m$
75.046	1.06	0.74	98.6	-0.1308	0.0253	1.3514	0.9434	-0.3011	2709959.6	0.0583	2.7100
114.686	35.28	0.79	69.2	-0.1024	1.5475	1.2658	0.0283	-0.2357	4780.5	3.5633	0.0048
135.24	58.53	0.77	56.7	-0.1135	1.7674	1.2987	0.0171	-0.2614	1764.7	4.0695	0.0018
145.137	125.43	0.2	13.6	-0.699	2.0984	5	0.008	-1.6094	389.7	4.8317	0.0004
147.28	126.59	0.21	14.1	-0.6778	2.1024	4.7619	0.0079	-1.5606	380.1	4.8410	0.0004

Table 4.34: Mn Adsorption by Oil Bean Carbonized at 800°C and Activated with H_2SO_4

C_o (mg/l)	C_e (mg/l)	q_e (mg/g)	E (%)	$logq_e$	$logC_e$	$1/q_e$	$1/C_e$	Inq_e	ε^2	InC_e	$\varepsilon^2/1m$
75.046	26.57	0.48	64.6	-0.3188	1.4244	2.0833	0.0376	-0.7340	8362.7	3.2798	0.0084
114.686	42.53	0.72	62.9	-0.1427	1.6287	1.3889	0.0235	-0.3285	3311.9	3.7502	0.0033
135.24	72.12	0.63	46.7	-0.2007	1.8581	1.5873	0.0139	-0.4620	1169.7	4.2783	0.0012
145.137	119.48	0.26	17.7	-0.585	2.0773	3.8462	0.0084	-1.3471	429.5	4.7831	0.0004
147.28	119.55	0.28	18.8	-0.5528	2.0775	3.5714	0.0084	-1.2730	429.5	4.7837	0.0004

Table 4.35: Ni Adsorption by Pea nut Carbonized at 600°C and Activated with HCl

C_o (mg/l)	C_e (mg/l)	q_e (mg/g)	E (%)	$logq_e$	$logC_e$	$1/q_e$	$1/C_e$	Inq_e	ε^2	InC_e	$\varepsilon^2/1m$
55.47	21.81	0.34	60.7	-0.47	1.34	2.94	0.0459	-1.0788	12362.7	3.0824	0.0124
52.67	19.38	0.33	63.2	-0.48	1.29	3.03	0.0516	-1.1087	15538.5	2.9642	0.0155
59.35	23.654	0.36	60.1	-0.44	1.37	2.78	0.0423	-1.0217	10536.1	3.1635	0.0105
64.96	38.59	0.26	40.6	-0.59	1.59	3.85	0.0257	-1.3471	3952.5	3.6530	0.0040
66.797	65.631	0.01	1.74	-0.82	1.82	100	0.0152	-4.6052	1396.9	4.1840	0.0014

Table 4.36: Ni Adsorption by Pea nut Carbonized at 600°C and Activated with H_3PO_4

C_o (mg/l)	C_e (mg/l)	q_e (mg/g)	E (%)	$logq_e$	$logC_e$	$1/q_e$	$1/C_e$	Inq_e	ε^2	InC_e	$\varepsilon^2/1m$
55.47	27.13	0.28	51	-0.55	1.43	3.57	0.0369	-1.2730	8059.7	3.3006	0.0081
52.67	22.33	0.3	57.6	-0.52	1.35	3.33	0.0448	-1.2040	11789.8	3.1059	0.0118
59.352	32.198	0.27	45.7	-0.57	1.51	3.7	0.0311	-1.3093	5757.6	3.4719	0.0058
64.96	53.406	0.12	17.8	-0.92	1.73	8.33	0.0187	-2.1203	2107.1	3.9779	0.0021
66.797	61.35	0.05	8.2	-1.3	1.79	20	0.0162	-2.9957	1585.2	4.1166	0.0016

Table 4.37: Ni Adsorption by Pea nut Carbonized at 600°C and Activated with H_2SO_4

C_o (mg/l)	C_e (mg/l)	q_e (mg/g)	E (%)	$\log q_e$	$\log C_e$	$1/q_e$	$1/C_e$	$\ln q_e$	ε^2	$\ln C_e$	$\varepsilon^2/1m$
55.47	23.46	0.32	57.7	-0.49	1.37	3.125	0.0426	-1.1394	10682.9	3.1553	0.0107
52.67	21.29	0.31	59.6	-0.51	1.33	3.226	0.047	-1.1712	12948.7	3.0582	0.0129
59.352	31.78	0.28	46.5	-0.55	1.5	3.571	0.0315	-1.2730	5904.3	3.4588	0.0059
64.96	34.91	0.3	46.3	-0.52	1.54	3.333	0.0286	-1.2040	4881.0	3.5528	0.0049
66.797	38.67	0.28	42.1	-0.55	1.59	3.571	0.0259	-1.2730	4013.5	3.6551	0.0040

Table 4.38: Ni Adsorption by Pea nut Carbonized at 800°C and Activated with HCl

C_o (mg/l)	C_e (mg/l)	q_e (mg/g)	E (%)	$\log q_e$	$\log C_e$	$1/q_e$	$1/C_e$	$\ln q_e$	ε^2	$\ln C_e$	$\varepsilon^2/1m$
55.47	23.56	0.32	57.5	-0.4949	1.3722	3.125	0.0424	-1.1394	10584.9	3.1596	0.0106
52.67	19.91	0.33	62.1	-0.4815	1.2991	3.0303	0.0502	-1.1087	14726.6	2.9912	0.0147
59.352	37.799	0.23	36.3	-0.6383	1.5775	4.3478	0.0265	-1.4697	4199.1	3.6323	0.0042
64.96	57.357	0.08	11.8	-1.0969	1.7586	12.5	0.0174	-2.5257	1826.6	4.0493	0.0018
66.797	21.296	0.46	68.1	-0.3372	1.3282	2.1739	0.047	-0.7765	12948.7	3.0585	0.0129

Table 4.39: Ni Adsorption by Pea nut Carbonized at 800°C and Activated with H_3PO_4

C_o (mg/l)	C_e (mg/l)	q_e (mg/g)	E (%)	$\log q_e$	$\log C_e$	$1/q_e$	$1/C_e$	$\ln q_e$	ε^2	$\ln C_e$	$\varepsilon^2/1m$
55.47	21.86	0.34	60.6	-0.4685	1.3397	2.9412	0.0457	-1.0788	12257.6	3.0847	0.0123
52.67	27.91	0.25	47	-0.6021	1.4458	4	0.0358	-1.3863	7594.5	3.3290	0.0076
59.352	30.18	0.29	49.1	-0.5376	1.4797	3.4483	0.0331	-1.2379	6509.2	3.4072	0.0065
64.96	46.88	0.18	27.8	-0.7447	1.671	5.5556	0.0213	-1.7148	2726.7	3.8476	0.0027
66.797	42.61	0.24	36.2	-0.6198	1.6295	4.1667	0.0235	-1.4271	3311.9	3.7521	0.0033

Table 3.40: Ni Adsorption by Pea nut Carbonized at 800°C and Activated with H_2SO_4

C_o (mg/l)	C_e (mg/l)	q_e (mg/g)	E (%)	$\log q_e$	$\log C_e$	$1/q_e$	$1/C_e$	$\ln q_e$	ε^2	$\ln C_e$	$\varepsilon^2/1m$
55.47	27.8	0.28	21.6	-0.5528	1.444	3.5714	0.036	-1.2730	7678.1	3.3250	0.0077
52.67	21.67	0.31	58.9	-0.5086	1.3359	3.2258	0.0461	-1.1712	12468.3	3.0759	0.0125
59.352	24.9	0.34	58.1	-0.4685	1.3962	2.9412	0.0402	-1.0788	9535.2	3.2149	0.0095
64.96	47.36	0.18	27	-0.7447	1.6754	5.5556	0.0211	-1.7148	2676.3	3.8578	0.0027
66.797	44.31	0.22	33.7	-0.6576	1.6465	4.5455	0.0226	-1.5141	3065.8	3.7912	0.0031

Table 4.41: Pb Adsorption by Pea nut Carbonized at 600°C and Activated with HCl

C_o (mg/l)	C_e (mg/l)	q_e (mg/g)	E (%)	$\log q_e$	$\log C_e$	$1/q_e$	$1/C_e$	$\ln q_e$	ε^2	$\ln C_e$	$\varepsilon^2/1m$
35.7	0.57	0.35	98.4	-0.46	-0.24	2.86	1.75	-1.0498	6281610.3	-0.5621	6.2816
37.6	2.05	0.36	92.9	-0.44	0.31	2.78	0.49	-1.0217	976137.2	0.7178	0.9761
43.9	4.77	0.39	89.1	-0.41	0.68	2.56	0.21	-0.9416	223044.3	1.5623	0.2230
57.2	0.56	0.57	99	-0.24	-0.25	1.75	1.79	-0.5621	6462231.4	-0.5798	6.4622
57.4	2.42	0.55	95.8	-0.26	0.38	1.82	0.41	-0.5978	724657.6	0.8838	0.7247

Table 4.42: Pb Adsorption by Pea nut Carbonized at 600°C and Activated with H_3PO_4

C_o (mg/l)	C_e (mg/l)	q_e (mg/g)	E (%)	$\log q_e$	$\log C_e$	$1/q_e$	$1/C_e$	$\ln q_e$	ε^2	$\ln C_e$	$\varepsilon^2/1m$
35.7	0.5	0.35	98.6	-0.46	-0.3	2.86	2	-1.0498	7408690.9	-0.6931	7.4087
37.6	1.16	0.36	96.9	-0.44	0.06	2.78	0.86	-1.0217	2363976.8	0.1484	2.3640
43.9	0.83	0.43	98.1	-0.37	-0.08	2.33	1.2	-0.8440	3816005.5	-0.1863	3.8160
57.2	3.43	0.54	94	-0.27	0.54	1.85	0.29	-0.6162	398027.8	1.2326	0.3980
57.4	4.87	0.53	91.5	-0.28	0.69	1.89	0.21	-0.6349	223044.3	1.5831	0.2230

Table 4.43: Pb Adsorption by Pea nut Carbonized at 600°C and Activated with H_2SO_4

C_o (mg/l)	C_e (mg/l)	q_e (mg/g)	E (%)	$logq_e$	$logC_e$	$1/q_e$	$1/C_e$	Inq_e	ε^2	InC_e	$\varepsilon^2/1m$
35.7	0.86	0.35	97.6	-0.45	-0.07	2.86	1.16	-1.0498	3640458.5	-0.1508	3.6405
37.6	0.87	0.37	97.7	-0.43	-0.06	2.7	1.15	-0.9943	3596718.7	-0.1393	3.5967
43.9	0.58	0.43	98.7	-0.37	-0.24	2.33	1.72	-0.8440	6146122.9	-0.5447	6.1461
57.2	5.23	0.52	90.9	-0.28	0.72	1.92	0.19	-0.6539	185745.3	1.6544	0.1857
57.4	2.64	0.55	95.4	-0.26	0.42	1.82	0.38	-0.5978	636780.2	0.9708	0.6368

Table 4.44: Pb Adsorption by Pea nut Carbonized at 800°C and Activated with HCl

C_o (mg/l)	C_e (mg/l)	q_e (mg/g)	E (%)	$logq_e$	$logC_e$	$1/q_e$	$1/C_e$	Inq_e	ε^2	InC_e	$\varepsilon^2/1m$
35.7	4.26	0.31	87.5	-0.5086	0.6294	3.2258	0.2347	-1.1712	272840.8	1.4493	0.2728
37.6	2.38	0.35	93.6	-0.4559	0.3766	2.8571	0.4202	-1.0498	755381.0	0.8671	0.7554
43.9	0.49	0.43	98.8	-0.3665	-0.3098	2.3256	2.0408	-0.8440	7592003.0	-0.7133	7.5920
57.2	0.58	0.57	98.9	-0.2441	-0.2366	1.7544	1.7241	-0.5621	6164639.9	-0.5447	6.1646
57.4	0.71	0.57	98.8	-0.2441	-0.1487	1.7544	1.4058	-0.5621	4730699.3	-0.3425	4.7307

Table 4.45: Pb Adsorption by Pea nut Carbonized at 800°C and Activated with H_3PO_4

C_o (mg/l)	C_e (mg/l)	q_e (mg/g)	E (%)	$logq_e$	$logC_e$	$1/q_e$	$1/C_e$	Inq_e	ε^2	InC_e	$\varepsilon^2/1m$
35.7	8.91	0.27	75	-0.5528	0.9499	3.5714	0.1122	-1.3093	69413.9	2.1872	0.0694
37.6	19.16	0.18	49	-0.7447	1.2824	5.5556	0.0522	-1.7148	15892.8	2.9528	0.0159
43.9	28.9	0.15	34.1	-0.8239	1.4609	6.6667	0.0346	-1.8971	7102.2	3.3638	0.0071
57.2	37.89	0.19	33.8	-0.7212	1.5785	5.2632	0.0264	-1.6607	4167.9	3.6347	0.0042
57.4	40.1	0.17	30.1	-0.7696	1.6031	5.8824	0.0249	-1.7720	3713.2	3.6914	0.0037

Table 4.46: Pb Adsorption by Pea nut Carbonized at 800°C and Activated with H_2SO_4

C_o (mg/l)	C_e (mg/l)	q_e (mg/g)	E (%)	$logq_e$	$logC_e$	$1/q_e$	$1/C_e$	Inq_e	ε^2	InC_e	$\varepsilon^2/1m$
35.7	7.89	0.27	77.8	-0.5686	0.8971	3.7037	0.1267	-1.3093	87353.9	2.0656	0.0874
37.6	12.91	0.25	65.7	-0.6021	1.1109	4	0.0775	-1.3863	34200.9	2.5580	0.0342
43.9	26.8	0.17	38.9	-0.7696	1.4281	5.8824	0.0373	-1.7720	8232.2	3.2884	0.0082
57.2	33.7	0.24	41	-0.6198	1.5276	4.1667	0.0297	-1.4271	5258.0	3.5175	0.0053
57.4	41.66	0.16	27.4	-0.7959	1.6199	6.25	0.024	-1.8326	3452.7	3.7295	0.0035

Table 4.47: Cd Adsorption by Pea nut Carbonized at 600°C and Activated with HCl

C_o (mg/l)	C_e (mg/l)	q_e (mg/g)	E (%)	$logq_e$	$logC_e$	$1/q_e$	$1/C_e$	Inq_e	ε^2	InC_e	$\varepsilon^2/1m$
53.66	20.32	0.33	62.1	-0.4815	1.3079	3.0303	0.0492	-1.1087	14159.3	3.0116	0.0142
53.06	28.59	0.24	46.1	-0.6198	1.4562	4.1667	0.035	-1.4271	7264.5	3.3531	0.0073
53.9	36.118	0.18	33	-0.7447	1.5577	5.5556	0.0277	-1.7148	4582.7	3.5868	0.0046
55.7	50.32	0.05	9.7	-1.301	1.7017	20	0.0199	-2.9957	2383.3	3.9184	0.0024
57.47	55.37	0.02	3.7	-1.699	1.7433	50	0.0181	-3.9120	1975.2	4.0140	0.0020

Table 4.48: Cd Adsorption by Pea nut Carbonized at 600°C and Activated with H_3PO_4

C_o (mg/l)	C_e (mg/l)	q_e (mg/g)	E (%)	$logq_e$	$logC_e$	$1/q_e$	$1/C_e$	Inq_e	ε^2	InC_e	$\varepsilon^2/1m$
53.66	34.38	0.19	36	-0.7212	1.5363	5.2632	0.0291	-1.6607	5050.7	3.5375	0.0051
53.06	31.3	0.22	41	-0.6576	1.4955	4.5455	0.0319	-1.5141	6052.9	3.4436	0.0061
53.9	30.5	0.23	43.4	-0.6383	1.4843	4.3478	0.0328	-1.4697	6393.6	3.4177	0.0064
55.7	49.06	0.07	11.9	-1.1549	1.6907	14.2857	0.0204	-2.6593	2503.4	3.8930	0.0025
57.47	55.03	0.02	4.2	-1.6889	1.7406	50	0.0182	-3.9120	1996.9	4.0079	0.0020

Table 4.49: Cd Adsorption by Pea nut Carbonized at 600°C and Activated with H_2SO_4

C_o (mg/l)	C_e (mg/l)	q_e (mg/g)	E (%)	$logq_e$	$logC_e$	$1/q_e$	$1/C_e$	Inq_e	ε^2	InC_e	$\varepsilon^2/1m$
53.66	34.8	0.19	35.1	-0.7212	1.5416	5.2632	0.0287	-1.6607	4914.7	3.5496	0.0049
53.06	35.6	0.17	32.9	-0.7696	1.5515	5.8824	0.0281	-1.7720	4714.1	3.5723	0.0047
53.9	36.5	0.17	32.3	-0.7696	1.5623	5.8824	0.0274	-1.7720	4485.3	3.5973	0.0045
55.7	49.66	0.06	10.9	-1.2218	1.696	16.6667	0.0201	-2.8134	2431.0	3.9052	0.0024
57.47	50.03	0.07	19.9	-1.1549	1.6992	14.2857	0.0199	-2.6593	2383.3	3.9126	0.0024

Table 4.50: Cd Adsorption by Pea nut Carbonized at 800°C and Activated with HCl

C_o (mg/l)	C_e (mg/l)	q_e (mg/g)	E (%)	$logq_e$	$logC_e$	$1/q_e$	$1/C_e$	Inq_e	ε^2	InC_e	$\varepsilon^2/1m$
53.66	20.56	0.33	61.7	-0.4815	1.313	3.0303	0.0486	-1.1087	13824.0	3.0233	0.0138
53.06	23.01	0.3	56.6	-0.5229	1.3619	3.3333	0.0435	-1.2040	11129.4	3.1359	0.0111
53.9	28.1	0.26	47.8	-0.585	1.4487	3.8462	0.0356	-1.3471	7511.3	3.3358	0.0075
55.7	49.6	0.06	10.9	-1.2218	1.6955	16.6667	0.0202	-2.8134	2455.0	3.9040	0.0025
57.47	55.5	0.02	3.4	-1.699	1.7443	50	0.018	-3.9120	1953.6	4.0164	0.0020

Table 4.51: Cd Adsorption by Pea nut Carbonized at 800°C and Activated with H_3PO_4

C_o (mg/l)	C_e (mg/l)	q_e (mg/g)	E (%)	$logq_e$	$logC_e$	$1/q_e$	$1/C_e$	Inq_e	ε^2	InC_e	$\varepsilon^2/1m$
53.66	32.61	0.21	39.2	-0.6778	1.5134	4.7619	0.0307	-1.5606	5612.6	3.4846	0.0056
53.06	40.3	0.13	24	-0.8861	1.6053	7.6923	0.0248	-2.0402	3683.8	3.6964	0.0037
53.9	39.16	0.15	27.3	-0.8239	1.5928	6.6667	0.0255	-1.8971	3892.0	3.6677	0.0039
55.7	46.7	0.09	16.1	-1.0458	1.6693	11.1111	0.0214	-2.4079	2752.1	3.8437	0.0028
57.47	41.9	0.16	27	-0.7959	1.6222	6.25	0.0239	-1.8326	3424.3	3.7353	0.0034

Table 4.52: Cd Adsorption by Pea nut Carbonized at 800°C and Activated with H_2SO_4

C_o (mg/l)	C_e (mg/l)	q_e (mg/g)	E (%)	$logq_e$	$logC_e$	$1/q_e$	$1/C_e$	Inq_e	ε^2	InC_e	$\varepsilon^2/1m$
53.66	28.36	0.25	47.1	-0.6021	1.4527	4	0.0353	-1.3863	7387.4	3.3450	0.0074
53.06	36.2	0.17	31.8	-0.7696	1.5587	5.8824	0.0276	-1.7720	4550.1	3.5891	0.0046
53.9	5.69	0.49	89.4	-0.3098	0.7551	2.0408	0.1757	-0.7133	160824.3	1.7387	0.1608
55.7	33.16	0.23	40.4	-0.6383	1.5206	4.3478	0.0302	-1.4697	5433.9	3.5013	0.0054
57.47	32.14	0.25	44	-0.6021	1.507	4	0.0311	-1.3863	5757.6	3.4701	0.0058

Table 4.53: Mn Adsorption by Pear nut Carbonized at 600°C and Activated with HCl

C_o (mg/l)	C_e (mg/l)	q_e (mg/g)	E (%)	$logq_e$	$logC_e$	$1/q_e$	$1/C_e$	Inq_e	ε^2	InC_e	$\varepsilon^2/1m$
75.05	30.03	0.45	60	-0.3468	1.4776	2.2222	0.0333	-0.7985	6586.8	3.4022	0.0066
114.69	34.65	0.8	69.8	-0.0969	1.5397	1.25	0.0289	-0.2231	4982.5	3.5453	0.0050
135.2	48.68	0.86	64	-0.0655	1.6874	1.1628	0.0205	-0.1508	2527.7	3.8853	0.0025
145.14	71.92	0.73	50.4	-0.1367	1.8568	1.3699	0.0139	-0.3147	1169.7	4.2756	0.0012
147.28	69.7	0.78	52.6	-0.1079	1.8432	1.2821	0.0143	-0.2485	1237.5	4.2442	0.0012

Table 4.54: Mn Adsorption by Pea nut Carbonized at 600°C and Activated with H_2SO_4

C_o (mg/l)	C_e (mg/l)	q_e (mg/g)	E (%)	$logq_e$	$logC_e$	$1/q_e$	$1/C_e$	Inq_e	ε^2	InC_e	$\varepsilon^2/1m$
75.05	37.19	0.38	50.4	-0.4202	1.5704	2.6316	0.0269	-0.9676	4325.2	3.6160	0.0043
114.69	59.25	0.55	48.3	-0.2596	1.7727	1.8182	0.0169	-0.5978	1724.0	4.0818	0.0017
135.2	91.25	0.44	32.5	-0.3565	1.9602	2.2727	0.011	-0.8210	734.7	4.5136	0.0007
145.14	128	0.17	11.8	-0.7696	2.1072	5.8824	0.0078	-1.7720	370.6	4.8520	0.0004
147.28	116.56	0.31	20.9	-0.5086	2.0665	3.2258	0.0086	-1.1712	450.1	4.7584	0.0005

Table 4.55: Mn Adsorption by Pea nut Carbonized at 600°C and Activated with H_3PO_4

C_o (mg/l)	C_e (mg/l)	q_e (mg/g)	E (%)	$logq_e$	$logC_e$	$1/q_e$	$1/C_e$	Inq_e	ε^2	InC_e	$\varepsilon^2/1m$
75.05	30.05	0.45	59.9	-0.3468	1.478	2.2222	0.0333	-0.7985	6586.8	3.4029	0.0066
114.69	67.81	0.47	40.9	-0.3279	1.8313	2.1277	0.0147	-0.7550	1307.2	4.2167	0.0013
135.2	68.66	0.67	49.2	-1739	1.8367	1.4925	0.0146	-0.4005	1289.6	4.2292	0.0013
145.14	142.75	0.24	1.6	-0.6198	2.1546	4.1667	0.007	-1.4271	298.7	4.9611	0.0003
147.28	118.4	0.29	19.6	-0.5376	2.0734	3.4483	0.0084	-1.2379	429.5	4.7741	0.0004

Table 4.56: Mn Adsorption by Pea nut Carbonized at 800°C and Activated with HCl

C_o (mg/l)	C_e (mg/l)	q_e (mg/g)	E (%)	$logq_e$	$logC_e$	$1/q_e$	$1/C_e$	Inq_e	ε^2	InC_e	$\varepsilon^2/1m$
75.05	30.162	0.45	59.8	-0.3468	1.4795	2.2222	0.0332	-0.7985	6548.0	3.4066	0.0065
114.69	46.61	0.68	59.5	-0.1675	1.6685	1.4706	0.0215	-0.3857	2777.6	3.8418	0.0028
135.2	76.34	0.59	43.6	-0.2291	1.8828	1.6949	0.0131	-0.5276	1039.8	4.3352	0.0010
145.14	132.2	0.13	8.9	-0.8861	2.1212	7.6923	0.0076	-2.0402	351.9	4.8843	0.0004
147.28	136.6	0.11	7.3	-0.9586	2.1355	9.091	0.0073	-2.2073	324.7	4.9171	0.0003

Table 4.57: Mn Adsorption by Pea nut Carbonized at 800°C and Activated with H_3PO_4

C_o (mg/l)	C_e (mg/l)	q_e (mg/g)	E (%)	$logq_e$	$logC_e$	$1/q_e$	$1/C_e$	Inq_e	ε^2	InC_e	$\varepsilon^2/1m$
75.05	21.67	0.53	71.1	-0.2757	1.3359	1.8868	0.0461	-0.6349	12468.3	3.0759	0.0125
114.69	42.6	0.72	62.9	-0.1427	1.6294	1.6294	0.0235	-0.3285	3311.9	3.7519	0.0033
135.2	72.5	0.63	46.4	-0.2007	1.8603	1.8603	0.0138	-0.4620	1153.1	4.2836	0.0012
145.14	117.9	0.27	18.8	-0.5686	2.0715	3.0715	0.0085	-1.3093	439.8	4.7698	0.0004
147.28	129.6	0.18	12.3	-0.7447	2.1126	5.1126	0.0077	-1.7148	361.2	4.8645	0.0004

Table 4.58: Mn Adsorption by Pea nut Carbonized at 800°C and Activated with H_2SO_4

C_o (mg/l)	C_e (mg/l)	q_e (mg/g)	E (%)	$logq_e$	$logC_e$	$1/q_e$	$1/C_e$	Inq_e	ε^2	InC_e	$\varepsilon^2/1m$
75.05	11.35	0.64	84.8	-0.1938	1.055	1.5625	0.0881	-0.4463	43760.0	2.4292	0.0438
114.69	22.29	0.92	80.6	-0.0362	1.3481	1.087	0.0449	-0.0834	11841.3	3.1041	0.0118
135.2	47.9	0.87	64.6	-0.0605	1.6803	1.1494	0.0209	-0.1393	2626.3	3.8691	0.0026
145.14	84.6	0.61	41.7	-0.2147	1.9274	1.6393	0.0118	-0.4943	844.7	4.4379	0.0008
147.28	136.8	0.1	7.1	-1	2.1361	10	0.0073	-2.3026	324.7	4.9185	0.0003

Table 4.59: Ni Adsorption by Palm Kernel shell Carbonized at 600°C and Activated with HCl

C_o (mg/l)	C_e (mg/l)	q_e (mg/g)	E (%)	$logq_e$	$logC_e$	$1/q_e$	$1/C_e$	Inq_e	ε^2	InC_e	$\varepsilon^2/1m$
55.47	32.6	0.23	41.2	-0.6383	1.5132	4.3478	0.0307	-1.4697	5612.6	3.4843	0.0056
52.67	33.56	0.19	36.2	-0.7212	1.5258	5.2632	0.0298	-1.6607	5293.0	3.5133	0.0053
59.35	35.62	0.24	39.9	-0.6198	1.5517	4.1667	0.0281	-1.4271	4714.1	3.5729	0.0047
64.96	52.08	0.13	19.8	-0.8861	1.7167	7.6923	0.0192	-2.0402	2220.2	3.9528	0.0022
66.79	60.64	0.06	9.2	-1.2218	1.7828	16.6667	0.0165	-2.8134	1644.0	4.1050	0.0016

Table 4.60: Ni Adsorption by Palm Kernel shell Carbonized at 600°C and Activated with H_3PO_4

C_o (mg/l)	C_e (mg/l)	q_e (mg/g)	E (%)	$logq_e$	$logC_e$	$1/q_e$	$1/C_e$	Inq_e	ε^2	InC_e	$\varepsilon^2/1m$
55.47	21.31	0.34	61.6	-0.4685	1.3285	2.9412	0.0469	-1.0788	12894.9	3.0592	0.0129
52.67	16.16	0.37	69.3	-0.4318	1.20844	2.7027	0.0619	-0.9943	22142.1	2.7825	0.0221
59.35	7.15	0.52	87.9	-0.284	0.8543	1.9231	0.1399	-0.6539	105244.8	1.9671	0.1052
64.96	17.79	0.47	72.6	-0.3279	1.2502	2.1277	0.0562	-0.7550	18351.5	2.8786	0.0184
66.79	45.74	0.21	31.5	-0.6778	1.6603	4.7619	0.0219	-1.5606	2880.8	3.8230	0.0029

Table 4.61: Ni Adsorption by Palm Kernel shell Carbonized at 600°C and Activated with H_2SO_4

C_o (mg/l)	C_e (mg/l)	q_e (mg/g)	E (%)	$logq_e$	$logC_e$	$1/q_e$	$1/C_e$	Inq_e	ε^2	InC_e	$\varepsilon^2/1m$
55.47	42.3	0.13	23.7	-0.8861	1.6263	7.6923	0.0236	-2.0402	3339.8	3.7448	0.0033
52.67	39.81	0.13	24.4	-0.8861	1.5999	7.6923	0.0251	-2.0402	3772.3	3.6841	0.0038
59.35	48.9	0.1	17.6	-1	1.6893	10	0.0204	-2.3026	2503.4	3.8898	0.0025
64.96	53.08	0.12	18.3	-1.9208	1.7249	8.3333	0.0188	-2.1203	2129.4	3.9718	0.0021
66.79	58.8	0.08	11.9	-1.0969	1.7694	12.5	0.017	-2.5257	1744.3	4.0741	0.0017

Table 4.62: Ni Adsorption by Palm Kernel shell Carbonized at 800°C and Activated with HCl

C_o (mg/l)	C_e (mg/l)	q_e (mg/g)	E (%)	$logq_e$	$logC_e$	$1/q_e$	$1/C_e$	Inq_e	ε^2	InC_e	$\varepsilon^2/1m$
55.47	25.56	0.3	53.9	-0.5229	1.4076	3.3333	0.0346	-1.2040	7102.2	3.2410	0.0071
52.67	28.96	0.24	45	-0.6198	1.4618	4.1667	0.0381	-1.4271	8582.5	3.3659	0.0086
59.35	30.44	0.29	48.7	-0.5376	1.4834	3.4483	0.0343	-1.2379	6981.6	3.4158	0.0070
64.96	49.68	0.15	23.5	-0.8239	1.6962	6.6667	0.0197	-1.8971	2336.1	3.9056	0.0023
66.79	64.15	0.03	3.96	-1.5229	1.8072	33.3333	0.0186	-3.5066	2084.8	4.1612	0.0021

Table 4.63: Ni Adsorption by Palm Kernel shell Carbonized at 800°C and Activated with H_3PO_4

C_o (mg/l)	C_e (mg/l)	q_e (mg/g)	E (%)	$logq_e$	$logC_e$	$1/q_e$	$1/C_e$	Inq_e	ε^2	InC_e	$\varepsilon^2/1m$
55.47	28.9	0.27	47.9	-0.5686	1.4609	3.7037	0.0346	-1.3093	7102.2	3.3638	0.0071
52.67	26.22	0.26	50.2	-0.585	1.4186	3.8462	0.0381	-1.3471	8582.5	3.2665	0.0086
59.35	29.12	0.3	50.9	-0.5229	1.4642	3.3333	0.0343	-1.2040	6981.6	3.3714	0.0070
64.96	50.77	0.14	21.9	-0.8539	1.7056	7.1429	0.0197	-1.9661	2336.1	3.9273	0.0023
66.79	53.81	0.13	19.4	-0.8861	1.7309	7.6923	0.0186	-2.0402	2084.8	3.9855	0.0021

Table 4.64: Ni Adsorption by Palm Kernel shell Carbonized at 800°C and Activated with H_2SO_4

C_o (mg/l)	C_e (mg/l)	q_e (mg/g)	E (%)	$logq_e$	$logC_e$	$1/q_e$	$1/C_e$	Inq_e	ε^2	InC_e	$\varepsilon^2/1m$
55.47	12.38	0.43	77.7	-0.3665	1.0927	2.3256	0.0808	-0.8440	37060.5	2.5161	0.0371
52.67	11.96	0.41	77.3	-0.3872	1.0777	2.439	0.0836	-0.8916	39569.7	2.4816	0.0396
59.35	14.49	0.45	75.6	-0.5468	1.1611	2.2222	0.069	-0.7985	27328.3	2.6735	0.0273
64.96	31.95	0.33	50.8	-0.4815	1.5044	3.0303	0.0313	-1.1087	5830.7	3.4642	0.0058
66.79	55.99	0.11	16.2	-0.9586	1.7481	9.0909	0.0179	-2.2073	1932.2	4.0252	0.0019

Table 4.65: Pb Adsorption by Palm Kernel shell Carbonized at 600°C and Activated with HCl

C_o (mg/l)	C_e (mg/l)	q_e (mg/g)	E (%)	$logq_e$	$logC_e$	$1/q_e$	$1/C_e$	Inq_e	ε^2	InC_e	$\varepsilon^2/1m$
35.7	0.5	0.35	98.6	-0.4559	-0.301	2.8571	2	-1.0498	7408690.9	-0.6931	7.4087
37.6	0.88	0.37	97.7	-0.4318	-0.0522	2.7027	1.1364	-0.9943	3537332.8	-0.1278	3.5373
43.9	1.67	0.42	96.2	-0.3768	0.2227	2.3809	0.5988	-0.8675	1351659.6	0.5128	1.3517
57.2	6.32	0.51	88.9	-0.2924	0.807	1.9608	0.1582	-0.6733	132404.1	1.8437	0.1324
57.4	7.1	0.5	87.6	-0.301	0.8513	2	0.1408	-0.6931	106517.4	1.9601	0.1065

Table 4.66: Pb Adsorption by Palm Kernel shell Carbonized at 600°C and Activated with H_3PO_4

C_o (mg/l)	C_e (mg/l)	q_e (mg/g)	E (%)	$logq_e$	$logC_e$	$1/q_e$	$1/C_e$	Inq_e	ε^2	InC_e	$\varepsilon^2/1m$
35.7	16.34	0.19	54.3	-0.7212	1.2133	5.2632	0.0612	-1.6607	21658.6	2.7936	0.0217
37.6	22.3	0.15	40.7	-0.8239	1.3483	6.6667	0.0448	-1.8971	11789.8	3.1046	0.0118
43.9	27.9	0.16	36.4	-0.7959	1.4456	6.25	0.0358	-1.8326	7594.5	3.3286	0.0076
57.2	38.11	0.19	33.3	-0.7212	1.581	5.2632	0.0262	-1.6607	4105.8	3.6405	0.0041
57.4	35.6	0.22	37.9	-0.6576	1.5515	4.5455	0.0281	-1.5141	4714.1	3.5723	0.0047

Table 4.67: Pb Adsorption by Palm Kernel shell Carbonized at 600°C and Activated with H_2SO_4

C_o (mg/l)	C_e (mg/l)	q_e (mg/g)	E (%)	$logq_e$	$logC_e$	$1/q_e$	$1/C_e$	Inq_e	ε^2	InC_e	$\varepsilon^2/1m$
35.7	5.81	0.29	83.7	-0.5376	0.7642	3.4483	0.1721	-1.2379	154788.0	1.7596	0.1548
37.6	7.15	0.3	80.9	-0.5229	0.8543	3.3333	0.1399	-1.2040	105244.8	1.9671	0.1052
43.9	16.2	0.28	63.1	-0.5528	1.2095	3.5714	0.0617	-1.2730	22003.5	2.7850	0.0220
57.2	29.7	0.27	40	-0.5686	1.4728	3.7037	0.0337	-1.3093	6743.4	3.3911	0.0067
57.4	28.3	0.29	43.7	-0.5376	1.4518	3.4483	0.0353	-1.2379	7387.4	3.3429	0.0074

Table 4.68: Pb Adsorption by Palm Kernel shell Carbonized at 800°C and Activated with HCl

C_o (mg/l)	C_e (mg/l)	q_e (mg/g)	E (%)	$logq_e$	$logC_e$	$1/q_e$	$1/C_e$	Inq_e	ε^2	InC_e	$\varepsilon^2/1m$
35.7	4.28	0.31	88	-0.5086	0.6314	3.2258	0.2336	-1.1712	270538.7	1.4540	0.2705
37.6	5.87	0.32	84.4	-0.4949	0.7686	3.125	0.1704	-1.1394	151971.3	1.7699	0.1520
43.9	11.38	0.33	74	-0.4815	1.0561	3.0303	0.0879	-1.1087	43569.7	2.4319	0.0436
57.2	19.98	0.37	65	-0.4318	1.3006	2.7027	0.0501	-0.9943	14669.4	2.9947	0.0147
57.4	18.77	0.39	67.3	-0.4089	1.2735	2.5641	0.0533	-0.9416	16552.3	2.9323	0.0166

Table 4.69: Pb Adsorption by Palm Kernel shell Carbonized at 800°C and Activated with H_3PO_4

C_o (mg/l)	C_e (mg/l)	q_e (mg/g)	E (%)	$logq_e$	$logC_e$	$1/q_e$	$1/C_e$	Inq_e	ε^2	InC_e	$\varepsilon^2/1m$
35.7	4.78	0.31	86.6	-0.5086	0.6794	3.2259	0.2092	-1.1712	221499.2	1.5644	0.2215
37.6	1.59	0.36	95.8	-0.4437	0.2014	2.7778	0.6289	-1.0217	1461244.9	0.4637	1.4612
43.9	6.96	0.37	84.1	-0.4318	0.8426	2.7027	0.1437	-0.9943	110662.8	1.9402	0.1107
57.2	14.2	0.43	75.1	-0.3665	1.1523	2.3256	0.0704	-0.8440	28410.9	2.6532	0.0284
57.4	16.77	41	70.8	-0.3872	1.2245	2.439	0.0596	3.7136	20572.3	2.8196	0.0206

Table 4.70: Pb Adsorption by Palm Kernel shell Carbonized at 800°C and Activated with H_2SO_4

C_o (mg/l)	C_e (mg/l)	q_e (mg/g)	E (%)	$logq_e$	$logC_e$	$1/q_e$	$1/C_e$	Inq_e	ε^2	InC_e	$\varepsilon^2/1m$
35.7	3.66	0.32	89.8	-0.4949	0.5635	3.125	0.2732	-1.1394	358102.2	1.2975	0.3581
37.6	6.81	0.31	81.9	-0.5086	0.8331	3.2258	0.1468	-1.1712	115169.7	1.9184	0.1152
43.9	13.9	0.3	68.3	-0.5229	1.143	3.3333	0.0719	-1.2040	29592.5	2.6319	0.0296
57.2	33.6	0.24	41.2	-0.6198	1.5263	4.1667	0.0298	-1.4271	5293.0	3.5145	0.0053
57.4	37.5	0.2	34.6	-0.699	1.574	5	0.0267	-1.6094	4261.9	3.6243	0.0043

Table 4.71: Cd Adsorption by Palm Kernel shell Carbonized at 600°C and Activated with HCl

C_o (mg/l)	C_e (mg/l)	q_e (mg/g)	E (%)	$logq_e$	$logC_e$	$1/q_e$	$1/C_e$	Inq_e	ε^2	InC_e	$\varepsilon^2/1m$
53.66	27.11	0.27	49.4	-0.5686	1.4331	3.7037	0.0369	-1.3093	8059.7	3.2999	0.0081
53.06	28.56	0.24	46.1	-0.6198	1.4558	4.1667	0.035	-1.4271	7264.5	3.3520	0.0073
53.93	30.27	0.24	43.9	-0.6198	1.481	4.1667	0.033	-1.4271	6470.6	3.4102	0.0065
55.73	48.61	0.07	12.7	-1.1549	1.6867	14.2857	0.0206	-2.6593	2552.2	3.8838	0.0026
57.47	55.57	0.02	3.3	-1.699	1.7448	50	0.018	-3.9120	1953.6	4.0176	0.0020

Table 4.72: Cd Adsorption by Palm Kernel shell Carbonized at 600°C and Activated with H_3PO_4

C_o (mg/l)	C_e (mg/l)	q_e (mg/g)	E (%)	$logq_e$	$logC_e$	$1/q_e$	$1/C_e$	Inq_e	ε^2	InC_e	$\varepsilon^2/1m$
53.66	2.41	0.51	95.5	-0.2924	0.382	1.9608	0.4149	-0.6733	739364.9	0.8796	0.7394
53.06	2.36	0.51	95.6	-0.2924	0.3729	1.9608	0.4237	-0.6733	766018.6	0.8587	0.7660
53.93	1.14	0.53	53.9	-0.2757	0.0569	1.8868	0.8772	-0.6349	2434625.1	0.1310	2.4346
55.73	6.46	0.49	88.4	-0.3098	0.8102	2.0408	0.1548	-0.7133	127156.4	1.8656	0.1272
57.47	19.84	0.38	65.4	-0.4202	1.2975	2.6316	0.0504	-0.9676	14841.3	2.9877	0.0148

Table 4.73: Cd Adsorption by Palm Kernel shell Carbonized at 600°C and Activated with H_2SO_4

C_o (mg/l)	C_e (mg/l)	q_e (mg/g)	E (%)	$logq_e$	$logC_e$	$1/q_e$	$1/C_e$	Inq_e	ε^2	InC_e	$\varepsilon^2/1m$
53.66	6.11	0.48	88.6	-0.3188	0.786	2.0833	0.1637	-0.7340	141083.8	1.8099	0.1411
53.06	5.72	0.47	89.2	-0.3279	0.7574	2.1277	0.1748	-0.7550	159306.1	1.7440	0.1593
53.93	8.99	0.45	83.3	-0.3467	0.9538	2.2222	0.1112	-0.7985	68244.5	2.1961	0.0682
55.73	15.12	0.41	72.8	-0.3872	1.1796	2.439	0.0661	-0.8916	25148.3	2.7160	0.0251
57.47	17.36	0.4	69.7	-0.3979	1.2395	2.5	0.0576	-0.9163	19251.4	2.8542	0.0193

Table 4.74: Cd Adsorption by Palm Kernel shell Carbonized at 800°C and Activated with HCl

C_o (mg/l)	C_e (mg/l)	q_e (mg/g)	E (%)	$logq_e$	$logC_e$	$1/q_e$	$1/C_e$	Inq_e	ε^2	InC_e	$\varepsilon^2/1m$
53.66	29.15	0.25	45.6	-0.6021	1.4646	4	0.0343	-1.3863	6981.6	3.3725	0.0070
53.06	30.66	0.22	42.2	-0.6576	1.4866	4.5455	0.0326	-1.5141	6317.1	3.4230	0.0063
53.93	32.07	0.22	40.5	-0.6576	1.5061	4.5455	0.0312	-1.5141	5794.1	3.4679	0.0058
55.73	49.14	0.66	11.8	-0.1805	1.6914	1.5152	0.0204	-0.4155	2503.4	3.8947	0.0025
57.47	55.34	0.02	3.7	-0.699	1.743	50	0.0181	-3.9120	1975.2	4.0135	0.0020

Table 4.75: Cd Adsorption by Palm Kernel shell Carbonized at 800°C and Activated with H_3PO_4

C_o (mg/l)	C_e (mg/l)	q_e (mg/g)	E (%)	$logq_e$	$logC_e$	$1/q_e$	$1/C_e$	Inq_e	ε^2	InC_e	$\varepsilon^2/1m$
53.66	5.28	0.48	90.1	-0.3188	0.7226	2.0833	0.1894	-0.7340	184669.9	1.6639	0.1847
53.06	6.77	0.46	87.2	-0.3372	0.8306	2.1739	0.1477	-0.7765	116492.6	1.9125	0.1165
53.93	8.1	0.46	84.9	-0.3372	0.9085	2.1739	0.1235	-0.7765	83238.2	2.0919	0.0832
55.73	9.1	0.47	83.6	-0.3279	0.959	2.1277	0.1099	-0.7550	66737.6	2.2083	0.0667
57.47	15.67	0.42	72.7	-0.3768	1.1951	2.381	0.0638	-0.8675	23479.9	2.7517	0.0235

Table 4.76: Cd Adsorption by Palm Kernel shell Carbonized at 800°C and Activated with H_2SO_4

C_o (mg/l)	C_e (mg/l)	q_e (mg/g)	E (%)	$logq_e$	$logC_e$	$1/q_e$	$1/C_e$	Inq_e	ε^2	InC_e	$\varepsilon^2/1m$
53.66	9.1	0.45	83.2	-0.3468	0.959	2.2222	0.1099	-0.7985	66737.6	2.2083	0.0667
53.06	8.76	0.44	83.4	-0.3565	0.9425	2.2727	0.1142	-0.8210	71779.2	2.1702	0.0718
53.93	7.32	0.47	86.4	-0.3279	0.8645	2.1277	0.1366	-0.7550	100635.9	1.9906	0.1006
55.73	4.49	0.51	91.9	-0.2757	0.6522	1.9608	0.2227	-0.6733	248147.9	1.5019	0.2481
57.47	4.14	0.03	5.8	-1.5229	1.7335	33.3333	0.0185	-3.5066	2062.6	1.4207	0.0021

Table 4.77: Mn Adsorption by Palm Kernel shell Carbonized at 600°C and Activated with HCl

C_o (mg/l)	C_e (mg/l)	q_e (mg/g)	E (%)	$logq_e$	$logC_e$	$1/q_e$	$1/C_e$	Inq_e	ε^2	InC_e	$\varepsilon^2/1m$
75.05	0.67	0.74	99.1	-0.1308	-0.1739	1.3514	1.4925	-0.3011	5119957.8	-0.4005	5.1200
114.69	16.16	0.99	85.9	-0.0044	1.2084	1.0101	0.0619	-0.0101	22142.1	2.7825	0.0221
135.2	28.3	1.07	79	0.0294	1.4518	0.9346	0.0353	0.0677	7387.4	3.3429	0.0074
145.14	40.65	1.04	71.9	0.017	1.6091	0.9615	0.0246	0.0392	3625.3	3.7050	0.0036
147.28	38.91	1.08	73.5	0.0334	1.5901	0.9259	0.0257	0.0770	3952.5	3.6613	0.0040

Table 4.78: Mn Adsorption by Palm Kernel shell Carbonized at 600°C and Activated with H_3PO_4

C_o (mg/l)	C_e (mg/l)	q_e (mg/g)	E (%)	$logq_e$	$logC_e$	$1/q_e$	$1/C_e$	Inq_e	ε^2	InC_e	$\varepsilon^2/1m$
75.05	28.12	0.47	62.5	-0.3279	1.449	2.1277	0.0356	-0.7550	7511.3	3.3365	0.0075
114.69	66.79	0.48	41.8	-0.3188	1.8247	2.0833	0.015	-0.7340	1360.7	4.2016	0.0014
135.2	86.79	0.48	35.9	-0.3188	1.9385	2.0833	0.0115	-0.7340	802.6	4.4635	0.0008
145.14	91.14	0.54	37.2	-0.2676	1.9597	1.8519	0.011	-0.6162	734.7	4.5124	0.0007
147.28	99.6	0.48	32.3	-0.3188	1.9983	2.0833	0.01	-0.7340	607.8	4.6012	0.0006

Table 4.79: Mn Adsorption by Palm Kernel shell Carbonized at 600°C and Activated with H_2SO_4

C_o (mg/l)	C_e (mg/l)	q_e (mg/g)	E (%)	$logq_e$	$logC_e$	$1/q_e$	$1/C_e$	Inq_e	ε^2	InC_e	$\varepsilon^2/1m$
75.05	12.4	0.63	83.4	-0.2007	1.0934	1.5873	0.0806	-0.4620	36884.2	2.5177	0.0369
114.69	16.8	0.98	85.3	-0.0088	1.2253	1.0204	0.0595	-0.0202	20505.2	2.8214	0.0205
135.2	51.4	0.84	61.9	-0.0757	1.711	1.1905	0.0195	-0.1744	2289.4	3.9396	0.0023
145.14	86.3	0.59	40.5	-0.2291	1.1963	1.6949	0.0116	-0.5276	816.5	4.4578	0.0008
147.28	103.2	0.44	29.9	-0.3565	2.0137	2.2727	0.0097	-0.8210	572.0	4.6367	0.0006

Table 4.80: Mn Adsorption by Palm Kernel shell Carbonized at 800°C and Activated with HCl

C_o (mg/l)	C_e (mg/l)	q_e (mg/g)	E (%)	$logq_e$	$logC_e$	$1/q_e$	$1/C_e$	Inq_e	ε^2	InC_e	$\varepsilon^2/1m$
75.05	56.65	0.22	29.8	-0.6576	1.7214	4.5455	0.019	-1.5141	2174.6	4.0369	0.0022
114.69	89.39	0.25	22.0	-0.6021	1.9513	4.0000	0.0112	-1.3863	761.5	4.4930	0.0008
135.20	120.30	0.15	11.0	-0.8239	2.0803	6.6667	0.0083	-1.8971	419.4	4.7900	0.0004
145.14	44.92	0.00	68.9	0.0000	1.6524	0.0000	0.0223	0.0000	2985.8	3.8049	0.0030
147.28	6.28	0.41	95.7	-0.1492	0.798	0.7092	0.1592	-0.8916	133964.8	1.8374	0.1340

Table 4.81: Mn Adsorption by Palm Kernel shell Carbonized at 800°C and Activated with H_3PO_4

C_o (mg/l)	C_e (mg/l)	q_e (mg/g)	E (%)	$logq_e$	$logC_e$	$1/q_e$	$1/C_e$	Inq_e	ε^2	InC_e	$\varepsilon^2/1m$
75.05	37.46	0.38	50.1	-0.4202	1.5736	2.6316	0.0267	-0.9676	4261.9	3.6233	0.0043
114.69	53.48	0.61	53.3	-0.2147	1.7282	1.6393	0.0187	-0.4943	2107.1	3.9793	0.0021
135.20	92.44	0.43	31.6	-0.3665	1.9659	2.3256	0.0108	-0.8440	708.3	4.5266	0.0007
145.14	116.55	0.29	19.7	-0.5376	2.0665	2.0665	0.0086	-1.2379	450.1	4.7583	0.0005
147.28	117.26	0.30	20.3	-0.5229	2.0691	2.0691	0.0085	-1.2040	439.8	4.7644	0.0004

Table 4.82: Mn Adsorption by Palm Kernel shell Carbonized at 800°C and Activated with H_2SO_4

C_o (mg/l)	C_e (mg/l)	q_e (mg/g)	E (%)	$logq_e$	$logC_e$	$1/q_e$	$1/C_e$	Inq_e	ε^2	InC_e	$\varepsilon^2/1m$
75.05	18.76	0.56	75	-0.2518	1.2732	1.7857	0.0533	-0.5798	16552.3	2.9317	0.0166
114.69	40.49	0.74	64.7	-0.1308	1.6073	1.3514	0.0247	-0.3011	3654.5	3.7011	0.0037
135.2	73.31	0.62	45.8	-0.2076	1.8652	1.6129	0.0136	-0.4780	1120.1	4.2947	0.0011
145.14	136.14	0.09	60.1	-1.0458	2.134	11.1111	0.0073	-2.4079	324.7	4.9137	0.0003
147.28	137.27	0.1	6.8	-1	2.1376	10	0.0073	-2.3026	324.7	4.9219	0.0003

Table 4.83: Ni Adsorption by Snail shell Carbonized at 600°C and Activated with HCl

C_o (mg/l)	C_e (mg/l)	q_e (mg/g)	E (%)	$logq_e$	$logC_e$	$1/q_e$	$1/C_e$	Inq_e	ε^2	InC_e	$\varepsilon^2/1m$
55.47	51.8	0.04	6.6	-1.3979	1.7143	25.0	0.0193	-3.2189	2243.1	3.9474	0.0022
52.67	50.11	0.03	4.9	-1.5229	1.6999	33.3	0.02	-3.5066	2407.1	3.9142	0.0024
59.35	58.96	0.01	0.7	-2	1.7706	100.0	0.017	-4.6052	1744.3	4.0769	0.0017
64.97	63.28	0.02	2.6	-1.699	1.8013	50.0	0.0158	-3.9120	1508.5	4.1476	0.0015
66.79	61.99	0.05	7.2	-1.301	1.7923	20.0	0.0161	-2.9957	1565.9	4.1270	0.0016

Table 4.84: Ni Adsorption by Snail shell Carbonized at 600°C and Activated with H_3PO_4

C_o (mg/l)	C_e (mg/l)	q_e (mg/g)	E (%)	$logq_e$	$logC_e$	$1/q_e$	$1/C_e$	Inq_e	ε^2	InC_e	$\varepsilon^2/1m$
55.47	49.96	0.06	9.9	-1.2218	1.6986	16.6667	0.02	-2.8134	2407.1	3.9112	0.0024
52.67	48.23	0.04	8.4	-1.3979	1.6833	25	0.0128	-3.2189	993.0	3.8760	0.0010
59.35	55.42	0.04	6.6	-1.3979	1.7437	25	0.018	-3.2189	1953.6	4.0149	0.0020
64.97	58.36	0.07	10.2	-1.1549	1.7661	14.2857	0.0172	-2.6593	1785.2	4.0666	0.0018
66.79	64.12	0.03	4	-1.5259	1.807	33.3333	0.0156	-3.5066	1470.9	4.1608	0.0015

Table 4.85: Ni Adsorption by Snail shell Carbonized at 600°C and Activated with H_2SO_4

C_o (mg/l)	C_e (mg/l)	q_e (mg/g)	E (%)	$logq_e$	$logC_e$	$1/q_e$	$1/C_e$	Inq_e	ε^2	InC_e	$\varepsilon^2/1m$
55.47	48.78	0.07	12.1	-1.1549	1.6882	14.2857	0.0205	-2.6593	2527.7	3.8873	0.0025
52.67	48.37	0.04	8.2	-1.3979	1.6846	25	0.0207	-3.2189	2576.8	3.8789	0.0026
59.35	56.79	0.03	4.3	-1.5229	1.7543	33.3333	0.0176	-3.5066	1868.5	4.0394	0.0019
64.97	62.38	0.03	4	-1.5229	1.795	33.3333	0.016	-3.5066	1546.6	4.1332	0.0015
66.79	65.49	0.01	1.9	-2	1.8162	100	0.0153	-4.6052	1415.2	4.1819	0.0014

Table 4.86: Ni Adsorption by Snail shell Carbonized at 800°C and Activated with HCl

C_o (mg/l)	C_e (mg/l)	q_e (mg/g)	E (%)	$logq_e$	$logC_e$	$1/q_e$	$1/C_e$	Inq_e	ε^2	InC_e	$\varepsilon^2/1m$
55.47	49.60	0.06	10.6	-1.2218	1.6955	16.6667	0.0202	-2.8134	2455.0	3.9040	0.0025
52.67	41.46	0.11	21.3	-0.9586	1.6176	9.0909	0.0241	-2.2073	3481.2	3.7247	0.0035
59.35	56.70	0.03	4.5	-1.5229	1.7536	33.3333	0.0176	-3.5066	1868.5	4.0378	0.0019
64.97	62.66	0.02	3..6	-1.699	1.797	50.0000	0.016	-3.9120	1546.6	4.1377	0.0015
66.79	63.57	0.03	4.8	-1.5229	1.8033	33.3333	0.0157	-3.5066	1489.6	4.1521	0.0015

Table 4.87: Ni Adsorption by Snail shell Carbonized at 800°C and Activated with H_3PO_4

C_o (mg/l)	C_e (mg/l)	q_e (mg/g)	E (%)	$logq_e$	$logC_e$	$1/q_e$	$1/C_e$	Inq_e	ε^2	InCe	$\varepsilon^2/1m$
55.47	51.09	0.04	7.9	-1.3979	1.7083	25	0.0196	-3.2189	2312.7	3.9336	0.0023
52.67	49.38	0.03	6.2	-1.5229	1.6936	33.3333	0.0202	-3.5066	2455.0	3.8995	0.0025
59.35	56.78	0.03	4.3	-1.5229	1.7542	33.3333	0.0176	-3.5066	1868.5	4.0392	0.0019
64.97	60.29	0.05	7.2	-1.301	1.7802	20	0.0166	-2.9957	1663.8	4.0992	0.0017
66.79	59.96	0.07	10.2	-1.1549	1.7779	14.2857	0.0167	-2.6593	1683.8	4.0937	0.0017

Table 4.88: Ni Adsorption by Snail shell Carbonized at 800°C and Activated with H_2SO_4

C_o (mg/l)	C_e (mg/l)	q_e (mg/g)	E (%)	$logq_e$	$logC_e$	$1/q_e$	$1/C_e$	Inq_e	ε^2	InC_e	$\varepsilon^2/1m$
55.47	42.32	0.13	23.7	-0.8861	1.6265	7.6923	0.0236	-2.0402	3339.8	3.7453	0.0033
52.67	50.19	0.02	4.7	-1.699	1.7006	50	0.0199	-3.9120	2383.3	3.9158	0.0024
59.35	54.89	0.04	7.5	-1.3979	1.7395	25	0.0182	-3.2189	1996.9	4.0053	0.0020
64.97	59.91	0.05	7.8	-1.301	1.7775	20	0.0167	-2.9957	1683.8	4.0928	0.0017
66.79	61.88	0.05	7.4	-1.301	1.7916	20	0.0162	-2.9957	1585.2	4.1252	0.0016

Table 4.89: Pb Adsorption by Snail shell Carbonized at 600°C and Activated with HCl

C_o (mg/l)	C_e (mg/l)	q_e (mg/g)	E (%)	$logq_e$	$logC_e$	$1/q_e$	$1/C_e$	Inq_e	ε^2	InC_e	$\varepsilon^2/1m$
35.7	13.89	0.52	61	-0.6576	1.1427	4.5455	0.072	-0.6539	29672.1	2.6312	-0.6539
37.6	21.67	0.16	42.3	-0.7959	1.3359	6.25	0.0461	-1.8326	12468.3	3.0759	-1.8326
43.91	15.67	0.28	64.3	-0.5528	1.1951	3.5714	0.0638	-1.2730	23479.9	2.7517	-1.2730
57.17	23.96	0.33	58	-0.4815	1.3795	3.0303	0.0417	-1.1087	10245.2	3.1764	-1.1087
57.58	24.69	0.33	56.9	-0.4815	1.3925	3.0303	0.0405	-1.1087	9675.3	3.2064	-1.1087

Table 4.90: Pb Adsorption by Snail shell Carbonized at 600°C and Activated with H_3PO_4

Co (mg/l)	Ce (mg/l)	qe (mg/g)	E (%)	logqe	logCe	1/qe	1/Ce	Inqe	ε^2	InCe	$\varepsilon^2/1m$
35.7	17.74	0.18	50.3	-0.7447	1.2489	5.5556	0.0564	-1.7148	18478.8	2.8758	0.0185
37.6	18.46	0.19	50.9	-0.7212	1.2662	5.2632	0.0542	-1.6607	17101.2	2.9156	0.0171
43.91	29.14	0.14	35.9	-0.8539	1.4685	7.1429	0.034	-1.9661	6862.0	3.3721	0.0069
57.17	33.46	0.24	41.4	-0.6198	1.5425	4.1667	0.0299	-1.4271	5328.1	3.5104	0.0053
57.58	30.67	0.27	46.5	-0.5686	1.4867	3.7037	0.0326	-1.3093	6317.1	3.4233	0.0063

Table 4.91: Pb Adsorption by Snail shell Carbonized at 600°C and Activated with H_2SO_4

C_o (mg/l)	C_e (mg/l)	q_e (mg/g)	E (%)	$logq_e$	$logC_e$	$1/q_e$	$1/C_e$	Inq_e	ε^2	InC_e	$\varepsilon^2/1m$
35.7	16.67	0.19	53.3	-0.7212	1.2219	5.2632	0.06	-1.6607	20841.4	2.8136	0.0208
37.6	28.13	0.09	25.2	-1.0458	1.4492	11.1111	0.0355	-2.4079	7469.9	3.3368	0.0075
43.91	32.92	0.11	25	-0.9586	1.5175	9.0909	0.0304	-2.2073	5505.1	3.4941	0.0055
57.17	44.8	0.12	21.6	-0.9208	1.6513	8.3333	0.0223	-2.1203	2985.8	3.8022	0.0030
57.58	45.6	0.12	20.5	-0.9208	1.659	8.3333	0.0219	-2.1203	2880.8	3.8199	0.0029

Table 4.92: Pb Adsorption by Snail shell Carbonized at 800°C and Activated with HCl

C_o (mg/l)	C_e (mg/l)	q_e (mg/g)	E (%)	$logq_e$	$logC_e$	$1/q_e$	$1/C_e$	Inq_e	ε^2	InC_e	$\varepsilon^2/1m$
35.7	32.1	0.04	10	-1.3979	1.5065	25	0.0312	-3.2189	5794.1	3.4689	0.0058
37.6	30.5	0.07	18.9	-1.1549	1.4843	14.2857	0.0328	-2.6593	6393.6	3.4177	0.0064
43.91	35.7	0.08	18.7	-1.0969	1.5527	12.5	0.028	-2.5257	4681.1	3.5752	0.0047
57.17	46.6	0.11	18.4	-0.9586	1.6684	9.0901	0.0215	-2.2073	2777.6	3.8416	0.0028
57.58	47.4	0.09	17.3	-1.0458	1.6758	11.1111	0.0211	-2.4079	2676.3	3.8586	0.0027

Table 4.93: Pb Adsorption by Snail shell Carbonized at 800°C and Activated with H_3PO_4

C_o (mg/l)	C_e (mg/l)	q_e (mg/g)	E (%)	$logq_e$	$logC_e$	$1/q_e$	$1/C_e$	Inq_e	ε^2	InC_e	$\varepsilon^2/1m$
35.7	31.4	0.04	12	-1.3979	1.4969	25	0.0318	-3.2189	6015.6	3.4468	0.0060
37.6	28.16	0.09	25.1	-1.0458	1.4496	11.1111	0.0355	-2.4079	7469.9	3.3379	0.0075
43.91	38.22	0.06	12.9	-1.2218	1.5823	16.6667	0.0262	-2.8134	4105.8	3.6434	0.0041
57.17	52.67	0.05	7.9	-1.301	1.7216	20	0.019	-2.9957	2174.6	3.9640	0.0022
57.58	49.91	0.07	13	-1.1549	1.6982	14.2857	0.02	-2.6593	2407.1	3.9102	0.0024

Table 4.94: Pb Adsorption by Snail shell Carbonized at 800°C and Activated with H_2SO_4

C_o (mg/l)	C_e (mg/l)	q_e (mg/g)	E (%)	$logq_e$	$logC_e$	$1/q_e$	$1/C_e$	Inq_e	ε^2	InC_e	$\varepsilon^2/1m$
35.7	33.6	0.02	5.9	-1.699	1.5263	50	0.0298	-3.9120	5293.0	3.5145	0.0053
37.6	29.9	0.08	20.4	-1.0969	1.4757	12.5	0.0334	-2.5257	6625.8	3.3979	0.0066
43.91	41.6	0.02	5.2	-1.699	1.6191	50	0.024	-3.9120	3452.7	3.7281	0.0035
57.17	50.1	0.07	12.3	-1.1549	1.6998	14.2857	0.02	-2.6593	2407.1	3.9140	0.0024
57.58	51.67	0.06	9.9	-1.2218	1.7132	16.6667	0.0194	-2.8134	2266.2	3.9449	0.0023

Table 4.95: Cd Adsorption by Snail shell Carbonized at 600°C and Activated with HCl

C_o (mg/l)	C_e (mg/l)	q_e (mg/g)	E (%)	$logq_e$	$logC_e$	$1/q_e$	$1/C_e$	Inq_e	ε^2	InC_e	$\varepsilon^2/1m$
53.66	50.87	0.03	5.2	-1.5229	1.7065	33.3333	0.0197	-3.5066	2336.1	3.9293	0.0023
53.06	51.65	0.01	2.7	-2	1.7131	100	0.0194	-4.6052	2266.2	3.9445	0.0023
53.9	50.59	0.03	6.1	-1.5229	1.7041	33.3333	0.0198	-3.5066	2359.7	3.9238	0.0024
55.7	51.67	0.04	7.2	-1.3979	1.7132	25	0.0194	-3.2189	2266.2	3.9449	0.0023
57.47	54.27	0.03	5.6	-1.5229	1.7346	33.3333	0.0184	-3.5066	2040.6	3.9940	0.0020

Table 4.96: Cd Adsorption by Snail shell Carbonized at 600°C and Activated with H_3PO_4

C_o (mg/l)	C_e (mg/l)	q_e (mg/g)	E (%)	$logq_e$	$logC_e$	$1/q_e$	$1/C_e$	Inq_e	ε^2	InC_e	$\varepsilon^2/1m$
53.66	51.89	0.02	3.3	-1.699	1.7151	50	0.0193	-3.9120	2243.1	3.9491	0.0022
53.06	49.91	0.03	5.9	-1.5229	1.6982	33.3333	0.2	-3.5066	204046.2	3.9102	0.2040
53.9	48.87	0.05	7.5	-1.301	1.698	20	0.0205	-2.9957	2527.7	3.8892	0.0025
55.7	53.19	0.03	4.5	-1.5229	1.7258	33.3333	0.0188	-3.5066	2129.4	3.9739	0.0021
57.47	50.99	0.06	11.3	-1.2218	1.7075	16.6667	0.0196	-2.8134	2312.7	3.9316	0.0023

Table 4.97: Cd Adsorption by Snail shell Carbonized at 600°C and Activated with H_2SO_4

C_o (mg/l)	C_e (mg/l)	q_e (mg/g)	E (%)	$logq_e$	$logC_e$	$1/q_e$	$1/C_e$	Inq_e	ε^2	InC_e	$\varepsilon^2/1m$
53.66	52.1	0.02	2.9	-1.699	1.7168	50	0.0192	-3.9120	2220.2	3.9532	0.0022
53.06	51.3	0.02	3.3	-1.699	1.7101	50	0.0195	-3.9120	2289.4	3.9377	0.0023
53.9	50.23	0.04	6.8	-1.3979	1.701	25	0.0199	-3.2189	2383.3	3.9166	0.0024
55.7	54.89	0.01	1.5	-2	1.7395	100	0.0182	-4.6052	1996.9	4.0053	0.0020
57.47	53.67	0.04	6.6	-1.3979	1.7297	25	0.0186	-3.2189	2084.8	3.9829	0.0021

Table 3.98: Cd Adsorption by Snail shell Carbonized at 800°C and Activated with HCl

C_o (mg/l)	C_e (mg/l)	q_e (mg/g)	E (%)	$logq_e$	$logC_e$	$1/q_e$	$1/C_e$	Inq_e	ε^2	InC_e	$\varepsilon^2/1m$
53.66	51.67	0.02	3.7	-1.699	1.7132	50	0.0194	-3.9120	2266.2	3.9449	0.0023
53.06	50.28	0.03	5.2	-1.5229	1.7014	33.3333	0.0199	-3.5066	2383.3	3.9176	0.0024
53.9	49.88	0.04	7.5	-1.3979	1.6979	25	0.02	-3.2189	2407.1	3.9096	0.0024
55.7	53.82	0.02	3.4	-1.699	1.7309	50	0.0186	-3.9120	2084.8	3.9856	0.0021
57.47	55.96	0.02	2.6	-1.699	1.7479	50	0.0179	-3.9120	1932.2	4.0246	0.0019

Table 4.99: Cd Adsorption by Snail shell Carbonized at 800°C and Activated with H_3PO_4

C_o (mg/l)	C_e (mg/l)	q_e (mg/g)	E (%)	$logq_e$	$logC_e$	$1/q_e$	$1/C_e$	Inq_e	ε^2	InC_e	$\varepsilon^2/1m$
53.66	49.92	0.04	7	-1.3979	1.6895	25	0.02	-3.2189	2407.1	3.9104	0.0024
53.06	51.28	0.02	3.4	-1.699	1.7099	50	0.0195	-3.9120	2289.4	3.9373	0.0023
53.9	51.22	0.03	5	-1.5229	1.7094	33.3333	0.0195	-3.5066	2289.4	3.9361	0.0023
55.7	53.91	0.02	3.2	-1.699	1.7317	50	0.0185	-3.9120	2062.6	3.9873	0.0021
57.47	56.89	0.01	1	-2	1.755	100	0.0176	-4.6052	1868.5	4.0411	0.0019

Table 4.100: Cd Adsorption by Snail shell Carbonized at 800°C and Activated with H_2SO_4

C_o (mg/l)	C_e (mg/l)	q_e (mg/g)	E (%)	$logq_e$	$logC_e$	$1/q_e$	$1/C_e$	Inq_e	ε^2	InC_e	$\varepsilon^2/1m$
53.66	52.19	0.01	2.7	-2	1.7176	100	0.0192	-4.6052	2220.2	3.9549	0.0022
53.06	51.92	0.01	2.1	-2	1.7153	100	0.0193	-4.6052	2243.1	3.9497	0.0022
53.9	50.55	0.03	6.2	-1.5229	1.7307	33.3333	0.0198	-3.5066	2359.7	3.9230	0.0024
55.7	51.24	0.04	6.9	-1.3979	1.7147	25	0.0193	-3.2189	2243.1	3.9365	0.0022
57.47	55.32	0.02	3.7	-1.699	1.7429	50	0.0181	-3.9120	1975.2	4.0131	0.0020

Table 4.101: Mn Adsorption by Snail shell Carbonized at 600°C and Activated with HCl

C_o (mg/l)	C_e (mg/l)	q_e (mg/g)	E (%)	$logq_e$	$logC_e$	$1/q_e$	$1/C_e$	Inq_e	ε^2	InC_e	$\varepsilon^2/1m$
75.05	8.48	0.67	88.7	-0.1739	0.9284	1.4925	0.1179	-0.4005	76247.9	2.1377	0.0762
114.69	112.51	0.02	1.9	-1.699	2.0512	50	0.0089	-3.9120	481.9	4.7230	0.0005
135.24	133.19	0.02	4.5	-1.699	2.1245	50	0.0075	-3.9120	342.7	4.8918	0.0003
145.14	75.63	0.69	47.9	-0.1612	1.8787	1.4493	0.0132	-0.3711	1055.6	4.3259	0.0011
147.28	145.12	0.02	1.47	-1.699	2.1617	50	0.0689	-3.9120	27251.7	4.9776	0.0273

Table 4.102: Mn Adsorption by Snail shell Carbonized at 600°C and Activated with H_3PO_4

C_o (mg/l)	C_e (mg/l)	q_e (mg/g)	E (%)	$logq_e$	$logC_e$	$1/q_e$	$1/C_e$	Inq_e	ε^2	InC_e	$\varepsilon^2/1m$
75.05	0.88	0.74	98.8	-0.1308	-0.0555	1.3514	1.1364	-0.3011	3537332.8	-0.1278	3.5373
114.69	7.47	1.07	93.4	0.0294	0.8733	0.9346	0.1339	0.0677	96932.1	2.0109	0.0969
135.24	19.58	1.16	85.5	0.0645	1.2918	0.8621	0.0511	0.1484	15246.2	2.9745	0.0152
145.14	11.95	1.33	91.8	0.1239	1.0774	0.7519	0.0837	0.2852	39660.7	2.4807	0.0397
147.28	46.45	1	68.4	0	1.667	1	0.0215	0.0000	2777.6	3.8384	0.0028

Table 4.103: Mn Adsorption by Snail shell Carbonized at 600°C and Activated with H_2SO_4

C_o (mg/l)	C_e (mg/l)	q_e (mg/g)	E (%)	$logq_e$	$logC_e$	$1/q_e$	$1/C_e$	Inq_e	ε^2	InC_e	$\varepsilon^2/1m$
75.05	2.16	0.73	97.1	-0.1367	0.3345	1.3699	0.463	-0.3147	888662.9	0.7701	0.8887
114.69	3.57	1.11	96.9	0.0453	0.5527	0.9009	0.2801	0.1044	374308.0	1.2726	0.3743
135.24	12.55	1.23	90.7	0.0899	1.0986	0.813	0.0797	0.2070	36095.5	2.5297	0.0361
145.14	26.19	1.19	81.9	0.0755	1.4181	0.8403	0.0382	0.1740	8626.8	3.2654	0.0086
147.28	57.8	0.89	60.8	-0.0506	1.7619	1.1236	0.0173	-0.1165	1805.9	4.0570	0.0018

Table 4.104: Mn Adsorption by Snail shell Carbonized at 800°C and Activated with HCl

C_o (mg/l)	C_e (mg/l)	q_e (mg/g)	E (%)	$logq_e$	$logC_e$	$1/q_e$	$1/C_e$	Inq_e	ε^2	InC_e	$\varepsilon^2/1m$
75.05	69.91	0.05	6.8	-1.301	1.8445	20	0.0143	-2.9957	1237.5	4.2472	0.0012
114.69	111.32	0.03	2.9	-1.5229	2.0466	33.3333	0.009	-3.5066	492.8	4.7124	0.0005
135.24	128.77	0.06	4.8	-1.2218	2.1098	16.6667	0.0078	-2.8134	370.6	4.8580	0.0004
145.14	141.87	0.03	2.3	-1.5229	2.1519	33.3333	0.007	-3.5066	298.7	4.9549	0.0003
147.28	146	0.01	0.9	-2	2.1647	100	0.0068	-4.6052	281.9	4.9836	0.0003

Table 4.105: Mn Adsorption by Snail shell Carbonized at 800°C and Activated with H_3PO_4

C_o (mg/l)	C_e (mg/l)	q_e (mg/g)	E (%)	$logq_e$	$logC_e$	$1/q_e$	$1/C_e$	Inq_e	ε^2	InC_e	$\varepsilon^2/1m$
75.05	70.38	0.05	6.2	-1.301	1.8474	20	0.0142	-2.9957	1220.4	4.2539	0.0012
114.69	109.4	0.05	4.6	-1.301	2.039	20	0.0091	-2.9957	503.7	4.6950	0.0005
135.24	128.37	0.07	5.1	-1.1549	2.1085	14.2857	0.0078	-2.6593	370.6	4.8549	0.0004
145.14	133.88	0.11	7.8	-0.9586	2.1267	9.0909	0.0075	-2.2073	342.7	4.8969	0.0003
147.28	140.76	0.07	4.4	-1.1549	2.1485	14.2857	0.0071	-2.6593	307.3	4.9471	0.0003

Table 43.106: Mn Adsorption by Snail shell Carbonized at 800°C and Activated with H_2SO_4

C_o (mg/l)	C_e (mg/l)	q_e (mg/g)	E (%)	$logq_e$	$logC_e$	$1/q_e$	$1/C_e$	Inq_e	ε^2	InC_e	$\varepsilon^2/1m$
75.05	67.89	0.07	9.5	-1.1549	1.8318	14.2857	0.0147	-2.6593	1307.2	4.2179	0.0013
114.69	109.48	0.05	4.5	-1.301	2.0393	20.0000	0.0091	-2.9957	503.7	4.6957	0.0005
135.24	121.36	0.14	10.2	-0.8539	2.0841	7.1429	0.0082	-1.9661	409.4	4.7988	0.0004
145.14	136.55	0.09	5.9	-1.0458	2.1353	11.1111	0.0073	-2.4079	324.7	4.9167	0.0003
147.28	146.75	0.01	0.4	-2.0000	2.1666	100.0000	0.0068	-4.6052	281.9	4.9887	0.0003

APPENDIX D

Table 4.123: Percentage Adsorption of Ni by OBAC

IMC	HCl/600˚C	HCl/800˚C	H_2SO_4/600˚C	H_2SO_4/800˚C	H_3PO4/600˚C	H_3PO4/800˚C
55.47	97.5	87.8	96.8	43.4	84.3	59.7
52.67	96.8	90.1	94.7	41.9	81.0	60.7
59.35	90.3	89.9	88.2	42.7	82.7	63.9
64.96	8.99	38.2	94.6	41.1	82.0	19.7
66.79	42.7	4.9	60.9	54.2	32.0	11.1

IMC = Initial Metal Conc.

Table 4.124: Percentage Adsorption of Cd by OBAC

IMC	HCl/600˚C	HCl/800˚C	H_2SO_4/600˚C	H_2SO_4/800˚C	H_3PO_4/600˚C	H_3PO_4/800 ^oC
53.662	71.7	63.3	98.9	39.9	58.4	30.5
53.057	61.6	78.6	97.6	29.9	55.6	24.8
53.930	60.3	77.7	99.1	27.6	59.2	23.8
55.728	17.9	36.4	96.9	9.2	18.0	4.90
57.470	7.04	6.96	71.3	3.4	14.8	12.3

IMC = Initial Metal Conc.

Table 4.125: Percentage Adsorption of Pb by OBAC

IMC	HCl/600˚C	HCl/800˚C	H_2SO_4/600˚C	H_2SO_4/800˚C	H_3PO_4/600˚C	H_3PO_4/800˚C
35.724	14.1	98.9	17.8	98.7	20.1	98.7
37.606	18.7	99.2	11.2	98.5	20.5	98.5
43.912	16.5	98.7	8.5	96.9	21.0	96.9
57.167	18.3	96.5	18.2	94.8	21.9	94.8
57.381	16.1	96.0	14.8	93.6	30.5	93.6

Table 4.126: Percentage Adsorption of Mn by OBAC

IMC	HCl/600˚C	HCl/800˚C	H_2SO_4/600˚C	H_2SO_4/800˚C	H_3PO_4/600˚C	H_3PO_4/800˚C
75.046	7.5	87.3	7.9	64.6	11.0	98.6
114.686	4.5	94.2	3.6	62.9	4.60	69.2
135.240	16.5	93.3	5.8	46.7	11.0	56.7
145.137	17.5	29.1	4.1	17.7	11.6	13.6
147.280	19.8	25.7	3.1	18.8	5.90	14.1

Table 4.127: Percentage Adsorption of Ni by PNAC

IMC	HCl/600˚C	HCl/800˚C	H_2SO_4/600˚C	H_2SO_4/800˚C	H_3PO_4/600˚C	H_3PO_4/800˚C
55.47	60.7	57.5	57.7	21.6	51.0	60.6
52.67	63.2	62.1	59.6	58.9	57.6	47.0
59.35	60.1	36.3	46.5	58.1	45.7	49.1
64.96	40.6	11.8	46.3	27.0	17.8	27.8
66.79	1.74	68.1	42.1	33.7	8.2	36.2

Table 4.128: Percentage Adsorption of Pb by PNAC

IMC	HCl/600˚C	HCl/800˚C	H_2SO_4/600˚C	H_2SO_4/800˚C	H_3PO_4/600˚C	H_3PO_4/800˚C
35.724	98.4	87.5	97.6	77.8	98.6	75.0
37.606	92.9	93.6	97.7	65.7	96.9	49.0
43.912	89.1	98.8	98.7	38.9	98.1	34.1
57.167	99.0	98.9	90.9	41.0	94.0	33.8
57.381	95.8	98.8	95.4	27.4	91.5	30.1

Table 4.129: Percentage Adsorption of Cd by PNAC

IMC	HCl/600°C	HCl/800°C	H_2SO_4/600°C	H_2SO_4/800°C	H_3PO_4/600°C	H_3PO_4/800°C
53.662	62.1	61.7	35.1	47.1	36.0	39.2
53.057	46.1	56.6	32.9	31.8	41.0	24.0
53.930	33.0	47.8	32.3	89.4	43.4	27.3
55.728	9.7	10.9	10.9	40.4	11.9	16.1
57.470	3.7	3.4	19.9	44.0	4.2	27.0

Table 4.130: Percentage Adsorption of Mn by PNAC

IMC	HCl/600°C	HCl/800°C	H_2SO_4/600°C	H_2SO_4/800°C	H_3PO_4/600°C	H_3PO_4/800°C
75.046	60.0	59.8	50.4	84.8	59.9	71.1
114.686	69.8	59.5	48.3	80.6	40.9	62.9
135.240	64.0	43.6	32.5	64.6	49.2	46.4
145.137	50.4	8.9	11.8	41.7	1.6	18.8
147.280	52.6	7.3	20.9	7.1	19.6	12.3

Table 4.131: Percentage Adsorption of Ni by PKAC

IMC	HCl/600°C	HCl/800°C	H_2SO_4/600°C	H_2SO_4/800°C	H_3PO_4/600°C	H_3PO_4/800°C
55.47	41.2	53.9	23.7	77.7	61.6	47.9
52.67	36.2	45.0	24.4	77.3	69.3	50.2
59.35	39.9	48.7	17.6	75.6	87.9	50.9
64.96	19.8	23.5	18.3	50.8	72.6	21.9
66.79	9.2	3.96	11.9	16.2	31.5	19.4

Table 4.132: Percentage Adsorption of Pb by PKAC

IMC	HCl/600°C	HCl/800°C	H_2SO_4/600°C	H_2SO_4/800°C	H_3PO_4/600°C	H_3PO_4/800°C
35.724	98.6	88.0	83.7	89.8	54.3	86.6
37.606	97.7	84.4	80.9	81.9	40.7	95.8
43.912	96.2	74.0	63.1	68.3	36.4	84.1
57.167	88.9	65.0	40.0	41.2	33.3	75.1
57.381	87.6	67.3	43.7	34.6	37.9	70.8

Table 4.133: Percentage Adsorption of Cd by PKAC

IMC	HCl/600°C	HCl/800°C	H_2SO_4/600°C	H_2SO_4/800°C	H_3PO_4/600°C	H_3PO_4/800°C
53.662	49.4	45.6	88.6	83.2	95.5	90.1
53.057	46.1	42.2	89.2	83.4	95.6	87.2
53.930	43.9	40.5	83.3	86.4	53.9	84.9
55.728	12.7	11.8	72.8	91.9	88.4	83.6
57.470	3.30	3.70	69.7	5.80	65.4	72.7

Table 4.134: Percentage Adsorption of Mn by PKAC

IMC	HCl/600°C	HCl/800°C	H_2SO_4/600°C	H_2SO_4/800°C	H_3PO_4/600°C	H_3PO_4/800°C
75.046	99.1	29.8	83.4	75.0	62.5	50.1
114.686	85.9	22.0	85.3	64.7	41.8	53.3
135.240	79.0	11.0	61.9	45.8	35.9	31.6
145.137	71.9	68.9	40.5	60.1	37.2	19.7
147.280	73.5	95.7	29.9	6.8	32.3	20.3

Table 4.135: Percentage Adsorption of Ni by SSAC

IMC	HCl/600 °C	HCl/800 °C	H_2SO_4/600 °C	H_2SO_4/800 °C	H_3PO_4/600 °C	H_3PO_4/800 °C
55.47	6.6	10.6	12.1	23.7	9.9	7.9
52.67	4.9	21.3	8.2	4.7	8.4	6.2
59.35	0.7	4.5	4.3	7.5	6.6	4.3
64.96	2.6	3..6	4.0	7.8	10.2	7.2
66.79	7.2	4.8	1.9	7.4	4.0	10.2

Table 4.136: Percentage Adsorption of Pb by SSAC

IMC	HCl/600 °C	HCl/800 °C	H_2SO_4/600 °C	H_2SO_4/800 °C	H_3PO_4/600 °C	H_3PO_4/800 °C
35.724	61.0	10.0	53.3	5.9	50.3	12.0
37.606	42.3	18.9	25.2	20.4	50.9	25.1
43.912	64.3	18.7	25.0	5.2	35.9	12.9
57.167	58.0	18.4	21.6	12.3	41.4	7.9
57.381	56.9	17.3	20.5	9.9	46.5	13.0

Table 4.137: Percentage Adsorption of Cd by SSAC

IMC	HCl/600 °C	HCl/800 °C	H_2SO_4/600 °C	H_2SO_4/800 °C	H_3PO_4/600 °C	H_3PO_4/800 °C
53.662	5.2	3.7	2.9	2.7	3.3	7.0
53.057	2.7	5.2	3.3	2.1	5.9	3.4
53.930	6.1	7.5	6.8	6.2	7.5	5.0
55.728	7.2	3.4	1.5	6.9	4.5	3.2
57.470	5.6	2.6	6.6	3.7	11.3	1.0

Table 4.138: Percentage Adsorption of Mn by SSAC

IMC	HCl/600 °C	HCl/800 °C	H_2SO_4/600 °C	H_2SO_4/800 °C	H_3PO_4/600 °C	H_3PO_4/800 °C
75.046	88.7	6.8	97.1	9.5	98.8	6.2
114.686	1.9	2.9	96.9	4.5	93.4	4.6
135.240	4.5	4.8	90.7	10.2	85.5	5.1
145.137	47.9	2.3	81.9	5.9	91.8	7.8
147.280	1.47	0.9	60.8	0.4	68.4	4.4

APPENDIX E

Table 4.140: Pearnut Seed Activated carbon -Pb/PNAC/H_3PO_4/600˚C

C_t	q_e	q_t	t(min)	Log(q_e-q_t)	t/q_t	t^$^{0.5}$
44.2	0.263	0.198	20	-1.187	101.0	4.47
40.3	0.263	0.214	40	-1.309	186.9	6.32
34.1	0.263	0.233	60	-1.523	257.5	7.75
23.2	0.263	0.171	80	-1.036	467.8	8.94
23.3	0.263	0.263	100	-	380.2	10.00

Table 4.141: Peanut Seed Activated carbon -Pb/PNAC/H_2SO_4/600˚C

C_t	q_e	q_t	t(min)	Log(q_e-q_t)	t/q_t	t^$^{0.5}$
45.3	0.263	0.182	20	-1.092	109.9	4.47
40.1	0.263	0.216	40	-1.328	185.2	6.32
35.1	0.263	0.223	60	-1.398	269.1	7.75
22.2	0.263	0.176	80	-1.060	454.5	8.94
22.3	0.263	0.263	100	-	380.2	10.00

Table 4.142: Peanut Activated carbon -Pb/PNAC/HCl/600˚C

C_t	q_e	q_t	t(min)	Log(q_e-q_t)	t/q_t	t^$^{0.5}$
37.2	0.353	0.303	20	-1.301	66.0	4.47
30.3	0.353	0.339	40	-1.854	117.9	6.32
23.0	0.353	0.344	60	-1.021	174.4	7.75
10.2	0.353	0.236	80	-0.932	338.9	8.94
10.3	0.353	0.353	100	-	283.3	10.00

Table 4.143: Peanut Activated Carbon -Pb/PNAC/HCl/800˚C

C_t	q_e	q_t	t(min)	Log(q_e-q_t)	t/q_t	t^$^{0.5}$
40.2	0.331	0.258	20	-1.137	77.5	4.47
36.1	0.331	0.266	40	-1.187	150.4	6.32
31.0	0.331	0.264	60	-1.174	227.3	7.75
13.2	0.331	0.221	80	-0.959	361.9	8.94
13.3	0.331	0.331	100	-	302.1	10.00

Table 4.144: Peanut Activated carbon -Pb/PNAC/H_2SO_4/800˚C

C_t	q_e	q_t	t(min)	Log(q_e-q_t)	t/q_t	t^$^{0.5}$
45.0	0.255	0.186	20	-1.161	107.5	4.47
40.4	0.255	0.213	40	-1.377	187.8	6.32
33.3	0.255	0.241	60	-1.854	248.9	7.75
23.3	0.255	0.171	80	-1.076	467.8	8.94
23.4	0.255	0.255	100	-	392.2	10.00

Table 4.145: Peanut Activated carbon -Pb/PNAC/H_3PO_4/800˚C

C_t	q_e	q_t	t(min)	Log(q_e-q_t)	t/q_t	t^$^{0.5}$
45.2	0.263	0.183	20	-1.097	109.3	4.47
40.0	0.263	0.218	40	-1.347	183.5	6.32
35.1	0.263	0.223	60	-1.398	269.1	7.75
22.3	0.263	0.176	80	-1.060	454.5	8.94
22.4	0.263	0.263	100	-	380.2	10.00

Table 4.146: Peanut Activated carbon -Ni/PNAC/HCl/600˚C

C_t	q_e	q_t	t(min)	Log(q_e-q_t)	t/q_t	t^$^{0.5}$
49.0	0.392	0.267	20	-0.903	74.9	4.47
47.4	0.392	0.243	40	-0.827	164.6	6.32
30.5	0.392	0.363	60	-1.538	165.3	7.75
14.5	0.392	0.262	80	-0.886	305.3	8.94
14.0	0.392	0.392	100	-	255.1	10.00

Table 4.147: Peanut Activated carbon -Ni/PNAC/H_2SO_4/600˚C

C_t	q_e	q_t	t(min)	Log(q_e-q_t)	t/q_t	t^$^{0.5}$
47.1	0.347	0.295	20	-1.284	67.8	4.47
40.0	0.347	0.335	40	-1.921	119.4	6.32
33.4	0.347	0.334	60	-1.886	179.6	7.75
20.5	0.347	0.232	80	-0.939	344.8	8.94
20.6	0.347	0.347	100	-	288.2	10.00

Table 4.148: Peanut Activated carbon -Ni/PNAC/H_3PO_4/600˚C

C_t	q_e	q_t	t(min)	Log(q_e-q_t)	t/q_t	t^$^{0.5}$
50.5	0.362	0.245	20	-0.932	81.6	4.47
44.5	0.362	0.279	40	-1.081	143.4	6.32
34.3	0.362	0.325	60	-1.432	184.6	7.75
18.3	0.362	0.243	80	-0.924	329.2	8.94
18.5	0.362	0.362	100	-	276.2	10.00

Table 4.149: Peanut Activated carbon -Ni/PNAC/HCl/800˚C

C_t	q_e	q_t	t(min)	Log(q_e-q_t)	t/q_t	t^$^{0.5}$
45.4	0.415	0.321	20	-1.027	62.3	4.47
40.5	0.415	0.329	40	-1.066	121.6	6.32
35.6	0.415	0.312	60	-0.987	192.3	7.75
11.4	0.415	0.277	80	-0.860	288.8	8.94
11.5	0.415	0.415	100	-	240.9	10.00

Table 4.150: Peanut Activated carbon -Ni/PNAC/H_2SO_4/800˚C

C_t	q_e	q_t	t(min)	Log(q_e-q_t)	t/q_t	t^$^{0.5}$
44.6	0.356	0.333	20	-1.638	60.1	4.47
39.3	0.356	0.344	40	-1.921	116.3	6.32
30.5	0.356	0.362	60	-1.620	165.7	7.75
18.4	0.356	0.356	80	-	224.7	8.94
18.3	0.356	0.243	100	-0.947	411.5	10.00

Table 4.151: Peanut Activated carbon -Ni/PNAC/H_3PO_4/800˚C

C_t	q_e	q_t	t(min)	Log(q_e-q_t)	t/q_t	t^$^{0.5}$
50.0	0.407	0.252	20	-0.810	79.4	4.47
40.2	0.407	0.333	40	-1.131	120.1	6.32
30.4	0.407	0.364	60	-1.367	164.8	7.75
12.4	0.407	0.272	80	-0.870	249.1	8.94
12.6	0.407	0.407	100	-	245.7	10.00

Table 4.152: Peanut Activated carbon -Cd/PNAC/HCl/600˚C

C_t	q_e	q_t	t(min)	Log(q_e-q_t)	t/q_t	t^$^{0.5}$
37.3	0.353	0.303	20	-1.301	66.0	4.47
30.4	0.353	0.339	40	-1.854	117.9	6.32
23.0	0.353	0.345	60	-1.019	173.9	7.75
10.3	0.353	0.236	80	-0.932	338.9	8.94
10.4	0.353	0.353	100	-	283.3	10.00

Table 4.153: Peanut Activated carbon -Cd/PNAC/H_2SO_4/600˚C

C_t	q_e	q_t	t(min)	Log(q_e-q_t)	t/q_t	t^$^{0.5}$
45.3	0.263	0.183	20	-1.097	109.3	4.47
40.1	0.263	0.218	40	-1.347	183.5	6.32
35.2	0.263	0.223	60	-1.398	269.1	7.75
22.3	0.263	0.176	80	-1.060	454.5	8.94
22.4	0.263	0.263	100	-	380.2	10.00

Table 4.154: Peanut Activated carbon -Cd/PNAC/ H_3PO_4/600˚C

C_t	q_e	q_t	t(min)	Log(q_e-q_t)	t/q_t	t^$^{0.5}$
45.2	0.264	0.185	20	-1.102	108.1	4.47
40.0	0.264	0.218	40	-1.337	183.5	6.32
35.1	0.264	0.223	60	-1.387	269.1	7.75
22.2	0.264	0.177	80	-1.060	451.9	8.94
22.3	0.264	0.264	100	-	378.8	10.00

Table 4.156: Peanut Activated carbon -Cd/PNAC/HCl/800˚C

C_t	q_e	q_t	t(min)	Log(q_e-q_t)	t/q_t	t^$^{0.5}$
40.3	0.331	0.258	20	-1.137	77.5	4.47
36.2	0.331	0.266	40	-1.187	150.4	6.32
31.1	0.331	0.264	60	-1.174	227.3	7.75
13.2	0.331	0.222	80	-0.963	360.4	8.94
13.4	0.331	0.331	100	-	302.1	10.00

Table 4.157: Peanut Activated carbon -Cd/PNAC/ H_2SO_4/800˚C

C_t	q_e	q_t	t(min)	Log(q_e-q_t)	t/q_t	t^$^{0.5}$
45.0	0.257	0.188	20	-1.161	106.4	4.47
40.5	0.257	0.213	40	-1.357	187.8	6.32
33.4	0.257	0.241	60	-1.796	248.9	7.75
23.1	0.257	0.172	80	-1.071	465.1	8.94
23.2	0.257	0.257	100	-	389.1	10.00

Table 4.158: Peanut Activated carbon-Cd/PNAC/ H_3PO_4/800˚C

C_t	q_e	q_t	t(min)	Log(q_e-q_t)	t/q_t	t^$^{0.5}$
45.3	0.263	0.183	20	-1.097	109.3	4.47
40.2	0.263	0.216	40	-1.328	185.2	6.32
34.1	0.263	0.234	60	-1.538	260.9	7.75
22.2	0.263	0.177	80	-1.066	451.9	8.94
22.4	0.263	0.263	100	-	380.2	10.00

Table 4.159: Peanut Activated carbon -Mn/PNAC/HCl/600˚C

C_t	q_e	q_t	t(min)	Log(q_e-q_t)	t/q_t	t^$^{0.5}$
60.0	0.383	0.254	20	-0.889	78.7	4.47
50.0	0.383	0.314	40	-1.161	127.4	6.32
40.0	0.383	0.351	60	-1.495	170.7	7.75
24.3	0.383	0.227	80	-0.807	352.4	8.94
24.1	0.383	0.383	100	-	261.1	10.00

Table 4.160: Peanut Activated carbon -Mn/PNAC/ H_2SO_4/600˚C

C_t	q_e	q_t	t(min)	Log(q_e-q_t)	t/q_t	t^$^{0.5}$
54.4	0.411	0.311	20	-1.000	64.3	4.47
44.3	0.411	0.385	40	-1.585	103.9	6.32
34.3	0.411	0.408	60	-1.007	147.1	7.75
20.4	0.411	0.274	80	-0.863	291.9	8.94
20.5	0.411	0.411	100	-	243.3	10.00

Table 4.161: Peanut Activated carbon -Mn/PNAC/ H_3PO_4/600˚C

C_t	q_e	q_t	t(min)	Log(q_e-q_t)	t/q_t	t^$^{0.5}$
55.4	0.411	0.296	20	-0.939	67.6	4.47
45.1	0.411	0.375	40	-1.444	106.7	6.32
35.4	0.411	0.397	60	-1.854	151.1	7.75
20.3	0.411	0.411	80	-	194.6	8.94
20.1	0.411	0.275	100	-0.866	363.6	10.00

Table 4.162: Peanut Activated carbon -Mn/PNAC/HCl/800˚C

C_t	q_e	q_t	t(min)	Log(q_e-q_t)	t/q_t	t^$^{0.5}$
50.0	0.455	0.377	20	-1.108	53.1	4.47
40.0	0.455	0.439	40	-1.796	91.1	6.32
30.4	0.455	0.447	60	-1.007	134.2	7.75
14.3	0.455	0.304	80	-0.821	263.2	8.94
14.5	0.455	0.455	100	-	219.8	10.00

Table 4.163: Peanut Activated carbon -Mn/PNAC/ H_2SO_4/800˚

C_t	q_e	q_t	t(min)	Log(q_e-q_t)	t/q_t	t^$^{0.5}$
55.3	0.410	0.297	20	-0.947	67.3	4.47
45.2	0.410	0.374	40	-1.444	106.9	6.32
35.3	0.410	0.398	60	-1.921	150.8	7.75
20.3	0.410	0.274	80	-0.866	291.9	8.94
20.4	0.410	0.410	100	-	243.9	10.00

Table 4.164: Peanut Activated carbon -Mn/PNAC/ H_3PO_4/800˚C

C_t	q_e	q_t	t(min)	Log(q_e-q_t)	t/q_t	t^$^{0.5}$
50.4	0.410	0.371	20	-1.409	53.9	4.47
45.2	0.410	0.374	40	-1.444	106.9	6.32
35.3	0.410	0.398	60	-1.921	150.8	7.75
20.3	0.410	0.274	80	-0.866	291.9	8.94
20.4	0.410	0.410	100	-	243.9	10.00

Table 4.165: Palm Kernel Shell-Ni/PKAC/HCl/600˚C

C_t	q_e	q_t	t(min)	Log(q_e-q_t)	t/q_t	t^$^{0.5}$
44.5	0.378	0.335	20	-1.367	59.7	4.47
38.2	0.378	0.358	40	-1.699	111.7	6.32
29.9	0.378	0.369	60	-2.046	162.6	7.75
16.8	0.378	0.250	80	-0.893	320.0	8.94
16.4	0.378	0.378	100	-	264.6	10.00

Table 4.166: Palm Kernel Shell- Ni/PKAC/ H_2SO_4/600˚C

C_t	q_e	q_t	t(min)	Log(q_e-q_t)	t/q_t	t^$^{0.5}$
51.3	0.292	0.233	20	-1.229	85.8	4.47
45.7	0.292	0.264	40	-1.553	151.5	6.32
39.8	0.292	0.270	60	-1.658	222.2	7.75
28.2	0.292	0.193	80	-1.004	414.5	8.94
27.9	0.292	0.292	100	-	342.5	10.00

Table 4.167: Palm Kernel Shell- Ni/PKAC/ H_3PO_4/600˚C

C_t	q_e	q_t	t(min)	Log(q_e-q_t)	t/q_t	t^$^{0.5}$
52.0	0.269	0.222	20	-1.328	90.1	4.47
47.3	0.269	0.244	40	-1.602	163.9	6.32
41.2	0.269	0.256	60	-1.886	234.4	7.75
31.1	0.269	0.179	80	-1.046	446.9	8.94
30.9	0.269	0.269	100	-	371.7	10.00

Table 4.168: Palm Kernel Shell- Ni/PKAC/HCl/800˚C

C_t	q_e	q_t	t(min)	Log(q_e-q_t)	t/q_t	t^$^{0.5}$
49.2	0.338	0.264	20	-1.131	75.8	4.47
43.8	0.338	0.288	40	-1.301	138.9	6.32
34.1	0.338	0.327	60	-1.959	183.5	7.75
22.0	0.338	0.224	80	-0.943	357.1	8.94
21.7	0.338	0.338	100	-	295.9	10.00

Table 4.169: Palm Kernel Shell- Ni/PKAC/ H_2SO_4/800˚C

C_t	q_e	q_t	t(min)	Log(q_e-q_t)	t/q_t	t^$^{0.5}$
48.4	0.320	0.276	20	-1.357	72.5	4.47
42.3	0.320	0.306	40	-1.854	130.7	6.32
35.5	0.320	0.313	60	-2.155	191.7	7.75
24.8	0.320	0.210	80	-0.959	380.9	8.94
24.1	0.320	0.320	100	-	312.5	10.00

Table 4.170: Palm Kernel Shell- Ni/PKAC/ H_3PO_4/800˚C

C_t	q_e	q_t	t(min)	Log(q_e-q_t)	t/q_t	t^$^{0.5}$
49.6	0.332	0.258	20	-1.131	77.5	4.47
42.9	0.332	0.299	40	-1.481	133.8	6.32
36.4	0.332	0.304	60	-1.553	197.4	7.75
22.8	0.332	0.220	80	-0.951	363.6	8.94
22.5	0.332	0.332	100	-	301.2	10.00

Table 4.171: Palm Kernel Shell- Pb/PKAC/HCl/600˚C

C_t	q_e	q_t	t(min)	Log(q_e-q_t)	t/q_t	t^$^{0.5}$
41.8	0.273	0.234	20	-1.401	85.5	4.47
37.2	0.273	0.252	40	-1.678	158.7	6.32
30.6	0.273	0.268	60	-2.301	223.9	7.75
21.8	0.273	0.178	80	-1.022	449.4	8.94
21.0	0.273	0.273	100	-	366.3	10.00

Table 4.172: Palm Kernel Shell- Pb/PKAC/ H_2SO_4/600˚C

C_t	q_e	q_t	t(min)	Log(q_e-q_t)	t/q_t	t^$^{0.5}$
43.9	0.256	0.202	20	-1.268	99.0	4.47
39.3	0.256	0.226	40	-1.523	176.9	6.32
32.8	0.256	0.246	60	-2.000	243.9	7.75
23.8	0.256	0.168	80	-1.056	476.2	8.94
23.2	0.256	0.256	100	-	390.6	10.00

Table 4.173: Palm Kernel Shell-Pb/PKAC/ H_3PO_4/600˚C

C_t	q_e	q_t	t(min)	Log(q_e-q_t)	t/q_t	t^$^{0.5}$
44.6	0.299	0.192	20	-1.432	104.2	4.47
40.8	0.299	0.207	40	-1.658	193.2	6.32
35.6	0.299	0.218	60	-1.959	275.2	7.75
27.2	0.299	0.151	80	-1.108	529.8	8.94
26.9	0.299	0.229	100	-	436.7	10.00

Table 4.174: Palm Kernel Shell- Pb/PKAC/HCl/800˚C

C_t	q_e	q_t	t(min)	Log(q_e-q_t)	t/q_t	t^$^{0.5}$
40.4	0.305	0.255	20	-1.301	78.4	4.47
35.1	0.305	0.279	40	-1.585	143.4	6.32
27.6	0.305	0.298	60	-2.155	201.3	7.75
16.5	0.305	0.204	80	-0.996	392.2	8.94
16.7	0.305	0.305	100	-	327.9	10.00

Table 4.175: Palm Kernel Shell- Pb/PKAC/ H_2SO_4/800˚C

C_t	q_e	q_t	t(min)	Log(q_e-q_t)	t/q_t	t^$^{0.5}$
42.1	0.268	0.229	20	-1.409	87.3	4.47
38.5	0.268	0.236	40	-1.495	169.5	6.32
31.9	0.268	0.255	60	-1.886	235.3	7.75
22.0	0.268	0.177	80	-1.041	451.9	8.94
21.7	0.268	0.268	100	-	373.1	10.00

Table 4.176: Palm Kernel Shell-Pb/PKAC/ H_3PO_4/800˚C

C_t	q_e	q_t	t(min)	Log(q_e-q_t)	t/q_t	t^$^{0.5}$
42.9	0.254	0.217	20	-1.432	92.2	4.47
38.4	0.254	0.237	40	-1.769	168.8	6.32
33.1	0.254	0.243	60	-1.959	246.9	7.75
23.9	0.254	0.167	80	-1.060	479.0	8.94
23.5	0.254	0.254	100	-	393.7	10.00

Table 4.177: Palm Kernel Shell- Cd/PKAC/HCl/600˚C

C_t	q_e	q_t	t(min)	Log(q_e-q_t)	t/q_t	t^$^{0.5}$
42.1	0.277	0.231	20	-1.337	86.6	4.47
36.6	0.277	0.261	40	-1.796	153.3	6.32
30.3	0.277	0.272	60	-2.301	220.6	7.75
20.9	0.277	0.183	80	-1.027	437.2	8.94
20.5	0.277	0.277	100	-	361.0	10.00

Table 4.178: Palm Kernel Shell- Cd/PKAC/ H_2SO_4/600˚C

C_t	q_e	q_t	t(min)	Log(q_e-q_t)	t/q_t	t^$^{0.5}$
44.3	0.258	0.198	20	-1.222	101.0	4.47
39.1	0.258	0.230	40	-1.553	173.9	6.32
32.2	0.258	0.253	60	-2.301	237.2	7.75
23.5	0.258	0.170	80	-1.056	470.6	8.94
23.0	0.258	0.258	100	-	387.6	10.00

Table 4.179: Palm Kernel Shell-Cd/PKAC/ H_3PO_4/600˚C

C_t	q_e	q_t	t(min)	Log(q_e-q_t)	t/q_t	t^$^{0.5}$
47.3	0.213	0.152	20	-1.215	131.6	4.47
43.1	0.213	0.180	40	-1.481	222.2	6.32
38.4	0.213	0.191	60	-1.658	314.1	7.75
29.5	0.213	0.140	80	-1.137	571.4	8.94
29.1	0.213	0.213	100	-	469.5	10.00

Table 4.180: Palm Kernel Shell-Cd/PKAC/HCl/800˚C

C_t	q_e	q_t	t(min)	Log(q_e-q_t)	t/q_t	t^$^{0.5}$
40.8	0.289	0.250	20	-1.409	80.0	4.47
35.4	0.289	0.276	40	-1.886	144.9	6.32
29.1	0.289	0.284	60	-2.301	211.3	7.75
18.7	0.289	0.194	80	-1.022	412.4	8.94
18.9	0.289	0.289	100	-	346.0	10.00

Table 4.181: Palm Kernel Shell- Cd/PKAC/ H_2SO_4/800˚C

C_t	q_e	q_t	t(min)	Log(q_e-q_t)	t/q_t	t^$^{0.5}$
42.7	0.273	0.222	20	-1.292	90.1	4.47
38.2	0.273	0.241	40	-1.495	165.9	6.32
31.3	0.273	0.262	60	-1.959	229.0	7.75
21.6	0.273	0.179	80	-1.027	446.9	8.94
21.1	0.273	0.273	100	-	366.3	10.00

Table 4.182: Palm Kernel Shell- Cd/PKAC/ H_3PO_4/800˚C

C_t	q_e	q_t	t(min)	Log(q_e-q_t)	t/q_t	t^$^{0.5}$
46.8	0.215	0.160	20	-1.260	125.0	4.47
42.1	0.215	0.192	40	-1.638	208.3	6.32
36.5	0.215	0.209	60	-2.222	287.1	7.75
29.1	0.215	0.142	80	-1.137	563.4	8.94
28.9	0.215	0.215	100	-	465.1	10.00

Table 4.183: Palm Kernel Shell- Mn/PKAC/HCl/600˚C

C_t	q_e	q_t	t(min)	Log(q_e-q_t)	t/q_t	t^$^{0.5}$
60.1	0.249	0.224	20	-1.602	89.3	4.47
56.3	0.249	0.234	40	-1.824	170.9	6.32
50.5	0.249	0.246	60	-2.523	243.9	7.75
41.6	0.249	0.167	80	-1.086	479.0	8.94
41.9	0.249	0.249	100	-	401.6	10.00

Table 4.184: Palm Kernel Shell- Mn/PKAC/ H_2SO_4/600˚C

C_t	q_e	q_t	t(min)	Log(q_e-q_t)	t/q_t	t^$^{0.5}$
61.3	0.248	0.206	20	-1.377	97.1	4.47
56.8	0.248	0.228	40	-1.699	175.4	6.32
51.1	0.248	0.239	60	-2.046	251.0	7.75
42.6	0.248	0.162	80	-1.066	493.8	8.94
42.0	0.248	0.248	100	-	403.2	10.00

Table 4.185: Palm Kernel Shell- Mn/PKAC/ H_3PO_4/600˚C

C_t	q_e	q_t	t(min)	Log(q_e-q_t)	t/q_t	t^$^{0.5}$
63.8	0.225	0.169	20	-1.252	118.3	4.47
58.2	0.225	0.211	40	-1.854	189.6	6.32
53.0	0.225	0.220	60	-2.301	272.7	7.75
45.8	0.225	0.146	80	-1.102	547.9	8.94
45.1	0.225	0.225	100	-	444.4	10.00

Table 4.186: Palm Kernel Shell-Mn/PKAC/HCl/800˚c

C_t	q_e	q_t	t(min)	Log(q_e-q_t)	t/q_t	t^$^{0.5}$
58.8	0.265	0.244	20	-1.678	81.9	4.47
54.5	0.265	0.257	40	-2.097	155.6	6.32
48.9	0.265	0.262	60	-2.523	229.0	7.75
39.3	0.265	0.179	80	-1.066	446.9	8.94
39.7	0.265	0.265	100	-	377.4	10.00

Table 4.187: Palm Kernel Shell-Mn/PKAC/ H_2SO_4/800˚C

C_t	q_e	q_t	t(min)	Log(q_e-q_t)	t/q_t	t^$^{0.5}$
60.0	0.262	0.226	20	-1.444	88.5	4.47
55.9	0.262	0.239	40	-1.638	167.4	6.32
49.8	0.262	0.253	60	-2.046	237.2	7.75
39.8	0.262	0.176	80	-1.066	454.5	8.94
40.1	0.262	0.262	100	-	381.7	10.00

Table 4.188: Palm Kernel Shell- Mn/PKAC/ H_3PO_4/800˚C

C_t	q_e	q_t	t(min)	Log(q_e-q_t)	t/q_t	t^$^{0.5}$
59.2	0.266	0.238	20	-1.553	84.0	4.47
55.4	0.266	0.246	40	-1.699	162.6	6.32
49.7	0.266	0.254	60	-1.921	236.2	7.75
39.6	0.266	0.266	80	-	300.8	8.94
39.0	0.266	0.180	100	-1.066	555.6	10.00

Table 4.189: Oil Bean- Pb/OBAC/HCl/600˚C

C_t	q_e	q_t	t(min)	Log(q_e-q_t)	t/q_t	t^$^{0.5}$
49.6	0.176	0.117	20	-1.229	170.9	4.47
46.2	0.176	0.139	40	-1.432	287.8	6.32
41.1	0.176	0.163	60	-1.886	368.1	7.75
34.2	0.176	0.115	80	-1.215	695.7	8.94
33.9	0.176	0.176	100	-	568.2	10.00

Table 4.190: Oil Bean-Pb/OBAC/ H_2SO_4/600˚C

C_t	q_e	q_t	t(min)	Log(q_e-q_t)	t/q_t	t^$^{0.5}$
44.2	0.244	0.197	20	-1.328	101.5	4.47
40.0	0.244	0.217	40	-1.569	184.3	6.32
34.6	0.244	0.228	60	-1.795	263.2	7.75
25.0	0.244	0.162	80	-1.086	493.8	8.94
24.9	0.244	0.244	100	-	409.8	10.00

Table 4.191: Oil Bean- Pb/OBAC/ H_3PO_4/600˚C

C_t	q_e	q_t	t(min)	Log(q_e-q_t)	t/q_t	t^$^{0.5}$
46.7	0.221	0.160	20	-1.215	125.0	4.47
41.4	0.221	0.199	40	-1.658	201.0	6.32
35.7	0.221	0.212	60	-2.398	283.0	7.75
28.2	0.221	0.146	80	-1.125	547.9	8.94
27.8	0.221	0.221	100	-	452.5	10.00

Table 4.192: Oil Bean- Pb/OBAC/HCl/800˚C

C_t	q_e	q_t	t(min)	Log(q_e-q_t)	t/q_t	t^$^{0.5}$
47.1	0.226	0.154	20	-1.143	129.9	4.47
44.8	0.226	0.157	40	-1.161	254.8	6.32
39.8	0.226	0.176	60	-1.301	340.9	7.75
27.9	0.226	0.147	80	-1.102	544.2	8.94
27.3	0.226	0.226	100	-	442.5	10.00

Table 4.193: Oil Bean-Pb/OBAC/ H_2SO_4/800˚C

C_t	q_e	q_t	t(min)	Log(q_e-q_t)	t/q_t	t^$^{0.5}$
42.5	0.269	0.223	20	-1.337	89.7	4.47
37.8	0.269	0.245	40	-1.619	163.3	6.32
31.1	0.269	0.263	60	-2.222	228.1	7.75
21.8	0.269	0.173	80	-1.018	462.4	8.94
21.5	0.269	0.269	100	-	371.7	10.00

Table 4.194: Oil Bean-Pb/OBAC/ H_3PO_4/800˚C

C_t	q_e	q_t	t(min)	Log(q_e-q_t)	t/q_t	t^$^{0.5}$
45.3	0.203	0.181	20	-1.658	110.5	4.47
42.8	0.203	0.182	40	-1.678	219.8	6.32
38.0	0.203	0.194	60	-2.046	309.3	7.75
30.6	0.203	0.134	80	-1.161	597.0	8.94
30.3	0.203	0.203	100	-	492.6	10.00

Table 4.195: Oil Bean-Ni/OBAC/HCl/600˚C

C_t	q_e	q_t	t(min)	Log(q_e-q_t)	t/q_t	t^$^{0.5}$
51.2	0.320	0.234	20	-1.066	85.5	4.47
47.1	0.320	0.246	40	-1.131	162.6	6.32
37.3	0.320	0.295	60	-1.602	203.4	7.75
24.8	0.320	0.210	80	-0.959	380.9	8.94
24.1	0.320	0.320	100	-	312.5	10.00

Table 4.196: Oil Bean-Ni/OBAC/ H_2SO_4/600˚C

C_t	q_e	q_t	t(min)	Log(q_e-q_t)	t/q_t	t^$^{0.5}$
47.2	0.380	0.294	20	-1.066	68.0	4.47
39.6	0.380	0.340	40	-1.398	117.6	6.32
29.0	0.380	0.378	60	-2.699	158.7	7.75
16.2	0.380	0.380	80	-	210.5	8.94
16.5	0.380	0.521	100	-0.889	191.9	10.00

Table 4.197: Oil Bean-Ni/OBAC/ H_3PO_4/600˚C

C_t	q_e	q_t	t(min)	Log(q_e-q_t)	t/q_t	t^$^{0.5}$
48.1	0.385	0.281	20	-0.983	71.2	4.47
41.2	0.385	0.320	40	-1.187	125.0	6.32
30.7	0.385	0.361	60	-1.619	166.2	7.75
25.6	0.385	0.206	80	-0.747	388.3	8.94
15.5	0.385	0.385	100	-	259.7	10.00

Table 4.198: Oil Bean-Ni/OBAC/HCl/800˚C

C_t	q_e	q_t	t(min)	Log(q_e-q_t)	t/q_t	t^$^{0.5}$
48.6	0.365	0.273	20	-1.036	73.3	4.47
38.6	0.365	0.351	40	-1.854	113.9	6.32
30.9	0.365	0.359	60	-2.222	167.1	7.75
18.3	0.365	0.243	80	-0.914	329.2	8.94
18.1	0.365	0.365	100	-	273.9	10.00

Table 4.199: Oil Bean-Ni/OBAC/ H_2SO_4/800˚C

C_t	q_e	q_t	t(min)	Log(q_e-q_t)	t/q_t	t^$^{0.5}$
41.3	0.445	0.385	20	-1.222	51.9	4.47
33.6	0.445	0.415	40	-1.523	96.4	6.32
22.6	0.445	0.442	60	-2.523	135.7	7.75
7.0	0.445	0.300	80	-0.839	266.7	8.94
7.5	0.445	0.445	100	-	224.7	10.00

Table 4.200: Oil Bean-Ni/OBAC/ $H_3PO_4$800˚C

C_t	q_e	q_t	t(min)	Log(q_e-q_t)	t/q_t	t^$^{0.5}$
46.1	0.347	0.311	20	-1.444	64.3	4.47
41.3	0.347	0.319	40	-1.553	125.4	6.32
33.8	0.347	0.330	60	-1.769	181.8	7.75
20.8	0.347	0.230	80	-0.932	347.8	8.94
20.6	0.347	0.347	100	-	288.2	10.00

Table 4.201: Oil Bean-Cd/OBAC/HCl/600˚C

C_t	q_e	q_t	t(min)	Log(q_e-q_t)	t/q_t	t^$^{0.5}$
48.2	0.178	0.138	20	-1.397	144.9	4.47
45.1	0.178	0.155	40	-1.638	258.1	6.32
40.0	0.178	0.175	60	-2.523	342.9	7.75
33.4	0.178	0.120	80	-2.237	666.7	8.94
33.7	0.178	0.178	100	-	561.8	10.00

Table 4.202: Oil Bean-Cd/OBAC/ H_2SO_4/600˚C

C_t	q_e	q_t	t(min)	Log(q_e-q_t)	t/q_t	t^$^{0.5}$
44.3	0.241	0.198	20	-1.367	101.0	4.47
40.8	0.241	0.208	40	-1.481	192.3	6.32
34.5	0.241	0.229	60	-1.921	262.0	7.75
25.0	0.241	0.162	80	-1.102	493.8	8.94
25.3	0.241	0.241	100	-	414.9	10.00

Table 4.203: Oil Bean-Cd/OBAC/ H_3PO_4/600˚C

C_t	q_e	q_t	t(min)	Log(q_e-q_t)	t/q_t	t^$^{0.5}$
45.9	0.264	0.173	20	-1.041	115.6	4.47
41.3	0.264	0.202	40	-1.208	198.0	6.32
36.4	0.264	0.211	60	-1.276	284.4	7.75
22.6	0.246	0.174	80	-1.046	459.8	8.94
22.3	0.246	0.264	100	-	378.8	10.00

Table 4.204: Oil Bean-Cd/OBAC/HCl/800˚C

C_t	q_e	q_t	t(min)	Log(q_e-q_t)	t/q_t	t^$^{0.5}$
47.4	0.223	0.151	20	-1.143	132.5	4.47
42.2	0.223	0.191	40	-1.494	209.4	6.32
37.5	0.223	0.199	60	-1.620	301.5	7.75
27.9	0.223	0.147	80	-1.119	544.2	8.94
27.3	0.223	0.223	100	-	448.4	10.00

Table 4.205: Oil Bean-Cd/OBAC/ H_2SO_4/800˚C

C_t	q_e	q_t	t(min)	Log(q_e-q_t)	t/q_t	t^$^{0.5}$
40.3	0.292	0.258	20	-1.469	77.5	4.47
36.5	0.292	0.262	40	-1.523	152.7	6.32
29.3	0.292	0.282	60	-2.000	212.8	7.75
18.6	0.292	0.292	80	-	274.0	8.94
18.3	0.292	0.192	100	-1.000	520.8	10.00

Table 4.206: Oil Bean-Cd/OBAC/ H_3PO_4/800˚C

C_t	q_e	q_t	t(min)	Log(q_e-q_t)	t/q_t	t^$^{0.5}$
41.9	0.283	0.234	20	-1.310	85.5	4.47
37.3	0.283	0.252	40	-1.509	158.7	6.32
30.8	0.283	0.267	60	-1.796	224.7	7.75
19.7	0.283	0.192	80	-1.041	416.7	8.94
19.7	0.283	0.283	100	-	353.4	10.00

Table 4.207: Oil Bean-Mn/OBAC/HCl/600˚C

C_t	q_e	q_t	t(min)	Log(q_e-q_t)	t/q_t	t^$^{0.5}$
63.8	0.244	0.214	20	-1.523	93.5	4.47
57.4	0.244	0.221	40	-1.638	180.9	6.32
51.3	0.244	0.238	60	-2.222	252.1	7.75
42.8	0.244	0.161	80	-1.081	496.9	8.94
42.5	0.244	0.244	100	-	409.8	10.00

Table 4.208: Oil Bean-Mn/OBAC/ H_2SO_4/600˚C

C_t	q_e	q_t	t(min)	Log(q_e-q_t)	t/q_t	t^$^{0.5}$
64.2	0.214	0.163	20	-1.292	122.7	4.47
60.9	0.214	0.177	40	-1.432	225.9	6.32
55.4	0.214	0.197	60	-1.770	304.6	7.75
46.9	0.214	0.141	80	-1.137	567.4	8.94
46.5	0.214	0.214	100	-	467.3	10.00

Table 4.209: Oil Bean-Mn/OBAC/ H_3PO_4/600˚C

C_t	q_e	q_t	t(min)	Log(q_e-q_t)	t/q_t	t^$^{0.5}$
62.7	0.261	0.185	20	-1.119	108.1	4.47
56.9	0.261	0.227	40	-1.469	176.2	6.32
50.1	0.261	0.250	60	-1.959	240.0	7.75
41.0	0.261	0.170	80	-1.041	470.6	8.94
40.2	0.261	0.261	100	-	383.1	10.00

Table 4.210: Oil Bean-Mn/OBAC/HCl/800˚C

C_t	q_e	q_t	t(min)	Log(q_e-q_t)	t/q_t	t^$^{0.5}$
61.9	0.255	0.197	20	-1.237	101.5	4.47
56.8	0.255	0.228	40	-1.569	175.4	6.32
56.2	0.255	0.249	60	-2.222	240.9	7.75
41.4	0.255	0.168	80	-1.060	476.2	8.94
41.1	0.255	0.255	100	-	392.2	10.00

Table 4.211: Oil Bean-Mn/OBAC/ H_2SO_4/800˚C

C_t	q_e	q_t	t(min)	Log(q_e-q_t)	t/q_t	t^$^{0.5}$
60.8	0.259	0.214	20	-1.347	93.5	4.47
57.0	0.259	0.226	40	-1.481	176.9	6.32
52.1	0.259	0.230	60	-1.538	260.9	7.75
40.9	0.259	0.171	80	-1.056	467.8	8.94
40.4	0.259	0.259	100	-	386.1	10.00

Table 4.212: Oil Bean-Mn/OBAC/H_3PO_4/800˚C

C_t	q_e	q_t	t(min)	Log(q_e-q_t)	t/q_t	t^$^{0.5}$
61.9	0.273	0.197	20	-1.119	101.5	4.47
55.7	0.273	0.242	40	-1.509	165.3	6.32
49.4	0.273	0.257	60	-1.796	233.5	7.75
39.1	0.273	0.180	80	-1.032	444.4	8.94
38.6	0.273	0.273	100	-	366.3	10.00

Table 4.213: Snail Shell-Ni/SSAC/HCl/600˚C

C_t	q_e	q_t	t(min)	Log(q_e-q_t)	t/q_t	t^$^{0.5}$
62.1	0.104	0.071	20	-1.481	281.7	4.47
60.3	0.104	0.081	40	-1.638	493.8	6.32
55.3	0.104	0.086	60	-1.745	930.2	7.75
54.9	0.104	0.060	80	-1.301	1666.7	8.94
56.4	0.104	0.104	100	-	576.9	10.00

Table 4.214: Snail Shell-Ni/SSAC/H_2SO_4/600˚C

C_t	q_e	q_t	t(min)	Log(q_e-q_t)	t/q_t	t^$^{0.5}$
63.0	0.088	0.057	20	-1.509	350.9	4.47
61.5	0.088	0.066	40	-1.658	606.1	6.32
58.3	0.088	0.085	60	-2.523	705.9	7.75
55.0	0.088	0.059	80	-1.538	1694.9	8.94
55.1	0.088	0.088	100	-	909.1	10.00

Table 4.215: Snail Shell-Ni/SSAC/H_3PO_4/600˚C

C_t	q_e	q_t	t(min)	Log(q_e-q_t)	t/q_t	t^$^{0.5}$
61.7	0.124	0.077	20	-1.328	259.7	4.47
58.2	0.124	0.108	40	-1.796	370.4	6.32
55.8	0.124	0.111	60	-1.854	545.5	7.75
50.3	0.124	0.083	80	-1.387	1204.8	8.94
50.3	0.124	0.124	100	-	645.2	10.00

Table 4.216: Snail Shell-Ni/SSAC/HCl/800˚C

C_t	q_e	q_t	t(min)	Log(q_e-q_t)	t/q_t	t^$^{0.5}$
60.0	0.147	0.102	20	-1.347	196.1	4.47
56.3	0.147	0.131	40	-1.796	305.3	6.32
53.3	0.147	0.101	60	-1.337	792.1	7.75
53.4	0.147	0.067	80	-1.097	1492.5	8.94
52.1	0.147	0.147	100	-	408.2	10.00

Table 4.217: Snail Shell-Ni/SSAC/ H_2SO_4/800˚C

C_t	q_e	q_t	t(min)	Log(q_e-q_t)	t/q_t	t^$^{0.5}$
62.4	0.085	0.066	20	-1.721	303.0	4.47
61.1	0.085	0.071	40	-1.854	563.4	6.32
55.8	0.085	0.083	60	-2.699	963.9	7.75
55.7	0.085	0.056	80	-1.538	1785.7	8.94
58.3	0.085	0.085	100	-	705.9	10.00

Table 4.218: Snail Shell-Ni/SSAC/ H_3PO_4/800˚C

C_t	q_e	q_t	t(min)	Log(q_e-q_t)	t/q_t	t^$^{0.5}$
60.9	0.114	0.089	20	-1.602	224.7	4.47
55.8	0.114	0.110	40	-2.398	545.5	6.32
51.7	0.114	0.113	60	-3.000	707.9	7.75
51.7	0.114	0.076	80	-1.420	1315.8	8.94
57.7	0.114	0.114	100	-	350.9	10.00

Table 4.219: Snail Shell-Pb/SSAC/HCl/600˚C

C_t	q_e	q_t	t(min)	Log(q_e-q_t)	t/q_t	t^$^{0.5}$
51.8	0.107	0.084	20	-1.638	238.1	4.47
49.3	0.107	0.101	40	-2.222	396.0	6.32
46.5	0.107	0.082	60	-1.602	975.6	7.75
46.1	0.107	0.057	80	-1.301	1754.4	8.94
46.7	0.107	0.107	100	-	560.7	10.00

Table 4.220: Snail Shell-Pb/SSAC/H_2SO_4/600˚C

C_t	q_e	q_t	t(min)	Log(q_e-q_t)	t/q_t	t^$^{0.5}$
52.6	0.121	0.072	20	-1.310	277.8	4.47
46.0	0.121	0.114	40	-2.155	526.3	6.32
45.1	0.121	0.092	60	-1.538	869.6	7.75
44.3	0.121	0.066	80	-1.260	1515.2	8.94
47.7	0.121	0.121	100	-	330.6	10.00

Table 4.221: Snail Shell-Pb/SSAC/H_3PO_4/600˚C

C_t	q_e	q_t	t(min)	Log(q_e-q_t)	t/q_t	t^$^{0.5}$
53.8	0.086	0.050	20	-1.444	400.0	4.47
51.3	0.086	0.076	40	-2.000	526.3	6.32
46.7	0.086	0.080	60	-2.222	1000.0	7.75
45.8	0.086	0.058	80	-1.553	1724.1	8.94
48.8	0.086	0.086	100	-	697.7	10.00

Table 4.222: Snail Shell-Pb/SSAC/HCl/800˚C

C_t	q_e	q_t	t(min)	Log(q_e-q_t)	t/q_t	t^$^{0.5}$
50.3	0.119	0.107	20	-1.921	186.9	4.47
48.7	0.119	0.109	40	-2.000	366.9	6.32
44.9	0.119	0.094	60	-1.602	851.1	7.75
43.0	0.119	0.072	80	-1.328	1388.9	8.94
45.5	0.119	0.119	100	-	504.2	10.00

Table 4.223: Snail Shell-Pb/SSAC/H_2SO_4/800˚C

C_t	q_e	q_t	t(min)	Log(q_e-q_t)	t/q_t	t^$^{0.5}$
49.9	0.125	0.113	20	-1.921	176.9	4.47
46.2	0.125	0.114	40	-1.035	285.7	6.32
43.1	0.125	0.107	60	-1.745	747.7	7.75
43.0	0.125	0.072	80	-1.276	1388.9	8.94
44.9	0.125	0.125	100	-	480.0	10.00

Table 4.224: Snail Shell-Pb/SSAC/ H_3PO_4/800˚C

C_t	q_e	q_t	t(min)	Log(q_e-q_t)	t/q_t	t^$^{0.5}$
52.7	0.416	0.071	20	-0.462	281.7	4.47
50.2	0.416	0.090	40	-0.487	444.4	6.32
42.4	0.416	0.113	60	-0.519	707.9	7.75
41.1	0.416	0.082	80	-0.476	1219.5	8.94
47.0	0.416	0.416	100	-	144.2	10.00

Table 4.225: Snail Shell-Cd/SSAC/HCl/600˚C

C_t	q_e	q_t	t(min)	Log(q_e-q_t)	t/q_t	t^$^{0.5}$
53.2	0.152	0.065	20	-1.060	307.7	4.47
51.0	0.152	0.098	40	-1.268	408.2	6.32
42.1	0.152	0.116	60	-1.444	698.7	7.75
43.0	0.152	0.133	80	-1.102	601.5	8.94
42.3	0.152	0.152	100	-	657.9	10.00

Table 4.226: Snail Shell-Cd/SSAC/ H_2SO_4/600˚C

C_t	q_e	q_t	t(min)	Log(q_e-q_t)	t/q_t	t^$^{0.5}$
55.0	0.099	0.038	20	-1.215	526.3	4.47
51.2	0.099	0.079	40	-1.699	506.3	6.32
44.9	0.099	0.095	60	-2.398	842.1	7.75
43.3	0.099	0.071	80	-1.553	1408.5	8.94
47.6	0.099	0.099	100	-	606.1	10.00

Table 4.227: Snail Shell-Cd/SSAC/ H_3PO_4/600˚C

C_t	q_e	q_t	t(min)	Log(q_e-q_t)	t/q_t	t^$^{0.5}$
51.8	0.138	0.086	20	-1.284	232.6	4.47
48.4	0.138	0.114	40	-1.620	350.9	6.32
42.6	0.138	0.112	60	-1.585	714.3	7.75
42.5	0.138	0.075	80	-1.201	1333.3	8.94
43.7	0.138	0.138	100	-	434.8	10.00

Table 4.228: Snail Shell-Cd/SSAC/HCl/800˚C

C_t	q_e	q_t	t(min)	Log(q_e-q_t)	t/q_t	t^$^{0.5}$
54.1	0.088	0.051	20	-1.432	392.2	4.47
50.3	0.088	0.090	40	-1.005	444.4	6.32
48.5	0.088	0.090	60	-1.005	666.7	7.75
45.8	0.088	0.088	80	-	909.1	8.94
45.7	0.088	0.059	100	-1.538	1695	10.00

Table 4.229: Snail Shell-Cd/SSAC/ H_2SO_4/800˚C

C_t	q_e	q_t	t(min)	Log(q_e-q_t)	t/q_t	t^$^{0.5}$
53.8	0.099	0.056	20	-1.367	357.1	4.47
49.9	0.099	0.095	40	-2.398	421.1	6.32
46.1	0.099	0.086	60	-1.886	697.7	7.75
46.0	0.099	0.058	80	-1.387	1379.3	8.94
47.6	0.099	0.099	100	-	1010.1	10.00

Table 4.230: Snail Shell-Cd/SSAC/ H_3PO_4/800˚C

C_t	q_e	q_t	t(min)	Log(q_e-q_t)	t/q_t	t^$^{0.5}$
54.0	0.103	0.053	20	-1.301	377.4	4.47
50.3	0.103	0.090	40	-1.886	444.4	6.32
48.1	0.103	0.094	60	-2.046	638.3	7.75
43.3	0.103	0.071	80	-1.495	1126.8	8.94
43.8	0.103	0.103	100	-	970.9	10.00

Table 4.231: Snail Shell-Mn/SSAC/HCl/600˚C

C_t	q_e	q_t	t(min)	Log(q_e-q_t)	t/q_t	t^$^{0.5}$
68.1	0.238	0.105	20	-0.876	190.5	4.47
62.3	0.238	0.160	40	-1.108	250.0	6.32
44.9	0.238	0.189	60	-1.310	317.5	7.75
49.8	0.238	0.127	80	-0.955	629.9	8.94
51.3	0.238	0.238	100	-	420.2	10.00

Table 4.232: Snail Shell-Mn/SSAC/ H_2SO_4/600˚C

C_t	q_e	q_t	t(min)	Log(q_e-q_t)	t/q_t	t^$^{0.5}$
67.8	0.168	0.110	20	-1.237	181.8	4.47
55.5	0.168	0.147	40	-1.678	272.1	6.32
54.3	0.168	0.104	60	-1.194	576.9	7.75
61.7	0.168	0.168	80	-	476.2	8.94
58.3	0.168	0.168	100	-	595.2	10.00

Table 4.233: Snail Shell-Mn/SSAC/ H_3PO_4/600˚C

C_t	q_e	q_t	t(min)	Log(q_e-q_t)	t/q_t	t^$^{0.5}$
65.8	0.185	0.140	20	-1.347	142.9	4.47
58.9	0.185	0.162	40	-1.638	246.9	6.32
56.4	0.185	0.140	60	-1.347	428.6	7.75
56.4	0.185	0.090	80	-1.041	888.9	8.94
60.3	0.185	0.185	100	-	540.5	10.00

Table 4.234: Snail Shell-Mn/SSAC/HCl/800˚C

C_t	q_e	q_t	t(min)	Log(q_e-q_t)	t/q_t	t^$^{0.5}$
65.8	0.138	0.078	20	-1.222	256.4	4.47
60.3	0.138	0.105	40	-1.481	380.9	6.32
56.4	0.138	0.072	60	-1.180	833.3	7.75
56.4	0.138	0.171	80	-1.174	470.6	8.94
58.9	0.138	0.138	100	-	724.6	10.00

Table 4.235: Snail Shell-Mn/SSAC/ H_2SO_4/800˚C

C_t	q_e	q_t	t(min)	Log(q_e-q_t)	t/q_t	t^$^{0.5}$
66.7	0.146	0.126	20	-1.699	158.7	4.47
63.8	0.146	0.141	40	-2.301	283.7	6.32
59.1	0.146	0.160	60	-1.854	375.0	7.75
55.6	0.146	0.100	80	-1.134	1000.0	8.94
55.7	0.146	0.146	100	-	547.9	10.00

Table 4.236: Snail Shell-Mn/SSAC/H_3PO_4/800˚C

C_t	q_e	q_t	t(min)	Log(q_e-q_t)	t/q_t	t^$^{0.5}$
64.9	0.173	0.153	20	-1.699	130.7	4.47
61.5	0.173	0.170	40	-2.523	235.3	6.32
56.7	0.173	0.138	60	-1.456	434.8	7.75
52.2	0.173	0.115	80	-1.237	869.6	8.94
52.1	0.173	0.173	100	-	462.4	10.00